

**The nature of mantle sources for Recent alkaline basalts
across the northern Canadian Cordillera**

Anne-Claude ABRAHAM

Department of Earth and Planetary Sciences

McGill University, Montréal

April 2002

A thesis submitted to

the Faculty of Graduate Studies and Research

in partial fulfilment of requirements of the degree of

Doctor of Philosophy

Copyright © Anne-Claude Abraham 2002



National Library
of Canada

Acquisitions and
Bibliographic Services

395 Wellington Street
Ottawa ON K1A 0N4
Canada

Bibliothèque nationale
du Canada

Acquisitions et
services bibliographiques

395, rue Wellington
Ottawa ON K1A 0N4
Canada

Your file Votre référence

Our file Notre référence

The author has granted a non-exclusive licence allowing the National Library of Canada to reproduce, loan, distribute or sell copies of this thesis in microform, paper or electronic formats.

L'auteur a accordé une licence non exclusive permettant à la Bibliothèque nationale du Canada de reproduire, prêter, distribuer ou vendre des copies de cette thèse sous la forme de microfiche/film, de reproduction sur papier ou sur format électronique.

The author retains ownership of the copyright in this thesis. Neither the thesis nor substantial extracts from it may be printed or otherwise reproduced without the author's permission.

L'auteur conserve la propriété du droit d'auteur qui protège cette thèse. Ni la thèse ni des extraits substantiels de celle-ci ne doivent être imprimés ou autrement reproduits sans son autorisation.

0-612-78635-8

Canada

Abstract

The Stikine Volcanic Belt is a lineament of Tertiary to Recent alkaline volcanic centres that cross disparate oceanic and continental terranes of the northern Canadian Cordillera, and extend onto the North America craton. This volcanic lineament thus offers an unique opportunity to probe the lithospheric mantle beneath these terranes and investigate the relative roles of lithospheric and asthenospheric mantle sources in the generation of alkaline lavas.

Alkaline lavas in twelve volcanic centres of the Stikine Volcanic Belt were sampled and studied for major and trace elements and Sr-Nd-Pb isotopic compositions. The primitive lavas of each volcanic centre define binary arrays between two compositional end-members, olivine nephelinite (NEPH) and hypersthene-normative olivine basalt (Hy-NORM). The NEPH end-member is characterized by large enrichments in incompatible trace elements with respect to primitive mantle, but is depleted in term of its isotopic composition. The presence of amphibole in its source suggests that this end-member is derived from the lithospheric mantle. The Hy-NORM end-member has lower incompatible trace element contents, but is still relatively enriched in incompatible elements compared to primitive mantle. Although this end-member has always more radiogenic Sr and Pb, and less radiogenic Nd isotopic ratios than the NEPH end-member, its isotopic signature varies with the tectonic belt in which it erupted, indicating a significant role for the lithospheric mantle in the derivation of the Hy-NORM basalts.

The Canadian Cordilleran, and other continental Hy-NORM basalts, have low Ca and high Na contents compared to their equivalents at oceanic hot spots such as Hawaii or associated with mid-ocean ridges. A comparison with experimental melts of mantle peridotite indicates that these characteristics reflect smaller degrees of partial melting (<10%) in continental regime. The range of observed lava compositions is explained by the melting of two distinct lithospheric components, a NEPH end-member representing the melting of amphibole-rich veins, and a Hy-NORM end-member resulting from small degrees of partial melting of their host garnet lherzolite. The high heat flow values reported in the northern Canadian Cordillera are consistent with a model in which ongoing melting and thinning of the lithospheric mantle is responsible for generating the mafic alkaline magmas.

Résumé

La ceinture volcanique Stikine est une chaîne de centres volcaniques alcalins Tertiaires et Récents qui recoupe les terrains disparates océaniques et continentaux du nord de la Cordillère Canadienne et se prolonge jusqu'au craton Nord Américain. Cette ceinture volcanique offre donc une occasion unique de sonder le manteau lithosphérique situé sous ces terrains et d'examiner les rôles relatifs joués par les sources mantelliques de type lithosphérique ou asthénosphérique dans la genèse des laves alcalines.

Les laves alcalines de douze centres volcaniques de la ceinture volcanique Stikine ont été échantillonnées et étudiées pour leurs éléments majeurs, en trace, et leur composition isotopique en Sr, Nd et Pb. Les laves primitives de chaque centre volcanique se répartissent entre deux pôles dont les compositions correspondent d'une part aux néphélinites à olivine (NEPH) et d'autre part aux basaltes à olivine à hypersthène normatif (Hy-NORM). Le pôle NEPH est caractérisé par de forts enrichissements en éléments en trace incompatibles par rapport au manteau primitif, mais possède une composition isotopique appauvrie. La présence d'amphibole dans la source de ce pôle suggère qu'il provient du manteau lithosphérique. Le pôle Hy-NORM a des concentrations plus faibles en éléments en trace incompatibles, tout en restant relativement enrichi par rapport au manteau primitif. Bien que ce pôle soit toujours plus radiogénique en Sr et en Pb, et moins radiogénique en Nd que le pôle NEPH, sa composition isotopique varie en fonction de la ceinture volcanique d'où il provient, indiquant un rôle important du manteau lithosphérique dans la génèse des basaltes de type Hy-NORM.

Les basaltes Hy-NORM de la Cordillère Canadienne et d'autres régions continentales ont des concentrations faibles en Ca et élevées en Na par rapport à leurs équivalents provenant de points chauds océaniques tels qu'Hawaii ou de ridges mid-océaniques. Une comparaison avec des liquides silicatés obtenus expérimentalement à partir de péridotite indique que ces caractéristiques reflètent de plus petits degrés de fusion partielle (<10%) en régime continental. L'entièvre gamme de composition des laves alcalines peut être expliquée par la fusion de deux composantes lithosphériques distinctes, le pôle NEPH représentant la fusion de veines riches en amphibole, et le pôle Hy-NORM résultant de petits degrés de fusion partielle de la lherzolite à grenat qui les entoure. Les hautes valeurs de flux de chaleur mesurées dans le nord de la Cordillère Canadienne sont

en accord avec un modèle où la fusion et l'amincissement du manteau lithosphérique seraient responsables de la genèse des magmas alcalins.

Acknowledgements

I would like to thank my supervisor Don Francis for offering me the chance to work on this project, for his advice and discussions, and for his patience in correcting my papers. I would also like to thank Mireille Polv , my un-official co-supervisor, who taught me her expertise in trace element and isotopic analysis, and provided me with advice and moral support during these years.

I am grateful to Georges Panagiotidis for producing thin sections, to Tariq Ahmedali and Glenna Keating for performing XRF analyses, to Bernard Reynier and Michel Valladon for helping me in acquiring the ICP-MS analyses, and to Pierre Brunet for training me in acquiring the TIMS analyses. I would like also to thank my brother Emmanuel Abraham and Fabien Rasselet for their assistance in the field.

Je n'aurais certainement jamais termin  cette th se sans le soutien de ma famille et de mes amis. Je tiens tout particulièrement  remercier mes parents Claude et Marie-France, et mon amie Jeanne Gendreau, qui ont t  pr s de moi pendant les plus durs moments, et qui ont tout fait pour que je finisse ce projet de longue haleine. Merci, papa et maman, pour votre amour et votre aide. Merci, Jeanne, pour ta confiance et les emails quotidiens que tu m'as envoy s pendant cette ann e 2001. Et merci  Marieke et Chouc qui nous ont permis de nous rencontrer. Merci aussi  ma 'petite soeur' Isabelle pour ses nombreux fax, et  mes fr res Emmanuel et Jean-S bastien pour leur soutien plus discret.

Je voudrais aussi remercier mes amis qui m'ont accueillie et log e  Montr al, Yann et Anik, ma colloc qui me gardait toujours une petite chambre dans ses logements successifs, ainsi que Brigitte et Hashem pour leur accueil chaleureux et les nombreux barbecues. Et bien s r, Jeanne et Virginie, pour leur accueil, et leur aide  d stresser, que ce soit au cours de nombreuses discussions autour d'un verre ou sur un terrain de squash.

Pour continuer avec Montr al, je voudrais remercier mes amis de McGill, Pierre Hudon pour son aide  s cher bien des larmes et ses nombreux emails 'Lâche pas!', Anne Peslier pour ses emails quotidiens lors de mes s jours  McGill, Annick Chouinard pour nos nombreuses discussions gastronomiques autour de soupers sympathiques, Peter Haas pour nos discussions sur les pyrox nites et ses cours de sushis. I would like to thank Sheldon Modeland for the coffee breaks, as well as all the students, staff and professors at McGill who made my stay much easier. Je veux aussi remercier mes amis 'hors McGill', entre autres Ginette Berube et la bande des biochimistes, ainsi que Val rie Hasik, Jean-Robert, Suzanne, Ben, Emilie et Daphn .

Je tiens  remercier mes coll gues et amis du LMTG de Toulouse, S bastien Aries, pour ses encouragements et sa confiance, David Baqu  pour ses cours sur les melons, Patricia et Fred Coppin pour leur convivialit  sans pareille, Samuel Deberdt, l'aventurier du grand Sud, et J r me Viers, pour son affection et son aide. Je voudrais galement remercier tous les autres 'vieux' et 'jeunes' th sards du LMTG, ainsi que les ITA, tout particulierement ma coll gue sur l'HPLC durant 6 mois, Jocelyne Escalier, et Bernard

Reynier pour ses petites histoires lors des pauses cafés. Merci aussi aux permanents du LMTG pour leur accueil et leurs encouragements lors de la rédaction de cette thèse.

J'aimerais également remercier Pierre Schiano pour avoir pris le temps de me rencontrer et m'avoir encouragée à finir cette thèse à un moment crucial.

Merci à tous mes amis toulousains qui ne m'ont pas oubliée malgré mes nombreux allers-retours Montréal-Amsterdam-Toulouse. Je ne peux pas nommer tout le monde, mais je tiens tout particulièrement à remercier Pédro, Chet et Fabienne, Xavier, la bande des DTT, c'est à dire Floflo, Christophe et Chloé et Marie, ainsi qu'Hailla, et Didier et Manue. Merci également au petit Nicolas barcelonais pour son soutien lors de mon oral de pré-doctorat.

J'aimerais finalement remercier Daan qui m'a aidée et soutenue moralement et financièrement pendant les 6 premières années de travail sur cette thèse, ainsi que ses parents Niek et Mechteld, et le reste de sa famille, en particulier Heleen et Frank, et Klaartje et Tiago. Danke jullie well!

Table of contents

Abstract.....	ii
Résumé.....	iii
Acknowledgments.....	v
Table of contents.....	vii
List of figures.....	x
List of tables.....	xvii
List of appendices.....	xviii
Preface.....	xx
Thesis outline.....	xxi
Originality.....	xxii
Contributions of co-authors.....	xxiii
Guidelines concerning thesis preparation.....	xxiii
CHAPTER I: General introduction.....	1
Introduction	2
The Stikine Volcanic Belt	5
References.....	8
CHAPTER II: Tertiary to Recent alkaline volcanoes of the Stikine Volcanic Belt, northern British Columbia.....	12
Abstract.....	13
1. Introduction.....	14
2. Tectonic setting.....	21
3. Classification of the lavas.....	22
4. Volcanic centres of the Stikine Volcanic Belt from S-W to N-E.....	23
4.1. <i>Mount Edziza</i>	23
4.2. <i>Level Mountain</i>	31
4.3. <i>Kawdy Mountain</i>	50
4.4. <i>Metahag Mountain</i>	62

4.5. <i>Metah Mountain</i>	73
4.6. <i>Tuya Butte</i>	85
4.7. <i>Tanzilla Volcano</i>	97
4.8. <i>Dome Mountain Volcanics</i>	108
4.9. <i>Jennings River</i>	118
4.10. <i>Nome Cone</i>	130
4.11. <i>Little Rancheria</i>	141
4.12. <i>Blue River</i>	152
4.13. <i>Caribou Tuya</i>	164
4.14. <i>Rancheria area</i>	175
4.15. <i>Watson Lake</i>	184
5. Discussion.....	191
5.1. <i>Magmatic groups</i>	191
5.2. <i>Spatial and temporal relationships</i>	194
5.3. <i>Volumes of the magma types</i>	195
5.4. <i>Volcanic-tectonic relationships</i>	196
6. Conclusion.....	197
References.....	199

CHAPTER III: Recent Alkaline Basalts as Probes of the Lithospheric Mantle Roots of the Northern Canadian Cordillera.....	203
Abstract.....	204
1. Introduction.....	205
2. Tectonic and geologic settings.....	209
3. Sample population and classification.....	211
4. Recent alkaline basalts.....	215
4.1. <i>Trace elements</i>	215
4.2. <i>Isotopes</i>	224
4.3. <i>Comparison with mantle xenoliths</i>	237
4.4. <i>Comparison with crustal granitoids</i>	240
5. Discussion.....	249

<i>5.1. Evaluation of crustal contamination.....</i>	249
<i>5.2. Evidence for distinct lithospheric mantle roots.....</i>	259
<i>5.3. Tectonic implications.....</i>	261
<i>5.3.1. Tintina Fault</i>	261
<i>5.3.2. Omineca Belt –Intermontane Belt transition.....</i>	263
<i>5.3.3. Intermontane Belt-Coast Belt transition.....</i>	264
6. Conclusion.....	265
Acknowledgements.....	266
References.....	267
CHAPTER IV: Origin of recent alkaline lavas by lithospheric thinning in the northern Canadian Cordillera.....	272
Abstract.....	273
1. Introduction.....	274
2. Tectonic setting.....	278
3. Magmatic end-members	281
3.1. NEPH lavas.....	282
3.2. Hy-NORM basalts.....	299
4. Discussion:	306
4.1. <i>Mantle source of NEPH lavas.....</i>	306
4.2. <i>Mantle source of Hy-NORM basalts.....</i>	326
4.3. <i>The composition range from Hy-NORM to AOB and BASAN... ..</i>	338
4.4. <i>Evidence for lithospheric thinning.....</i>	342
5. Conclusion.....	344
Acknowledgements.....	345
References.....	346
CHAPTER V: General conclusion.....	360
Appendices.....	365

List of figures

CHAPTER II	12
Figure 1.1: Location map of the Stikine Volcanic Belt and other Tertiary to Recent alkaline volcanic centres in the northern Canadian Cordillera.....	16
Figure 1.2: Enlargement of the northern part of the Stikine Volcanic Belt.....	18
Figure 2.1: a) $\text{Na}_2\text{O} + \text{K}_2\text{O}$ versus SiO_2 , and b) FeO (total) versus MgO in wt.% for Mount Edziza alkaline lavas.....	25
Figure 2.2: a) Trace element patterns of Mount Edziza mafic lavas ($\text{MgO} > 5$ wt.%) and hawaiites normalized to the primitive mantle values of Sun and McDonough (1989). b) Trace element patterns of Mount Edziza rhyolite normalized to the primitive mantle values of Sun and McDonough (1989).....	27
Figure 2.3: a) $^{143}\text{Nd}/^{144}\text{Nd}$ versus $^{87}\text{Sr}/^{86}\text{Sr}$, and b) $^{208}\text{Pb}/^{204}\text{Pb}$ versus $^{206}\text{Pb}/^{204}\text{Pb}$ for Mount Edziza mafic alkaline lavas.	29
Figure 3.1: Photos of the lava plateau forming the base of Level Mountain: a) from a distance, b) closer view of the sampled section, c) closer view of the lava flows.....	32
Figure 3.2: Photos of the strato volcano constituting the top of Level Mountain: a) the eastern part, b) Messah Peak.....	34
Figure 3.3: Location of our sections on section #3 of Hamilton (1981).....	36
Figure 3.4: a) $\text{Na}_2\text{O} + \text{K}_2\text{O}$ versus SiO_2 , and b) FeO (total) versus MgO in wt.% for Level Mountain alkaline lavas compared to Hamilton (1981)'s data set.....	39
Figure 3.5: a) Trace element patterns of Level Mountain mafic lavas with $\text{MgO} > 5$ wt.% normalized to the primitive mantle values of Sun and McDonough (1989). b) Trace element patterns of Level Mountain hawaiites normalized to the primitive mantle values of Sun and McDonough (1989).....	42
Figure 3.6: Trace element patterns of Level Mountain felsic lavas normalized to the primitive mantle values of Sun and McDonough (1989).....	44
Figure 3.7: a) $^{143}\text{Nd}/^{144}\text{Nd}$ versus $^{87}\text{Sr}/^{86}\text{Sr}$ for Level Mountain lavas compared to other mafic lavas erupted in the northern Canadian Cordillera. b) $^{143}\text{Nd}/^{144}\text{Nd}$ versus $^{87}\text{Sr}/^{86}\text{Sr}$ for Level Mountain lavas compared to granitoid samples from the northern Canadian Cordillera.....	46
Figure 3.8: $^{208}\text{Pb}/^{204}\text{Pb}$ versus $^{206}\text{Pb}/^{204}\text{Pb}$ for Level Mountain lavas.....	48
Figure 4.1: a) Pyroclastic tuff forming the summit of Kawdy Mountain. b) Pillow lava and dike at the base of Kawdy Mountain. c) Closer view of a dike.....	51
Figure 4.2: Stratigraphic column of Kawdy Mountain indicating the position of each analyzed sample.	54
Figure 4.3: a) SiO_2 , b) TiO_2 , c) CaO , and d) Al_2O_3 versus MgO in wt.% for Kawdy Mountain basalts.....	56

Figure 4.4:	Trace element patterns of Kawdy Mountain basalts normalized to the primitive mantle values of Sun and McDonough (1989).....	58
Figure 4.5:	a) $^{143}\text{Nd}/^{144}\text{Nd}$ versus $^{87}\text{Sr}/^{86}\text{Sr}$ and b) $^{208}\text{Pb}/^{204}\text{Pb}$ versus $^{206}\text{Pb}/^{204}\text{Pb}$ for Kawdy Mountain basalts.....	60
Figure 5.1:	a) Long view of the cirque to the north of Metahag Mountain; b) Thick lava flows at the top of the cirque. c) Unconsolidated pillow lava at the top of Metahag Mountain.....	63
Figure 5.2:	Stratigraphic column of Metahag Mountain indicating the position of each analyzed sample.....	65
Figure 5.3:	a) SiO_2 , b) TiO_2 , c) CaO , and d) Al_2O_3 versus MgO in wt.% for Metahag Mountain basalts.....	67
Figure 5.4:	Trace element patterns of Metahag Mountain basalts normalized to the primitive mantle values of Sun and McDonough (1989).....	69
Figure 5.5:	a) $^{143}\text{Nd}/^{144}\text{Nd}$ versus $^{87}\text{Sr}/^{86}\text{Sr}$ and b) $^{208}\text{Pb}/^{204}\text{Pb}$ versus $^{206}\text{Pb}/^{204}\text{Pb}$ for Metahag Mountain basalts.....	71
Figure 6.1:	a) Long view of Metah Mountain, with Isspah Butte in the forefront. b) Closer view of Isspah Butte. c) Sampling of the lava flows of Isspah Butte.....	74
Figure 6.2:	Stratigraphic column of Metah Mountain indicating the position of each analyzed sample.....	77
Figure 6.3:	a) SiO_2 , b) TiO_2 , c) CaO , and d) Al_2O_3 versus MgO in wt.% for Metah Mountain basalts.....	79
Figure 6.4:	Trace element patterns of Metah Mountain basalts normalized to the primitive mantle values of Sun and McDonough (1989).....	81
Figure 6.5:	a) $^{143}\text{Nd}/^{144}\text{Nd}$ versus $^{87}\text{Sr}/^{86}\text{Sr}$ and b) $^{208}\text{Pb}/^{204}\text{Pb}$ versus $^{206}\text{Pb}/^{204}\text{Pb}$ for Metah Mountain basalts.....	83
Figure 7.1:	a) Long distance view of Tuya Butte, a typical flat topped volcano that grew in the ice. b) Closer view of the lava flows forming the top of the tuya.....	86
Figure 7.2:	Stratigraphic column of Tuya Butte indicating the position of each analyzed sample.....	89
Figure 7.3:	a) SiO_2 , b) TiO_2 , c) CaO , and d) Al_2O_3 versus MgO for Tuya Butte basalts. Symbols as in Fig. 7.2.....	91
Figure 7.4:	Trace element patterns of Tuya Butte basalts normalized to the primitive mantle values of Sun and McDonough (1989).....	93
Figure 7.5:	a) $^{143}\text{Nd}/^{144}\text{Nd}$ versus $^{87}\text{Sr}/^{86}\text{Sr}$ and b) $^{208}\text{Pb}/^{204}\text{Pb}$ versus $^{206}\text{Pb}/^{204}\text{Pb}$ for Tuya Butte basalts.....	95
Figure 8.1:	a) Long distance view of Tanzilla Volcano. b) Closer view of the small lava flows that erupted at the base of the centre. c) Closer view of the bedded pillow lavas that constitute the top of the cone...	98
Figure 8.2:	Stratigraphic column of Tanzilla Volcano indicating the position of each analyzed sample.....	100
Figure 8.3:	a) SiO_2 , b) TiO_2 , c) CaO , and d) Al_2O_3 versus MgO in wt.% for Tanzilla Volcano basalts.....	102
Figure 8.4:	Trace element patterns of Tanzilla Volcano basalts normalized to the primitive mantle values of Sun and McDonough (1989).....	104

Figure 8.5:	a) $^{143}\text{Nd}/^{144}\text{Nd}$ versus $^{87}\text{Sr}/^{86}\text{Sr}$ and b) $^{208}\text{Pb}/^{204}\text{Pb}$ versus $^{206}\text{Pb}/^{204}\text{Pb}$ for Tanzilla Volcano basalts.....	106
Figure 9.1:	a) Long distance view of Dome Mountain. b) Closer view of the bedded lapilli tuff that constitute most of the centre. c) Unconsolidated pillow lavas at the base of Dome Mountain.....	109
Figure 9.2:	a) SiO_2 , b) TiO_2 , c) CaO , and d) Al_2O_3 versus MgO in wt.% for Dome Mountain basalts.....	112
Figure 9.3:	a) Trace element patterns of Dome Mountain lavas normalized to the primitive mantle values of Sun and McDonough (1989). b) Trace element patterns of Dome Mountain and Hirschfeld BASAN and NEPH magmas normalized to the primitive mantle values of Sun and McDonough (1989).....	114
Figure 9.4:	a) $^{143}\text{Nd}/^{144}\text{Nd}$ versus $^{87}\text{Sr}/^{86}\text{Sr}$ and b) $^{208}\text{Pb}/^{204}\text{Pb}$ versus $^{206}\text{Pb}/^{204}\text{Pb}$ for Dome Mountain lavas.....	116
Figure 10.1:	a) Lava flows at the top of the lower section of Jennings River. b) Pillow lavas and small lava flows at the base of Jennings River. c) Pillow lavas at the base of the upper section.....	119
Figure 10.2:	Stratigraphic column of Jennings River indicating the position of each analyzed sample.....	122
Figure 10.3:	a) SiO_2 , b) TiO_2 , c) CaO , and d) Al_2O_3 versus MgO in wt.% for Jennings River basalts.....	124
Figure 10.4:	a) Trace element patterns of Jennings River basalts normalized to the primitive mantle values of Sun and McDonough (1989). b) Trace element patterns of BASAN erupted at Jennings River, compared to BASAN erupted at Dome Mountain, and at Hirschfeld.	126
Figure 10.5:	a) $^{143}\text{Nd}/^{144}\text{Nd}$ versus $^{87}\text{Sr}/^{86}\text{Sr}$ and b) $^{208}\text{Pb}/^{204}\text{Pb}$ versus $^{206}\text{Pb}/^{204}\text{Pb}$ for Jennings River basalts.....	128
Figure 11.1:	a) Long distance view of Nome Cone. b) Small lava flows and pillow lavas at the base of the cone. c) Closer view of interbedded lava flows and pillow lavas.....	131
Figure 11.2:	Stratigraphic column of Nome Cone indicating the position of each analyzed sample.....	133
Figure 11.3:	a) SiO_2 , b) TiO_2 , c) CaO , and d) Al_2O_3 versus MgO in wt.% for Nome Cone basalts.....	135
Figure 11.4:	Trace element patterns of Nome Cone basalts normalized to the primitive mantle values of Sun and McDonough (1989).....	137
Figure 11.5:	a) $^{143}\text{Nd}/^{144}\text{Nd}$ versus $^{87}\text{Sr}/^{86}\text{Sr}$ and b) $^{208}\text{Pb}/^{204}\text{Pb}$ versus $^{206}\text{Pb}/^{204}\text{Pb}$ for Nome Cone basalts.....	139
Figure 12.1:	a) Northern side of Little Rancheria, walking on the lava tops. b) Long distance view of the lava flows forming the top of the tuya. c) Closer view of two different lava flows.....	142
Figure 12.2:	Stratigraphic column of Little Rancheria indicating the position of each analyzed sample.....	144
Figure 12.3:	a) SiO_2 , b) TiO_2 , c) CaO , and d) Al_2O_3 versus MgO in wt.% for Little Rancheria basalts.....	146
Figure 12.4:	Trace element patterns of Little Rancheria basalts normalized to the primitive mantle values of Sun and McDonough (1989).	148

Figure 12.5: a) $^{143}\text{Nd}/^{144}\text{Nd}$ versus $^{87}\text{Sr}/^{86}\text{Sr}$ and b) $^{208}\text{Pb}/^{204}\text{Pb}$ versus $^{206}\text{Pb}/^{204}\text{Pb}$ for Little Rancheria basalts.....	150
Figure 13.1: a) Pyroclastic tuff in the middle of Blue River volcanic centre. b) Lava flows at the top of the tuya. c) Giant steps belonging certainly to a lava lake formed to the south.....	153
Figure 13.2: Stratigraphic column of Blue River indicating the position of each analyzed sample.....	156
Figure 13.3: a) SiO_2 , b) TiO_2 , c) CaO , and d) Al_2O_3 versus MgO in wt.% for Blue River basalts.....	158
Figure 13.4: Trace element patterns of Blue River basalts normalized to the primitive mantle values of Sun and McDonough (1989).....	160
Figure 13.5: a) $^{143}\text{Nd}/^{144}\text{Nd}$ versus $^{87}\text{Sr}/^{86}\text{Sr}$ and b) $^{208}\text{Pb}/^{204}\text{Pb}$ versus $^{206}\text{Pb}/^{204}\text{Pb}$ for Blue River basalts.....	162
Figure 14.1: a) Long distance view of Caribou Tuya, a typical tuya erupted in the Cassiar Batholith. b) Sampling the pillow lavas forming the lower part of the tuya.....	165
Figure 14.2: Stratigraphic column of Caribou Tuya indicating the position of each analyzed sample.....	167
Figure 14.3: a) SiO_2 , b) TiO_2 , c) CaO , and d) Al_2O_3 versus MgO in wt.% for Caribou Tuya basalts.....	169
Figure 14.4: Trace element patterns of Caribou Tuya basalts normalized to the primitive mantle values of Sun and McDonough (1989).....	171
Figure 14.5: a) $^{143}\text{Nd}/^{144}\text{Nd}$ versus $^{87}\text{Sr}/^{86}\text{Sr}$ and b) $^{208}\text{Pb}/^{204}\text{Pb}$ versus $^{206}\text{Pb}/^{204}\text{Pb}$ for Caribou Tuya basalts.....	173
Figure 15.1: a) SiO_2 , b) TiO_2 , c) CaO , and d) Al_2O_3 versus MgO in wt.% for Rancheria areas basalts.....	177
Figure 15.2: Trace element patterns normalized to the primitive mantle values of Sun and McDonough (1989) of mafic lavas at: a) Swan Lake and Rancheria River, and b) Big Creek and Liard River.....	179
Figure 15.3: a) $^{143}\text{Nd}/^{144}\text{Nd}$ versus $^{87}\text{Sr}/^{86}\text{Sr}$ and b) $^{208}\text{Pb}/^{204}\text{Pb}$ versus $^{206}\text{Pb}/^{204}\text{Pb}$ for basalts of the Rancheria area.....	181
Figure 16.1: a) SiO_2 , b) TiO_2 , c) CaO , and d) Al_2O_3 versus MgO in wt.% for the Watson Lake basalts compared to Rancheria area basalts.	185
Figure 16.2: Trace element patterns of Watson Lake basalts normalized to the primitive mantle values of Sun and McDonough (1989), a) compared to the range in Hy-NORM lavas with $\text{MgO} > 8$ wt.% from small volcanic centres from the Intermontane Belt, and b) compared to the range in AOB from the Rancheria area.....	187
Figure 16.3: a) $^{143}\text{Nd}/^{144}\text{Nd}$ versus $^{87}\text{Sr}/^{86}\text{Sr}$ and b) $^{208}\text{Pb}/^{204}\text{Pb}$ versus $^{206}\text{Pb}/^{204}\text{Pb}$ for Watson Lake basalts.....	189

CHAPTER III	203
Figure 1: Location map for the Tertiary to Recent alkaline centres in the Northern Canadian with respect to the different accreted terranes that constitute the Cordillera.....	207
Figure 2: a) Trace element concentrations of representative samples from each magma type, normalized to the composition of the primordial mantle (Sun and McDonough, 1989), showing the compositional spectrum from NEPH to Hy-NORM. b) Average trace element concentrations for Hy-NORM from the Omineca Belt and from the Coast Belt, normalized to the average value of Hy-NORM from the Intermontane Belt.....	222
Figure 3: $^{87}\text{Sr}/^{86}\text{Sr}$ versus $^{206}\text{Pb}/^{204}\text{Pb}$ for 3 individual centres from the Intermontane Belt compared to Alligator Lake from the Coast Belt and to the range in Rancheria, Omineca Belt.....	226
Figure 4: $^{87}\text{Sr}/^{86}\text{Sr}$ versus $^{143}\text{Nd}/^{144}\text{Nd}$ for Recent alkaline volcanic rocks.....	228
Figure 5: Pb-Pb isotopes diagrams for alkaline volcanic rocks and granitoids..	230
Figure 6: Projection of isotopic analyses along the Stikine Volcanic Belt with respect to distance from Tintina fault, a) $^{87}\text{Sr}/^{86}\text{Sr}$ and b) $^{143}\text{Nd}/^{144}\text{Nd}$	233
Figure 7: $^{206}\text{Pb}/^{204}\text{Pb}$, $^{207}\text{Pb}/^{204}\text{Pb}$ and $^{208}\text{Pb}/^{204}\text{Pb}$ versus distance from Tintina Fault.....	235
Figure 8: a) $^{87}\text{Sr}/^{86}\text{Sr}$ versus $^{208}\text{Pb}/^{204}\text{Pb}$ for Recent alkaline volcanic rocks compared to the fields of Northern Cordilleran upper mantle xenoliths and Carmacks volcanics.....	238
Figure 9: Trace element concentrations of crustal batholiths and xenoliths from Table 3, normalized to the composition of the primordial mantle (Sun and McDonough, 1989). a) samples from Omineca Belt, b) samples from the Intermontane Belt and c) samples from the Coast Belt.....	244
Figure 10: Sr isotopic signatures in Recent alkaline basalts compared to contoured Sr initial ratios in Cenozoic granitoids and to the location of the isotopic discontinuity observed in the Carmacks volcanics....	247
Figure 11: $^{87}\text{Sr}/^{86}\text{Sr}$ versus MgO (wt%).	251
Figure 12: $^{87}\text{Sr}/^{86}\text{Sr}$ versus Nb/La for for Hy-NORM basalts erupted in the Intermontane Belt and Omineca Belt.....	253
Figure 13: a) $^{87}\text{Sr}/^{86}\text{Sr}$ and b) $^{208}\text{Pb}/^{204}\text{Pb}$ versus MgO (wt%) for Hy-NORM basalts erupted in the Intermontane Belt and Omineca Belt.....	256

CHAPTER IV.....	272
Figure 1: Nb versus SiO ₂ for the northern Cordilleran mafic alkaline volcanic suites.....	276
Figure 2: a) Location map showing mid-Tertiary to Recent alkaline volcanic centres described in this paper.....	279
Figure 3: CaO/Al ₂ O ₃ versus MgO in wt.% for Hy-NORM basalts and NEPH lavas from Recent alkaline centres of the Canadian Cordillera.....	285
Figure 4: Major elements versus SiO ₂ in wt.% for NEPH lavas from the northern Canadian Cordillera compared to NEPH lavas from other oceanic and continental areas.....	288
Figure 5: Average trace elements concentrations normalized to primitive mantle of Sun and McDonough (1989) for Hy-NORM and NEPH lavas from Recent alkaline centres of the Canadian Cordillera and for MORB.....	290
Figure 6: a) TiO ₂ , b) Zr, c) Ba, and d) Y versus Nb for Hy-NORM and NEPH lavas in NEPH-bearing suites of the northern Canadian Cordillera.....	292
Figure 7: ⁸⁷ Sr/ ⁸⁶ Sr versus ²⁰⁶ Pb/ ²⁰⁴ Pb for lavas erupted in the Rancheria area and in individual NEPH-bearing vents from the northern Canadian Cordillera.....	295
Figure 8: ⁸⁷ Sr/ ⁸⁶ Sr versus SiO ₂ for primitive alkaline lavas (MgO > 8 wt.%) in the northern Canadian Cordillera and in other continental margins and oceanic hot spot areas.....	297
Figure 9: a) CaO, and b) Al ₂ O ₃ versus Na ₂ O for primitive Hy-NORM lavas (MgO > 8 wt.%) of the northern Canadian Cordillera, other continental areas, and hot spots corrected for olivine fractionation or accumulation to MgO = 12 wt.%.....	303
Figure 10: K ₂ O and TiO ₂ versus La in high MgO (> 8 wt.%) lavas from Hirschfeld.....	309
Figure 11: Calculated source concentrations that could produce the composition of the melts at the kink in the K versus La diagram (Fig. 10), assuming that it corresponds to exhaustion of amphibole..	317
Figure 12: a) K versus La, b) Sr versus La, c) Th versus La and d) Yb versus La for the Hirschfeld's data set.....	320
Figure 13: Nb versus Sr variations during partial melting of amphibole-bearing pyroxenites in the spinel stability field, with labels indicating the proportion of amphibole in the pyroxenites, compared to the Hirschfeld data set.....	323
Figure 14: a) CaO, b) Na ₂ O, c) MgO, and d) Al ₂ O ₃ versus degree of partial melting (F) for experimental melts produced by dry melting of peridotite at 15 and 30 kbars.....	330

Figure 15:	a) REE concentrations calculated from 4, 8 and 12% partial melting of a garnet peridotite using the REE concentrations in Cordilleran mantle xenoliths for the source composition (Peslier, 1999) and the melting mode of Ottonello et al. (1984), compared to average primitive Hy-NORM from the Intermontane and Omineca belts. b) Calculated sources for the Intermontane and Omineca Hy-NORM basalts assuming that the Hy-NORM basalts were generated by 8% partial melting of a garnet peridotite.....	334
Figure 16:	P versus T diagram showing the conditions in the northern Cordilleran mantle.....	340

List of tables

CHAPTER III	203
Table 1: Classification of Cordillera alkaline basalts, following Francis and Ludden (1995).....	213
Table 2: Major, trace and isotopic compositions of representative alkaline volcanic samples from Watson Lake, the Omineca, Intermontane and Coast belts.....	216
Table 3: Major and trace elements of representative samples from Cassiar Batholith, Coast Belt crustal xenoliths and batholiths, and Intermontane Belt batholiths.....	241
CHAPTER IV	272
Table 1: Major and trace element compositions of NEPH lavas that have erupted to the southeast of Fort Selkirk, near Minto Landing, and at Table Hill and Fire Mountain in the Atlin field.....	283
Table 2: Major, trace and isotopic compositions of Hy-NORM basalts that have erupted in different centres from the Stikine Volcanic Belt.....	300
Table 3: Composition of the different components used in the least-square calculations to determine the melting reactions of amphibole in the spinel and garnet stability fields.....	312
Table 4: Partition coefficients used in melting calculations.....	315
Table 5: Calculated compositions of the enriched mantle sources for Hy-NORM basalts from the Intermontane and Omineca belts.....	336

List of appendices

Appendix A.....	365
Table A-1-a: Classification of Mount Edziza mafic volcanic samples.....	A-1
Table A-1-b: Classification of Mount Edziza hawaiites and felsic volcanic samples.....	A-2
Table A-2-a: Location and classification of Level Mountain mafic volcanic samples.....	A-3
Table A-2-b: Location and classification of Level Mountain hawaiites and felsic volcanic samples.....	A-4
Table A-3: Location and classification of Kawdy Mountain volcanic samples...	A-5
Table A-4: Location and classification of Metahag Mountain volcanic samples.	A-6
Table A-5: Location and classification of Metah Mountain volcanic samples....	A-7
Table A-6: Location and classification of Tuya Butte volcanic samples.....	A-8
Table A-7: Location and classification of Tanzilla Volcano samples.....	A-9
Table A-8: Location and classification of Dome Mountain volcanic samples....	A-10
Table A-9: Location and classification of Jennings River volcanic samples.....	A-11
Table A-10: Location and classification of Nome Cone volcanic samples.....	A-12
Table A-11: Location and classification of Little Rancheria volcanic samples....	A-13
Table A-12: Location and classification of Blue River volcanic samples.....	A-14
Table A-13: Location and classification of Caribou Tuya volcanic samples.....	A-15
Table A-14: Location and classification of Rancheria area volcanic samples.....	A-16
Table A-15: Location and classification of Watson Lake volcanic samples.....	A-17

Appendix B

Table B-1-a: Whole rock analyses of Mount Edziza mafic volcanic samples.....	B-1
Table B-1-b: Whole rock analyses of Mount Edziza hawaiites and felsic volcanic samples.....	B-6
Table B-2-a: Whole rock analyses of Level Mountain mafic volcanic samples....	B-11
Table B-2-b: Whole rock analyses of Level Mountain hawaiites and felsic volcanic samples.....	B-14
Table B-3: Whole rock analyses of Kawdy Mountain volcanic samples.....	B-17
Table B-4: Whole rock analyses of Metahag Mountain volcanic samples.....	B-20
Table B-5: Whole rock analyses of Metah Mountain volcanic samples.....	B-23
Table B-6: Whole rock analyses of Tuya Butte volcanic samples.....	B-26
Table B-7: Whole rock analyses of Tanzilla Volcano samples.....	B-29
Table B-8: Whole rock analyses of Dome Mountain volcanic samples.....	B-32
Table B-9: Whole rock analyses of Jennings River volcanic samples.....	B-34
Table B-10: Whole rock analyses of Nome Cone volcanic samples.....	B-37
Table B-11: Whole rock analyses of Little Rancheria volcanic samples.....	B-39
Table B-12: Whole rock analyses of Blue River volcanic samples.....	B-42
Table B-13: Whole rock analyses of Caribou Tuya volcanic samples.....	B-46
Table B-14: Whole rock analyses of Rancheria area volcanic samples.....	B-49
Table B-15: Whole rock analyses of Watson Lake volcanic samples.....	B-52

Appendix C

Table C: Whole rock analyses of granitoid samples from the northern Canadian Cordillera..... C-1

Preface

Thesis outline

This thesis is presented as a collection of three manuscripts, one that may not be published, one published in Chemical Geology, and one submitted to the Journal of Petrology. Each of these manuscripts contains an introduction, a presentation of the results, a discussion and a conclusion. The published and submitted papers contain additional abstracts. The references are placed at the end of each chapter, and the tables and figures have been incorporated in the text.

Chapter I is an introduction, that presents the controversies on the origin of mafic alkaline lavas in the literature, and states the objectives of the study. Chapter II describes each sampled volcano of the Stikine Volcanic Belt, and presents their chemical and isotopic characteristics centre by centre. In addition, this chapter reviews the chemical and isotopic characteristic of Mount Edziza, a large bimodal volcanic complex of the Stikine Volcanic Belt, and of alkaline basalts erupted in the Rancheria area and across the Tintina fault. Chapter III describes the chemical and isotopic variations observed in alkaline basalts erupted across the Stikine Volcanic Belt and demonstrates the existence of a distinct isotopic discontinuity at the boundary between the Intermontane and Omineca belts that can not be explained by crustal contamination and indicates the existence of a major lithospheric mantle discontinuity in the northern Canadian Cordillera. Chapter III has already been published in Chemical Geology (Abraham et al. 2001). Chapter IV examines the petrogenesis of the Cordilleran mafic alkaline lavas and

the implication for their derivation from lithospheric sources. This paper highlights the low CaO and high Na₂O contents of continental margin basalts compared to oceanic alkaline basalts and proposes that these characteristics reflect low degrees of melting of the continental lithospheric upper mantle associated with lithospheric thinning. Chapter IV has been submitted to Journal of Petrology. Chapter V is a general conclusion that summarizes the main results of the study, presents their implications, and suggestions for future work.

Originality

The main contributions of this thesis are presented in two manuscripts. One manuscript has already been published, and shows that alkaline basalts from previously unsampled volcanic centres of the northern Canadian Cordillera exhibit a terrane dependence in their isotopic signature, indicating that their mantle source must be situated in the unconvecting lithosphere, and that a major lithospheric mantle discontinuity is present at the boundary between the Intermontane and Omineca belts. The other manuscript has been submitted to Journal of Petrology, and shows that primitive alkaline basalts in the northern Canadian Cordillera, and in continental margin areas in general, have lower Ca and higher Na contents than their equivalents in oceanic hot spots or associated with mid-ocean ridges. This worldwide signature of continental alkaline lavas has not previously been recognized and is interpreted to represent smaller degrees of partial melting of continental lithospheric mantle.

Contributions of co-authors

This study involved two summers of fieldwork during which I sampled 12 volcanic centres in the Stikine Volcanic Belt. More than 200 representative lava samples were studied petrographically and geochemically. The petrographic characterization involved thin sections, that were prepared by Georges Panagiotidis at McGill University. The geochemical data set includes analyses of major and trace elements, and Sr, Nd, and Pb isotopic ratios. The major elements were obtained by XRF, by Tariq Ahmedali and Glenna Keating, at McGill University, Montréal. The trace elements were obtained by ICP-MS by myself, at Université Paul Sabatier, Toulouse, with the assistance of Bernard Reynier and Michel Valladon. The Sr, Nd and Pb isotopic ratios were obtained by TIMS by myself, at Université Paul Sabatier, Toulouse, with the training of Pierre Brunet. The chemical procedure for the Sr, Nd and Pb isotopic analyses was set up in Toulouse by the co-author Mireille Polv  and myself. The numerical modeling and interpretations of the analytical data are my own, but have benefited from numerous discussions with my co-authors, Don Francis and Mireille Polv .

Guidelines concerning thesis preparation

The following is an excerpt from the "Guidelines Concerning Thesis Preparation" as required by the Faculty of Graduate Studies and Research at McGill University:

Candidates have the option of including, as part of the thesis, the text of one or more papers submitted, or to be submitted, for publication, or the clearly-duplicated text

of one or more published papers. These must be bound together as an integral part of the thesis and connecting texts that provide logical bridges between the different papers are mandatory.

The thesis must conform to all other requirements of the "Guidelines for Thesis Preparation" and should be in a literary form that is be more than a mere collection of manuscripts published or to be published. The thesis must include: a table of contents, a general abstract in English and French, an introduction which clearly states the rational and objectives of the research, a comprehensive review of the literature, and a general conclusion and summary.

Additional material must be provided when appropriate (e.g., in appendices) and in sufficient detail to allow a clear and precise judgement to be made of the importance and originality of the research reported in the thesis.

In the case of manuscripts co-authored by the candidate and others, the candidate is required to make an explicit statement in the thesis as to who contributed to such work and to what extent. The supervisor must attest to the accuracy of this statement at the doctoral oral defense. Since the task of the examiners is made more difficult in these cases, it is in the candidate's interest to clearly specify the responsibilities of all the authors of the co-authored papers.

CHAPTER I

General introduction

Introduction

Mafic alkaline magmas erupt in both oceanic and continental settings and there is still considerable debate as to whether they are derived from the melting of lithospheric or asthenospheric mantle sources, or a mixture of the two. The term "lithosphere" designates both the crust and the attached part of the upper mantle, unaffected by convection, that has been depleted by previous partial melting, but may have been re-enriched by the infiltration of melts and fluids from deeper levels. The term "asthenosphere" designates the convecting part of the upper mantle below the lithosphere, representing the depleted source of mid-ocean ridge basalts, but may also incorporate blobs of enriched material of a variety of origins. Even in extensively studied areas, the nature of the mantle source (s) of mafic alkaline lavas is controversial. In Hawaii, post-erosional alkaline basalts at the terminal stage of volcanism have been explained by partial melting of the metasomatized lithosphere (Chen and Frey, 1985), by very small degrees of partial melting of the asthenosphere (Sims et al., 1995), and by mixing between low degree partial melts of the asthenosphere and higher degree partial melts of pyroxenite veins (Lassiter et al., 2000). Along the Cameroon Line, similarities between oceanic and continental alkaline volcanic suites have led to the generally held opinion that the source of intraplate alkaline magmatism lies in the asthenospheric mantle (Fitton, 1987). More recent isotopic studies have concluded that a mantle plume might be present beneath the Cameroon line (Halliday et al., 1988 and 1990), and Marzoli et al. (2000) have concluded that a continental lithospheric signature overprints the asthenospheric

signature in the alkaline lavas of the Cameroon Line. These examples illustrate the lack of consensus concerning the source of alkaline lavas, and the need for better targeted chemical and isotopic studies to resolve the roles of lithospheric and asthenospheric mantle in the origin of mafic alkaline lavas.

Mafic alkaline suites often comprise highly alkaline lavas, olivine nephelinites and/or basanites, associated with other less alkaline lava types, such as alkali olivine basalts and hypersthene-normative basalts (e.g. Francis & Ludden, 1990 and 1995; Hoernle and Schmincke, 1993; Class and Goldstein, 1997; Beccaluva et al., 1998; Marzoli et al., 2000; Gorring and Kay, 2001; Zhang et al., 2001). These volcanic suites commonly display compositional spectra between the olivine nephelinite (NEPH) and hypersthene-normative (Hy-NORM) basalt end-members, that have been explained by either increasing degrees of partial melting of one single lithospheric or asthenospheric source (e.g. Class and Goldstein, 1997; Gorring and Kay, 2001), or by mixing between at least two mantle components (e.g. Francis and Ludden, 1990 and 1995; Hoernle and Schmincke, 1993; Beccaluva et al., 1998; Marzoli et al., 2000; Zhang et al., 2001). In many continental volcanic suites, the two end-members exhibit additional isotopic differences, the NEPH end-member being generally less radiogenic than the Hy-NORM end-member (Francis and Ludden, 1990; Beccaluva et al., 1998; Zhang et al., 2001). In areas where primitive lavas show little evidence of crustal contamination, these isotopic differences require the existence of at least two isotopically distinct mantle sources (e.g. Francis and Ludden, 1990; Zhang et al., 2001).

The mantle source of the NEPH end-member might be the depleted asthenospheric mantle, in which case extremely small degrees of partial melting (less than 0.25%; Sims et al., 1995) would be required to explain their enriched trace element concentrations. Evidence for the presence of amphibole and/or phlogopite in the mantle source regions of highly alkaline lavas in both oceanic and continental terranes suggests, however, that their chemical signatures were established within the lithosphere (Francis & Ludden, 1990 & 1995; Wilson et al., 1995; Class and Goldstein, 1997; Beccaluva et al., 1998; Zhang et al., 2001). Current debate concerns whether the amphibole-rich component is present as amphibole-bearing peridotite or amphibole-rich pyroxenite vein (Francis and Ludden, 1990 and 1995; Class and Goldstein, 1997; Zhang et al., 2001).

The mantle source of the Hy-NORM end-member is poorly constrained, and may be situated either in the lithospheric or sub-lithospheric mantle (asthenosphere or plume). The continental lithospheric mantle is often considered to be refractory and anhydrous, rarely heated above its solidus, and so large volumes of magmas were considered to originate in the underlying asthenospheric mantle (e.g. McKenzie and Bickle, 1988; Arndt and Christensen, 1992). In the presence of small amounts of water (~ 0.4 %), however, significant quantities of melt may be generated entirely within the lithospheric mantle (Gallagher and Hawkesworth, 1992), and an asthenospheric source is not necessarily required.

The Stikine Volcanic Belt

The Stikine Volcanic Belt is an excellent place to investigate the role of lithospheric and sub-lithospheric mantle sources because this Tertiary to Recent alkaline volcanic lineament crosses three of the five tectonic belts (from east to west, the Omineca, Intermontane, and Coast belts) that compose the northern Canadian Cordillera. These major tectonic belts are composed of terranes of different ages and origins that have been displaced along and/or accreted to the North American craton to form the northern Canadian Cordillera (Monger et al., 1982). Numerous small volcanic centres from the Stikine Volcanic belt cross the boundary between the Intermontane and the Omineca belts, composed respectively of terranes of oceanic and continental origin. In addition, some recent alkaline lavas have erupted to the east of the Tintina fault, a major transcurrent feature that separates the Omineca Belt from the North American craton. The existence of a terrane dependence in the geochemical signatures of alkaline lavas erupted along the Stikine Volcanic Belt would indicate that the lavas were not derived from a purely asthenospheric source, and that the lithospheric mantle and/or crust contributed significantly to their geochemical signature.

Previous studies have suggested the existence of a terrane dependence in the chemical and isotopic signatures of alkaline basalts from the northern Cordilleran volcanic province. For example, Carignan et al. (1994) showed that alkaline lavas erupted in the Coast Belt have more radiogenic Sr and less radiogenic Nd signatures than their equivalents in the Intermontane Belt. As crustal contamination does not appear to

have significantly modified the trace element and isotopic signatures of these mafic alkaline lavas (Carignan et al., 1994), the observed chemical and isotopic changes were interpreted to be present in their mantle sources, suggesting the involvement of distinctive lithospheric mantles. The most interesting terrane dependence, however, was documented across the Tintina fault in the Watson Lake area, where lavas to the east of the fault have higher Zr contents and Sm/Yb ratios than their equivalents just to the west of the fault (Hasik, 1994). Hasik (1994) interpreted this change as reflecting a major lithospheric mantle discontinuity, indicating that the Tintina fault is a steeply dipping suture.

In parallel with the geochemical work presented in this thesis, the northern Canadian Cordillera has been the subject of one of the most intensive geophysical surveys ever carried out as part of the Lithoprobe Slave-NORthern Cordillera Lithospheric Evolution (SNORCLE) transect (Clowes, 1993). Seismic refraction and wide-angle reflection surveys of this transect provide detailed images of the geometry and structure of the lithosphere of most of the terranes composing the Canadian Cordillera (Clowes et al., 2001). A low-velocity anomaly has been detected by teleseismic tomography in the northwestern part of the northern Cordillera (Frederiksen et al., 1998), which is interpreted to represent a zone of hot mantle produced either by a mantle plume, or by asthenospheric upwelling associated with the opening of a slab window beneath the northern Cordillera (Shi et al., 1998; Frederiksen et al., 1998). In addition, thermal studies have measured very high surface heat flows in the Canadian Cordillera, that have been interpreted in terms of a thin lithospheric mantle (Hyndman and Lewis, 1999). Finally, Hasik's (1994) interpretation that the Tintina fault is a steeply dipping major

lithospheric suture has been recently confirmed by seismic (Welford et al., 2001) and magnetotelluric surveys (Ledo et al., 2001). The Stikine Volcanic Belt offers thus an unique opportunity to probe the mantle and crust that lie beneath the Canadian Cordillera because it crosses a number of different types of lithospheres, whose properties and structures are well constrained by recent high-quality geophysical data.

The preliminary geochemical results inspired a systematic sampling of alkaline volcanic centres erupted in the Stikine Volcanic Belt in order to investigate the terrane dependence in the chemical and isotopic characteristics of the lavas across the boundary between the Intermontane and the Omineca belts. The lavas of one large bimodal volcanic complex, Level Mountain, and of eleven smaller volcanic centres of the Stikine Volcanic Belt were sampled, and analyzed for major and trace element and Sr-Nd-Pb isotopic compositions. This data set, and that from previous studies (Francis and Ludden, 1990 and 1995; Carignan et al., 1994; Hasik, 1994), were used to identify and quantify the roles of the different components (crust, lithospheric and asthenospheric mantle, plume) involved in the genesis of the alkaline basalts of the Stikine Volcanic Belt.

The results of this study are presented in the three following chapters. Chapter II describes the field, chemical and isotopic characteristics of each sampled volcanic centre of the Stikine Volcanic Belt. Chapter III deals with the tectonic implications of a comparison of the geochemical characteristics of the centres from different terranes and documents the existence of a distinct isotopic discontinuity at the boundary between the Intermontane and Omineca belts that cannot be explained by crustal contamination and indicates the existence of a major discontinuity in the lithospheric mantle of the northern

Canadian Cordillera. Chapter IV examines the petrogenesis of the Cordilleran mafic alkaline lavas and documents a previously unrecognized low CaO and high Na₂O signature of alkaline basalts along continental margin compared to oceanic alkaline basalts, that is interpreted to reflect smaller degrees of partial melting of continental lithospheric mantle associated with lithospheric thinning.

References

- Arndt, N.T., Christensen, U., 1992. The role of lithospheric mantle in continental flood volcanism; thermal and geochemical constraints. *J. Geophys. Res.* 97, 10967-10981.
- Beccaluva, L., Siena, F., Coltorti, M. Di Grande, A., Lo Giudice, A., Macciotta, G., Tassinari, R., Vaccaro, C., 1998. Nephelinitic to tholeiitic magma generation in a transtensional tectonic setting : an integrated model for the Iblean volcanism, Sicily. *J. Petrol.* 39, 1547-1576.
- Carignan, J., Ludden, J., Francis, D., 1994. Isotopic constraints on the mantle sources for Quaternary continental alkaline magmas in the northern Canadian Cordillera. *Earth Planet. Sci. Lett.* 128, 271-286.
- Chen, C.Y., Frey, F.A., 1985. Trace element and isotopic geochemistry of lavas from Haleakala Volcano, East Maui, Hawaii; implications for the origin of Hawaiian basalts. *J. Geophys. Res.* 90, 8743-8768.
- Class, C., Goldstein, S.L., 1997. Plume-lithosphere interactions in the ocean basins: constraints from the source mineralogy. *Earth Planet. Sci. Lett.* 150, 245-260.
- Clowes, R.M., 1993. Lithoprobe phase IV Proposal – Studies of the Evolution of a Continent. Published by the LITHOPROBE Secretariat, The University of British Columbia, Vancouver, B.C. 290 p.
- Cousens, B.L., Bevier, M.L., 1995. Discerning asthenospheric, lithospheric and crustal influences on the geochemistry of Quaternary basalts from Iskut-Unuk rivers area, northwestern British Columbia. *Can. J. Earth Sci.* 32, 1451-1461.

- D'Orazio, M., Agostini, S., Mazzarini, F., Innocenti, F., Manetti, P., Haller, M.J., Lahsen, A., 2000. The Pali Aike Volcanic Field, Patagonia: slab-window magmatism near the tip of South America. *Tectonophys.* 32, 407-427.
- Edwards, B.R., Russell, J.K., 2000. Distribution, nature, and origin of Neogene-Quaternary magmatism in the northern Cordilleran volcanic province, Canada. *Geol. Soc. of Am. Bulletin* 112, 1280-1295.
- Fitton, J.G., 1987. The Cameroon Line west Africa: a comparison between oceanic and continental alkaline volcanism. In: *Alkaline Igneous Rocks*, Fitton J.G. & Upton B.G. (eds), 273-291.
- Francis, D., Ludden, J., 1990. The mantle source for Olivine Nephelinite, Basanite, and Alkaline olivine basalt at Fort Selkirk, Yukon, Canada. *J. Petrol.* 31, 371-400.
- Francis, D., Ludden, J., 1995. The signature of amphibole in mafic alkaline lavas, a study in the northern Canadian Cordillera. *J. Petrol.* 36, 1171-1191.
- Frederiksen, A.W., Bostock, M.G., Van Decar, J. C., Cassidy, J., 1998. Seismic structure of the upper mantle beneath the northern Canadian Cordillera from teleseismic travel-time inversion. *Tectonophys.*, 294, 43-55.
- Gabrielse, H., Monger, J.W.H., Wheeler, J.O., Yorath, C.J., 1991. Part A. Morphogeological belts, tectonic assemblages and terranes. In: Chapter 2 of *Geology of the Cordilleran Orogen in Canada* H. Gabrielse and C.J. Yorath (Eds.). *Geol. Soc. Am., The Geology of North America*, G-2, 15-28.
- Gallagher, K., Hawkesworth, C., 1992. Dehydration melting and the generation of continental flood basalts. *Nature* 358, 57-59.
- Gehrels, G.E., McClelland, W.C., Samson, S.D., Patchett, P.J., Jackson, J.L., 1990. Ancient continental margin assemblage in the northern Coast Mountains, southeast Alaska and northwest Canada. *Geology* 18, 208-211.
- Gorring, M.L., Kay, S.M., 2001. Mantle processes and sources of Neogene slab window magmas from southern Patagonia, Argentina. *J. of Petrol.* 42, 1067-1094.
- Halliday, A.N., Dickin, A.P., Fallick, A.E., Fitton, J.G., 1988. Mantle dynamics; a Nd, Sr, Pb and O isotopic study of the Cameroon line volcanic chain. *J. of Petrol.* 29, 181-211.

- Halliday, A.N., Davidson, J.P., Holden, P., DeWolf, C., Lee, D.C., Fitton, J.G., 1990. Trace-element fractionation in plumes and the origin of HIMU mantle beneath the Cameroon Line. *Nature* 347, 523-528.
- Hasik, V., 1994. Volcanic evidence for a compositional contrast in the lithospheric upper mantle across the Tintina Trench, Southeastern Yukon, Canada, M.Sc. thesis, McGill University, Montreal, Canada.
- Hoernle, K., Schmincke, H.U., 1993. The petrology of the tholeiites through melilite nephelinites on Gran Canaria, Canary Islands: crystal fractionation, accumulation, and depths of melting. *J. Petrol.* 34, 573-597.
- Hyndman, R. D., Lewis, T.J., 1999. Geophysical consequences of the Cordillera-Craton thermal transition in southwestern Canada. *Tectonophysics* 306, 397-422.
- Ionov, D.A., Griffin, W.L., O'Reilly, S.Y., 1997. Volatile-bearing minerals and lithophile trace elements in the upper mantle. *Chem. Geol.* 141, 153-184.
- Lassiter, J.C., Hauri, E.H., Reiners, Garcia, P.W., M.O. 2000. Generation of Hawaiian post-erosional lavas by melting of a mixed lherzolite/ pyroxenite source. *Earth and Planet. Sci. Lett.* 178, 269-284.
- Ledo, J., Jones, A.G., Ferguson, I.J., Wennberg, G., 2001. Electromagnetic images of the Tintina fault. *Lithoprobe Report* 79, 67-73.
- Marzoli, A., Piccirillo, E.M., Renne, P.R., Bellieni, G., Iacumin, M., Nyobe, J.B., Tongwa, A.T., 2000. The Cameroon Volcanic Line revisited: petrogenesis of continental basaltic magmas from lithospheric and asthenospheric mantle sources. *J. Petrol.* 41, 87-109.
- McKenzie, D., Bickle, M.J., 1988. The volume and composition of melt generated by extension of the lithosphere. *J. Petrol.* 29, 625-679.
- Monger, J.W.H., Price, R.A. Tempelman-Kluit, D.J., 1982. Tectonic accretion and the origin of the two major metamorphic and welts in the Canadian Cordillera. *Geology* 10, 70-75.
- O'Reilly, S.Y., Zhang, M., 1995. Geochemical characteristics of lava-field basalts from eastern Australia and inferred sources: connections with the subcontinental lithospheric mantle?. *Contrib. Mineral. Petrol.* 121, 148-170.

- Shi, L., Francis, D., Ludden, J., Frederiksen, A., Bostock, M., 1998. Xenolith evidence for lithospheric melting above anomalously hot mantle under the northern Canadian Cordillera. *Contrib. Mineral. Petrol.* 131, 38-53.
- Sims, K.W.W., DePaolo, D.J., Murrell, M.T., Baldridge, W.S., Goldstein, S.J., Clague, D.A., 1995. Mechanisms of magma generation beneath Hawaii and mid-ocean ridges; uranium/ thorium and samarium/neodymium isotopic evidence. *Science* 267, 508-512.
- Song, Y., Frey, F.A., Zhi, X., 1990. Isotopic characteristics of Hannuoba basalts, eastern China: implications for their petrogenesis and the composition of the subcontinental mantle. *Chem. Geol.* 88, 35-52.
- Welford, J.K., Clowes, R.M., Ellis, R.M., Spence, G.D., Asudeh, I., Hajnal, Z., 2001. Lithospheric structure across the craton-Cordilleran transition of northeastern British Columbia. *Can. J. Earth Sci.* 38, 1169-1189.
- Wilson, M., Downes, H., Cebria, J.M., 1995. Contrasting fractionation trends in coexisting continental alkaline magmas series; Cantal, Massif Central, France. *J. Petrol.* 36, 1729-1753.
- Zhang, M., Stephenson, P.J., O'Reilly, S.Y., McCullough, M.T., Norman M., 2001. Petrogenesis and geodynamic implications of Late Cenozoic basalts in North Queensland, Australia: trace-element and Sr-Nd-Pb isotope evidence. *J. Petrol.* 42, 685-719.

Chapter II

Tertiary to Recent alkaline volcanoes of the Stikine Volcanic Belt, northern British Columbia

Abstract

The Stikine Volcanic Belt is a major Tertiary to Recent alkaline volcanic structure that crosses most of the accreted terranes of the northern Cordillera and extends onto the North American craton. Most of the alkaline magmatism in the Stikine Volcanic Belt occurred as small monogenetic cinder cones and tuyas, scattered to the northeast of the large volcanic complexes of Level Mountain and Mount Edziza. Level Mountain, as well as a series of eleven small tuyas and cones that cross the tectonic boundary between two major lithospheric blocks of the northern Canadian Cordillera, the Intermontane and Omineca belts, have been systematically sampled and geochemically analyzed for major, trace and Sr-Nd-Pb isotopic compositions.

The small alkaline centres of the Stikine Volcanic Belt have erupted mainly alkaline olivine basalts (AOB) and hypersthene normative olivine basalts (Hy-NORM), the most Si-undersaturated lavas being basanite lavas that were found at only three volcanic centres. In most individual volcanic centres, the lavas define at least two different magmatic series, with distinct trace element and isotopic compositions, defining distinct olivine-control lines. The trace element and isotopic compositions change systematically with the degree of Si-saturation, from Hy-NORM basalts, with generally the least enriched incompatible trace elements, but the most radiogenic Sr and Pb isotopic ratios, to AOB and basanite, with the most enriched incompatible trace elements and the least radiogenic Sr and Pb ratios. A range of parental magmas with different Si-saturations is required at most centres to explain the range in the major and trace element compositions

of the lavas. The range of parental magmas might be produced, on one hand, by different degrees of partial melting of one source, in which case the isotopic range of the magmas would indicate subsequent crustal contamination. On the other hand, both the chemical and isotopic ranges of the lavas at each centre might be explained by melting and mixing of two different mantle components, one responsible for the Si-undersaturated end-member represented by either basanites or unseen olivine nephelinites, and the other for the Si-saturated Hy-NORM basalts.

A comparison of the isotopic composition of Hy-NORM basalts of the Intermontane and Omineca belts indicates that Hy-NORM basalts of the Omineca Belt have more radiogenic Sr and Pb and less radiogenic Nd isotopic ratios than those of the Intermontane Belt. This terrane dependence requires either that the Omineca belt Hy-NORM basalts have been contaminated on their way to the surface, or that they were derived from a more radiogenic mantle source than the Intermontane Belt Hy-NORM basalts

1. Introduction

The name Stikine Volcanic Belt has been used by different authors to designate groups of Tertiary to Recent alkaline volcanic centres that have erupted in northern British Columbia and Yukon, Canada. In this paper, we have kept the definition given by Souther (1977) for the Stikine Volcanic Belt, as a southwest-northeast segment of the Tertiary to Recent northern Cordilleran volcanic province, that comprises numerous

monogenic vents, in addition to the large composite shield volcanoes of Level Mountain (Hamilton, 1981), Mount Edziza (Souther, 1992), Heart Peaks (Casey and Scarfe, 1980), Hoodoo Mountain (Edwards, 1997), and Maitland (Souther, 1990). The monogenic vents erupted valley-filling lavas, and built small lapilli cones or tuyas to the northeast of Level Mountain (Fig. 1.1), as far as the Watson Lake area (Hasik, 1994), and to the southwest of Level Mountain to the Iskut-Unuk volcanic field (Cousens and Bevier, 1995), and Aiyansh (Sutherland Brown, 1969; not shown in Fig. 1.1). Valley-filling lavas may once have covered relatively large areas, such as between Kawdy Mountain and Tanzilla Volcano (Fig. 1.2), where scattered erosional remnants of lavas are abundant (Gabrielse, 1969).

In addition to the Stikine Volcanic Belt, Tertiary to Recent alkaline volcanism has occurred discontinuously to the northwest, in the Atlin field (Francis and Ludden, 1995), and at Alligator Lake (Eiché et al., 1987), Miles Canyon (Hart and Villeneuve, 1999), Fort Selkirk field (Francis and Ludden, 1990), West Dawson (Fig. 1.1) and Prindle Volcano in eastern Alaska (Foster, 1981). This series of volcanic centres forms a striking lineament, perhaps following a zone of weakness, which roughly corresponds to the location of the tectonic boundary between the Intermontane and Coast belts (Monger et al., 1982).

The oldest alkaline lavas erupted in the northern Cordilleran volcanic province are found in the Atlin region (Fig. 1.1) and have been dated at approximately 27 Ma (Bloodgood and Bellefontaine, 1990), whereas the youngest lavas are found in the south, at Aiyansh, dated at 250 ± 130 y.b.p. (Sutherland-Brown, 1969). In the Stikine Volcanic

Figure 1.1:

Location map of the Stikine Volcanic Belt and other Tertiary to Recent alkaline volcanic centres in the northern Canadian Cordillera. Abbreviations: AL = Alligator Lake (Eiché et al., 1987); ED = Mount Edziza; HF = Hirschfeld (Francis and Ludden, 1995); IS = Iskut-Unuk (Cousens and Bevier, 1995); LG = Llangorse; LM = Level Mountain (Hamilton, 1981); MC = Miles Canyon; MI = Minto Landing; WD = West Dawson. Modified after Wheeler and Mcfeely (1991).

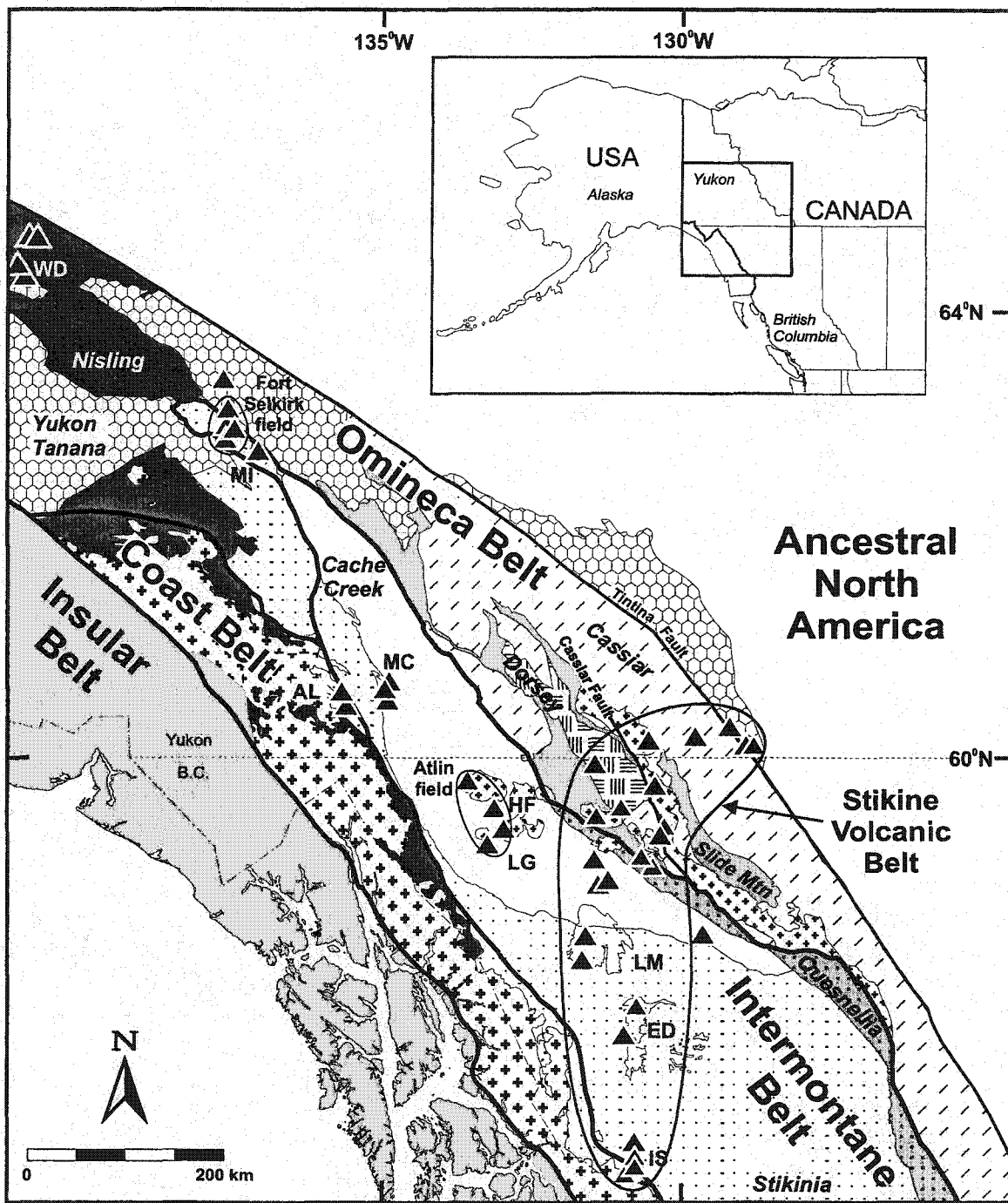
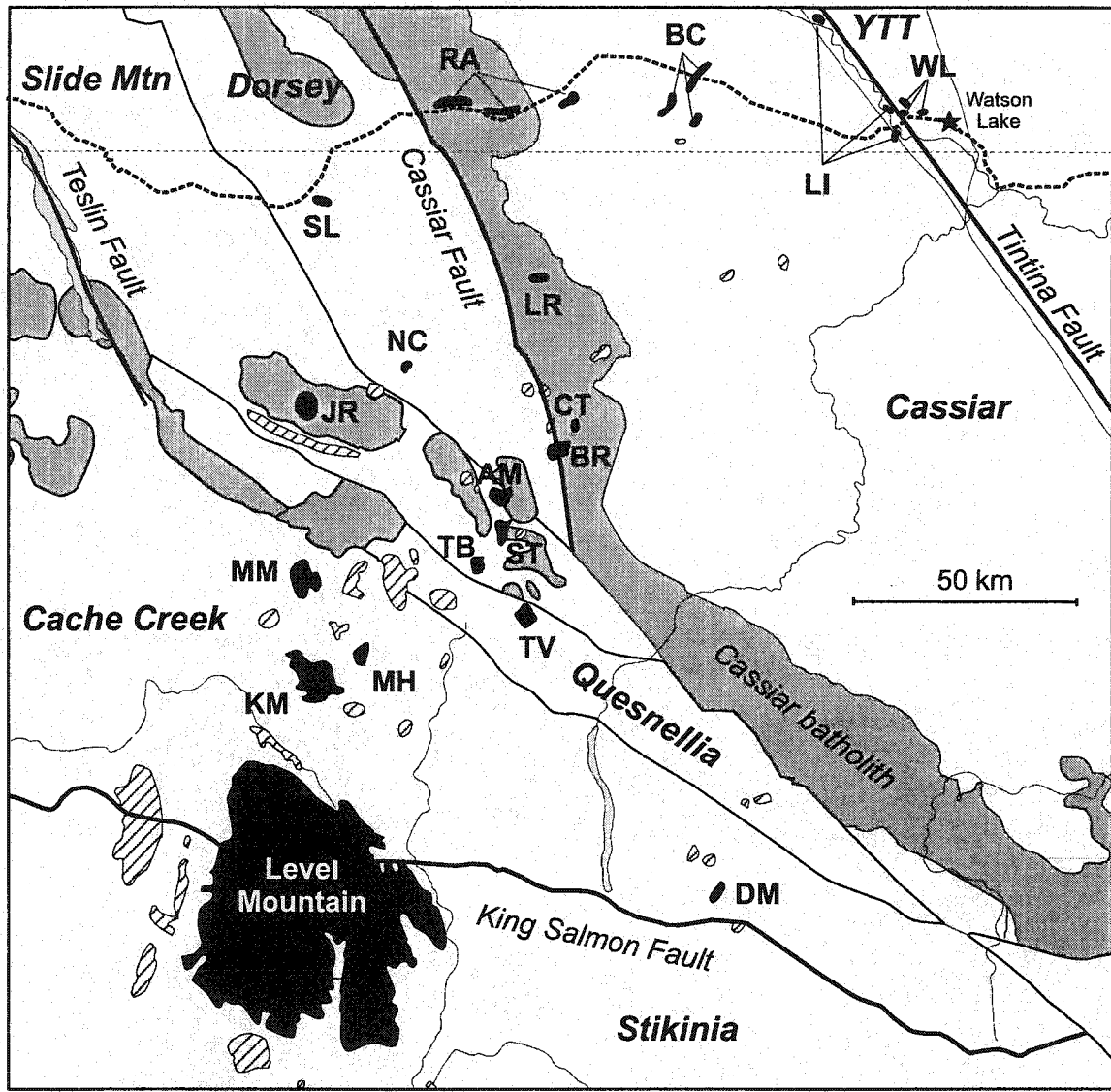


Figure 1.2: Enlargement of the northern part of the Stikine Volcanic Belt. Black centres: Tertiary to Recent volcanic centres that have been sampled for this study or previously (Hasik, 1994; Moore et al., 1995). Lined centres: unsampled Recent alkaline volcanic centres. Grey areas: Cretaceous plutons. Abbreviations: AM = Ash Mountain (Moore et al., 1995); BC= Big Creek; BR = Blue River; CT = Caribou Tuya; DM = Dome Mountain; JR = Jennings River; KM = Kawdy Mountain; LI = Liard River; LR = Little Rancheria; MH = Metahag Mountain; MM = Metah Mountain; NC = Nome Cone; RA = Rancheria River; SL = Swan Lake; ST = South Tuya (Moore et al. 1995); TB = Tuya Butte; TV = Tanzilla Volcano, WL = Watson Lake. Modified after Wheeler and Mcfeely (1991).



Belt itself, alkaline lavas first erupted at Level Mountain (14.9 Ma; Hamilton, 1981), then at Mount Edziza (7.4 Ma; Souther, 1992), and continued to Recent times (Pleistocene to Quaternary; Gabrielse, 1969) in these large volcanic complexes as well as at numerous small volcanic centres. The available dates for the small volcanic centres of the Stikine Volcanic Belt range from 0.232 to 0.765 Ma in the Watson Lake area (Klassen, 1987) and from 8780 to 360 y.b.p. in the Iskut-Unuk area (Elliot et al., 1979). A summary of ages for alkaline basalt centres in the northern Cordilleran volcanic province can be found in Edwards and Russell (2000).

Recent alkaline volcanism of the northern Canadian Cordillera may be the result of transtension created by the dextral relative movement between the Pacific and North America plates (Souther, 1977; Edwards and Russell, 1999). The presence of a mantle plume under Mount Edziza and Level Mountain has also been proposed, based on the HIMU affinity of basalts at Mount Edziza (Carignan et al., 1994). Finally, high heat flow values measured in the northern Canadian Cordillera (Hyndman and Lewis, 1999) indicate that incipient melting might now be occurring in the Cordilleran lithospheric mantle, and that lithospheric thinning might be responsible for the alkaline volcanism.

With a total length of 400-500 km, the Stikine Volcanic Belt crosses many of the accreted terranes constituting the northern Canadian Cordillera, from the Stikinia terrane in the west to the Cassiar terrane in the east (Fig. 1.1). In addition, Recent alkaline lavas have erupted to the east of the Tintina fault, a major transcurrent feature that separates the Cordilleran terranes from the North American craton (Fig. 1.1; Hasik, 1994). The goal of this project is to use this series of Recent volcanic centres to probe the Cordilleran upper

mantle. For that purpose, Level Mountain, as well as eleven small volcanic centres of the Stikine Volcanic belt that cross the boundary between the Intermontane and the Omineca belts, were systematically sampled during the field seasons of 1995 and 1996. This paper describes the individual centres that were sampled along the Stikine Volcanic Belt, and presents their major, trace element and isotopic characteristics in light of their field occurrence. In addition, it reviews the main chemical and isotopic characteristics of mafic lavas erupted at Mount Edziza (Souther, 1992; D. Francis, unpublished data), in the Rancheria area, and across the Tintina fault in the Watson Lake area (Hasik, 1994).

2. Tectonic setting

The Canadian Cordillera is composed of a series of terranes of different ages and origins that have been displaced along and accreted to the North American craton to form the northern Canadian Cordillera (Monger et al., 1982). The terranes have been divided into five morphological belts, which are, from west to east, the Insular, Coast, Intermontane, Omineca and Foreland belts (Fig. 1.1). Tertiary to Recent alkaline volcanism has occurred in the Coast, Intermontane, and Omineca belts, as well as across the Tintina Fault, which separates the Omineca Belt from the North American Craton. The Coast Belt consists mainly of metamorphic and plutonic rocks of the Coast Plutonic Complex that appear to have formed during the mid-Cretaceous subduction and accretion of two allochthonous belts of oceanic origin, the Insular and Intermontane belts (Gabrielse et al., 1991). A small terrane containing Proterozoic rocks with continental affinities (Gehrels et al., 1990), the Nisling terrane, lies to the north of the Coast Belt. The Intermontane Belt consists of late Paleozoic to Mesozoic allochthonous terranes of

oceanic origin (Gabrielse et al., 1991), that were accreted in Early to Middle Jurassic time to the continental margin of North America, represented at that time by the Omineca Belt. The Omineca Belt consists of autochthonous rocks derived from North America, but displaced northward several hundred kilometers along northwest-trending dextral faults in Late Cretaceous and Early Tertiary time (Gabrielse et al., 1991).

3. Classification of the lavas

Recent alkaline centres in the northern Canadian Cordillera have erupted olivine-phryic lavas with $MgO > 5$ wt.% that can be classified into four types (Francis and Ludden, 1990). Lavas with more than 15 wt.% normative nepheline (Ne) and no modal feldspar have been classified as olivine nephelinites (NEPH). This magma type occurs in a number of Tertiary to Recent centres situated to the northwest of the Stikine Volcanic Belt, such as in the Fort Selkirk (Francis and Ludden, 1990) and Atlin fields (Francis and Ludden, 1995). The crystallizing sequence in the NEPH magmas is olivine, followed by Ti-magnetite, and then clinopyroxene (Francis and Ludden, 1990 and 1995). Lavas with 5 to 15 wt.% normative Ne have been classified as basanites (BASAN) and are separated from the NEPH lavas by a distinct minimum in population. In BASAN magmas, the crystallization sequence is olivine, followed by clinopyroxene, and then plagioclase, and unlike the other magma types, most BASAN lavas have olivine and clinopyroxene as phenocrysts. The most common lavas are alkali olivine basalts (AOB) with 0-5 wt.% normative Ne, and hypersthene-normative basalts (Hy-NORM) with normative hypersthene (Hy), which appear to constitute a continuous compositional group with

distinctively lower incompatible element contents than the BASAN lavas. In AOB and Hy-NORM magmas, the crystallization sequence is olivine, followed by plagioclase in lavas with less than 8 wt.% MgO, and then clinopyroxene.

Lower-Mg mafic and felsic lavas, which are restricted to the large volcanic complexes of Level Mountain and Mount Edziza, have been classified following the scheme of Charland (1994; chap IV). Lavas with $1.5 < \text{MgO} < 5$ wt.% and both normative and modal andesine feldspar (An_{30-50}) are termed hawaiites. Felsic lavas, with $\text{MgO} < 1.5$ wt.%, are termed trachytes if they contain less than 5 wt.% normative nepheline (Ne) or quartz (Qtz), phonolitic trachytes if they contain between 5 and 15 wt.% Ne, quartz-trachytes if they contain 5 to 15 wt.% Qtz, and rhyolites if they contain more than 15 wt.% Qtz.

4. Volcanic centres of the Stikine Volcanic Belt from S-W to N-E

4.1. Mount Edziza ($57.5^\circ\text{N}, 130.6^\circ\text{W}$; NTS 104 G)

The Mount Edziza volcanic complex lies in the Stikinia terrane of the Intermontane Belt (Figure 1.1) and is associated with northerly trending normal faults indicating an extensional tectonic setting (Souther and Hickson, 1984). The Mount Edziza complex records a long history of episodic eruptions ranging in age from at least 7.5 Ma to less than 2000 B.P. (Souther et al., 1984). This volcanic complex covers about 665 km^3 and has been extensively studied by Souther and co-workers (e.g. Souther and Hickson, 1984; Souther et al., 1984; Souther and Yorath, 1991; Souther, 1992). The lavas from five of

the Mount Edziza formations, Raspberry (7.4 Ma), Armadillo (6.3 Ma), Nido (4.4 Ma), Ice Peak (~ 1 Ma) and Big Raven (0.002 Ma), were sampled by Don Francis and John Ludden and studied chemically (Tables B-1-a and B-1-b of appendix B) and isotopically (Carignan et al., 1994). The Mount Edziza complex displays a bimodal distribution of mafic and felsic lavas (Fig. 2.1.a ; Souther, 1992), with the most abundant lavas types being hawaiites and low-MgO Hy-NORM and AOB basalts (Souther and Hickson, 1984). The mafic lavas range in MgO from 1.5 to 12 wt.%, but only five samples in our dataset have more than 8 wt.% MgO (Fig. 2.1.b).

The trace element patterns of Mount Edziza mafic lavas are characterized by an enrichment in large ion lithophile elements (LILE) and light rare earth elements (LREE) compared to heavy rare earth elements (HREE) when normalized to primitive mantle, and negative Sr and Rb, but positive Nb anomalies compared to elements with similar compatibilities (Fig. 2.2.a). The two AOB samples analyzed for trace elements are more enriched in most trace elements than the Hy-NORM basalts. One of the two hawaiites analyzed for trace elements has similar trace elements patterns to the more primitive mafic magmas, whereas the other is characterized by a large positive K anomaly (Fig. 2.2.a). The rhyolite sample is more enriched in most trace elements than primitive Hy-NORM basalts from the Intermontane Belt, except in Sr, P and Ti (Fig. 2.2.b). In contrast to the mafic lavas, this sample exhibits positive Rb and K anomalies compared to Ba and Nb respectively when normalized to primitive mantle. Its trace element pattern is similar to those of felsic lavas at Level Mountain, with large negative Sr, P, Eu and Ti anomalies (Fig. 2.2.b).

Figure 2.1: a) $\text{Na}_2\text{O} + \text{K}_2\text{O}$ versus SiO_2 , and b) FeO (total) versus MgO in wt.% for Mount Edziza alkaline lavas. The lavas have been classified following the scheme of Charland (1994; chap IV), and the total alkali-silica (TAS) classification of Le Bas et al. (1986) has been drawn for comparison in Fig. 2.1.a. Symbols: white squares = AOB; black diamonds = Hy-NORM basalts; fine crosses = hawaiites; thick cross = Qtz trachyte; inverted triangles = rhyolites. Data in tables B-1-a and B-1-b of appendix B.

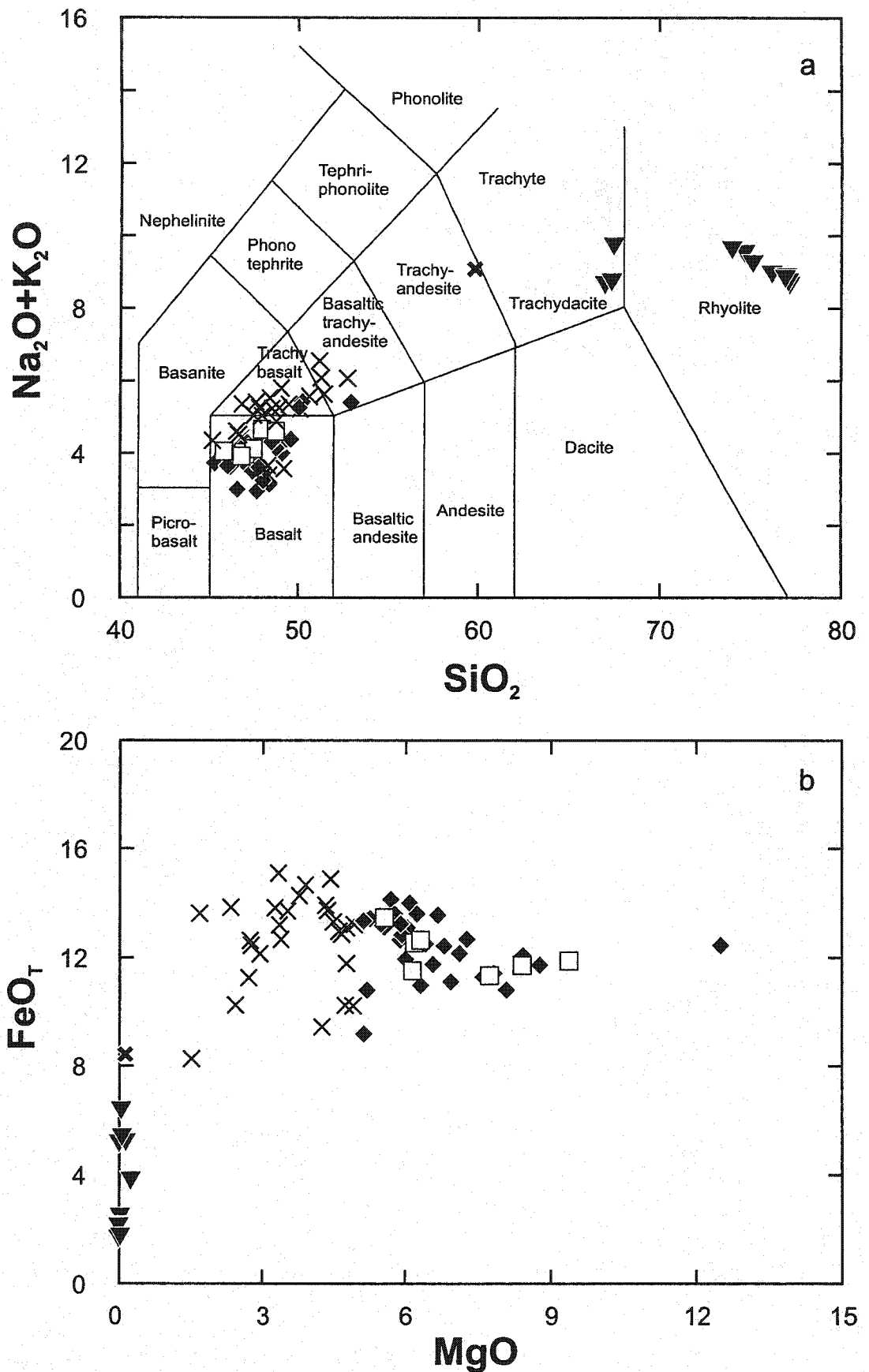


Figure 2.2: a) Trace element patterns of Mount Edziza mafic lavas ($MgO > 5$ wt.%) and hawaiites normalized to the primitive mantle values of Sun and McDonough (1989). Symbols as in Fig. 2.1. The shaded field corresponds to the range in Hy-NORM lavas with $MgO > 8$ wt.% from small volcanic centres from the Intermontane Belt (Kawdy Mountain, Metahag Mountain, and Metah Mountain). b) Trace element patterns of Mount Edziza rhyolite normalized to the primitive mantle values of Sun and McDonough (1989). Symbol as in Fig. 2.1. Shaded field as in Fig. 2.2.a. The streaked field corresponds to the range in felsic lavas from Level Mountain (Table B-2-b of appendix B).

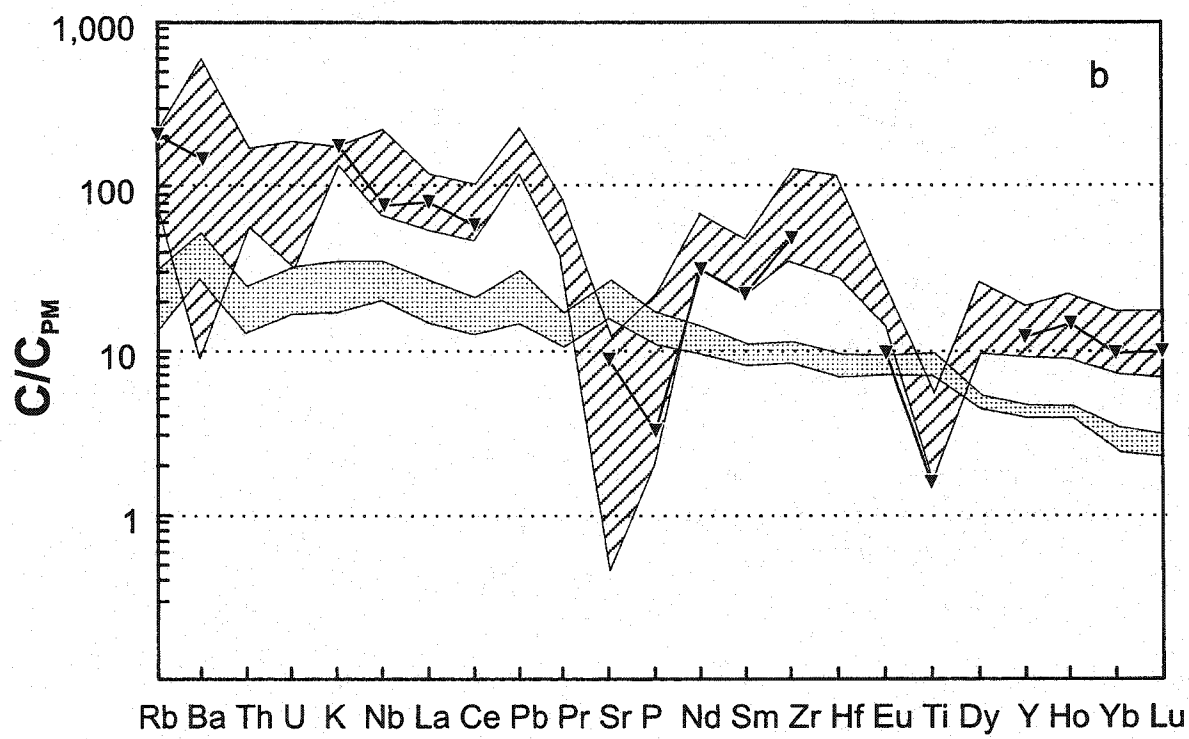
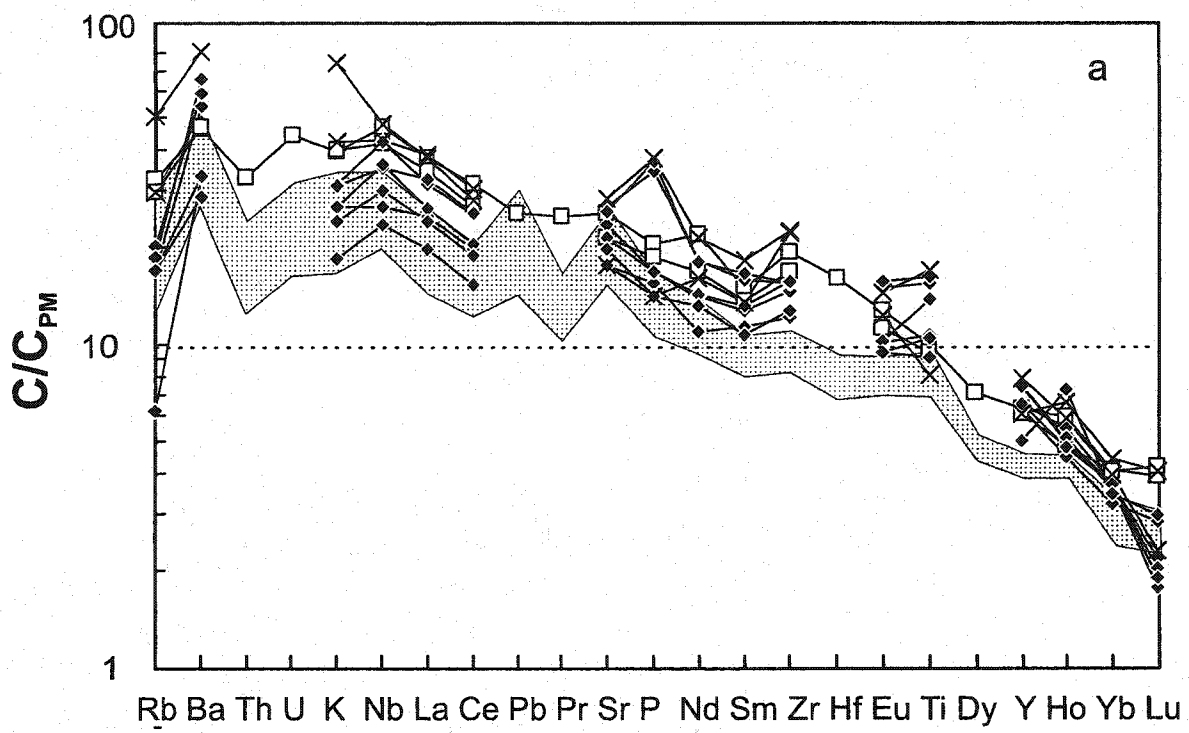
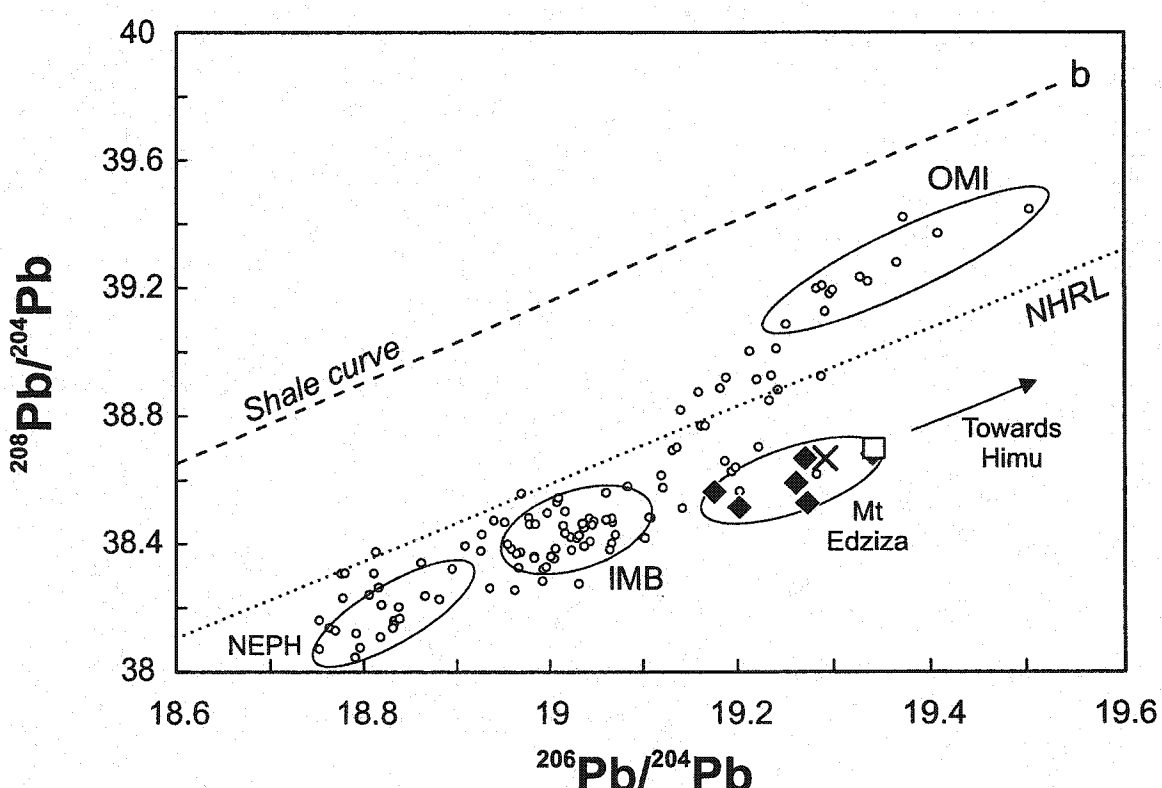
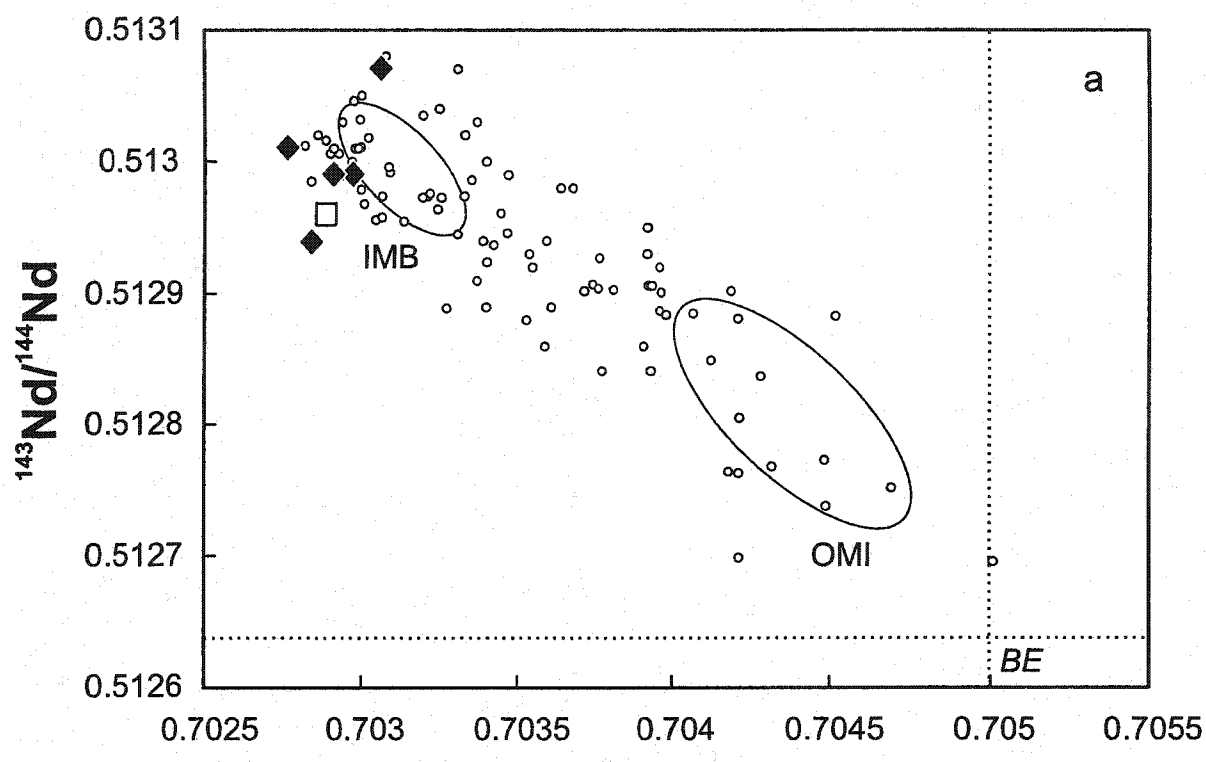


Figure 2.3:

a) $^{143}\text{Nd}/^{144}\text{Nd}$ versus $^{87}\text{Sr}/^{86}\text{Sr}$, and b) $^{208}\text{Pb}/^{204}\text{Pb}$ versus $^{206}\text{Pb}/^{204}\text{Pb}$ for Mount Edziza mafic alkaline lavas. Symbols as in Fig. 2.1., except for small circles which correspond to mafic lavas from the northern Canadian Cordillera. BE corresponds to bulk Earth values. The north hemisphere reference line (NHRL) is from Hart (1984), the shale curve from Godwin and Sinclair (1982). The fields labeled IMB and OMI correspond to the isotopic range in primitive Hy-NORM basalts ($\text{MgO} > 8$ wt.%) at small volcanic centres of the Intermontane Belt (Hirschfeld, Kawdy Mountain, Metahag Mountain, and Metah Mountain) and the Omineca Belt (Rancheria area, Blue River, and Caribou Tuya) respectively. The field labeled NEPH corresponds to the isotopic range of primitive NEPH lavas from the northern Canadian Cordillera (Francis and Ludden, 1990; Carignan et al., 1994). Data for Mount Edziza from Carignan et al. (1994).



The Mount Edziza mafic lavas that have been studied isotopically (Carignan et al., 1994; Table B-1-a of appendix B) display a restricted isotopic range characterized by unradiogenic Sr and radiogenic Nd isotopic ratios, similar to those of primitive H-NORM basalts at small volcanic centres in the Intermontane Belt (Fig. 2.3.a). Their Pb isotopic signatures, however, define an end-member in a Pb-Pb isotopic plot with high $^{206}\text{Pb}/^{204}\text{Pb}$, and relatively low $^{207}\text{Pb}/^{204}\text{Pb}$ and $^{208}\text{Pb}/^{204}\text{Pb}$ (Fig. 2.3.b), that trends towards the HIMU mantle component of Zindler and Hart (1986). Because of its large volume and the similarity between Mount Edziza and Pacific seamounts isotopic signatures, Carignan et al. (1994) proposed that Mount Edziza might be centered on a HIMU-type mantle plume.

4.2. *Level Mountain (58.48°N, 131.43°W; NTS 104-J/3, J/4, J/5, and J/6)*

With an aerial extent of approximately 860 km³ (Hamilton, 1981), Level Mountain is the largest volcanic centre of the Stikine Volcanic Belt. It is located to the northwest of Mount Edziza at the boundary between the Stikinia and the Cache Creek terranes of the Intermontane Belt (Fig. 1.1). This area corresponds to the height of land in the northern Cordillera, separating drainage systems which flow to the Bering Sea via the Yukon River towards the north, from those which flow to the Pacific Ocean via the Stikine River towards the southwest. Level Mountain has a long-lived volcanic history initiated 14.9 Ma ago with the formation of a large basaltic plateau (Fig. 3.1), and ended 2.5 Ma ago, with the construction of a bimodal stratovolcano (Fig. 3.2; Hamilton, 1981). The late Tertiary uplift that has affected the drainage and morphology of the area (Kerr,

Figure 3.1: Photos of the lava plateau forming the base of Level Mountain: **a)** from a distance, **b)** closer view of the sampled section, **c)** closer view of the lava flows.

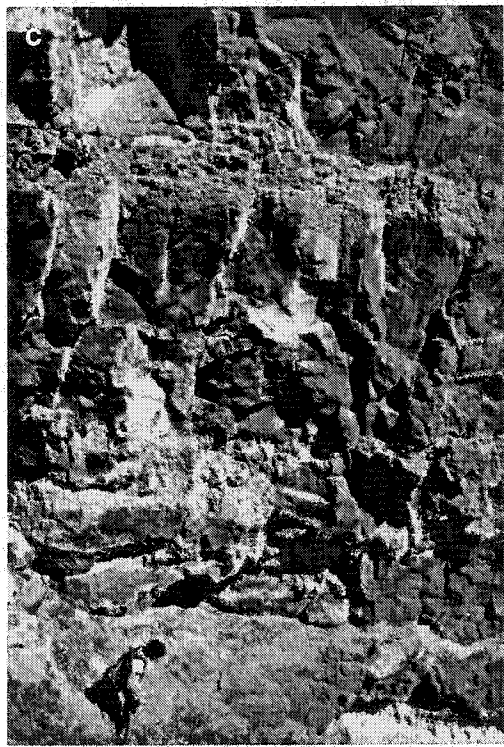
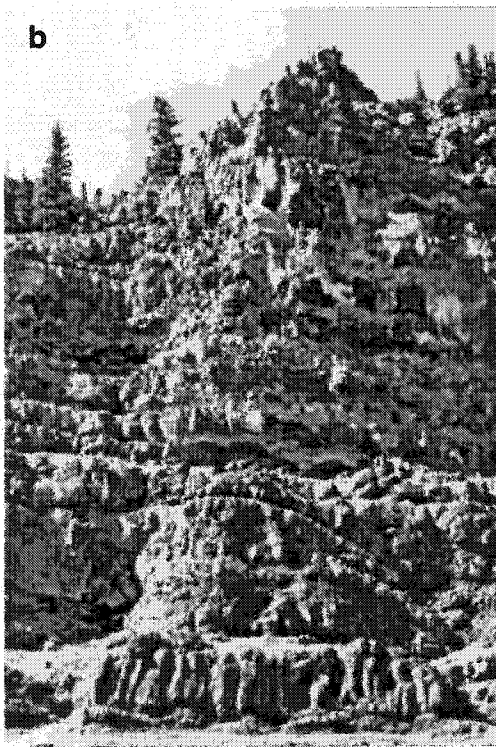
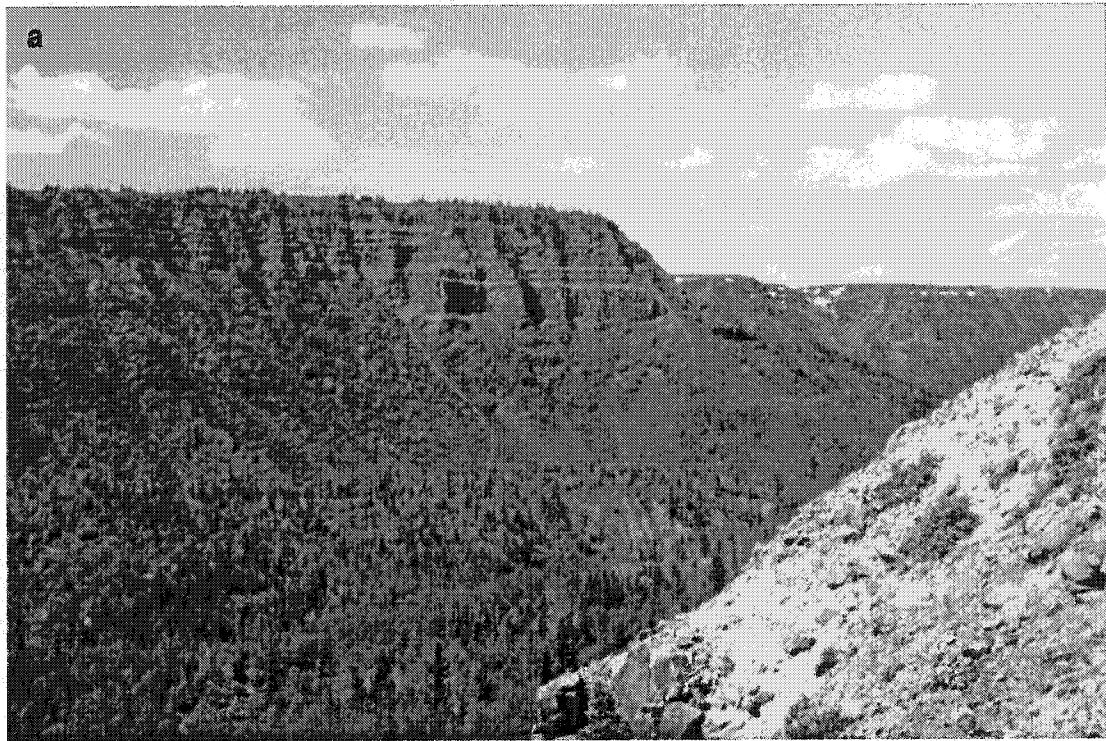


Figure 3.2: Photos of the strato volcano constituting the top of Level Mountain: a) the eastern part, b) Meszah Peak.

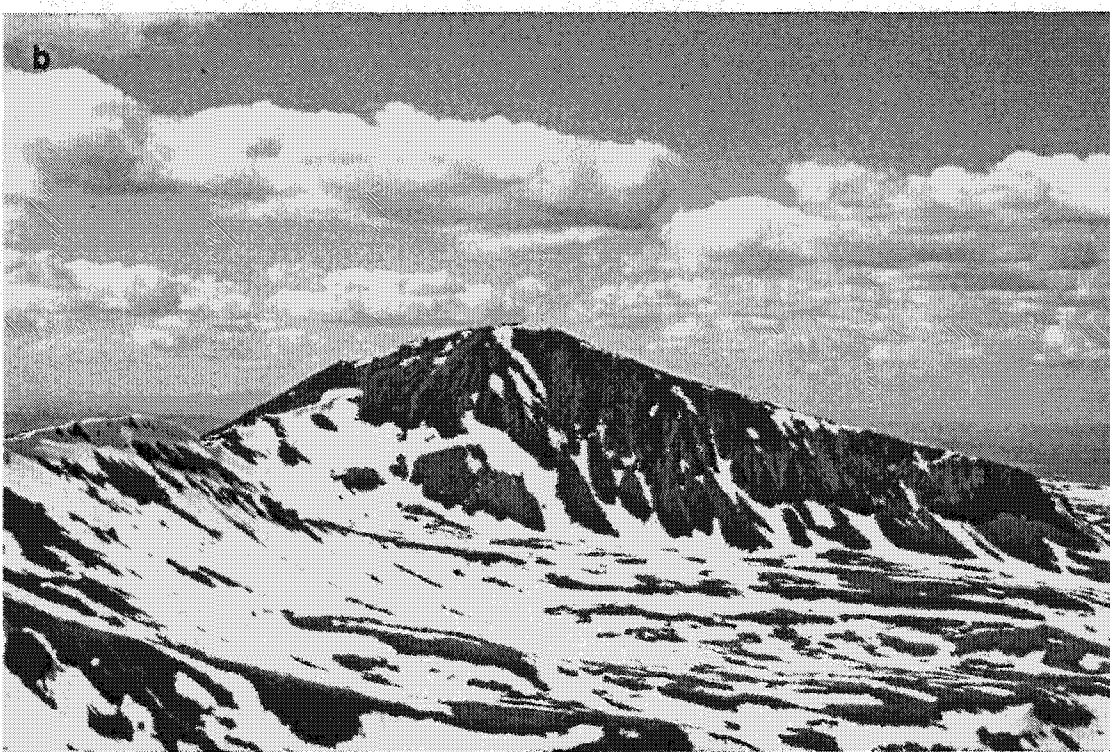
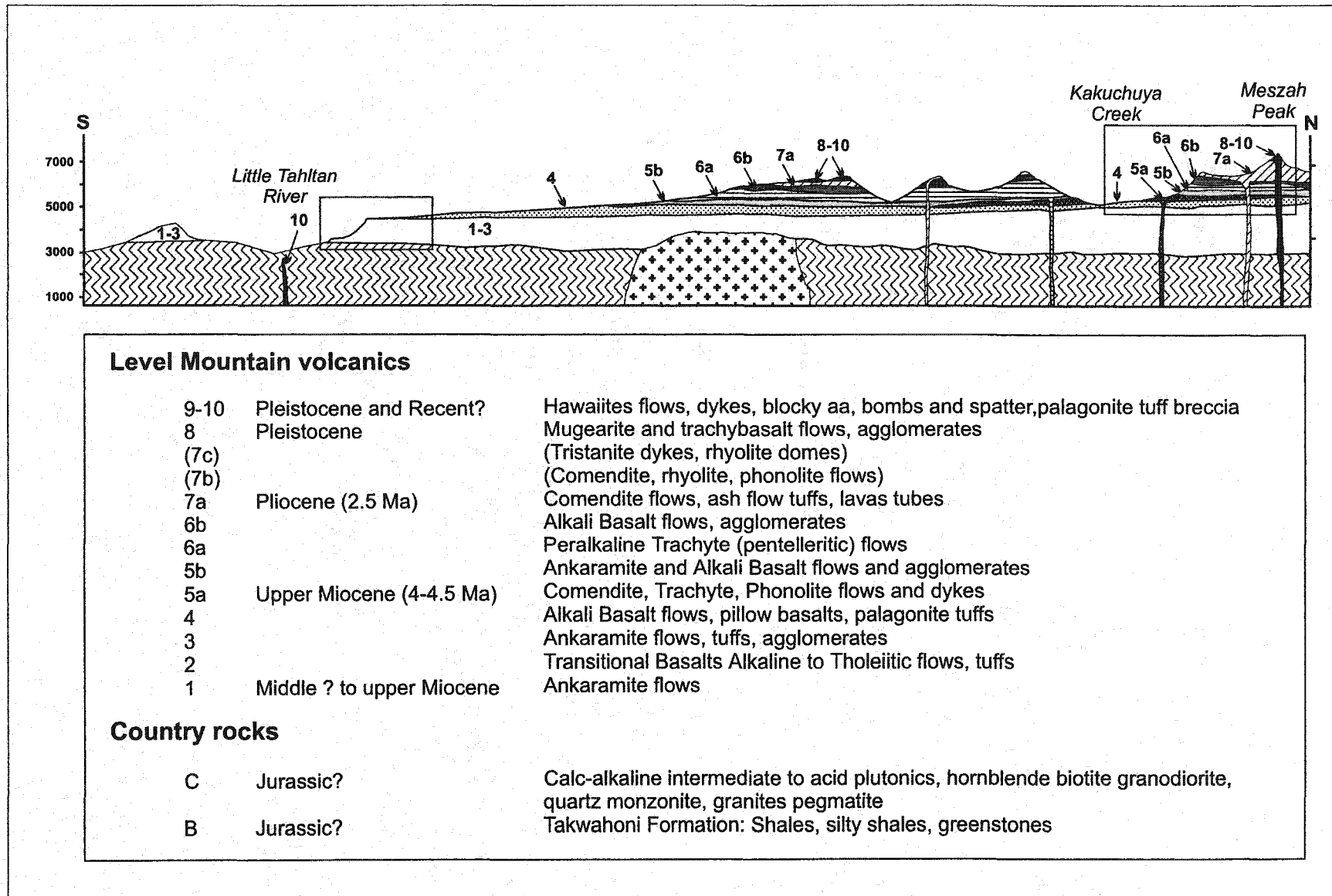


Figure 3.3: Location of our sections on section #3 of Hamilton (1981). Our sections are represented by boxes. The units in brackets in the legend correspond to units recognized by Hamilton that have not been sampled in this study.

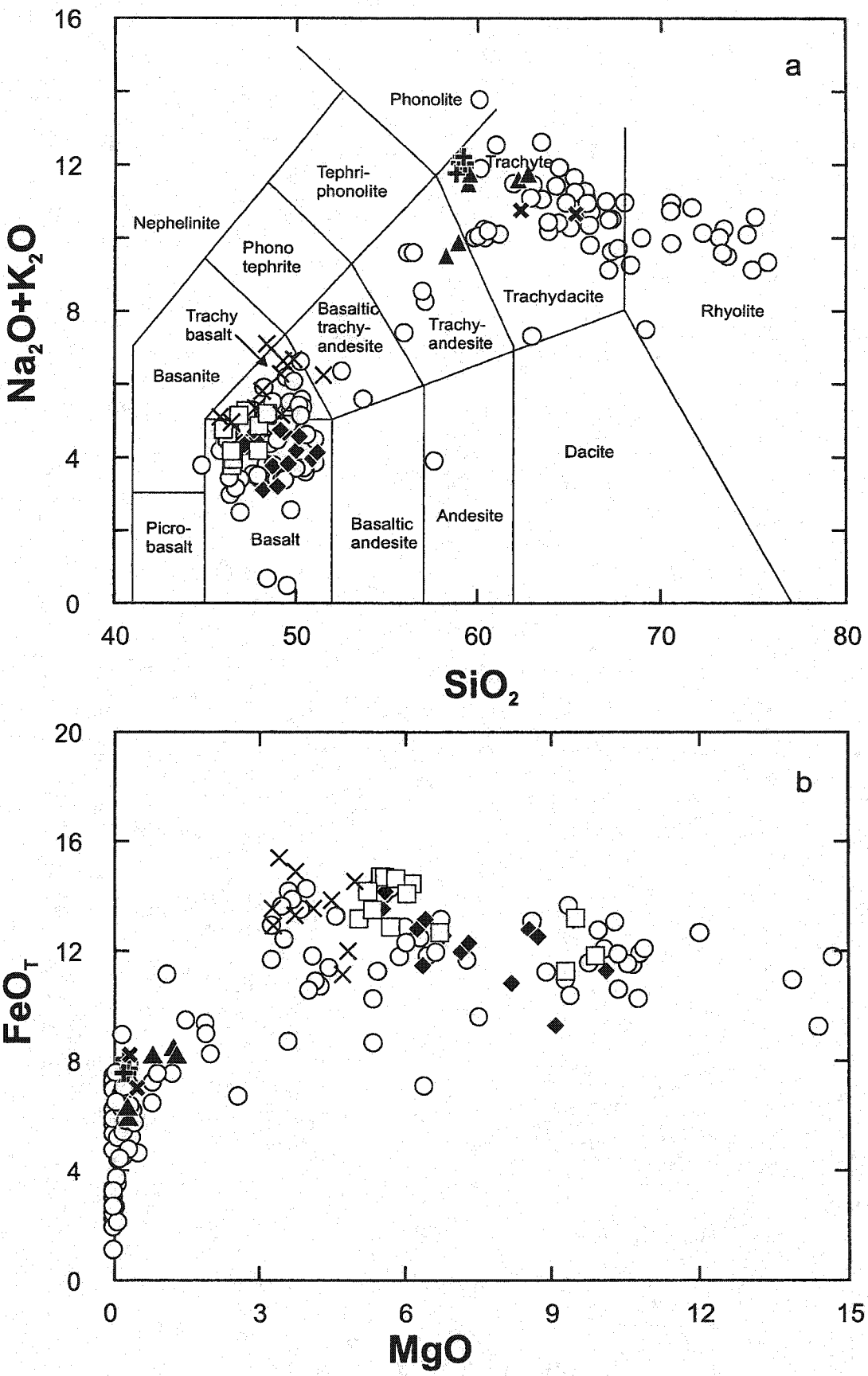


1936) may be related to the tectonic process responsible for Level Mountain alkaline volcanism.

The Level Mountain volcanic complex has been studied by Hamilton (1981), who produced a detailed map and the first petrochemical study of the lavas. At least four sequences of alkaline basalt flows and tuffs erupted during the early plateau-building stage, whereas a bimodal population of alkaline basalts and peralkaline felsic lavas and tuffs have erupted repetitively during the later stratovolcano-building stage (Hamilton, 1981; Fig. 3.3). Samples were collected for this study from most of the volcanic units recognized by Hamilton (1981). Four stratigraphic sections were systematically sampled, with 40 of 70 samples collected from the mafic volcanic plateau that constitutes the base of the shield volcano. The locations of our sections on Hamilton's cross-section #3 are shown in Fig. 3.3. Precise location of the samples can be found in table A-2 of appendix A and chemical analyses for 54 samples are in tables B-2-a and B-2-b of appendix B.

As can be seen in Fig. 3.4.a, our data set comprises a large number of mafic to intermediate lavas, separated from the felsic lavas by a distinct "Daly gap" (Daly, 1925) between 51 and 58 wt.% SiO₂. All the felsic lavas, except one sample, are metaluminous with agpaitic indices (molar $(\text{Na}_2\text{O} + \text{K}_2\text{O})/\text{Al}_2\text{O}_3$) < 1. Mafic olivine basalts with MgO > 5 wt.% are AOB and Hy-NORM basalts, and constitute about 80% of the volume of the plateau. They have MgO contents that range from 10 wt.% down to 5 wt.% MgO and grade continuously to hawaiites down to 3 wt.% MgO (Fig. 3.4.b).

Figure 3.4: a) $\text{Na}_2\text{O} + \text{K}_2\text{O}$ versus SiO_2 , and b) FeO (total) versus MgO in wt.% for Level Mountain alkaline lavas compared to Hamilton (1981)'s data set. The lavas have been classified following the scheme of Charland (1994; chap IV), and the total alkali-silica (TAS) classification of Le Bas et al. (1986) has been drawn for comparison. Symbols: squares = AOB; diamonds = Hy-NORM basalts; fine crosses = hawaiites; triangles = trachytes; thick cross = Qtz trachyte; thick straight crosses = phonolitic trachytes; circles = Hamilton (1981)'s dataset.



The trace element patterns of Level Mountain AOB and Hy-NORM basalts are characterized by an enrichment in LILE and LREE compared to HREE when normalized to primitive mantle, positive Pb and Sr, and negative Rb and Th anomalies (Fig. 3.5.a). AOB and Hy-NORM basalts exhibit a large range in LILE and LREE, but they have a tendency to converge in the HREE end of the diagram. All but one sample exhibit small positive Nb anomalies compared to La. The U contents of Level Mountain basalts are highly variable compared to other incompatible elements, resulting in both negative and positive anomalies compared to Th. Although the AOB lavas tend to be more enriched in some incompatible trace elements than the Hy-NORM basalts in Level Mountain, the distinction between AOB and Hy-NORM basalts does not correspond to systematic differences in the trace element contents (Fig. 3.5.a). The trace element patterns of Level Mountain mafic lavas are similar to those of primitive Hy-NORM from small volcanic centres in the Intermontane Belt, except for those of two Hy-NORM basalts (LM-42 and LM-44) that erupted at the end of the plateau-building stage and have lower K and Rb concentrations than the other basalts (Fig. 3.5.a). One of these samples, LM-42, has one of the least enriched trace element pattern in terms of LILE and LREE, but still exhibits large positive Pb and Sr anomalies (Fig. 3.5.a). The hawaiites are more enriched in most trace elements than the mafic lavas (Fig. 3.5.b), but display similar trace element patterns, except for a lack of large positive Pb and negative Sr anomalies, and the presence of positive P anomalies (Fig. 3.5.b). The trace element patterns of the felsic lavas are characterized by strong negative Sr, P and Ti anomalies, and positive Pb anomalies, and slight positive Nb anomalies compared to La, when normalized to primitive mantle (Fig. 3.6). They are more enriched in most incompatible trace elements than mafic lavas, except in Sr, P and Ti.

Figure 3.5: a) Trace element patterns of Level Mountain mafic lavas with $\text{MgO} > 5$ wt.% normalized to the primitive mantle values of Sun and McDonough (1989). b) Trace element patterns of Level Mountain hawaiites normalized to the primitive mantle values of Sun and McDonough (1989). Symbols as in Fig. 3.4. Shaded field as in Fig. 2.2.a.

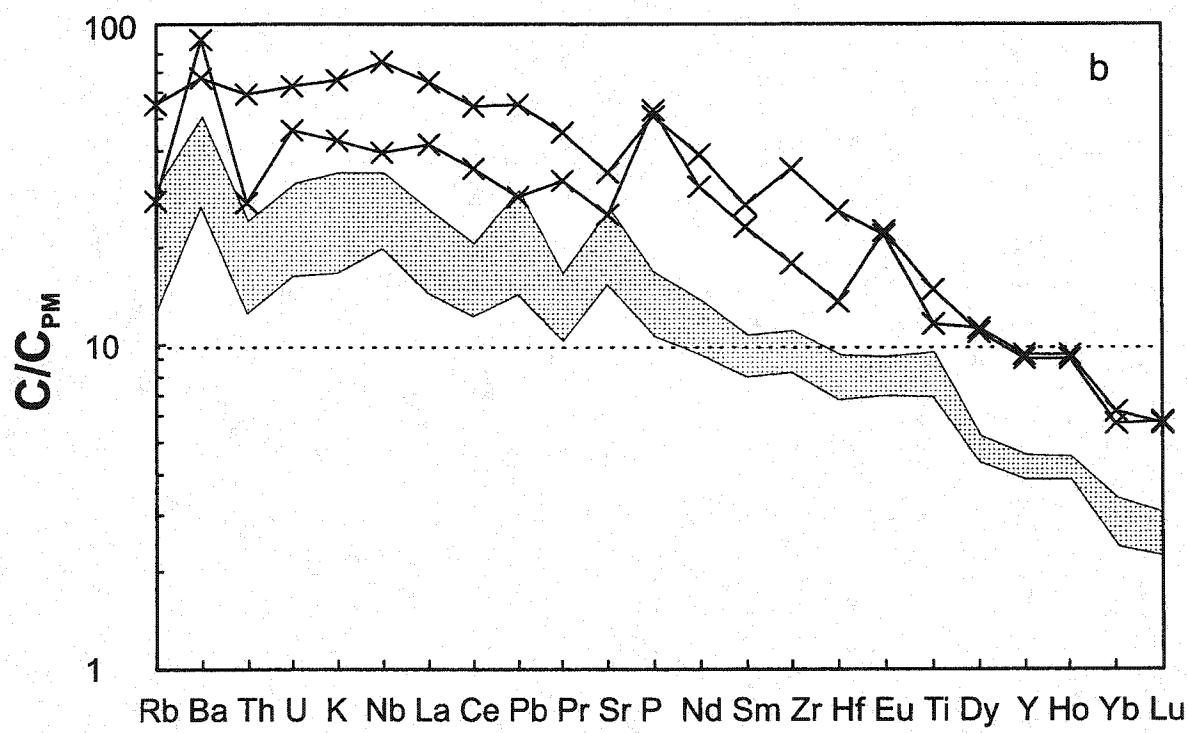
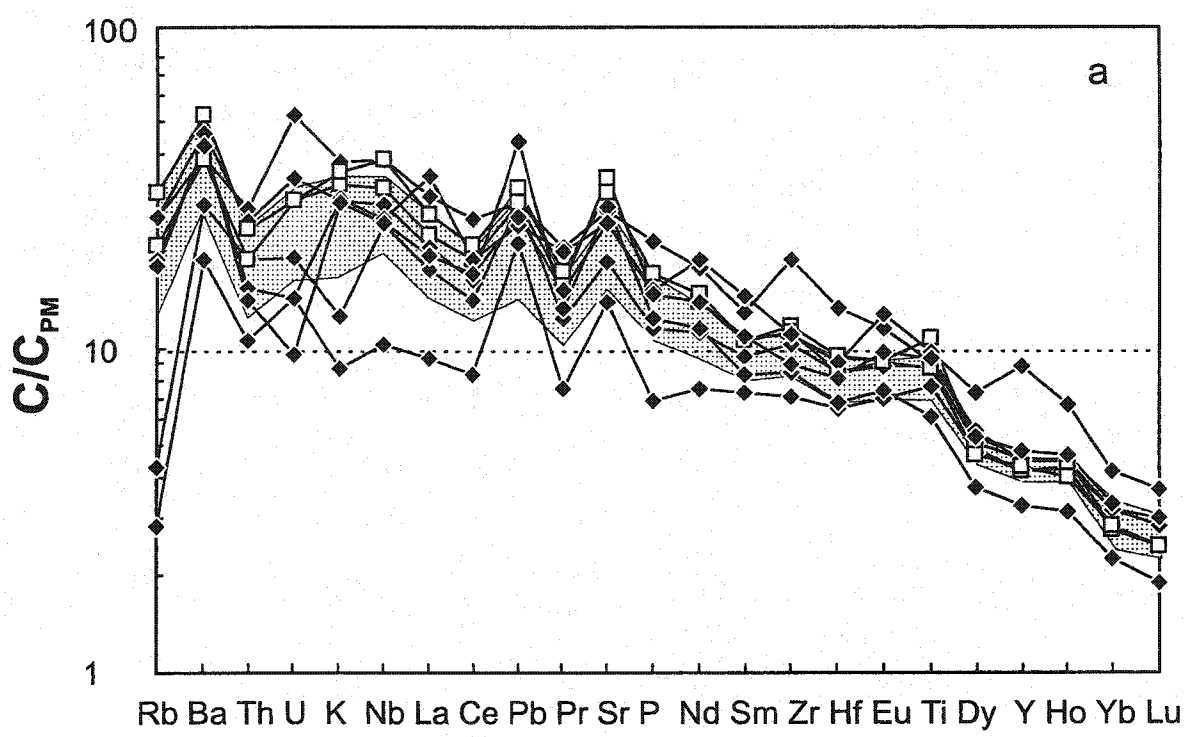


Figure 3.6: Trace element patterns of Level Mountain felsic lavas normalized to the primitive mantle values of Sun and McDonough (1989). Symbols as in Fig. 3.4. Shaded field as in Fig. 2.2.a.

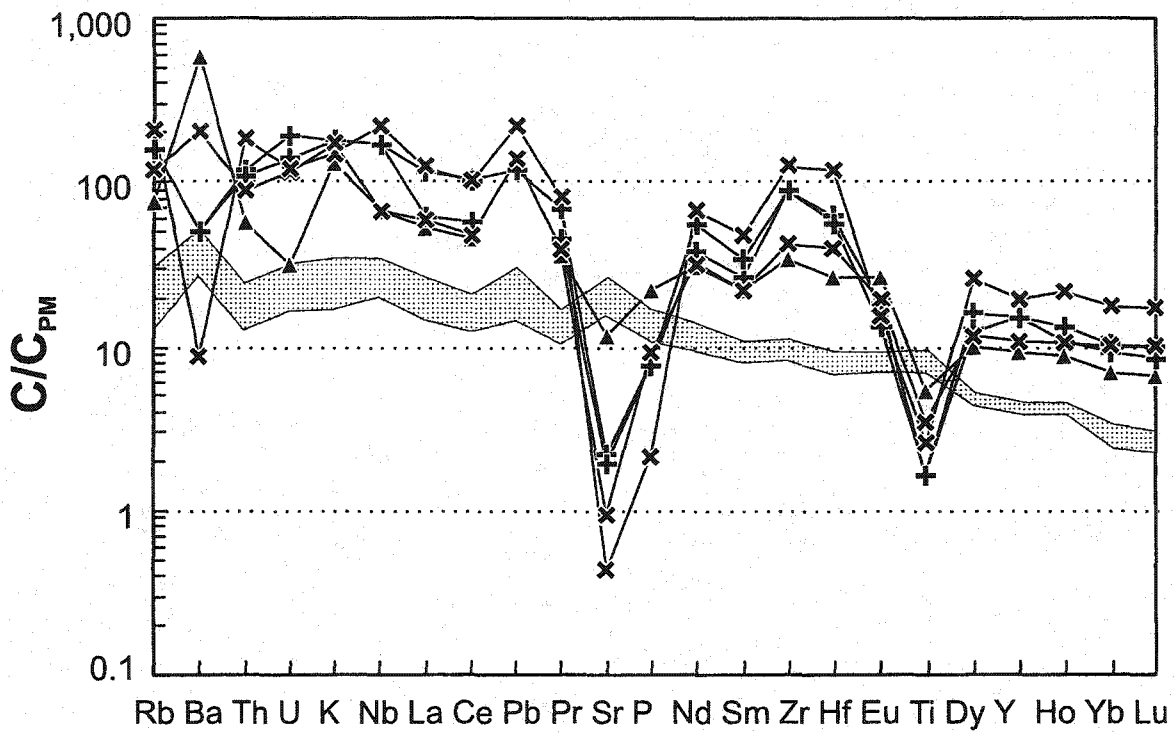


Figure 3.7:

a) $^{143}\text{Nd}/^{144}\text{Nd}$ versus $^{87}\text{Sr}/^{86}\text{Sr}$ for Level Mountain lavas compared to other mafic lavas erupted in the northern Canadian Cordillera. Symbols as in Fig. 3.4, except for white circles that correspond to all Cordilleran mafic lavas. Fields as in Fig. 2.3. b) $^{143}\text{Nd}/^{144}\text{Nd}$ versus $^{87}\text{Sr}/^{86}\text{Sr}$ for Level Mountain lavas compared to granitoid samples from the northern Canadian Cordillera. Symbols as in Fig. 3.4, except for crosses that correspond to Cordilleran granitoid samples (Appendix C; Driver et al., 2000).

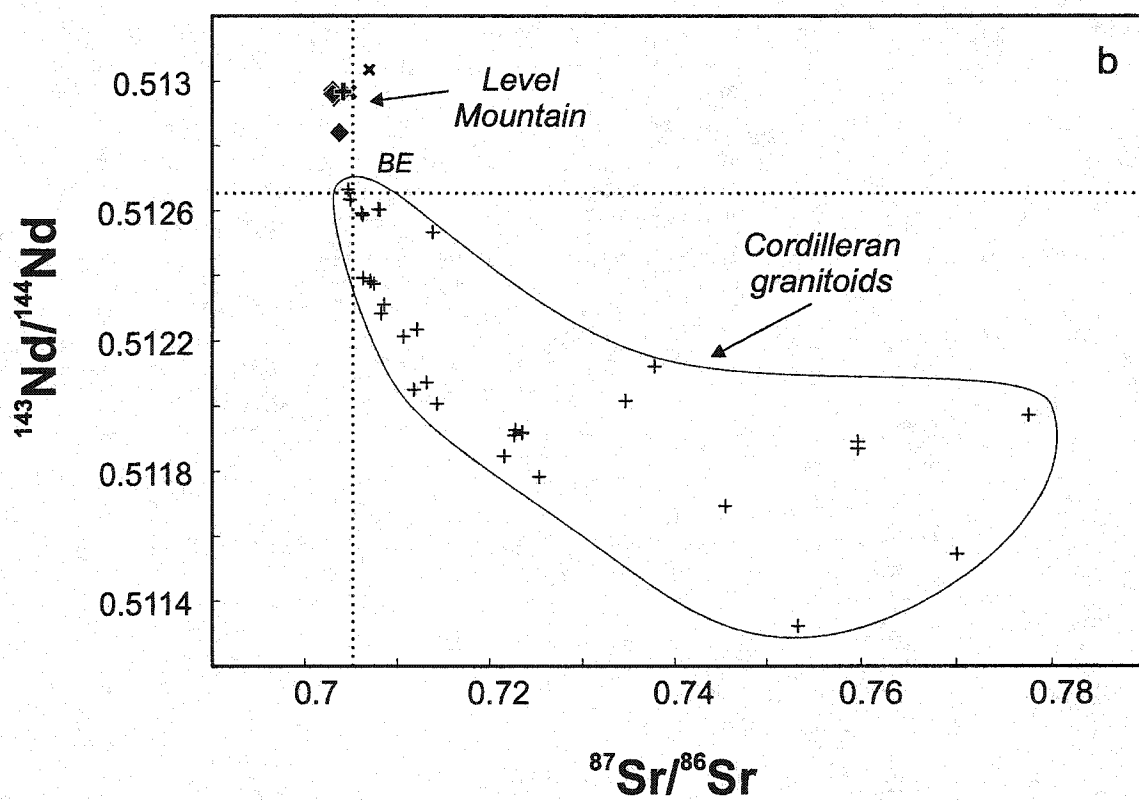
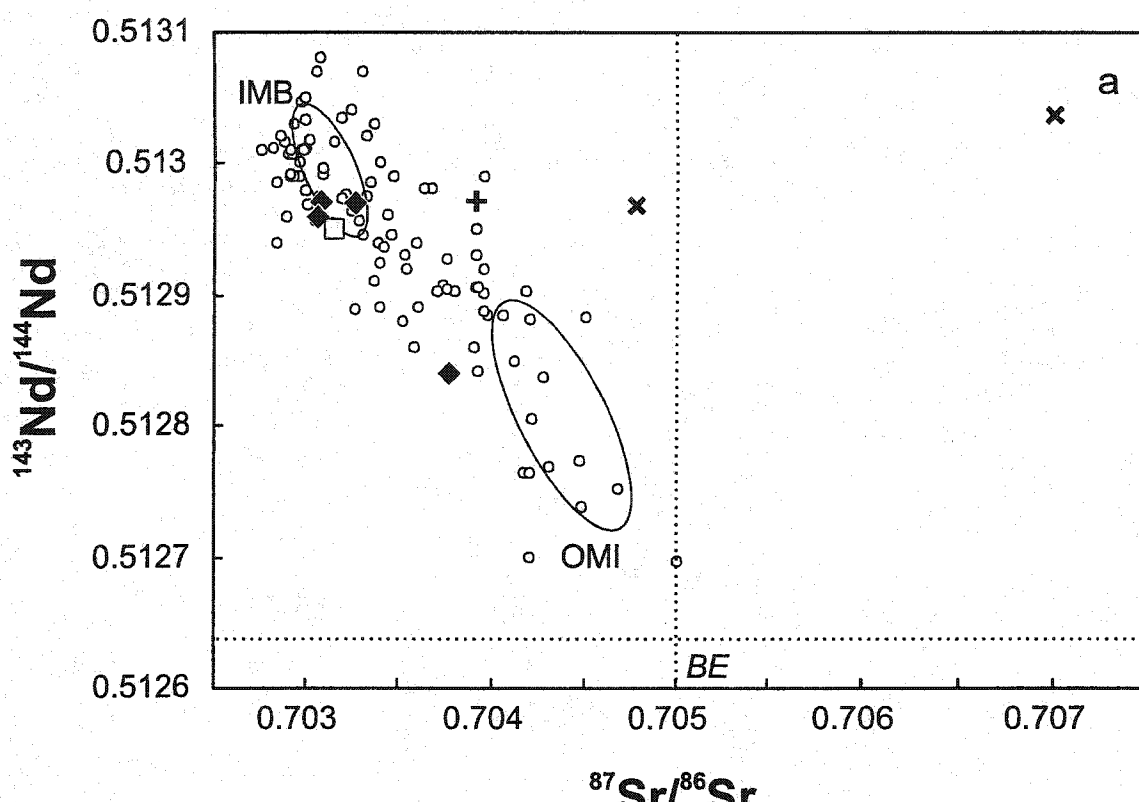
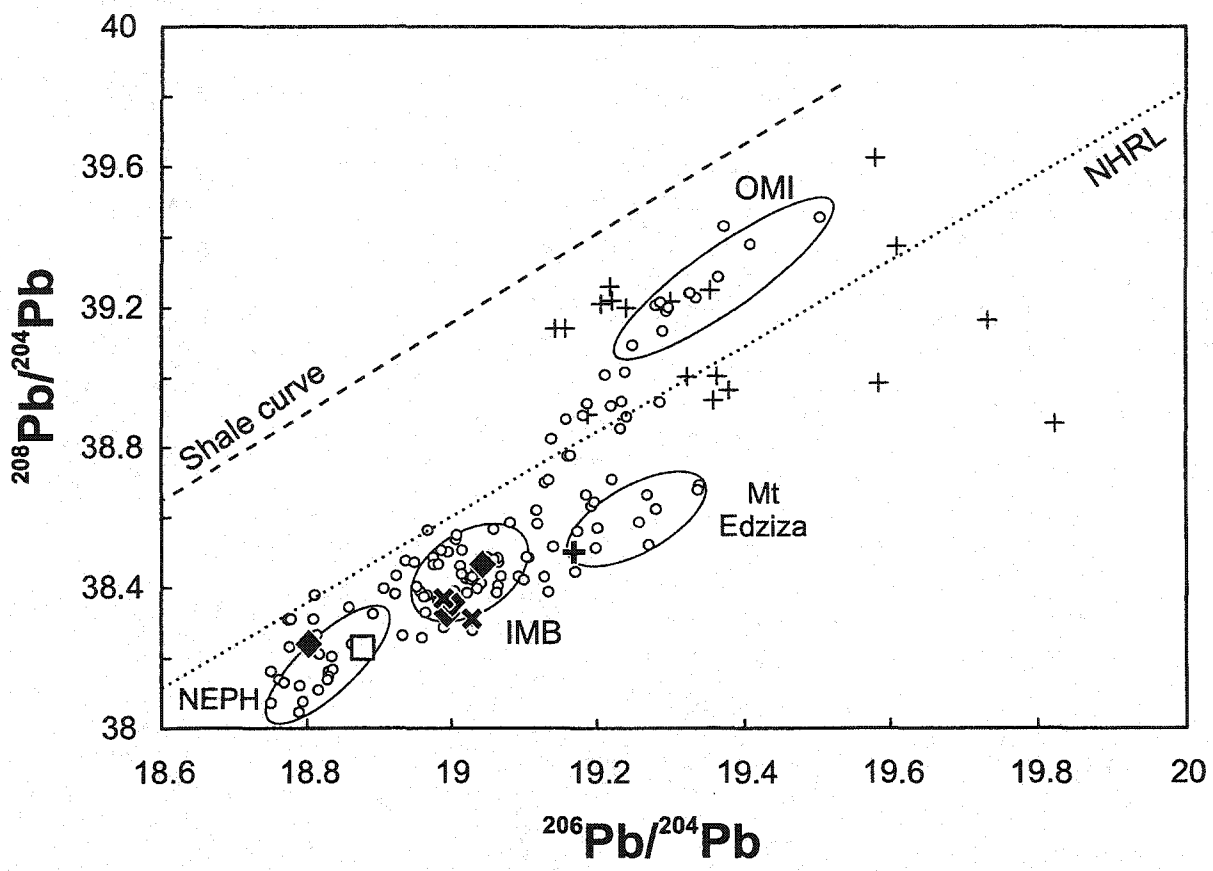


Figure 3.8: $^{208}\text{Pb}/^{204}\text{Pb}$ versus $^{206}\text{Pb}/^{204}\text{Pb}$ for Level Mountain lavas. Symbols as in Fig. 3.4, except for white circles and small crosses that correspond to Cordilleran mafic lavas and granitoid samples, respectively. Fields and explanations as in Fig. 2.3. Data for granitoid samples: appendix C and Driver et al. (2000).

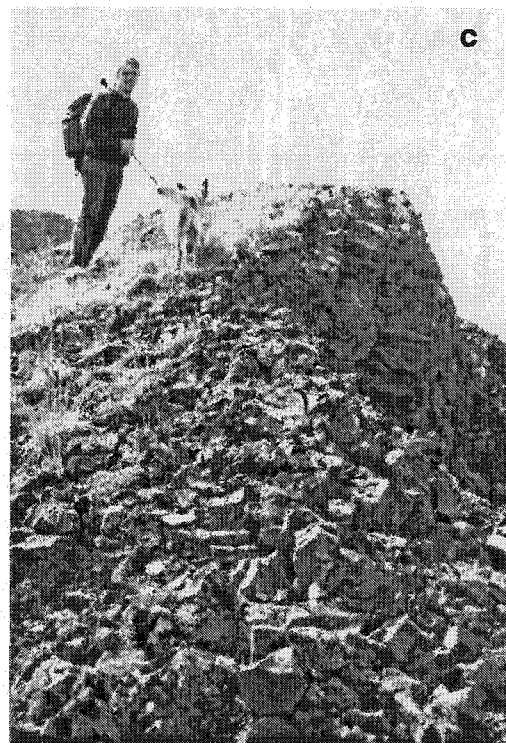


All the Level Mountain mafic lavas, except the lowest one in the stratigraphy (LM-70), have unradiogenic Sr and Pb, but radiogenic Nd isotopic ratios, characteristic of a relatively isotopically depleted mantle (Fig. 3.7.a). They do not share the HIMU-type affinities of Mount Edziza mafic lavas, having distinctly lower $^{206}\text{Pb}/^{204}\text{Pb}$ isotopic ratios (Fig. 3.8). An AOB and one of the Hy-NORM samples have even less radiogenic Pb isotopes than primitive Hy-NORM basalts from small volcanic centres in the Intermontane Belt (Fig. 3.8). The few isotopic measurements of Level Mountain felsic lavas indicate that they are significantly more radiogenic in Sr than the mafic lavas (Fig. 3.7.a). However, they have similar Nd and Pb isotopic ratios to the mafic lavas (Fig. 3.7.a and 3.8), and do not trend towards crustal isotopic compositions in a Sr-Nd space (Fig. 3.7.b). These features suggest that, despite the presence of granitic xenoliths in some lavas and the enrichment in ^{18}O in some rhyolites (Hamilton 1981), the Level Mountain felsic magmas did not strongly interact with upper crustal granitic rocks. Their high $^{87}\text{Sr}/^{86}\text{Sr}$ and ^{18}O might be explained by contamination by seawater-altered oceanic crust or oceanic sediments that might be present in the Intermontane Belt.

4.3. Kawdy Mountain (58.88°N , 131.22°W ; NTS 104-J/14)

Kawdy Mountain is part of a field of small cones and tuyas situated to the north of Level Mountain in the Cache Creek terrane of the Intermontane Belt (Fig. 1.2). This volcanic centre is comprised of a clastic cone constructed on a base consisting of a succession of pillow lava (about 100 m; Fig. 4.1.b and 4.2) overlaid by hyaloclastite tuff (about 200 m), with interbeds of ash and lapilli tuffs, then by polymictic breccia (about 70

Figure 4.1: a) Pyroclastic tuff forming the summit of Kawdy Mountain. b) Pillow lava and dike at the base of Kawdy Mountain. c) Closer view of a dike.



m), and capped by another layer of hyaloclastic tuff (Fig. 4.1.a). Numerous dikes cut the whole structure (Fig. 4.1.c). The volume of the centre is estimated to be approximately 14 km³ (Edwards and Russell, 2000). The entire volcanic centre has apparently erupted in an englacial lake, and the absence of capping flows suggests that the volcanic pile never reached the water surface (Allen et al., 1982). Although no age has been determined for this field, a late Tertiary to Recent (perhaps mainly Pleistocene) age has been proposed by Gabrielse (1969) for these alkaline volcanic centres and appears consistent with the evidence for subglacial eruption at this centre.

The basalts sampled at Kawdy Mountain are relatively fractionated, as only six of the 20 samples have MgO contents greater than 8 wt.% (Fig. 4.3). They can be divided into two stratigraphically separate groups, that define distinct olivine-control lines in plots of SiO₂ and TiO₂ versus MgO (Fig. 4.3.a and b). One group comprises Hy-NORM basalts from the lower part of the centre, and the other comprises both AOB and Hy-NORM basalts from blocks in the upper tuff and breccia (Fig. 4.2). Both groups have similar CaO and Al₂O₃ contents at similar MgO contents (Fig. 4.3.c and 4.3.d), and trace element patterns that are enriched in LILE and LREE compared to HREE, when normalized to primitive mantle, with positive Ti, Sr and Nb anomalies and negative Th and Rb anomalies compared to elements with similar compatibilities (Fig. 4.4). The Hy-NORM basalts at the base of the centre, however, are less enriched in LILE and LREE than the other basalts, but they all converge to similar HREE values (Fig. 4.4). The Hy-NORM basalts at the base of Kawdy Mountain are the only high MgO Hy-NORM basalts from the Intermontane Belt that do not exhibit systematic positive Pb anomalies (Fig.

Figure 4.2: Stratigraphic column of Kawdy Mountain indicating the position of each analyzed sample. Bold sample labels correspond to samples that have been isotopically studied. Symbols: squares = AOB; diamonds = Hy-NORM basalts. The black and white colors correspond the two stratigraphically separated groups that define distinct olivine-control lines identified in this centre. Data in table B-3 of appendix B.

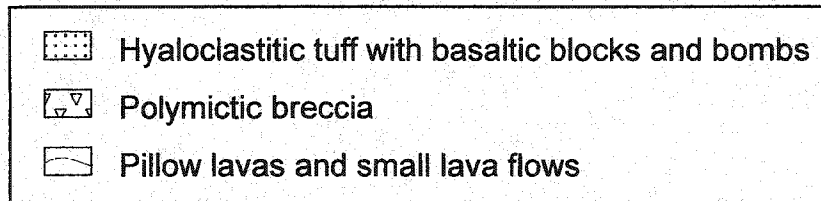
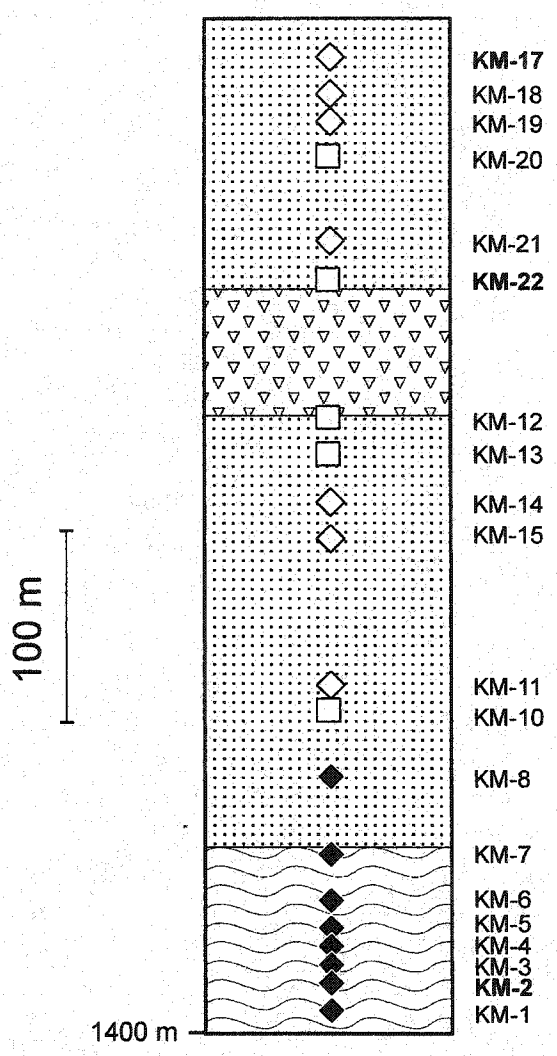




Figure 4.3: a) SiO_2 , b) TiO_2 , c) CaO , and d) Al_2O_3 versus MgO in wt.% for Kawdy Mountain basalts. Symbols as in Fig. 4.2. The arrow corresponds to the trend expected for olivine fractionation from sample KM-2.

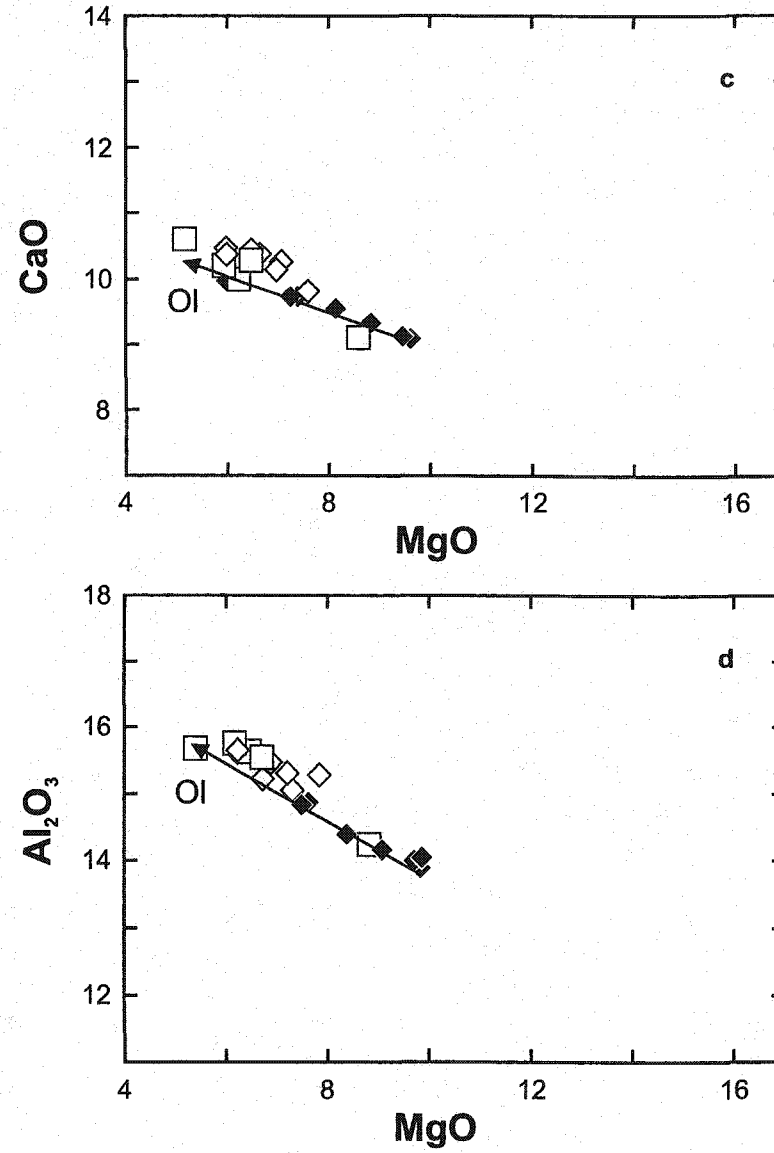
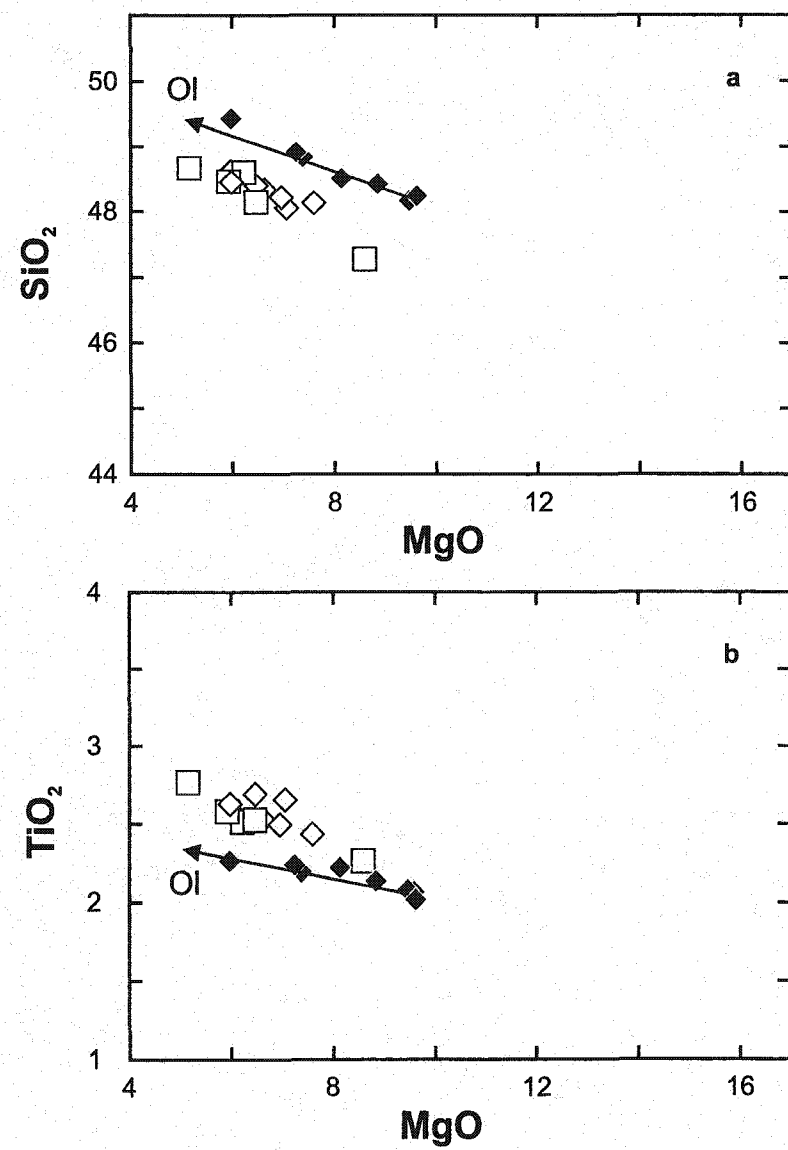




Figure 4.4: Trace element patterns of Kawdy Mountain basalts normalized to the primitive mantle values of Sun and McDonough (1989). Symbols as in Fig. 4.2. Shaded field as in Fig. 2.2.a.

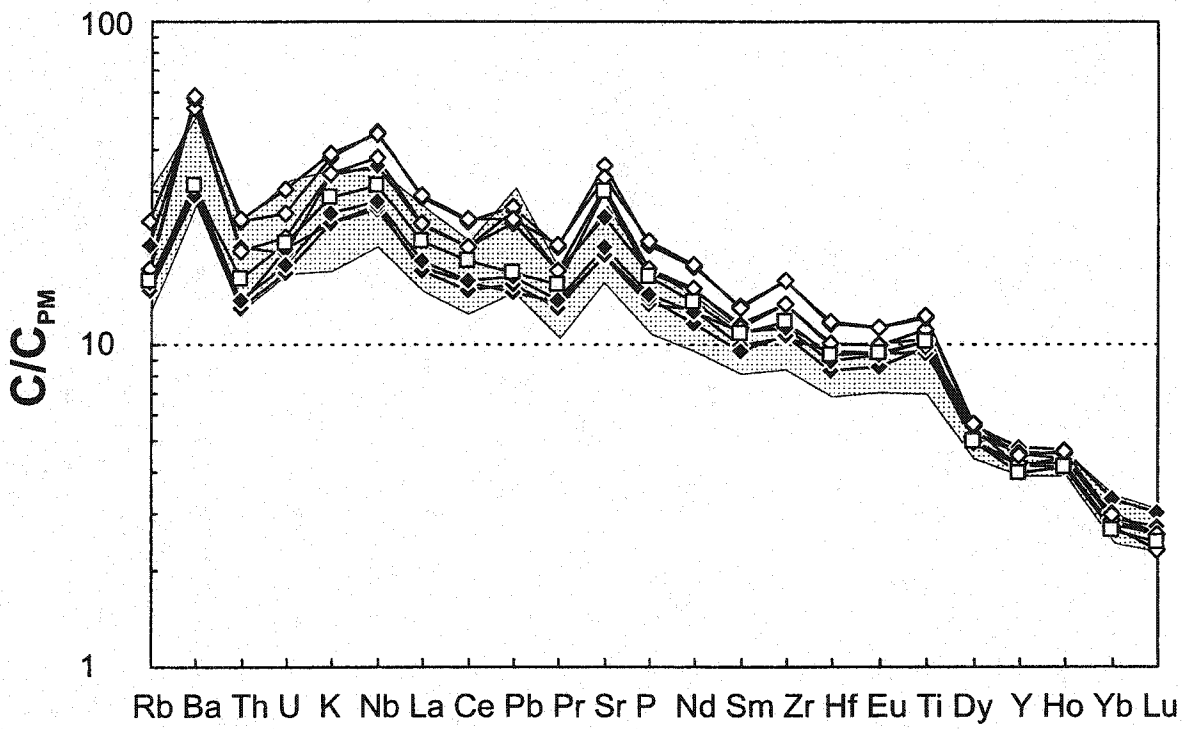
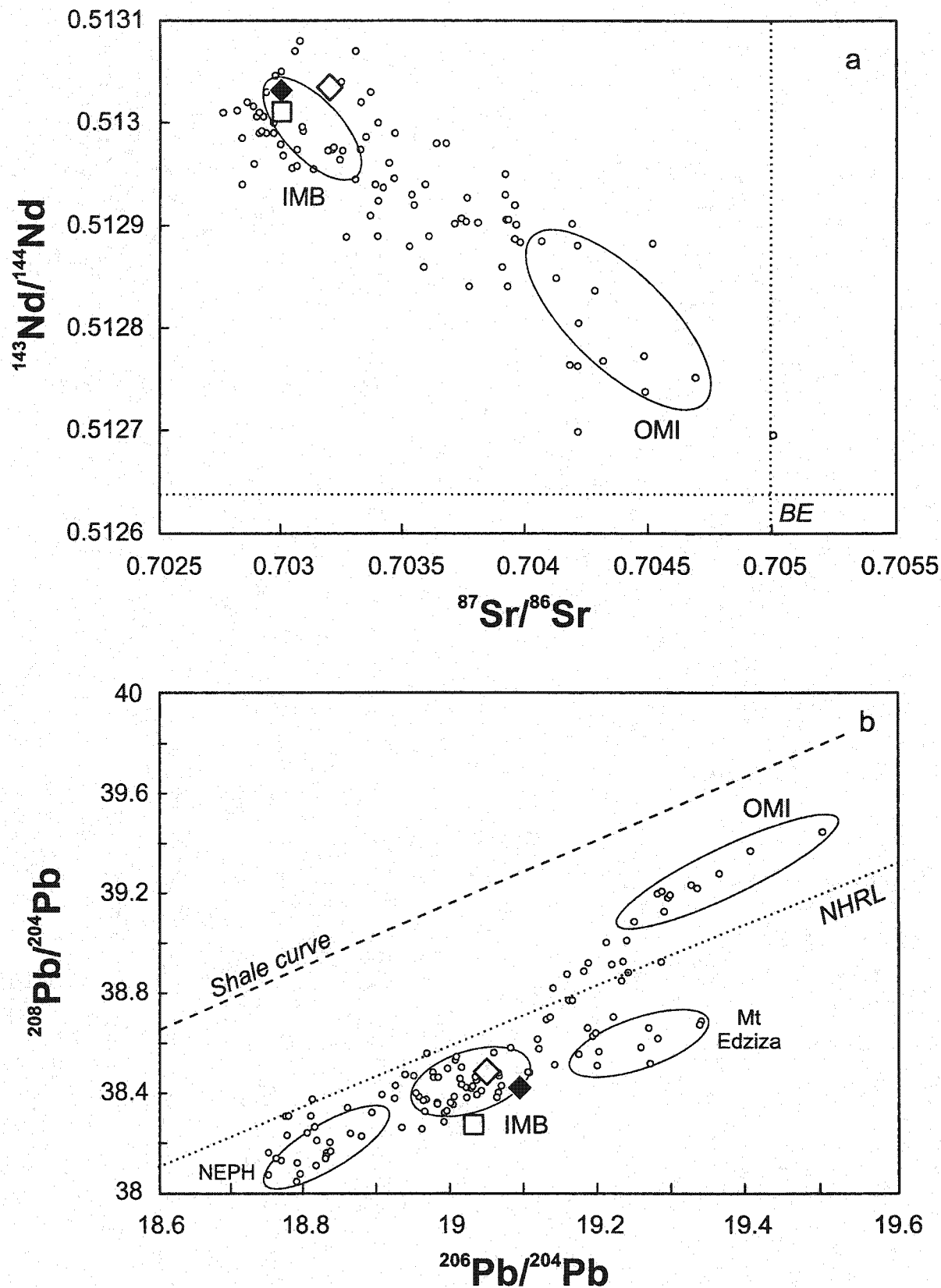


Figure 4.5: a) $^{143}\text{Nd}/^{144}\text{Nd}$ versus $^{87}\text{Sr}/^{86}\text{Sr}$ and b) $^{208}\text{Pb}/^{204}\text{Pb}$ versus $^{206}\text{Pb}/^{204}\text{Pb}$ for Kawdy Mountain basalts. Large symbols as in Fig. 4.2. Fields, small circles and explanations as in Fig. 2.3.



4.4). The more fractionated Hy-NORM basalts that erupted with AOB in the upper part of Kawdy Mountain, however, do exhibit positive Pb anomalies (Fig. 4.4).

Isotopic measurements (Sr, Nd and Pb) were performed on three Kawdy Mountain basalts, two Hy-NORM basalts and one AOB (Fig. 4.2). There is no apparent correlation between Si-saturation and isotopic ratios, with all three Kawdy Mountain basalts having relatively unradiogenic Sr and Pb, but radiogenic Nd isotopic ratios (Fig. 4.5).

4.4. Metahag Mountain (58.92°N , 131.08°W ; NTS 104-J/14)

Metahag Mountain is situated about 5 km to the northeast of Kawdy Mountain (Fig. 1.2) and erupted onto the sedimentary rocks of the Cache Creek terrane of the Intermontane Belt in Pleistocene to Quaternary times (Gabrielse, 1969). This volcanic centre consists of a tuya (Fig. 5.1.a) capped on its eastern side by an unconsolidated cone of small pillows (Fig. 5.1.c), with a total volume of erupted lavas of approximately 3 km^3 . The base of the tuya consists of pillow lava followed by 150 m of mixed massive lava flows and pillows that are overlaid by 100 m of thicker lava flows ($> 10\text{m}$) forming a capping plateau to the tuya (Fig. 5.1.a and 5.1.b). An absence of massive tuff units at this centre (Fig. 5.2) indicates a less explosive eruption style than that at Kawdy Mountain.

As in the case of Kawdy Mountain, the Metahag lavas can be divided into two stratigraphically separated groups that define distinct olivine-control lines in plots of SiO_2 and TiO_2 versus MgO (Fig. 5.3). One group is comprised of Hy-NORM basalts and a few AOB, and constitutes the major part of the centre. This lava group has higher SiO_2 ,

Figure 5.1: a) Long view of the cirque to the north of Metahag Mountain; b) Thick lava flows at the top of the cirque. c) Unconsolidated pillow lava at the top of Metahag Mountain.

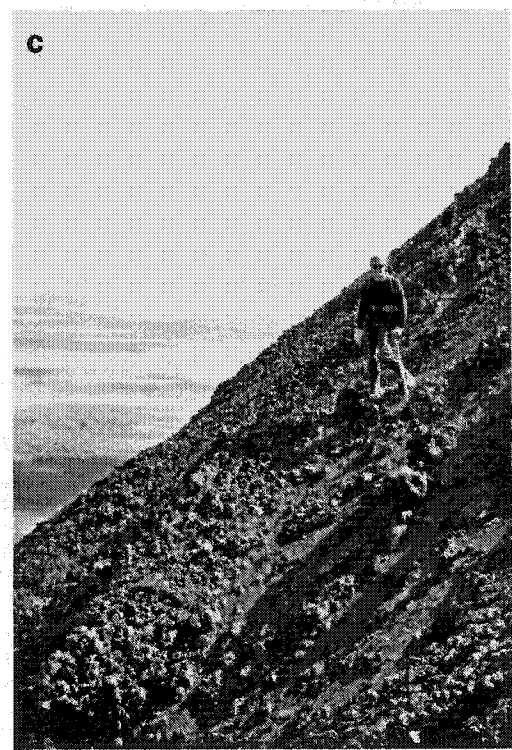
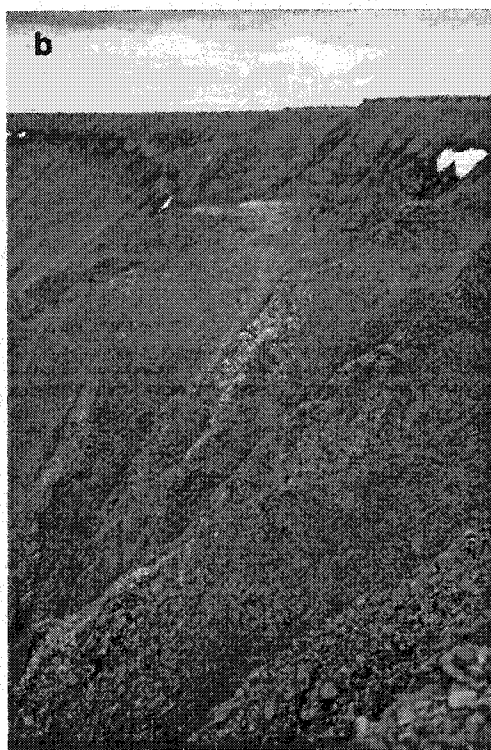


Figure 5.2: Stratigraphic column of Metahag Mountain indicating the position of each analyzed sample. Bold sample labels correspond to samples that have been isotopically studied. Symbols: squares = AOB; diamonds = Hy-NORM basalts. Data in table B-4 of appendix B.

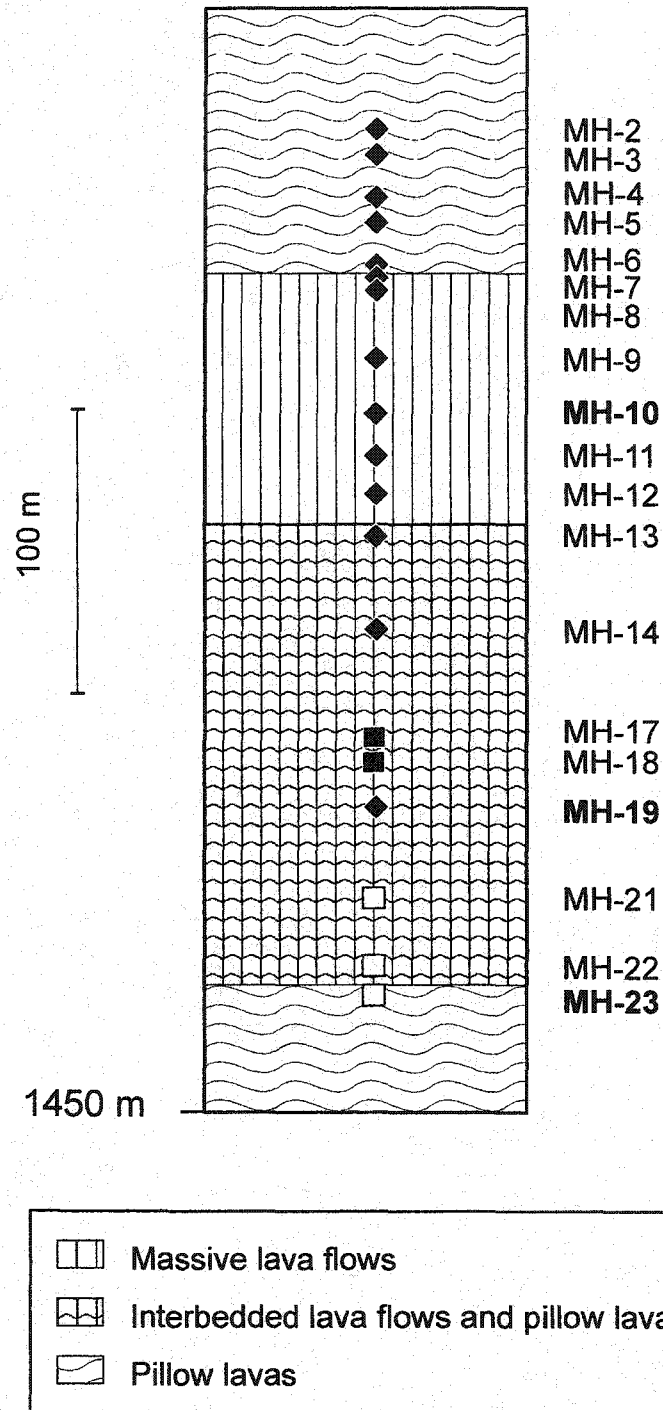




Figure 5.3: a) SiO_2 , b) TiO_2 , c) CaO , and d) Al_2O_3 versus MgO in wt.% for Metahag Mountain basalts. Symbols as in Fig. 5.2. The arrow corresponds to trend expected for olivine fractionation from sample MH-17.

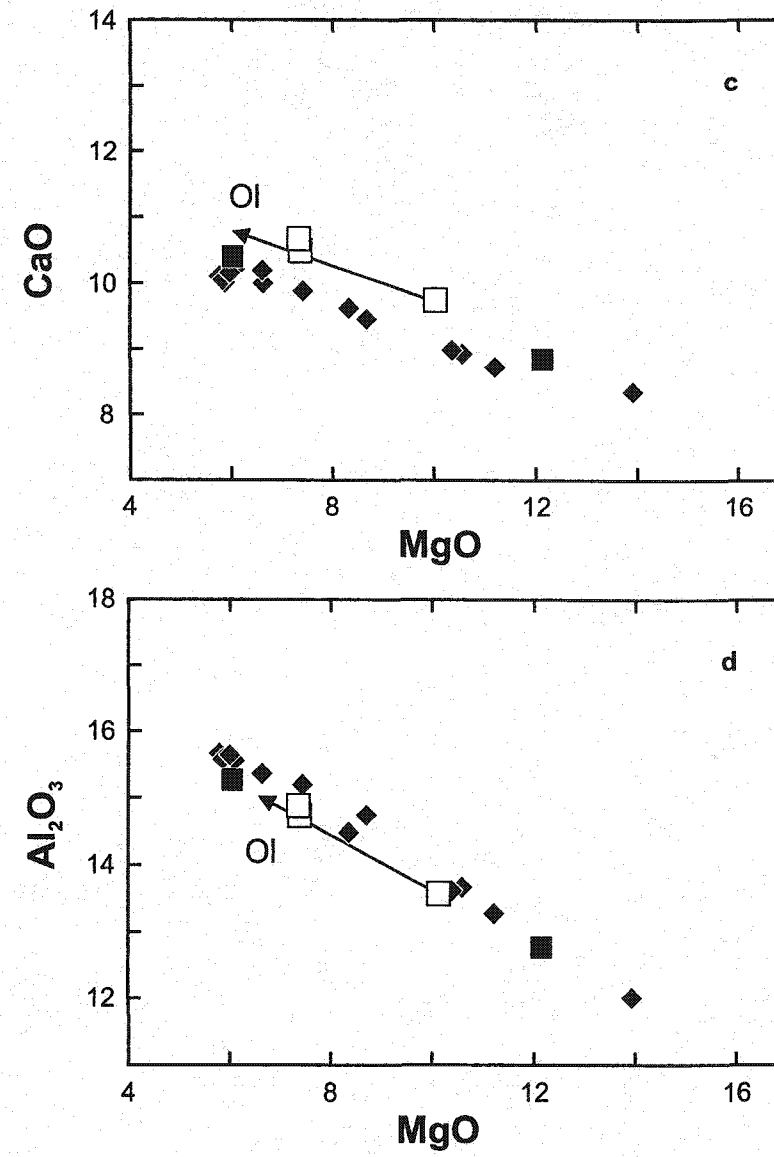
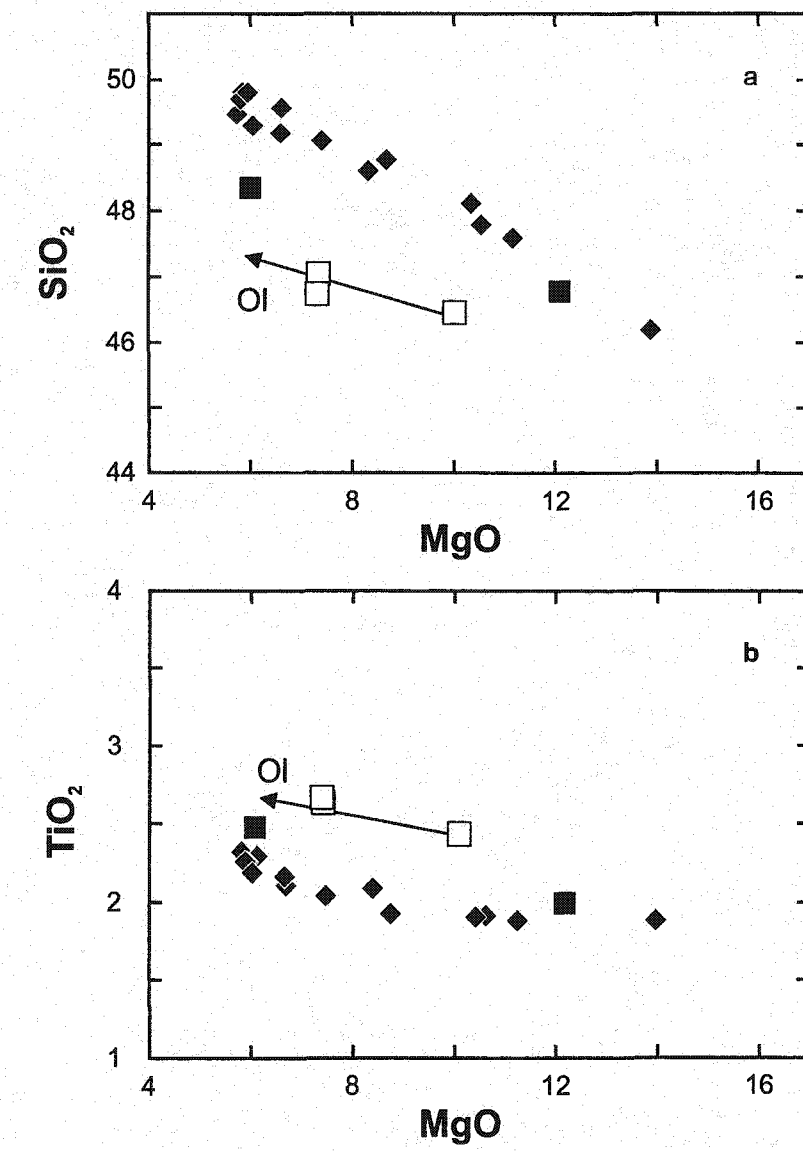


Figure 5.4: Trace element patterns of Metahag Mountain basalts normalized to the primitive mantle values of Sun and McDonough (1989). Symbols as in Fig. 5.2. Shaded field as in Fig. 2.2.a.

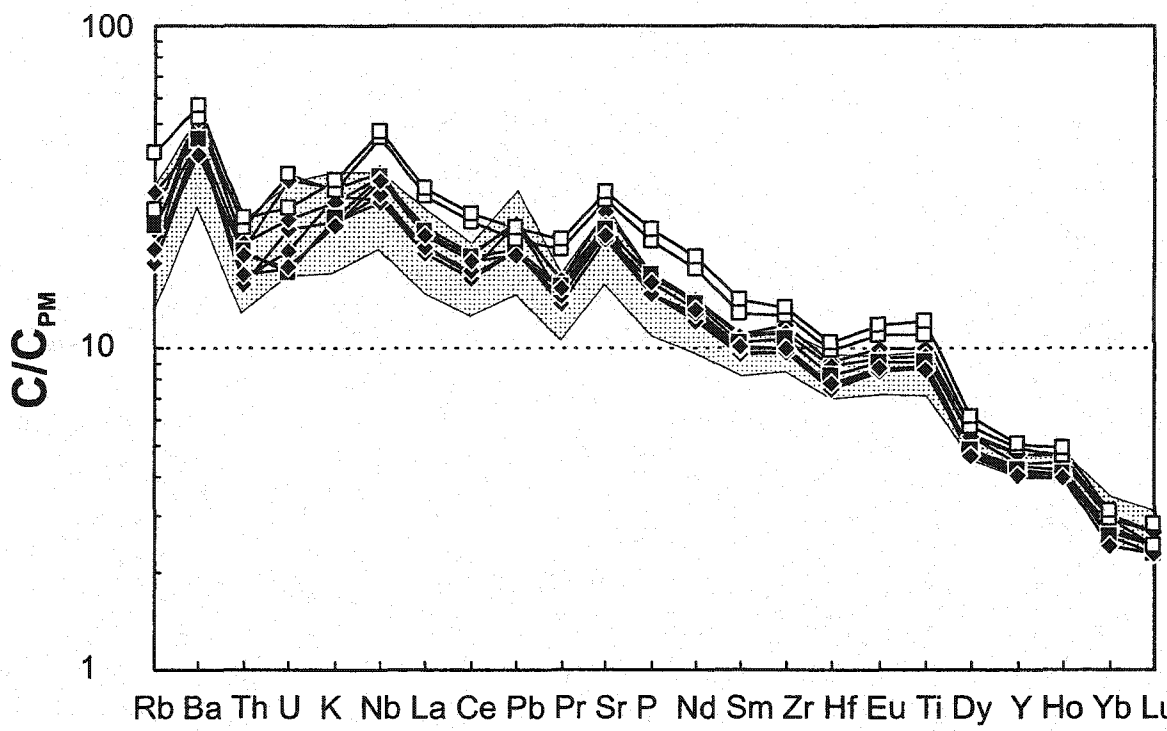
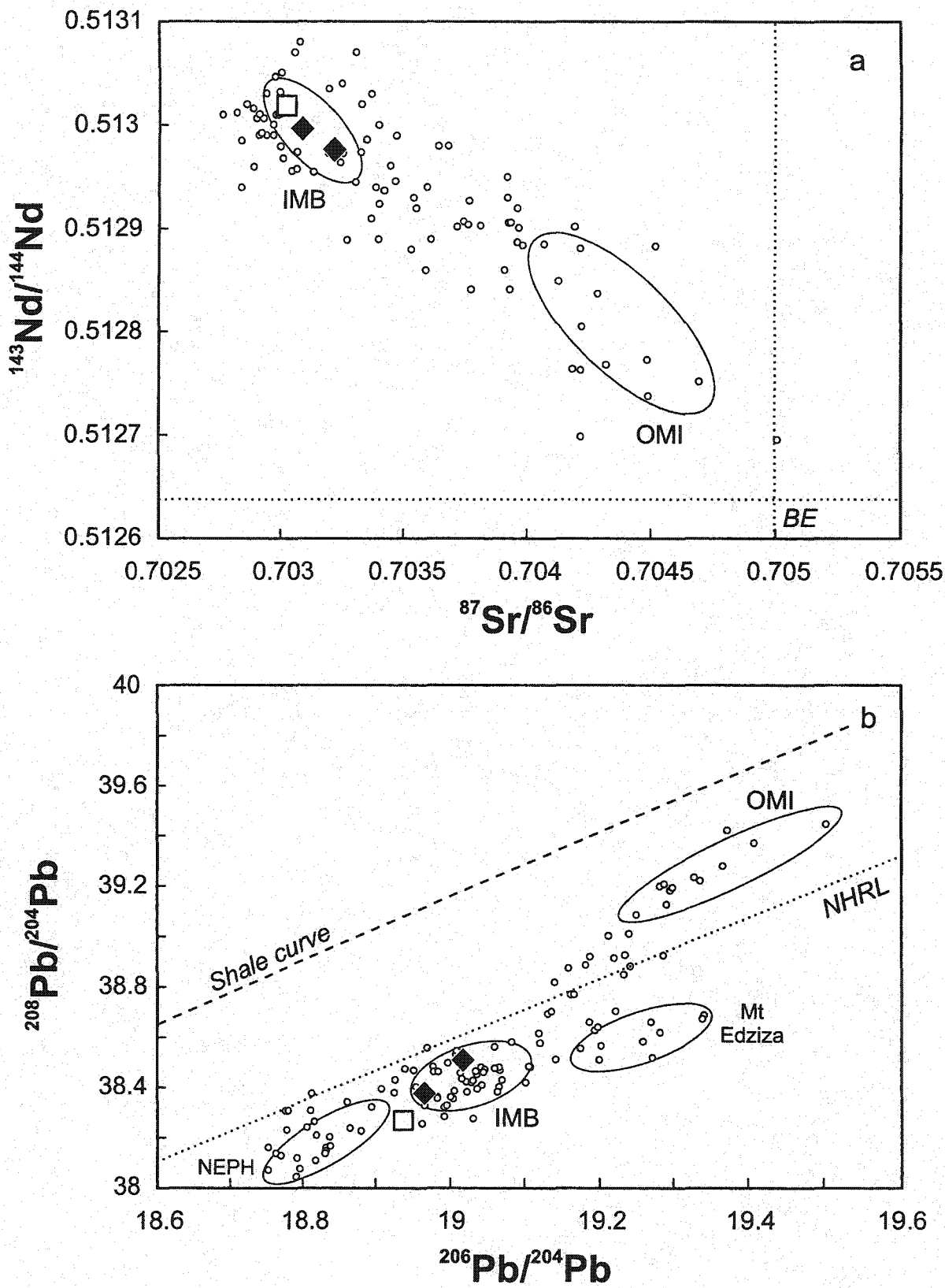




Figure 5.5: a) $^{143}\text{Nd}/^{144}\text{Nd}$ versus $^{87}\text{Sr}/^{86}\text{Sr}$ and b) $^{208}\text{Pb}/^{204}\text{Pb}$ versus $^{206}\text{Pb}/^{204}\text{Pb}$ for Metahag Mountain basalts. Large symbols as in Fig. 5.2. Fields, small circles and explanations as in Fig. 2.3.



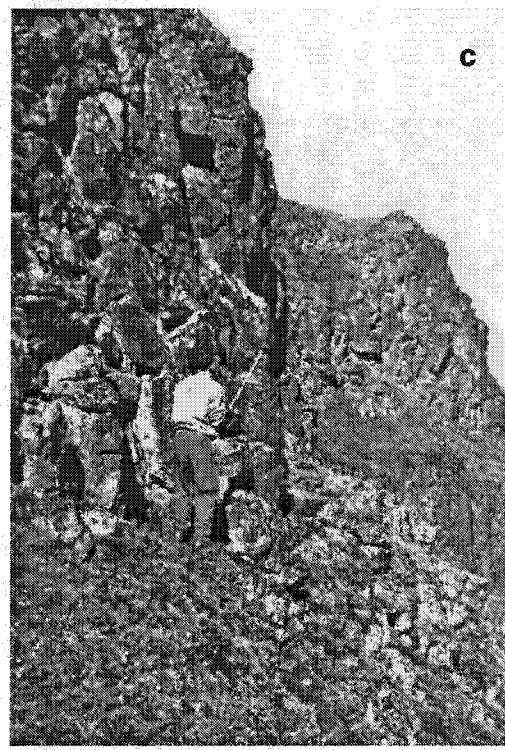
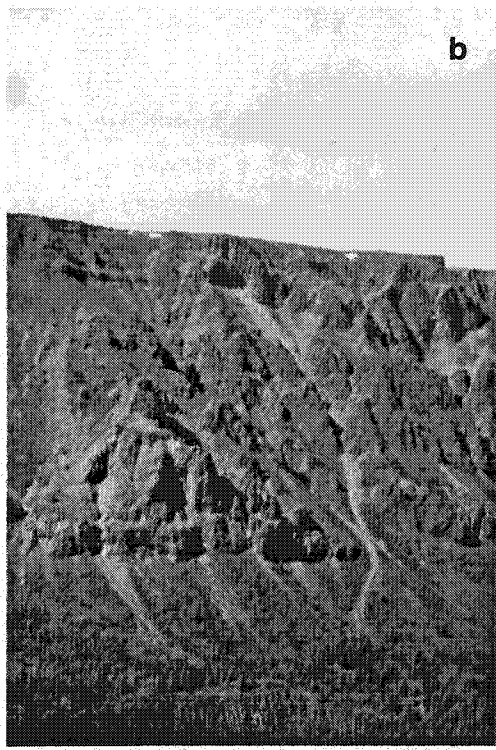
and lower TiO_2 and CaO contents (Fig. 5.3) than the other group, that is comprised only of AOB and constitutes the first 100 m of the base (Fig. 5.2). Although the AOB lavas in each group appear to define distinct olivine-control lines, the Hy-NORM basalts deviate from the olivine-control line to higher SiO_2 and lower TiO_2 values at low MgO (Fig. 5.3.a and b). Both groups have similar trace element patterns characterized by a general enrichment in LILE and LREE compared to HREE, when normalized to primitive mantle, and positive Ti, Sr and Nb and negative Th and Rb anomalies compared to elements with similar compatibilities (Fig. 5.4). The AOB lavas at the base, however, are slightly more enriched in most of the incompatible trace elements than the upper basalts, and do not exhibit positive Pb anomalies. The trace element patterns of the Hy-NORM basalts are characteristic of high- MgO Hy-NORM basalts from the Intermontane Belt (Fig. 5.4).

Metahag Mountain as a whole is characterized by unradiogenic Sr and Pb, but radiogenic Nd isotopic ratios (Fig. 5.5), which are characteristics of a relatively depleted mantle source. The Hy-NORM basalts, however, are slightly more radiogenic in Sr and Pb, and less radiogenic in Nd isotopes than the AOB sample (Fig. 5.5).

4.5. *Metah Mountain (59.08°N, 131.3°W, NTS 104-O/3)*

Metah Mountain is situated to the north of Kawdy Mountain, in the Cache Creek terrane of the Intermontane belt (Fig. 1.2) and is thought to have erupted in Pleistocene to Quaternary times (Gabrielse, 1969). This volcanic centre is made up of two parts, a lapilli cone in the north, and a tuya, Isspah Butte, in the south (Fig. 6.1), with a total volume of volcanic rocks of about 5 km^3 . The lapilli cone is typical of the lapilli cones

Figure 6.1: a) Long view of Metah Mountain, with Isspah Butte in the forefront. b) Closer view of Isspah Butte. c) Sampling of the lava flows of Isspah Butte.



developed in this area (Allen et al., 1982), with a basal pillow lava unit overlaid by a breccia of fore-set pillows and flows, and a cap of pillow lava in unconsolidated palagonized lapilli. Isspah Butte consists of a 50 m basal layer of lava flows, the uppermost of which are highly altered and oxidized, overlaid by 80 m of tuff, 70 m of mafic lava flows, 200 m of hyaloclastite tuff with large lava fragments, and a cap of thick lava flows (Fig. 6.2). This stratigraphy indicates that Isspah Butte grew by alternating episodes of subaerial and subaqueous eruption.

Most of the samples from this centre are AOB, except for a few Hy-NORM basalts with Hy < 5 wt.%. The samples from the lapilli cone exhibit a range in MgO (5-13.5 wt.), and appear to follow one olivine liquid line of descent (Fig. 6.3). The lavas erupted at Isspah Butte exhibit a smaller range in MgO (6- 10 wt.%) and can be divided into three stratigraphically separated groups, that exhibit distinct SiO₂, TiO₂ and CaO contents suggesting the existence of at least three liquid lines of descent from a range of parental magmas (Fig. 6.3). One group consists of Hy-NORM basalts that occur as flows at the base of Isspah Butte, the second group comprises AOB lavas from the middle part of Isspah Butte, whereas the third group consists of AOB and a few Hy-NORM basalts that form the top of the Isspah Butte. The lavas at Metah Mountain have similar trace element patterns, characterized by an enrichment in LILE and LREE compared to HREE, when normalized to primitive mantle, and positive Ti, Sr and Nb, and negative Th and Ba anomalies compared to elements with similar compatibilities (fig. 6.4). The relatively primitive (MgO ~ 9 wt.%) Hy-NORM sample from the base of Isspah Butte exhibits a large positive Pb anomaly, a characteristic of many Cordilleran Hy-NORM basalts (Fig.

Figure 6.2: Stratigraphic column of Metah Mountain indicating the position of each analyzed sample. Symbols: squares = AOB; diamonds = Hy-NORM basalts. Bold sample labels correspond to samples that have been isotopically studied. Black, white and grey symbols correspond to the stratigraphically controlled lava groups (see text for explanation) that erupted at the base, centre and top of Isspah Butte respectively, whereas crossed symbols correspond to samples from the lapilli cone. Data in table B-5 of appendix B.

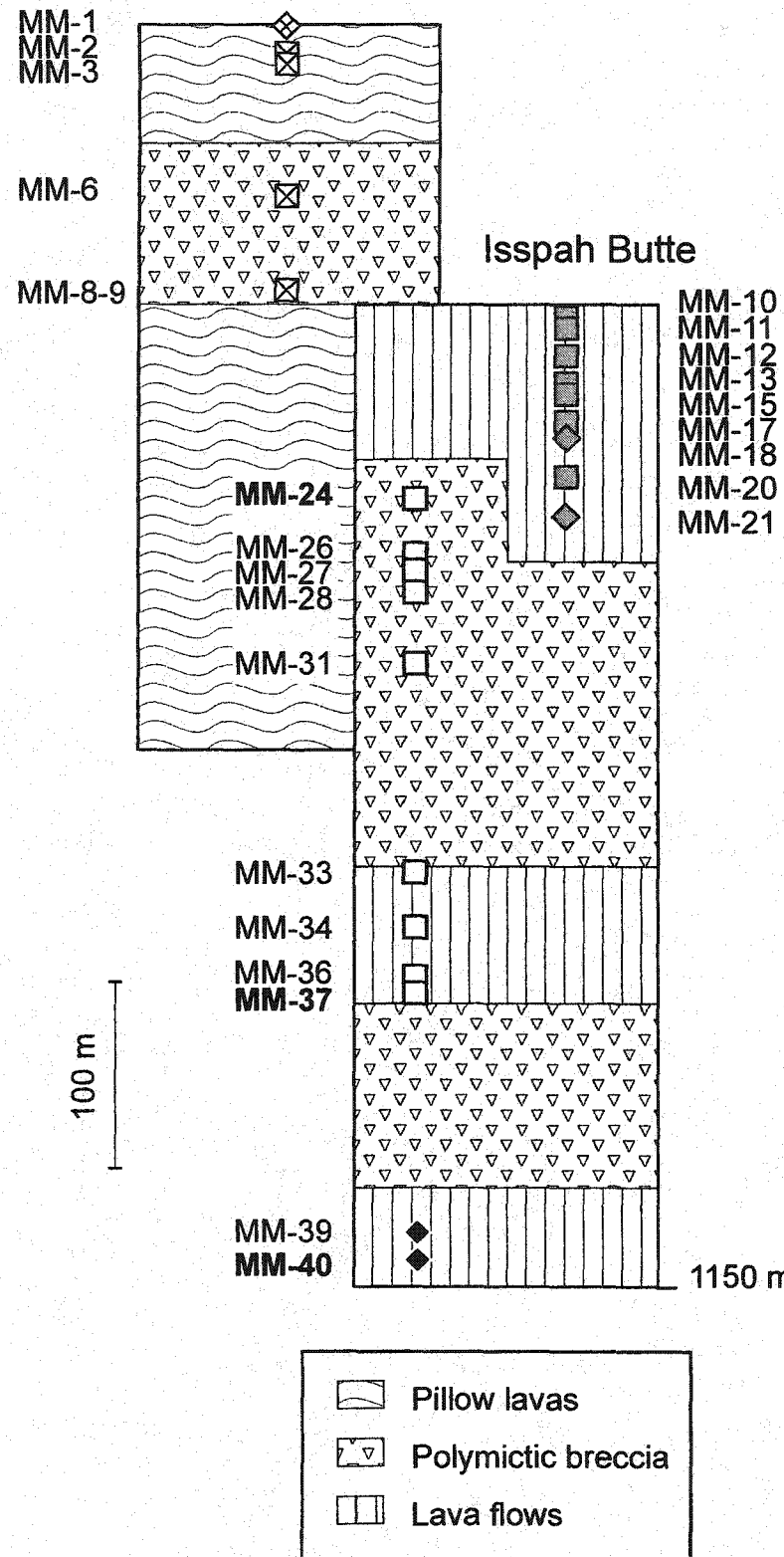


Figure 6.3: a) SiO_2 , b) TiO_2 , c) CaO , and d) Al_2O_3 versus MgO in wt.% for Metah Mountain basalts. Symbols as in Fig. 6.2. The arrow corresponds to the trend expected for olivine fractionation from sample MM-8.

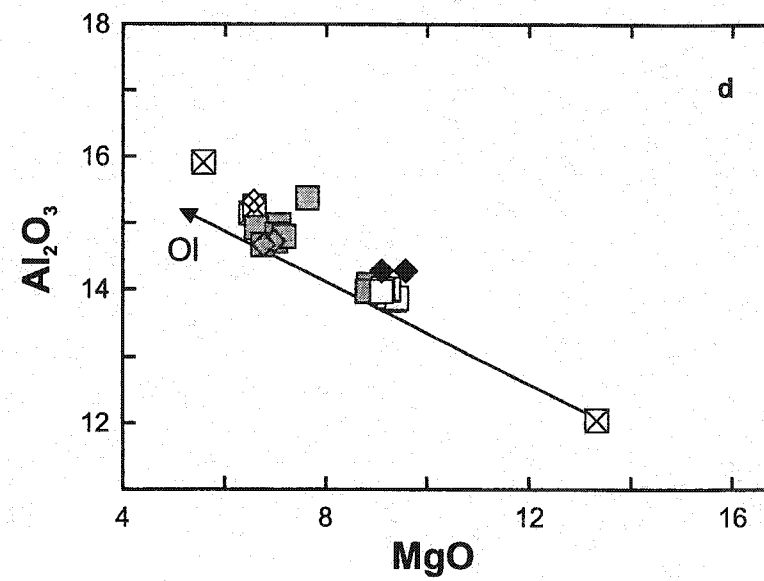
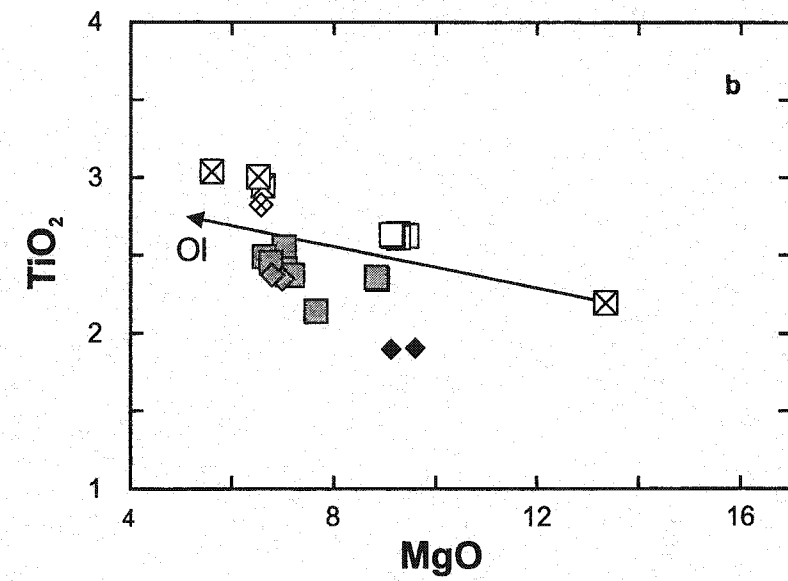
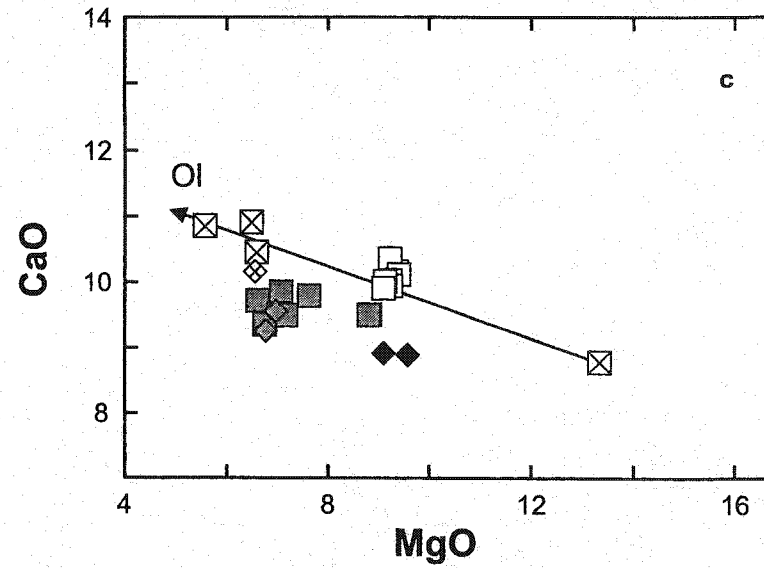
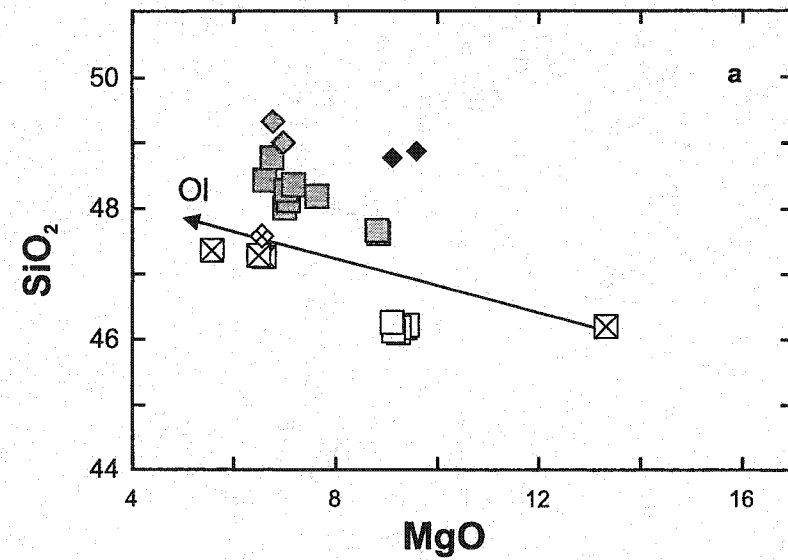


Figure 6.4: Trace element patterns of Metah Mountain basalts normalized to the primitive mantle values of Sun and McDonough (1989). Same symbols as Fig. 6.2. Shaded field as in Fig. 2.2.a.

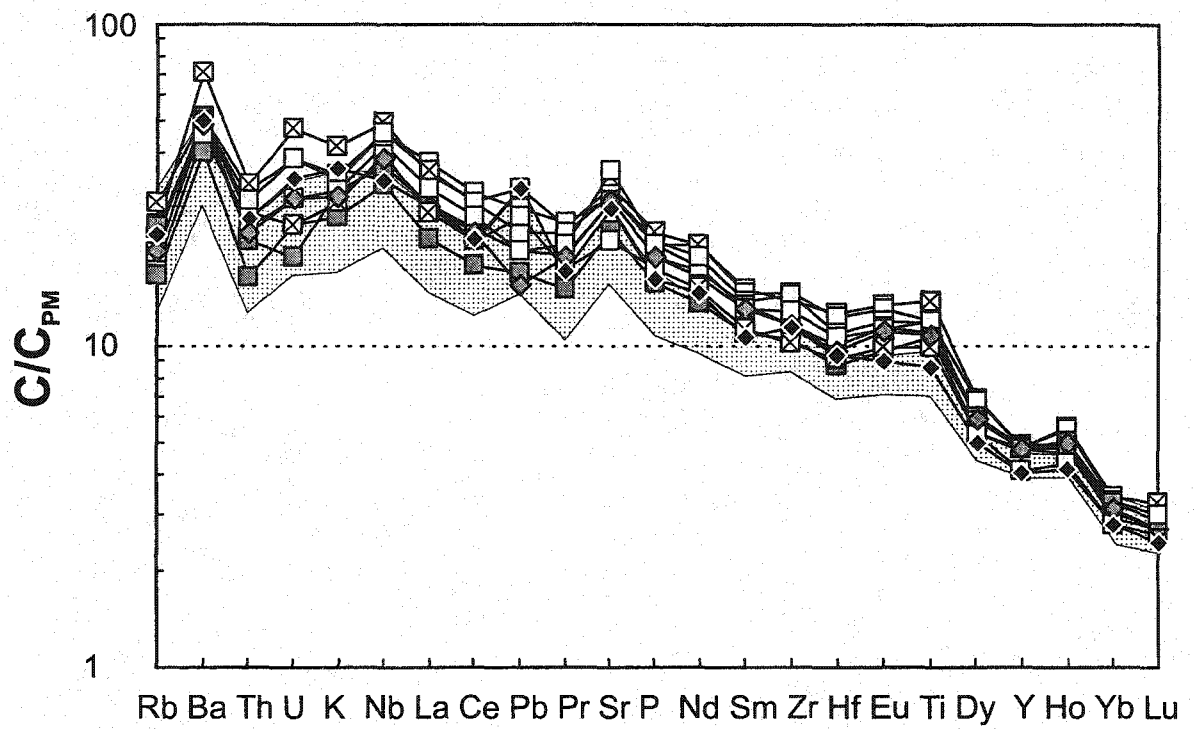
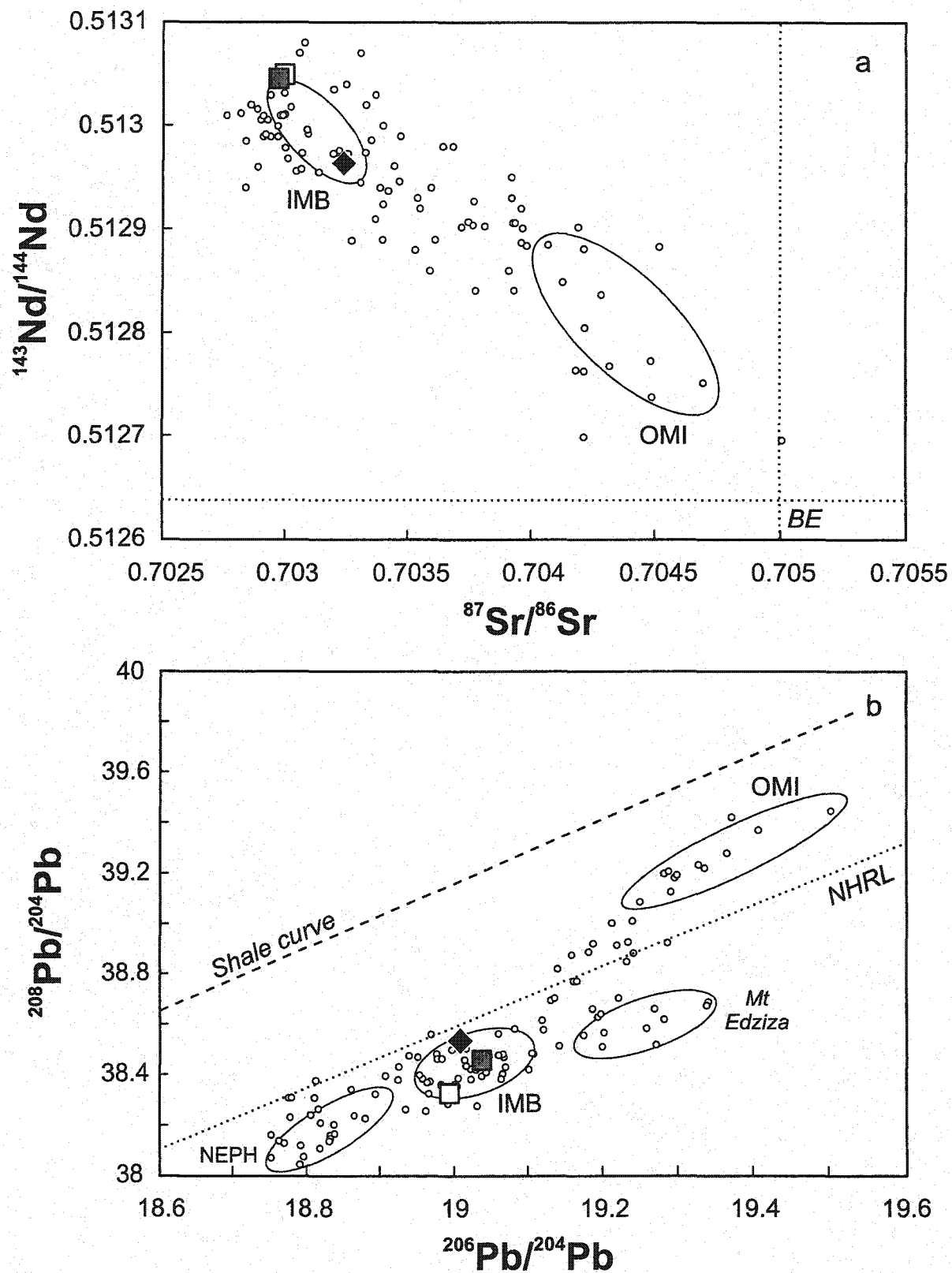


Figure 6.5: a) $^{143}\text{Nd}/^{144}\text{Nd}$ versus $^{87}\text{Sr}/^{86}\text{Sr}$ and b) $^{208}\text{Pb}/^{204}\text{Pb}$ versus $^{206}\text{Pb}/^{204}\text{Pb}$ for Metah Mountain basalts. Large symbols as in Fig. 6.2. Fields, small circles and explanations as in Fig. 2.3.



6.4), but is amongst the most trace element enriched of the high-MgO Hy-NORM basalts in the Intermontane Belt.

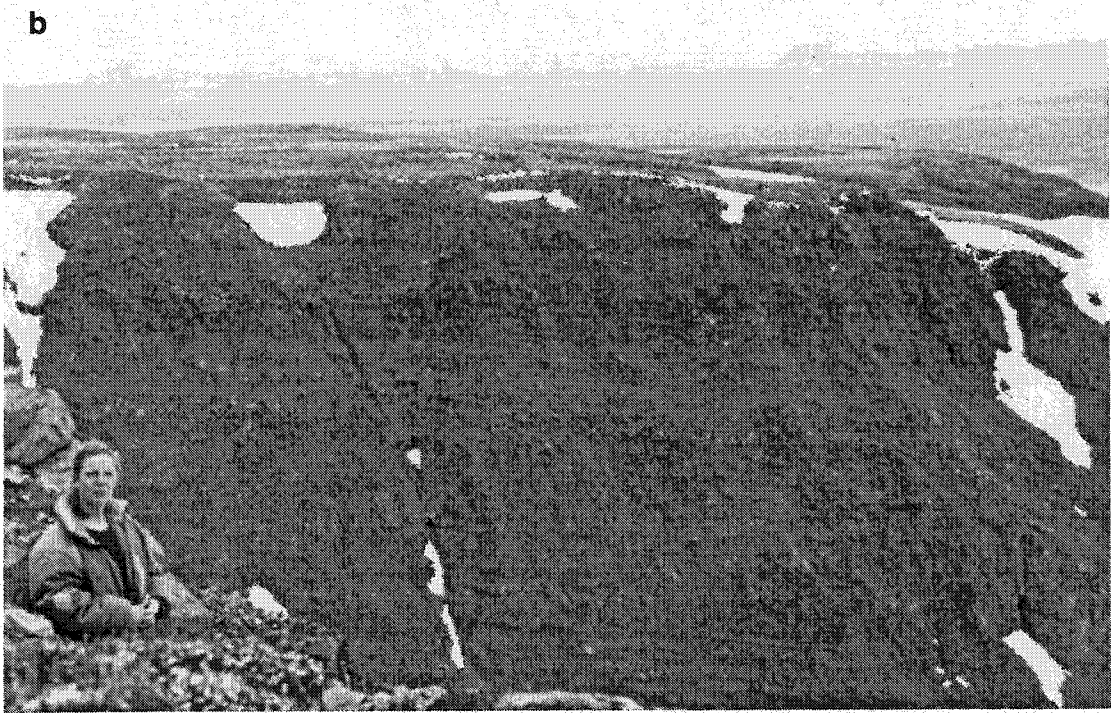
Three lavas in the Isspah Butte succession were analyzed isotopically, one from each group (Fig. 6.2). The Hy-NORM sample from the base of Isspah Butte has more radiogenic Sr and less radiogenic Nd isotopes than the AOB samples, but they all have similar Pb isotopic ratios. The overall low Sr and Pb, but high Nd isotopic ratios (Fig. 6.5) are suggestive of a relatively depleted source.

4.6. *Tuya Butte* ($59.13^{\circ}N$, $130.55^{\circ}W$; NTS 104-O/2)

Tuya Butte is located at the transition between the Intermontane and the Omineca belts (Fig. 1.2), in the Slide Mountain terrane, a thin slice of oceanic origin that is thought to have been thrust onto the Omineca Belt (Gabrielse et al., 1991). No precise date is available for this centre, but Allen (1991) proposed a Late Pleistocene age. Tuya Butte is a flat-topped, steep-sided volcano that has been extensively described by Mathews (1947), Allen et al. (1982), and Moore et al. (1995). The base consists of pillow lava in palagonized hyaloclastite, capped by about 80 m of thick massive lava flows (Fig. 7.1.a and b). The total volume of Tuya Butte is estimated to be about 2.6 km^3 (Moore et al., 1995).

The lavas from Tuya Butte can be divided into two stratigraphically distinct groups. One group consists of Hy-NORM basalts that have Hy contents of 15-17%, and that erupted as pillow lava at the base of the centre, whereas the other groups consists of Hy-

Figure 7.1: a) Long distance view of Tuya Butte, a typical flat topped volcano that grew in the ice. b) Closer view of the lava flows forming the top of the tuya.



NORM basalts that have less than 5% Hy and one AOB, that erupted both as upper pillow lava and as the capping lava flows. Moore et al. (1995) noted a change from low alkalinity in the subglacial pillow lavas of the base to higher alkalinity in the subaerial capping lavas. In our sampling, however, the change occurs within the pillow lava pile, and not at the transition to the capping flows. Tuya Butte lavas display a relatively low range in MgO (5.4-8.3 wt.%), and appear to lie on a variety of olivine-control lines in a plot of SiO₂ versus MgO (Fig. 7.3.a). Although the two groups have distinct SiO₂ and TiO₂ contents (Fig. 7.3.a and b), they define similar trends in plots of CaO and Al₂O₃ versus MgO (Fig. 7.3.c and d). Tuya Butte basalts have trace element patterns that are enriched in LILE and LREE compared to HREE, when normalized to primitive mantle, and that are characterized by positive Pb and negative Rb anomalies compared to elements with similar compatibilities, but with otherwise relatively smooth trace element patterns (Fig. 7.4). Hy-NORM basalts at the base of the centre are less enriched in incompatible trace elements than the other lavas, and are similar to other primitive Hy-NORM basalts in the Intermontane Belt, except that they have smaller positive Sr, and negative Th and Rb anomalies, and more pronounced positive Pb anomalies. Although the upper lavas are also Hy-NORM basalts, they have higher incompatible trace element concentrations than primitive Hy-NORM of the Intermontane Belt (Fig. 7.4).

The three Tuya Butte Hy-NORM basalts that have been studied isotopically appear to have similar Sr and Nd isotopic ratios (Fig. 7.5.a), but the Hy-NORM sample at the base of the centre has more radiogenic Pb isotopic ratios than the two upper samples (Fig. 7.5.b). Tuya Butte lavas have slightly more radiogenic Sr and Pb, and less radiogenic Nd isotopic ratios than high MgO Hy-NORM from other volcanic centres in the Intermontane



Figure 7.2: Stratigraphic column of Tuya Butte indicating the position of each analyzed sample. Two sections were sampled in this centre. Symbols: squares = AOB; diamonds = Hy-NORM basalts. Bold sample labels correspond to samples that have been isotopically studied. Data in table B-6 of appendix B.

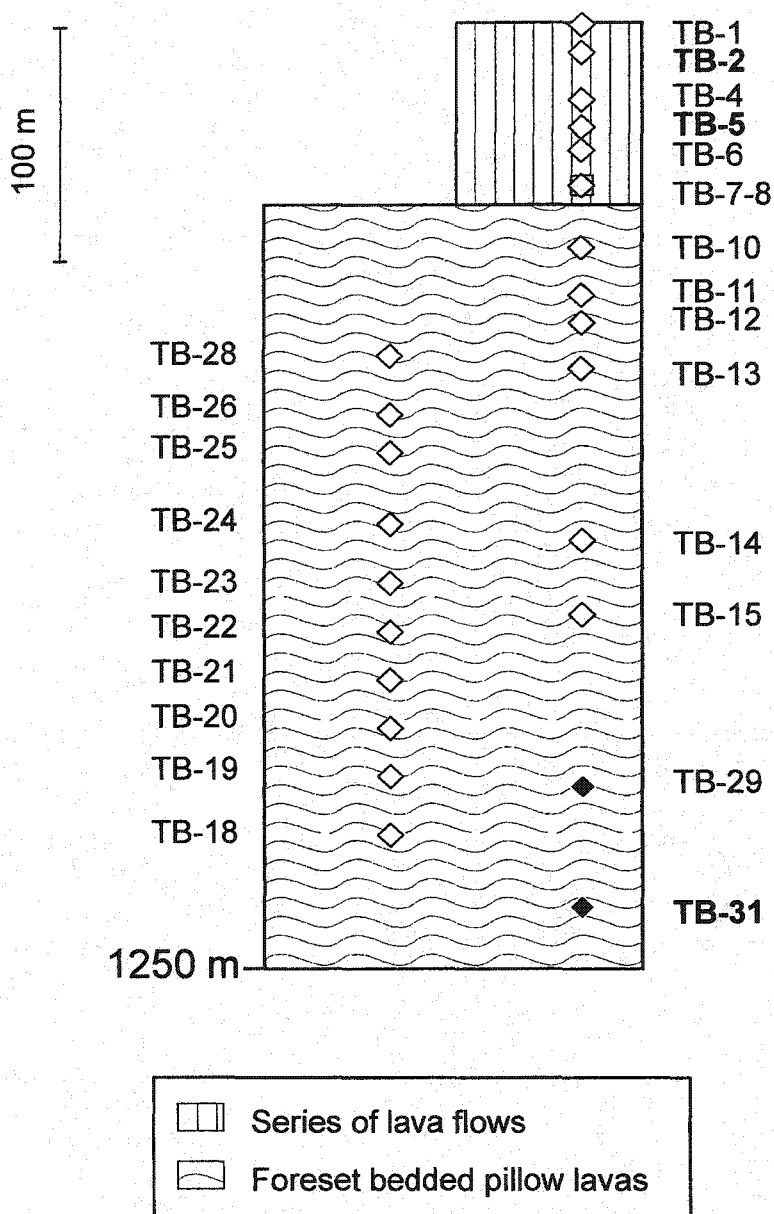


Figure 7.3: a) SiO_2 , b) TiO_2 , c) CaO , and d) Al_2O_3 versus MgO for Tuya Butte basalts. Symbols as in Fig. 7.2. The arrow corresponds to the trend expected for olivine fractionation from sample TB-7.

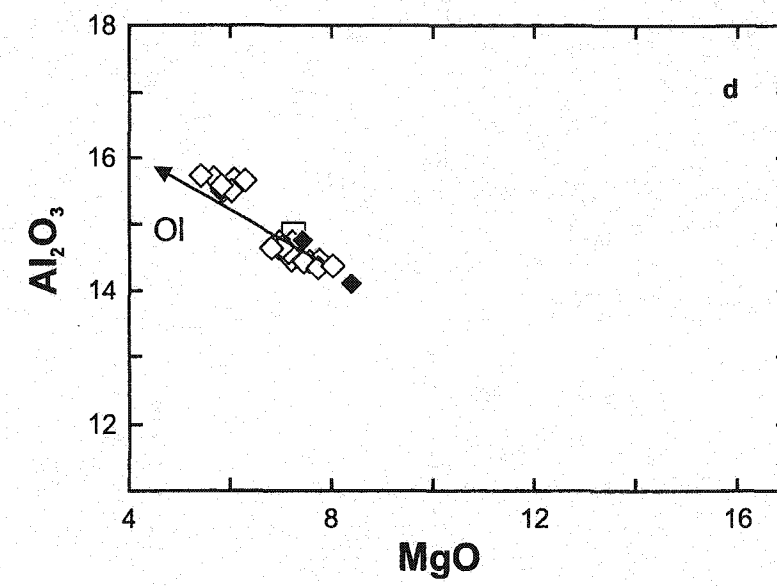
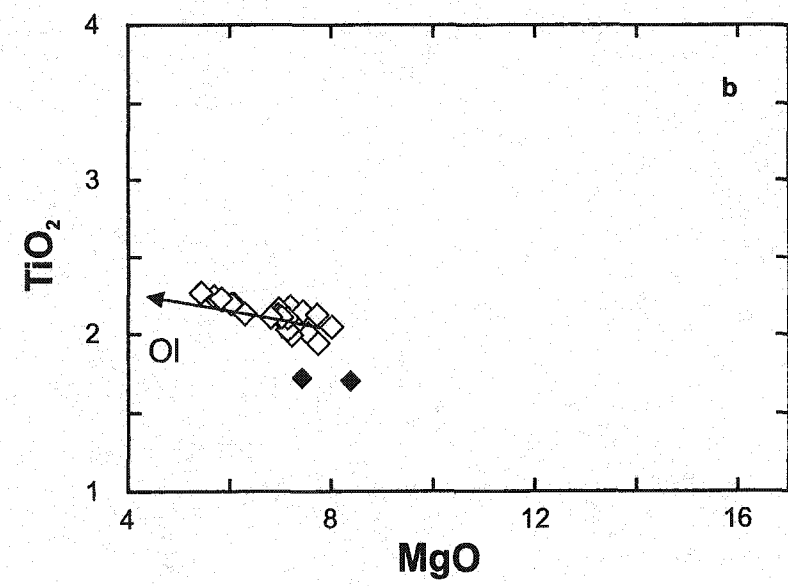
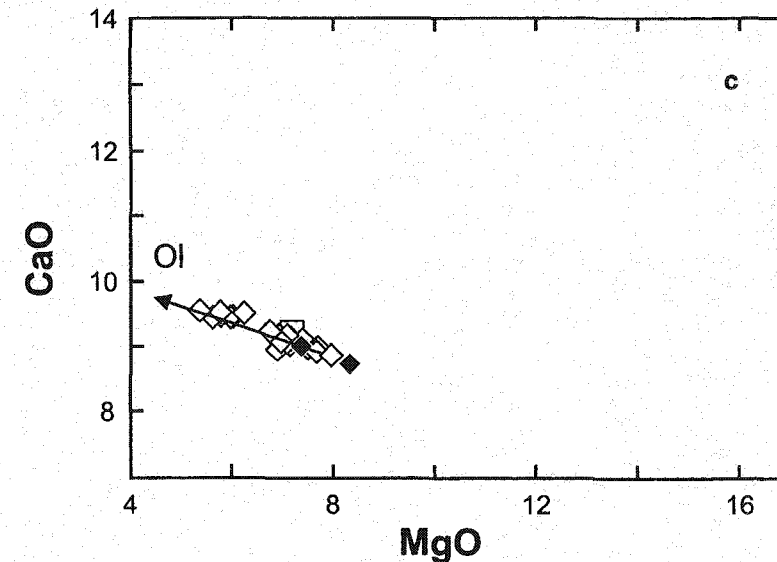
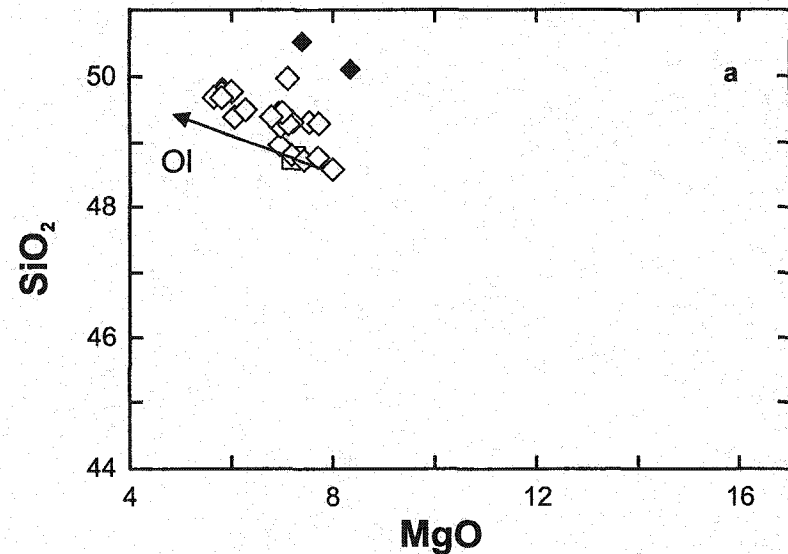


Figure 7.4: Trace element patterns of Tuya Butte basalts normalized to the primitive mantle values of Sun and McDonough (1989). Same symbols as Fig. 7.2. Shaded field as in Fig. 2.2.a.

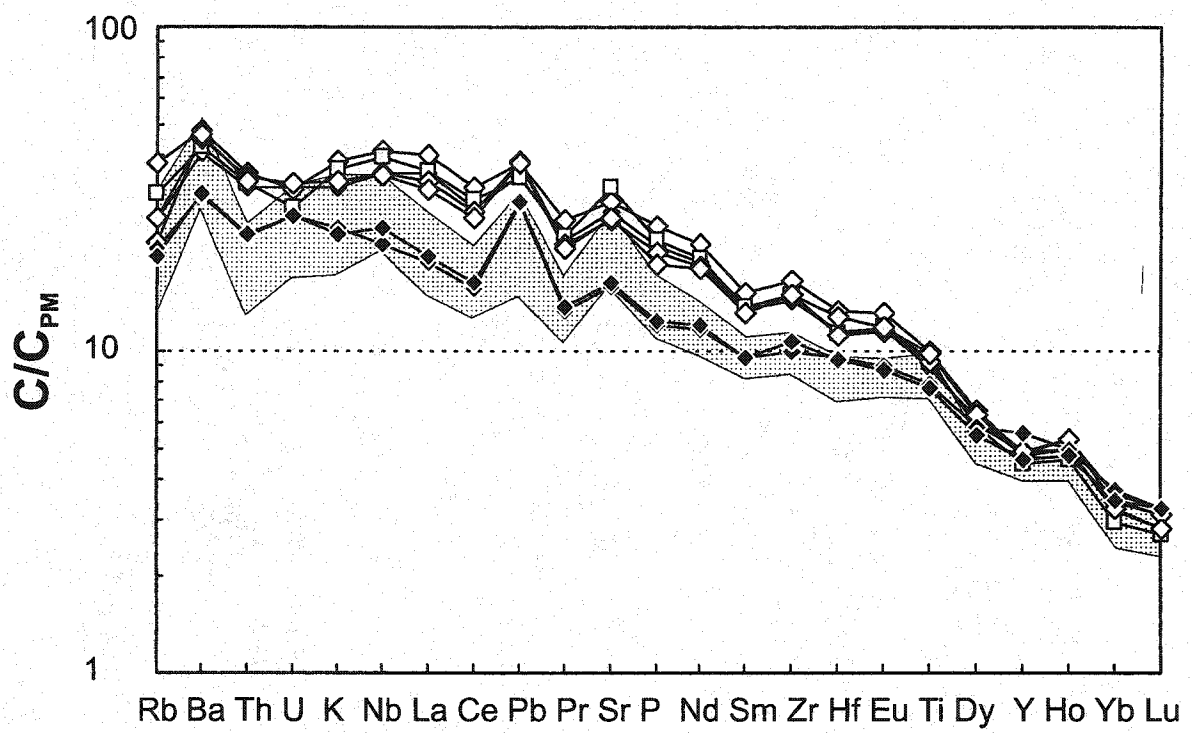
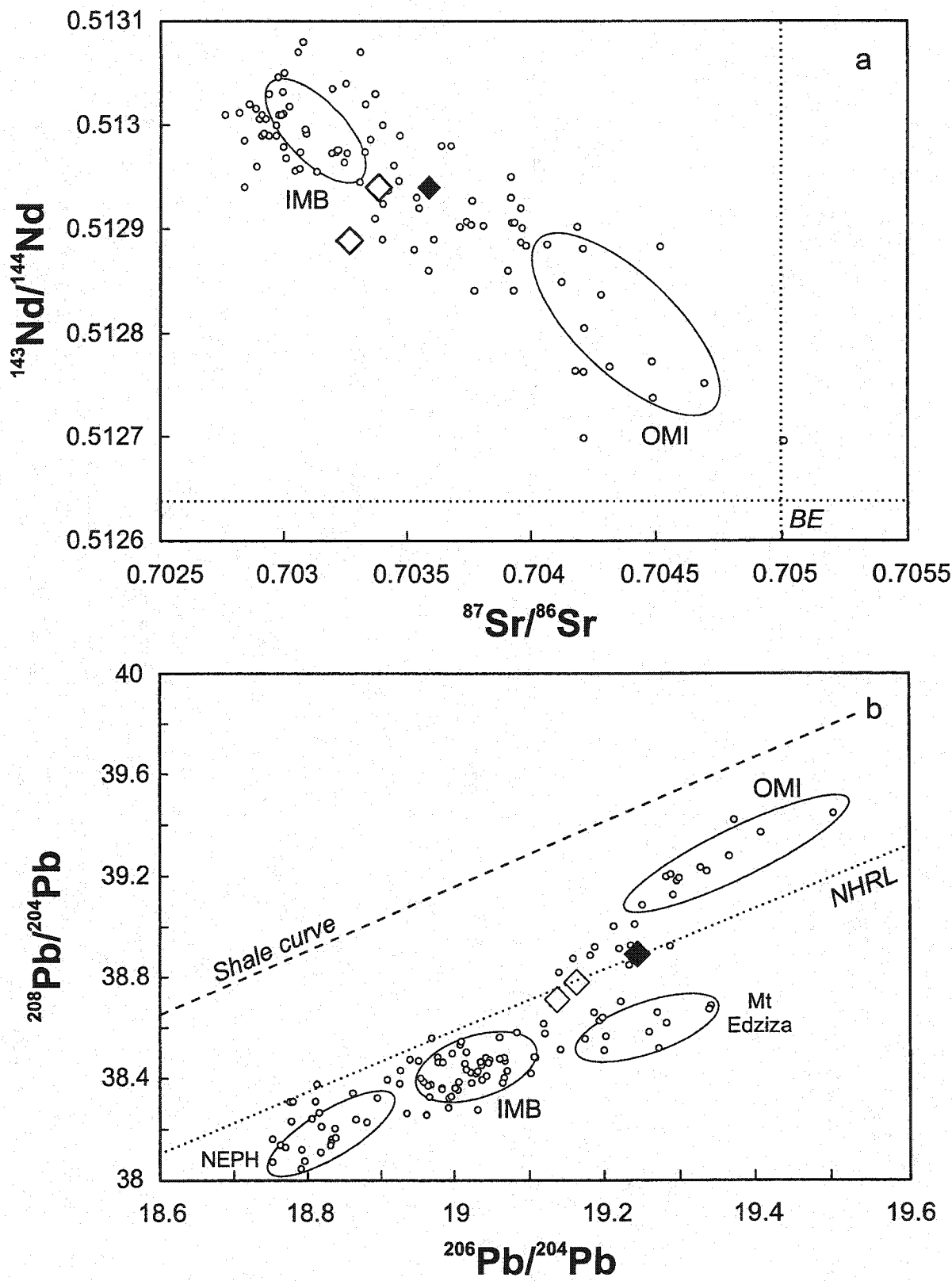


Figure 7.5: a) $^{143}\text{Nd}/^{144}\text{Nd}$ versus $^{87}\text{Sr}/^{86}\text{Sr}$ and $^{208}\text{Pb}/^{204}\text{Pb}$ versus $^{206}\text{Pb}/^{204}\text{Pb}$ for Tuya Butte basalts. Large symbols as in Fig.7.2. Fields, small circles and explanations as in Fig. 2.3.



Belt (Fig. 7.5.a and b). They are, however, less radiogenic Sr and Pb, but more radiogenic Nd than high-MgO Hy-NORM of the Omineca Belt (Fig. 7.5.a and b). The Tuya Butte lavas appear thus to have an intermediate isotopic signature between those of the Intermontane and Omineca belts, consistent with their location at the transition between the two belts.

4.7. *Tanzilla Volcano (59.05N, 130.38W; map 104-O/1)*

Tanzilla Volcano is situated to the southeast of Tuya Butte and is named after the Tanzilla Plateau on which it lies. It is located in the Quesnellia terrane, to the west of the Dorsey Terrane, at the transition between the Intermontane and Omineca belts (Fig. 1.2). Like the Slide Mountain terrane, the Quesnellia terrane is thought to represent a thin slice of oceanic crust thrust onto the Omineca Belt (Gabrielse et al., 1991). The Parallel Creek Batholith, a Late Cretaceous quartz monzonite pluton, lies just to the north of Tanzilla Volcano. Tanzilla volcano probably erupted in the Pleistocene to Quaternary (Gabrielse, 1969), and has a volume of about 4 km³. It is constructed on a base consisting of a series of thin lava flows (around 2 m; Fig. 8.1.b) interbedded with layers of pillow lava, overlain by a unit of lava flows, and capped by bedded pillow lava (Fig. 8.1.c) cut by basaltic dykes.

The Tanzilla Volcano lavas can also be divided into two stratigraphically separate groups, one consisting of Hy-NORM basalts that erupted in the interbedded lava flows and pillow lava at the base, and the other consisting of AOB that erupted mainly as pillow lava in the upper part of the centre (Fig. 8.2). Although the lavas of these two groups



Figure 8.1: a) Long distance view of Tanzilla Volcano. b) Closer view of the small lava flows that erupted at the base of the centre. c) Closer view of the bedded pillow lavas that constitute the top of the cone.

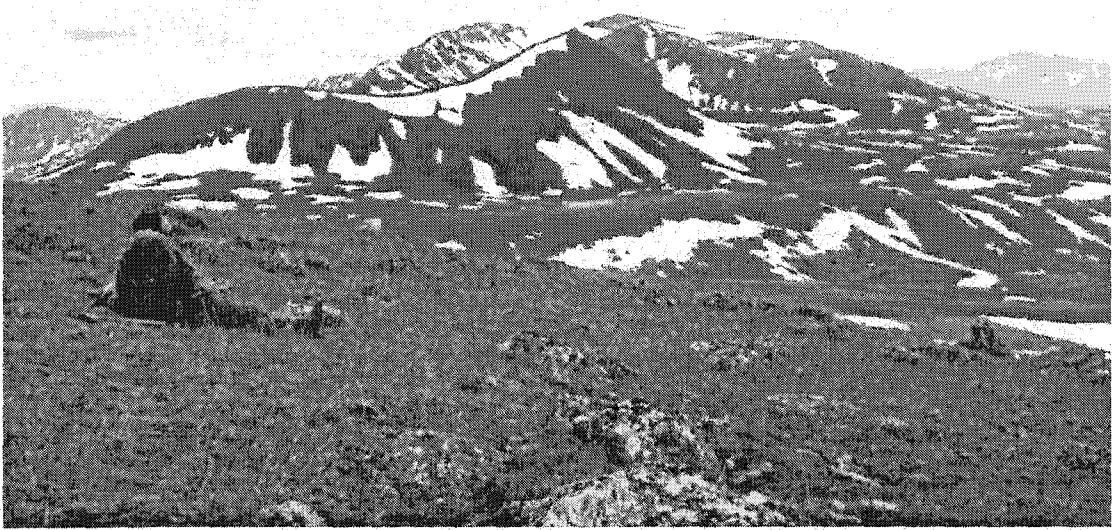
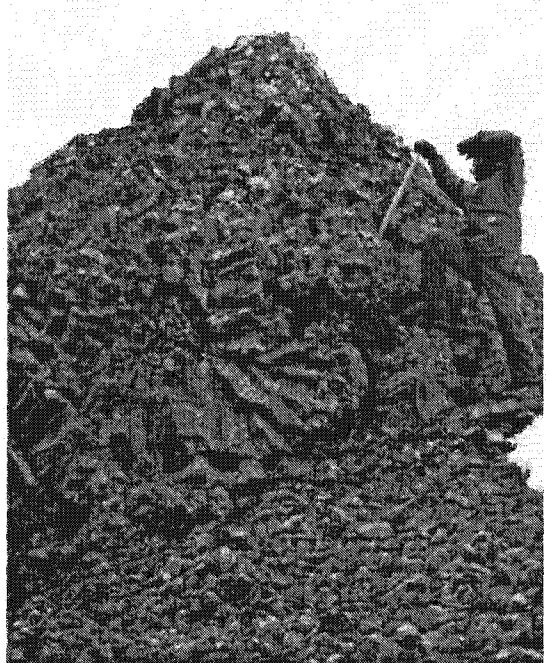
a**b****c**

Figure 8.2: Stratigraphic column of Tanzilla Volcano indicating the position of each analyzed sample. Symbols: squares = AOB; diamonds = Hy-NORM basalts. Bold sample labels correspond to samples that have been isotopically studied. Data in table B-7 of appendix B.

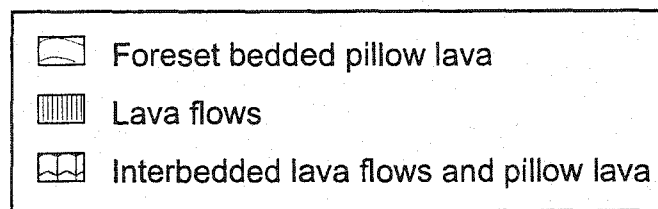
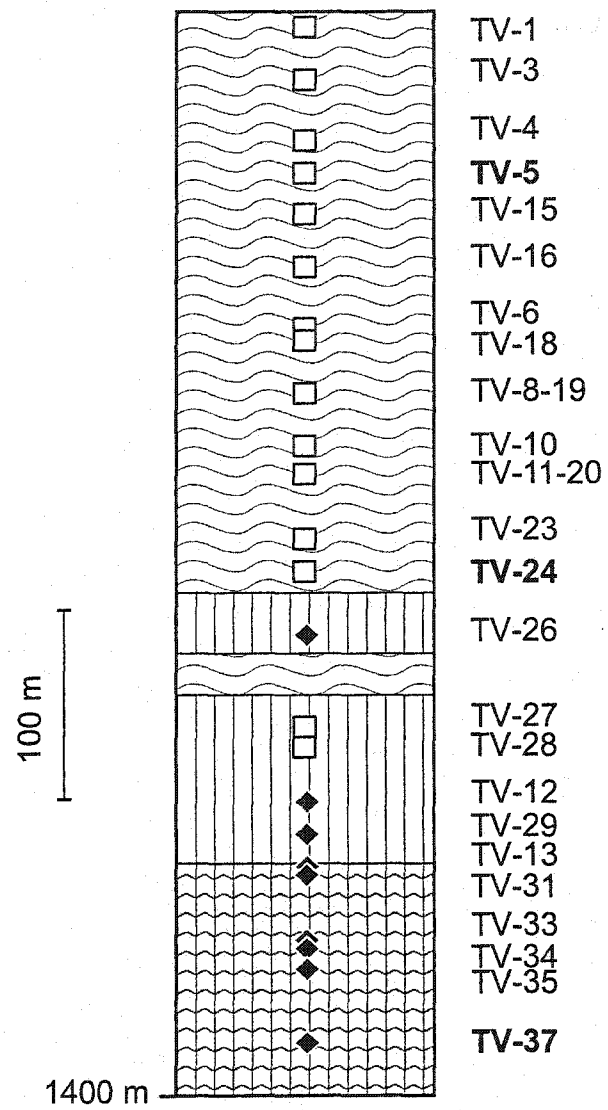


Figure 8.3: a) SiO_2 , b) TiO_2 , c) CaO , and d) Al_2O_3 versus MgO in wt.% for Tanzilla Volcano basalts. Symbols as in Fig. 8.2. The arrow corresponds to the trend expected for olivine fractionation from sample TV-28.

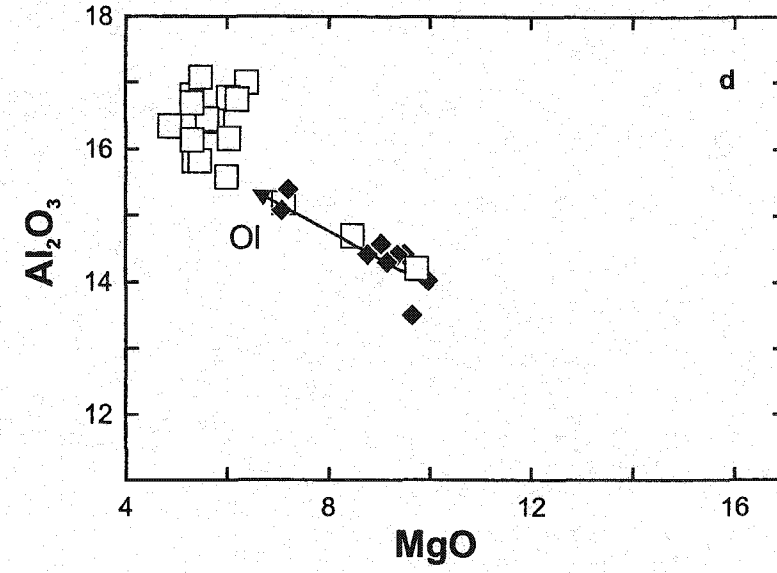
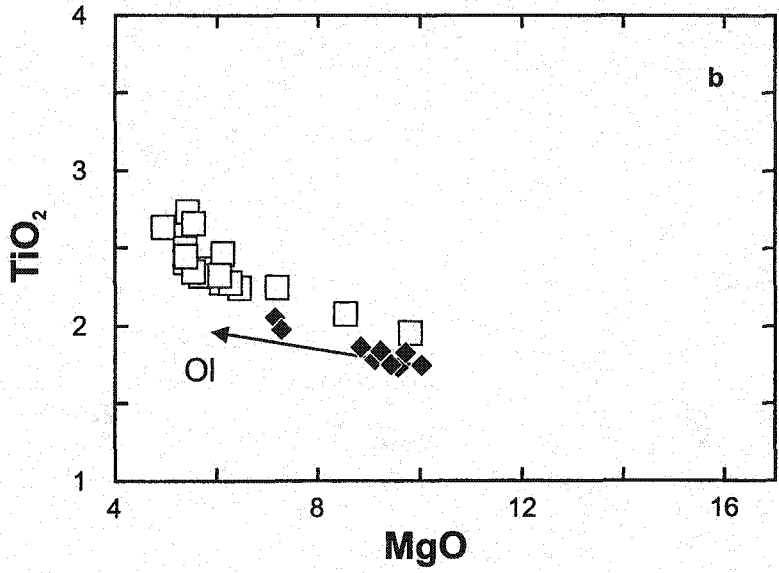
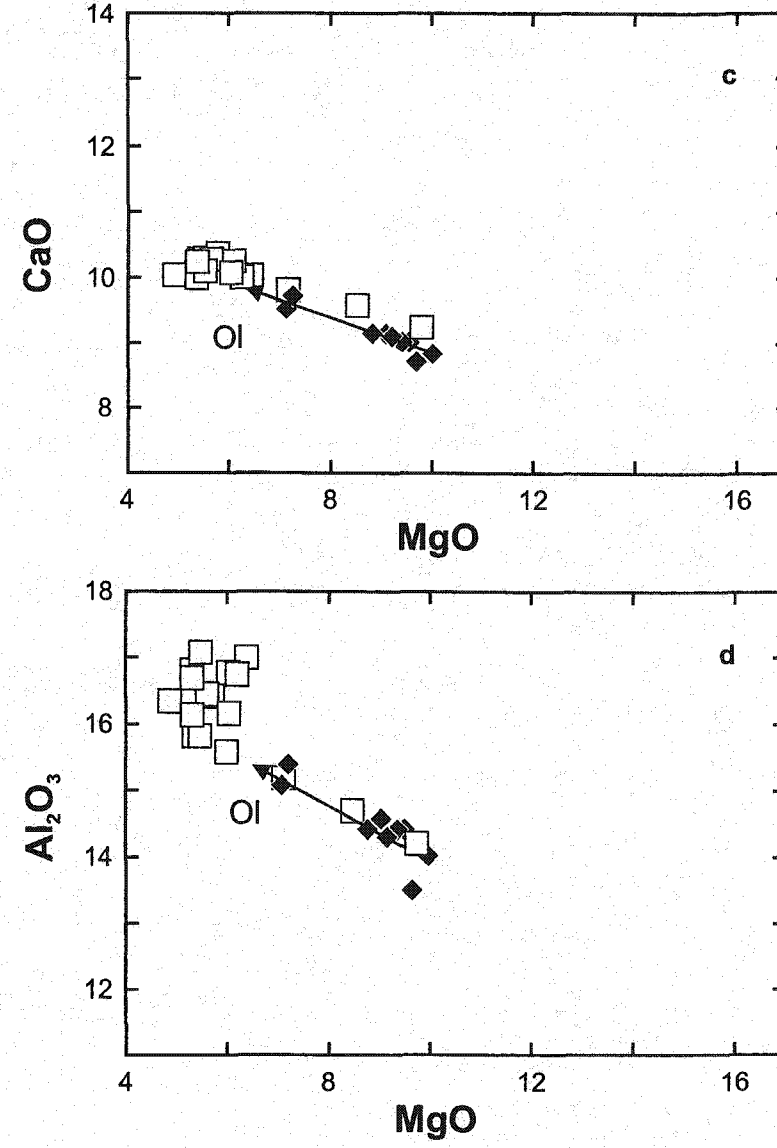
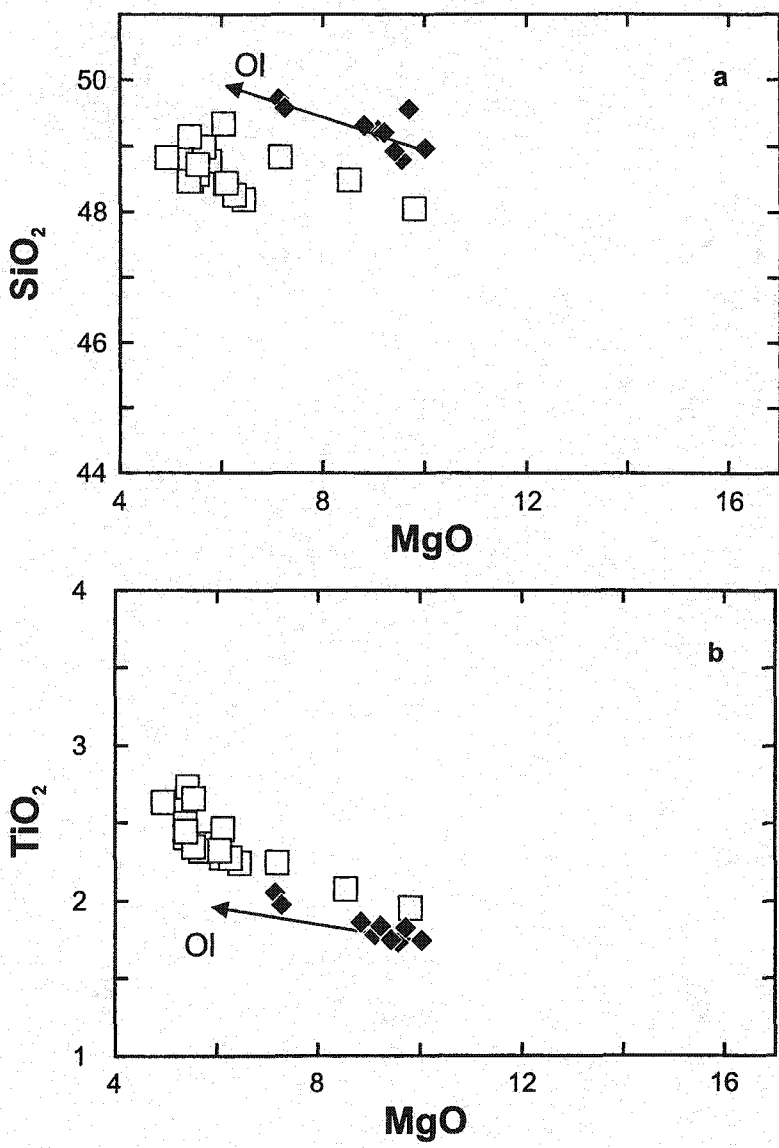


Figure 8.4: Trace element patterns of Tanzilla Volcano basalts normalized to the primitive mantle values of Sun and McDonough (1989). Same symbols as Fig. 8.2. Shaded field as in Fig. 2.2.a.

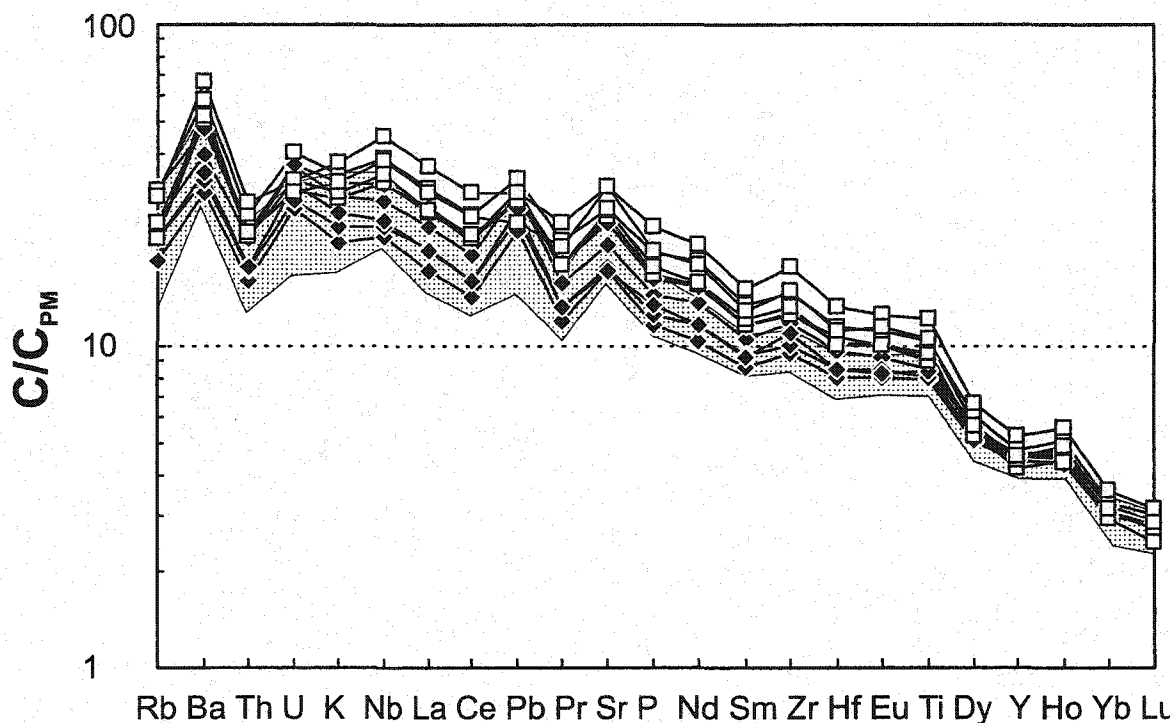
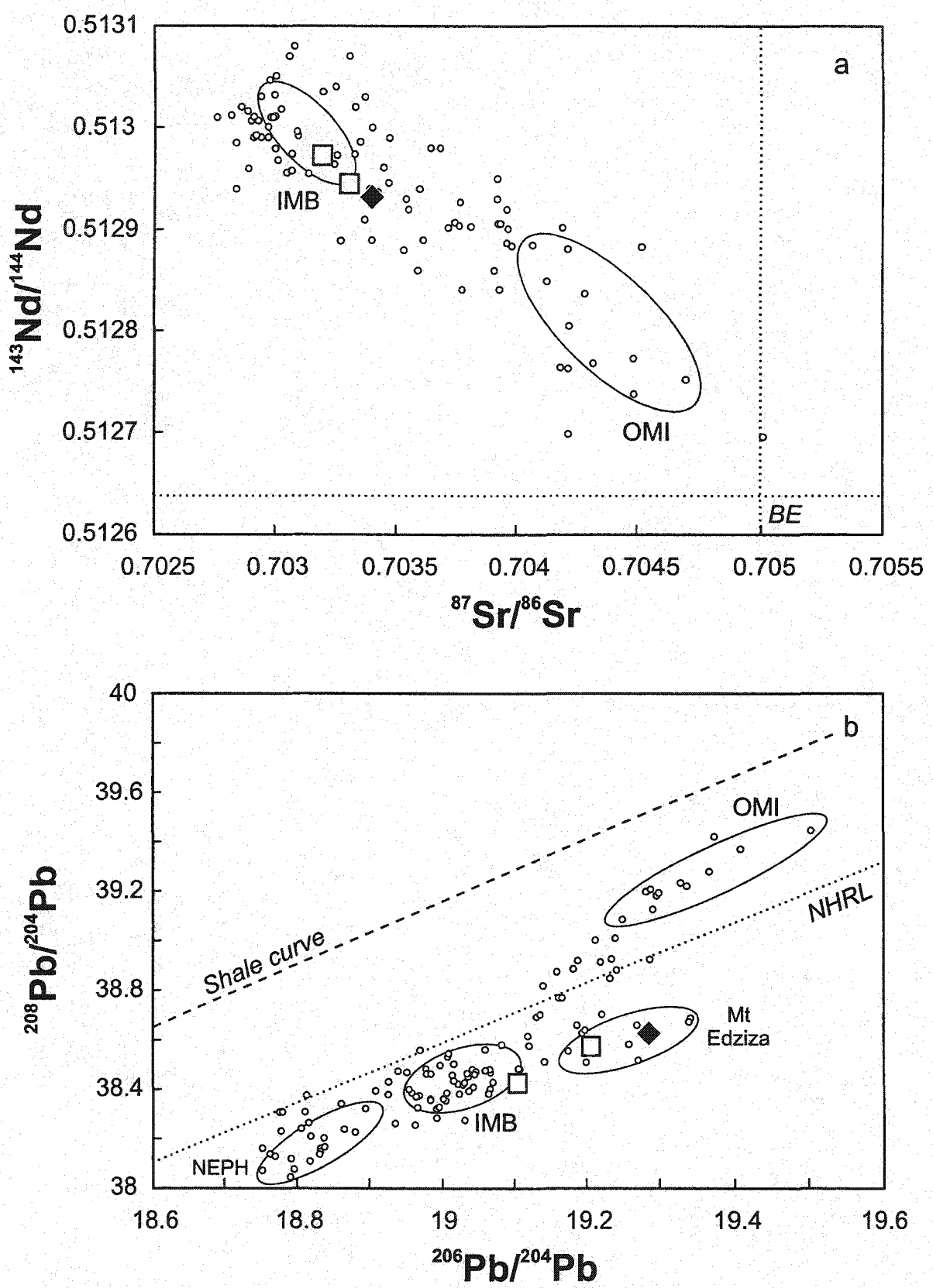


Figure 8.5: a) $^{143}\text{Nd}/^{144}\text{Nd}$ versus $^{87}\text{Sr}/^{86}\text{Sr}$ and b) $^{208}\text{Pb}/^{204}\text{Pb}$ versus $^{206}\text{Pb}/^{204}\text{Pb}$ for Tanzilla Volcano basalts. Large symbols as in Fig.8.2. Fields, small circles and explanations as in Fig. 2.3.



have distinct SiO₂ contents and appear to lie along distinct olivine-control lines at high MgO (Fig. 8.3), they have relatively similar TiO₂, CaO and Al₂O₃ contents (Fig. 8.3). Furthermore, the low-MgO AOB lavas exhibit a large range in SiO₂ and Al₂O₃ that cannot be related to low-pressure fractionation of olivine. Both groups have trace element patterns characterized by an enrichment in LILE and LREE compared to HREE, when normalized to primitive mantle, with positive Ti, Sr, Pb, Nb and negative Th and Rb anomalies compared to elements with similar compatibilities (Fig. 8.4). The trace element patterns of the Hy-NORM basalts are similar to those of primitive Hy-NORM basalts erupted in the Intermontane Belt.

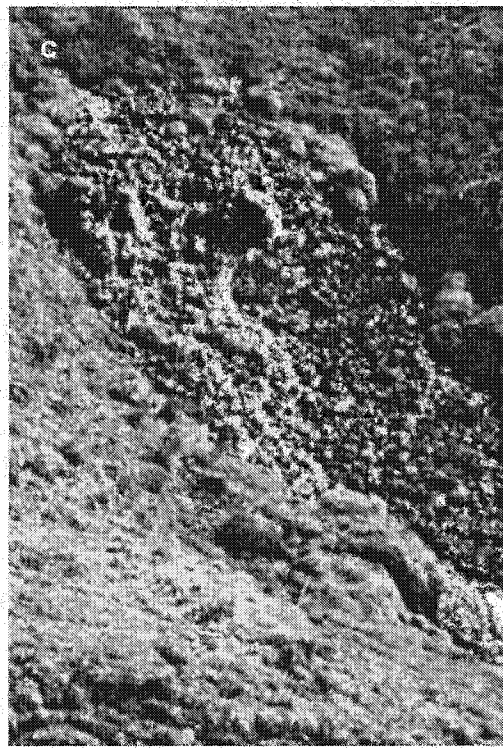
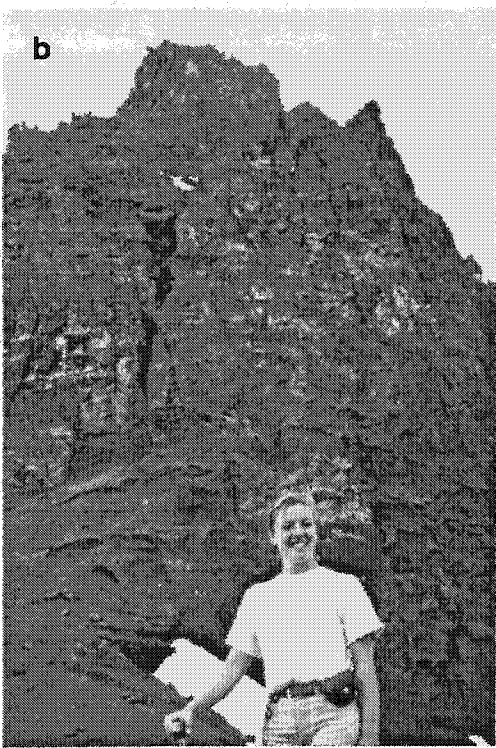
Tanzilla Volcano lavas define a small range of unradiogenic Sr and radiogenic Nd isotopic ratios (Fig. 8.5.a), but trend towards the high ²⁰⁶Pb/²⁰⁴Pb end-member defined by Mount Edziza lavas in a Pb-Pb isotopic plot (Fig. 8.5.b). Despite having a higher MgO content (Table 8), the Hy-NORM basalt is slightly more radiogenic in Sr and Pb, but less radiogenic in Nd isotopic ratios than the AOB lavas (Fig. 8.5). Although Tanzilla Volcano is located close to Tuya Butte, at the transition between the Intermontane and Omineca belts, its lavas have Pb isotopic signatures that are distinct from those of Tuya Butte, and do not appear to reflect mixing between Intermontane and Omineca belt lavas.

4.8. Dome Mountain Volcanics (58.45N, 129.58W; map 104-I/5).

This volcanic centre is situated to the east of Dome Mountain, in the eastern part of the Stikine terrane of the Intermontane Belt (Fig. 1.2). Although no age was determined for this centre, it cannot be younger than Pleistocene owing to the presence of boulder



Figure 9.1: a) Long distance view of Dome Mountain. b) Closer view of the bedded lapilli tuff that constitute most of the centre. c) Unconsolidated pillow lavas at the base of Dome Mountain.



erratics on its upper slopes. This occurrence consists of a well-bedded lapilli and ash tuff unit (Fig. 9.1.a and 9.1.b) that overlies a base consisting of pillow breccia (Fig. 9.1.c) cut by numerous mafic dykes. The eruption appears to have been entirely subglacial and very explosive. Approximately 2 km³ of volcanics are preserved. Because of the absence of true flows at this locality, sampling was restricted to fragments of pillow breccia and dykes. Numerous mantle xenoliths that occur in the tuffs were also sampled.

All the collected samples are BASAN in composition (Table B-8 of appendix B), except for one NEPH sample, DM-1, which has distinctly lower SiO₂ and higher TiO₂ contents than the other BASAN samples (Fig. 9.2 a and b). The Dome Mountain BASAN lavas form a homogeneous group characterized by high MgO, high TiO₂, and the lowest CaO contents of all BASAN lavas erupted in the northern Cordillera (Fig. 9.2.c). All the Dome Mountain BASAN lavas contain numerous small mantle-derived xenoliths that could not all be removed before whole rock analysis, so that the high MgO and low CaO contents of these lavas might reflect contamination by mantle fragments. Dome Mountain lavas form a homogeneous group in terms of trace elements, characterized by enrichments in LILE and LREE compared to HREE, when normalized to primitive mantle, but a relatively large spread in HREE (Fig. 9.3.a). The NEPH sample has the most fractionated HREE pattern. The Dome Mountain lavas have intermediate REE concentrations between those of BASAN and NEPH sampled from Hirschfeld, a high level volcanic plug from the Intermontane Belt (Fig. 9.3.b; Francis and Ludden, 1995). They are, however, more enriched in HFSE (Nb, Zr, and Hf) and in Rb and K than the BASAN at Hirschfeld, with values more similar to those of the Hirschfeld NEPH lavas (Fig. 9.3.b).

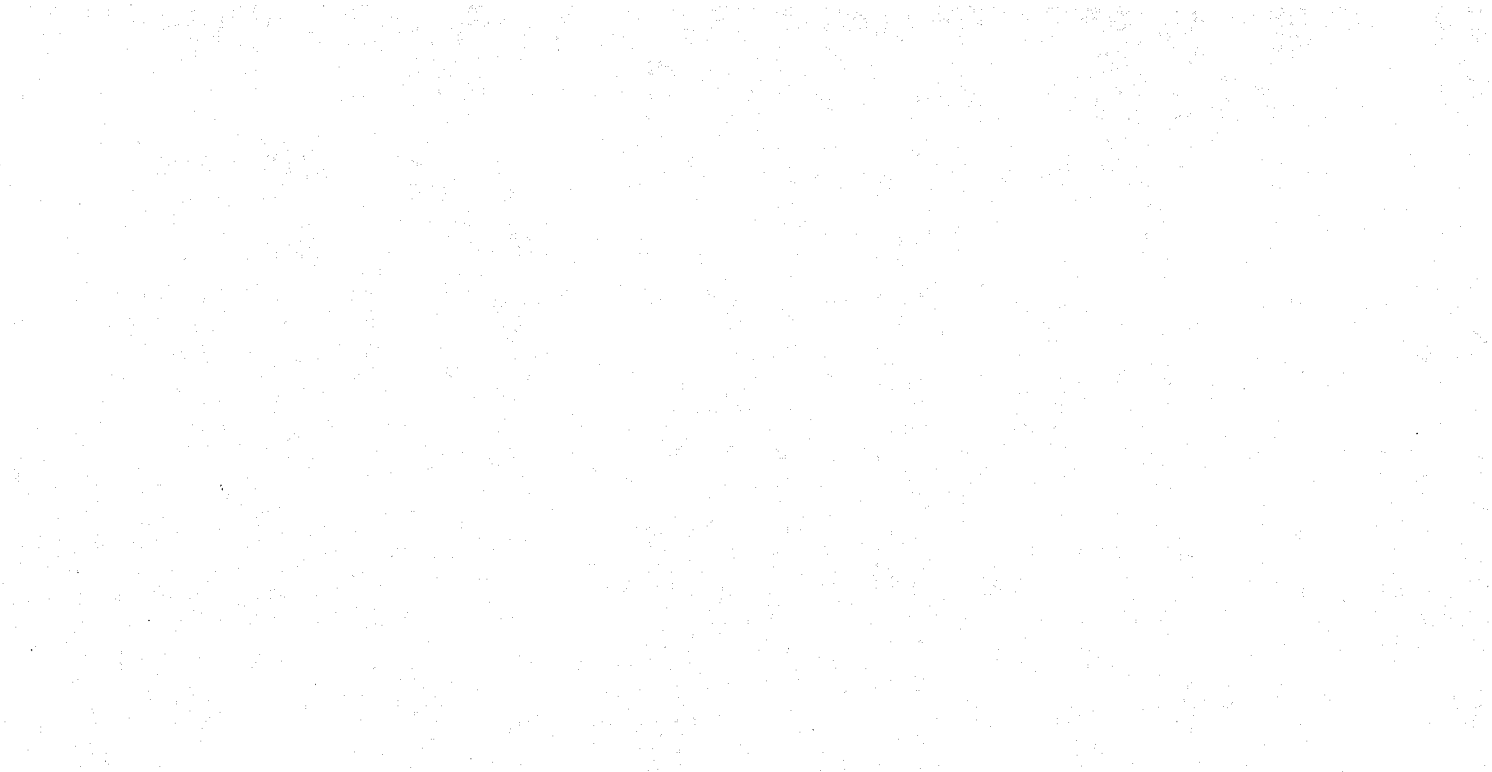
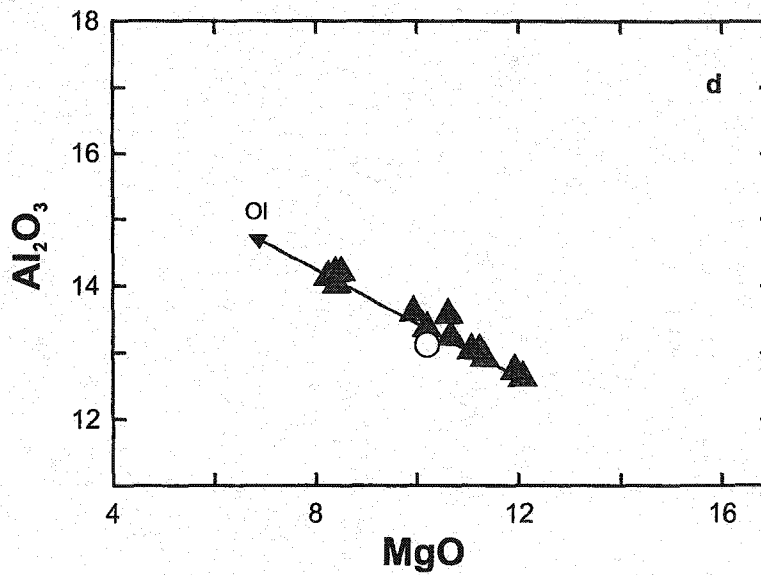
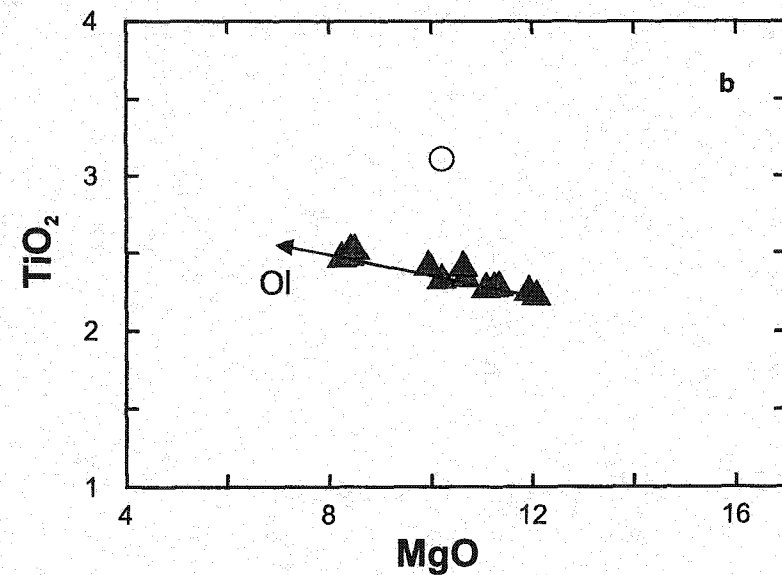
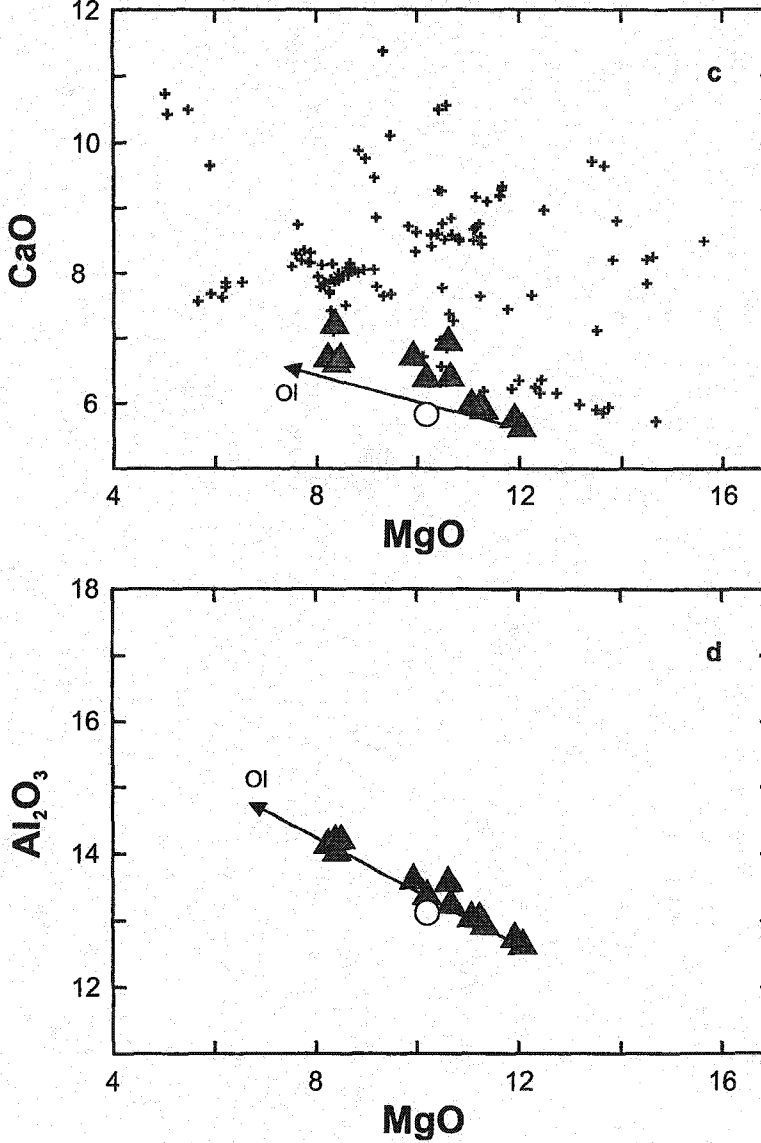
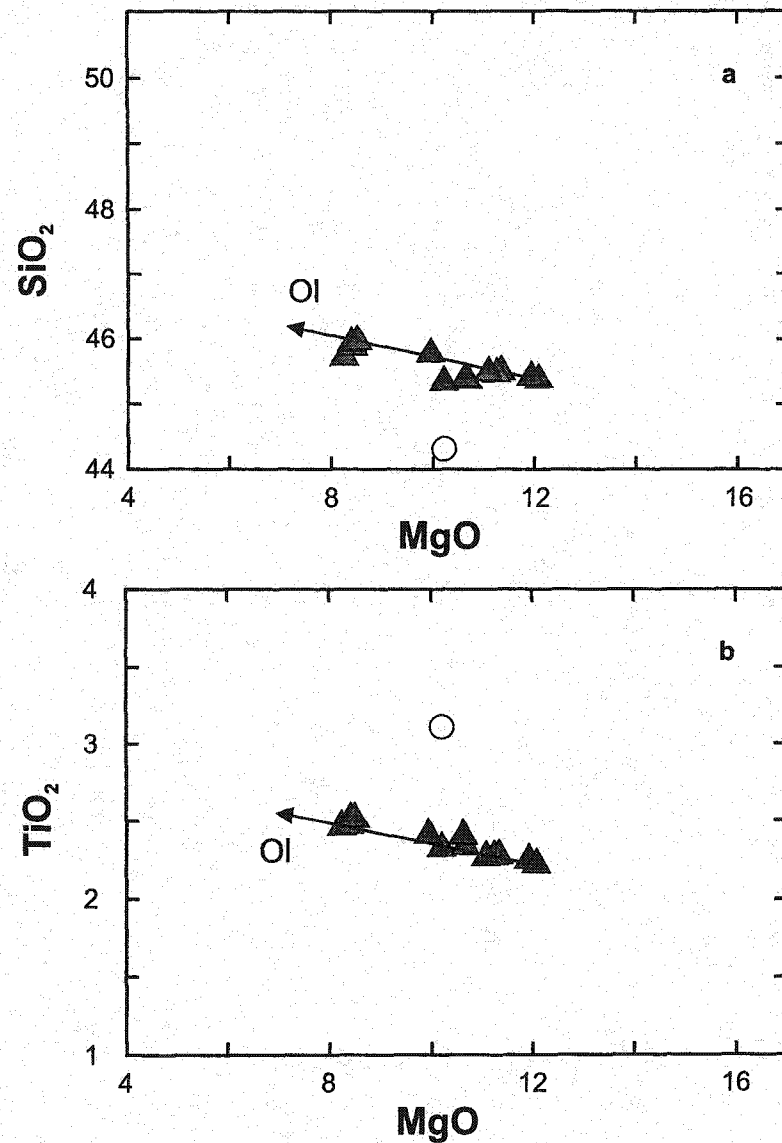


Figure 9.2:

a) SiO_2 , b) TiO_2 , c) CaO , and d) Al_2O_3 versus MgO in wt.% for Dome Mountain basalts. Symbols: triangles = BASAN, circle = NEPH. In Fig. 9.2.c, the crosses correspond to the composition of BASAN lavas erupted in other volcanic centres from the northern Canadian Cordillera (Eiché et al., 1987; Francis and Ludden, 1990 and 1995; this study and unpublished data from Don Francis). The arrow corresponds to the trend expected for olivine fractionation from sample DM-11.



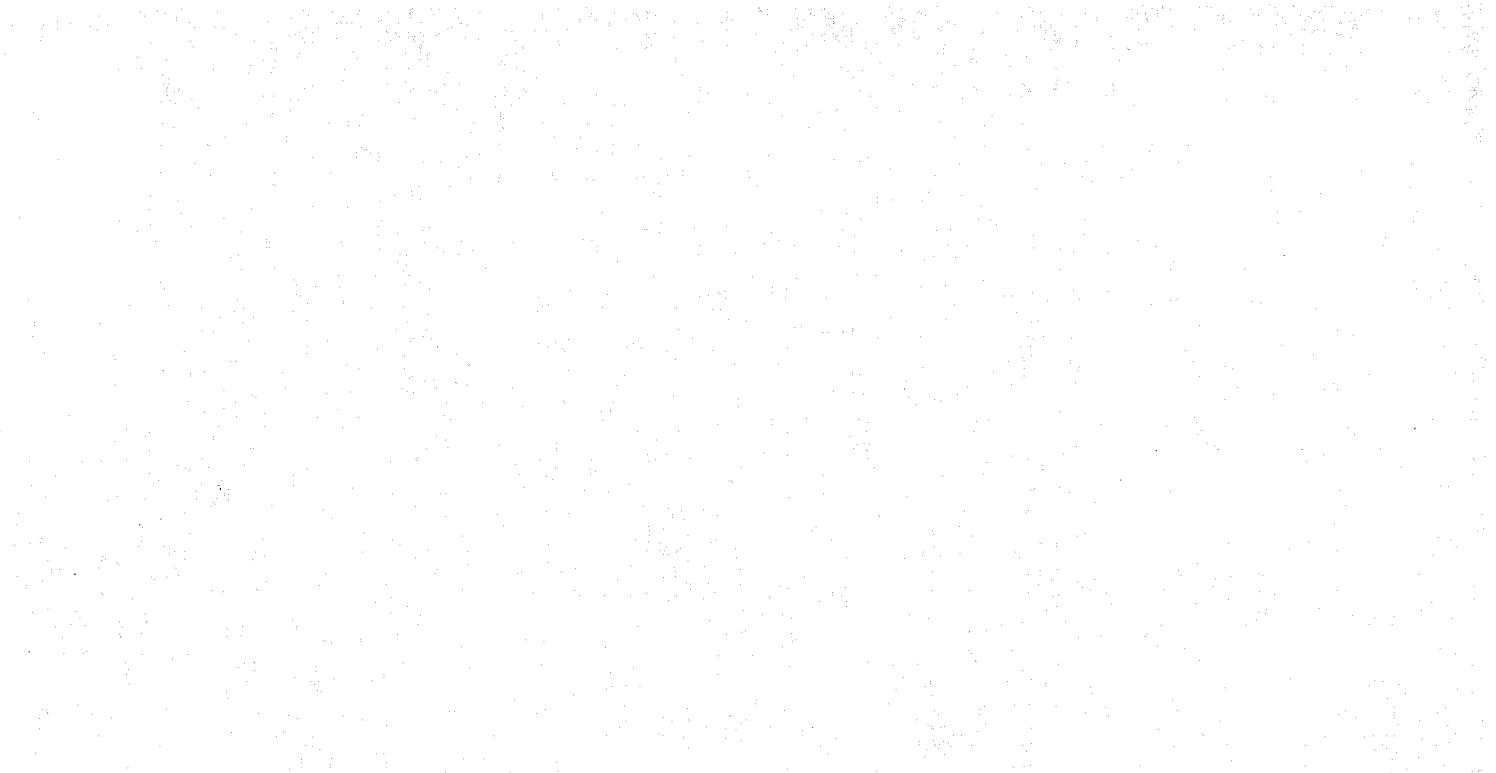


Figure 9.3:

- a) Trace element patterns of Dome Mountain lavas normalized to the primitive mantle values of Sun and McDonough (1989). Symbols as in Fig. 9.2. Shaded field as in Fig. 2.2.a. b) Trace element patterns of Dome Mountain and Hirschfeld BASAN and NEPH magmas normalized to the primitive mantle values of Sun and McDonough (1989). Symbols: triangles = BASAN at Hirschfeld, circles = NEPH at Hirschfeld. The shaded area corresponds to the range of trace elements at Dome Mountain. Data for Hirschfeld from Francis and Ludden (1995).

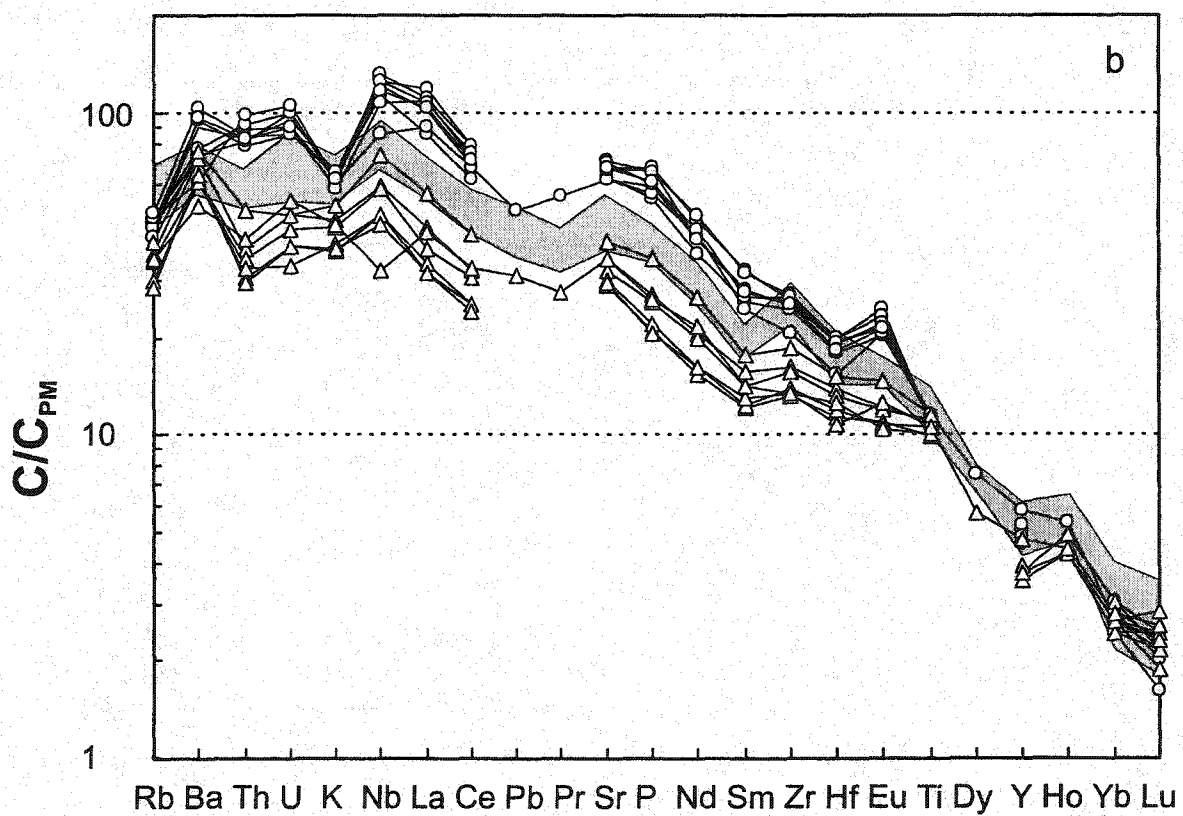
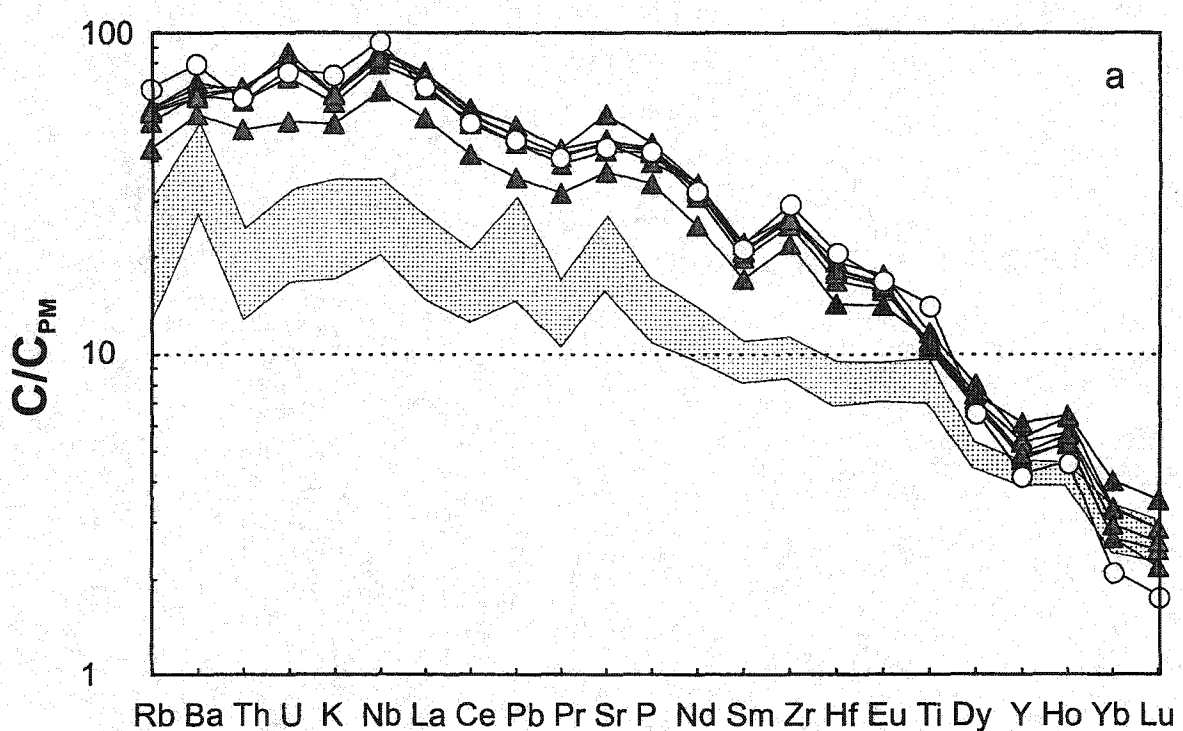
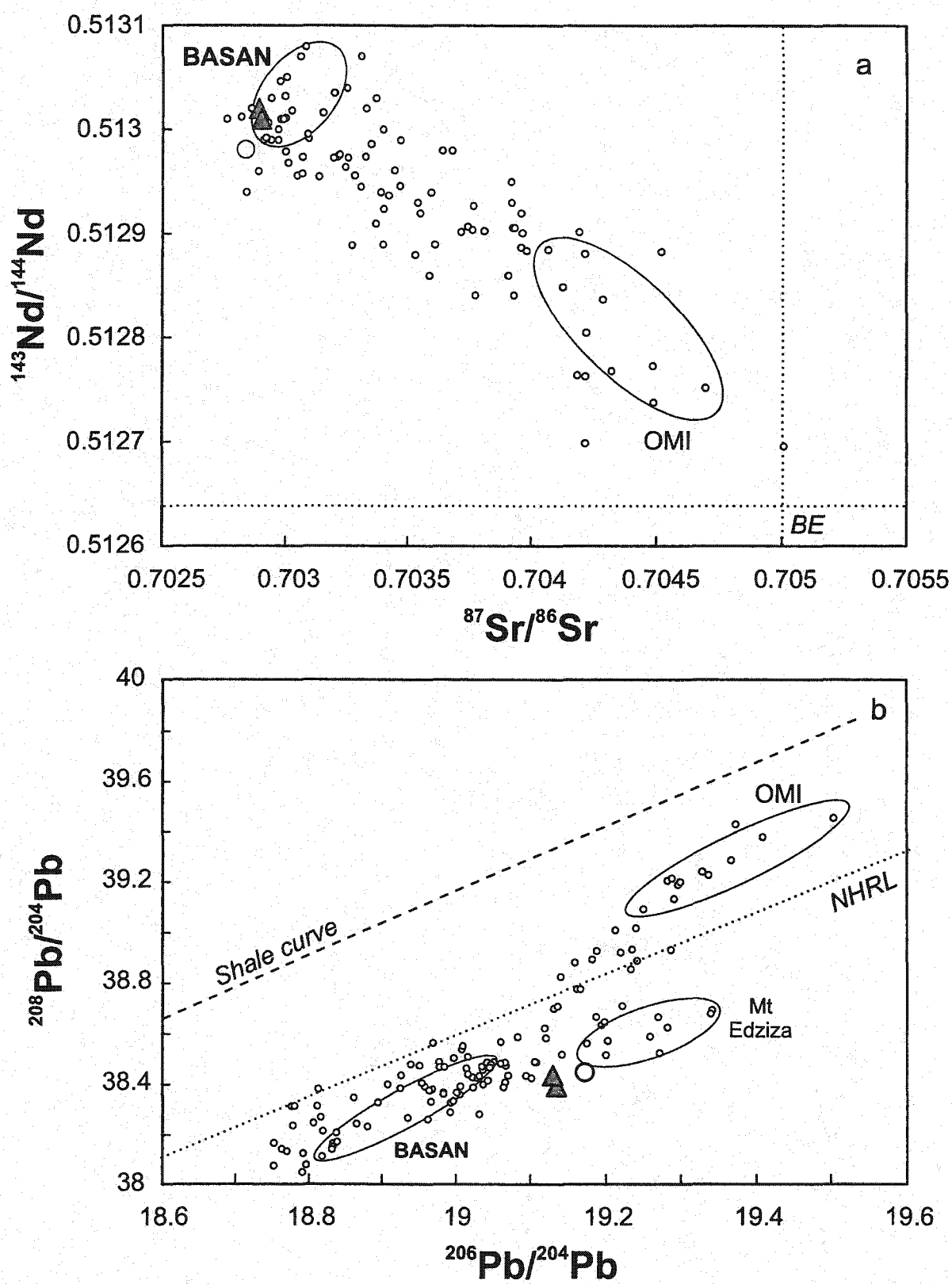


Figure 9.4: a) $^{143}\text{Nd}/^{144}\text{Nd}$ versus $^{87}\text{Sr}/^{86}\text{Sr}$ and b) $^{208}\text{Pb}/^{204}\text{Pb}$ versus $^{206}\text{Pb}/^{204}\text{Pb}$ for Dome Mountain lavas. Symbols as in Fig. 9.2. BE corresponds to bulk Earth values, the NHRL is from Hart (1984) and the shale curve is from Godwin and Sinclair (1982). The field labeled BASAN corresponds to the range in BASAN erupted in volcanic centres from the northern Canadian Cordillera (Eiché et al., 1987; Francis and Ludden, 1990 and 1995; this study and unpublished data from Don Francis). The fields labeled OMI and Mt Edziza correspond to the range in primitive Hy-NORM basalts from the Omineca Belt and Mount Edziza, respectively.



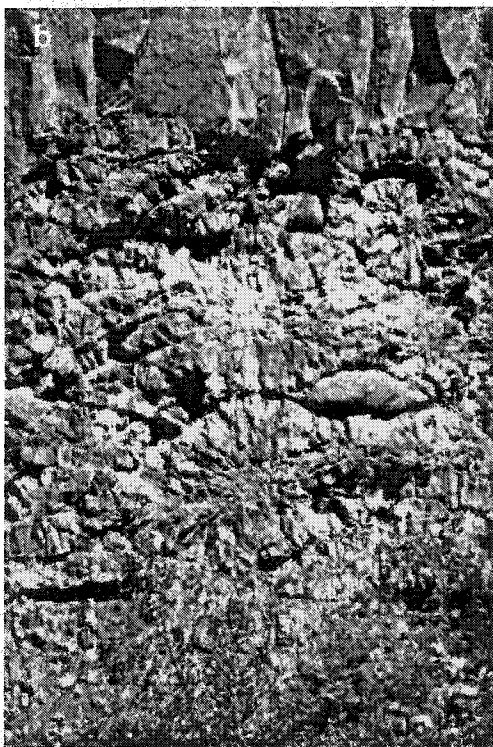
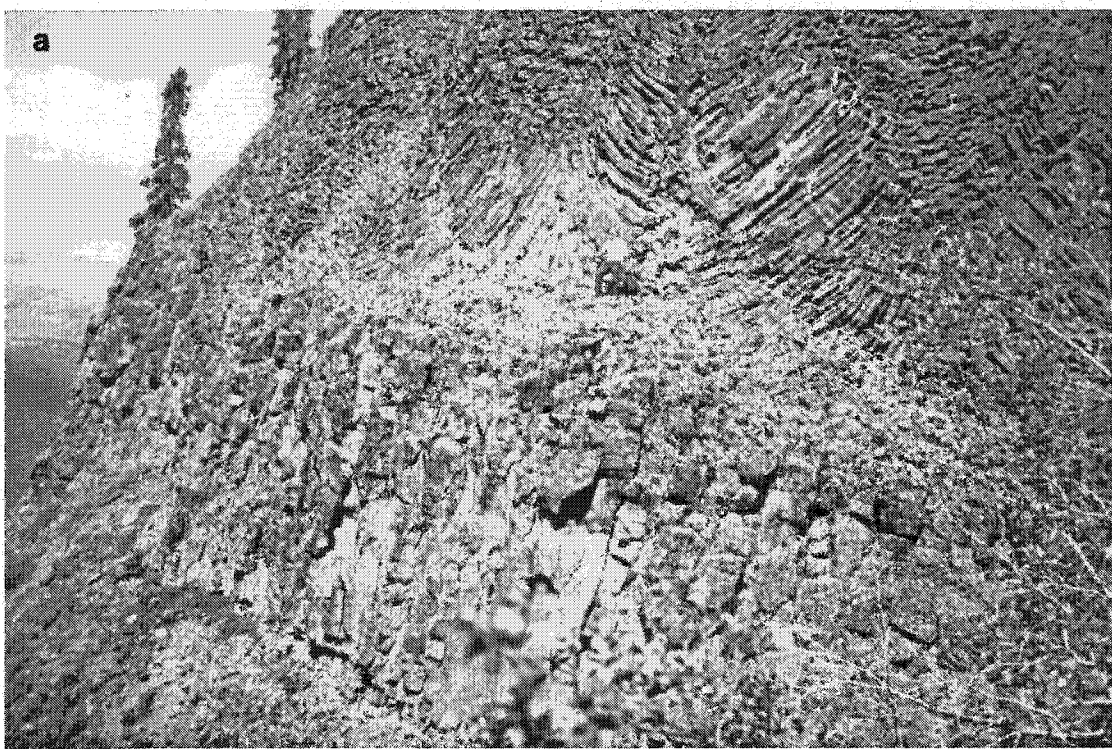
The Dome Mountain lavas form a homogeneous isotopic group characterized by low $^{87}\text{Sr}/^{86}\text{Sr}$, high $^{143}\text{Nd}/^{144}\text{Nd}$, low $^{207}\text{Pb}/^{204}\text{Pb}$ and $^{208}\text{Pb}/^{204}\text{Pb}$ ratios, but relatively high $^{206}\text{Pb}/^{204}\text{Pb}$ (Fig. 9.4). They have similar Sr and Nd isotopic signatures to other BASAN lavas erupted in the Intermontane (Fig. 9.4.a), but have higher Pb isotopic ratios that trend towards the high $^{206}\text{Pb}/^{204}\text{Pb}$ end-member defined by Mount Edziza lavas (Fig. 9.4.b).

4.9. Jennings River ($59.47^\circ\text{N}, 130.30^\circ\text{W}$; NTS 104-O/6)

This unnamed volcanic centre originally mapped by Gabrielse (1969) is situated at the junction between Jennings River and Klinkit Creek, in the Slide Mountain terrane, to the east of the Teslin fault, a major lineament thought to separate the Intermontane Belt from the Omineca Belt (Fig. 1.2). The lavas erupted through the Cretaceous Klinkit Batholith, which consists mainly of biotite quartz monzonite (Gabrielse, 1969). No age has been determined for this centre, but the presence of boulder erratics indicate that it has been covered by ice, and cannot be younger than Pleistocene. We estimate the volume of the centre to be about 4 km^3 . The base of the centre consists mainly of pillow lava, interbedded with massive lava flows with well-developed columnar joints (Fig. 10.1.b), capped by thick massive flows (Fig. 10.1.a). The upper part of the centre consists of small pillow lava in hyaloclastic tuff (Fig. 10.1.c), capped by bedded lapilli tuff.

The lavas of the base grade upwards from Hy-NORM basalts to AOB, while the bombs in the upper tuffaceous unit are BASAN. These three lava types are clearly distinct in terms of major (Fig. 10.3) and trace elements (Fig. 10.4), and define distinct olivine-control lines (Fig. 10.3), indicating that they have evolved separately since their

Figure 10.1: **a)** Lava flows at the top of the lower section of Jennings River. **b)** Pillow lavas and small lava flows at the base of Jennings River. **c)** Pillow lavas at the base of the upper section.



extraction of their mantle source (s). The high-MgO BASAN lavas are characterized by high CaO contents compared to BASAN lavas erupted in Dome Mountain and in other Cordilleran volcanic centres (Fig. 9.2). The low CaO contents of the low-MgO BASAN lavas (Fig. 10.3) indicate that they may have undergone some fractionation of clinopyroxene, consistent with the presence of clinopyroxene phenocrysts in thin sections. Jennings River lavas define trace element patterns characterized by an enrichment in LILE and LREE compared to HREE, when normalized to primitive mantle, with positive Sr and Pb and negative Nb, K, U, Th and Rb anomalies compared to elements with similar compatibilities (Fig. 10.4). From Hy-NORM to BASAN, there is a decrease in the positive Pb anomaly, and an increase in the positive Nb and negative U anomalies. The lavas exhibit a large spread in LILE and LREE, but converge towards common HREE values. The Hy-NORM basalts have trace element patterns similar to those of high-MgO Hy-NORM basalts of the Intermontane Belt (Fig. 10.4.a). The BASAN lavas are generally less enriched in most incompatible trace elements than the Dome Mountain BASAN, but have similar patterns to Hirschfeld BASAN (Fig. 10.4.b).

The three magma types have relatively unradiogenic Sr and Pb, and radiogenic Nd isotopic ratios that fall within the range of high-MgO Hy-NORM lavas of the Intermontane Belt (Fig. 10.5.a). There is a general decrease in the Sr and Pb isotopic ratios, and an increase in the Nd isotopic ratios from the BASAN, through the AOB, to the Hy-NORM lavas. These characteristics are similar to those documented at Hirschfeld and Fort Selkirk (Francis and Ludden, 1990 and 1995; Carignan et al., 1994). The BASAN sample falls within the isotopic range of NEPH lavas from the northern

Figure 10.2: Stratigraphic column of Jennings River indicating the position of each analyzed sample. Symbols: Triangles = BASAN; squares = AOB; diamonds = Hy-NORM basalts. Bold sample labels correspond to samples that have been isotopically studied. Data in table B-9 of appendix B.

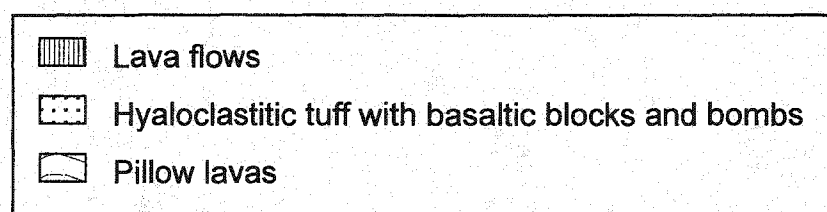
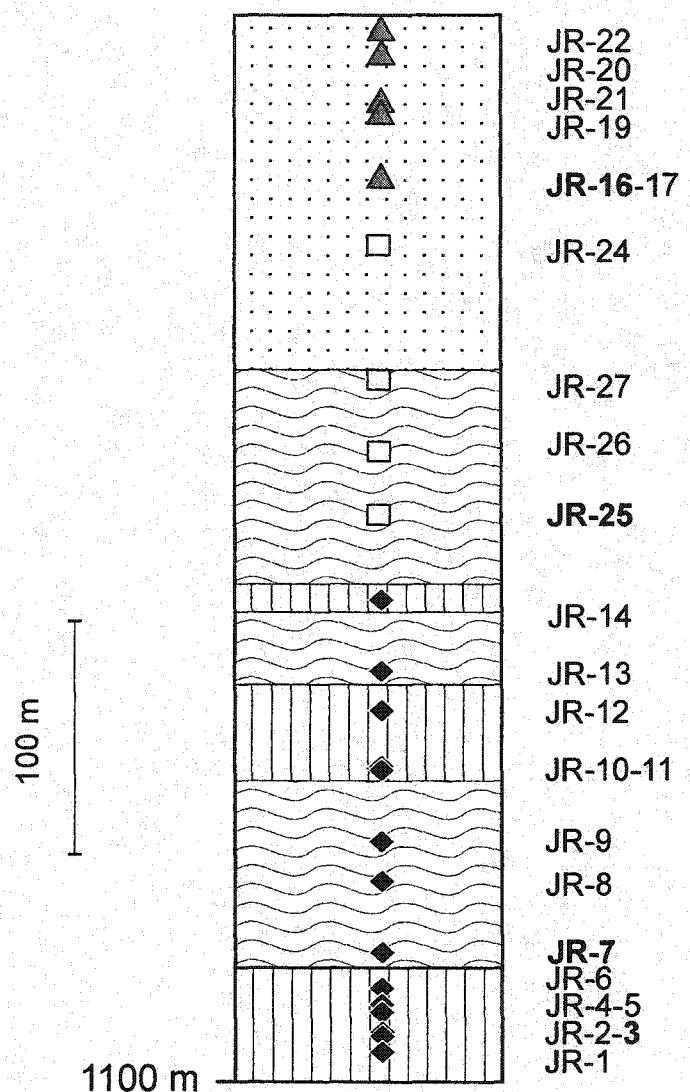




Figure 10.3: a) SiO_2 , b) TiO_2 , c) CaO , and d) Al_2O_3 versus MgO in wt.% for Jennings River basalts. Symbols as in Fig. 10.2. The arrows labeled Ol and Ol + Cpx correspond to the trends expected for olivine fractionation from sample JR-3 and 50% Olivine + 50% clinopyroxene fractionation from sample JR-16, respectively.

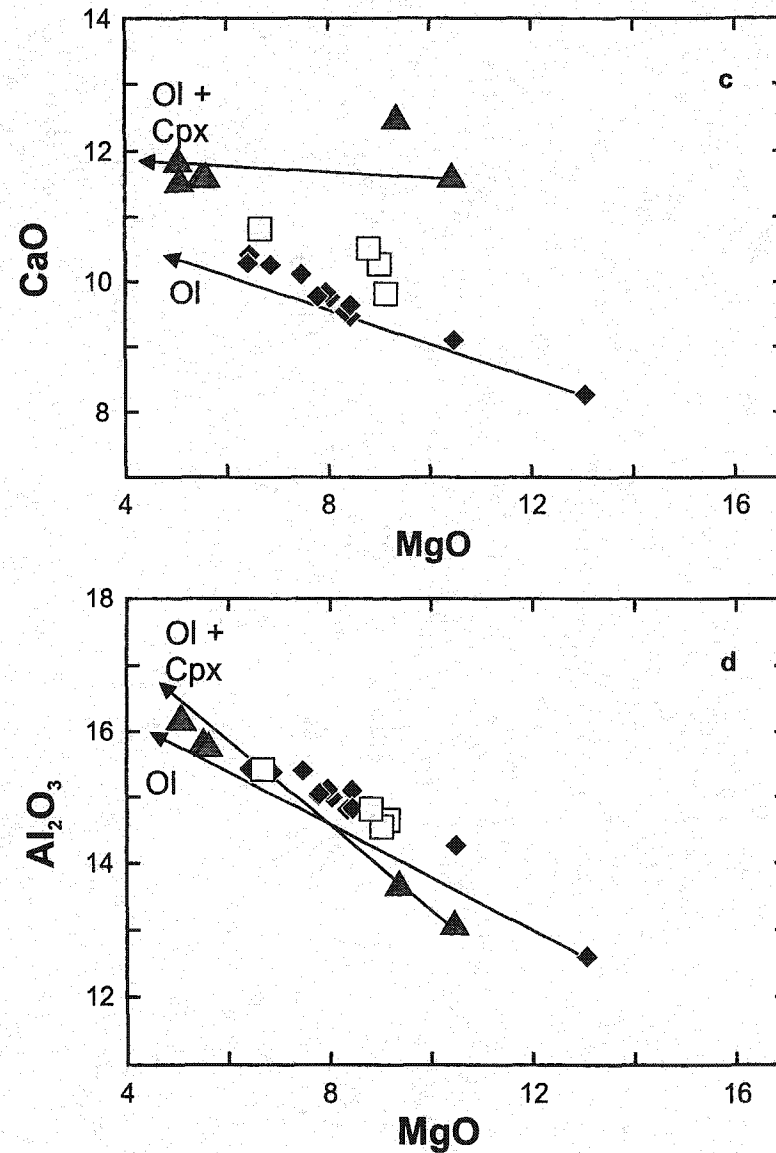
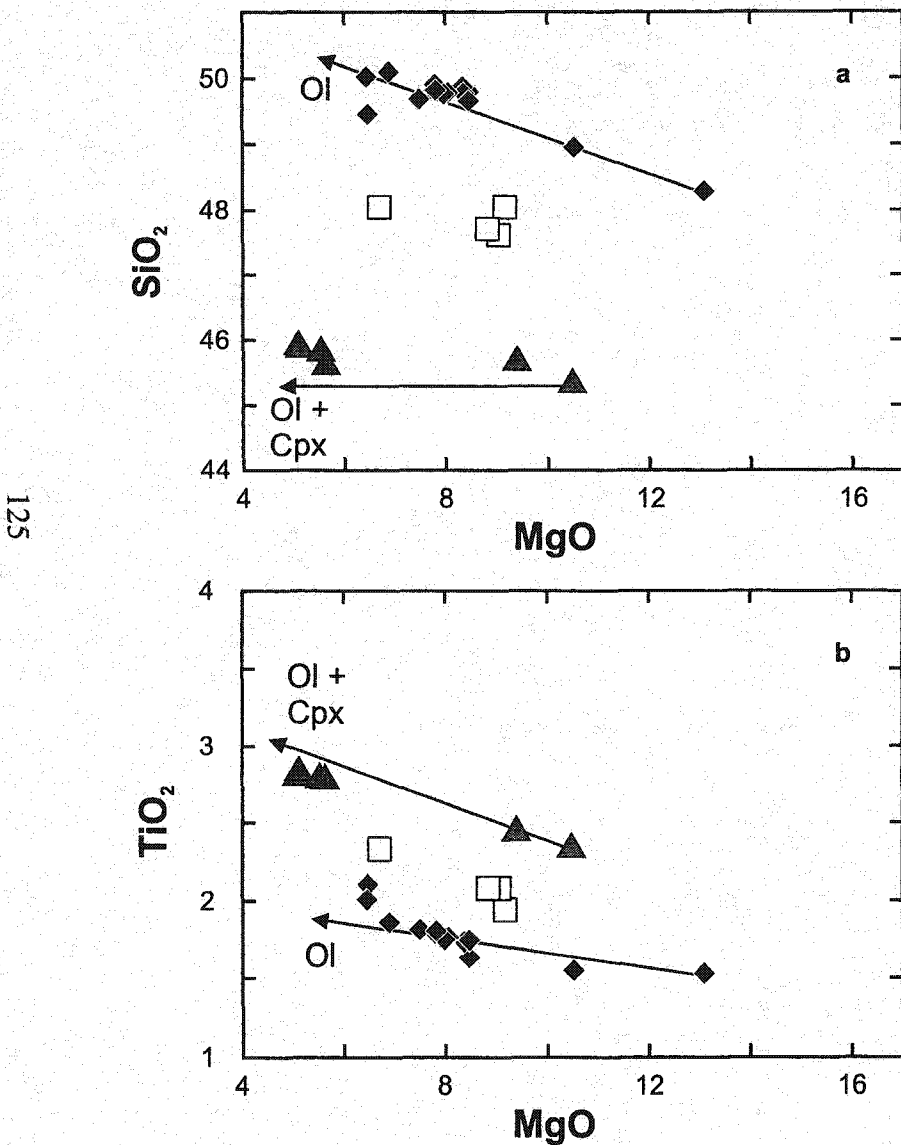


Figure 10.4: a) Trace element patterns of Jennings River basalts normalized to the primitive mantle values of Sun and McDonough (1989). Same symbols as Fig. 10.2. Shaded field as in Fig. 2.2.a. b) Trace element patterns of BASAN erupted at Jennings River (thick curve), compared to BASAN erupted at Dome Mountain (grey field), and at Hirschfeld (white triangles). All data are normalized to the primitive mantle values of Sun and McDonough (1989).

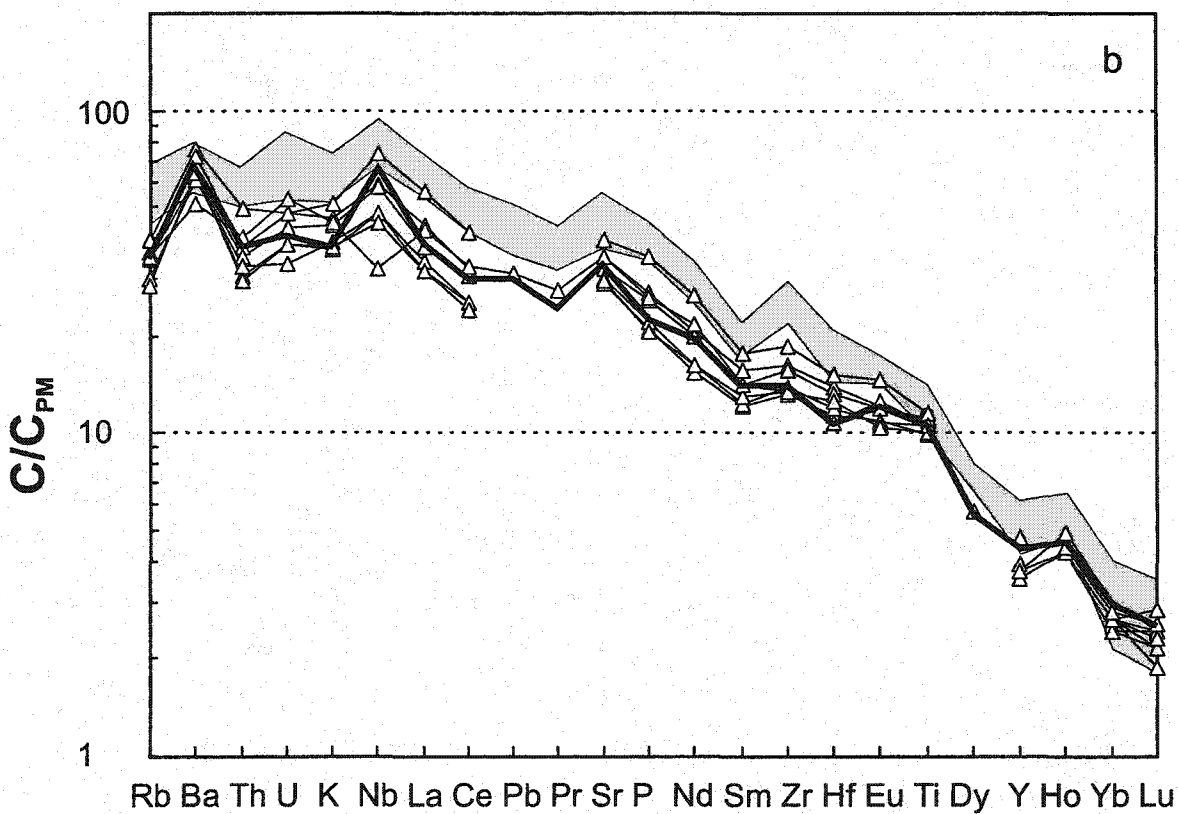
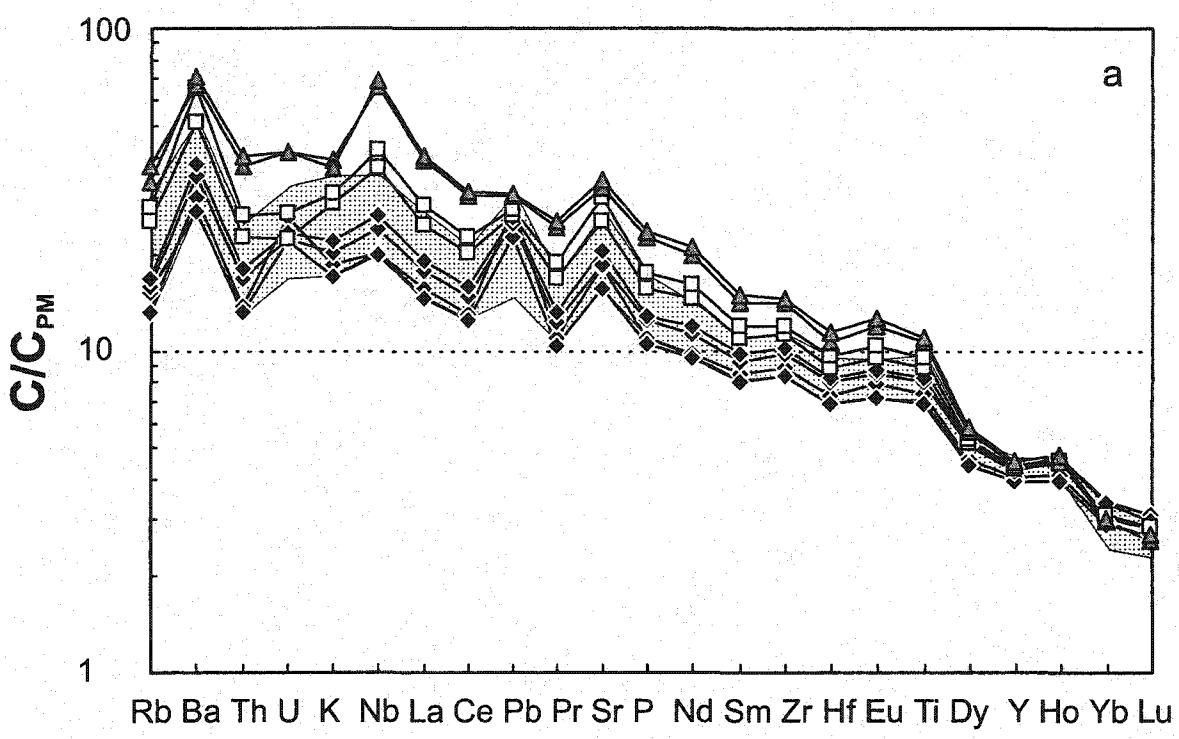
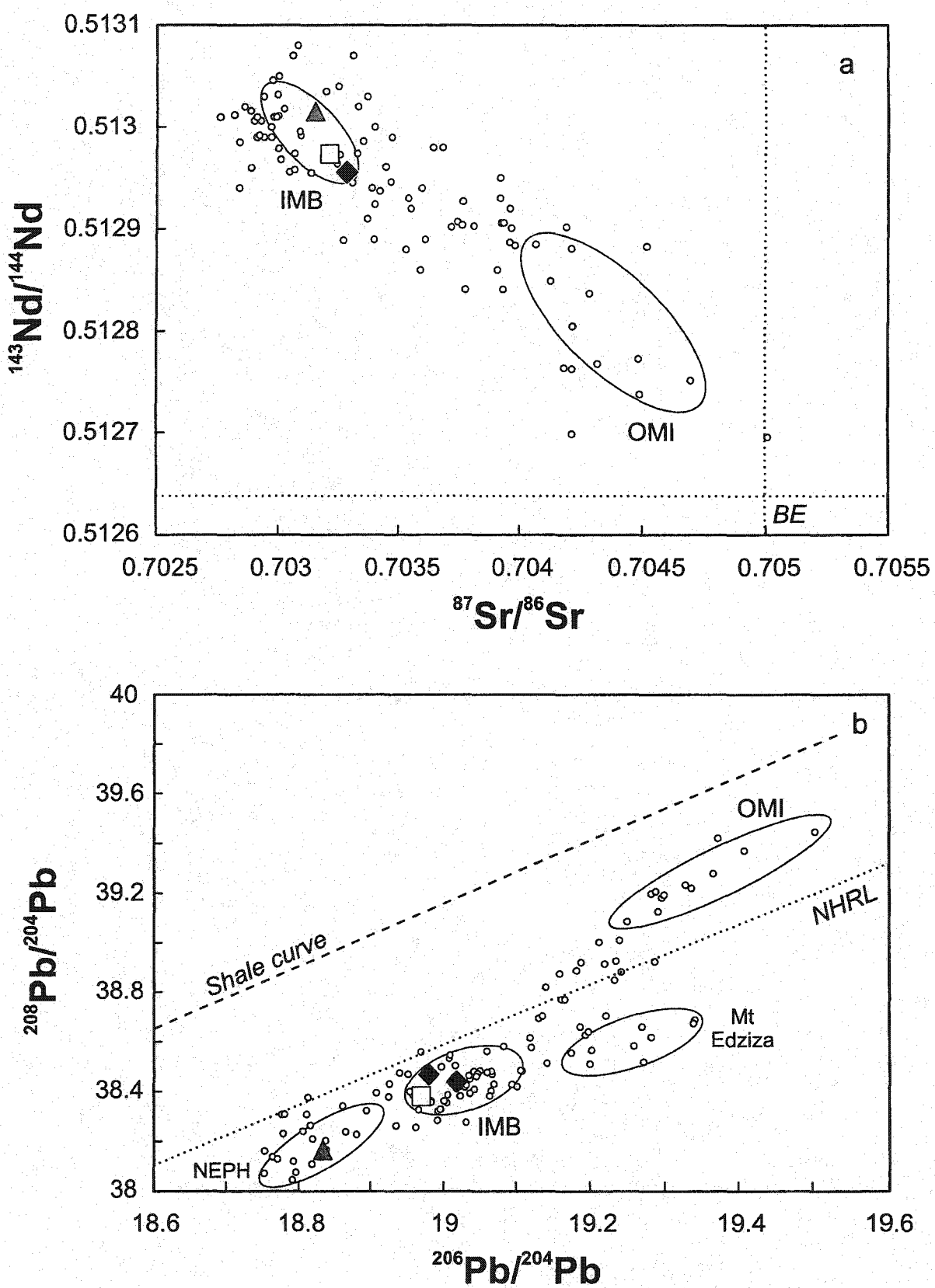


Figure 10.5: a) $^{143}\text{Nd}/^{144}\text{Nd}$ versus $^{87}\text{Sr}/^{86}\text{Sr}$ and b) $^{208}\text{Pb}/^{204}\text{Pb}$ versus $^{206}\text{Pb}/^{204}\text{Pb}$ for Jennings River basalts. Large symbols as in Fig.10.2. Fields, small circles and explanations as in Fig. 2.3.



Cordillera, with significantly less radiogenic Pb isotopic ratios than the AOB and Hy-NORM lavas (Fig. 10.5.b).

4.10. Nome Cone (59.55°N, 130.88°W, NTS 104-O/10)

Nome Cone, first mapped by Gabrielse (1969), erupted through Carboniferous metamorphic rocks of the Slide Mountain terrane of the Intermontane Belt, just south of the Jurassic Nome Lake batholith (Fig. 1.2), probably in the Pleistocene to Quaternary (Gabrielse, 1969). Nome Cone has a volume of less than 2 km³ and is composed of a base of pillow lava interbedded with more massive lava flows (Fig. 11.1.a and b), and an upper cone of bedded lapilli tuff. Most of the eruption appears to have been subglacial.

Nome Cone lavas have a restricted range of MgO contents (7-9 wt.%), and most are Hy-NORM basalts, except for a thin (2m) lapilli tuff layer in which AOB fragments with distinct chemical signatures, such as higher TiO₂, and lower Al₂O₃, occur (Fig. 11.3). The trace element patterns of the Nome Cone lavas are characterized by an enrichment in LILE and LREE compared to HREE, when normalized to primitive mantle, and a convergence towards relatively similar HREE values (Fig. 11.4). The AOB and Hy-NORM basalts have distinct trace element patterns, the AOB lavas being more enriched in incompatible trace elements than the Hy-NORM basalts, except in the HREE. Both lavas types have positive Sr and Nb anomalies compared to elements with similar compatibilities, but only the Hy-NORM lavas exhibit strong positive Pb anomalies, a feature observed in most primitive Hy-NORM lavas of the Intermontane Belt (Fig. 11.4.a). Nome Cone Hy-NORM basalts have similar trace element patterns to high MgO



Figure 11.1: a) Long distance view of Nome Cone. b) Small lava flows and pillow lavas at the base of the cone. c) Closer view of interbedded lava flows and pillow lavas.

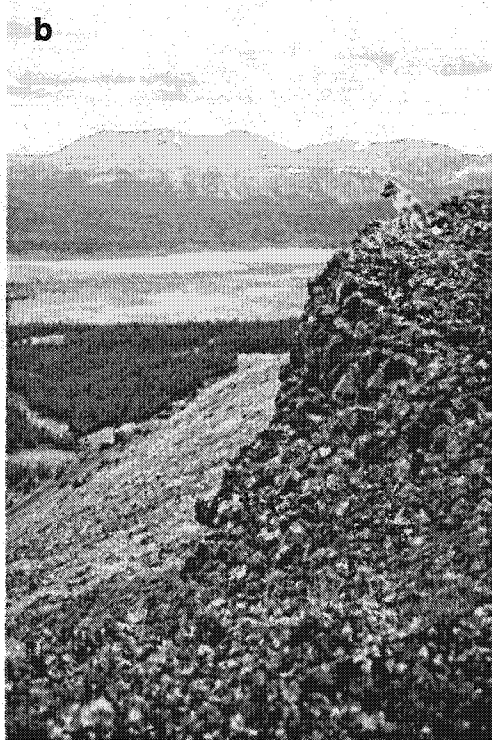
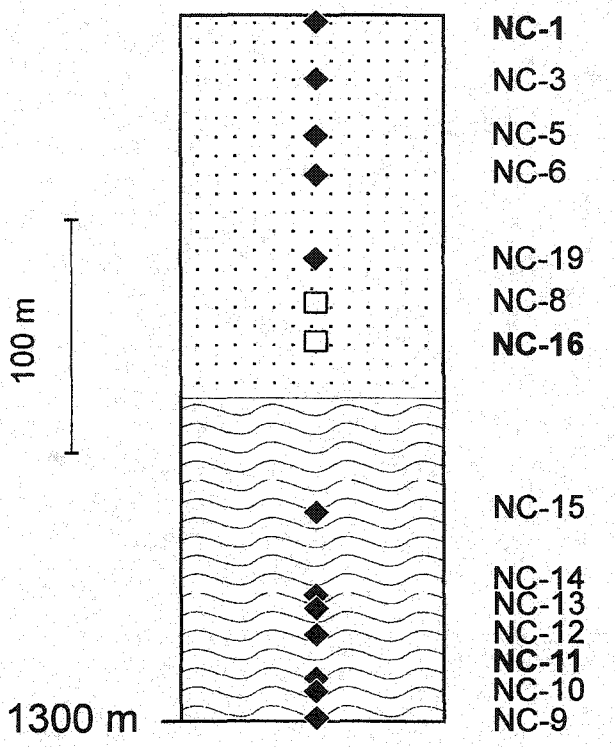


Figure 11.2: Stratigraphic column of Nome Cone indicating the position of each analyzed sample. Symbols: squares = AOB; diamonds = Hy-NORM basalts. Bold sample labels correspond to samples that have been isotopically studied. Data in table B-10 of appendix B.



••• Hyaloclastitic tuff with basaltic blocks and bombs
— Pillow lavas and small lava flows

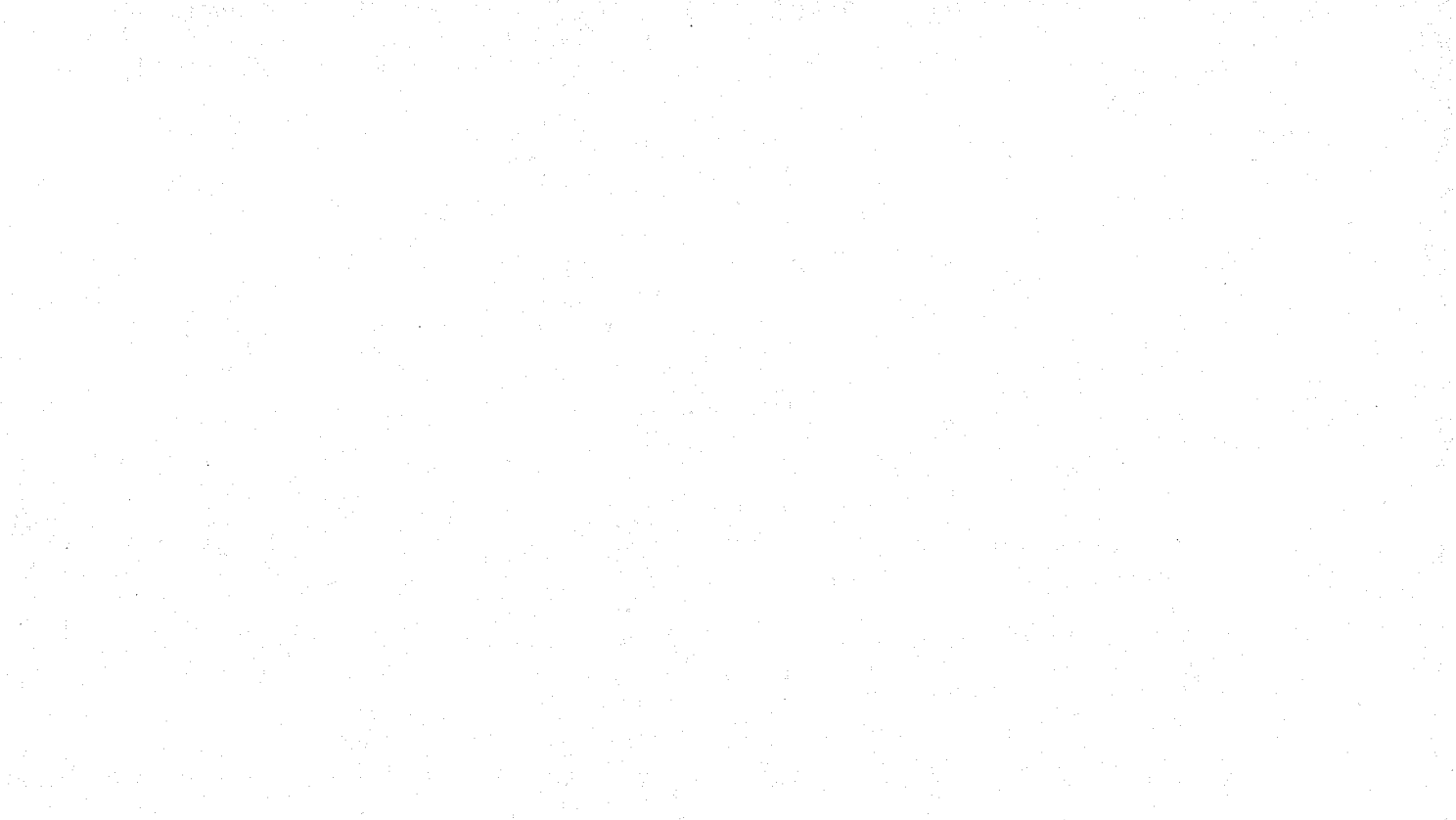


Figure 11.3: a) SiO_2 , b) TiO_2 , c) CaO , and d) Al_2O_3 versus MgO in wt.% for Nome Cone basalts. Symbols as in Fig. 11.2.

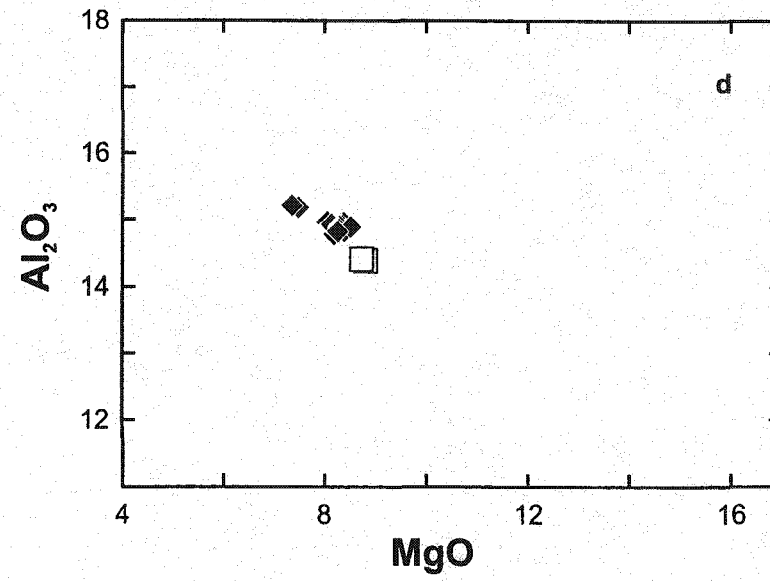
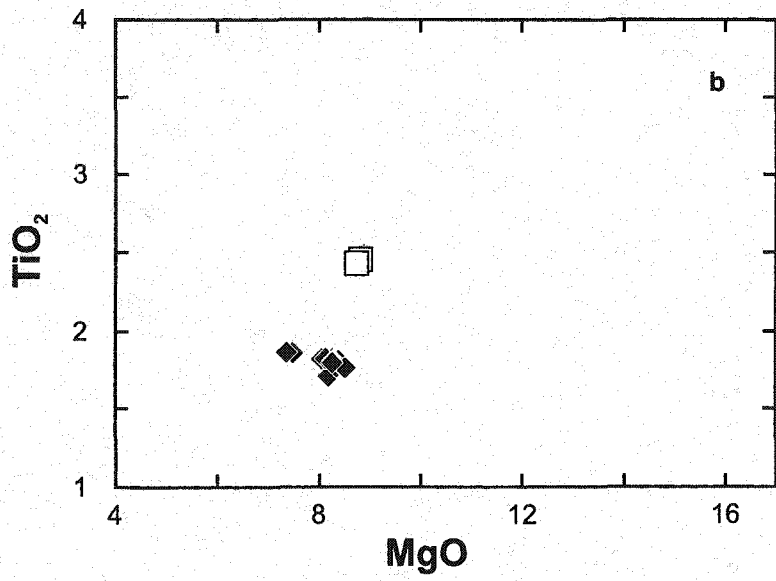
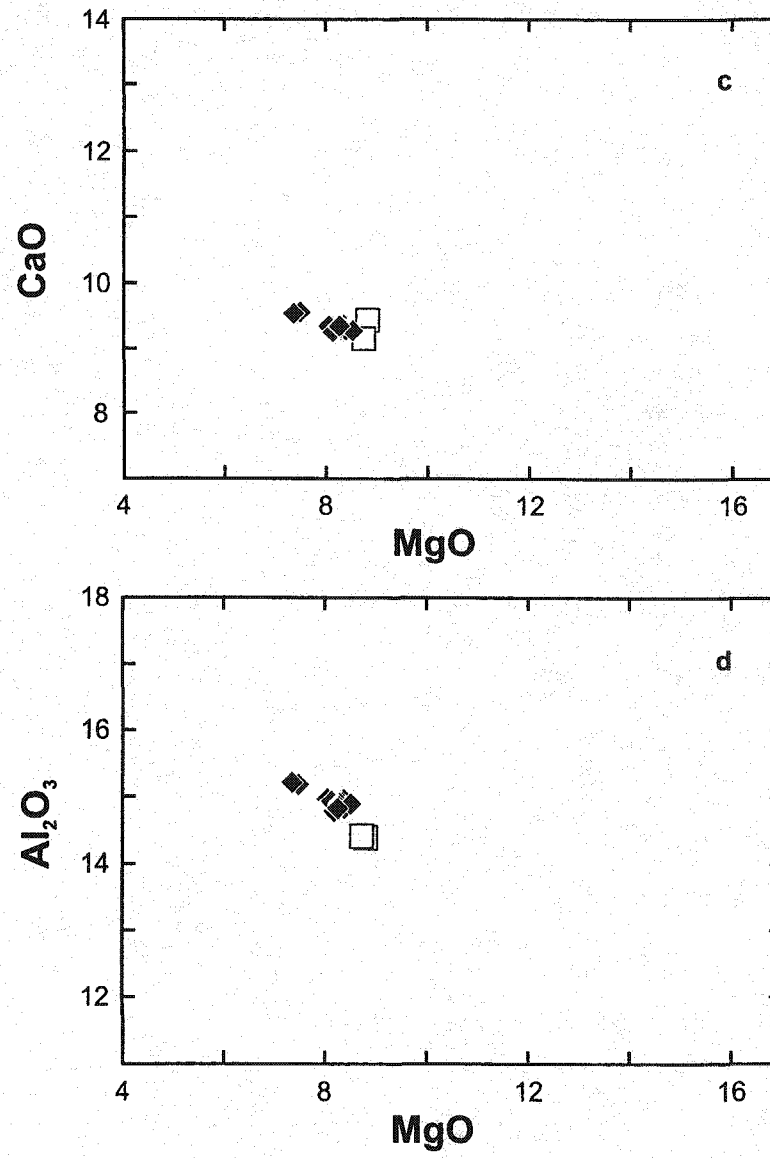
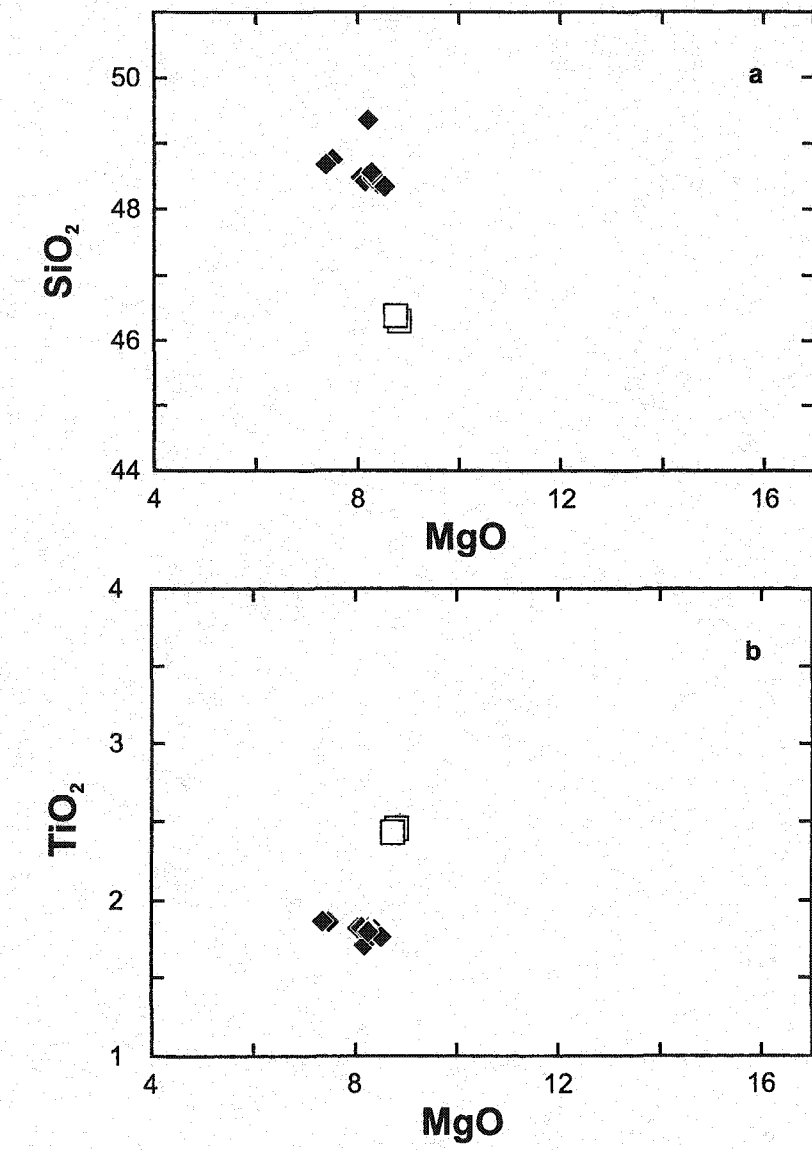
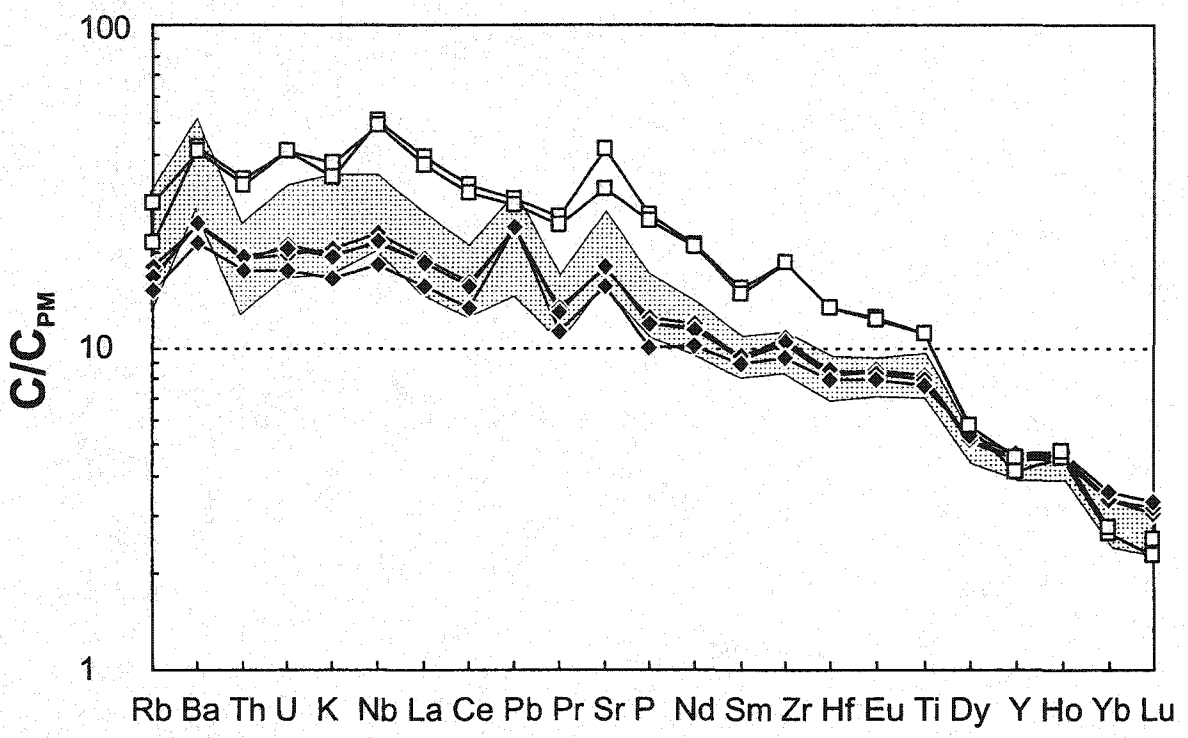


Figure 11.4: Trace element patterns of Nome Cone basalts normalized to the primitive mantle values of Sun and McDonough (1989). Same symbols as Fig. 11.2. Shaded field as in Fig. 2.2.a.





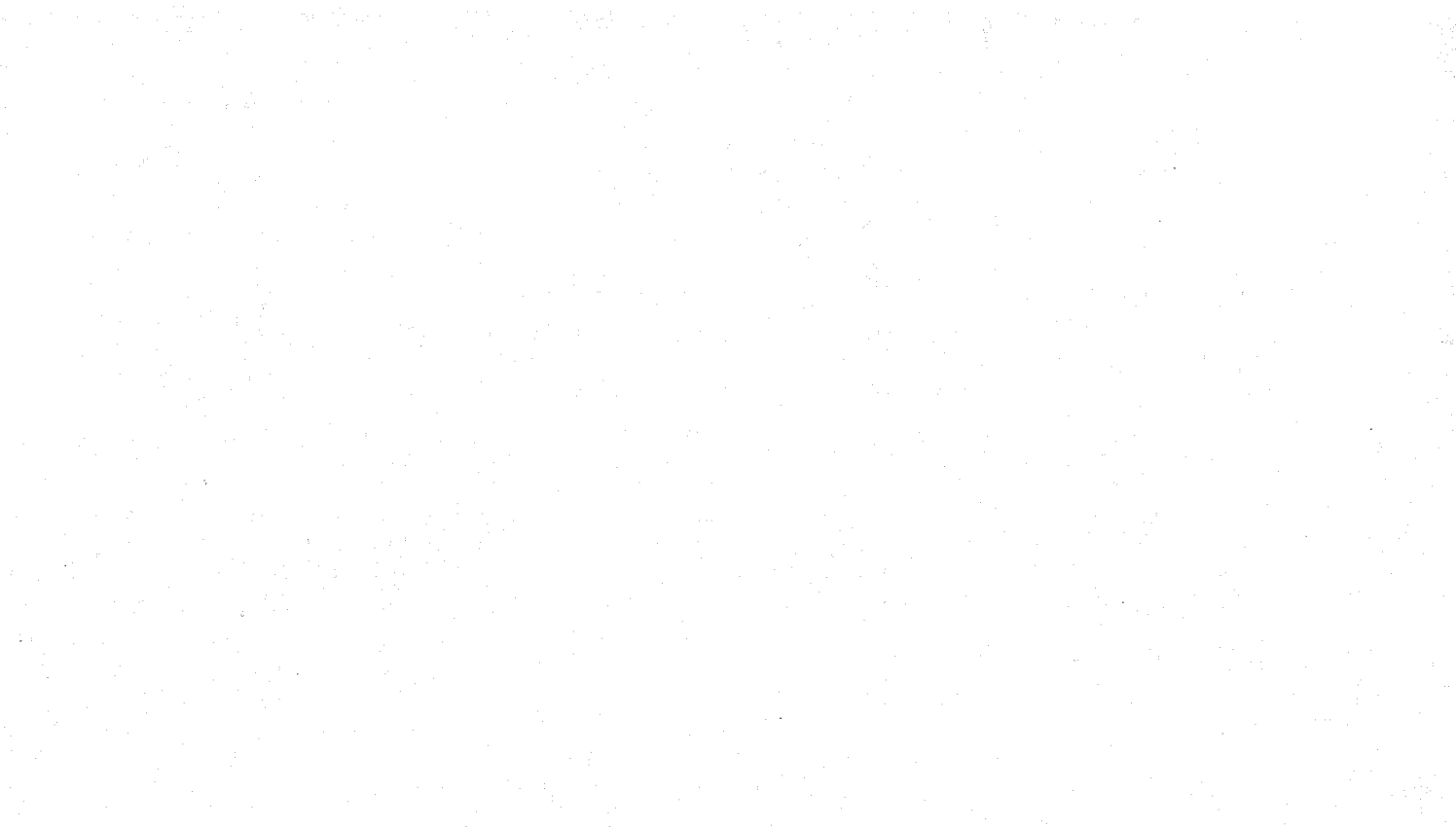
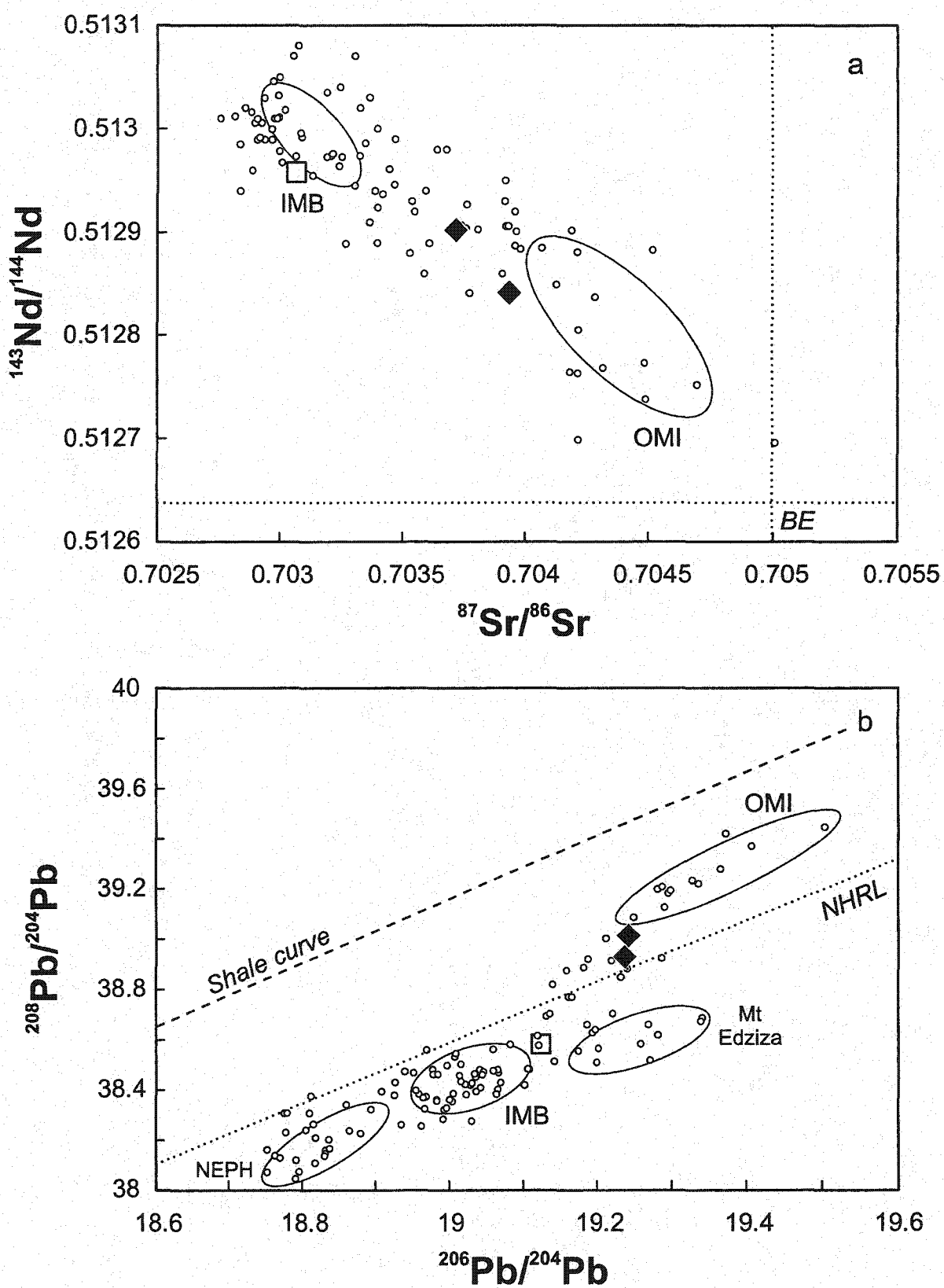


Figure 11.5: a) $^{143}\text{Nd}/^{144}\text{Nd}$ versus $^{87}\text{Sr}/^{86}\text{Sr}$ and b) $^{208}\text{Pb}/^{204}\text{Pb}$ versus $^{206}\text{Pb}/^{204}\text{Pb}$ for Nome Cone basalts. Large symbols as in Fig.11.2. Fields, small circles and explanations as in Fig. 2.3.



Hy-NORM basalts erupted in the Intermontane Belt, except for significantly lower Ba contents.

The AOB sample is distinctly less radiogenic in Sr, Pb, but more radiogenic in Nd isotopic ratios than the Hy-NORM lavas (Fig. 11.5). In Sr-Nd and Pb-Pb isotopic plots, the AOB sample falls within the range of primitive Hy-NORM lavas of the Intermontane Belt, whereas the Hy-NORM samples trend towards the field of primitive Hy-NORM lavas of the Omineca Belt (Fig. 11.5).

4.11. Little Rancheria (59.72°N, 130.38°W; NTS 104-O/9)

The Little Rancheria centre is located in the Cassiar Batholith of the Omineca Belt (Fig. 1.2). Once again, the presence of boulder erratics on its summit indicates that the volcanic centre cannot be younger than Pleistocene. This centre is a tuya that appears to have erupted two successive sequences (Fig. 12.2), each comprised of a base of pillow lava (\pm hyaloclastic tuff) erupted in a subglacial environment, and a top of massive lava flows erupted in a subaerial environment (Fig. 12.1). The total volume of Little Rancheria is estimated to be about 2 km³.

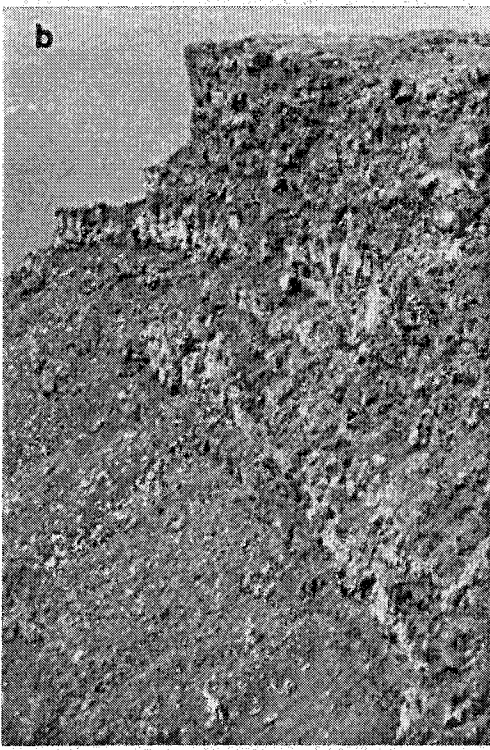
The Little Rancheria lavas are more evolved than those of the other centers of the Stikine Volcanic Belt, with the highest MgO content being approximately 7 wt.% (Fig. 12.3). They range from AOB to Hy-NORM basalts that exhibit a range in SiO₂ and TiO₂ (Fig. 12.3). The trace element patterns of the Little Rancheria basalts are characterized by an enrichment in LILE and LREE compared to HREE, when normalized to primitive

Figure 12.1: a) Northern side of Little Rancheria, walking on the lava tops. b) Long distance view of the lava flows forming the top of the tuya. c) Closer view of two different lava flows.

a



b



c





Figure 12.2: Stratigraphic column of Little Rancheria indicating the position of each analyzed sample. Symbols: squares = AOB; diamonds = Hy-NORM basalts. Bold sample labels correspond to samples that have been isotopically studied. Data in table B-11 of appendix B.

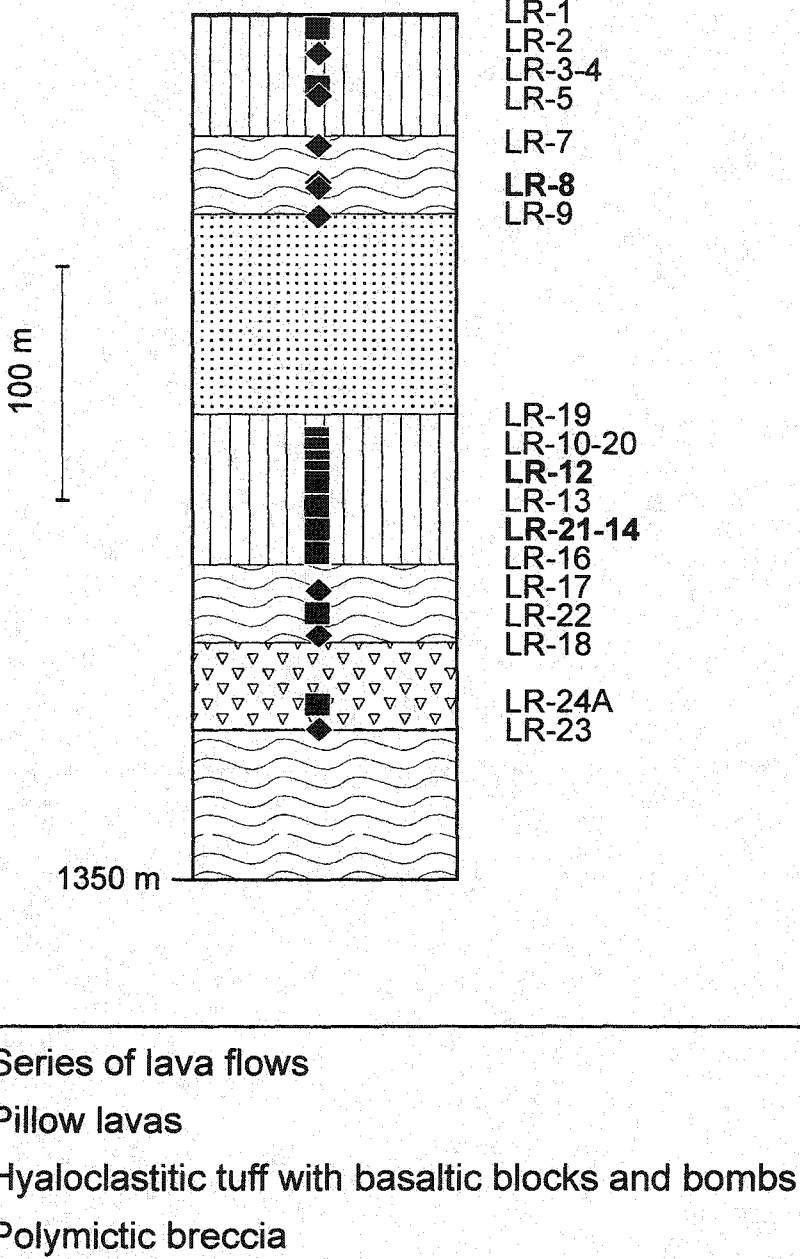


Figure 12.3: a) SiO_2 , b) TiO_2 , c) CaO , and d) Al_2O_3 versus MgO in wt.% for Little Rancheria basalts. Symbols as in Fig. 12.2

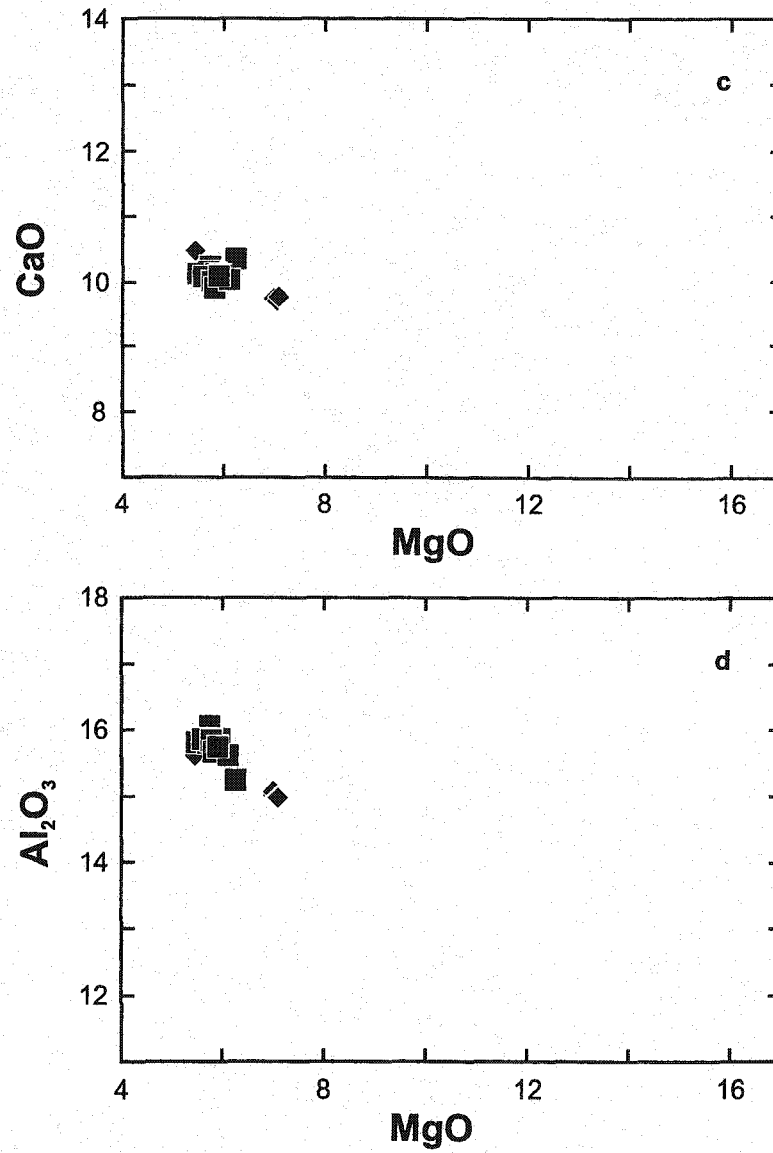
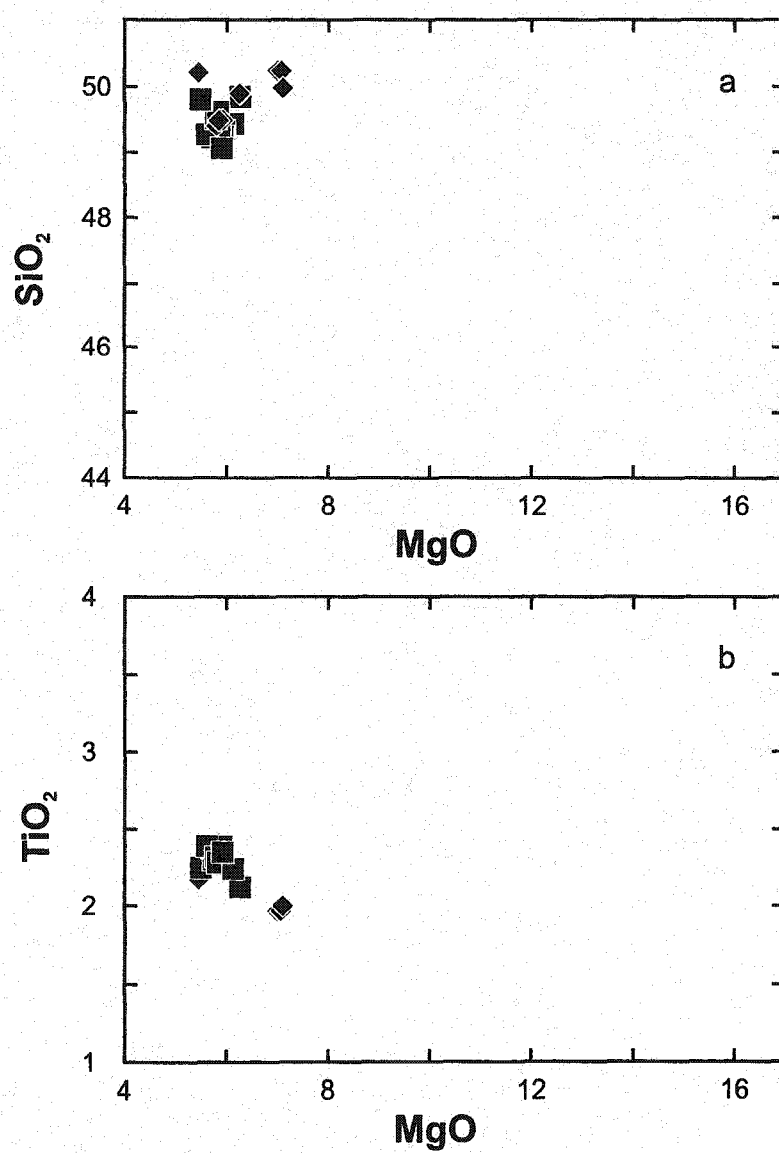


Figure 12.4: Trace element patterns of Little Rancheria basalts normalized to the primitive mantle values of Sun and McDonough (1989). Same symbols as Fig. 11.2. Shaded field as in Fig. 2.2.a.



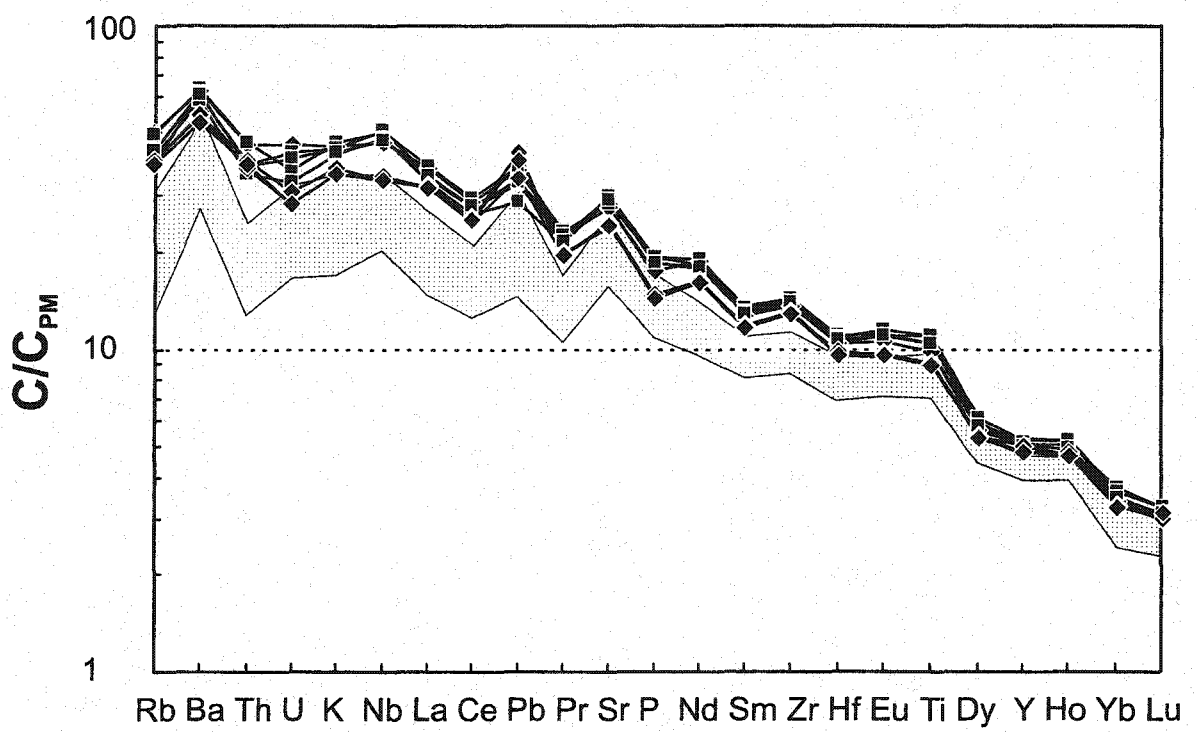
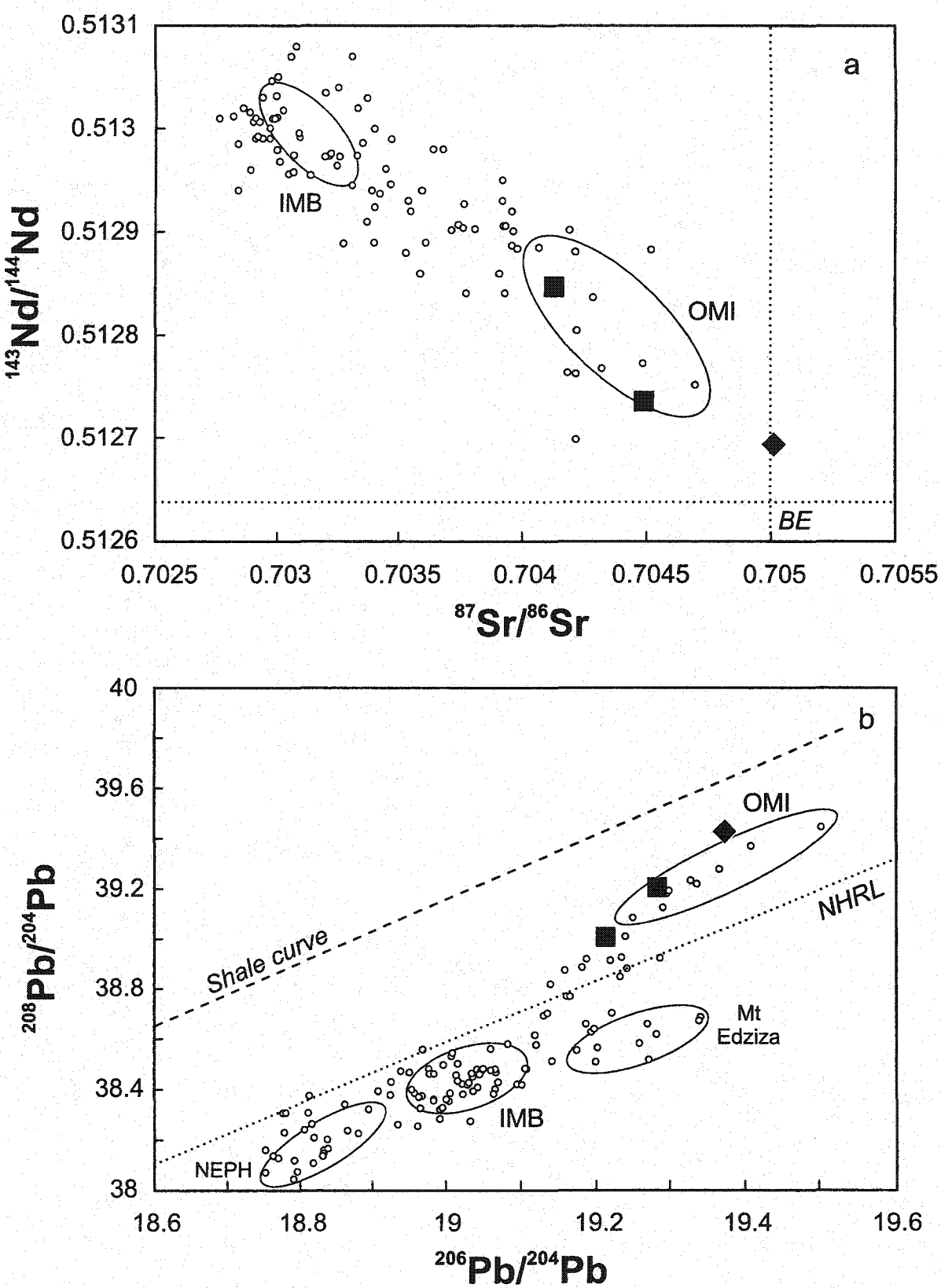


Figure 12.5: a) $^{143}\text{Nd}/^{144}\text{Nd}$ versus $^{87}\text{Sr}/^{86}\text{Sr}$ and b) $^{208}\text{Pb}/^{204}\text{Pb}$ versus $^{206}\text{Pb}/^{204}\text{Pb}$ for Little Rancheria basalts. Large symbols as in Fig.12.2. Fields, small circles and explanations as in Fig. 2.3.



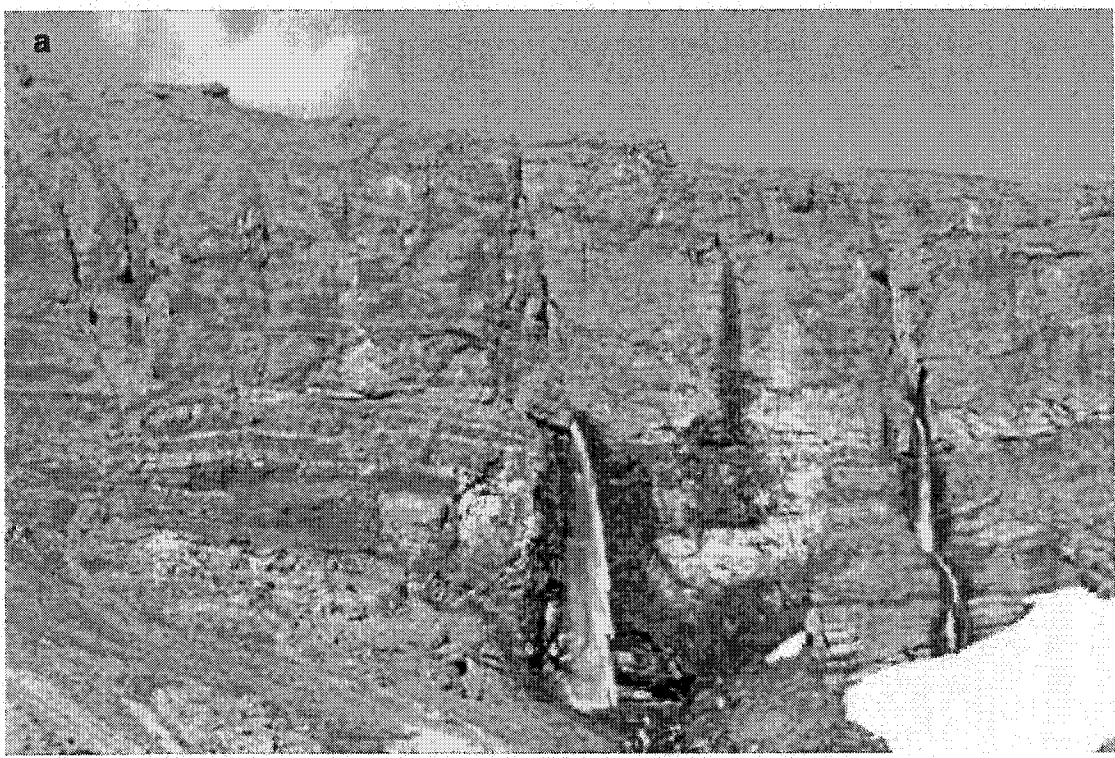
mantle, and positive Sr and Pb anomalies compared to elements with similar compatibilities (Fig. 12.4). The Little Rancheria lavas are more enriched in incompatible trace elements than primitive Hy-NORM basalts from the Intermontane Belt, but they have similar trace element patterns. The less evolved Hy-NORM basalts that erupted in the upper pillow lava sequence (LR-7-8-9 in Fig. 12.2) have lower Nb and higher Pb concentrations than the more evolved AOB and Hy-NORM basalts (Fig. 12.4; Table B-11 of appendix B).

The Little Rancheria basalts have radiogenic Sr and Pb, and unradiogenic Nd isotopic ratios compared to primitive basalts from the Intermontane Belt, similar to those of primitive basalts of the Omineca Belt (Fig. 12.5). They display the largest ranges in isotopic composition observed in the Stikine Volcanic Belt, despite their restricted compositional range (Fig. 12.5), with their Pb isotopic composition trending towards the shale curve of Godwin and Sinclair (1982). The Hy-NORM basalt analyzed isotopically is more radiogenic in Sr and Pb, and less radiogenic in Nd than the AOB samples.

4.12. Blue River (59.30°N, 130.25°W; NTS 104-O/8)

The Blue River centre erupted through the Cassiar Batholith, to the east of the Cassiar fault in the Omineca Belt (Fig. 1.2). It has not been dated, but likely erupted in Pleistocene to Quaternary (Gabrielse, 1969). The Blue River centre is a tuya that can be divided in two parts in terms of volcanic style and lava type (Fig. 13.2). The base consists of pillow lava (~ 100 m), followed by a succession of lapilli tuff layers and pillow lava of more than 200 m in thickness (Fig. 13.1.a). The upper part begins with 100

Figure 13.1: a) Pyroclastic tuff in the middle of Blue River volcanic centre. b) Lava flows at the top of the tuya. c) Giant steps belonging certainly to a lava lake formed to the south.



m of massive lava flows overlain by a thick breccia of more than 200 m in thickness, and capped by approximately 100 m of small massive lava flows (Fig. 13.1.b). The total volume of Blue River is estimated to be about 4 km³.

The Blue River lavas are relatively primitive, ranging from 7 to 9.5 wt.% MgO (Fig. 13.3). They can be divided into two stratigraphically separated groups, that define distinct olivine-control lines in plots of SiO₂ and TiO₂ versus MgO (Fig. 13.3.a and b).

One group consists of Hy-NORM basalts that occur in the lowest part of the Blue River volcanic centre, whereas the other consists of AOB and Hy-NORM basalts from the upper part of the centre (Fig. 13.2). Both groups have incompatible trace element patterns characterized by an enrichment in LILE and LREE compared to HREE, when normalized to primitive mantle, and small positive Sr and large positive Pb anomalies compared to elements with similar compatibilities (Fig. 13.4). The Hy-NORM basalts from the base differs from the other basalts from the upper part of the centre, however, in having lower incompatible trace element concentrations and no negative Th and Rb anomalies. Compared to primitive Hy-NORM basalts of the Intermontane Belt, Hy-NORM basalts from the base of the centre have smaller positive Sr anomalies, larger positive Pb anomalies, smaller negative Th and Rb anomalies, and no negative K and U anomalies (Fig. 13.4).

Blue River lavas have relatively radiogenic Sr and Pb, and unradiogenic Nd isotopic signatures compared to basalts of the Intermontane Belt, and they trend towards the shale curve in a Pb-Pb diagram (Fig. 13.5). The Hy-NORM basalt from the base of Blue River has a more radiogenic Sr and Pb isotopic ratio than the Hy-NORM basalt from the upper

Figure 13.2: Stratigraphic column of Blue River indicating the position of each analyzed sample. Symbols: square = AOB; diamonds = Hy-NORM basalts. Data in table B-12 of appendix B.

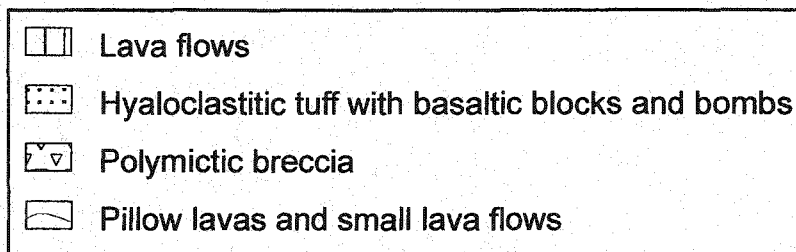
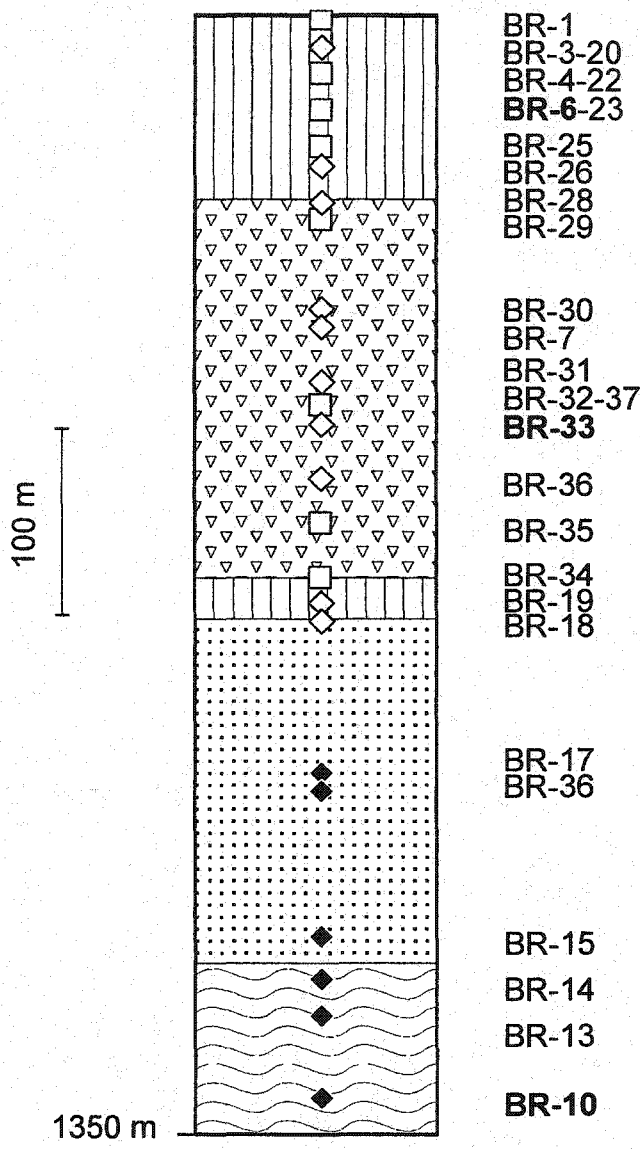


Figure 13.3: a) SiO_2 , b) TiO_2 , c) CaO , and d) Al_2O_3 versus MgO in wt.% for Blue River basalts. The arrow corresponds to the trend expected for olivine + clinopyroxene fractionation from sample BR-22.

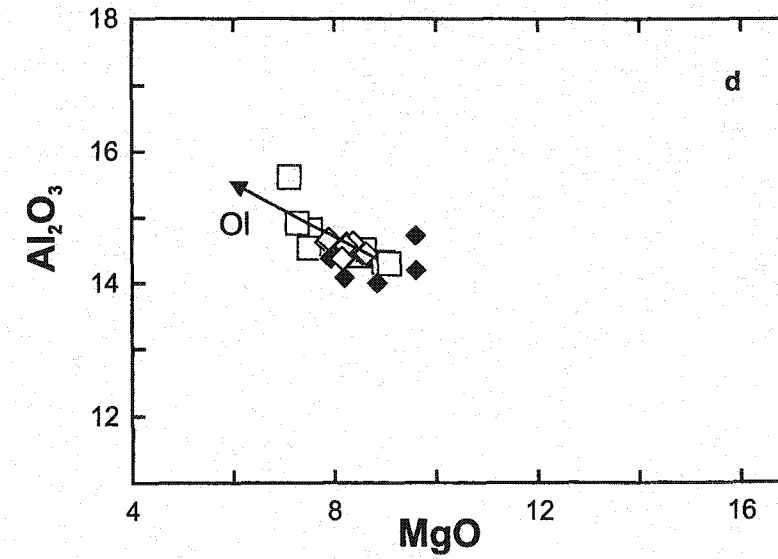
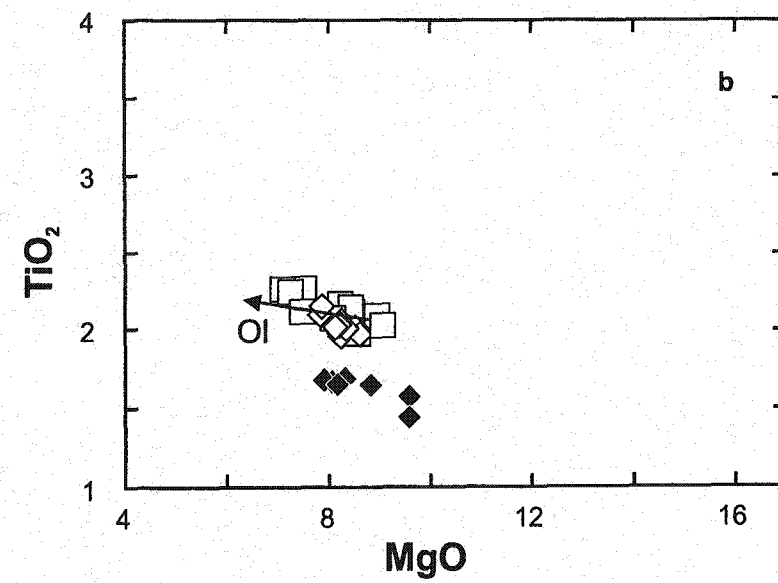
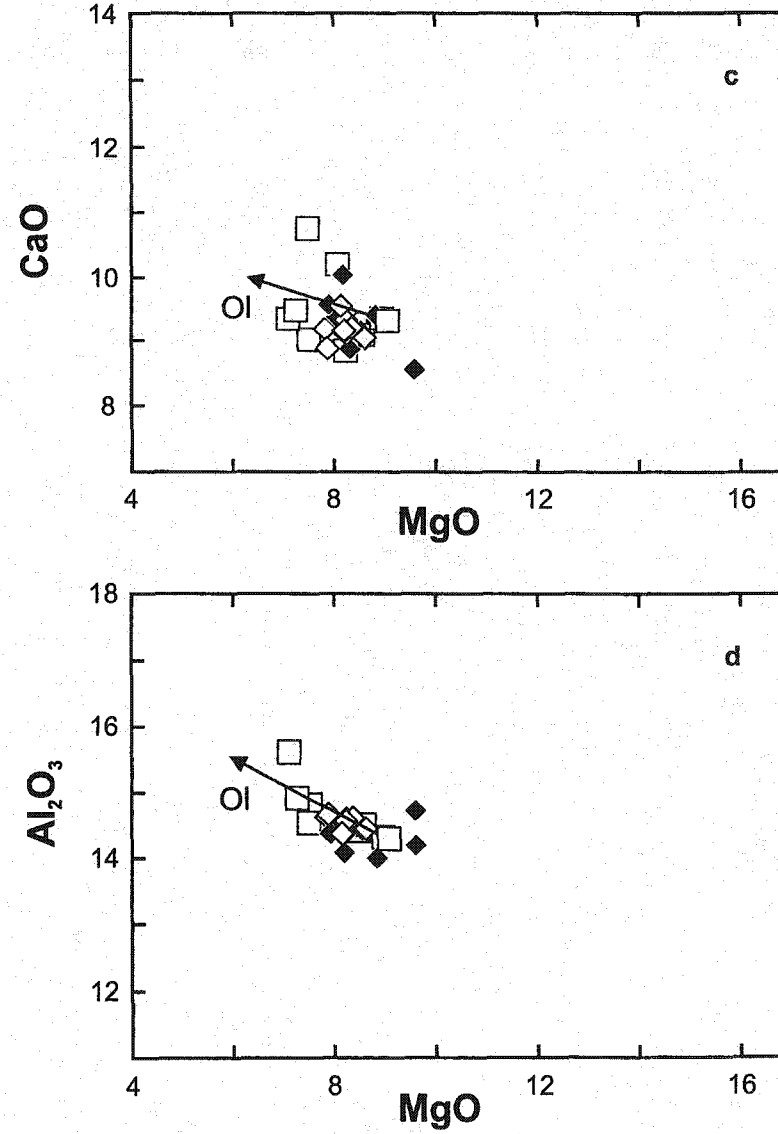
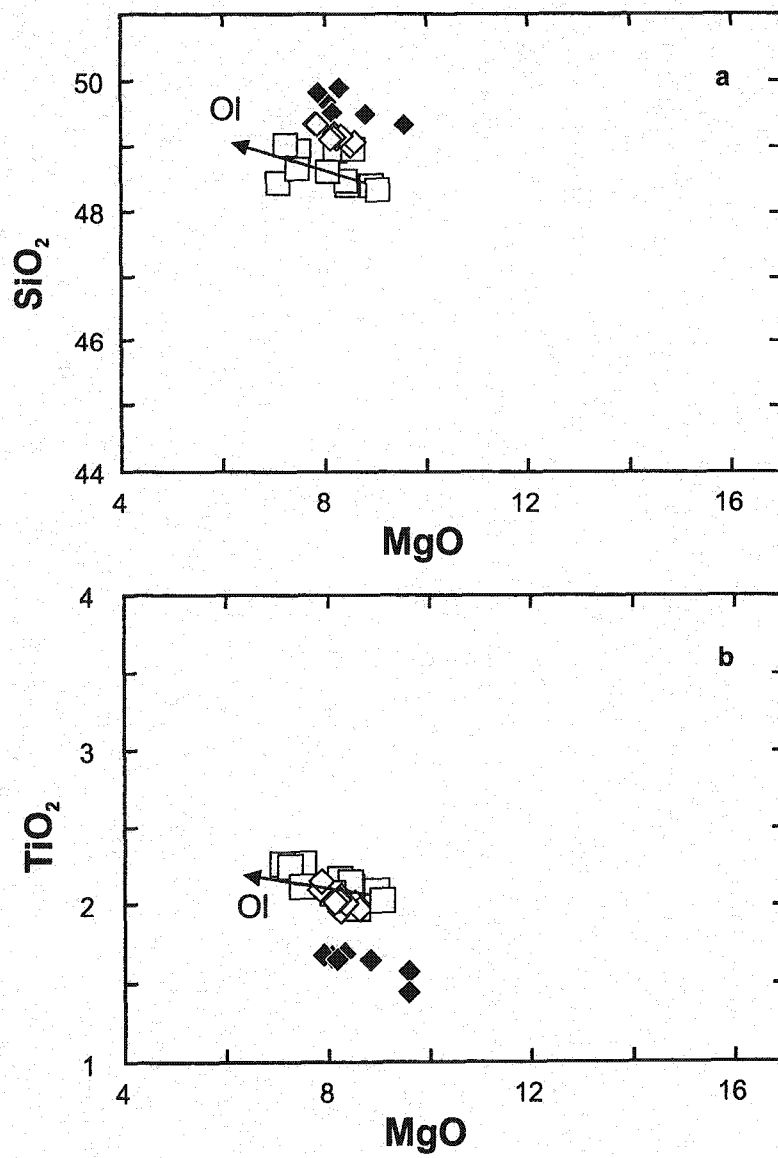


Figure 13.4: Trace element patterns of Blue River basalts normalized to the primitive mantle values of Sun and McDonough (1989). Same symbols as Fig. 13.2. Shaded field as in Fig. 2.2.a.

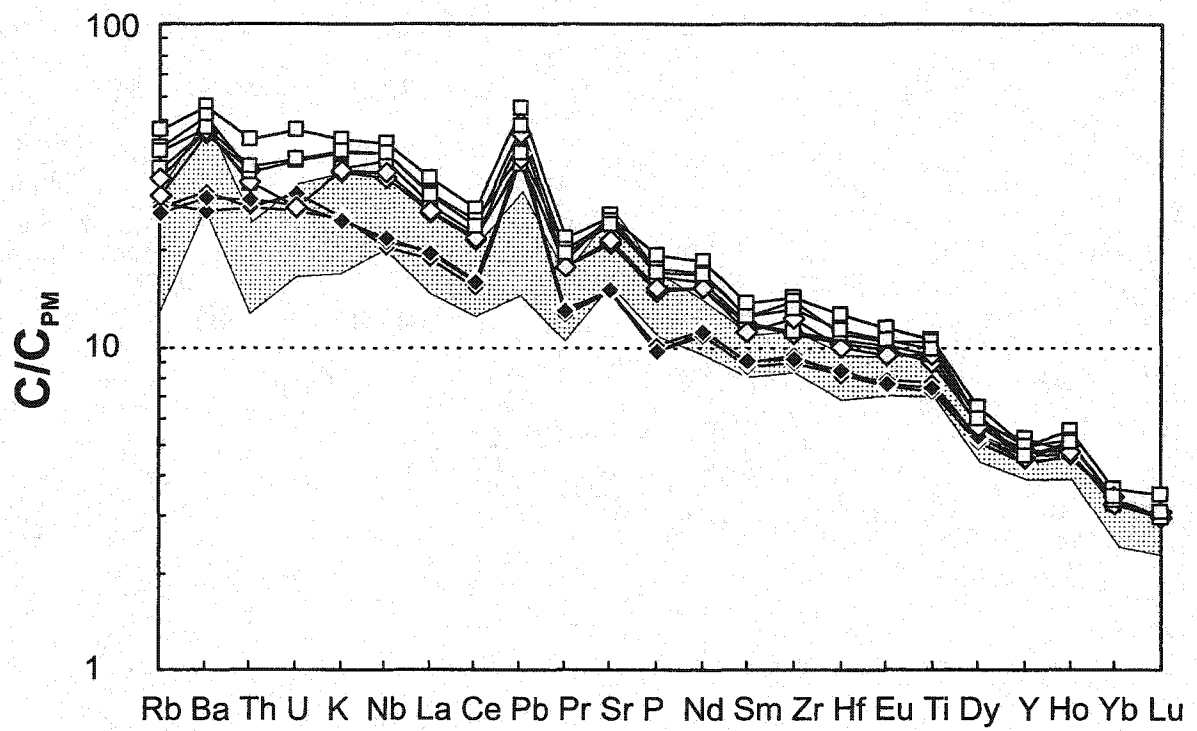
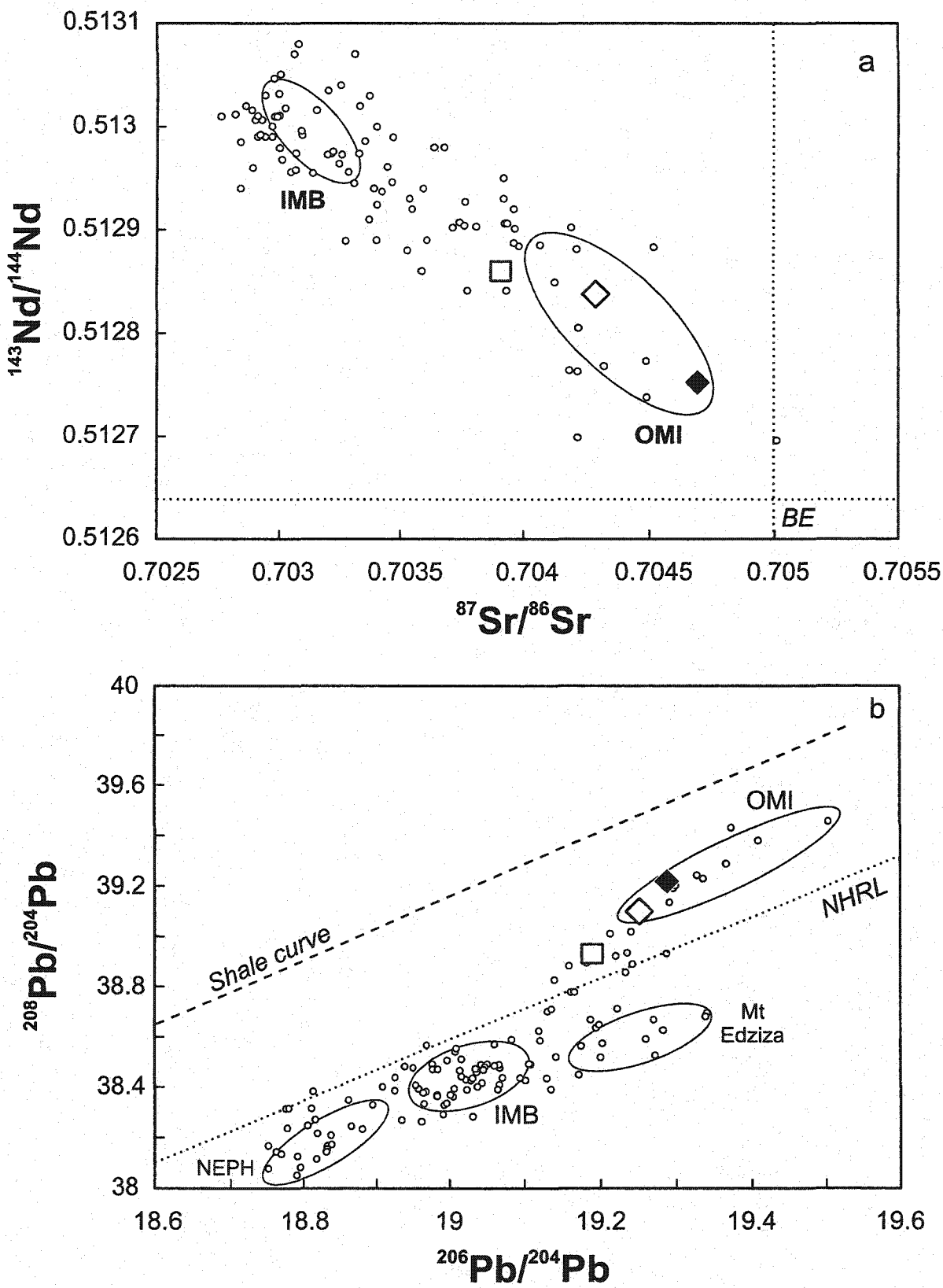


Figure 13.5: a) $^{143}\text{Nd}/^{144}\text{Nd}$ versus $^{87}\text{Sr}/^{86}\text{Sr}$ and b) $^{208}\text{Pb}/^{204}\text{Pb}$ versus $^{206}\text{Pb}/^{204}\text{Pb}$ for Blue River basalts. Large symbols as in Fig.13.2. Fields, small circles and explanations as in Fig. 2.3.



part despite its higher MgO content (Table B-12 of appendix B), but they both have more radiogenic Sr and Pb isotopic ratios than the AOB sample.

4.13. Caribou Tuya (59.16N, 130.16W; map 104-O/8)

Caribou Tuya is located in the Cassiar Batholith (Fig. 1.2), to the north of Blue River, in the Omineca Belt. It has not been precisely dated, but likely erupted in the Pleistocene to Quaternary (Gabrielse, 1969). It is a small tuya of less than 2 km³ of lavas that can be divided into three parts in terms of eruption style (Fig. 14.2). The base consists of a series of small lava flows, with a few layers of breccia and pillow lava. The middle consists of a thick (100 m) breccia unit, with fragments of small pillow lava (Fig. 14.1.b), capped by thick lava flows (>5 m). Finally, the upper part consists of a 50 m succession of thin lava flows forming the top of the tuya.

The Caribou Tuya lavas exhibit a limited range in MgO, between 6 and 8 wt.% (Fig. 14.3). They are all Hy-NORM basalts and relatively homogeneous in term of their major elements (Fig. 14.3). Their trace element patterns are characterized by a general enrichment in LILE and LREE compared to HREE, when normalized to primitive mantle, and positive Sr and Pb anomalies compared to elements with similar compatibilities (Fig. 14.4). The most primitive lavas at Caribou Tuya have similar trace element patterns to primitive Hy-NORM basalts of the Intermontane Belt, except for a lack of K, Th, U and Rb negative anomalies. They also lack the positive Nb anomalies compared to La of most Cordilleran alkaline basalts.

Figure 14.1: a) Long distance view of Caribou Tuya, a typical tuya erupted in the Cassiar Batholith. b) Sampling the pillow lavas forming the lower part of the tuya.



b



Figure 14.2: Stratigraphic column of Caribou Tuya indicating the position of each analyzed sample. Symbols: diamonds = Hy-NORM basalts. Data in table B-13 of appendix B.

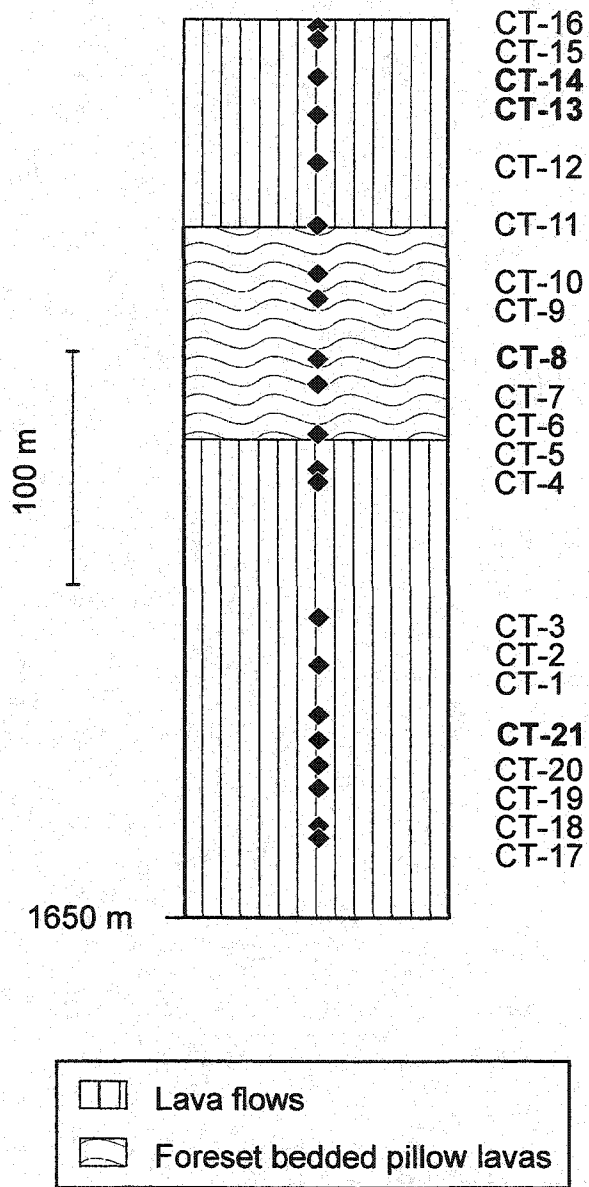




Figure 14.3: a) SiO_2 , b) TiO_2 , c) CaO , and d) Al_2O_3 versus MgO in wt.% for Caribou Tuya basalts. The arrow corresponds to the trend expected for olivine fractionation from sample CT-13.

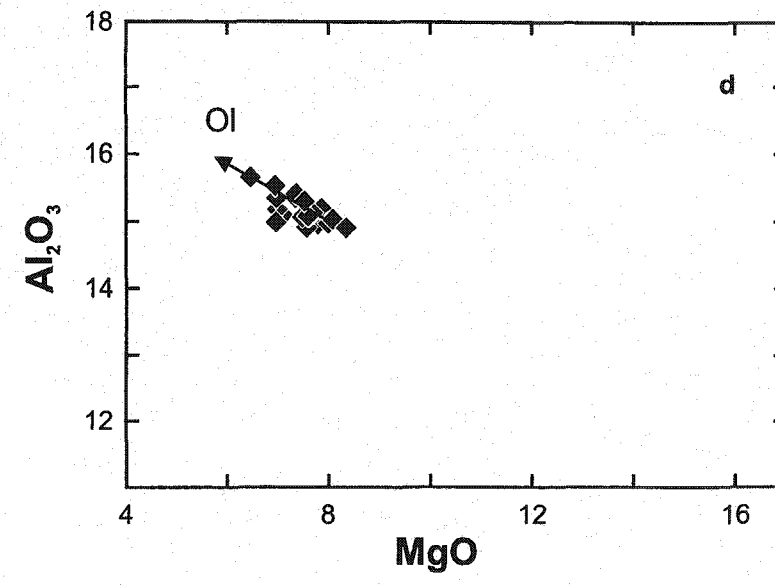
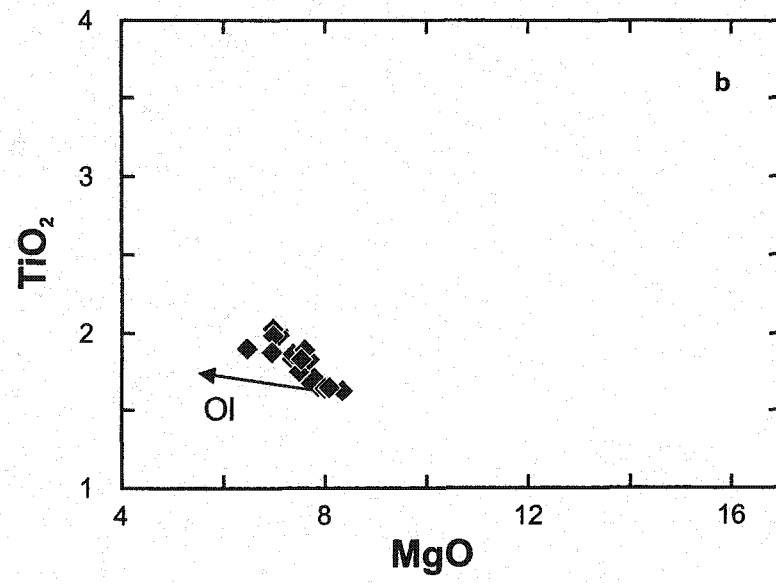
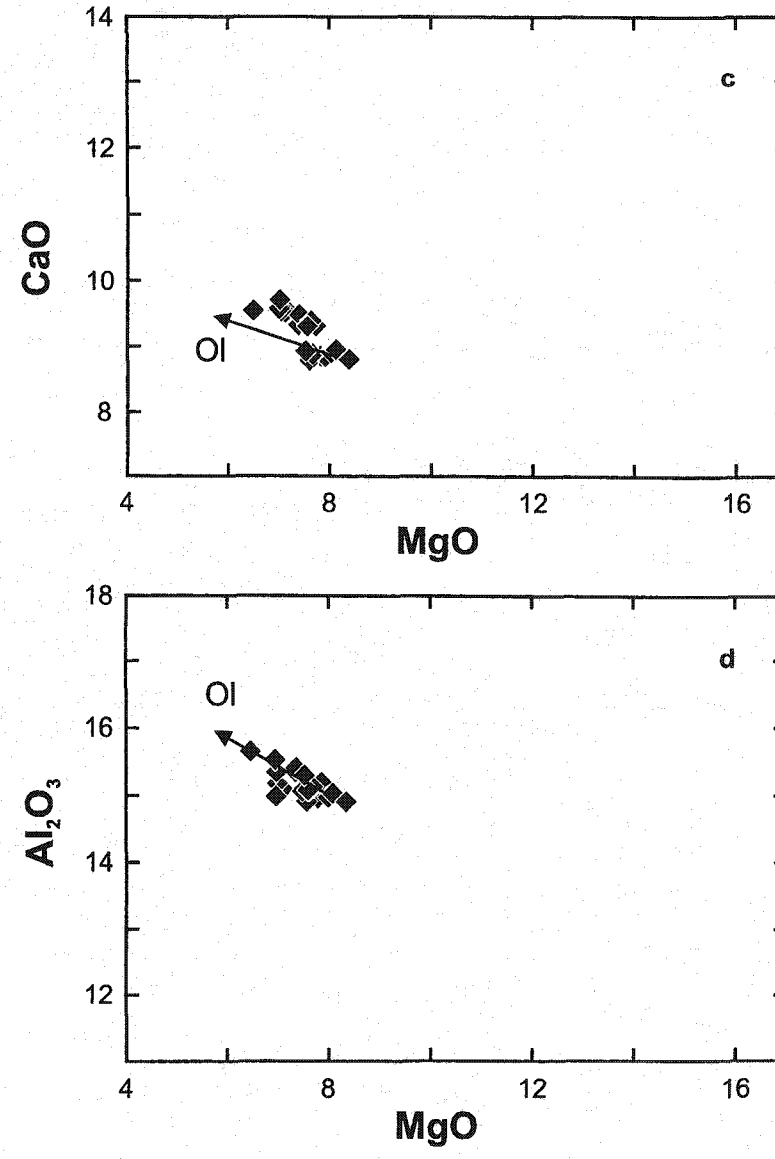
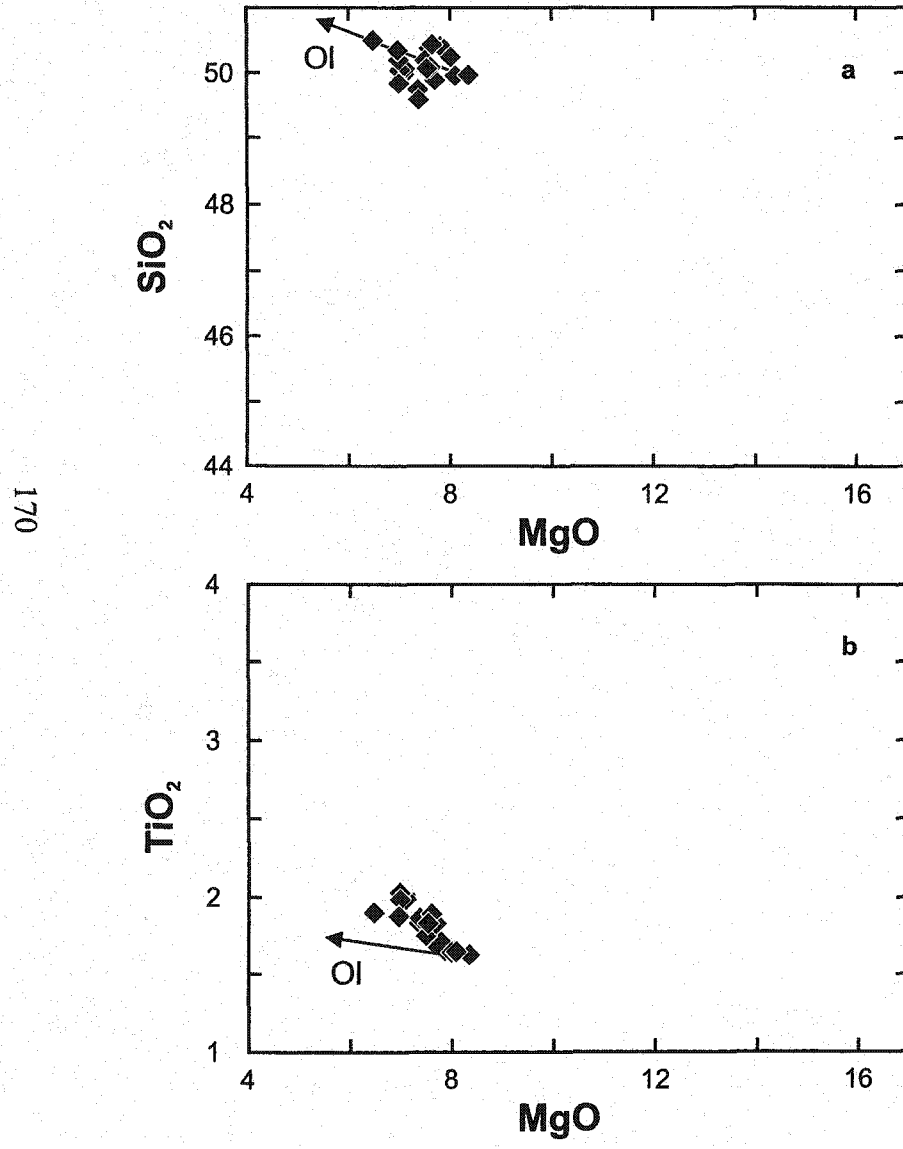


Figure 14.4: Trace element patterns of Caribou Tuya basalts normalized to the primitive mantle values of Sun and McDonough (1989). Same symbols as Fig. 14.2. Shaded field as in Fig. 12.2.a.

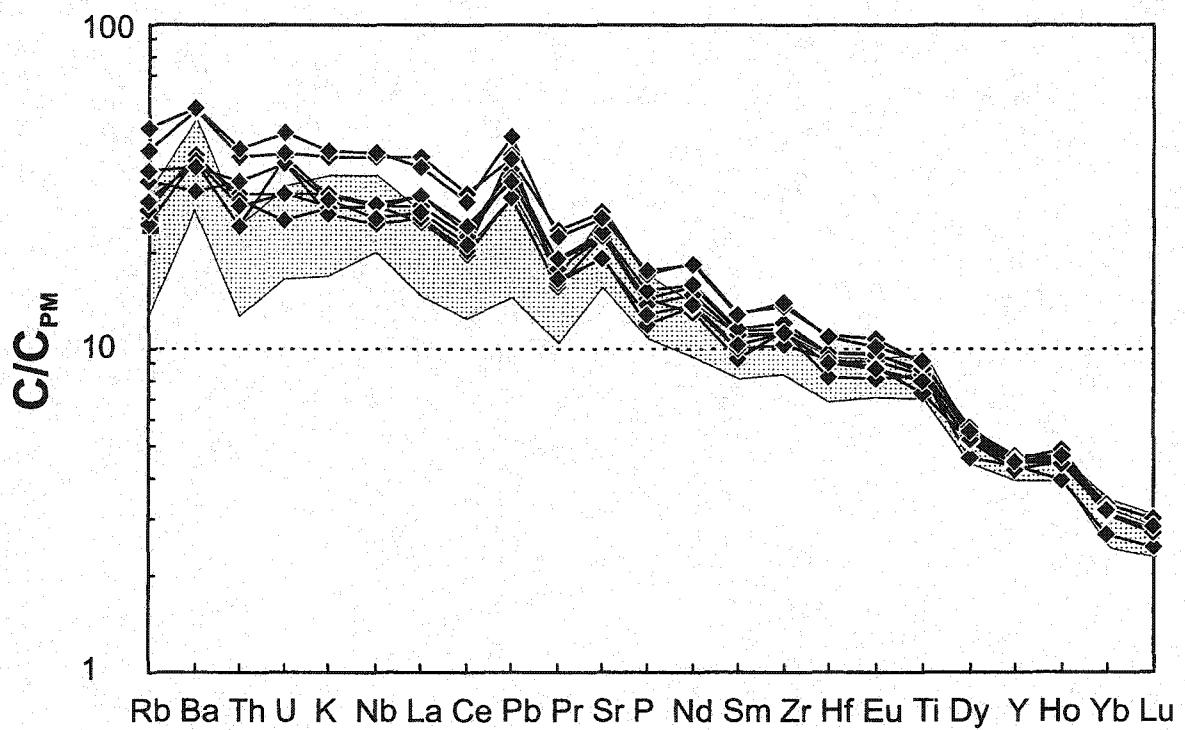
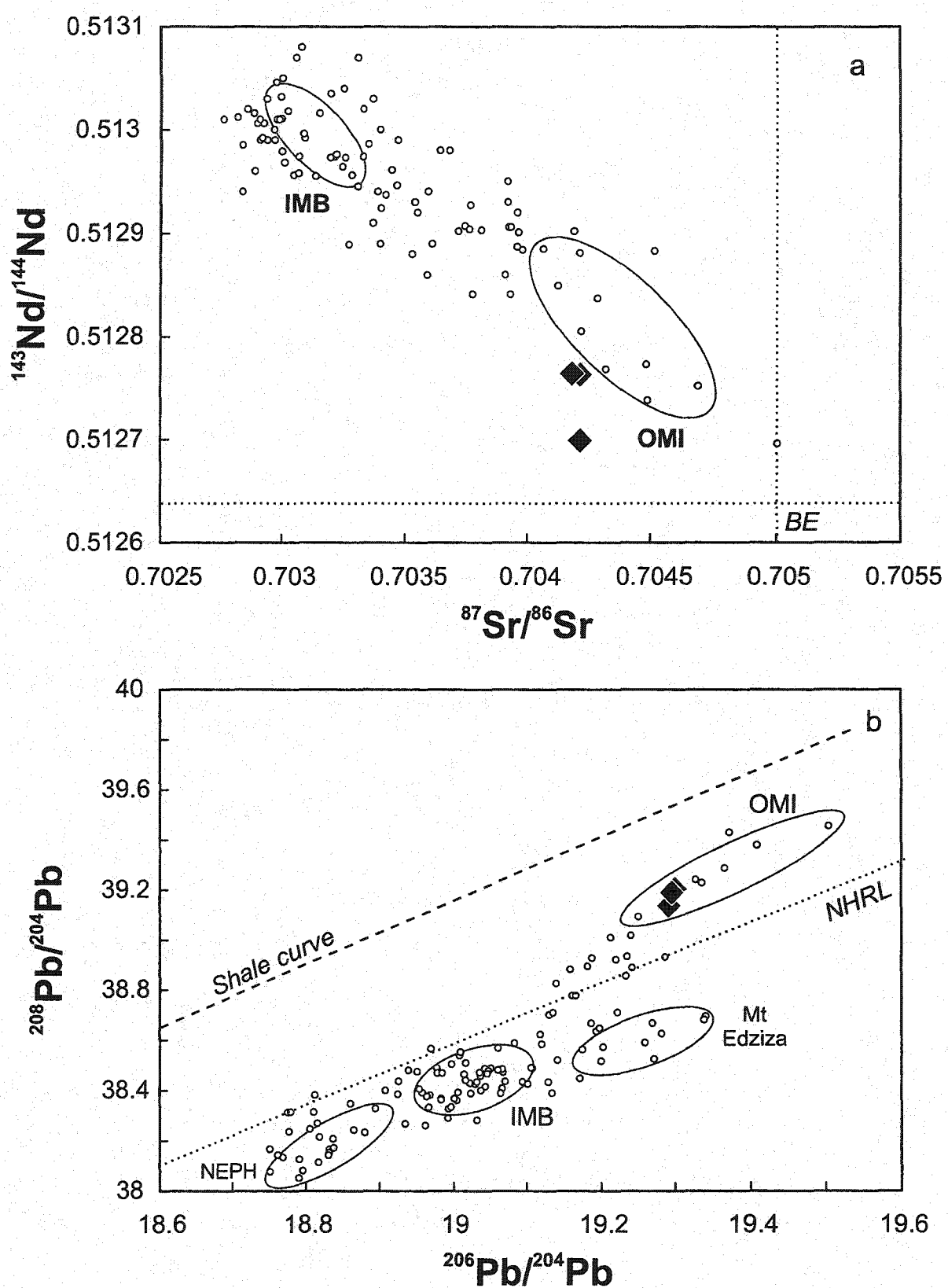




Figure 14.5: a) $^{143}\text{Nd}/^{144}\text{Nd}$ versus $^{87}\text{Sr}/^{86}\text{Sr}$ and b) $^{208}\text{Pb}/^{204}\text{Pb}$ versus $^{206}\text{Pb}/^{204}\text{Pb}$ for Caribou Tuya basalts. Large symbols as in Fig.14.2. Fields, small circles and explanations as in Fig. 2.3.



The Hy-NORM lavas at Caribou Tuya are isotopically homogeneous, having both radiogenic Sr and Pb, and unradiogenic Nd isotopic ratios, with values similar to those of high-MgO Hy-NORM basalts of the Omineca Belt (Fig. 14.5).

4.14. Rancheria area

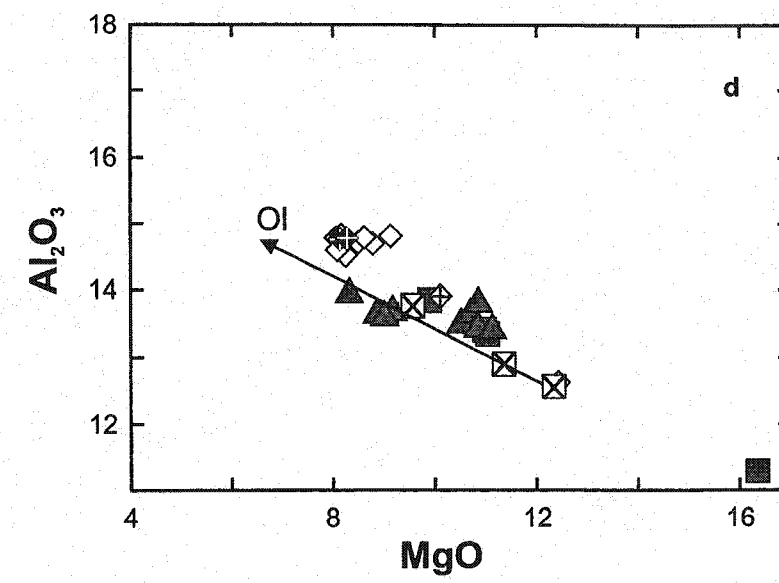
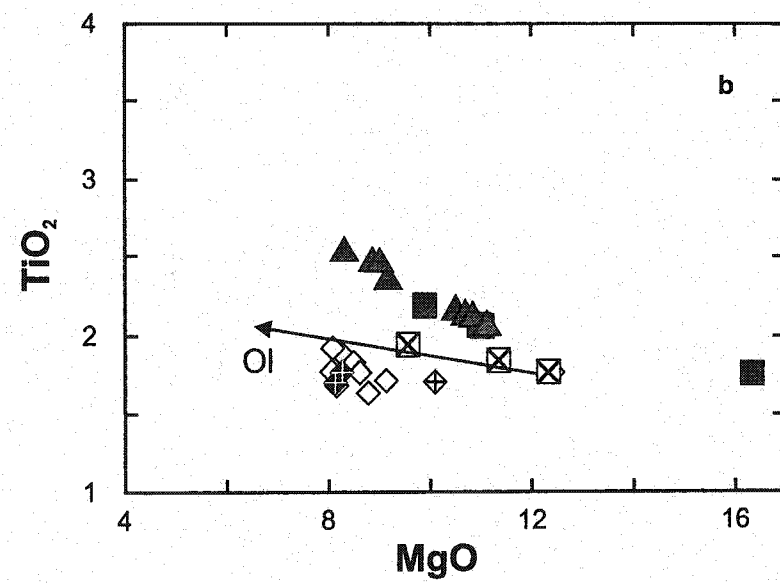
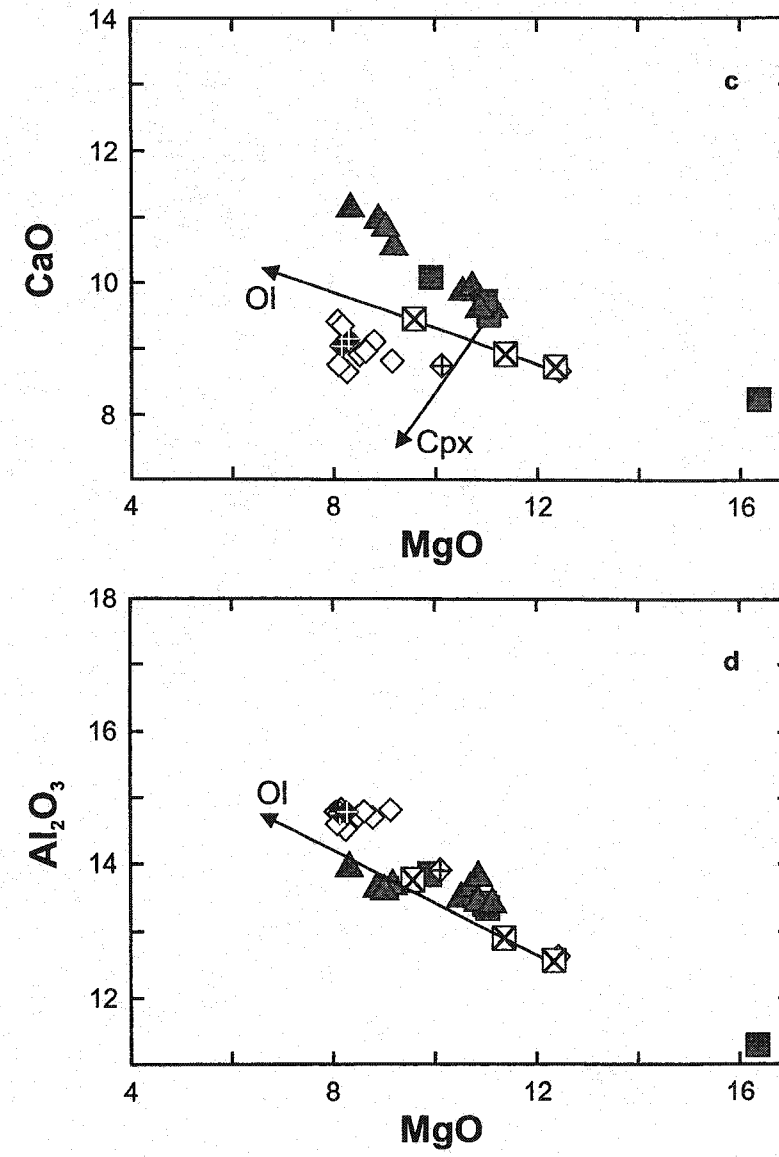
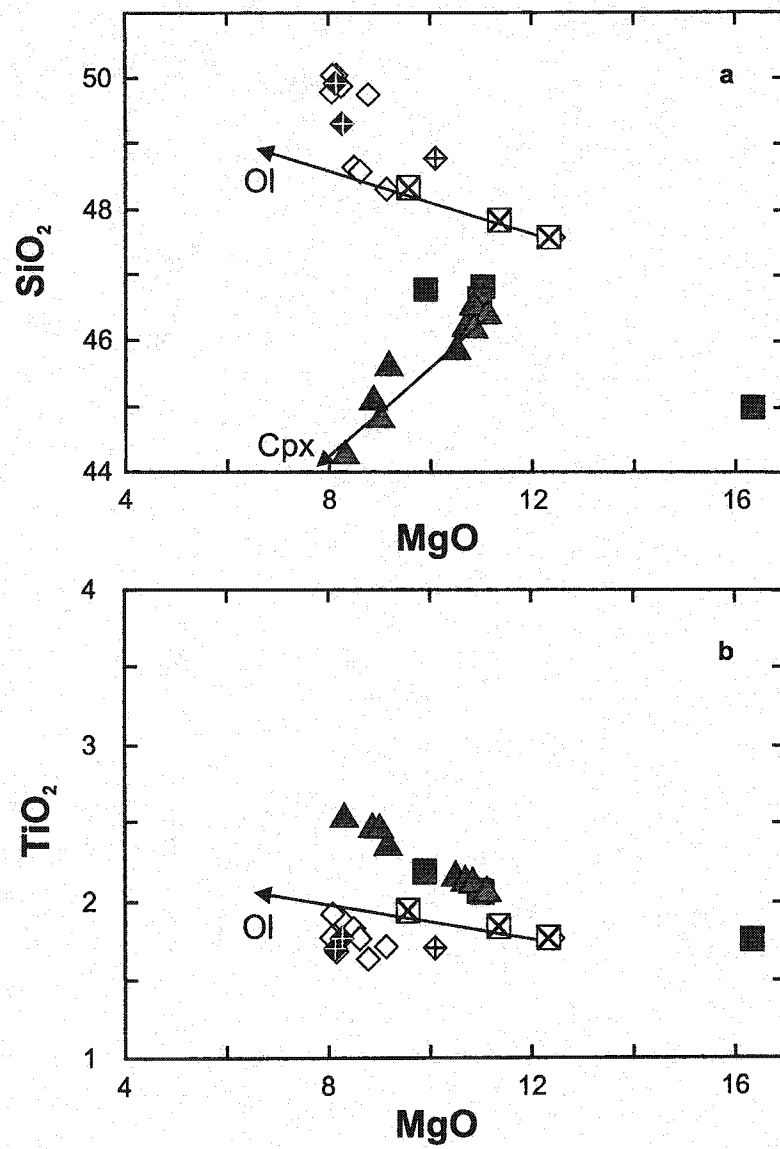
Erosional remnants of Quaternary alkaline basalts continue along a west-east trend across the Omineca Belt in the southern Yukon (Fig. 1.2). They overlie a variety of rock types, ranging from Carboniferous chert and clastics of the Dorsey terrane (Swan Lake; Fig. 1.2), Mesozoic to Cenozoic granodiorite plutons of the Cassiar Batholith (Rancheria River; Fig. 1.2), Upper Proterozoic to Upper Triassic sediments of the Cassiar Terrane (Big Creek; Fig. 1.2), and Proterozoic to Triassic metamorphic rocks of the Yukon Tanana pericratonic terrane (Liard River; Fig. 1.2). The volcanism in this area is characterized by flat-lying massive valley-filling flows (Hasik, 1994), in contrast to the cones and tuyas of the southern Stikine Volcanic Belt. The numerous erosional remnants sampled in the Rancheria area, and studied petrographically and chemically by Hasik (1994), have been grouped into four locations: Swan Lake, Rancheria River, Big Creek, and Liard River (Fig. 1.2). Representative samples for each locality have been studied isotopically in this study (Table B-14 of appendix B).

The two samples from Swan Lake are Hy-NORM basalts, with high SiO₂, and low TiO₂ and CaO compared to AOB and BASAN from the Rancheria area (Fig. 15.1). The Swan Lake sample analyzed for trace element and isotopic composition exhibits a trace element pattern similar to high-MgO Hy-NORM basalts of the Intermontane Belt, except

for a lack of negative Th and positive Nb anomalies when normalized to primitive mantle (Fig. 15.2). The Swan Lake Hy-NORM basalt has more radiogenic Sr and Pb, but less radiogenic Nd isotopic ratios than primitive Hy-NORM basalts of the Intermontane Belt, and fall within the field of primitive Hy-NORM basalts of the Omineca Belt.

The lavas erupted along the Rancheria River range from AOB to BASAN (Table B-14 of appendix B). One sample, RA-3, might be considered a NEPH because of its high normative Ne content (16.8 wt.%), but feldspar is present in its groundmass, and RA-3 has thus been classified as a BASAN. The Rancheria River samples are relatively primitive, ranging from 8 to 16 wt.% MgO (Fig. 15.1). Although the AOB lavas along the Rancheria River appear to lie along an olivine-control line in a SiO₂ versus MgO diagram (Fig. 15.1), the positive trend of the BASAN lavas from Rancheria River requires the existence of another process. This trend cannot have been produced by fractionation of clinopyroxene because of the negative trends displayed by all the lavas in the CaO versus MgO diagram (Fig. 15.1.c), but might represent a range in alkalinity of parental magmas. The BASAN and AOB along the Rancheria River have trace element patterns characterized by an enrichment in LILE and LREE compared to HREE, when normalized to primitive mantle, and positive Sr, Pb and negative Th and Rb anomalies compared to elements with similar compatibilities (Fig. 15.2.a). They are more enriched in LILE and LREE than primitive Hy-NORM basalts, but have similar HREE contents. The Rancheria River AOB and BASAN lavas have radiogenic Sr and Pb, and unradiogenic Nd isotopic ratios compared to primitive Hy-NORM basalts of the Intermontane Belt, except for the most Si-undersaturated BASAN lava that has less radiogenic Sr and Pb, and more radiogenic Nd isotopic ratios than coexisting BASAN and

Figure 15.1: a) SiO_2 , b) TiO_2 , c) CaO , and d) Al_2O_3 versus MgO in wt.% for Rancheria areas basalts. Symbols: diamonds = Hy-NORM basalts; squares = AOB; triangle = BASAN. Crossed black symbols correspond to Swan Lake samples, grey symbols to Rancheria River samples, crossed white symbols to Big Creek samples, and white symbols to Liard River samples. The arrows correspond to the trend expected for olivine fractionation from sample RA-18 and clinopyroxene fractionation from sample RA-6.



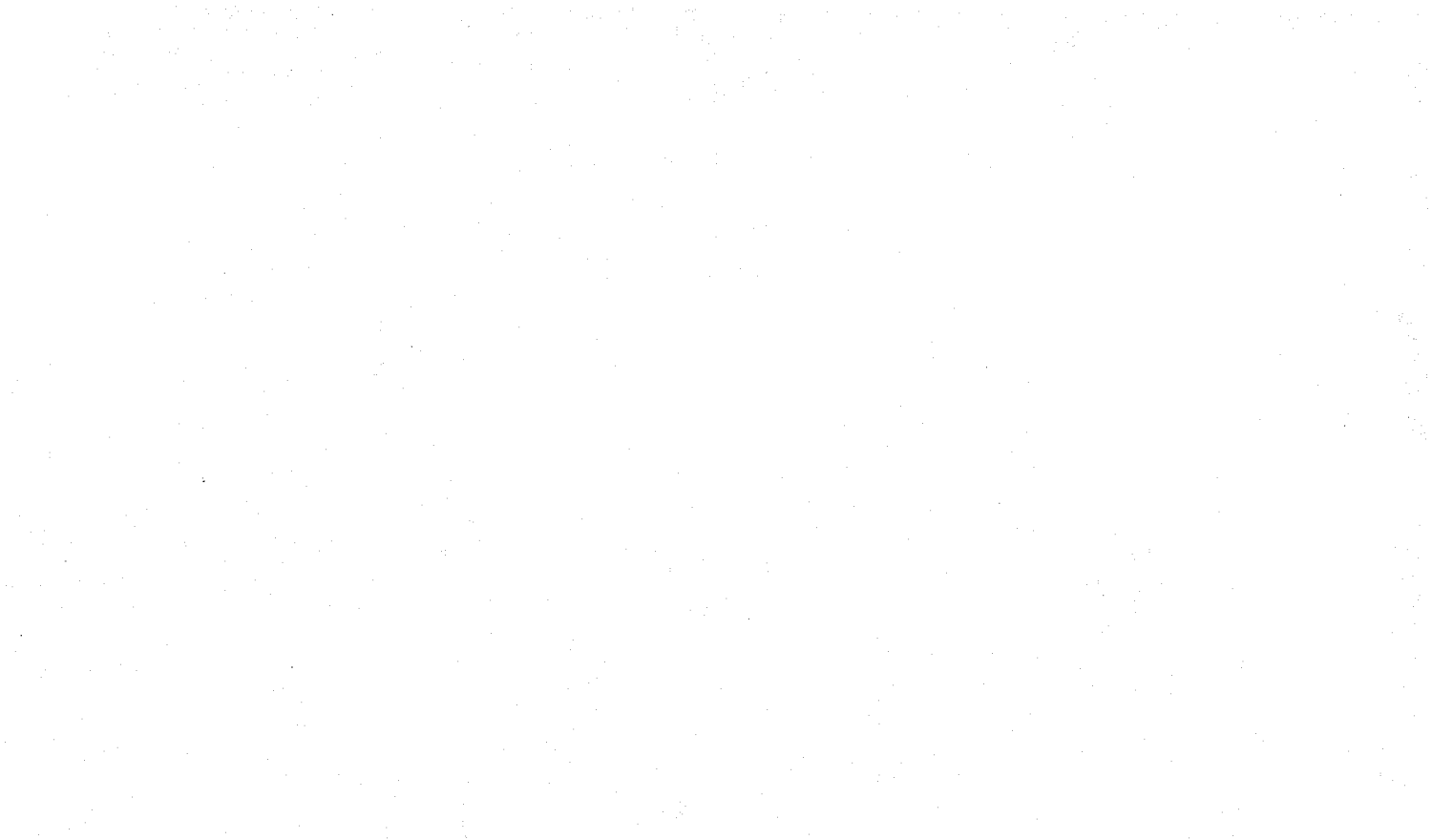


Figure 15.2: Trace element patterns normalized to the primitive mantle values of Sun and McDonough (1989) of mafic lavas at: a) Swan Lake and Rancheria River, and b) Big Creek and Liard River. Symbols as in Fig. 15.1. Shaded field as in Fig. 2.2.a.

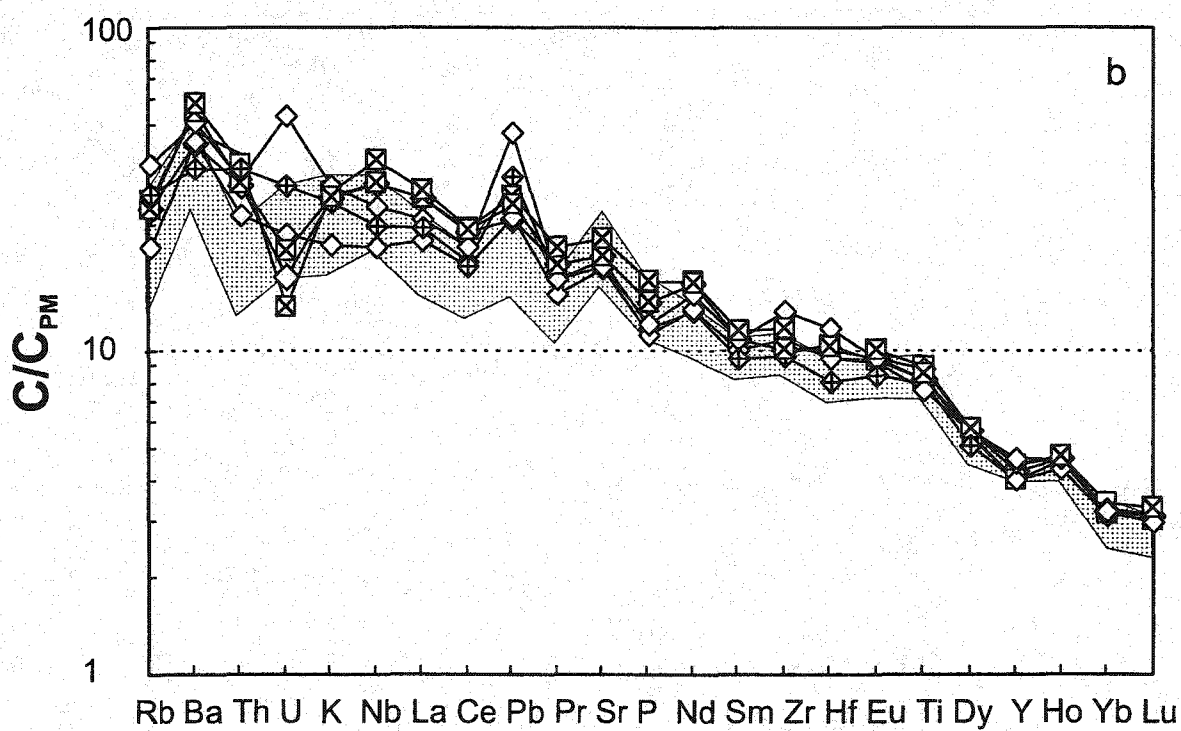
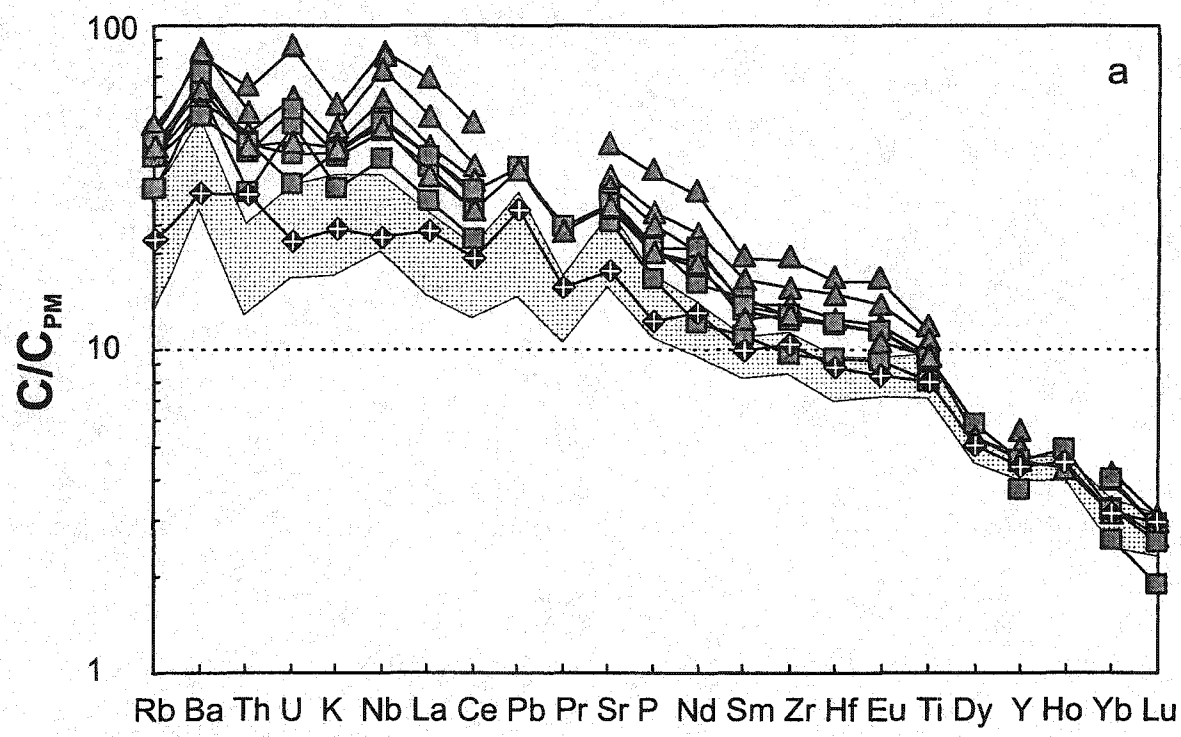
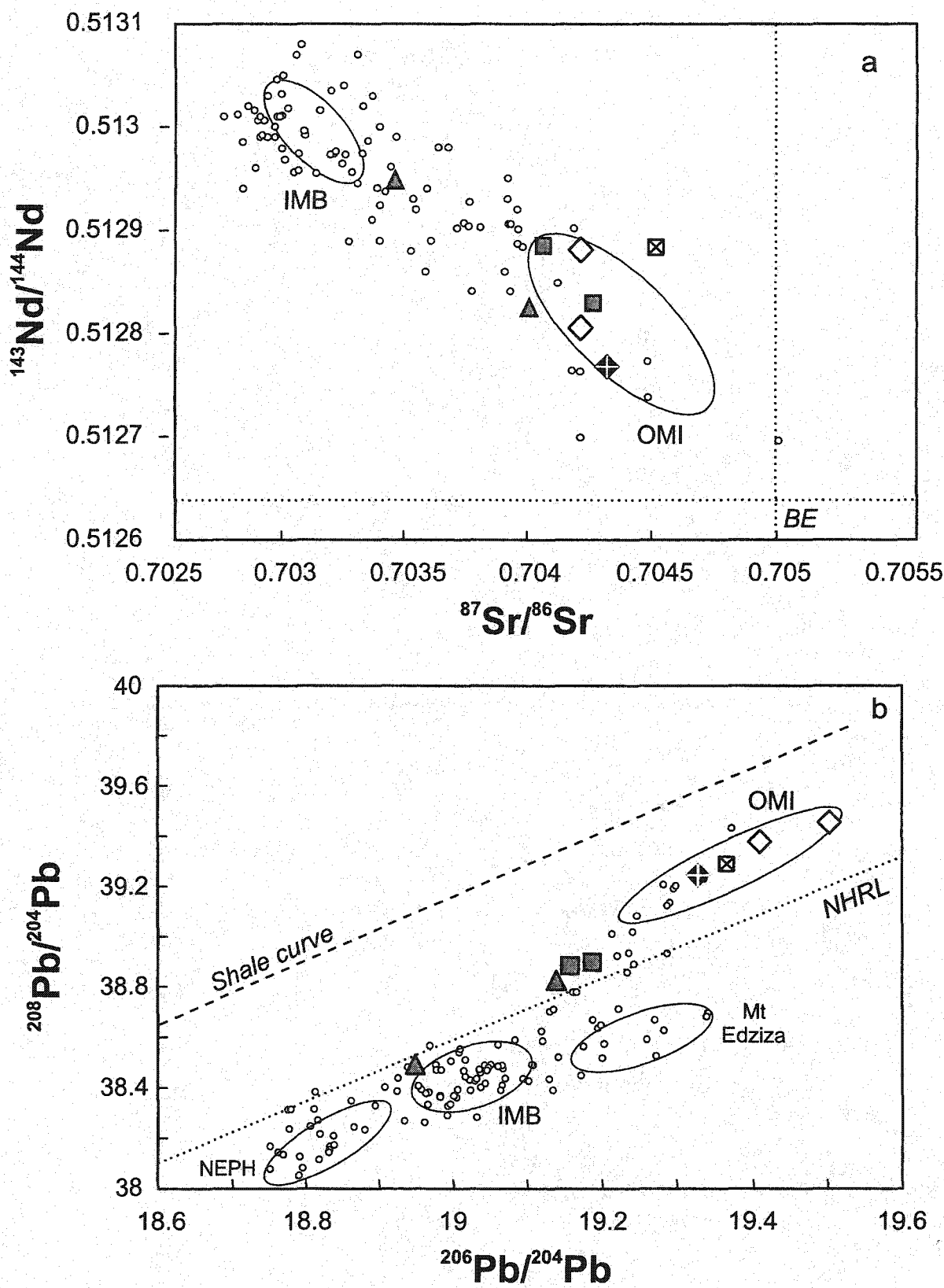


Figure 15.3: a) $^{143}\text{Nd}/^{144}\text{Nd}$ versus $^{87}\text{Sr}/^{86}\text{Sr}$ and b) $^{208}\text{Pb}/^{204}\text{Pb}$ versus $^{206}\text{Pb}/^{204}\text{Pb}$ for Rancheria area basalts. Symbols as in Fig. 15.1. Fields, small circles and explanations as in Fig. 2.3.



AOB lavas, and approaches the composition of the NEPH end-member of the Intermontane Belt in a Pb-Pb isotopic plot (Fig. 15.3.b).

The lavas erupted at Big Creek range from Hy-NORM basalts to AOB. They are relatively primitive in composition (9 to 13 wt.% MgO), and the AOB lavas appear to define an olivine-control line in SiO_2 and TiO_2 versus MgO plots (Fig. 15.1). The trace element patterns of the Big Creek lavas are characterized by an enrichment in LILE and LREE compared to HREE with, when normalized to primitive mantle, with positive Sr and Pb, but negative Th and Rb anomalies compared to elements with similar compatibilities (Fig. 15.2). Compared to primitive Hy-NORM basalts of the Intermontane Belt, the Hy-NORM lavas at Big Creek exhibit smaller negative Th anomalies, and a large range in U, that exhibits both negative and positive anomalies. The one AOB sample that has been isotopically analyzed has relatively radiogenic Sr and Pb, and unradiogenic Nd isotopic ratios, typical of primitive Hy-NORM basalts from the Omineca Belt (Fig. 15.3)

The lavas erupted along the Liard River are Hy-NORM basalts that exhibit a small range in MgO (8-9.5 wt.%), but a relatively large range in SiO_2 (Fig. 15.1). The Liard River Hy-NORM lavas have trace element patterns characterized by an enrichment in LILE and LREE compared to HREE, when normalized to primitive mantle, and positive Sr and Pb, and negative Th and Rb anomalies compared to elements with similar compatibilities (Fig. 15.2.b). Compared to primitive Hy-NORM basalts of the Intermontane Belt, the Hy-NORM lavas along the Liard River are more enriched in Th, and exhibit a larger range in U. They are characterized by radiogenic Sr and Pb, but

unradiogenic Nd isotopic ratios, and represent the most radiogenic end-member in a Pb-Pb isotopic plot of all primitive Hy-NORM basalts of the Omineca Belt (Fig. 15.3).

4.15. Watson Lake

Flat-lying valley-filling flows have erupted through Proterozoic to Triassic metamorphic rocks of the Yukon Tanana pericratonic terrane, on the eastern side of the Tintina Fault in the Watson Lake area (Fig. 1.2). The alkaline lavas that have erupted at Watson Lake are AOB, except for one sample that is slightly Hy normative (Table B-15 of appendix B). They define a small range in MgO, between 8 and 9 wt.%, and have similar SiO₂ and TiO₂ contents to their equivalents in the Omineca Belt to the west (Fig. 16.1). They have, however, lower CaO (Fig. 16.1.c) and Sc contents (Table B-15 of appendix B), which may suggest that they have experienced the fractionation of clinopyroxene. This is in agreement with the presence of clinopyroxene phenocrysts, which have crystallized before plagioclase, in addition to olivine phenocrysts in the Watson Lake lavas (Hasik, 1994).

The Watson Lake AOB have trace element patterns characterized by an enrichment in LILE and LREE compared to HREE, when normalized to primitive mantle, and small positive Sr and Pb anomalies compared to elements with similar compatibilities (Fig. 16.2). They are more enriched in most trace elements than primitive Hy-NORM basalts from the Intermontane Belt, and have no negative Th and Rb anomalies (Fig. 16.2). They have lower Nb/Zr and higher Zr/Y and Sm/Yb ratios than their equivalents in the Omineca Belt just to the west (Hasik, 1994). The Watson Lake lava are characterized by



Figure 16.1: a) SiO₂, b) TiO₂, c) CaO, and d) Al₂O₃ versus MgO in wt.% for the Watson Lake basalts compared to Rancheria area basalts. Symbols: diamonds = Hy-NORM basalts; squares = AOB. Black symbols correspond to Watson Lake basalts, other symbols as in Fig. 15.1.

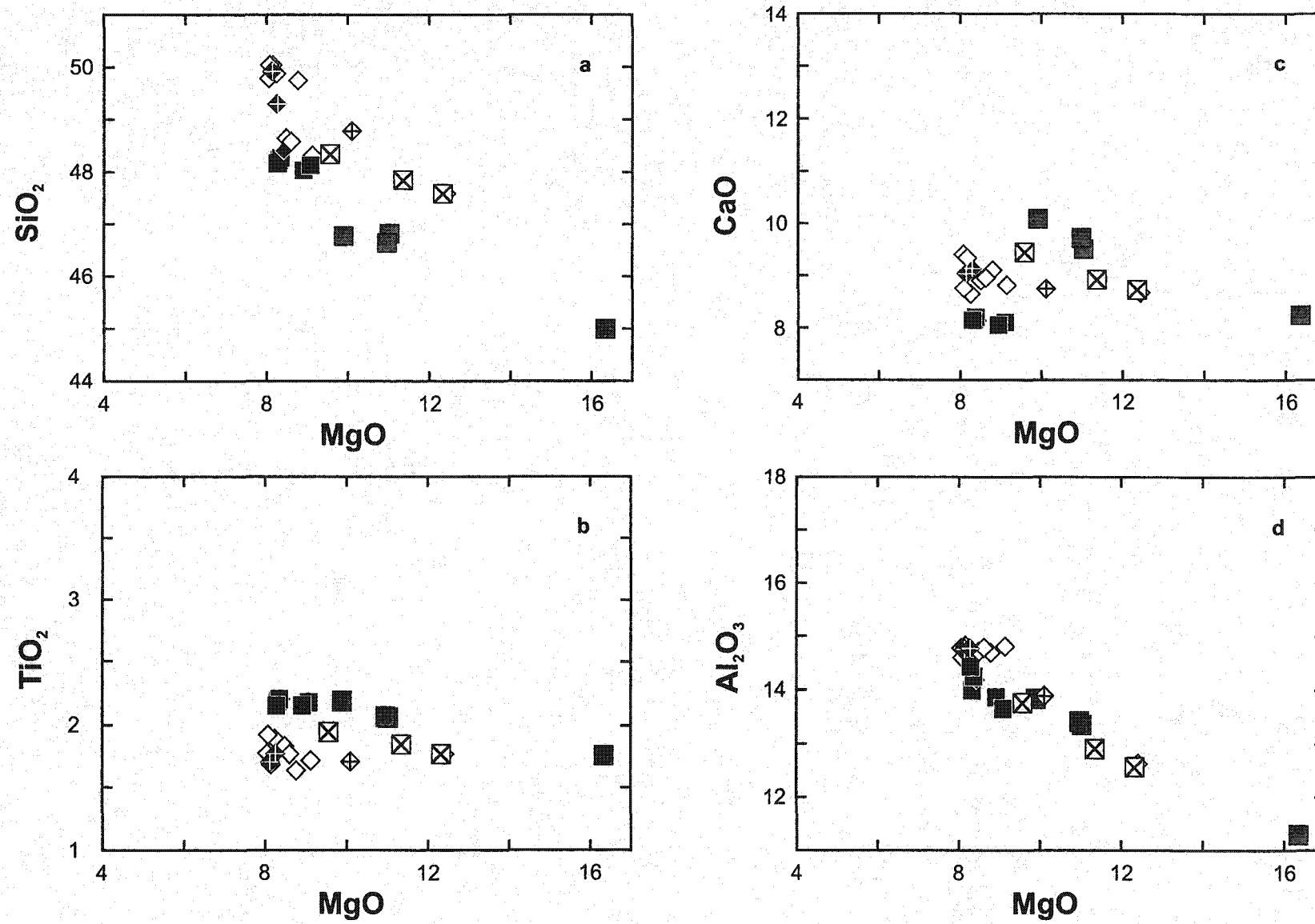


Figure 16.2: Trace element patterns of Watson Lake basalts (black squares) normalized to the primitive mantle values of Sun and McDonough (1989) a) compared to the range in Hy-NORM lavas with $\text{MgO} > 8$ wt.% from small volcanic centres from the Intermontane Belt (shaded area), and b) compared to the range in AOB from the Rancheria area (Fig. 15.2; grey area).

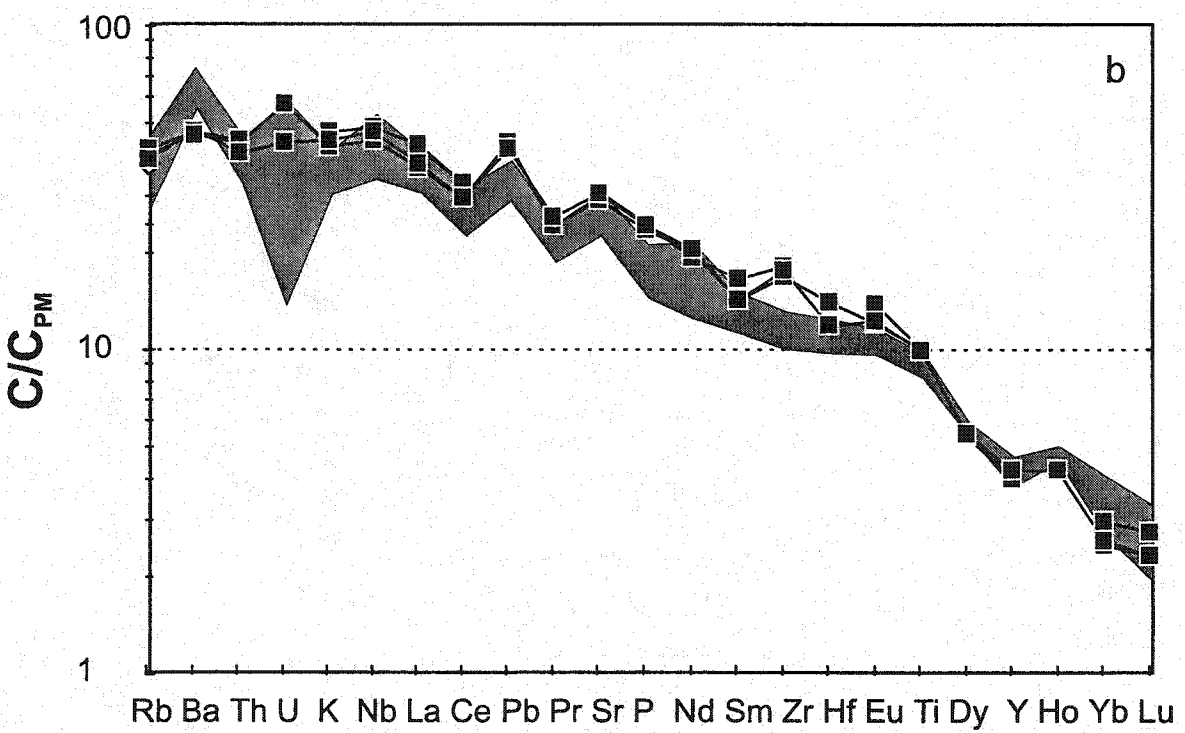
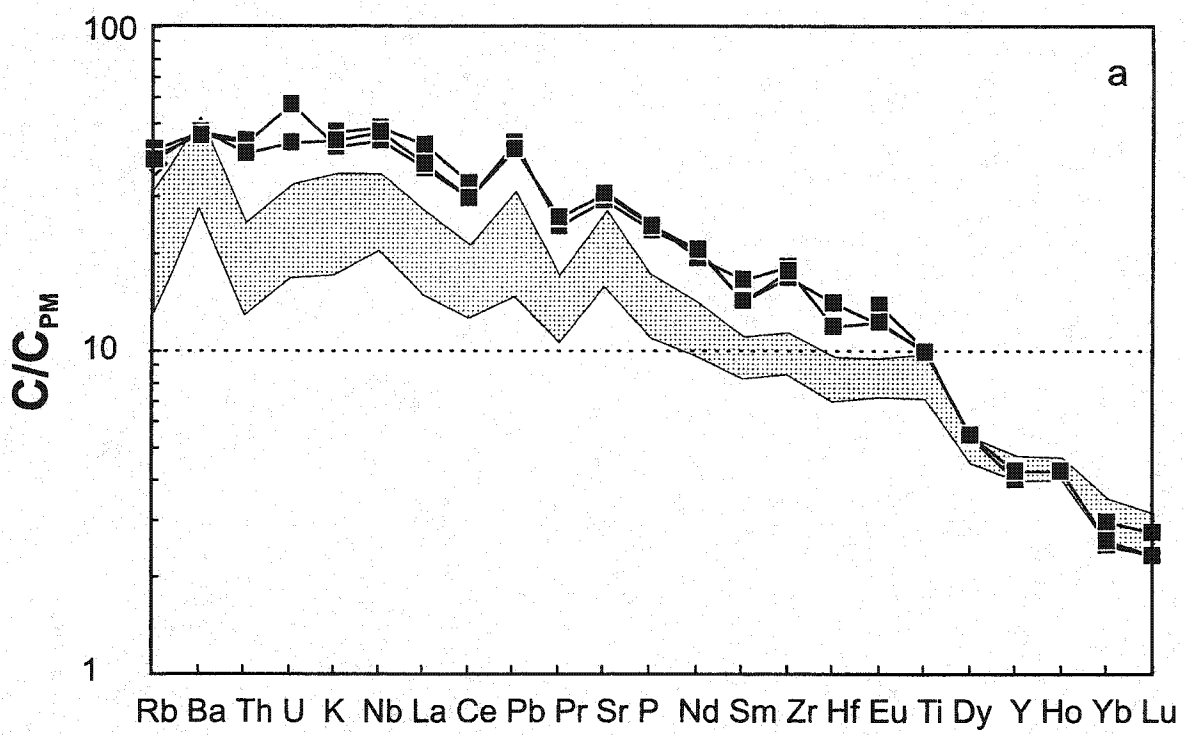
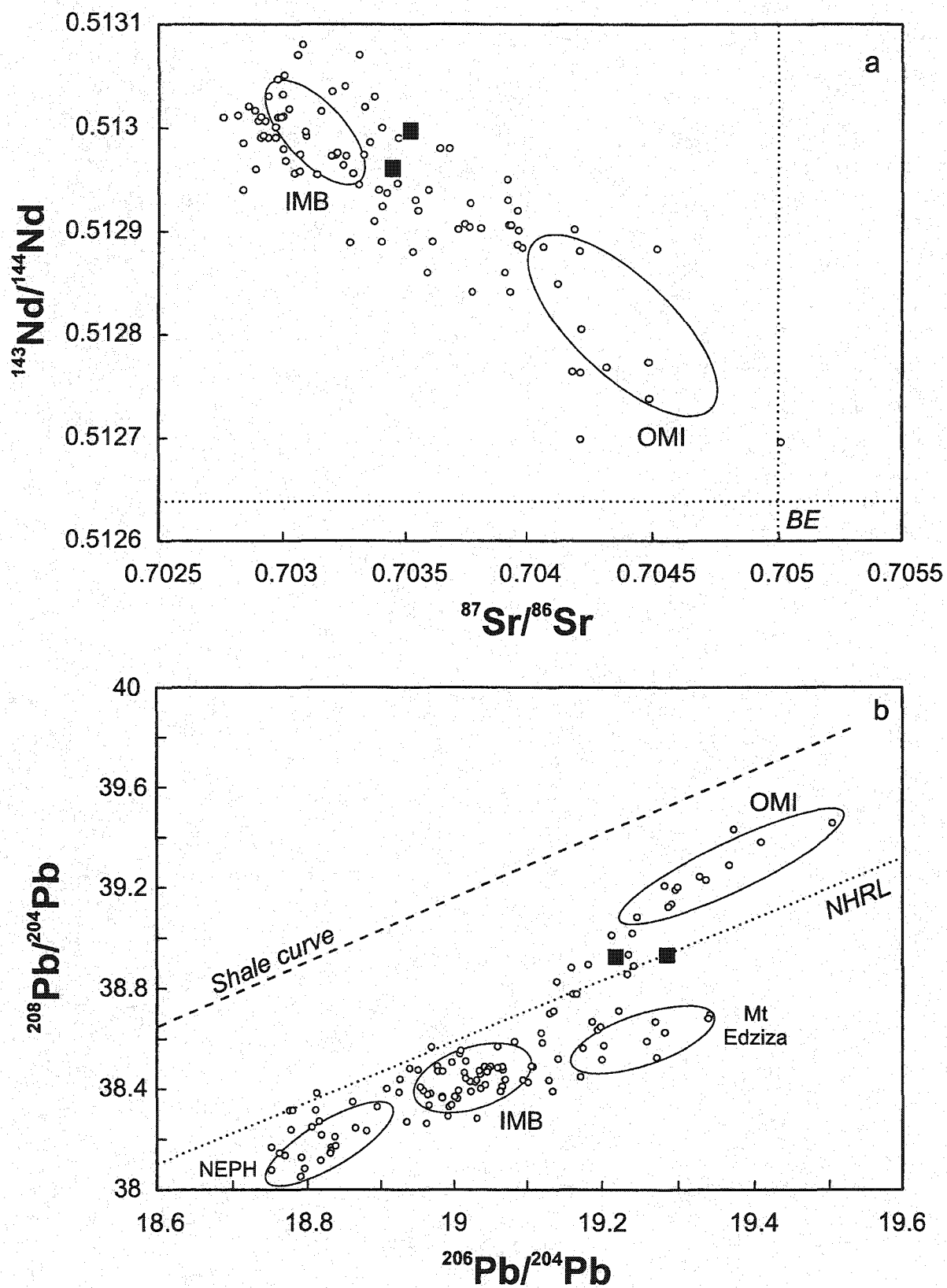




Figure 16.3: a) $^{143}\text{Nd}/^{144}\text{Nd}$ versus $^{87}\text{Sr}/^{86}\text{Sr}$ and b) $^{208}\text{Pb}/^{204}\text{Pb}$ versus $^{206}\text{Pb}/^{204}\text{Pb}$ for Watson Lake basalts. Symbols as in Fig. 16.2. Fields, small circles and explanations as in Fig. 2.3.



relatively unradiogenic Sr and radiogenic Nd isotopic ratios, that fall close to the field of primitive Hy-NORM basalts of the Intermontane Belt (Fig. 16.3.a). They have, however, relatively radiogenic Pb isotopic ratios (Fig. 16.3.b), similar to that of AOB lavas from Rancheria River (Fig. 15.3.b). The discontinuous changes in both the trace elements (Hasik, 1994) and the isotopic signatures in AOB basalts across the Tintina fault (Fig. 15.3) suggest that the Rancheria and Watson Lake lavas either sampled distinct lithospheric mantles, or were contaminated by distinct crustal material.

5. Discussion

5.1. Magmatic groups

In most centres of the Stikine Volcanic Belt, two to three distinct magmatic series can be distinguished based on stratigraphy, and major and trace element compositions. One series comprises the least Si-undersaturated lavas, usually Hy-NORM basalts, although locally some AOB may be included (e.g. in Metahag Mountain). These Hy-NORM lavas have the lowest Ti, K, P and incompatible trace element concentrations, the largest positive Pb anomalies (e.g. Fig. 7.4 and 11.4), and represent the most radiogenic end-member in Sr or Pb isotopes, and the least radiogenic end-member in Nd isotopes (e.g. Fig. 11.5 and 13.5). The second series consists of less silica-rich and more incompatible element-enriched lavas, which are either AOB, such as at Metahag Mountain, Tanzilla Volcano, Jennings River, and Nome Cone, or both Hy-NORM and AOB such as at Kawdy Mountain, Metah Mountain, Tuya Butte, and Blue River. These lavas usually have less radiogenic Sr and Pb and more radiogenic Nd isotopic ratios than

the Hy-NORM group lavas with which they are associated (e.g. Fig. 6.5 and 7.5). At some centres of the Stikine Volcanic Belt, such as at Jennings River and Rancheria River, a third series, made of BASAN lavas, is present. These lavas are more strongly Si-undersaturated and incompatible element-enriched, and less radiogenic in Sr and Pb isotopes, but more radiogenic in Nd isotopes than coexisting AOB and Hy-NORM lavas (e.g. Fig. 10.5 and 15.3). At most centres, such as at Tanzilla Volcano, Jennings River, or Nome Cone, the formally defined magma types (Hy-NORM, AOB and BASAN) closely correspond to natural clustering in the compositional data (Fig. 8.2, Fig. 10.2, and Fig. 11.2), despite the common presence of a few orthopyroxene-poor Hy-NORM basalts within the enriched group.

Although olivine-control lines are apparent in the data of most centres of the Stikine Volcanic Belt, there is often significant scatter about these lines at low MgO contents. The crystallization sequence of AOB and Hy-NORM basalts is olivine, plagioclase, clinopyroxene and opaques (Francis and Ludden, 1990), with plagioclase appearing as a phenocryst phase at about 8 wt% MgO. There are, however, no obvious inflections in Al_2O_3 versus MgO plots at this MgO content, implying a limited role for plagioclase fractionation in these magmas. The scatter at low MgO contents might reflect either a range of parental magmas producing multiple lines of descent, or the effect of combined crustal assimilation and fractional crystallization.

The Hy-NORM basalts commonly have similar to higher MgO contents (Fig. 4.3, 5.3, 7.3, 8.3, 10.3), and lower Ba or Rb contents (Fig. 4.4, 5.4, 7.4, 10.4), than AOB or BASAN magmas. These characteristics indicate that it is highly unlikely that the Hy-

NORM basalts were derived from AOB or BASAN lavas by crustal contamination, which would decrease the MgO and increase the Rb or Ba contents of the melt (Francis and Ludden, 1990). High MgO lavas (> 8 wt.%) in each individual volcanic centre commonly define convincing olivine-control lines (Fig. 4.3, 6.3, 8.3, 9.2, 10.2 and 15.1). The presence of two to three distinct liquid lines of descent at most centres requires the existence of a range of parental magmas, with different Si, Ti, P, alkalis and trace element compositions. The chemical range of the parental magmas could be derived, on one hand, by different degrees of partial melting of a common source, in which case the isotopic range in each centre must reflect subsequent crustal contamination. On the other hand, both the isotopic and chemical ranges in most centres could be explained by the presence of two mantle components. The melting of one of these components would produce the Si-saturated Hy-NORM basalts that are present in almost all the Canadian Cordillera volcanic centres, and represent an end-member in terms of major and trace elements and isotopic compositions, whereas the melting of the other component would produce the more Si-undersaturated and isotopically depleted lavas. The Si-undersaturated end-member is thought to be represented by the NEPH lavas, whereas BASAN and AOB lavas would represent mixtures between the Hy-NORM basalts and the NEPH lavas. This is the model adopted by Francis and Ludden (1990) and Carignan et al. (1994) to explain the chemical and isotopic signatures of mafic alkaline lavas erupted at Hirschfeld, Llangorse, Alligator Lake and Fort Selkirk, in which the mantle source producing the Si-undersaturated NEPH lavas is considered to be amphibole-rich.

5.2. Spatial and temporal relationships

In most alkaline centres of the Stikine Volcanic Belt, such as Jennings River, Kawdy Mountain, Metah Mountain, Tuya Butte, Tanzilla Volcano and Blue River, there is an evolution from early Hy-NORM basalts to later AOB, and sometimes BASAN. This evolution is reversed, however, at Metahag Mountain, where the base consists of AOB, and the top consists of Hy-NORM basalts (Fig. 5.2). Moore et al. (1995) proposed that magma compositions changed from hypersthene to nepheline normative at the transition from subglacial to shallow water or subaerial eruptions at Tuya Butte. Our data, however, suggest that the switch from Hy-NORM to AOB at Tuya Butte occurred during the sub-glacial stage (Fig. 7.2). Furthermore, Hy-NORM basalts have erupted both as pillow lava and subaerial lava flows, whereas AOB lavas have erupted as pillow lava at Jennings River (Fig. 10.2), indicating that there is no systematic change in alkalinity with the style of magmatic eruption.

At other volcanic centres of the northern Canadian Cordillera, the temporal evolution is generally similar to that of Metahag Mountain, evolving from early alkaline to late Hy-NORM basalts. This temporal sequence applies to centres erupted in the Atlin field, for example to Hirschfeld, where early NEPH is followed by late AOB in the same volcanic conduit (Francis and Ludden, 1995), and Table Hill, near Mount Llangorse (D. Francis, unpublished data). In the Fort Selkirk field, two continuous volcanic sequences have evolved from early alkaline to late Hy-NORM basalts (Francis and Ludden, 1990). However, Volcano Mountain, the most recent vent in the Fort Selkirk field, first erupted Hy-NORM, but ended with NEPH lavas (Francis and Ludden, 1990), and at Alligator

Lake in the southern Yukon, there appears to be two successive sequences of Hy-NORM basalts followed by concomitant eruption of AOB and BASAN (Eiché et al., 1987).

In summary, most of the volcanic centres in the northern Canadian Cordillera exhibit a temporal evolution from early Hy-NORM to more Si-undersaturated alkaline lavas (AOB and or BASAN). In contrast, however, the few NEPH-bearing volcanic centres commonly evolve from early alkaline to more Si-saturated lavas. In either case, in most of the northern Cordillera volcanic centres, magmas of different Si-saturation are intimately related in both time and space.

5.3. Volumes of the magma types

AOB and Hy-NORM basalts have erupted in most centres of the northern Canadian Cordillera and are volumetrically the most abundant volcanic rock types. They dominate the mafic volcanic plateau that constitutes the base of the shield volcano of Level Mountain, as well as much of the Tertiary to Recent volcanic centres of the Stikine Volcanic Belt. BASAN lavas are less volumetrically abundant, but they still occur in many volcanic centres of the northern Cordillera, and constitute in some places the only lava type, such as at Dome Mountain, or West Dawson (Fig. 1.1). NEPH lavas are present only in two different volcanic fields of the northern Canadian Cordillera, in the Fort Selkirk field at the transition between the Intermontane Belt and the Omineca Belt in central Yukon (Francis and Ludden, 1990), and in the Atlin field, in the Intermontane Belt (Francis and Ludden, 1995). The NEPH lavas occur in much smaller volumes than the other lava types; for example, in the Fort Selkirk volcanic field, the volume of NEPH

lavas is less than 2 km³ compared to approximately 40 km³ for the other lava types (Francis and Ludden, 1990).

5.4. Volcanic-tectonic relationships

Most of the alkaline volcanism in the northern Canadian Cordillera occurred in the Intermontane Belt (Fig. 1.1), where many volcanic centres contain abundant peridotite xenoliths that range from fertile lherzolites to refractory harzburgites (Shi et al. 1998). The mafic lavas range from NEPH to Hy-NORM, with the NEPH lavas being restricted to the northwest of the Stikine Volcanic Belt, in the Atlin and Fort Selkirk fields (Francis and Ludden, 1990 and 1995). The Intermontane Belt mafic lavas have relatively unradiogenic and restricted $^{87}\text{Sr}/^{86}\text{Sr}$ and $^{208}\text{Pb}/^{204}\text{Pb}$ isotopic ratios ($0.703 < ^{87}\text{Sr}/^{86}\text{Sr} < 0.7035$ and $38.1 < ^{208}\text{Pb}/^{204}\text{Pb} < 38.6$), but exhibit relatively larger ranges in $^{206}\text{Pb}/^{204}\text{Pb}$ and $^{207}\text{Pb}/^{204}\text{Pb}$ ratios ($18.8 < ^{206}\text{Pb}/^{204}\text{Pb} < 19.4$ and $15.5 < ^{207}\text{Pb}/^{204}\text{Pb} < 15.6$). NEPH lavas erupted at different centres in the Intermontane Belt have a common unradiogenic Sr and Pb isotopic signature (Francis and Ludden, 1990; Carignan et al. 1994). Where different magma types coexist in the same volcanic centre, the less strongly silica-undersaturated lavas are typically slightly more radiogenic in Sr or Pb isotopic ratios than the more silica-undersaturated lavas (e.g. Fig. 10.5).

In contrast to the Intermontane Belt, no NEPH lavas nor mantle xenoliths have been found in the Omineca Belt alkaline lavas. The Hy-NORM basalts of the Omineca Belt are characterized by generally larger positive Pb anomalies, and less pronounced negative Rb and Th anomalies than their equivalents in the Intermontane Belt. They define an

end-member in term of their isotopic compositions characterized by unradiogenic Nd and radiogenic Sr and Pb isotopic composition (e.g. Fig. 15.3). These geochemical features indicate either that the Omineca belt Hy-NORM basalts have been contaminated on their way to the surface, or that they were derived from a more radiogenic mantle source than the Intermontane Belt Hy-NORM basalts.

Unlike their counterparts to the west, AOB lavas erupted to the east of the Tintina Fault are characterized by clinopyroxene phenocrysts, lower CaO contents, higher Zr/Nb and Sm/Yb ratios (Hasik, 1994), and less radiogenic Sr and Pb isotopic signatures (Fig. 15.3 and 16.3). These compositional and isotopic differences might reflect the juxtaposition of two distinct lithospheres, indicating that the Tintina Fault is a high angle feature that penetrates at least the crustal part of the lithosphere, and perhaps the entire lithospheric mantle.

6. Conclusion

Most of the Tertiary to recent alkaline volcanism of the Stikine Belt occurred as small monogenetic cinder cones and tuyas scattered to the northeast of the large volcanic complexes of Level Mountain and Mount Edziza. The small alkaline centres of the Stikine Volcanic Belt have erupted mainly Hy-NORM and AOB basalts, with the most Si-undersaturated lavas being BASAN lavas that have been found at only three volcanic centres. In most individual volcanic centres, the lavas appear to define at least two different groups with distinct trace element and isotopic compositions that define distinct olivine-control lines. The less Si-undersaturated group consists mainly of Hy-NORM

basalts that are less incompatible trace element enriched, but more radiogenic in Sr and Pb than the more Si-undersaturated group, which consists mostly of AOB, but commonly includes a few Hy-NORM basalts. Where BASAN are present, they form a distinct group, more enriched in incompatible trace elements and less radiogenic in Sr and Pb than the other magma types. Despite occasional exceptions, there is a good correspondence between natural groupings in terms of liquid lines of descent and the formally defined magmas types.

A range of parental magmas with different Si-saturation and alkalinity must be present in the mantle source of each centre to explain the distinct chemical and isotopic character of the distinct lava groups. The range of parental magmas might be produced, on one hand, by different degrees of partial melting of one source, in which case the isotopic range of the magmas would indicate subsequent crustal contamination. On the other hand, both the chemical and isotopic ranges of the lavas at each centre might be explained by melting and mixing of two different mantle components, one responsible for the Si-undersaturated end-member represented by either basanites or unseen olivine nephelinites, and the other for the Si-saturated Hy-NORM basalts.

A terrane dependence has been detected in the most Si-saturated Hy-NORM basalts erupted in the Intermontane and Omineca belts, with the Hy-NORM basalts of the Omineca Belt having more radiogenic Sr and Pb but less radiogenic Nd isotopic ratios than Hy-NORM basalts of the Intermontane Belt. Some Hy-NORM basalts from the Omineca Belt exhibit additional enrichments in trace elements, such as Rb, Th, U or Pb, compared to Hy-NORM basalts from the Intermontane Belt with similar MgO contents.

This trace element and isotopic terrane dependence indicates either that the mantle sources of the Intermontane and Omineca belts are chemically and isotopically different, or that the lavas have been contaminated by distinct crustal material on their way through the surface.

References

- Allen, C., 1991. Tuya Butte. In: Volcanoes of North America, Wood, C.A., and Kienle, J. (Eds.), New York, Cambridge University Press, 119-120.
- Allen, C.C., Jercinovic, M.J., Allen, J.S.B., 1982. Subglacial volcanism in north-central British Columbia and Iceland. *J. Geol.* 90, 699-715.
- Bloodgood, M.A., Bellefontaine, K.A., 1990. The geology of the Atlin area (Dixie Lake and Teresa Island) (104N/6 and parts of 104N/5 and 12): In Geological Fieldwork 1989, British Columbia Ministry of Energy, Mines, and Petroleum Resources Paper 1990-1, 205-215.
- Carignan, J., Ludden, J., Francis, D., 1994. Isotopic characteristics of mantle sources for Quaternary continental alkaline magmas in the northern Canadian Cordillera. *Earth Planet. Sci. Lett.* 128, 271-286.
- Casey, J.J., Scarfe, C.M., 1980. Summary of the petrology of the Heart Peaks volcanic centre, northwestern British Columbia. *Current Research Geol. Surv. Can. Paper 80-1A*, 356.
- Charland, A., 1994. Stratigraphy, geochemistry, and petrogenesis of the Itcha Volcanic Complex, central British Columbia. Ph.D. dissertation, McGill University, Canada.
- Cousens, B.L., Bevier, M.L., 1995. Discerning asthenospheric, lithospheric and crustal influences on the geochemistry of Quaternary basalts from Iskut-Unuk rivers area, northwestern British Columbia. *Can. J. Earth Sci.* 32, 1451-1461.
- Daly, R.A., 1925. The geology of Ascension Island. *Proc. Amer. Acad. Arts Sci.* 60, 1-80.
- Driver, L.A., Creaser, R.A., Chacko, T., Erdmer, P., 2000. Petrogenesis of the Cretaceous Cassiar batholith, Yukon-British Columbia, Canada: Implications for magmatism in the North American Cordilleran Interior. *Geol. Surv. Am. Bull.* 112, 1119-1133.

- Edwards, B.R., 1997. Field, kinetic, and thermodynamic studies of magmatic assimilation in the Northern Cordilleran Volcanic Province, northwestern British Columbia. Ph.D. dissertation, Univ. of British Columbia, Canada.
- Edwards, B.R., Russell, J.K., 1999. Northern Cordilleran volcanic province; a northern Basin and Range? *Geology* 27, 243-246.
- Edwards, B.R., Russell, J.K., 2000. Distribution, nature, and origin of Neogene-Quaternary magmatism in the northern Cordilleran volcanic province, Canada. *Geol. Soc. Am. Bulletin* 112, 1280-1295.
- Eiché, G., Francis, D., Ludden, J., 1987. Primary alkaline magmas in the Quaternary Alligator Lake volcanic complex, Yukon, Canada. *Contrib. Mineral. Petrol.* 95, 191-201.
- Elliot, R.L., Koch, R.D., Robinson, S.W., 1981. Age of basalt flows in the Blue River valley, Bradfield Canal quadrangle. In The United States Geological Survey in Alaska: Accomplishments during 1979: USGS Circ 823-B, B115-B116.
- Foster, H.L., 1981. A minimum age for Prindle Volcano, Yukon-Tanana Upland. U. S. Geological Survey Circular 37-38.
- Francis, D., Ludden, J., 1990. The mantle source for Olivine Nephelinite, Basanite, and Alkaline olivine basalt at Fort Selkirk, Yukon, Canada. *J. Petrol.* 31, 371-400.
- Francis, D., Ludden, J., 1995. The signature of amphibole in mafic alkaline lavas, a study in the northern Canadian Cordillera. *J. Petrol.* 36, 1171-1191.
- Gabrielse, H., 1969. Geology of the Jennings River map-area, British Columbia: Geological Survey of Canada Paper 68-55, 37p.
- Gabrielse, H., Monger, J.W.H., Wheeler, J.O., Yorath, C.J., 1991. Part A. Morphogeological belts, tectonic assemblages and terranes; In: Chap. 2 of Geology of the Cordilleran Orogen in Canada, H. Gabrielse and C.J. Yorath (Eds.); Geological Survey of Canada, Geology of Canada 4, 15-28.
- Gehrels, G.E., McClelland, W.C., Samson, S.D., Patchett, P.J., Jackson, J.L., 1990. Ancient continental margin assemblage in the northern Coast Mountains, southeast Alaska and northwest Canada. *Geology* 18, 208-211.
- Godwin, C.I., Sinclair, A.J., 1982. Average lead isotope growth curves for shale-hosted zinc-lead deposits, Canadian Cordillera. *Econ. Geol.* 77, 675-690.

- Hamilton, T.S., 1981. Late Cenozoic alkaline volcanics of the Level Mountain Range, northwestern British Columbia. Ph.D. thesis, University of Alberta, Canada.
- Hart, S.R., 1984. A large-scale isotope anomaly in the Southern Hemisphere mantle. *Nature* 309, 753-757.
- Hart, C.J.R., Villeneuve, M., 1999. Geochronology of Neogene alkaline volcanic rocks (Miles Canyon Basalt), southern Yukon Territory, Canada; the relative effectiveness of laser $^{40}\text{Ar}/^{39}\text{Ar}$ and K-Ar geochronology. *Can. J. Earth Sci.* 36, 1495-1507.
- Hasik, V., 1994. Volcanic evidence for a compositional contrast in the lithospheric upper mantle across the Tintina Trench, southeastern Yukon, Canada, M.Sc. thesis, McGill University, Canada.
- Hyndman, R. D., Lewis, T.J., 1999. Geophysical consequences of the Cordillera-Craton thermal transition in southwestern Canada. *Tectonophys.* 306, 397-422.
- Kerr, F.A., 1936. The physiography of the Cordilleran region of northern B.C. Royal Society of Canada, 3rd series, 30.
- Klassen, R.W., 1987. The Tertiary-Pleistocene stratigraphy of the Liard Plain, southeastern Yukon Territory. Geological Survey of Canada Paper 86-17.
- Le Bas, M.J., Le Maitre, R.W., Streckeisen, A., Zanettin, B., 1986. A chemical classification of volcanic rocks based on the total alkali-silica diagram. *J. Petrol.* 27, 745-750.
- Mathews, W.H., 1947. "Tuyas," flat-topped volcanoes in northern British Columbia. *Am. J. Sci.* 245, 560-569.
- Monger, J.W.H., Price, R.A., Tempelman-Kluit, D.J., 1982. Tectonic accretion and the origin of the two major metamorphic and welts in the Canadian Cordillera. *Geology* 10, 70-75.
- Moore, J.G., Hickson, C.J., Calk, L.C., 1995. Tholeitic - alkalic transition at subglacial volcanoes, Tuya Region, British Columbia, Canada. *J. Geophys. Res.* 100, 24577-24592.
- Shi, L., Francis, D., Ludden, J., Frederiksen, A., Bostock, M., 1998. Xenolith evidence for lithospheric melting above anomalously hot mantle under the northern Canadian Cordillera. *Contrib. Min. Pet.* 131, 38-53.

- Souther, J.G., 1977. Volcanic and tectonic environments in the Canadian Cordillera - second look. In: *Volcanic Regimes in Canada*, Baragar, W.R.A., Coleman, L.C. and Hall, J.M. (Eds). *Geol. Assoc. Canada Spec. Paper 16*, 3-24.
- Souther, J.G., 1990. Volcano tectonics of Canada. In: *Volcanoes of North America*, Wood, C.A. and Kienle, J. (Eds.), United States and Canada, 126-127.
- Souther, J.G., 1992. The late Cenozoic Mount Edziza Volcanic Complex, British Columbia. *Geol. Surv. Can. Mem. 420*, 320p.
- Souther, J.G., Hickson, C.J., 1984. Crystal fractionation of the basalt comendite series of the Mount Edziza Volcanic Complex, British Columbia: major and trace elements. *J. Volcan. Geotherm. Res. 21*, 79-106.
- Souther, J.G., Yorath, C.J., 1991. Neogene assemblages, Chapter 10. In: *Geology of the Cordilleran Orogen in Canada*, Gabrielse, H., and Yorath, C.J. (Eds.). *Geol. Surv. Can., Geology of Canada*, 373-401.
- Souther, J.G., Armstrong, R.L., Harakal, J., 1984. Chronology of the peralkaline, late Cenozoic Mount Edziza volcanic complex, northern British Columbia, Canada. *Geol. Soc. Am. Bull. 95*, 337-49.
- Sun, S.S., McDonough, W.F., 1989. Chemical and isotopic systematics of oceanic basalts: implications for mantle composition and processes. In: *Magmatism in the ocean basins*, Saunders, A.D., and Norry, M.J. (Eds.). *Geol. Soc. London Special Publication 42*, 313-345.
- Wheeler, J.O., McFeely, P., 1991. Tectonic assemblage map of the Canadian Cordillera and adjacent parts of the United States of America. *Geol. Surv. Canada Map 1712A*, scale 1:2000000.
- Sutherland-Brown, A., 1969. Aiyansh lava flow, British Columbia: *Can. J. Earth Sci. 6*, 1460-1468.
- Zindler, A., Hart, S.R., 1986. Chemical geodynamics. *Annu. Rev. Earth Planet. Sci. Lett. 14*, 493-571.

CHAPTER III

Recent Alkaline Basalts as Probes of the Lithospheric Mantle Roots of the Northern Canadian Cordillera.

Anne-Claude Abraham ^{a,b,*}, Don Francis ^a, and Mireille Polv ^b

^a Earth and Planetary Sciences, McGill University
3450, University Street
Montr al, Qu bec, H3A 2A7, Canada

^b UMR 5563, Universit  Paul Sabatier
38 rue des 36 Ponts
31400 Toulouse, France

Published in Chemical Geology, June 2001

Abstract

Tertiary to Recent alkaline lavas across the Northern Canadian Cordillera display chemical and isotopic characteristics that can be correlated with their position with respect to three of the five major tectonic belts that constitute the Canadian Cordillera: the Omineca Belt, the Intermontane Belt, and the Coast Belt. There is a discontinuous change in the $^{87}\text{Sr}/^{86}\text{Sr}$ and $^{143}\text{Nd}/^{144}\text{Nd}$ ratios in Recent alkaline basalts across the Tintina Fault, a major Mesozoic to Tertiary strike-slip fault separating the Omineca Belt from North America. Important changes are also identified across both boundaries of the Intermontane Belt. Lavas erupted within the Intermontane Belt have lower $^{87}\text{Sr}/^{86}\text{Sr}$, higher $^{143}\text{Nd}/^{144}\text{Nd}$, and lower Rb concentrations compared to their equivalents in the Omineca Belt to the East, and in the Coast Belt to the West. Recent alkaline basalts in the Coast Belt, however, have distinctly lower Pb isotopic ratios and Th concentrations than Omineca Belt lavas.

The changes observed in the signatures of the alkaline basalts correspond approximately to isotopically distinctive upper crustal domains defined on the basis of granitoids in the Northern Cordillera. Some lavas might have suffered small amounts of crustal contamination; however, the distinctive isotopic signatures of lavas erupted in each belt cannot be explained by crustal contamination and appear to be inherited from the lithospheric mantle.

The chemical and isotopic changes across the Tintina Fault indicate that it is a deep

feature that juxtaposes two distinct lithospheric mantles. There is spatial correspondence of isotopic discontinuities in both the Cretaceous Carmacks volcanics and the Recent alkaline basalts, suggesting that the Omineca-Intermontane Belt lithospheric mantle boundary has been conserved since the accretion of the Intermontane Belt to the North American continental margin, represented by the Omineca Belt. An eastern displacement from the tectonic boundary at the surface for the inferred mantle transition between the Intermontane Belt and the Coast Belt indicates that enriched lithosphere related to the Coast Belt basalts extends partly beneath the Intermontane Belt at latitude 60°N.

keywords: alkaline basalts, Canadian Cordillera, lithospheric mantle, Sr-Nd-Pb isotopes, isotopic composition.

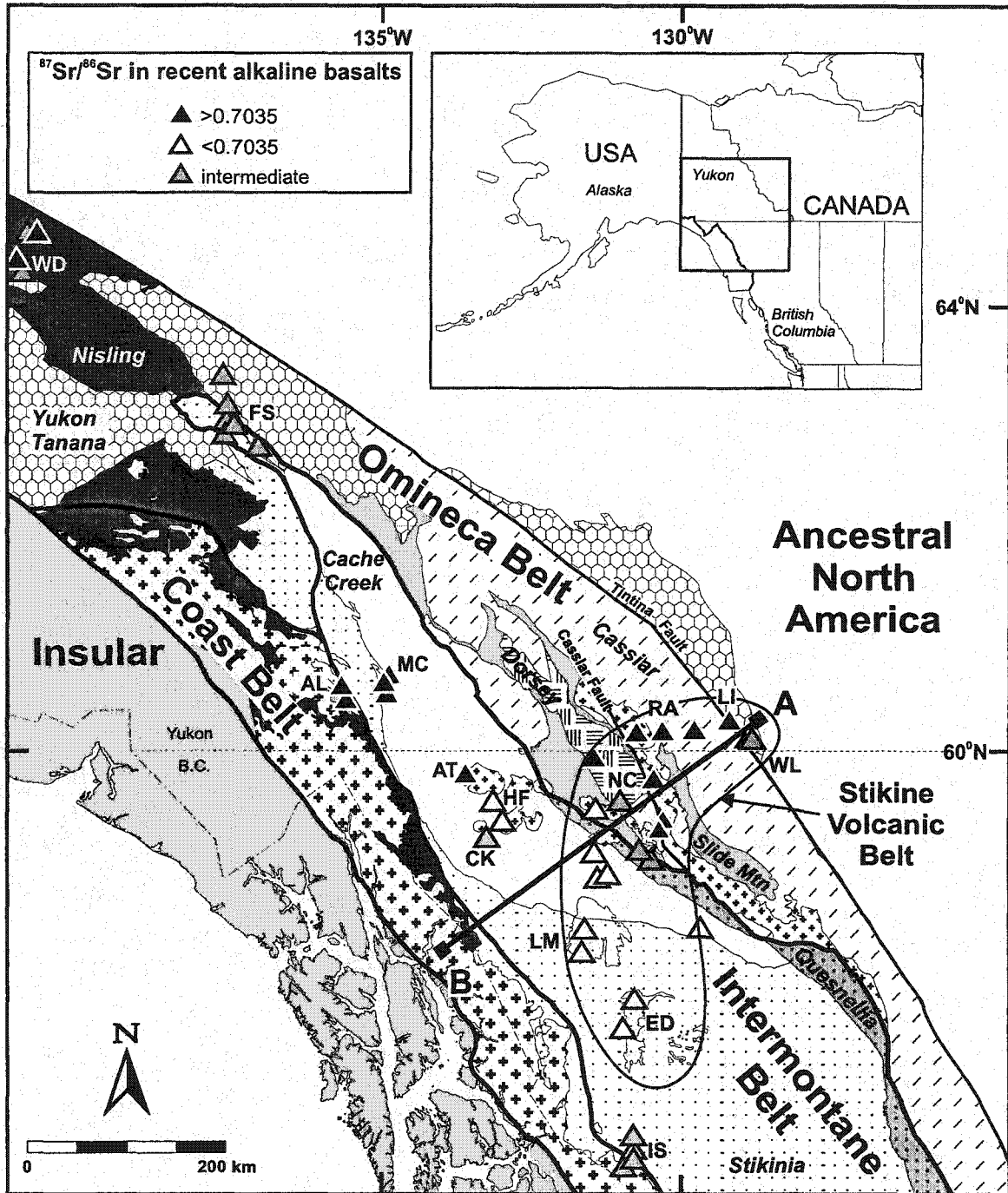
1. Introduction

Although alkaline volcanic rocks have been described as “windows on the Earth's interior” (Menzies, 1987), their chemical and isotopic signatures can not obviously be used to characterize the underlying upper mantle in continental areas because they might have experienced crustal contamination on their way through thick continental crust. This contamination process is commonly associated with crystal fractionation (e.g., AFC; DePaolo, 1981) so that basalts rapidly lose their primitive chemical and isotopic signatures. In extensional or trans-tensional continental environments, however, alkaline basalts are commonly primitive and show little evidence of crystal fractionation or crustal contamination (e.g., in Australia, O'Reilly and Zhang, 1995; Price et al., 1997).

Furthermore, they often carry dense mantle xenoliths, implying a relatively rapid ascent from their mantle source regions. This is the case in the Northern Canadian Cordillera, where numerous Recent to Tertiary volcanic centres have erupted relatively primitive alkaline lavas (Francis and Ludden, 1990, 1995) across the entire Northern Cordillera, many of which contain mantle xenoliths (Francis, 1987; Shi et al., 1998).

These small alkaline volcanic centres, known collectively as the Northern Cordillera Volcanic Province (NCVP; Edwards and Russell, 1999), provide a regional sampling of the upper mantle underlying many of the Cordilleran terranes (Fig. 1). In particular, the Stikine Volcanic Belt crosscuts most of the elongated tectonic blocks of diverse origins that were accreted to the North American craton in the Mesozoic. In this paper, we present the chemical and isotopic variations of lavas from alkaline centres from the NCVP, in particular along the Stikine Volcanic Belt, in relation to their tectonic position across the Northern Canadian Cordillera. We show that there are discontinuous changes in the character of these alkaline lavas that are associated with boundaries between major tectonic blocks. As some of these changes appear to represent changes in the lithospheric mantle underneath the Cordillera, they imply that distinct mantle roots were conserved during the accretion of the major terranes composing the Canadian Cordillera.

Figure 1: Location map for the Tertiary to Recent alkaline centres in the Northern Canadian Cordillera (modified from Wheeler and McFeely, 1991) with respect to the different accreted terranes that constitute the Cordillera. Volcanic centres containing samples analyzed for Sr, Nd and Pb isotopic ratios are represented by triangles. Line AB indicates the trace of the plane onto which the volcanic centres have been projected in Fig. 6 and Fig. 7. Abbreviations: AL = Alligator Lake, AT = Atlin area, CK = Chikoida, ED = Mount Edziza, FS = Fort Selkirk, HF = Hirschfeld, IS = Iskut-Unuk, LI = Liard River, LM = Level Mountain, MC = Miles Canyon, NC = Nome Cone, WD = West Dawson, WL = Watson Lake.



2. Tectonic and geologic settings

The Canadian Cordillera consists of juxtaposed terranes of different ages and origins, that have been accreted to western North America during the Mesozoic (before mid-Cretaceous, Monger et al., 1982; Armstrong, 1988), and have since been displaced northward along large dextral strike-slip faults due to the motion between the Pacific ocean basin and the North American continent (Gabrielse, 1985). These terranes can be divided into five morphogeologic belts that are, from east to west, the Foreland Belt, the Omineca Belt, the Intermontane Belt, the Coast Belt, and the Insular Belt (Fig. 1). It is generally accepted that the Canadian Cordillera was formed by consecutive accretion to North America of two composite superterrane, corresponding roughly to the Intermontane and the Insular belts (Monger et al., 1982; Irving et al., 1996). The Intermontane Belt is composed of terranes with oceanic affinities (Stikine, Cache Creek, Quesnellia and Slide Mountain). On the western side of the Intermontane Belt, a terrane containing Proterozoic rocks (Gehrels et al., 1990) with continental margin affinities lies between the Intermontane Belt and the Coast Belt. This lithospheric fragment, assigned either to the Nisling terrane (Currie and Parrish, 1993; Wheeler and Mcfeely, 1991) or the Yukon-Tanana terrane (Gehrels and Kapp, 1998; Samson et al., 1991), is particularly important in the Northern Cordillera because it may have been involved in the formation of both the granitoid batholiths (Samson et al., 1991) and the Recent alkaline basalts of the CPB. At the time of accretion of the Intermontane Belt, the North American margin, represented by the Omineca Belt, was composed of the Cassiar Terrane, a displaced continental margin, and fragments of the pericratonic Yukon-Tanana terrane.

Subsequently, slices of the Slide Mountain and Quesnellia terranes have been thrust onto the Omineca Belt (Gabrielse et al., 1991).

By the Mid-Tertiary, the earliest alkaline lavas of the Northern Cordillera began to erupt in the large volcanic complexes of Level Mountain ($58^{\circ}31'N$, $131^{\circ}20'W$; Hamilton, 1981) and Mount Edziza ($57^{\circ}42'N$, $130^{\circ}42'W$; Souther, 1992) in a tectonic regime similar to the present. In addition to these shield complexes, primitive alkaline lavas have erupted more recently from numerous small volcanic centres across most of the accreted terranes of the Northern Cordillera and onto the North America craton (Fig. 1; Francis and Ludden, 1990, 1995). These alkaline to peralkaline, Neogene to Recent, volcanic centres of the NCVP define two branches: one extends along the edge of the CPB from the Iskut-Unuk volcanic field in the South ($56^{\circ}30'N$, $130^{\circ}40'W$; Cousens and Bevier, 1995) to the Alaska-Yukon border in the North (West Dawson area; $64^{\circ}22'N$, $140^{\circ}39'W$), the other, the Stikine Volcanic Belt (Fig. 1), extends from Mount Edziza onto the North American Craton to the East (Watson Lake area; $60^{\circ}05'N$, $128^{\circ}50'W$). This mid-Tertiary to Recent alkaline volcanism is considered to have originated in response to trans-tensional stresses related to movements between the Pacific and the North America plates (Souther, 1977; Francis and Ludden, 1990). However, recent heat flow measurements (Hyndman and Lewis, 1999) indicate that the temperature just below the Moho might be extremely high beneath the Cordillera ($\sim 900^{\circ}C$), above the wet solidus of fertile mantle, so that incipient melting might be occurring in the upper mantle now.

In the northwestern part of the Northern Cordillera, a low-velocity anomaly centered under the Alligator Lake volcanic field ($60^{\circ}25'N$, $135^{\circ}25'W$; Eiché et al., 1987)

has been detected by teleseismic tomography (Frederiksen et al., 1998). This 500 km deep anomaly has been interpreted to represent a zone of mantle, 100-200°C hotter than its surroundings (Shi et al., 1998; Frederiksen et al., 1998), produced either by a mantle plume associated with the Late Cretaceous volcanism in the Yukon (Johnston et al., 1996), or by an asthenospheric upwelling associated with the opening of a slab window beneath the Northern Cordillera (Frederiksen et al., 1998). In either case, the source of the basalts may have been affected by the presence of this hot mantle.

3. Sample population and classification

Our volcanic data set comprises new collections from more than twelve different eruption centres along the Stikine Volcanic Belt, as well as previously described centres from the NCVP (Eiché et al., 1987; Francis and Ludden, 1990, 1995; Hasik, 1994). The location of the individual centres are shown with respect to the terranes in Figure 1. Typically, approximately 30 lava samples were analyzed from each centre for major and trace element by XRF so as to characterize its entire volcanic succession. In this paper, we compare the characteristics of lavas from four tectonic domains, the Coast Belt, Omineca Belt, Intermontane Belt, and the Watson Lake area (Fig. 1).

Lavas from these Recent volcanic centres range from basalt to olivine nephelinite in composition (Le Bas, 1986) and previous studies (Francis and Ludden, 1990, 1995) have identified four distinct magma types on petrological and chemical grounds, which are summarized in Table 1. The olivine nephelinites (NEPH) are the most Si-undersaturated

rocks, containing no modal plagioclase and more than 15 wt.% normative nepheline. The basanites (BASAN) and alkaline olivine basalts (AOB) have respectively 5-15 and 0-5 wt.% normative nepheline. Hypersthene-normative (Hy-NORM) basalts are the most Si-saturated rocks and define the end-member of the suite that is the least enriched in incompatible elements. In many cases, there is a continuous gradation between AOB and Hy-NORM basalts and their distinction is somewhat artificial.

A number of individual centres in the Intermontane Belt display a complete range in composition from Hy-NORM basalt to NEPH, all occurring in close relation in space and time (Francis and Ludden, 1995). However, NEPH lavas have not been found in the Coast Belt, the Omineca Belt, nor in the Watson Lake area, and BASAN lavas are rare in the Omineca Belt and have not been found in the Watson Lake area. Hy-NORM basalts occur in all the Cordilleran terranes except in the Watson Lake area and define an end-member in terms of major, trace and isotopic compositions.

In order to better constrain the possibility of crustal contamination, we have also sampled granitoids from batholiths located close to the Recent volcanic centres in the Intermontane, Omineca, and northern Coast Belts, and crustal xenoliths found in the lavas of Alligator Lake, Coast Belt (Eiché et al., 1987). These granitoid samples, ranging from granodiorite to granite in composition, have been analyzed for major, trace, and isotopic compositions (Table 3).

Table 1: Classification of Cordillera alkaline basalts, following Francis and Ludden (1995). Normative mineralogy calculated in oxygen units assuming $\text{Fe}^{3+}/\text{Fe}_{\text{tot}}=0.15$.

Table 1: Classification of Cordilleran alkaline basalts

Rock name	Nephelinite	Basanite	Alkali Olivine Basalt	Hypersthene normative Olivine Basalt
Abbreviation	NEPH	BASAN	AOB	Hy-NORM
Modal plag	no	yes	yes	yes
Normative ne	> 15 %	> 5 %	0-5 %	0%
Normative hy	0%	0%	0%	>0%

4. Recent alkaline basalts

4.1. Trace elements

A subset of samples containing more than 6.5 wt.% MgO, chosen so as to span the width of the Cordillera, were analyzed for trace elements and Sr-Nd-Pb isotopic ratios (Table 2). The Northern Cordilleran alkaline lavas have trace element patterns showing an overall enrichment in incompatible elements, with normalized concentrations decreasing with increasing compatibility (Fig. 2a). The most undersaturated rocks (NEPH) and some BASAN have low large ion lithophile element (LILE, such as K, Rb, Ba) concentrations compared to Nb, Th, and U and the light rare earth elements (LREE). In addition, they are always more depleted in heavy rare earth elements (HREE) than the AOB and Hy-NORM magma types. There is a progressive decrease in incompatible element enrichment from the NEPH to BASAN, AOB and Hy-NORM magmas, and the Hy-NORM basalts do not exhibit negative K, Ba and Rb anomalies. The trace element patterns do not show significant negative Nb anomalies with respect to La and Th, suggesting that the source of these basalts has not been significantly modified by subduction-related fluids, and that these primitive basalts have not been strongly contaminated by upper crustal material.

Table 2:

Representative samples from Watson Lake, Omineca Belt, Intermontane Belt and Coast Belt. Major elements and the trace elements Rb, Sr, Ba, V, Cr, Zn, Ga, Y, Zr and Nb were determined by X-ray fluorescence (XRF) spectrometry at McGill University, Montréal, Canada with a Philips PW 1400 spectrometer. FeO and Fe₂O₃ were calculated from FeO_T assuming Fe³⁺/Fe_{tot}=0.15. LOI: loss on ignition. REE and other trace elements (Sc, Hf, U, Th, Pb) were analyzed by inductively coupled plasma mass spectrometer (ICP-MS) at (1) Université Paul Sabatier, Toulouse, France, with either a Perkin Elmer Elan 5000 or a Perkin Elmer Elan 6000 or (2) at Université de Montréal by INAA using a SLOWPOKE II reactor and two Ge detectors. Analytical precision for these elements is less than 5%. Sr, Nd and Pb isotopic ratios were analysed by TIMS at Université Paul Sabatier, Toulouse, France. A Pb fractionation correction on the order of 0.12%/uma was applied to the measured ratios and 1 σ reproducibility was 0.1%. 2 σ reproducibilities for Nd and Sr are 10⁻⁵ and 2.10⁻⁵ respectively. Sr, Nd and Pb blanks were typically less than 150, 350, and 70 pg, respectively.

Table 2: Major, trace and isotopic compositions of representative alkaline volcanic samples from Watson Lake, the Omineca, Intermontane and Coast belts.

	Watson L. Intermontane Belt												Intermediate	
Sample	RA-20	JR-25	MH-19	MH-23	MM-40	KM-2	LM-57	EZ-39	LG-2	HF-23	HF-3	NC-8		
Rock type	AOB	AOB	Hy-NORM	AOB	Hy-NORM	Hy-NORM	Hy-NORM	AOB	BASAN	AOB	NEPH	AOB		
Site	Watson L.	Jennings	Metahag	Metahag	Metah M.	Kawdy M.	Level M.	Mtn Edz.	Llangorse	Hirschfeld	Hirschfeld	Nome Cone		
Lat	60°15'	59°27'	58°55'	58°55'	59°05'	58°53'	58°25'	57°42'	59°22'	59°32'	59°32'	59°32'		
Long	128°50'	131°20'	131°05'	131°05'	131°18'	131°15'	131°21'	130°42'	132°47'	132°56'	132°56'	130°52'		
SiO ₂	48.01	47.92	46.02	46.25	48.14	48.05	50.92	46.53	42.38	46.36	41.16	46.02		
TiO ₂	2.15	1.92	1.87	2.63	1.86	2.03	1.33	2.2	2.84	2.12	2.39	2.4		
Al ₂ O ₃	13.59	14.56	11.94	14.7	14.05	13.8	15.02	15.2	13.04	13.8	11.47	14.27		
FeO	11	9.65	11.5	10.85	9.68	10.88	11.10	9.75	11.36	10.21	11.55	11.13		
Fe ₂ O ₃	2.16	1.89	2.26	2.13	1.9	2.13	2.18	1.91	2.23	2	2.26	2.18		
MnO	0.16	0.17	0.19	0.18	0.17	0.17	0.14	0.17	0.19	0.18	0.21	0.18		
MgO	9.08	9.14	13.89	7.28	9.44	9.59	9.08	8.64	10.27	10.07	11.72	8.7		
CaO	8.05	9.75	8.29	10.53	8.72	9	9.47	9.32	10.08	9.49	10.79	9.05		
Na ₂ O	3.62	3.31	2.41	2.68	2.92	2.82	3.06	3.01	3.2	3.03	4.4	3.41		
K ₂ O	1.26	0.87	0.73	1	1.07	0.71	0.86	1.21	1.19	1.07	1.74	1.13		
P ₂ O ₅	0.5	0.34	0.35	0.51	0.35	0.29	0.27	0.45	0.54	0.41	1.44	0.54		
LOI	0.01	-	-	0.54	0.97	-	0.17	0.3	-	-	0.76	0.4		
Total	99.59	99.52	99.45	99.29	99.26	99.47	99.38	98.69	97.32	98.74	99.89	99.41		
ne	2.36	2.39	-	0.61	-	-	-	2.18	8.57	3.30	25.96	4.66		
hy	-	-	1.07	-	4.70	7.09	11.18	-	-	-	-	-		
Rb	25	16.1	13	25.7	14	9.4	16.2	21	27.1	16.3	28	17.9		
Cs	0.45	0.19	0.12	0.29	0.14	0.16	0.22	0.23	0.31	0.25	0.46	0.18		
Sr	604	535.2	475.7	644.1	567.2	389.1	579.5	548	724.6	510.5	1392	655.6		
Ba	215.9	360	278.5	395	350.6	211.5	322.2	331	520.4	266.5	502.4	284.4		
Sc	16.7	19	16	17	23	22	16	23	17.2	21	15	21		
V	209	222	205	254	199	202	158	-	267	235	225	210		
Cr	280.5	450.2	340	247.7	343.5	268.9	236.7	311	238.8	283.3	341.4	224.4		
Co	61.5	55	80	48	-	50	55	51	70	60	54.3	62		
Ni	245	119	346	107	215	224	220	104	219	239	300	194		
Zn	150	117	135	136	-	138	105	64	113	103	-	151		
Cu	69	55	61	77	-	66	59	31	52	50	-	88		
Ga	25.5	20.3	18.8	22.9	21	22	19.6	-	20.9	21.2	-	23.1		
Y	18	19.6	18.3	23	18.2	18.8	14.9	29	20.5	18.8	23	21		

Table 2: continued

Table 2: continued

	Omineca Belt						Coast Belt					
Sample	WT-3	RA-16	RA-13	CT-8	BR-6	BR-10	LR-8	RB-11	AL-8	AL-119	AL-171	WD-7
Rock type	Hy-NORM	Hy-NORM	AOB	Hy-NORM	AOB	Hy-NORM	Hy-NORM	BASAN	Hy-NORM	BASAN	AOB	BASAN
Site	Liard R.	Saw M.	Spencer C	Caribou T.	Blue Riv.	Blue Riv.	Lit. Ranch.	Ruby Mtn.	Miles C.	Alligator L.	Alligator L.	W. Dawson
Lat	60°13'	60°15'	60°07'	59°24'	59°18'	59°18'	59°43'	59°42'	60°40'	60°25'	60°25'	64°24'
Long	129°09'	129°37'	130°13'	130°10'	130°13'	130°13'	130°22'	133°22'	135°01'	135°25'	135°25'	140°39'
SiO ₂	49.68	47.47	46.53	49.61	48.52	49.08	50.06	47.32	49.95	48.03	47.09	43.36
TiO ₂	1.61	1.74	2.04	1.98	2.12	1.57	1.94	2.12	1.72	2.26	1.91	3.07
Al ₂ O ₃	14.64	12.57	13.36	14.95	14.4	14.06	14.9	13.95	15.11	15.64	13.61	12.71
FeO	10.12	10.61	10.26	9.2	10.08	10.52	9.39	9.29	9.38	9.16	9.77	2.04
Fe ₂ O ₃	1.98	2.08	2.01	1.8	1.98	2.06	1.84	1.82	1.84	1.8	1.92	10.38
MnO	0.18	0.18	0.18	0.16	0.17	0.18	0.17	0.15	0.16	0.15	0.17	0.17
MgO	8.79	12.42	10.97	7.05	8.5	9.56	7.09	9.3	8.81	6.52	11.47	11.33
CaO	9.05	8.61	9.66	9.48	9.16	8.45	9.62	8.93	8.62	8.85	8.78	8.89
Na ₂ O	2.8	2.75	2.87	3.3	3.48	2.85	3.09	4.09	3.23	3.79	3.1	3.61
K ₂ O	0.63	0.87	1.23	1.23	1.21	0.76	1.08	1.46	0.64	2.11	1.33	2.14
P ₂ O ₅	0.24	0.3	0.45	0.38	0.37	0.21	0.32	0.78	0.25	0.67	0.43	0.8
LOI	-	0.01	0.01	-	-	0.31	-	-	0.39	-	-	0.59
Total	99.72	99.61	99.57	99.14	99.99	99.61	99.5	99.21	100.1	98.98	99.58	99.09
ne	-	-	3.82	-	2.37	-	-	7.58	-	5.81	3.66	14.18
hy	15.41	0.19	-	2.72	-	12.07	8.46	-	11.39	-	-	-
Rb	13	17	25	30.3	25.5	17.6	24.3	27	9	41	-	31
Cs	0.14	0.05	0.15	0.41	0.30	0.29	0.23	0.52	0.07	0.17	-	0.50
Sr	369.3	405	600	538.5	503.5	313.2	499.6	1053	392	1040	-	890
Ba	303.6	301	497.1	384.8	334.6	183.9	365.9	-	-	674	391	603.7
Sc	20.6	22	24	21	23	22	25	17.7	18.5	-	-	18.4
V	184	185	236	211	229	181	220	-	-	202	217	260
Cr	271.6	396.8	374.3	309.3	299.7	286	321.6	314.7	289	168	472	357.8
Co	55	63.7	60.5	-	-	-	50	-	-	-	-	75.8
Ni	181	322	232	93	177	246	61	133.6	206	71	385	310
Zn	105	124	124	-	-	-	124	-	-	-	-	-
Cu	103	58	56	-	-	-	58	-	-	-	-	-
Ga	20.9	20	20.3	21.6	20.4	20.1	20.8	20.2	21.0	-	-	-
Y	20.4	19	21	20.2	20.9	19.7	22.7	22.7	20.0	21	-	24

Table 2: continued

Sample	WT-3	RA-16	RA-13	CT-8	BR-6	BR-10	LR-8	RB-11	AL-8	AL-119	AL-171	WD-7
Zr	119	111	144	155.3	145.9	99.2	142.2	-	-	174	-	248
Nb	14.6	23	36	28.8	28.4	14.4	23.6	46.0	14.3	42	-	65
Hf	2.91	3.08	3.76	3.39	3.48	2.54	3.01	3.93	2.68	4.12	2.3	5.4
Th	2.2	2.7	3.7	3.54	3.08	2.31	3.22	3.93	1.34	3.21	2.4	4.7
U	0.47	0.35	0.84	0.98	0.80	0.63	0.64	1.37	0.50	0.75	-	1.40
Pb	1.79	1.78	2.60	3.22	3.41	2.71	2.85	3.00	1.50	3.19	-	-
La	14.67	19.91	27.09	25.04	20.16	12.80	21.75	37.92	11.28	36.10	24.30	39.90
Ce	31.67	40.65	55.26	50.87	42.14	26.99	44.79	77.04	24.97	72.75	46.70	78.00
Pr	4.03	5.03	6.66	6.20	5.40	3.44	5.48	9.46	3.34	8.56	-	-
Nd	17.78	21.39	28.22	24.73	22.75	14.58	21.88	39.88	15.77	35.25	18.80	38.00
Sm	4.39	4.77	6.07	5.64	5.50	3.84	5.20	8.04	4.18	6.93	5.53	9.55
Eu	1.53	1.56	1.92	1.70	1.77	1.27	1.60	2.58	1.51	2.19	1.62	2.62
Gd	4.55	4.71	5.38	5.20	5.16	3.85	4.58	6.92	4.38	5.68	-	-
Tb	0.71	0.71	0.77	0.76	0.79	0.63	0.71	0.94	0.68	0.76	0.40	1.02
Dy	4.09	4.09	4.39	4.11	4.41	3.75	3.93	4.87	3.89	4.17	-	-
Ho	0.76	0.75	0.81	0.76	0.83	0.75	0.76	0.82	0.73	0.72	0.82	0.00
Er	1.99	1.97	2.02	1.89	2.06	1.88	1.93	2.01	1.88	1.73	-	-
Tm	0.26	0.25	0.26	0.23	0.25	0.24	0.24	0.25	0.24	0.21	-	-
Yb	1.58	1.56	1.57	1.57	1.69	1.69	1.63	1.46	1.51	1.24	1.59	1.90
Lu	0.23	0.23	0.22	0.21	0.23	0.22	0.23	0.20	0.22	0.17	0.18	0.27
Rb/Sr	0.035	0.042	0.042	0.056	0.051	0.056	0.049	0.026	0.023	0.039	-	0.035
Th/U	4.68	7.71	4.40	3.61	3.85	3.67	5.03	2.87	2.68	-	-	3.36
Nb/La	1.00	1.16	1.33	1.15	1.41	1.13	1.09	1.21	1.27	1.16	-	1.63
$^{87}\text{Sr}/^{86}\text{Sr}$	0.704212	0.704484	0.704067	0.704182	0.703909	0.704693	0.705007	0.703981	0.703743	0.703960	0.703860	0.703590
$^{143}\text{Nd}/^{144}\text{Nd}$	0.512881	0.512773	0.512885	0.512764	0.512860	0.512752	0.512696	0.512884	0.512907	0.512920	-	-
eNd	4.7	2.6	4.8	2.5	4.3	2.2	1.1	4.8	5.2	5.5	-	-
$^{206}\text{Pb}/^{204}\text{Pb}$	19.408	19.336	19.182	19.296	19.189	19.289	19.372	19.022	19.108	18.862	18.926	18.813
$^{207}\text{Pb}/^{204}\text{Pb}$	15.666	15.627	15.644	15.650	15.626	15.669	15.664	15.558	15.580	15.538	15.573	15.555
$^{208}\text{Pb}/^{204}\text{Pb}$	39.379	39.228	38.894	39.190	38.931	39.219	39.430	38.428	38.488	38.269	38.436	38.382
	(1)	(1)	(1)	(1)	(1)	(1)	(1)	(1)	(1)	(1)	(2)	(2)

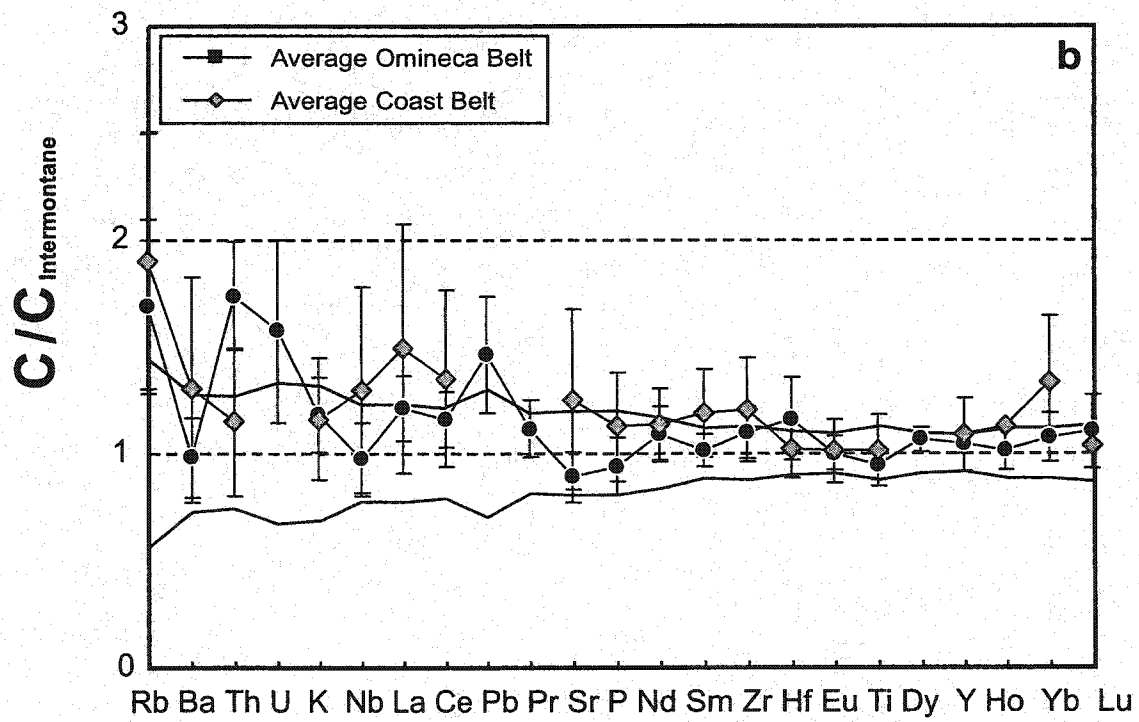
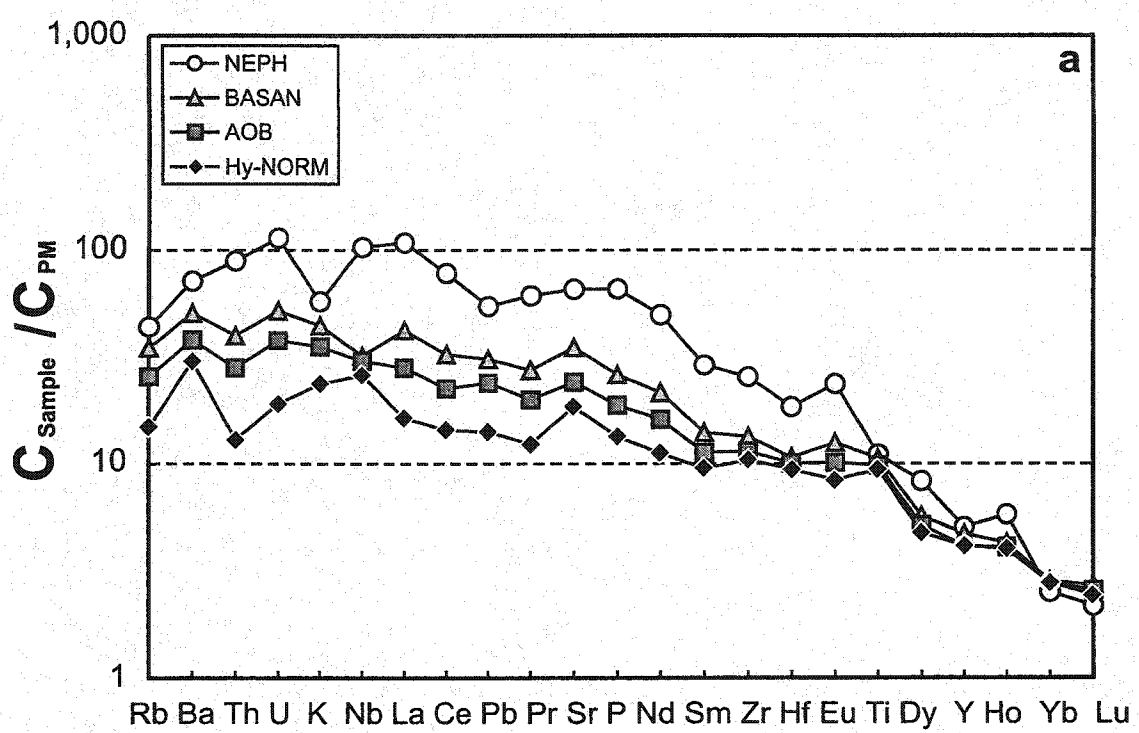
The range from Hy-NORM to NEPH can not be explained by fractional crystallization from a common parent or by partial melting of a homogeneous source (Francis and Ludden, 1995). Furthermore, the relative behavior of LILE and LREE in NEPH and BASAN lavas of some suites requires the presence of amphibole in their mantle source. The compositional spectrum has thus been interpreted to reflect the dilution of melts derived from the amphibole-rich veins by melts of the host lithospheric mantle (Francis and Ludden, 1995). As the Hy-NORM lavas are ubiquitous and define an end-member in terms of their major, trace and isotopic compositions, we will focus on this magma type to identify possible terrane dependence.

Hy-NORM basalts of the Omineca Belt, Intermontane Belt and Coast Belt are similar in terms of many trace elements, the main differences being observed in the most incompatible trace elements (Fig. 2b). Hy-NORM of the Omineca Belt have generally higher concentrations of Rb, Th, U and Pb and higher Rb/Sr and Th/U ratios compared to those of the Intermontane Belt, but they have similar Ba and K contents and slightly lower Nb/La ratios (Fig. 2b and table 2). Hy-NORM basalts of the Coast Belt (Eiché et al., 1987; this study) are generally slightly more enriched in incompatible trace elements compared to those of the Intermontane Belt. They have high Rb contents similar to Omineca Belt basalts, but low Th concentrations, similar to the Intermontane Belt basalts.

There is a discontinuous change in the chemical signatures of Recent alkaline basalts (Hasik, 1994) across the Tintina fault, a major Mesozoic to Tertiary transcurrent fault separating North America from the Cordilleran accreted terranes. AOB samples erupted in the Watson Lake area (Fig. 1) have clinopyroxene phenocrysts and are

Figure 2:

a) Trace element concentrations of representative samples from each magma type, normalized to the composition of the primordial mantle (Sun and McDonough, 1989), showing the compositional spectrum from NEPH to Hy-NORM. The NEPH, BASAN and AOB are from Hirschfeld (Francis and Ludden, 1995) and the Hy-NORM is sample KM-2 (Table 2). b) Average trace element concentrations for Hy-NORM from the Omineca Belt and from the Coast Belt, normalized to the average value of Hy-NORM from the Intermontane Belt. Samples from Intermontane Belt and Omineca Belt have $MgO > 7.5$ wt.%, and from the Coast Belt have $MgO > 6.5$ wt.%. Error bars for the Omineca Belt and Coast Belt, and field for the Intermontane Belt correspond to 1σ around the average.



characterized by lower CaO and Sc contents than their equivalents in the Omineca Belt (Table 2), which may suggest that they have experienced the fractionation of clinopyroxene. In addition, they have lower Nb/Zr ratios and higher Zr/Y and Sm/Yb ratios than their equivalents in the Omineca Belt. These trace element features are, however, not unique to basalts of the Watson Lake area, because AOB erupted at two centres situated at the transition between the Intermontane and Omineca Belt, Nome Cone (Table 2) and Fort Selkirk (Francis and Ludden, 1990), have similar characteristics. Hasik (1994) proposed that the alkaline basalts sampled chemically distinct lithospheric mantles, separated by the Tintina fault.

4.2. Isotopes

Sr, Nd and Pb isotopic ratios were determined on at least three samples for each of 15 volcanic centres along the Stikine Volcanic Belt. At centres where more than one magma type is present, there is generally a progressive variation in isotopic signature from NEPH through BASAN and AOB to Hy-NORM lava types, with NEPH magmas being the least radiogenic in Sr and Pb (Fig. 3) and the most radiogenic in Nd. Despite having a larger range of SiO₂ contents, the within centre isotopic variations in the Intermontane Belt are less important than those in the Omineca Belt, where a large range of Sr, Nd and Pb isotopic ratios are observed despite the limited range in SiO₂. In the Coast Belt, on the other hand, individual centres do not display any isotopic variation, despite a wide range in degree of Si-saturation (Fig. 3).

In a $^{87}\text{Sr}/^{86}\text{Sr}$ - $^{143}\text{Nd}/^{144}\text{Nd}$ diagram (Fig. 4), all samples fall on the mantle array (e.g., Zindler and Hart, 1986) in the depleted quadrant between the field of MORB and Bulk earth. In the Pb-Pb diagrams (Fig. 5), the basalts cross the North Hemisphere Reference Line (NHRL) defined by Hart (1984), and trend towards the shale evolution curve of Godwin and Sinclair (1982). These two figures clearly indicate that Omineca Belt and Coast Belt basalt samples define distinct isotopic domains from those of the Intermontane Belt. Intermontane Belt basalts have isotopic characteristics comparable to those of MORB, with low $^{87}\text{Sr}/^{86}\text{Sr}$ and Pb isotopic ratios, but high $^{143}\text{Nd}/^{144}\text{Nd}$ ratios, whereas Coast Belt basalts have higher $^{87}\text{Sr}/^{86}\text{Sr}$, lower $^{143}\text{Nd}/^{144}\text{Nd}$, and low Pb isotopic ratios. Finally, Omineca Belt basalts have the highest $^{87}\text{Sr}/^{86}\text{Sr}$ and Pb isotopic ratios and lowest $^{143}\text{Nd}/^{144}\text{Nd}$.

The regional variations in $^{87}\text{Sr}/^{86}\text{Sr}$ indicate the existence of three discontinuities that roughly correlate with tectonic boundaries between distinct Cordilleran belts (Fig. 6a). From east to west, the first change occurs near the Tintina Fault. AOB basalts erupted in the Watson Lake area have lower $^{87}\text{Sr}/^{86}\text{Sr}$ (0.7035) than equivalent AOB basalts to the west of the fault in the Omineca Belt (>0.704). The second change occurs in the western portion of the Omineca Belt. Lavas erupted in the Intermontane Belt have lower $^{87}\text{Sr}/^{86}\text{Sr}$ values (0.7028-0.7035) than lavas erupted in the Omineca Belt. The change in Sr isotopic values from the Omineca Belt to the Intermontane Belt occurs across a zone between the Cassiar and Teslin faults, in the Dorsey terrane (Wheeler and McFeely, 1991) where three volcanic centres have Sr isotopic signatures (0.703-0.704) intermediate between those of the Omineca Belt and Intermontane Belt (Fig. 1). The last

Figure 3: $^{87}\text{Sr}/^{86}\text{Sr}$ versus $^{206}\text{Pb}/^{204}\text{Pb}$ for 3 individual centres from the Intermontane Belt (white symbols) compared to Alligator Lake from the Coast Belt (grey symbols; Carignan et al., 1994) and to the range in Rancheria, Omineca Belt (black symbols).

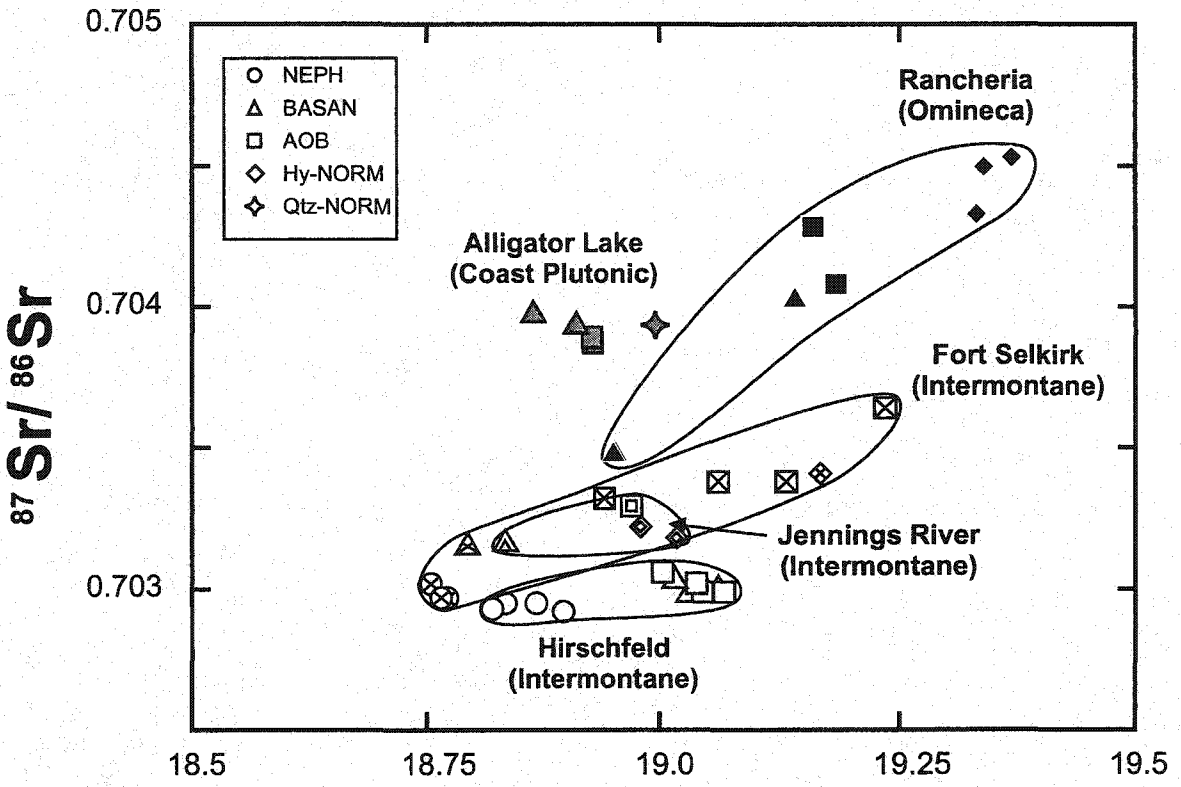


Figure 4: $^{87}\text{Sr}/^{86}\text{Sr}$ versus $^{143}\text{Nd}/^{144}\text{Nd}$ for Recent alkaline volcanic rocks. Fields corresponding to N-MORB and Oceanic Island Basalts (OIB) are drawn for comparison. Intermediate centres, identified by the grey symbols in Fig. 1, have erupted both lavas with relatively radiogenic and unradiogenic isotopic signatures. Symbols: Intermontane Belt lavas = white squares, Intermediate lavas = white triangles, Omineca Belt lavas = black circles, Coast Belt lavas = grey diamonds, Watson Lake area lavas = grey triangles. Data sources: Carignan et al. (1994), Cousens and Bevier (1995), Francis and Ludden (1990), Hart (1995), this study, and unpublished data from Carignan and Abraham.

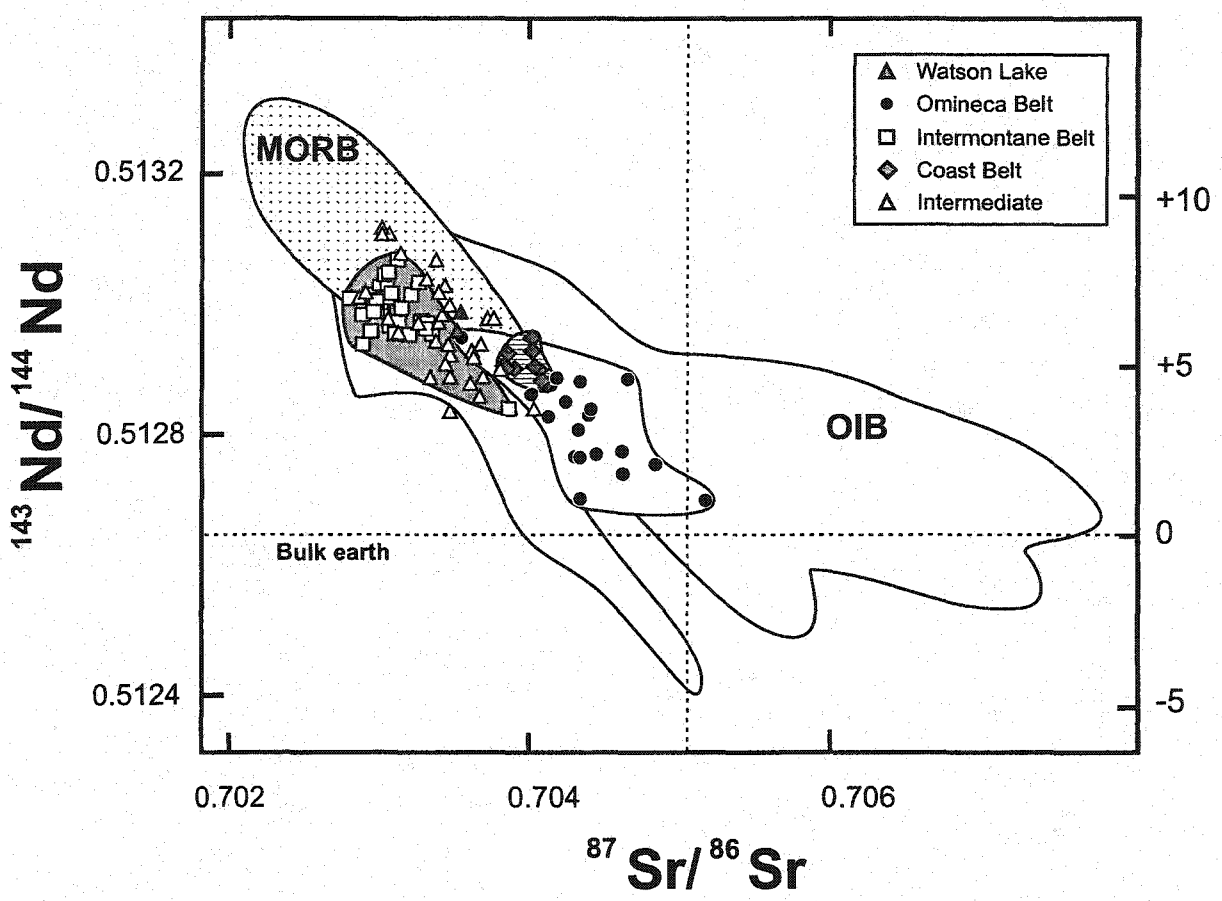
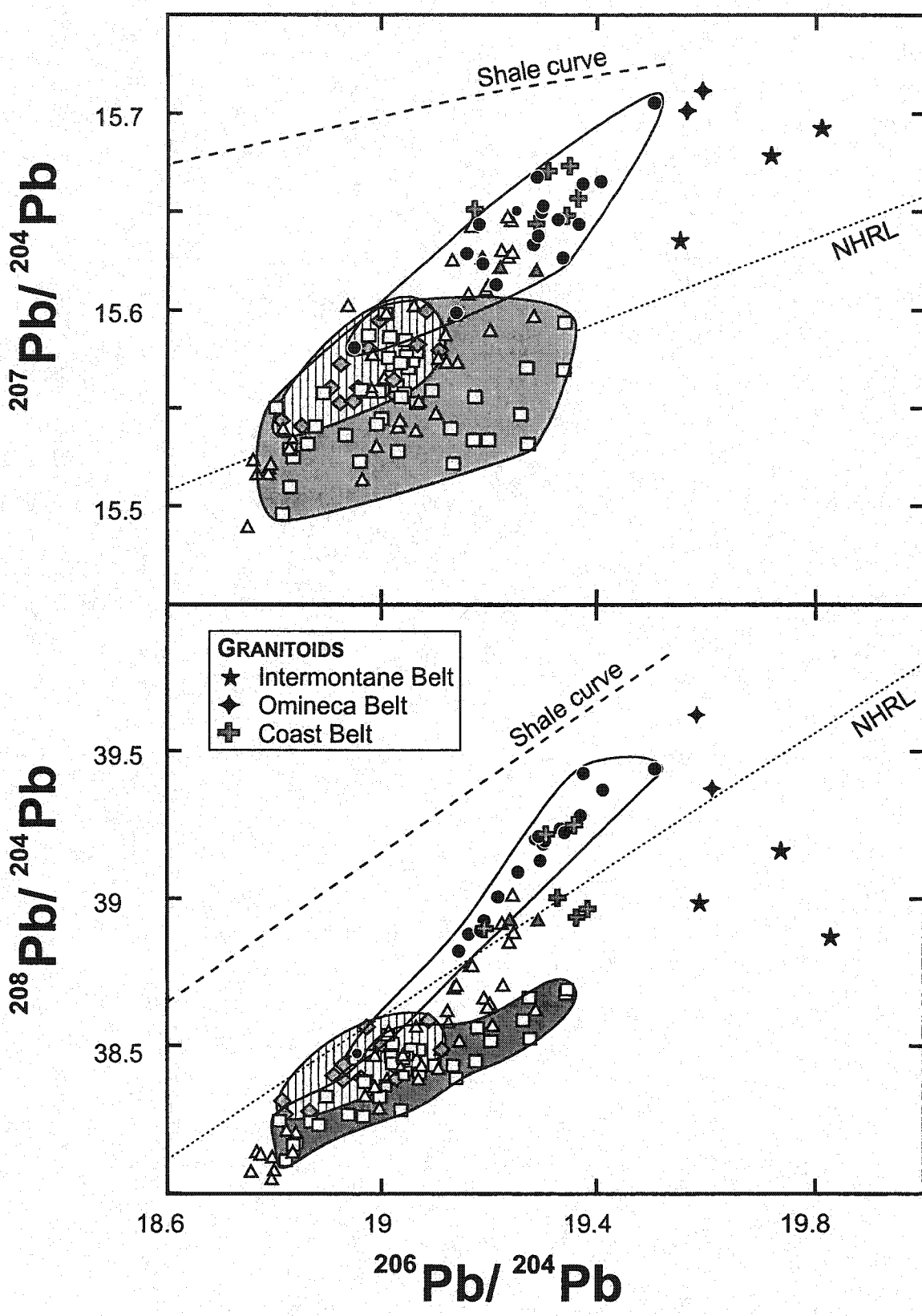


Figure 5: Pb-Pb isotopes diagrams for alkaline volcanic rocks and granitoids. No age correction was applied to the granitoids. The shale curve is from Godwin and Sinclair (1982) and the North Hemisphere Reference Line (NHRL) from Hart (1984). Alkaline volcanic symbols as in Fig. 4.



transition occurs to the east of the tectonic boundary between the Intermontane Belt and the Coast Belt around latitude 60°N, and may coincide with the Intermontane-Coast Belt boundary further South, near latitude 56°N (Fig. 1). The alkaline lavas of the Coast Belt have higher $^{87}\text{Sr}/^{86}\text{Sr}$ values (0.7034-0.704) than those of the Intermontane Belt. In addition, BASAN erupted at West Dawson (Fig. 1), in the North, have high $^{87}\text{Sr}/^{86}\text{Sr}$ ratios and low Pb isotopic signatures, suggesting that they are related to the Coast Belt.

The regional variations in Nd isotopes mirrors that of the Sr isotopes (Fig. 6b) with corresponding discontinuities at the Tintina Fault and on both sides of the Intermontane Belt. AOB in the Watson Lake area have higher $^{143}\text{Nd}/^{144}\text{Nd}$ (0.51295) than those of the Omineca Belt (0.51275-0.51285), more similar to AOB of the Intermontane Belt. In the Coast Belt, the lavas have intermediate $^{143}\text{Nd}/^{144}\text{Nd}$ values, between those of the Omineca and Intermontane Belt basalts (0.51292-0.513).

Regional variations can also be observed in the Pb isotopic system, with more pronounced changes for the $^{207}\text{Pb}/^{204}\text{Pb}$ and $^{208}\text{Pb}/^{204}\text{Pb}$ ratios than for the $^{206}\text{Pb}/^{204}\text{Pb}$ ratio (Fig. 7). The lavas can be divided into two groups in term of their Pb isotopic composition, basalts from the Omineca Belt and Watson Lake area being clearly more radiogenic in Pb than basalts from the Intermontane Belt and Coast Belt. The Watson Lake basalts have high Pb isotopic ratios, in contrast to their low $^{87}\text{Sr}/^{86}\text{Sr}$ and high $^{143}\text{Nd}/^{144}\text{Nd}$. Basalts from the Omineca Belt have radiogenic Pb compositions, except for one BASAN sample, which have lower Pb isotopic ratios, similar to BASAN from the Intermontane Belt. Basalts from the Intermontane Belt have generally low Pb isotopic ratios, the large overall range in the $^{206}\text{Pb}/^{204}\text{Pb}$ signatures being essentially due to high

Figure 6: Projection of isotopic analyses along the Stikine Volcanic Belt with respect to distance from Tintina fault, a) $^{87}\text{Sr}/^{86}\text{Sr}$ and b) $^{143}\text{Nd}/^{144}\text{Nd}$. All centres have been projected onto line AB (Fig. 1). The dotted lines correspond to major Belt boundaries. Symbols: NEPH = circles, BASAN = triangles, AOB = squares and Hy-NORM = diamonds. Colors are similar to that used in Fig. 1 for the Recent alkaline centres.

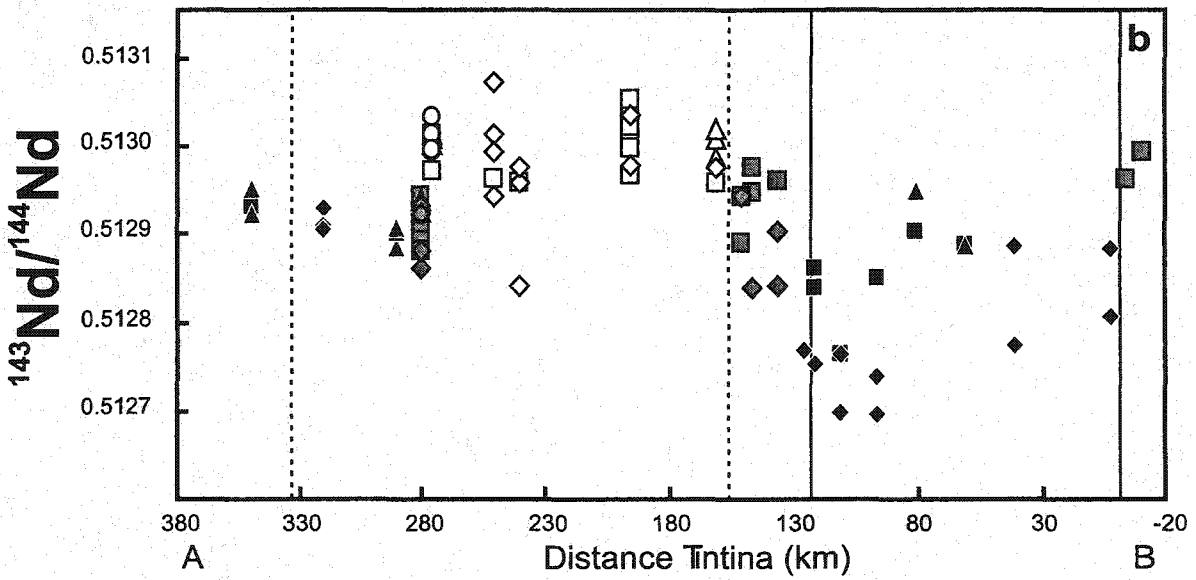
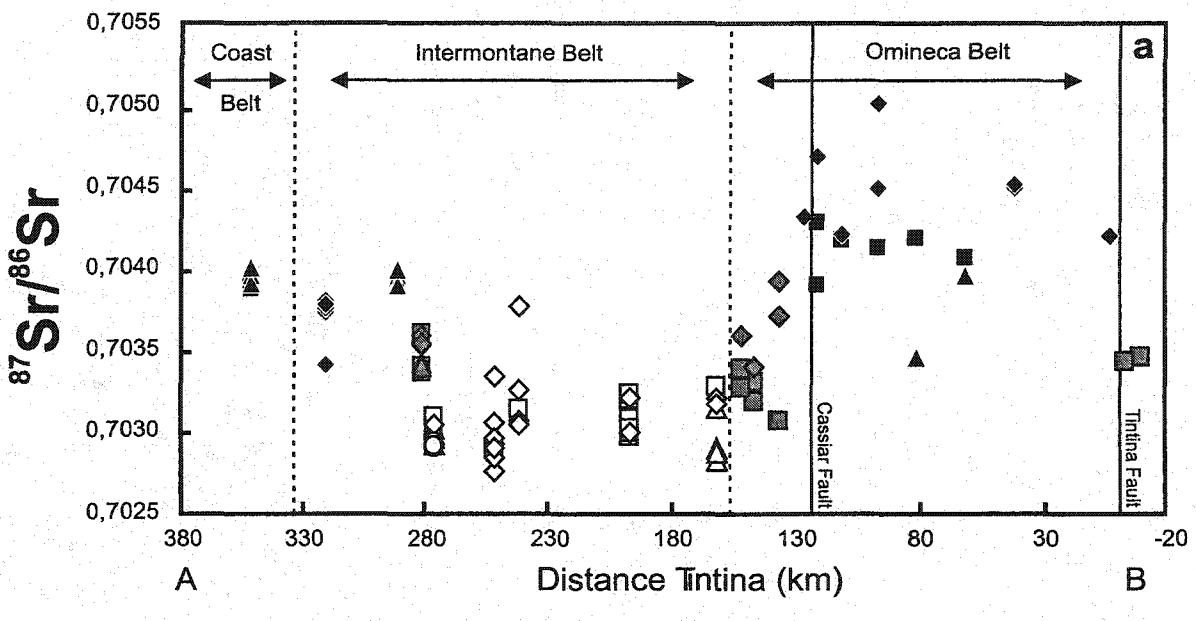
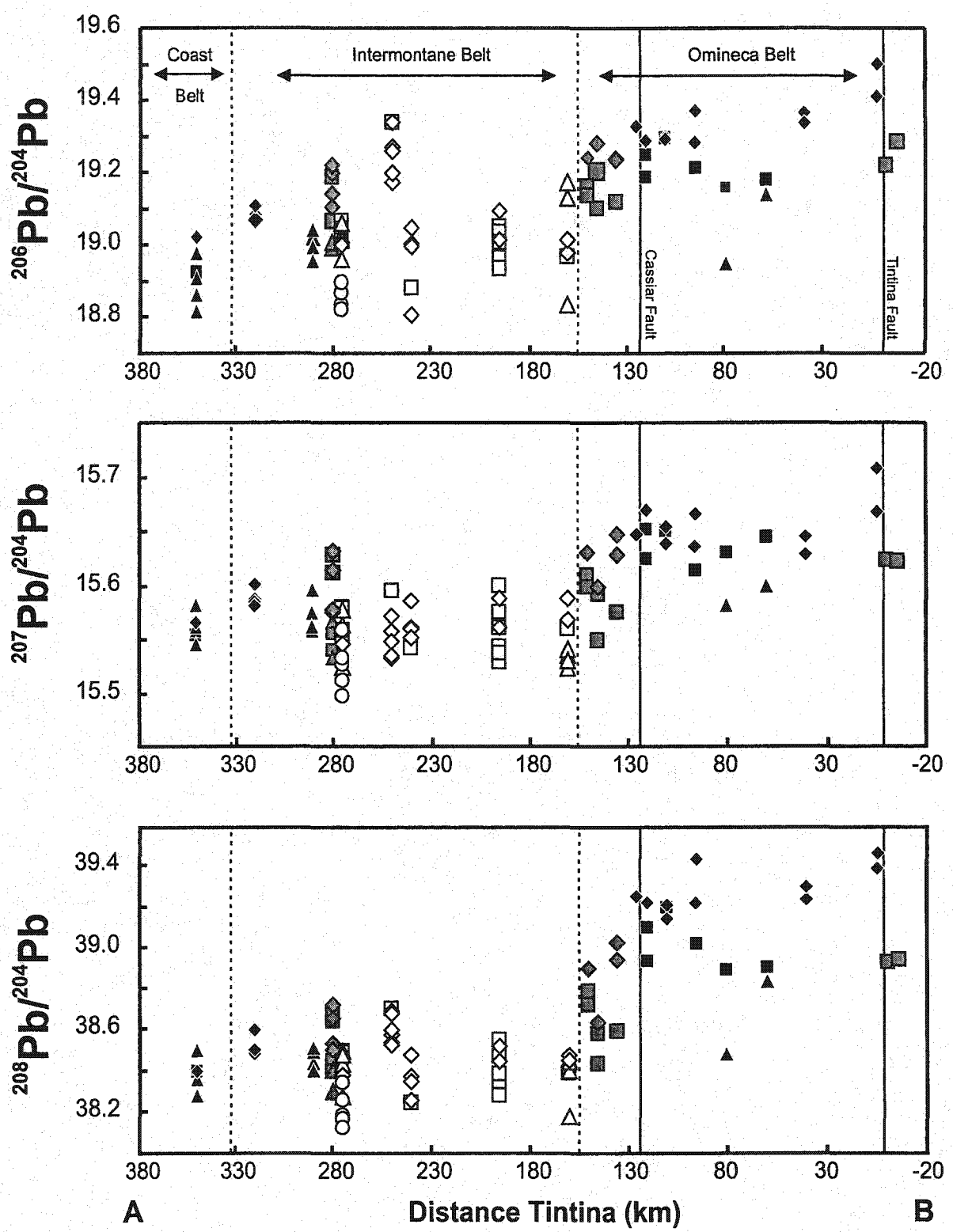


Figure 7: $^{206}\text{Pb}/^{204}\text{Pb}$, $^{207}\text{Pb}/^{204}\text{Pb}$ and $^{208}\text{Pb}/^{204}\text{Pb}$ versus distance from Tintina Fault. Same symbols and explanations as in Fig. 6.



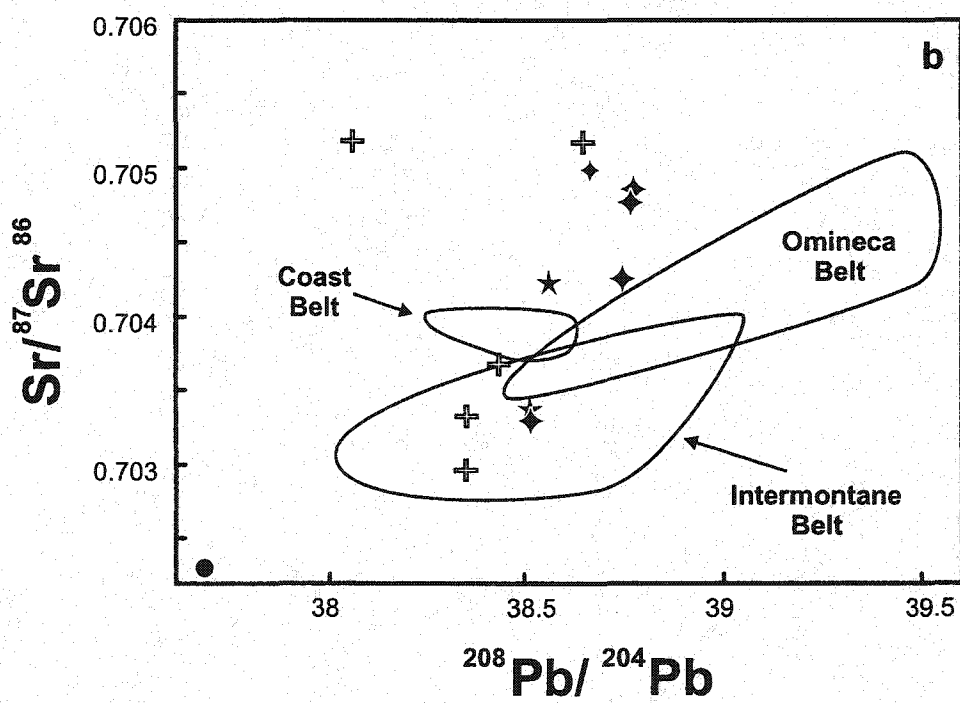
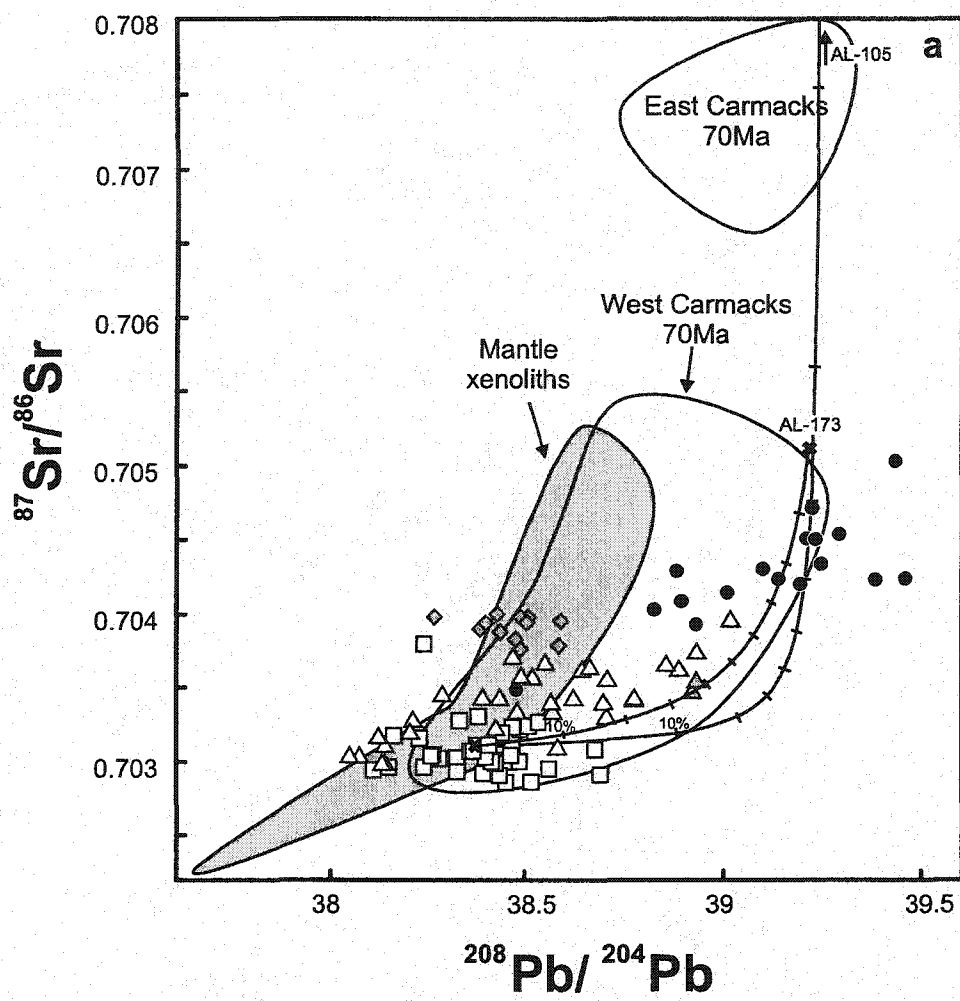
values in the Edziza volcanic complex (Carignan et al., 1994). Finally, although alkaline lavas erupted in the Coast Belt are more radiogenic in Sr compared to Intermontane Belt lavas, they have comparable low Pb isotopic ratios.

4.3. Comparison with mantle xenoliths.

A number of alkaline centres from the Northern Cordillera contain numerous mantle xenoliths that have been the subject of parallel studies (Francis, 1987; Carignan et al., 1996; Shi et al., 1998; Peslier et al., 2000). All of the mantle xenoliths occurrences in the Northern Cordillera are in centres from the Coast Belt and Intermontane Belt (Shi et al., 1998). The Sr isotopic composition of leached whole rocks and clinopyroxenes from Cordilleran harzburgite and lherzolite xenoliths range from 0.70233 to 0.7052 (Fig. 8b) with no simple correlation with indices of fertility such as calcium or aluminum content (Carignan et al., 1996). This large range in mantle xenolith $^{87}\text{Sr}/^{86}\text{Sr}$ values encompasses the range of the Cordilleran lava values. Nd isotopic compositions have only been determined on four lherzolite xenoliths from the Coast Belt (Peslier, 1999), three of which have similar values (0.51274-0.51279) corresponding to a relatively enriched mantle. These $^{143}\text{Nd}/^{144}\text{Nd}$ values are distinctly lower than those of their host lavas. Pb isotopes have also been measured for whole rocks and clinopyroxenes of mantle xenoliths from the Coast Belt (Carignan et al., 1996), plus seven samples from the Intermontane Belt (J. Carignan's unpublished data). These mantle xenoliths have similar Pb isotopic ratios as the Intermontane Belt and Coast Belt alkaline lavas, but lower values than those of the Omineca Belt alkaline basalts (Fig. 8b). No correlation is observed between the

Figure 8:

a) $^{87}\text{Sr}/^{86}\text{Sr}$ versus $^{208}\text{Pb}/^{204}\text{Pb}$ for Recent alkaline volcanic rocks compared to the fields of Northern Cordilleran upper mantle xenoliths (Carignan et al. 1996 and unpublished data) and Carmacks volcanics (D. Francis, unpublished data). Symbols and data source for alkaline volcanic rocks as in Fig. 4. The mixing lines correspond to results of bulk mixing between MH-19 and two crustal fragments from Alligator Lake lavas. b) $^{87}\text{Sr}/^{86}\text{Sr}$ versus $^{208}\text{Pb}/^{204}\text{Pb}$ in clinopyroxenes and whole rocks from Cordilleran xenoliths (Carignan et al. 1996 and unpublished data). Symbols: Alligator Lake clinopyroxenes = black diamonds, Alligator Lake whole rocks = black stars, Llangorse volcanic field clinopyroxenes = white crosses, Fort Selkirk clinopyroxene = black circle. The fields correspond to the range in Cordilleran alkaline lavas.



isotopic signature of the mantle xenoliths and the tectonic belts in which they are found. In general, the mantle xenoliths do not define the same isotopic domains as the basalts, except for Coast Belt lavas which fall on the Sr-Pb isotopic domain defined by the mantle xenoliths (Fig. 8b).

4.4. Comparison with crustal granitoids.

The granitoids sampled in the Omineca Belt, Intermontane Belt and Coast Belt range from granite to granodiorite (Table 3), with apparently no correlation between the rock types and the terranes in which they occur. They display a large range in trace element concentrations that are generally characterized by incompatible element enriched patterns with negative Nb, Sr, P and Ti anomalies and positive Pb anomalies with respect to elements of similar incompatibility (Fig. 9).

Omineca Belt granitoids display a large range of present day Sr and Nd isotopic compositions (Table 3; Driver, 1998), whereas Intermontane Belt granitoid values are much more restricted and generally lower, the differences being similar to, but more pronounced than, the isotopic differences observed between the alkaline basalts of these two belts. Coast Belt granitoids and crustal xenoliths span a large range of present-day Sr isotopic ratios, but a more restricted range in present-day Nd isotopic values. In comparison, the alkaline lavas erupted through the Coast Belt have restricted range in both $^{87}\text{Sr}/^{86}\text{Sr}$ and $^{143}\text{Nd}/^{144}\text{Nd}$ ratios (Fig. 4). The granitoids we have examined define three groups in terms of their present-day Pb isotopic composition (Fig. 5). The samples

Table 3: Representative samples from Cassiar Batholith, Coast Belt crustal xenoliths and batholith, and Intermontane Belt batholiths. Analytical procedures as for basalts.

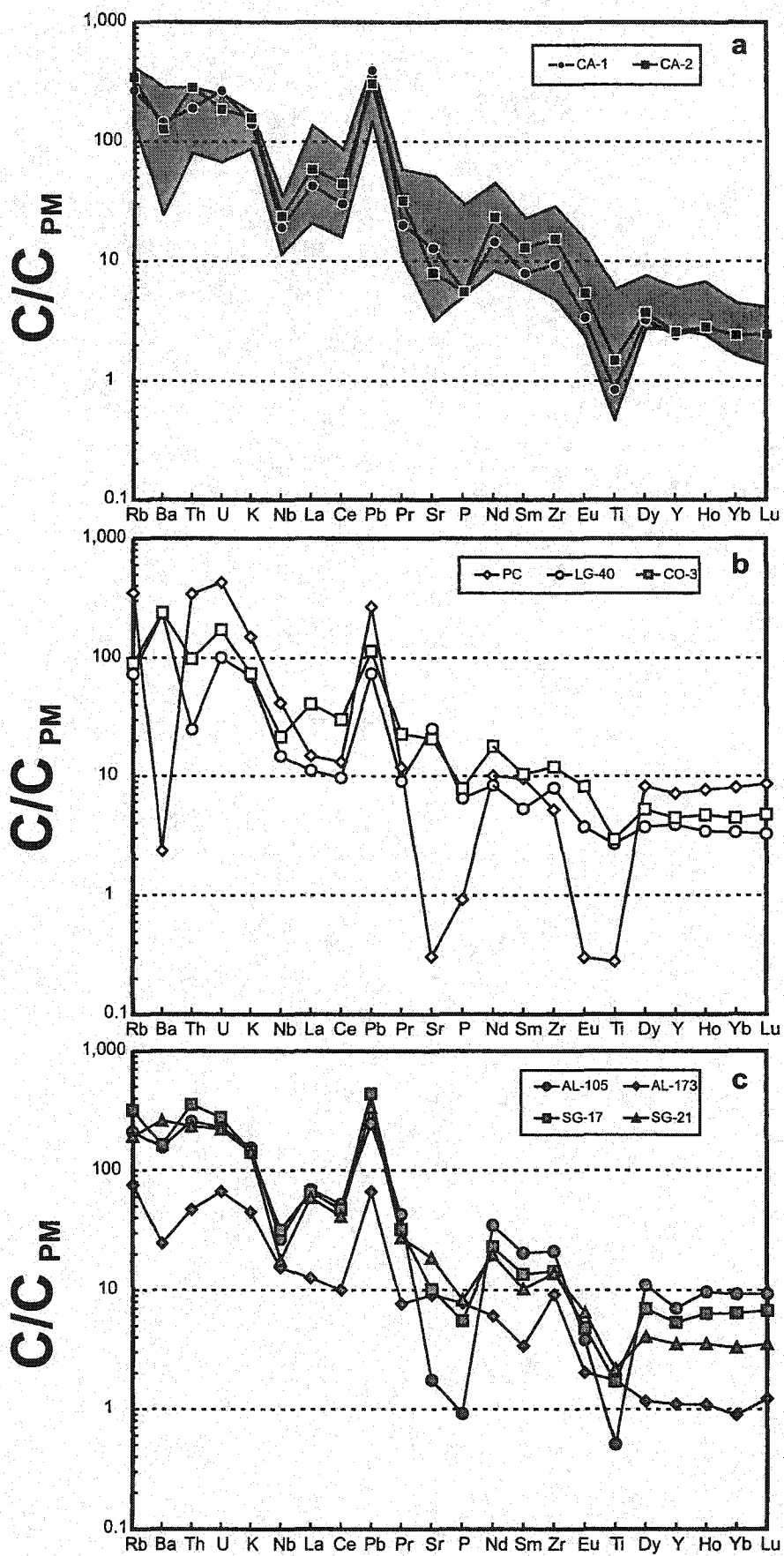
Table 3 : Major and trace elements of representative samples from Cassiar Batholith, Coast Belt crustal xenoliths and batholiths, and Intermontane Belt batholiths.

Sample Rock: Site	Omineca Belt		Intermontane Belt			Coast Belt			
	CA-1 Gr Pluton	CA-2 Gr Pluton	PC Gr Pluton	LG-40 Gd Pluton	CO-3 MsGd Pluton	AL-105 Gr Xenolith	AL-173 Gr Xenolith	SG-17 BtGr Pluton	SG-21 BtGd Pluton
	Cassiar	Cassiar	Parallel Creek	Llangorse	Chikoida Mtn	Alligator Lake	Alligator Lake	Skagway Road	Skagway Road
SiO ₂	73.66	72.42	76.16	64.14	64.42	75.05	72.22	70.32	67.86
TiO ₂	0.18	0.32	0.06	0.58	0.63	0.11	0.38	0.37	0.47
Al ₂ O ₃	14.52	14.69	12.91	16.11	15.93	12.78	15.93	14.75	15.8
FeO _T	1.29	1.77	1.12	4.94	4.44	1.49	1.63	2.49	3.14
MnO	0.04	0.04	0.08	0.12	0.10	0.03	0.01	0.06	0.07
MgO	0.29	0.45	0.06	2.08	1.95	0	0.58	0.68	1.1
CaO	1.33	1.42	0.48	5.46	4.82	0.2	0.51	1.95	2.75
Na ₂ O	3.45	3	4.3	2.99	3.09	4.04	5.73	3.91	3.9
K ₂ O	4.19	4.74	4.48	2.08	2.21	4.66	1.35	4.39	4.26
P ₂ O ₅	0.12	0.12	0.02	0.14	0.17	0.02	0.17	0.12	0.18
LOI	0.62	0.63	0.32	0.96	1.27	0.65	1.77	0.25	0.32
Total	99.68	99.6	99.98	99.6	99.02	99.03	100.28	99.29	99.84
Rb	169.7	217.3	219.4	46.2	56.7	133	48	201.2	121.7
Cs	-	-	-	1.5	1.5	-	-	4.76	2.46
Sr	269.2	166.5	6.4	529.7	434.3	37	192	214.3	393.9
Ba	1014	880	16.4	1635	1660	1087	172	1139	1817
V	-	23	-	90	67	-	50	25	54
Cr	-	-	13	17.1	26	-	64	-	-
Co	-	-	-	-	-	-	-	11	13
Ni	-	-	6	-	3	-	33	3	7.25
Zn	-	-	-	-	71	-	-	55	59
Cu	-	-	-	-	-	-	-	4	21
Ga	17.2	18.7	17.1	16	16.4	-	-	17.8	16
Y	10.8	11.6	32.2	17.6	20.1	32	5	24.3	16
Zr	103.4	169.8	57.7	88.2	133.3	237	103	161.2	153.8
Nb	13.6	16.8	29.5	10.5	15.3	19	11	22.7	12.7
Hf	-	-	-	-	5.1	6.7	-	-	-
Ta	-	2.3	1.2	-	1.06	-	-	-	-

Table 3: continued

Sample	CA-1	CA-2	PC	LG-40	CO-3	AL-105	AL-173	SG-17	SG-21
Th	16.1	24.1	28.9	2.1	8.31	21.8	4	30.1	19.80
U	5.6	3.9	8.9	2.1	3.58	4.8	1.4	5.8	4.64
Pb	28	21.6	18.7	5.2	7.99	17.4	4.7	31.1	23.58
La	28.91	39.88	10.16	7.64	27.82	47.33	8.69	45.39	40.66
Ce	52.85	77.93	23.23	17.08	53.11	92.73	17.83	83.40	73.22
Pr	5.5	8.7	3.25	2.49	6.24	11.84	2.12	8.92	7.61
Nd	19.49	31.25	13.55	11.22	24.07	47.11	8.23	31.14	26.70
Sm	3.5	5.73	4.2	2.33	4.57	9.08	1.5	6.02	4.56
Eu	0.56	0.9	0.05	0.62	1.36	0.64	0.34	0.81	1.10
Gd	2.58	4.16	4.9	2.7	4.14	8.52	0.98	5.20	3.59
Tb	0.4	0.53	0.93	0.43	0.64	1.27	0.13	0.85	0.51
Dy	2.36	2.72	6	2.73	3.84	8.13	0.86	5.14	2.98
Ho	0.46	0.46	1.25	0.56	0.77	1.59	0.18	1.05	0.58
Er	1.35	1.34	3.7	1.78	2.24	4.61	0.5	3.13	1.71
Tm	0.19	0.18	0.58	0.27	0.32	0.68	0.07	0.45	0.24
Yb	1.18	1.18	3.93	1.65	2.18	4.58	0.44	3.16	1.62
Lu	0.18	0.18	0.63	0.24	0.35	0.69	0.09	0.50	0.26
$^{87}\text{Sr}/^{86}\text{Sr}$	0.714022	0.723522	0.96327	0.704719	0.704940	0.713998	0.705095	0.707977	0.706159
$^{143}\text{Nd}/^{144}\text{Nd}$	-	0.511916	0.512867	0.512665	0.512634	0.512532	-	0.512604	0.512592
$^{206}\text{Pb}/^{204}\text{Pb}$	19.609	19.580	19.585	19.823	19.732	19.355	19.302	19.359	19.380
$^{207}\text{Pb}/^{204}\text{Pb}$	15.713	15.703	15.637	15.694	15.680	15.673	15.645	15.649	15.658
$^{208}\text{Pb}/^{204}\text{Pb}$	39.373	39.624	38.986	38.871	39.165	39.25	39.218	38.937	38.966

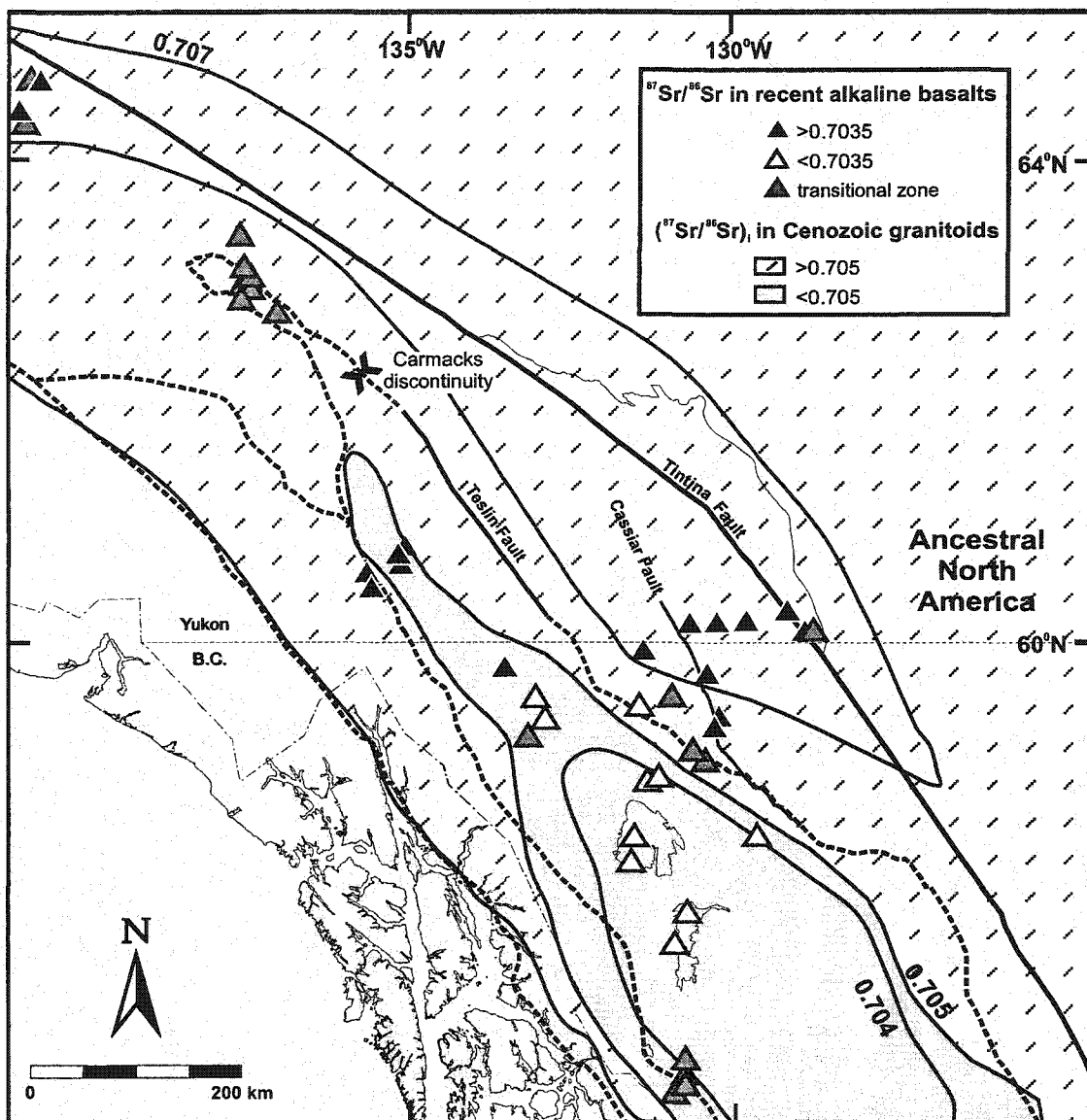
Figure 9: Trace element concentrations of crustal batholiths and xenoliths from Table 3, normalized to the composition of the primordial mantle (Sun and McDonough, 1989). a) samples from Omineca Belt. The shaded field corresponds to the range of Cassiar Batholith (Driver, 1998) b) samples from the Intermontane Belt and c) samples from the Coast Belt.



in the Omineca Belt have high $^{206}\text{Pb}/^{204}\text{Pb}$, $^{207}\text{Pb}/^{204}\text{Pb}$, and $^{208}\text{Pb}/^{204}\text{Pb}$ ratios (above the NHRL), whereas granitoids within the Intermontane Belt have similar $^{206}\text{Pb}/^{204}\text{Pb}$ ratios, but lower $^{207}\text{Pb}/^{204}\text{Pb}$ and $^{208}\text{Pb}/^{204}\text{Pb}$ ratios, only slightly above the NHRL. Finally, Coast Belt granitoids have $^{207}\text{Pb}/^{204}\text{Pb}$ and $^{208}\text{Pb}/^{204}\text{Pb}$ ratios comparable to those of the Intermontane Belt granitoids, but distinctly lower $^{206}\text{Pb}/^{204}\text{Pb}$ ratios. In comparison, alkaline basalts erupted in the Omineca Belt, Intermontane Belt and Coast Belt define two distinct groups rather than three in terms of their Pb isotopic compositions, Intermontane Belt and Coast Belt basalts having low Pb isotopic ratios and those in the Omineca Belt having much higher values (Fig. 5).

The existence of distinct initial isotopic domains in the Canadian Cordillera has already been established for upper crustal granitoids and a wide variety of crustal lithologies (Armstrong, 1988; Samson et al., 1989, 1991; Gehrels et al., 1990; Gehrels and Kapp, 1998). There is a rough correspondence between the $^{87}\text{Sr}/^{86}\text{Sr}$ variations in the Recent alkaline volcanic rocks in the Northern Cordillera and the "Sr lines" defined by Armstrong (1988) on the basis of initial Sr ratios in Mesozoic and Cenozoic granitoids (Fig. 10). Across the tectonic boundary between the Intermontane Belt and the Omineca Belt, the initial $^{87}\text{Sr}/^{86}\text{Sr}$ isotopic ratios in crustal granitoids increase from less than about 0.705 to the West to higher than 0.705 to the East (Armstrong, 1988; Fig. 10). Across the Intermontane-Coast Belt tectonic boundary, in the Northern Cordillera, there is a change in the $^{87}\text{Sr}/^{86}\text{Sr}$ initial ratios of crustal granitoids from values lower than 0.705 to the East to values higher than 0.705 to the West, accompanied by a corresponding change in initial $^{143}\text{Nd}/^{144}\text{Nd}$ ratios (Samson et al., 1991). The geographic coincidence of the isotopic changes in crustal granitoids and Recent alkaline basalts across the

Figure 10: Sr isotopic signatures in Recent alkaline basalts compared to contoured Sr initial ratios in Cenozoic granitoids (Armstrong, 1988) and to the location of the isotopic discontinuity observed in the Carmacks volcanics.



Intermontane-Omineca Belt boundary suggests that either the alkaline magmas have been contaminated by crustal granitoids on their way to the surface, or the existence of a genetic link in the magma sources for these 2 suites of igneous rocks.

5. Discussion

5.1. Evaluation of crustal contamination.

Alkaline basalts erupted in the Intermontane Belt have lower $^{87}\text{Sr}/^{86}\text{Sr}$ and higher $^{143}\text{Nd}/^{144}\text{Nd}$ ratios than their equivalents erupted in the Coast Belt and Omineca Belt. At the same time, both the Intermontane Belt and Coast Belt lavas have unradiogenic Pb signatures compared to the Omineca Belt basalts (Fig. 8a). There are several possible explanations for this terrane dependence. First, all the basalts may have originated from a similar mantle source, and their differences may reflect contamination by different crustal material. This is the model adopted by Cousens and Bevier (1995) to explain the Iskut-Unuk volcanic field characteristics, such as positive Ba and negative Nb anomalies that increase in size with increasing SiO₂. Their proposed contaminants are Stikine Terrane metavolcanic rocks of the Stuhini and Hazelton Groups (Thorkelson, 1992). A second possible model is that the different signatures of the basalts reflect differences in their mantle sources. This interpretation was proposed by Eiché et al. (1987) for the Alligator Lake centre in the Coast Belt, and used by Carignan et al. (1994) to explain the isotopic differences between Alligator Lake basalts and basalts erupted in the Intermontane Belt.

A third possibility is that both mantle source differences and crustal contamination play a role in producing the differences in the isotopic signatures of the Omineca Belt, Intermontane Belt and Coast Belt basalts.

The shift in isotopic composition of lavas in the Omineca Belt compared to the Intermontane Belt (Fig. 11a) could suggest that Omineca Belt alkaline lavas have suffered more crustal contamination than Intermontane Belt lavas, or have been contaminated by a more radiogenic crust. In addition, simple bulk mixing calculations indicate that the slightly lower Nb/La ratios of Intermontane Belt Hy-NORM compared to Omineca Belt Hy-NORM could be explained by approximately 15% bulk contamination of a primitive Intermontane Belt Hy-HORM (MH-19, see table 2) by Cassiar granitoid (Fig. 12). It is difficult, however, to reconcile the high MgO content (>10 wt.%) of some of the Omineca Hy-Norm with 15% contamination by upper crustal material, and thus the Nb/La difference might well be a source characteristic.

Within each belt, there is a tendency for the range of Sr and Pb isotopic compositions to decrease with increasing MgO (Fig. 11), especially if attention is restricted to the Hy-NORM end-member (Fig. 13), but there is no overlap or convergence between the Intermontane Belt and Omineca Belt lavas. This suggests that the lavas of both belts may have experienced some AFC style contamination. We quantitatively tested the effects of crustal contamination during crystal fractionation within each belt using a model for fractional crystallization and assimilation (FCA) similar to that of Cribb and Barton (1996), in which the assimilated material is added step-by-step to the

Figure 11: $^{87}\text{Sr}/^{86}\text{Sr}$ versus MgO (wt.%). Symbols and data source as in Fig. 4.

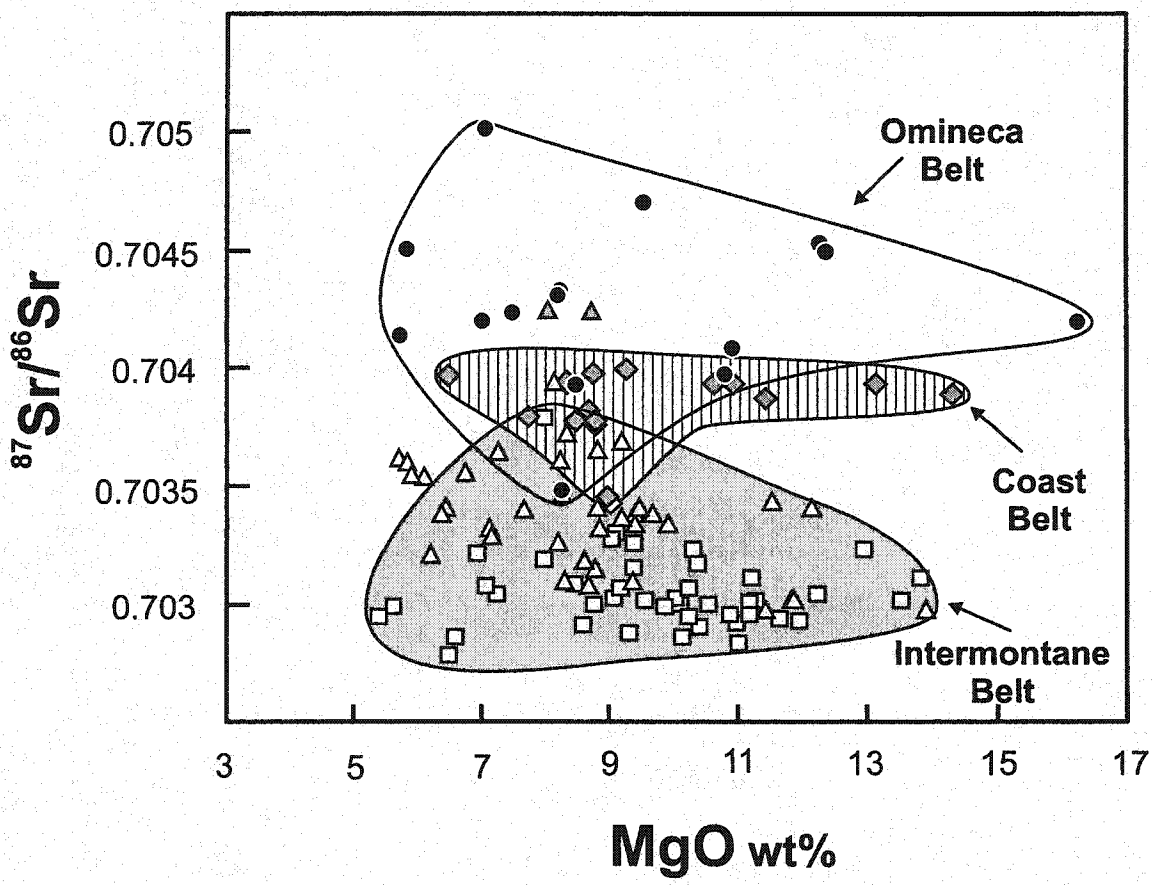
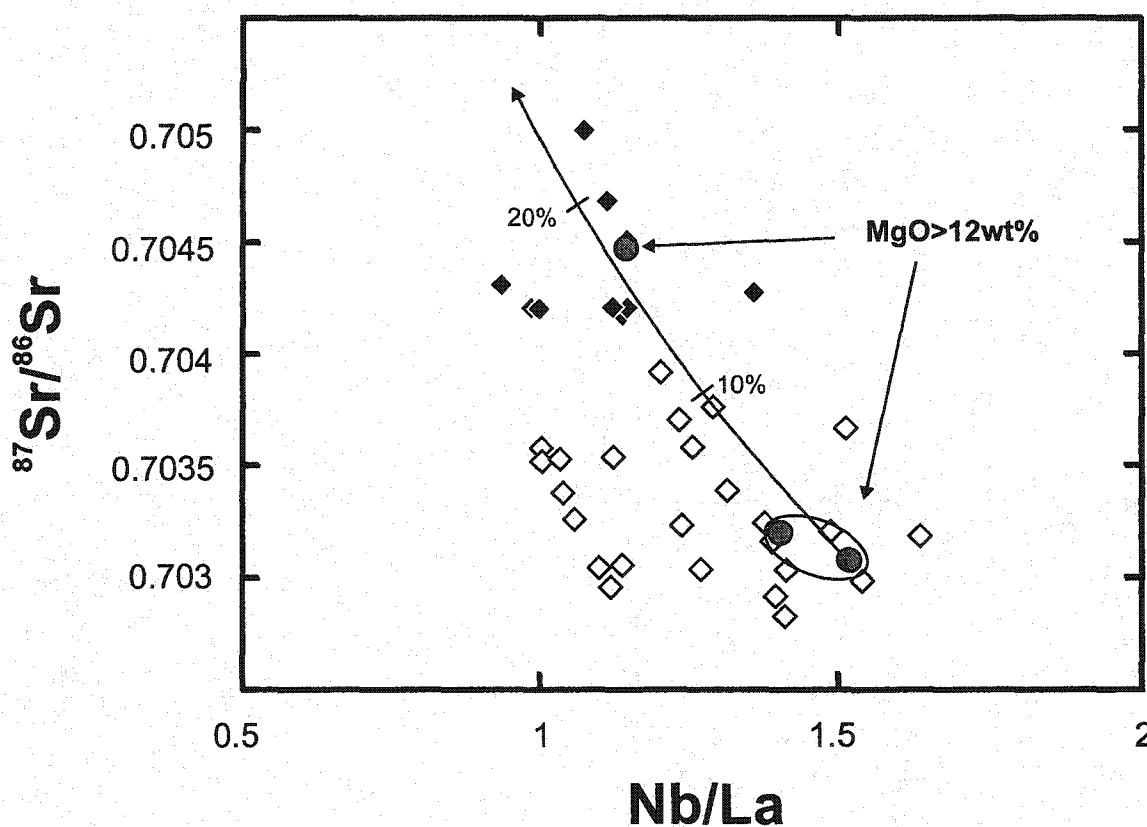
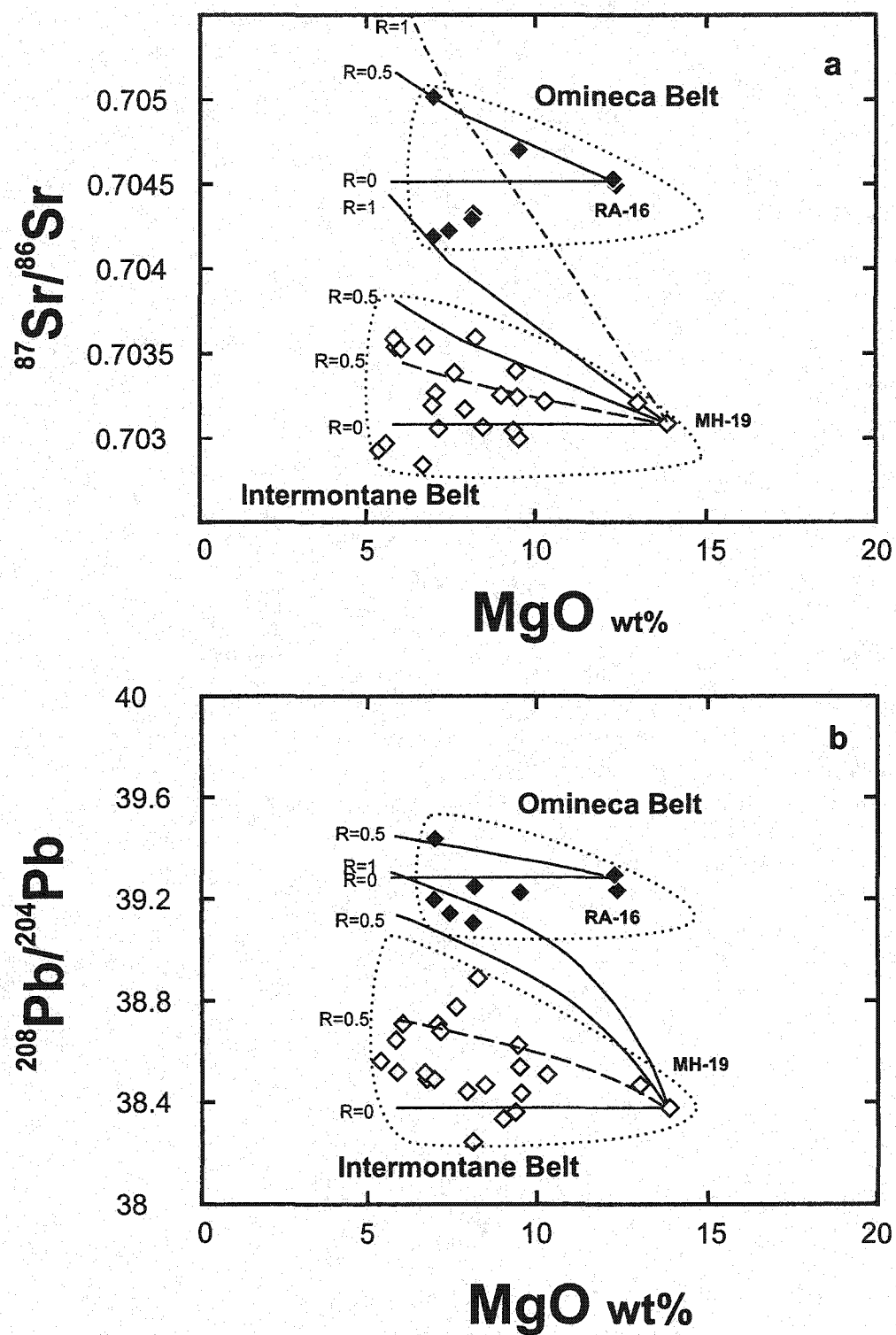


Figure 12: $^{87}\text{Sr}/^{86}\text{Sr}$ versus Nb/La for Hy-NORM basalts erupted in the Intermontane Belt (white symbols) and Omineca Belt (black symbols). The line correspond to simple bulk mixing between MH-19 (Table 2) and CA-2 (Table 3).



fractionated magma, with a constant ratio R of material assimilated versus solid crystallized. This allows us to model major, trace, and isotopic ratios together. MH-19 and RA-16 (Table 2) were used as parental magmas for Intermontane Belt and Omineca Belt Hy-NORM basalts, respectively. The upper crustal contaminants are PC, a granite from Parallel Creek batholith in the Intermontane Belt and CA-2, a granite from the Cassiar batholith in the Omineca Belt. These two upper crustal samples were chosen because they are the most efficient samples in each belt in producing changes in Sr isotopic composition by bulk mixing. This selection takes into account the effects of both the $^{87}\text{Sr}/^{86}\text{Sr}$ ratio and the Sr concentration in the contaminant. Lower crustal xenoliths are rarely found in Northern Cordillera (Edwards et al., 1999) and thus the possibility that the lower crust in this area might have an isotopic and chemical signature capable of explaining the characteristics of the Omineca Belt and Coast Belt samples cannot be excluded. Indeed, although the lower crust is thought to be less radiogenic in Sr and Pb than the upper crust, it may acquire a radiogenic signature by incorporation of upper crustal material during and after accretion (Rudnick, 1990; Rudnick and Goldstein, 1990; Chen and Arculus, 1995). Although mafic granulite xenoliths with high $^{87}\text{Sr}/^{86}\text{Sr}$ are statistically rare and usually have low Sr concentrations, we again used bulk mixing contamination calculations to select a lower crustal mafic contaminant from the literature (83-140; Rudnick, 1990), that would be the most efficient in producing changes in Sr isotopic composition.

Figure 13: a) $^{87}\text{Sr}/^{86}\text{Sr}$ and b) $^{208}\text{Pb}/^{204}\text{Pb}$ versus MgO (wt.%) for Hy-NORM basalts erupted in the Intermontane Belt (white symbols) and Omineca Belt (black symbols). The lines correspond to results of FCA calculation (see text) with different R and different contaminants (full lines = CA-2, dotted lines = PC, short and long dottes lines = granulite 83-140).



A range of FCA models using the upper crustal xenoliths, in which R varied from 0 to 0.5, can explain the increase in range of isotopic composition with decreasing MgO within both the Intermontane Belt and Omineca Belt lavas (Fig. 13a). This corresponds to a minimum value of 5% of contamination for the low MgO basalts by upper crustal granites. However, using Intermontane Belt basalt MH-19 as parent and unrealistic R values as high as 1, we could not reproduce the signature of the primitive Omineca Belt basalts using these felsic granitoids. Models using 83-140 as a possible lower crustal contaminant were also not effective in accounting for the differences between the Omineca Belt and Intermontane Belt basalts (Fig. 13a). We thus argue that, although some lavas in both suites have suffered assimilation and crystal fractionation processes, the isotopic shift between Intermontane Belt and Omineca Belt lavas must have been generated prior to fractionation processes recorded in the lavas, i.e., before their ascent through the crust.

The alkaline basalts erupted at Alligator Lake in the Coast Belt (Eiché et al., 1987) are characterized by a very small range in Sr, Nd and Pb isotopic compositions, despite a large range in SiO₂ and MgO (Carignan et al., 1994). These lavas, as well as lavas from Miles Canyon and the Atlin area (Fig. 1), form a distinct isotopic group characterized by high ⁸⁷Sr/⁸⁶Sr, low ¹⁴³Nd/¹⁴⁴Nd and Pb isotopic ratios. In order to evaluate the effects of upper crustal contamination, we analyzed crustal fragments from Alligator Lake and Coast Range batholith samples (Table 3). Although bulk mixing is highly improbable, we use bulk mixing models between MH-19 and these granitoids to illustrate the relative variation in the Sr and Pb isotopic values that would be produced from upper crustal contamination (Fig. 8a). These calculations demonstrate that the Coast Belt granitoids are

too radiogenic in Pb to explain the systematically low Pb isotopic signatures of the Coast Belt lavas despite their high $^{87}\text{Sr}/^{86}\text{Sr}$ ratios (Fig. 8a). In addition, the very restricted range in $^{87}\text{Sr}/^{86}\text{Sr}$ ratios of the three different magma types of the Coast Belt lavas argues against contamination, which would be less effective in the Sr-rich BASAN than the relatively Sr-poor Hy-NORM. The high $^{87}\text{Sr}/^{86}\text{Sr}$ signature of the Coast Belt lavas is thus also thought to have been acquired before passage through the crust.

We conclude that, although some basalts may have been affected by small degrees of contamination during their ascent through the crust, the distinctive Sr, Nd, and Pb isotopic characteristics of the high-MgO Hy-NORM basalts of the Omineca Belt, Coast Belt and Intermontane Belt reflect differences in their mantle source regions. These results suggest that the lithospheric mantle roots of the Omineca Belt and Coast Belt are isotopically enriched compared to that of the Intermontane Belt.

5.2. Evidence for distinct lithospheric mantle roots.

If the isotopic differences between the Recent alkaline basalts of the Intermontane Belt, Omineca Belt, and Coast Belt originated in their mantle source regions, then lithospheric mantle roots were preserved beneath the large superterranea constituting the Canadian Cordillera during their accretion to the North American continental margin. These results seem inconsistent with the interpretation of recent Os isotopic results on mantle xenoliths by Peslier et al. (2000), which suggest the possibility of a single age of formation for the Cordilleran lithospheric mantle around 1.1 Ga, independent of tectonic

terranes. However, given the possible uncertainties in Os model ages and the fact that similar Proterozoic Os model ages predominate in Post-Archean mantle peridotites, the significance of these Proterozoic model ages must be interpreted with caution. In addition, these Os results do not preclude the possibility that the lithospheric mantle roots beneath the different tectonic belts of the Cordillera have experienced different metasomatic events since their stabilization.

The Omineca Belt lithospheric mantle must have been enriched to account for the Sr, Nd and Pb signatures of its alkaline basalts. The occurrence of isotopically enriched signatures in Late Cretaceous high-MgO ankaramites and in mantle xenoliths sampled by the Recent alkaline lavas (Francis and Johnson, 1998; Carignan et al., 1996) also suggests that parts of the lithospheric mantle beneath the Northern Cordillera have been modified. The timing of the enrichment of the mantle source region of the Omineca Belt alkaline basalts is not well constrained, but presumably occurred before the accretion of the Intermontane Belt to the Omineca Belt (i.e., before Mid Jurassic; Monger et al., 1982). One possible way to isotopically enrich the mantle would be to incorporate small amounts of terrigenous sediment in the upper mantle during the collision of the Intermontane Belt and the paleomargin of North America. The slightly lower Nb/La ratios in the Hy-NORM from the Omineca Belt compared to the Intermontane Belt (Fig. 12) would be consistent with addition of small amounts of crustal material in the source of Omineca Belt Hy-NORM. This possibility will be explored in a following paper.

The source region of the Coast Belt basalts may have been enriched either before the accretion of the Insular Belt to the Intermontane Belt (i.e., before mid-Cretaceous,

Monger et al., 1982), or more recently (post mid-Cretaceous) if related to the mantle thermal anomaly situated under the Yukon (Frederiksen et al., 1998). This latter interpretation would be consistent with the U-Pb systematics of mantle xenoliths that suggest an age of <30 Ma for the enrichment of the Coast Belt subcontinental lithosphere beneath Alligator Lake (Carignan et al., 1996). This would also be in agreement with the fact that enrichment in $^{87}\text{Sr}/^{86}\text{Sr}$ is not accompanied by strong Pb isotopic enrichments in either the lavas or mantle xenoliths at Alligator Lake, suggesting that the Coast Belt and western Intermontane Belt lithospheric mantle may have been affected by one major enrichment event. The differences in isotopic composition between alkaline basalts and the xenoliths they carry in the Llangorse volcanic field (Carignan et al. 1996, Fig. 8b) indicate that the xenoliths sample parts of the lithospheric mantle that are different from the lavas source regions. In addition, the similar isotopic trends of Alligator Lake and the Llangorse mantle xenoliths might indicate that the enriched lithosphere related to the Coast Belt extends partly beneath the Intermontane Belt, under the Llangorse volcanic field.

5.3. Tectonic implications

5.3.1. Tintina Fault

The distinct change in the Zr content in Recent alkaline basalts across the Tintina Fault, along with lower HREE abundances in the lavas erupted on the east side of the fault, has been interpreted to reflect a change to a more garnet-rich cratonic peridotite

($K_D^{Gnt/Melt}$ (HREE)>1) or greater depth of origin of the basalts on the east side of the Tintina fault than under the Cassiar Terrane to the West (Hasik, 1994). In addition, the changes in Sr, and Nd isotopic compositions in the AOB across the fault indicate that the mantle source of samples erupted on the east side of the fault, in the Watson Lake area, was isotopically more depleted than the mantle source of the Omineca Belt basalts.

These source differences must be situated in the lithosphere because the isotopic signature of the asthenospheric mantle should not be related to lithospheric terrane boundaries. However, the nature and origin of the lithosphere underlying the Watson Lake area are not well constrained, in part because this part of the Yukon Tanana terrane has been translated at least 400 km south along the Tintina Fault (Roddick, 1967). There are at least two possible origins for the lithospheric upper mantle in this area. First, as the upper crustal part of the Yukon Tanana terrane near Watson Lake has clearly been thrust over the North American craton margin before its southward translation (Tempelman-Kluit, 1979), the underlying lithospheric mantle might be that of the North American craton. However, another possibility is that either the Yukon Tanana or Intermontane Belt lithospheric mantle may have been transported South along the Tintina fault, and been juxtaposed with the isotopically enriched lithospheric mantle beneath the Cassiar terrane.

The changes in isotopic signatures of basalts on either side of the Tintina Fault are observed in volcanic centres situated in the Tintina Trench separated by less than 5 km from each other. Regardless of the origins of the chemical and isotopic differences observed in the alkaline basalts across the fault, the data indicate that the Tintina Fault is

a high-angle feature that penetrates the lithosphere and juxtaposes two isotopically distinct lithospheric mantles.

5.3.2. *Omineca Belt –Intermontane Belt transition*

The change in Sr, Nd and Pb isotopic signatures of basalts from the Omineca Belt to the Intermontane Belt occurs slightly to the east of the accepted tectonic boundary between the two Belts at the surface, at the western edge of the Dorsey terrane (Wheeler and McFeely, 1991; Fig. 1), and between Armstrong's 0.705 and 0.707 Sr-lines defined on the basis of initial $^{87}\text{Sr}/^{86}\text{Sr}$ ratios in Mesozoic and Cenozoic granitoids (Fig. 10).

Further North (latitude 62°N), Francis and Johnson (1998) have shown the existence of a discontinuous change in the $^{87}\text{Sr}/^{86}\text{Sr}$ (Fig. 8a) and $^{143}\text{Nd}/^{144}\text{Nd}$ initial ratios at the Yukon River in the late Cretaceous Carmacks volcanics (Fig. 10). Initial $^{87}\text{Sr}/^{86}\text{Sr}$ ratio of these high MgO lavas change from less than 0.705 west of the Yukon River to more than 0.706 east of the Yukon River. This discontinuity corresponds to the Northern extension of the Teslin fault, in the tectonically equivalent position to the isotopic discontinuity observed in the Recent alkaline magmas of the Stikine Volcanic Belt at the Intermontane-Omineca Belt boundary to the South (Fig. 10). Thus, the isotopic signature of both the Recent alkaline basalts and late Cretaceous Carmacks lavas appear to have detected a lithospheric transition between the Omineca Belt and the Intermontane Belt. The Carmacks volcanic rocks and the Mesozoic and Cenozoic plutons (Armstrong, 1988) are isotopically similar, whereas the alkaline basalt signatures are significantly less

radiogenic in Sr. The intermediate isotopic signatures of Fort Selkirk basalts (Fig. 1) and of the three Recent alkaline volcanic centres situated in the Dorsey and Quesnellia terranes (Fig. 1; Fig. 6; Fig. 7) may reflect an east dipping contact between Intermontane Belt and Omineca Belt, or the existence of a zone of mixing near this tectonic boundary.

5.3.3. *Intermontane Belt-Coast Belt transition*

Alkaline basalts erupted in the Coast Belt and in the western part of the Intermontane Belt are characterized by a very small range in Sr, Nd and Pb isotopic compositions, despite a large range in SiO₂ and MgO. As these signatures cannot be explained by crustal contamination of parental magmas with Intermontane Belt signatures, they appear to represent the underlying lithospheric mantle signatures. It is unclear, however, what the Coast Belt -Intermontane Belt boundary represents. On one hand, it may reflect the boundary between two juxtaposed lithospheric blocks with different isotopic signatures. Samson et al. (1991) argued that a Proterozoic crustal component is needed to explain the Nd isotopic characteristics of some Coast Mountain batholiths in the Northern Cordillera. Their best candidates were rocks of the Yukon Crystalline Terrane, which were later assigned to the Nisling or Yukon-Tanana terranes. This old lithosphere situated on the western side of the Intermontane Belt may have been preserved and been sampled by the Recent alkaline basalts. In that case, the high ⁸⁷Sr/⁸⁶Sr ratios reflect an old Rb enrichment in the lithosphere and the suture between the Coast Belt and the Intermontane Belt lithospheres would appear to dip to the east at latitude 60°N, where isotopically enriched alkaline basalts extend well into the

Intermontane Belt (Fig. 1). On the other hand, the distinctive signature in the Recent alkaline basalts of the northern Coast Belt may be related to modification of the lithosphere by underlying hot asthenospheric mantle that has recently been discovered teleseismically under this area (Fredericksen et al., 1998), and which might be related to late Cretaceous Carmacks volcanism (Johnson et al., 1996) or the Eocene magmatic event. This hot mantle anomaly has been interpreted as representing either a thermal plume (Shi et al., 1998) or asthenospheric material rising to fill the gap created by a slab window (Fredericksen et al., 1998). In this case, the isotopic data cannot be used to infer the dip of the suture between the Coast Belt and Intermontane Belt lithospheric blocks.

6. Conclusion

Alkaline basalts in the northern Canadian Cordillera are reliable probes of the underlying lithospheric mantle because they have erupted at the surface with little interaction with the crust. A systematic study of alkaline volcanic centres across the Northern Cordillera has detected domains with distinct isotopic signatures. A change in Sr and Nd isotopic ratios across the Tintina fault indicates that it has a steep dip, and separates two different lithospheric mantles. The tectonic correspondence of isotopic discontinuities in Cretaceous Carmacks volcanics and Recent alkaline basalts suggests that the Omineca Belt-Intermontane Belt boundary is a major lithospheric feature that juxtaposes distinct mantle roots and that has been conserved since the accretional tectonics that assembled the Northern Canadian Cordillera. A change in the isotopic signatures between Intermontane Belt and Coast Belt occurs in the western part of the

Intermontane Belt. The eastern displacement in this change from the tectonic boundary at the surface indicates that enriched lithosphere related to the Coast Belt basalts extends partly beneath the Intermontane Belt.

Acknowledgements

We thank Tariq Ahmedali and Glenna Jackson for performing the XRF analyses, Bernard Reynier and Michel Valladon for assistance in obtaining the ICP-MS analysis, and especially Pierre Brunet for training and help with the TIMS analysis. We thank Jean Carignan for making available his unpublished isotopic data for both alkaline lavas and mantle xenoliths. The editor, N. Arndt, and the reviewers J. Dostal and R. Kerrich are thanked for their reviews. This research was supported by NSERC and LITHOPROBE grants to D. F. and CNRS funds to M. P. Lithoprobe Publication No. 1153.

References

- Armstrong, R.L., 1988. Mesozoic and early Cenozoic magmatic evolution of the Canadian Cordillera. *Geol. Soc. Am. Spec. Pap.* 218, 55-91.
- Carignan, J., Ludden, J., Francis, D., 1994. Isotopic constraints on the mantle sources for Quaternary continental alkaline magmas in the northern Canadian Cordillera. *Earth Planet. Sci. Lett.* 128, 271-286.
- Carignan, J., Ludden, J., Francis, D., 1996. On the Recent enrichment of the subcontinental lithosphere: A detailed U-Pb study of spinel lherzolite xenoliths, Yukon, Canada. *Geochim. Cosmochim. Acta* 60, 4241-4252.
- Chen, W., Arculus, R. J., 1995. Geochemical and isotopic characteristics of lower crustal xenoliths, San Francisco volcanic field, Arizona, U.S.A. *Lithos* 36, 203-225.
- Cousens, B.L., Bevier, M.L., 1995. Discerning asthenospheric, lithospheric and crustal influences on the geochemistry of Quaternary basalts from Iskut-Unuk rivers area, northwestern British Columbia. *Can. J. Earth Sci.* 32, 1451-1461.
- Cribb, J.W., Barton, M., 1996. Geochemical effects of decoupled fractional crystallization and crustal assimilation. *Lithos*, 37, 293-307
- Currie, L., Parrish, R.R., 1993. Jurassic accretion of Nisling terrane along the western margin of Stikinia, Coast Mountains, northwestern British Columbia. *Geology* 21, 235-238.
- DePaolo, D.J., 1981. Trace element and isotopic effects of combined wallrock assimilation and fractional crystallization. *Earth Planet. Sci. Lett.* 53, 189-202.
- Driver, L.A., 1998. Petrogenesis of the Cretaceous Cassiar Batholith, Yukon-B.C., Canada: Implications for Magmatism in the North American Cordilleran Interior. M.Sc. thesis, University of Alberta, Canada.
- Edwards, B.R., Russell, J.K., 1999. Northern Cordilleran volcanic province; a northern Basin and Range? *Geology* 27, 243-246.
- Eiché, G., Francis, D., Ludden, J., 1987. Primary alkaline magmas in the Quaternary Alligator Lake volcanic complex, Yukon, Canada. *Contrib. Mineral. Petrol.* 95, 191-201.

- Francis, D., 1987. Mantle-melt interaction recorded in spinel lherzolite xenoliths from the Alligator Lake Volcanic Complex, Yukon, Canada. *J Petrol.* 28, 569-597.
- Francis, D., Johnston, S.T., 1998. Isotopic constraints on lithospheric melting near the Yellowstone hotspot, Carmacks Volcanics, Yukon. *Geol. Soc. Am. Abstr. Programs* A90.
- Francis, D., Ludden, J., 1990. The mantle source for Olivine Nephelinite, Basanite, and Alkaline olivine basalt at Fort Selkirk, Yukon, Canada. *J. Petrol.* 31, 371-400.
- Francis, D., Ludden, J., 1995. The signature of amphibole in mafic alkaline lavas, a study in the northern Canadian Cordillera. *J. Petrol.* 36, 1171-1191.
- Frederiksen, A.W., Bostock, M.G., Van Decar, J. C., Cassidy, J., 1998. Seismic structure of the upper mantle beneath the northern Canadian Cordillera from teleseismic travel-time inversion. *Tectonophysics*, 294, 43-55.
- Gabrielse, H., 1985. Major dextral transcurrent displacements along the Northern Rocky Mountain Trench and related lineaments in north-central British Columbia. *Geol. Soc. Am. Bull.* 96, 1-14.
- Gabrielse, H. Yorath, C.J., 1991. Tectonic synthesis. In: H. Gabrielse and C.J. Yorath (Editors), *Geology of the Cordilleran Orogen in Canada*. Geol. Surv. Can., *Geology of Canada*, pp. 677-705.
- Gehrels, G.E., Kapp, P.A., 1998. Detrital zircon geochronology and regional correlation of metasedimentary rocks in the Coast Mountains, southeastern Alaska. *Can. J. Earth Sci.* 35, 269-279.
- Gehrels, G.E., McClelland, W.C., Samson, S.D., Patchett, P.J., Jackson, J.L., 1990. Ancient continental margin assemblage in the northern Coast Mountains, southeast Alaska and northwest Canada. *Geology* 18, 208-211.
- Godwin, C.I., Sinclair, A.J., 1982. Average lead isotope growth curves for shale-hosted zinc-lead deposits, Canadian Cordillera. *Econ. Geol.* 77, 675-690.
- Hamilton, T.S., 1981. Late Cenozoic alkaline volcanics of the Level Mountain Range, northwestern British Columbia. Ph.D. thesis, University of Alberta, Canada.
- Hart, C.J.R., 1995. Magmatic and tectonic evolution of the Intermontane Superterrane and Coast Complex in southern Yukon Territory. M.Sc. thesis, University of British Columbia, Canada.

- Hart, S.R., 1984. A large-scale isotope anomaly in the Southern Hemisphere mantle. *Nature* 309, 753-757.
- Hasik, V., 1994. Volcanic evidence for a compositional contrast in the lithospheric upper mantle across the Tintina Trench, Southeastern Yukon, Canada, M.Sc. thesis, University of McGill, Canada.
- Hyndman, R. D., Lewis, T.J., 1999. Geophysical consequences of the Cordillera-Craton thermal transition in southwestern Canada. *Tectonophysics* 306, 397-422.
- Irving, E., Wynne, P.J., Thorkelson, D.J., Schiarizza, P., 1996. Large (1000 to 4000 km) northward movements of tectonic domains in the northern Cordillera, 83 to 45 Ma. *J. of Geophys. Res.* 101, 17901-17916.
- Johnston, S.T., Wynne, P.J., Francis, D., Hart, C.J., Enkin, R.J., Engebretson, D.C., 1996. Yellowstone in Yukon: the Late Cretaceous Carmacks Group. *Geology* 24, 997-1000.
- Le Bas, M.J., Le Maitre, R.W., Streckeisen, A., Zanettin, B., 1986. A chemical classification of volcanic rocks based on the total alkali-silica diagram. *J. Petrol.* 27, 745-750.
- Menzies, M., 1987. Alkaline rocks and their inclusions: a window on the Earth's interior. In: J.G. Fitton and B.G. Upton (Editors), *Alkaline Igneous Rocks*, pp. 15-27.
- Monger, J.W.H., Price, R.A. Tempelman-Kluit, D.J., 1982. Tectonic accretion and the origin of the two major metamorphic and welts in the Canadian Cordillera. *Geology*, 10, 70-75.
- O'Reilly, S.Y. Zhang, M., 1995. Geochemical characteristics of lava-field basalts from eastern Australia and inferred sources: connections with the subcontinental lithospheric mantle?. *Contrib. Mineral. Petrol.* 121, 148-170.
- Peslier, A.H., 1999. Pétrologie et géochimie isotopique de xénolites mantelliques de la Cordillère Canadienne. Ph.D thesis, Université de Montréal, Canada.
- Peslier, A.H., Reisberg, L., Ludden, J., Francis, D., 2000. Os isotopic systematics in mantle xenoliths; age constraints on the Canadian Cordillera lithosphere. *Chem. Geol.* 166, 85-101.
- Price, R.C., Gray, C.M., Frey, F.A., 1997. Strontium isotopic and trace element heterogeneity in the plains basalts of the Newer Volcanic Province, Victoria,

- Australia. *Geochim. Cosmochim. Acta* 61, 171-192.
- Roddick, J.A., 1967. Tintina Trench. *J. of Geol.* 75, 23-33.
- Rudnick, R.L., 1990. Nd and Sr isotopic compositions of lower-crustal xenoliths from north Queensland, Australia: Implications for Nd model ages and crustal growths processes. *Chem. Geol.* 83, 195-208.
- Rudnick, R.L., Goldstein, S.L., 1990. The Pb isotopic compositions of lower crustal xenoliths and the evolution of lower crustal Pb. *Earth Planet. Sci. Lett.* 98, 192-207.
- Samson, S.D., McClelland, W.C., Patchett P.J., Gehrels, G.E., Anderson, R.G., 1989. Evidence from neodymium isotopes for mantle contributions to Phanerozoic crustal genesis in the Canadian Cordillera. *Nature* 337, 705-709.
- Samson, S.D., Patchett, P.J., McClelland, W.C. Gehrels, G.E., 1991. Nd isotopic characterization of metamorphic rocks in the Coast Mountains, Alaskan and Canadian Cordillera: ancient crust bounded by juvenile terranes. *Tectonics* 10, 770-780.
- Shi, L., Francis, D., Ludden, J., Frederiksen, A., Bostock, M., 1998. Xenolith evidence for lithospheric melting above anomalously hot mantle under the northern Canadian Cordillera. *Contrib. Mineral. Petrol.* 131, 38-53.
- Souther, J.G., 1977. Volcanism and tectonic environments in the Canadian Cordillera - a second look. *Geol. Ass. Can. Spec. Pap.* 16, 3-24.
- Souther, J.G., 1992. The late Cenozoic Mount Edziza Volcanic Complex, British Columbia. *Geol. Surv. Can. Mem.* 420, 320p.
- Sun, S.S, McDonough, W.F., 1989. Chemical and isotopic systematics of oceanic basalts: implications for mantle composition and processes. In: A.D. Saunders and M.J. Norry (Editors), *Magmatism in the ocean basins*. *Geol. Soc. Lond. Spec. Publ.* 42, pp. 313-345.
- Tempelman-Kluit, D.J., 1979. Transported cataclasite, ophiolite and granodiorite in Yukon: evidence for arc-continent collision. *Geol. Surv. Can. Pap.* 79-14, 27p.
- Thorkelson, D.J., 1992. Volcanic and tectonic evolution of the Hazelton Group in Spatsizi River (104H) map area, North-Central British Columbia. Ph.D. thesis, Carleton University, Canada.
- Wheeler, J.O. McFeely, P., 1991 Tectonic assemblage map of the Canadian Cordillera

and adjacent parts of the United States of America. Geol. Surv. Canada Map
1712A, scale 1:2000000.

Zindler, A., Hart, S.R., 1986. Chemical geodynamics. Annu. Rev. Earth Planet. Sci. Lett.
14, 493-571.

CHAPTER IV

Origin of recent alkaline lavas by lithospheric thinning in the northern Canadian Cordillera.

Anne-Claude Abraham ^{a,b,*}, Don Francis ^a, and Mireille Polv ^b

^a Earth and Planetary Sciences, McGill University
3450, University St.
Montr al, Qu bec, H3A 2A7, Canada

^b Laboratoire des M canismes de Transfert en G ologie, UMR 5563
38 rue des 36 Ponts
31400 Toulouse, France

Submitted to the Journal of Petrology, January 2002.

Abstract

Recent primitive alkaline lavas in the northern Canadian Cordillera define two compositional end-members, olivine nephelinite (NEPH) and hypersthene-normative olivine basalt (Hy-NORM). The NEPH end-member is characterized by large enrichments in incompatible trace elements with respect to primitive mantle, but is depleted in term of its Sr, Nd, and Pb isotopic ratios. The presence of amphibole in its source suggests that this end-member is derived from the lithospheric mantle. The Hy-NORM end-member is characterized by the lowest incompatible trace element contents, but is still relatively enriched in the most incompatible elements compared to primitive mantle. Although the Hy-NORM end-member is more radiogenic in Pb and Sr isotopes and less radiogenic in Nd isotopes than the NEPH end-member, its isotopic signature varies with the tectonic belt in which it erupted, which is interpreted to reflect the existence of distinct lithospheric mantles.

The Cordilleran, and other continental Hy-NORM basalts, have low Ca and high Na contents compared to their equivalents in oceanic hot spots such as Hawaii or associated with mid-ocean ridges. A comparison with experimental melts of mantle peridotite indicates that these characteristics reflect smaller degrees of partial melting (<10%) in continental regime. A two-stage model is refined in which the NEPH end-member results from relatively large degrees of partial melting (>15%) of amphibole-rich veins, while the Hy-NORM end-member represents smaller degrees of melting of the surrounding garnet-bearing lithospheric mantle. This model suggests that, contrary to the conclusion that is

commonly drawn from simplistic interpretations of experimental results, the NEPH lavas might be derived from similar or shallower depths than coeval Hy-NORM basalts.

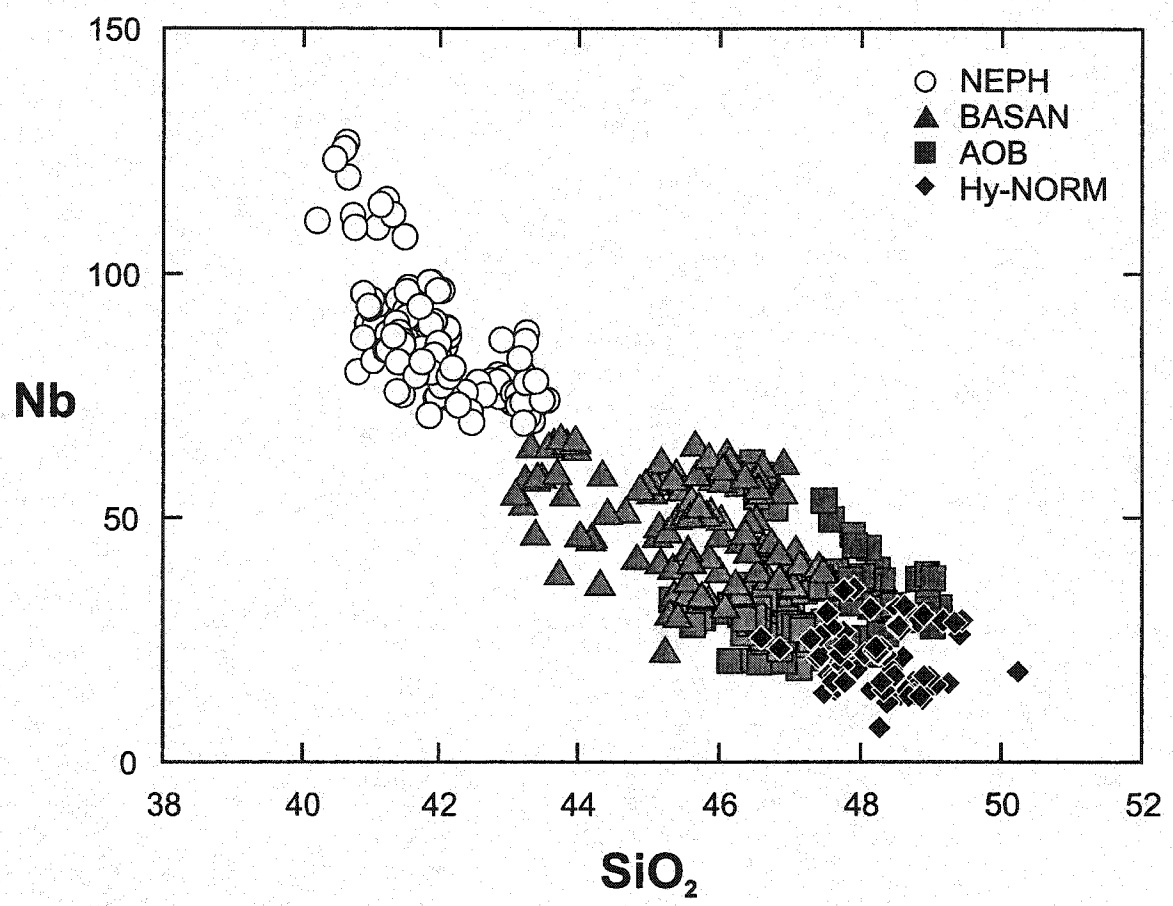
1. Introduction

Although a general consensus has been reached on the genesis of mid-ocean ridge tholeiites, there is still little agreement concerning the origin of primitive alkaline lavas. Primitive alkaline lavas are found in many tectonic settings and, whether oceanic or continental, they are systematically enriched in incompatible trace elements compared to primitive mantle, but display a large range in isotopic composition, from unradiogenic to radiogenic compositions. Experimental studies have suggested that very Siundersaturated lavas, such as olivine nephelinites (NEPH), may be derived by melting of mantle peridotite. If the peridotite is anhydrous, the NEPH lavas must be derived from extremely small degrees of partial melting (< 0.25 %; Sims et al., 1995) at very high pressure ($P \sim 3$ kbar; Green and Ringwood, 1967), whereas in the presence of H_2O-CO_2 fluids (e.g. Holloway, 1973; Olafsson and Eggler, 1983; Hirose, 1997), NEPH lavas may be produced by more reasonable degrees of partial melting (~ 5%). On the other hand, NEPH lavas may also be derived from melting of ultramafic veins, consisting principally of hydrous minerals and clinopyroxene (Foley et al., 1999). These different proposals imply different P-T conditions of melting, different degrees of partial melting, and different mantle source compositions for primitive alkaline lavas.

Si-undersaturated lavas such as NEPH are often associated with other mafic magma types, such as basanites, alkali olivine basalts, and hypersthene-normative olivine basalts (Hy-NORM) (e.g. Embey-Isztin et al., 1993; Hoernle and Schmincke, 1993; Francis and Ludden, 1990 and 1995; Beccaluva et al., 1998; Marzoli et al., 2000; Zhang et al., 2001). These mafic alkaline lavas commonly define continuous arrays in major and trace elements between the most Si-undersaturated NEPH lavas and the Hy-NORM basalts (Fig. 1; Francis and Ludden, 1995).

In this paper, the problem of the origin of mafic alkaline lavas is addressed in recent alkaline lavas that have erupted along the northern Canadian Cordillera (Francis and Ludden, 1990 & 1995; Carignan et al., 1994; Abraham et al., 2001). A two-stage model is refined, in which the NEPH end-member results from melting of amphibole-rich veins, while the Hy-NORM end-member represents a relatively small degree of melting (<10 %) of the surrounding garnet-bearing lithospheric mantle. We establish that Hy-NORM basalts erupted in continental areas like the Cordillera have systematically low Ca and high Na contents compared to their equivalents in oceanic environments, consistent with derivation by smaller degrees of partial melting. A synthesis of our results with recent Lithoprobe geophysical data leads to the conclusion that the partial melting that produced the Recent alkaline lavas of the Canadian Cordillera reflects ongoing melting and thinning of the northern Cordilleran lithospheric mantle.

Figure 1: Nb versus SiO_2 for the northern Cordilleran mafic alkaline volcanic suites. Data sources: Eiché et al. (1987), Francis and Ludden (1990 and 1995); Cousens and Bevier (1995); Abraham et al. (2001); this study and unpublished data from D. Francis.



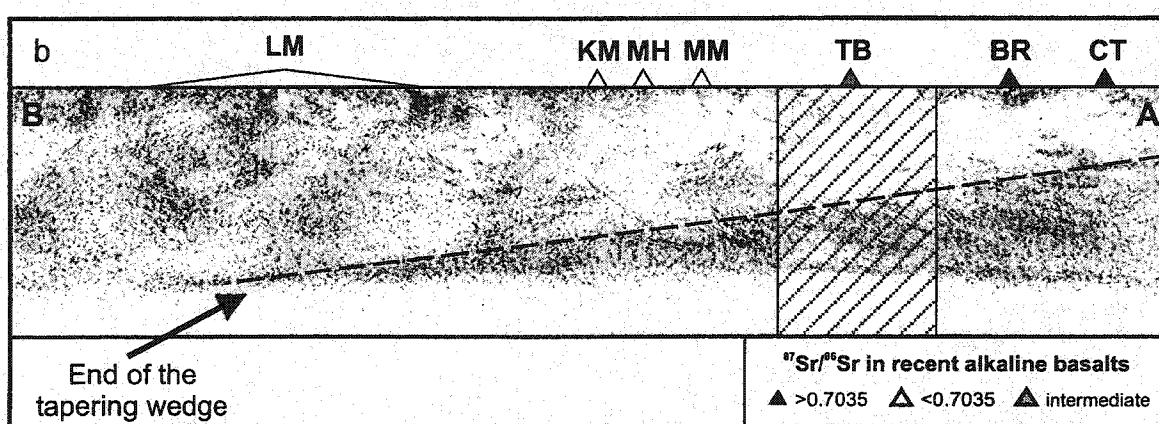
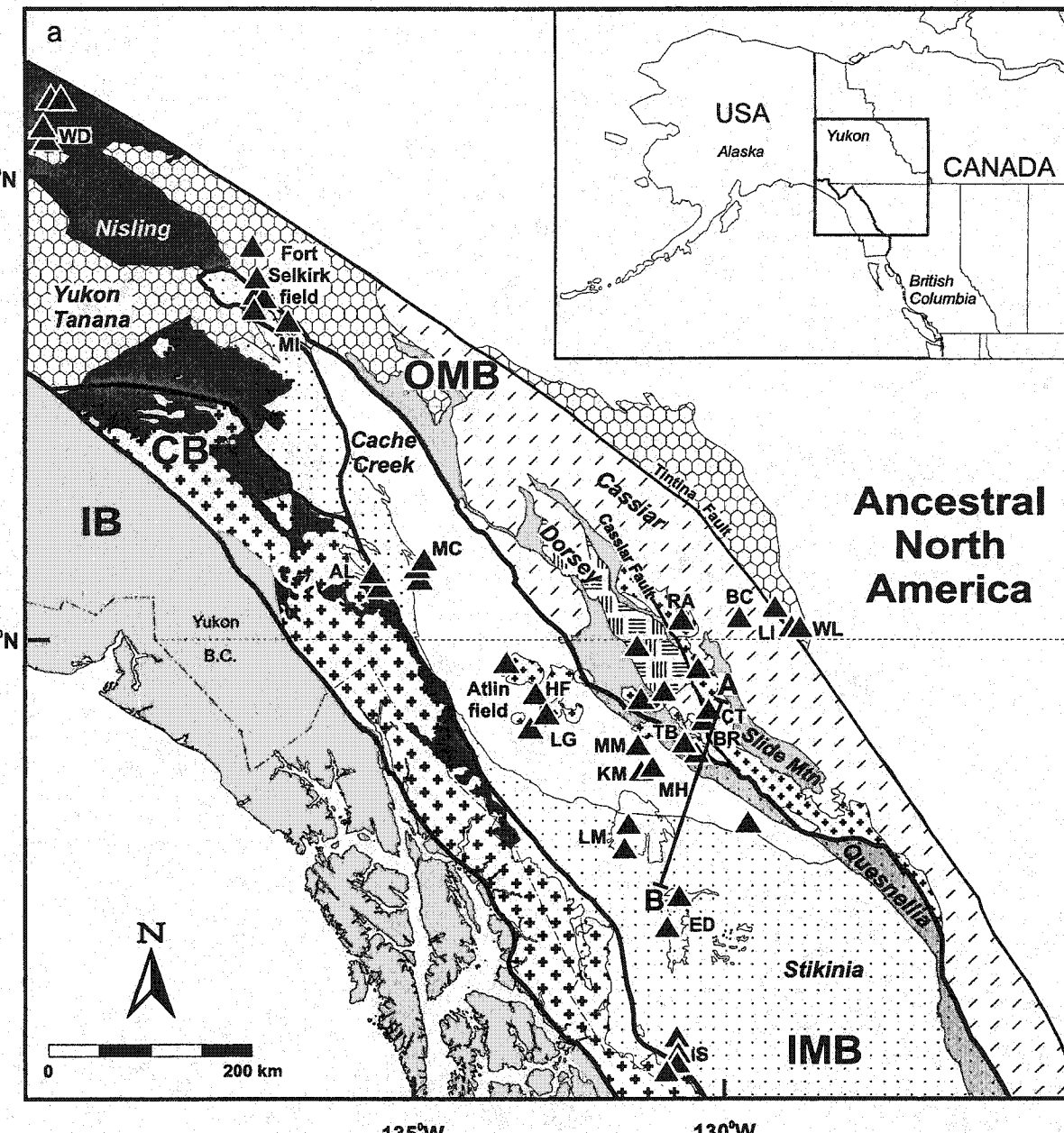
2. Tectonic setting

Recent alkaline lavas have erupted through three of the five sub-parallel morphotectonic belts that constitute the northern Canadian Cordillera: the Coast, the Intermontane, and the Omineca belts (Fig. 2a). The Intermontane Belt consists of terranes of oceanic origin that were accreted onto the continental margin represented by the Omineca Belt in Jurassic time (about 180 Ma ago), whereas the plutons of the Coast Belt are considered to result from the accretion of the Insular Belt, consisting of terranes of oceanic origin, onto the Intermontane Belt in Cretaceous time (about 100 Ma ago) (Monger et al., 1982).

The northern Canadian Cordillera has been the subject of numerous recent geophysical studies as part of the Lithoprobe Slave-NORthern Cordillera Lithospheric Evolution (SNORCLE) transect (Clowes, 1993), that has imaged the crustal part of the lithosphere. The results relevant to this study are:

- 1) Seismic reflection data reveal the presence of a westward tapering wedge (Fig. 2b) in the lower crust of the Omineca Belt and the eastern part of the Intermontane Belt (Cache Creek terrane) that has been interpreted as North American Precambrian lower crust (Cook et al., 2001).
- 2) Heat flow measurements indicate that the temperature just below the Moho may be relatively high beneath the entire Cordillera ($\sim 900 \pm 100$ °C; Hyndman et al., 2000), above the wet solidus of fertile mantle, suggesting that

Figure 2: **a)** Location map showing mid-Tertiary to Recent alkaline volcanic centres described in this paper (modified from Wheeler and McFeely, 1991). The heavy line AB corresponds to the approximate location of the Lithoprobe seismic cross-section in Fig. 2b. Abbreviations for the tectonic belts: OMB = Omineca Belt, IMB = Intermontane Belt, CB = Coast Belt, IB = Insular Belt. Abbreviations for the alkaline volcanic centres: AL = Alligator Lake, BC = Big Creek, BR = Blue River, CT = Caribou Tuya, ED = Mount Edziza, FS = Fort Selkirk, HF = Hirschfeld, IS = Iskut-Unuk, KM = Kawdy Mountain, LG = Llangorse, LI = Liard River, LM = Level Mountain, MC = Miles Canyon, MH = Metahag Mountain, MI = Minto Landing, MM = Metah Mountain, RA = Rancheria, TB = Tuya Butte, WD = West Dawson, WL = Watson Lake. **b)** Location of the westward tapering wedge detected seismically in the lower crust (Cook et al., 2001) compared to the location of the isotopic discontinuity observed in recent alkaline volcanic centres from the northern Canadian Cordillera (shaded area; Abraham et al., 2001). Abbreviations as in Fig. 2.a.



lithospheric thinning might be actively occurring. Furthermore, higher heat flow values in the Omineca Belt ($86 \pm 20 \text{ mW m}^{-2}$) compared to the Intermontane Belt ($73 \pm 6 \text{ mW m}^{-2}$) in the southern Cordillera indicate that the temperature at the base of the crust in the Omineca Belt might be up to 150°C hotter than that beneath the Intermontane Belt (Hyndman and Lewis, 1999).

3. Magmatic end-members

The NEPH end-member is defined by highly silica-undersaturated olivine-nephelinite lavas with no feldspar in the groundmass (Francis and Ludden, 1995) that occur in small volumes, as lava flows and pyroclastic deposits. These lavas are separated by a natural population minimum at 15% normative nepheline from the other mafic lavas that have feldspars in the groundmass at Fort Selkirk (Francis and Ludden, 1990) and Hirschfeld (Francis and Ludden, 1995), so that 15 wt.% normative nepheline was chosen to distinguish the NEPH lavas from the other mafic lavas. The Hy-NORM end-member is comprised of olivine basalts that have hypersthene in their normative mineralogy and dominate the mafic parts of larger volcanic constructs, such as Level Mountain (Hamilton, 1981) and Mount Edziza (Souther, 1992). Two intermediate magma types have been defined according to their percentage of normative nepheline, basanite (BASAN) with 5-15 wt.% normative nepheline, and alkali olivine basalts (AOB) with less than 5 wt.% normative nepheline. AOB are always associated with Hy-NORM basalts and there appears to be a continuous gradation between these two magma types.

3.1. NEPH lavas

NEPH lavas occur mainly in two different areas of the northern Canadian Cordillera (Fig. 2a). The first occurrence is at the transition between the Intermontane Belt and the Omineca Belt in the northern Yukon, in the Fort Selkirk field (Francis and Ludden, 1990) and near Minto Landing (Fig. 2a; Table 1). The second occurrence comprises at least five different vents in the Atlin field in the Intermontane Belt of northern British Columbia, one of them, Hirschfeld, already extensively studied by Francis and Ludden (1995). Chemical data for two others, Table Hill ($59^{\circ}20'N$, $132^{\circ}54'W$), and Fire Mountain ($59^{\circ}27'N$, $132^{\circ}47'W$) are presented in Table 1. NEPH lavas represent much smaller volumes than the other alkaline magma types of the Cordillera. In the Fort Selkirk volcanic field, for example, the NEPH lavas represent a volume of less than 2 km^3 compared to approximately 40 km^3 of the other magma types (Francis and Ludden, 1990).

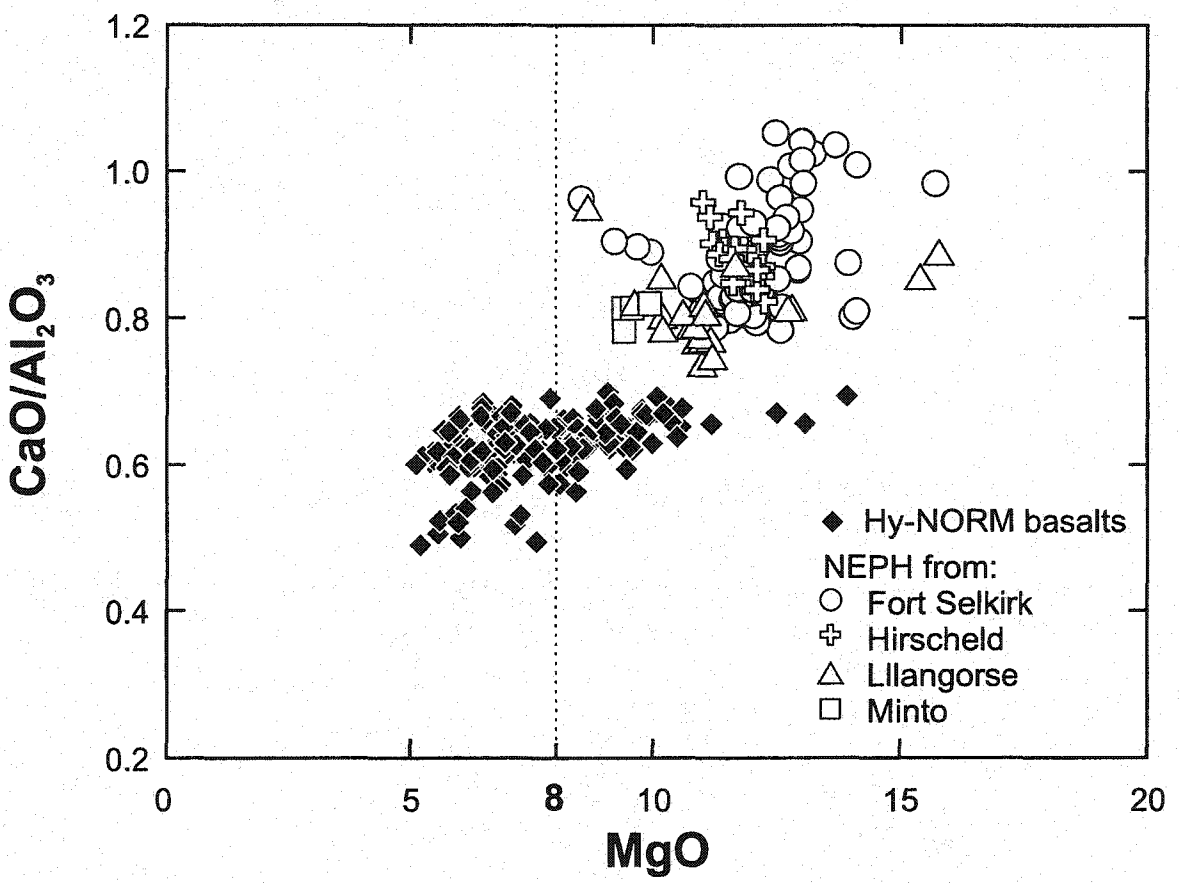
The northern Canadian Cordillera NEPH lavas display a range in MgO between 8 and 16 wt.% (Fig. 3) and are characterized by high FeO contents (13.25 ± 0.6 ; Table 1), despite their relatively high MgO contents. Because of the large number of entrained mantle xenoliths, the most magnesian compositions probably reflect contamination by mantle material, and do not represent liquid compositions. The majority of the northern Cordillera NEPH lavas, however, cluster around 12 wt.% MgO (Fig. 3) and have relatively low Mg# (≈ 0.6) (Francis and Ludden, 1990 and 1995). Compared to other NEPH lavas erupted in oceanic and other continental areas, Cordilleran NEPH lavas

Table 1: Major and trace element compositions of NEPH lavas that have erupted to the southeast of Fort Selkirk, near Minto Landing, and at Table Hill and Fire Mountain in the Atlin field. A description of these volcanic centres can be found in Francis and Ludden (1995).

Table 1: Major and trace element compositions of NEPH lavas that have erupted to the southeast of Fort Selkirk, near Minto Landing, and at Table Hill and Fire Mountain in the Atlin field.

Sample Site	MI-14 Minto	MI-16 Minto	LG-30 Table	LG-31 Table	LG-33 Table	LG-43 Table	LG-48 Table	LG-51 Table	FM-1 Fire M.	FM-7 Fire M.
SiO ₂	42.44	42.85	40.93	40.95	40.63	40.99	42.92	40.9	41.72	41.22
TiO ₂	2.55	2.58	2.81	2.79	2.84	2.68	2.51	2.83	2.41	2.72
Al ₂ O ₃	13.95	13.85	12.1	12.18	12.1	11.98	13.1	12.1	10.56	11.19
FeO	9.38	9.31	11.53	11.71	11.63	11.49	10.73	11.41	11.23	11.72
Fe ₂ O ₃	1.84	1.83	2.26	2.3	2.28	2.25	2.1	2.24	2.2	2.3
MnO	0.2	0.19	0.2	0.2	0.2	0.2	0.19	0.19	0.19	0.21
MgO	9.15	9.73	10.56	9.93	10.66	10.5	10.89	10.32	15.19	12.52
CaO	11.31	11.31	9.69	9.69	9.3	9.36	9.57	9.68	8.96	9.01
Na ₂ O	4.25	3.81	3.82	4.24	4.21	4.62	3.92	3.97	3.6	4.53
K ₂ O	1.41	1.61	1.98	2.08	1.88	1.93	2.02	2.16	1.31	1.6
P ₂ O ₅	0.8	0.75	1.12	1.16	1.13	1.18	0.84	1.13	1.08	1.14
LOI	1.87	1.84	-	-	-	1.98	0.57	2.12	1.11	-
Total	99.16	99.65	97	97.21	96.85	99.17	99.36	99.05	99.56	98.17
Rb	53	56	26.45	24.6	26.83	34	24.8	32.1	42	39.15
Cs	-	-	0.35	-	0.49	-	-	-	-	0.56
Sr	988	953	1274	1452	1215	1369	1023	1347	1104	1207
Ba	763.9	767.5	645.7	671.8	492.1	510.5	391.4	549	524.8	581.5
Sc	-	-	12	14.5	14.5	13	22	17	-	15
V	271	286	212.5	202	207.5	192	227	206	223	205
Cr	325.7	347.6	296.3	263.8	277.8	303.1	293.5	249.7	-	364.7
Co	-	-	62	57	59.5	55	55	56	0	61
Ni	170	186	291.5	258	287.5	293	275	268	555	420
Zn	-	-	148	155	146.5	189	169	185	-	142
Cu	-	-	60.5	50	71	65	76	72	-	49
Ga	-	-	24.55	25.35	25.25	25.4	21.4	24.8	-	21.3
Y	24	23	22.6	23.35	22.11	19.2	19.9	18.9	18	22.95
Zr	240	234	324.9	348.6	294.4	344.8	225.3	319.3	258	263.7
Nb	82	77	84.2	92.7	74.37	98	58.5	87.5	62	53.8
Hf	4.45	4.47	6	-	6.27	-	-	-	-	5.84
Th	9.21	8.76	6.6	-	6.99	-	-	-	-	7.01
U	2.35	2.3	2.13	-	2.21	-	-	-	-	2.24
Pb	3.88	3.76	3.67	-	3.61	-	-	-	-	1.25
La	67.98	64.72	56.78	-	58.48	-	-	-	-	60.26
Ce	116.2	112.6	112.2	-	114.9	-	-	-	-	117.4
Pr	13.62	13.12	14.14	-	14.5	-	-	-	-	14.97
Nd	49.49	47.65	52.33	-	54.94	-	-	-	-	56.37
Sm	9.11	9.07	10.56	-	10.84	-	-	-	-	10.91
Eu	2.78	2.7	3.27	-	3.37	-	-	-	-	3.43
Gd	1.13	1.13	8.59	-	8.87	-	-	-	-	9
Tb	0.76	0.75	1.15	-	1.18	-	-	-	-	1.2
Dy	5.55	5.47	5.02	-	5.28	-	-	-	-	5.43
Ho	1.04	1.01	0.75	-	0.8	-	-	-	-	0.84
Er	2.59	2.53	1.68	-	1.71	-	-	-	-	1.85
Tm	0.35	0.35	0.2	-	0.19	-	-	-	-	0.21
Yb	2.01	1.96	0.99	-	1.03	-	-	-	-	1.16
Lu	0.3	0.29	0.13	-	0.13	-	-	-	-	0.15

Figure 3: CaO/Al₂O₃ versus MgO in wt.% for Hy-NORM basalts and NEPH lavas from Recent alkaline centres of the Canadian Cordillera. Data sources as in Fig. 1.



represent an end-member in terms of their low CaO and high FeO and alkalis contents at otherwise similar major element compositions (Fig. 4). The low CaO content of Cordilleran NEPH lavas is associated with low Sc contents (16 ± 2 ppm in Cordilleran NEPH lavas compared to 24 ± 6 ppm for worldwide NEPH lavas). No systematic chemical differences are apparent between NEPH lavas erupted in continental versus oceanic areas.

The NEPH lavas are characterized by large enrichments in incompatible trace elements when normalized to primitive mantle (Fig. 5), but relatively low concentrations of large ion lithophile elements (LILE), such as Rb, Ba and K, compared to other incompatible elements such as Nb, Th, U, and the light rare earth elements (LREE). The NEPH lavas have more pronounced negative anomalies LILE and lower heavy rare earth elements (HREE) concentrations than associated Hy-NORM basalts (Fig. 5). The NEPH magma end-member appears to have distinct chemical compositions at different centres. For example, NEPH lavas erupted at Fort Selkirk, Hirschfeld and Llangorse in the northern Cordillera define trends with different slopes in Ti or Zr versus Nb diagrams (Fig. 6a and 6b). In addition, the NEPH lavas that have erupted at Llangorse, Hirschfeld or Minto have higher Ba, and lower Y contents than the NEPH lavas that have erupted at Fort Selkirk (Fig. 6c and 6d). At Fort Selkirk, the lavas display much larger ranges in most major and trace elements than at other volcanic centres (Fig. 6) that might be in part due to the presence of a number of distinct vents (Francis and Ludden, 1990).

Figure 4:

Major elements versus SiO_2 in wt.% for NEPH lavas from the northern Canadian Cordillera compared to NEPH lavas from other oceanic and continental areas. All data have $\text{MgO} > 8$ wt.%. Symbols : white circles = NEPH lavas from Cordillera, Black diamonds = NEPH lavas from other areas. Data sources for NEPH lavas from continental areas: western Australia (Frey et al., 1978; Ewart et al., 1980; O'Reilly and Zhang, 1995; Adam, 1990), Europe (Wilson and Downes, 1991; Cebria and Lopez Ruiz, 1995; Wilson et al., 1995; Beccaluva et al., 1998; Jung and Masberg, 1998), China (Zou et al., 2000), Kenya rift (Baker, 1987; Class et al. 1994), western USA (Kempton et al., 1991; Beard and Johnson, 1997; Fitton et al., 1991). Data sources for NEPH from hot spots: Hawaii (Clague and Frey, 1982; Garcia et al., 1986; Maaloe et al., 1992), the Comores (Strong, 1972; Späth et al., 1996; Class and Goldstein, 1997; Class et al., 1998), the Canaries (Schmincke, 1982; Hoernle, et al. 1991; Hoernle and Schmincke, 1993).

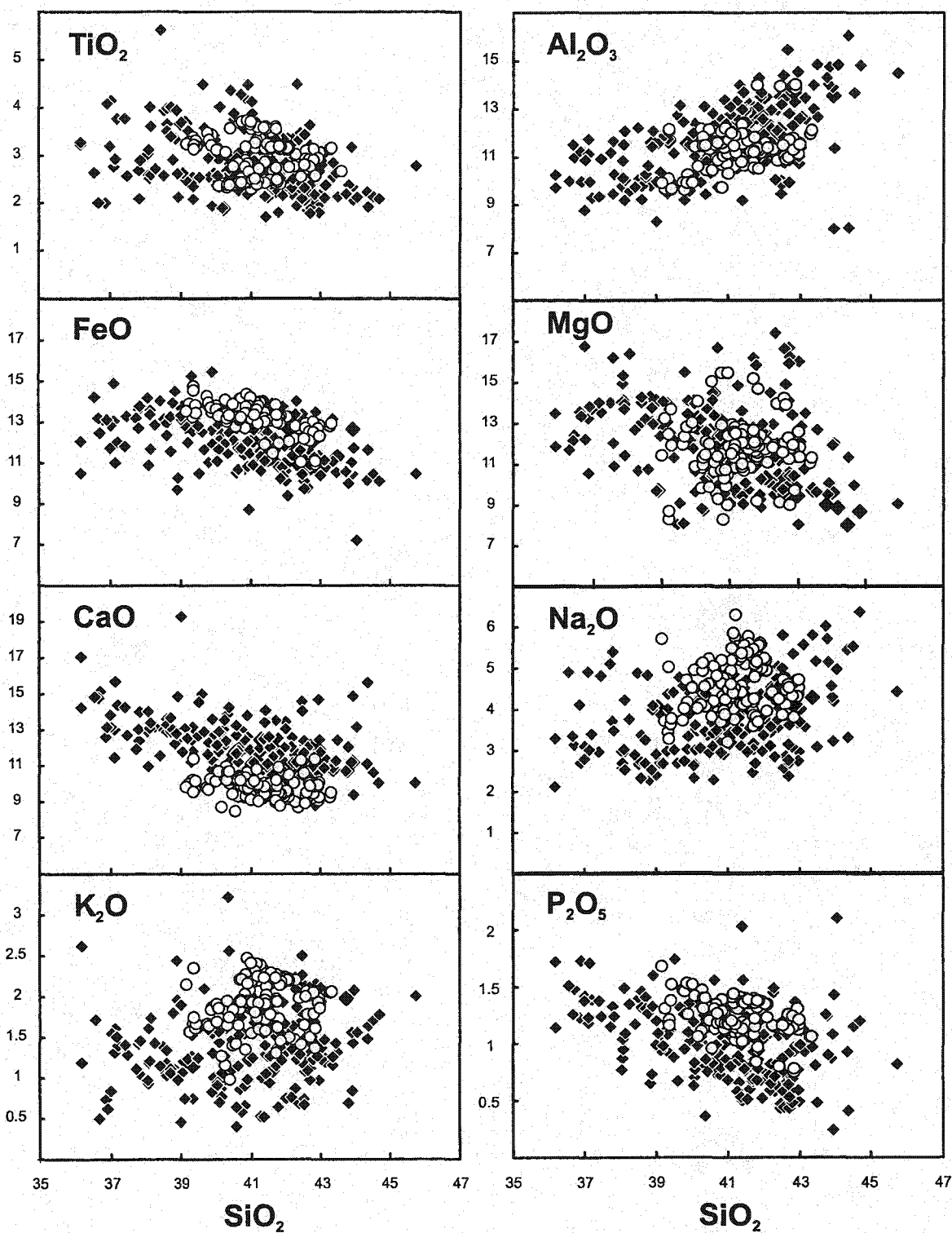


Figure 5: Average trace elements concentrations normalized to primitive mantle of Sun and McDonough (1989) for Hy-NORM and NEPH lavas from Recent alkaline centres of the Canadian Cordillera and for MORB. All data have MgO > 8 wt.%. Data sources as in Fig. 1, except for the average MORB values that are from Sun and McDonough (1989).

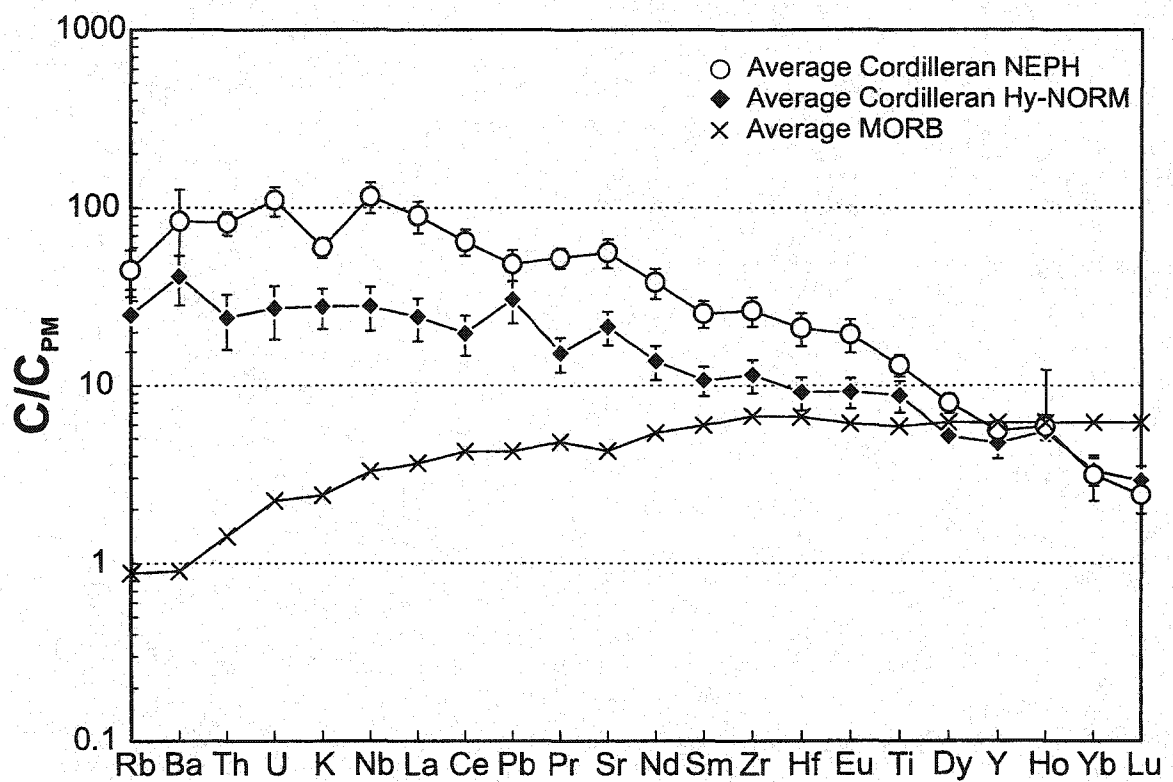
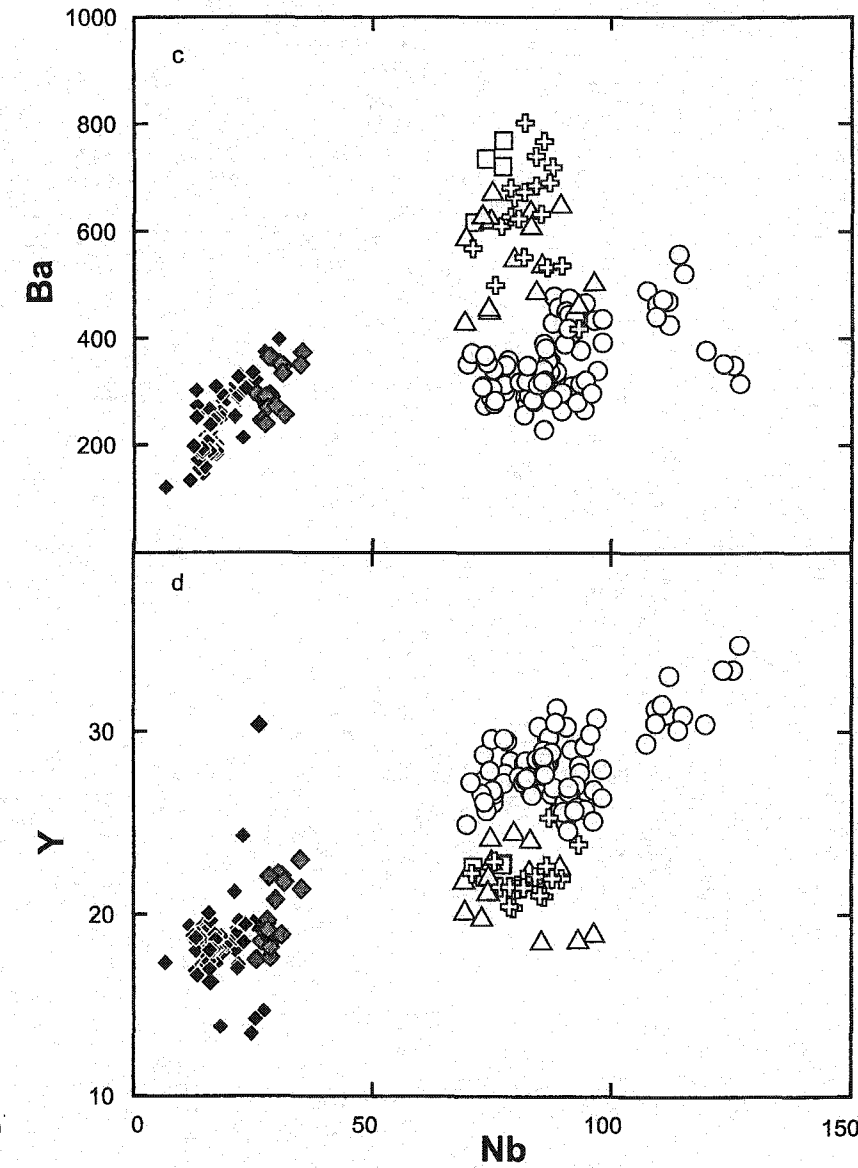
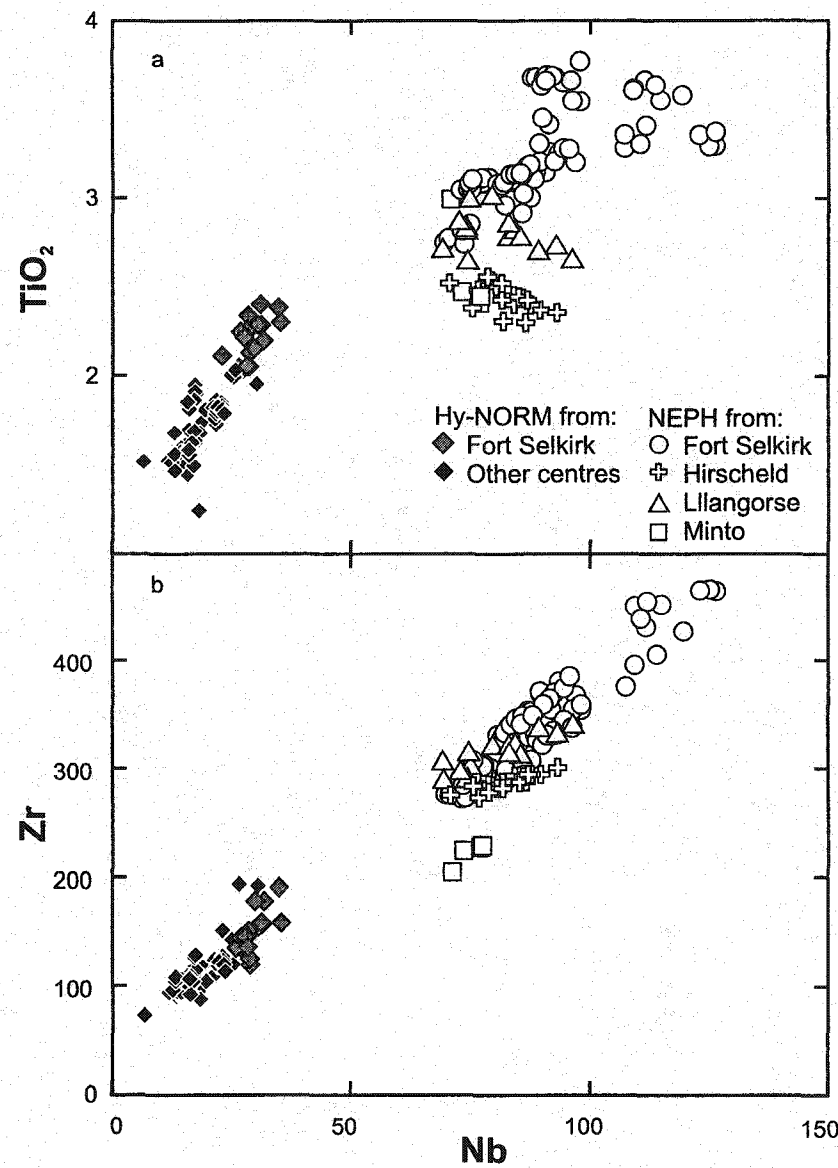
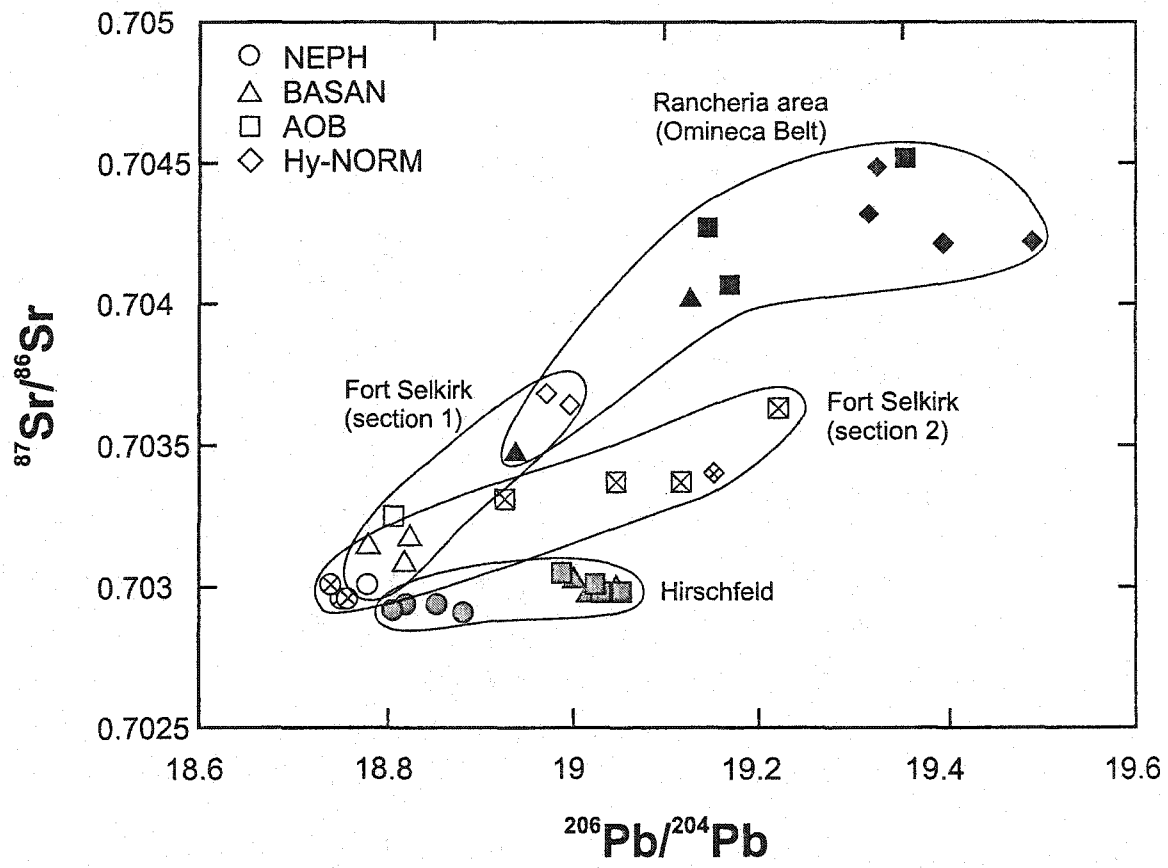


Figure 6: a) TiO_2 , b) Zr, c) Ba, and d) Y versus Nb for Hy-NORM and NEPH lavas in NEPH-bearing suites of the northern Canadian Cordillera. All data have $\text{MgO} > 8 \text{ wt.\%}$. Data sources as in Fig. 1.



The NEPH end-member in the northern Canadian Cordillera has a very restricted and depleted isotopic signature with the least radiogenic Sr and Pb isotopic ratios and the most radiogenic Nd isotopic ratios compared to other Cordilleran alkaline magma types (Carignan et al., 1994; Abraham et al., 2001) (Fig. 7). Although no NEPH lavas have been documented in the Omineca Belt, the BASAN lavas in the Omineca Belt trend towards the Sr-Nd-Pb isotopic values of NEPH lavas from the Intermontane Belt (Fig. 7), suggesting the existence of a NEPH end-member in the Omineca Belt that is isotopically similar to that of the Intermontane Belt. In most other mafic continental alkaline suites, the most Si-undersaturated lavas define an isotopic end-member that is more isotopically depleted than associated magma types (Fig. 8). This is the case in Australia (McDonough et al., 1985), in China (Zhi et al., 1990, Song et al., 1990), and in southern Kenya (Späth et al., 2001). In Sicily (Beccaluva et al., 1998), however, the NEPH lavas are slightly more isotopically enriched than the associated magma types, and in northern Kenya, the isotopic difference between the two end-member is small. In most oceanic areas, such as the Comores (Class et al., 1998), and the Canaries (Hoernle and Schmincke, 1993), NEPH lavas have similar isotopically depleted signatures to associated mafic alkaline lavas (Fig. 8). The Hawaiian lavas represent an exception, however, defining an isotopic variation similar to that of the Cordillera, with the post-erosional alkaline lavas being more isotopically depleted than the shield-building tholeiites and associated pre-erosional alkaline lavas (e.g. Chen and Frey, 1985; Clague and Dalrymple, 1988). In summary, the Cordilleran NEPH lavas share the isotopically depleted signature of many mafic alkaline suites, from both oceanic and continental areas.

Figure 7: $^{87}\text{Sr}/^{86}\text{Sr}$ versus $^{206}\text{Pb}/^{204}\text{Pb}$ for lavas erupted in the Rancheria area (RA, BC and LI in Fig. 2.a) and in individual NEPH-bearing vents from the northern Canadian Cordillera. Fort Selkirk section 1 corresponds to the Wootton's Cone and the Wolverine Sequence, whereas Fort Selkirk section 2 corresponds to Volcano Mountain and the Pelly Sequence (Francis and Ludden, 1990). Data sources: Francis and Ludden (1990), Carignan et al. (1994), Abraham et al. (2001) and unpublished data from A.-C. Abraham and J. Carignan.



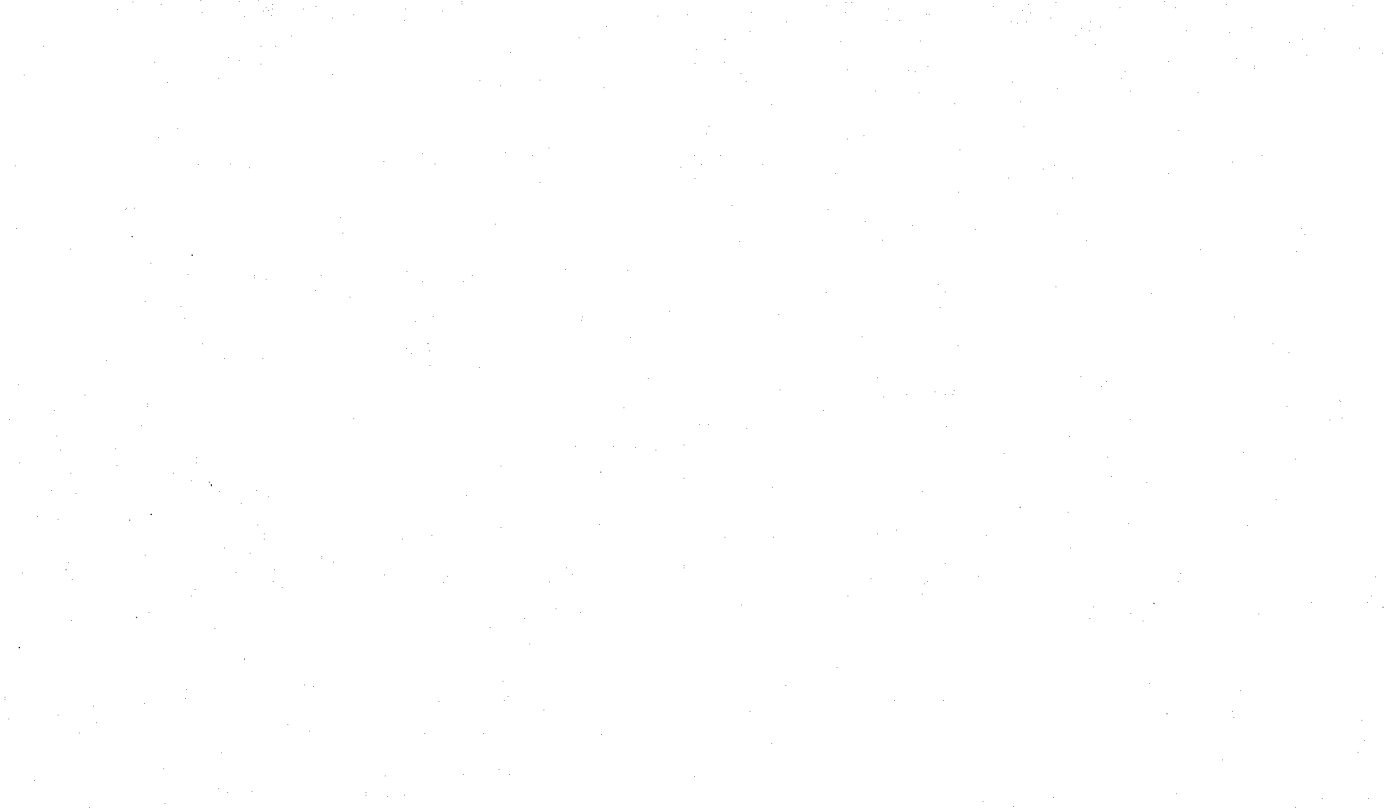
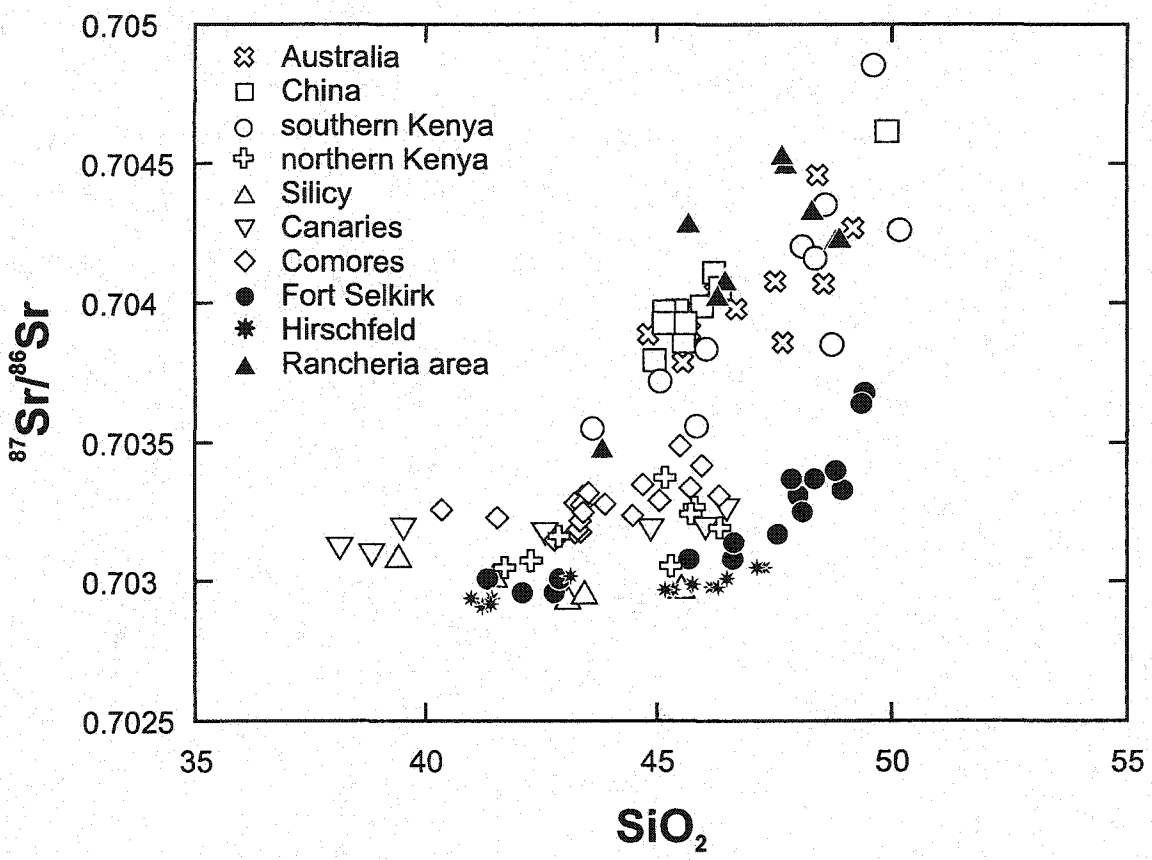


Figure 8: $^{87}\text{Sr}/^{86}\text{Sr}$ versus SiO_2 for primitive alkaline lavas ($\text{MgO} > 8$ wt.%) in the northern Canadian Cordillera and in other continental margins and oceanic hot spot areas. Data sources: Australia (McDonough et al., 1985), China (Zhi et al., 1990; Song et al., 1990), southern Kenya rift (Rogers et al., 2000; Späth et al., 2001), northern Kenya (Class et al., 1994; Rogers et al., 2000), Sicily (Beccaluva et al., 1998), Canaries (Hoernle et al., 1991), and Comores (Späth et al., 1996; Class and Goldstein, 1997). Data sources as in Fig. 7 for Fort Selkirk, Hirschfeld, and the Rancheria area.



3.2. Hy-NORM basalts

Hy-NORM basalts have erupted at most of the Tertiary to Recent volcanic centres of the northern Canadian Cordillera (Fig. 2a). In the Stikine Volcanic Belt, they are always associated with AOB, and sometimes also with BASAN. They rarely carry mantle xenoliths, and, except for a few samples, have relatively low MgO, Ni and Cr contents (Table 2). They range from 5 and 13.5 wt.% MgO, and have low CaO/Al₂O₃ ratios that do not vary with MgO (Fig. 3). The Hy-NORM basalts have generally low Fe contents (average total FeO = 11.6 ± 0.7 wt.%) compared to NEPH lavas (13.3 ± 0.6) with MgO greater than 8 wt.%.

The major element compositions of Hy-NORM basalts from the Canadian Cordillera have been compared to the compositions of their equivalents from other continental margin areas, such as eastern Australia, eastern China, Sicily, southern Kenya, or the Cameroon Line, from oceanic hot spots such as Hawaii, Comores, Canaries, La Reunion, or St Helena, and from mid-ocean ridges (MOR). For this comparison, Hy-NORM basalts with less than 20 wt.% hypersthene and more than 8 wt.% MgO were normalized to an arbitrary MgO content of 12 wt.% by olivine addition or subtraction. The comparison indicates that Hy-NORM basalts from the northern Cordillera, and other continental margin areas, have similar major element compositions, characterized by low CaO and high Na₂O contents (Fig. 9a). Hy-NORM basalts from MOR and oceanic hot spots, on the other hand, have higher CaO and lower Na₂O contents, and define a larger

Table 2:

Major, trace and isotopic compositions of Hy-NORM basalts that have erupted in different centres from the Stikine Volcanic Belt. See Fig. 2a for locations.

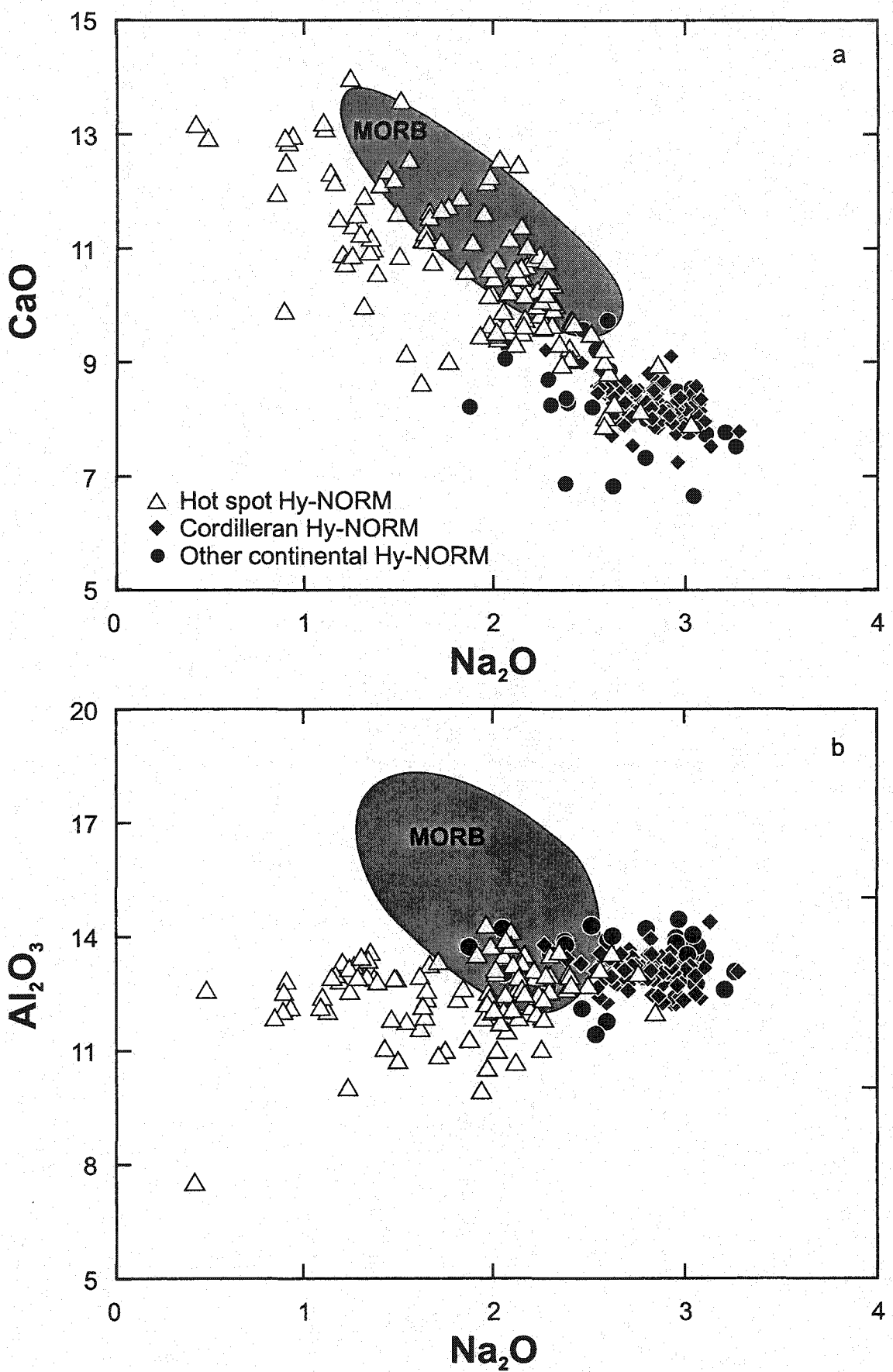
Table 2: Major, trace and isotopic compositions of Hy-NORM basalts that have erupted in different centres from the Stikine Volcanic Belt.

Sample Site	MH-10 Metahag	MH-12 Metahag	JR-7 Jennings R.	LM-44 Level Mtn.	NC-11 Nome Cone	TV-37 Tanzilla V.	CT-13 Caribou T.	BR-33 Blue Riv.	RA-8 Swan Lake	RA-19 Big Creek
SiO ₂	47.92	47.49	49.59	47.07	48.2	48.61	49.68	49.12	49.12	48.69
TiO ₂	1.89	1.87	1.74	1.91	1.78	1.71	1.59	2.03	1.74	1.68
Al ₂ O ₃	13.55	13.23	14.88	14.18	14.74	14.31	14.79	14.5	14.69	13.85
FeO	10.6	10.84	9.65	10.84	10.88	10.48	9.89	10	10.41	10.39
Fe ₂ O ₃	2.08	2.13	1.89	2.13	2.13	2.05	1.94	1.96	2.04	2.04
MnO	0.17	0.18	0.17	0.18	0.18	0.17	0.17	0.17	0.17	0.16
MgO	10.35	11.2	8.02	9.21	8.39	9.5	8.33	8.23	8.26	10.11
CaO	8.92	8.68	9.68	8.42	9.21	8.94	8.73	9.1	9.06	8.69
Na ₂ O	2.9	2.94	2.95	2.62	3.08	2.84	3.18	3.22	3.06	3
K ₂ O	0.75	0.75	0.61	0.38	0.62	0.63	0.79	1.06	0.72	0.85
P ₂ O ₅	0.32	0.32	0.27	0.25	0.27	0.25	0.26	0.33	0.27	0.25
LOI	-	-	-	1.5	-	0.12	-	-	0.01	0.01
Total	99.45	99.63	99.46	98.67	99.48	99.61	99.34	99.72	99.55	99.72
Rb	11.7	12.8	10.1	2.7	11.4	11.7	21	21	14	19
Cs	0.1	0.18	0.15	0.16	0.16	0.18	0.32	0.18	0.51	0.26
Sr	464	479.1	393.5	393.5	377.1	357.7	406.8	453.5	370	395
Ba	299.6	307.6	245	194.8	168.5	209.3	215.9	329.5	215	251.7
Sc	14	24	32	21	31	23	25	25	23.61	-
V	214	204	208	207	198	185	173	220	201	203
Cr	315.4	312.7	320.9	338	258.6	290.8	271.6	327	253.2	353.7
Co	66	62	52	57	52	-	-	-	54.93	-
Ni	200	242	115	276	172	267	141	156	139	194
Zn	129	132	121	137	141	-	-	-	-	-
Cu	59	70	57	77	81	-	-	-	-	-
Ga	20.5	19.9	20	21.2	21.5	19.8	20.6	20.9	-	-
Y	19.2	18.6	19.3	20.7	21.1	19.9	19.3	21.9	20	18
Zr	109.4	112	109.1	115.2	120.7	106.1	115.7	136.8	118	106
Nb	20.4	21.6	17	17.1	16.3	15.6	17.5	24.7	16	17
Hf	2.32	2.4	2.49	2.65	2.6	2.44	2.86	3.05	3.64	2.43
Th	1.35	1.44	1.43	1.58	1.62	1.35	2.8	2.75	2.44	3.06
U	0.49	0.37	0.47	0.38	0.41	0.56	0.79	0.57	0.76	0.67
Pb	1.42	1.74	1.76	1.98	1.68	1.61	2.81	2.71	1.93	2.38

Table 2: continued

Sample	MH-10	MH-12	JR-7	LM-44	NC-11	TV-37	CT-13	BR-33	RA-8	RA-19
La	13.63	14.29	12.14	12.01	13.09	11.77	17.54	18.03	16.93	16.03
Ce	29.36	31.13	26.19	24.99	28.64	24.98	35.85	38.43	32.74	32.54
Pr	3.8	4	3.38	3.43	3.68	3.26	4.43	4.91	-	4.49
Nd	16.55	17.44	15.2	15.26	16.18	13.99	18.2	20.6	20.44	17.74
Sm	4.25	4.45	4.13	4.21	4.17	3.79	4.45	4.91	4.57	4.17
Eu	1.42	1.46	1.43	1.47	1.45	1.33	1.48	1.57	1.65	1.4
Gd	4.12	4.2	4.1	4.32	4.15	3.83	4.14	4.56	-	4.11
Tb	0.61	0.61	0.65	0.65	0.66	0.61	0.64	0.72	0.43	0.63
Dy	3.46	3.47	3.76	3.74	3.86	3.69	3.78	4.15	-	3.7
Ho	0.66	0.67	0.76	0.73	0.76	0.7	0.73	0.78	-	0.7
Er	1.63	1.63	1.9	1.87	1.97	1.77	1.81	1.91	-	1.75
Tm	0.2	0.2	0.24	0.23	0.24	0.22	0.23	0.24	-	0.26
Yb	1.34	1.32	1.69	1.56	1.71	1.46	1.55	1.6	1.9	1.51
Lu	0.18	0.18	0.23	0.21	0.23	0.21	0.2	0.22	0.27	0.23
$^{87}\text{Sr}/^{86}\text{Sr}$	0.703219	-	0.703173	0.703047	0.703716	0.703401	-	0.704284	0.704318	-
$^{143}\text{Nd}/^{144}\text{Nd}$	0.512976	-	-	0.512956	0.512902	0.512837	-	0.512837	0.512768	-
e Nd	6.6	-	-	6.2	5.1	3.9	-	3.9	2.5	-
$^{206}\text{Pb}/^{204}\text{Pb}$	19.016	-	19.016	19.005	19.235	19.282	19.3	19.251	19.328	-
$^{207}\text{Pb}/^{204}\text{Pb}$	15.587	-	15.567	15.56	15.628	15.597	15.655	15.652	15.646	-
$^{208}\text{Pb}/^{204}\text{Pb}$	38.509	-	38.441	38.361	38.933	38.625	39.205	39.098	39.242	-

Figure 9: a) CaO, and b) Al₂O₃ versus Na₂O for primitive Hy-NORM lavas (MgO > 8 wt.%) of the northern Canadian Cordillera, other continental areas, and hot spots corrected for olivine fractionation or accumulation to MgO = 12 wt.%. The shaded field corresponds to MOR Hy-NORM basalts. Data sources for Hy-NORM basalts from continental areas: Cameroon Line (Fitton, 1987), western Australia (Frey et al., 1978; Ewart et al., 1980; McDonough et al., 1985; O'Reilly and Zhang, 1995; Price et al., 1997), Europe (Beccaluva et al., 1998; Jung and Masberg, 1998), China (Zhi et al., 1990; Song et al., 1990; Zou et al., 2000), southern Kenya (Späth et al., 2001), western USA (Lum et al., 1989; Kempton et al., 1991; Fitton et al., 1991; Beard and Johnson, 1997), and Patagonia (D'Orazio et al., 2000; Gorring and Kay, 2001). Data sources for Hy-NORM basalts from hot spots: Hawaii (Clague and Beeson, 1980; Frey and Clague, 1983; Feigenson et al., 1983; Feigenson, 1984; Frey et al., 1990 and 1991; Fodor et al., 1992; Maaloe et al., 1992; Reiners et al., 1998), St Helena (Barsikov et al., 1979; Chaffey et al., 1989), Reunion (Albarede et al., 1988; Fisk et al., 1988), the Comores (Strong, 1972), and the Canaries (Schmincke, 1982; Hoernle and Schmincke, 1993). Data sources for MOR Hy-NORM basalts: Blanchard et al., 1976; Jakobsson et al., 1978; Zindler et al., 1979; Bryan et al., 1981; Le Roex et al., 1981; Bender et al., 1984; Cousens et al., 1984; Devey et al., 1994; Cousens et al., 1995.



range in both elements (Fig. 9.a). In addition, Hy-NORM basalts from oceanic hot spots have similar to slightly lower Al₂O₃ contents compared to continental margin basalts, but they all have lower Al₂O₃ contents than MOR Hy-NORM basalts (Fig. 9b).

The trace element patterns of primitive Cordilleran Hy-NORM basalts are characterized by a general enrichment in the most incompatible elements compared to HREE, and systematic negative Rb and Th, and positive Sr and Pb anomalies, compared to elements of similar compatibility (Fig. 5). Hy-NORM basalts are less enriched than NEPH lavas in all elements except HREE, which are, however, still significantly lower than those of MOR (Fig. 5). The Hy-NORM basalts display a more restricted range in most incompatible elements than the NEPH lavas (Fig. 6). Hy-NORM basalts from different Cordilleran volcanic centres have similar trace element signatures, except for higher concentrations of Rb, Th, U, and Pb in most Omineca Belt centres compared to Intermontane Belt centres (Abraham et al., 2001), and higher concentrations of high field strength elements (Nb, Zr and Ti) at Fort Selkirk (Fig. 6).

Hy-NORM basalts in the northern Canadian Cordillera have systematically higher Pb isotopic ratios than associated NEPH lavas (Fig. 7) (Carignan et al., 1994; Abraham et al., 2001), but their Sr, Nd and Pb signatures vary significantly between the different tectonic belts (Abraham et al., 2001). Hy-NORM basalts erupted within the Intermontane Belt have lower ⁸⁷Sr/⁸⁶Sr, and higher ¹⁴³Nd/¹⁴⁴Nd ratios compared to their equivalents in the Omineca Belt to the east (Fig. 7), and the Coast Belt to the west. They also have lower Pb isotopic ratios than those of the Omineca Belt Hy-NORM basalts, but similar to those of the Coast Belt. The Sr isotopic compositions of Hy-NORM basalts in the

northern Cordillera define a range similar to that of Hy-NORM basalts from other mafic alkaline suites of the world (Fig. 8). Hy-NORM basalts from the Omineca Belt have high Sr isotopic ratios, similar to Hy-NORM basalts that have erupted in Australia (McDonough et al., 1985), China (Zhi et al., 1990; Song et al., 1990), and southern Kenya (Späth et al., 2001). On the other hand, Hy-NORM basalts from the Intermontane Belt have lower Sr isotopic ratios, similar to Hy-NORM basalts from the Comores (Class et al., 1998), the Canaries (Hoernle and Schmincke, 1993), and Sicily (Beccaluva et al., 1998). In a broad sense, the Omineca and Intermontane belts Hy-NORM basalts display isotopic characteristics of continental margin versus oceanic Hy-NORM basalts respectively.

4. Discussion:

4.1. *Mantle source of NEPH lavas*

The observed crystallization sequence of the NEPH lavas is olivine, ulvöspinel, and then clinopyroxene (Francis and Ludden, 1990), and has been confirmed in low pressure experiments (Dalpé, 1997). The low, but relatively constant, CaO (Fig. 4) and Sc contents of the northern Cordilleran NEPH lavas indicate either that all these lavas have fractionated a similar amount of clinopyroxene (Cpx), or are characteristic of their mantle sources. As Cpx phenocrysts are absent, and CaO/Al₂O₃ and MgO are not positively correlated in the NEPH lavas with MgO > 8 wt.% (Fig. 3), it is unlikely that Cpx has

fractionated from these lavas and therefore the low CaO content of the northern Cordilleran NEPH lavas must originate in their mantle source regions. In the following, only primitive lavas with MgO contents greater than 8 wt.% are considered, in order to eliminate the possible effects of low pressure Cpx fractionation.

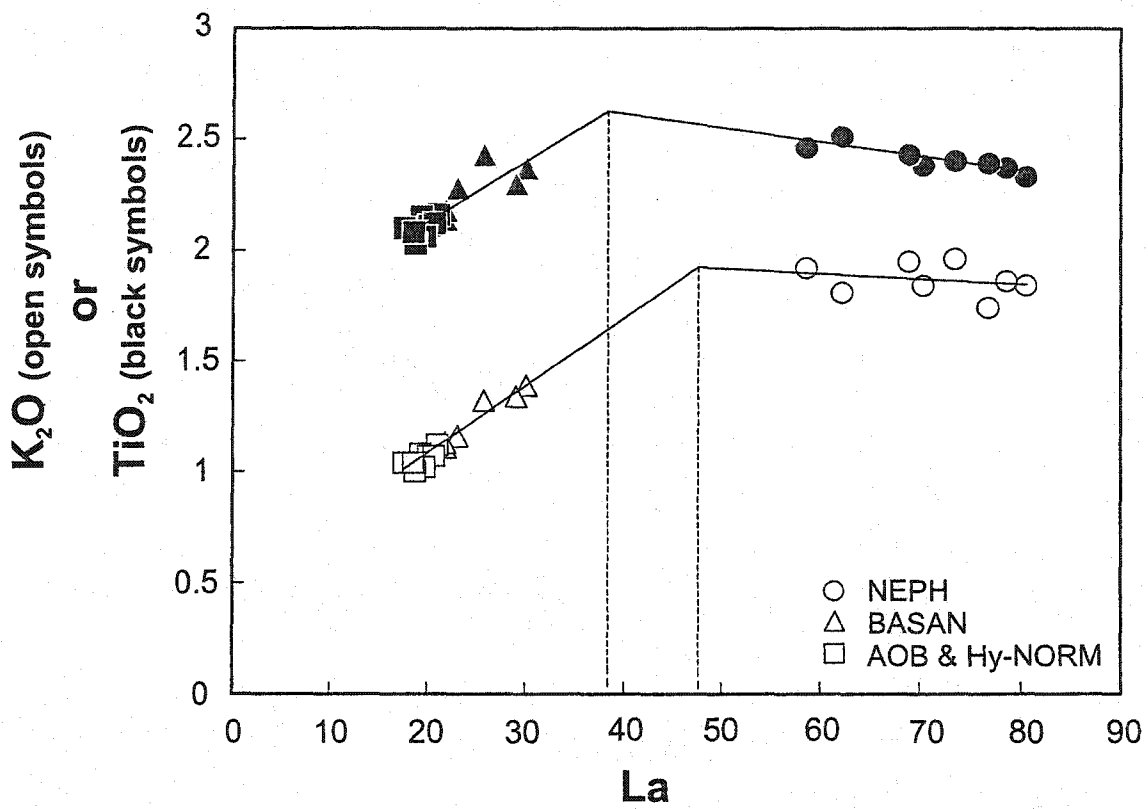
Francis and Ludden (1990 and 1995) demonstrated that amphibole was an important residual phase during the production of NEPH lavas at Hirschfeld and Fort Selkirk, explaining the low concentrations of K, Rb and Ba compared to other incompatible elements (Fig. 5). The NEPH lavas are isotopically homogeneous, and isotopically depleted compared to associated Hy-NORM lavas in the northern Canadian Cordillera (Fig. 7). Despite their isotopic homogeneity, however, the NEPH lavas have distinct major and trace element signatures at different volcanic centres, such as higher Ti and Y, and lower Ba at Fort Selkirk than at Hirschfeld, Llangorse or Minto Landing (Fig. 6). These observations indicate that an isotopically depleted mantle component rich in amphibole, but with variable trace element abundances must be present in the northern Cordilleran mantle.

The Fo content calculated for olivine in equilibrium with Cordilleran NEPH with $\text{MgO} \approx 12$ wt.% is 86 ± 1 , assuming that $\text{Fe}^{3+}/\text{total Fe} = 0.15$ and an olivine-liquid Kd $\text{Fe/Mg}=0.3$ (Roeder and Emslie, 1970). This value is well below the values typical of fertile pyrolite-like mantle (Fo_{89-90} ; Ringwood, 1975), and of actual mantle xenoliths entrained in the NEPH lavas (Fo_{89-92} ; Francis, 1987; Shi et al., 1998). The 12 wt.% MgO NEPH lavas may be either primary, or the result of olivine fractionation from more magnesian primary lavas. An olivine Mg# value of 90 ± 1 can be obtained by the

fractional addition of 2 to 20 % olivine until the lava composition reaches an MgO content of ~ 16 wt.%. If the NEPH lavas last equilibrated with amphibole, as suggested by the behavior of K, the amphibole coexisting with a 12 wt.% MgO NEPH magma would have a Mg# value of 0.83 ± 1 , assuming an amphibole-melt Fe/Mg Kd of 0.38 (LaTourrette et al., 1995), whereas they would have a Mg# value 0.87 ± 1 if primary NEPH magmas contained 16 wt.% MgO. In either case, these Mg# values are lower than those of amphibole in mantle peridotites, that typically have Mg# > 0.88 (e.g. Francis, 1976a; O'Reilly et al., 1991; Witt-Eickschen and Harte, 1994; Ionov and Hofmann, 1995; Ionov et al., 1997; Xu Y. et al., 1997). On the other hand, amphiboles in veins cutting peridotites generally have lower Mg# than those in peridotites (e.g. Francis, 1976b; Frey and Prinz, 1978; Xu X. et al., 1997; Ionov and Hofmann, 1995; Ionov et al., 1997) and would be suitable candidates for the mantle source of the NEPH end-member.

Experimental studies indicate that, where present, amphibole will be the first phase to melt under H_2O -undersaturated conditions (Olafsson and Eggler, 1983) and will control the K content in the melt. A recent experimental study on ultramafic vein assemblages containing Ca-amphibole indicates that the melting reaction is controlled largely by the incongruent melting of amphibole to produce Cpx, and that the melt composition resembles nepheline or melilite at pressures greater than 15 kbar (Foley et al., 1999). The kink that occurs in a plot of K versus La at La \approx 50 ppm in the Hirschfeld dataset (Fig. 10), where primitive NEPH are in direct continuous contact with BASAN and AOB in a high-level volcanic plug, has been proposed to represent the exhaustion of

Figure 10: K_2O (white symbols) and TiO_2 (black symbols) versus La in high MgO (> 8 wt.%) lavas from Hirschfeld (Francis and Ludden, 1995).



amphibole in the mantle source (Francis and Ludden, 1995) and the beginning of melting of the host mantle. The negative trend displayed by the NEPH lavas at Hirschfeld in a Ti versus La plot (Fig. 10) indicates that Ti is buffered by a residual Ti-rich phase. This trend displays a kink similar to that in a K versus La plot (Fig. 10), except that the kink occurs at a lower La content (~40 ppm) than that for K (La)~50 ppm. This discrepancy suggests that Ti and K are not controlled by the same phase and that the phase that controlled Ti melted out after amphibole. Ti might be controlled by ilmenite, which is present in many amphibole-rich pyroxenites (Lorand et al., 1990; Zack and Brumm, 1998).

Experimental studies have shown that incongruent melting of amphibole can produce nepheline-normative lavas, either at relatively low pressure in the spinel stability field (~13.5 kbar; Olafsson and Eggler, 1983), or at higher pressures, in the garnet stability field (above ~20 kbar; Merrill and Wyllie, 1975). In both cases, Cpx is produced at the expense of amphibole during progressive melting. From these results, Francis and Ludden (1995) calculated a melting reaction for amphibole (1 Amph = 0.6 Liq + 0.3 Grt + 0.1 Cpx) by mass-balancing the major elements of average NEPH, amphibole, Cpx and garnet. We followed a similar approach, adding ilmenite as a residual phase, and calculated two melting reactions, involving spinel and garnet respectively, by mass-balancing Ti, Al, Ca, Na and K using the average compositions of NEPH lavas from Hirschfeld (Francis and Ludden, 1995) and amphibole, ilmenite, Cpx, garnet and spinel in amphibole-bearing pyroxenites from Kakanui (Table 3). In the spinel stability field, the calculated incongruent melting reaction for amphibole is Amph \rightarrow 0.72

Table 3: Composition of the different components used in the least-square calculations to determine the melting reactions of amphibole in the spinel and garnet stability fields.

--

Table 3: Composition of the different components used in the least-square calculations to determine the melting reactions of amphibole in the spinel and garnet stability fields

	NEPH	Spinel	Cpx	Ilmenite	Amph	Residuals
TiO ₂	2.4	0.7	1.3	51.5	5	0.1
Al ₂ O ₃	11.6	61	9.8	1	14.2	0.1
CaO	10.25	-	16	-	9.5	0.22
Na ₂ O	4.7	-	1.5	-	3.2	0.41
K ₂ O	1.8	-	-	-	1.45	-0.15
% component	72%	7%	15%	6%	100%	0.26

	NEPH	Garnet	Cpx	Ilmenite	Amph	Residuals
TiO ₂	2.4	0.4	1.3	51.5	5	-0.28
Al ₂ O ₃	11.6	23.00	9.8	1	14.2	-0.52
CaO	10.25	5.00	16	-	9.5	-0.55
Na ₂ O	4.7	-	1.5	-	3.2	-0.36
K ₂ O	1.8	-	-	-	1.45	-0.43
% component	57%	26%	11%	6%	100%	0.97

$\text{NEPH} + 0.15 \text{ Cpx} + 0.07 \text{ Sp} + 0.06 \text{ Ilm}$ (1). In reality, the spinel and ilmenite would probably be combined in a single oxide phase. At higher pressures, garnet replaces spinel as a residual phase and the best melting reaction becomes: $\text{Amph} \rightarrow 0.57 \text{ NEPH} + 0.26 \text{ Gnt} + 0.11 \text{ Cpx} + 0.06 \text{ Ilm}$ (2), similar to that of Francis and Ludden (1995), except for the additional ilmenite.

Potential amphibole-bearing source compositions for the NEPH lavas in Hirschfeld have been recalculated using Shaw (1970)'s non-modal melting equation $C_0 = C_L * [D + F * (1 - P)]$, and assuming that the kink in the K versus La plot (Fig. 10) corresponds to exhaustion of amphibole. In a first step, we assumed a pure amphibole source, in which case this point represents 57% melting in the garnet stability field, as compared to 72% melting in the spinel stability field. The values of P in Shaw's equation were calculated using Kd values in Table 4 and the proportion of each mineral given by the two melting reactions. The calculated source composition for Hirschfeld NEPH lavas in the spinel stability field is similar to that of natural amphibole in mantle veins (average from data from Ionov and Hoffman (1995), Vaselli et al., (1995), Ionov et al. (1997), Witt-Eickschen et al. (1998), and Francis' unpublished Kakanui data for amphiboles), except that it contains higher Th (~ 3 ppm as compared to 0.17 ± 0.1 ppm in natural amphibole in veins), LREE (~ 30 ppm as compared to 11 ± 8 ppm in natural amphibole in veins), and P contents (Fig. 11). Using the average composition of metasomatic apatite from O'Reilly and Griffin (2000), the differences between natural amphibole in veins and the calculated source for the Hirschfeld NEPH in the spinel stability field can be explained by the presence of as little as 1% apatite in the veins (Fig. 11). The calculated source for

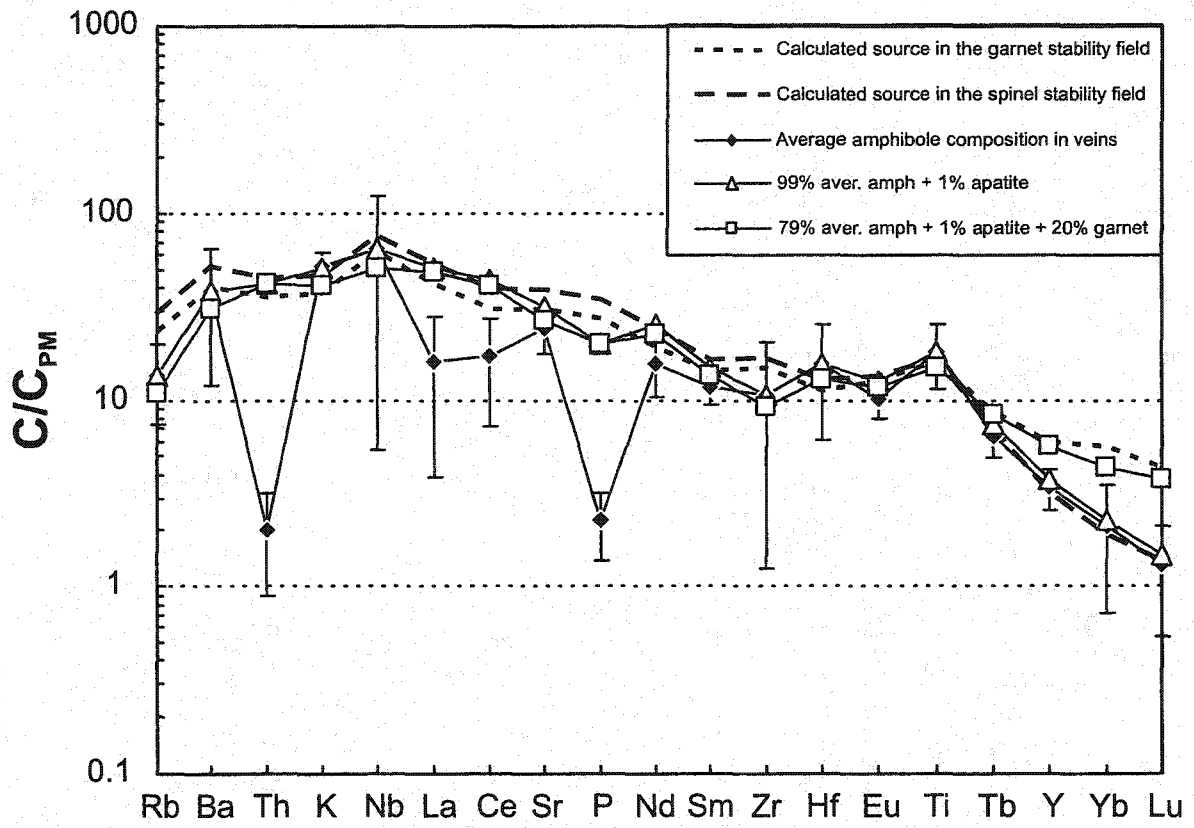
Table 4:

Partition coefficients used in melting calculations. Clinopyroxene / melt partition coefficients are from Hart and Dunn (1993), except for Rb (Foley et al., 1996), Th (Hauri et al., 1994) and Eu, Tb and Ho (interpolated). Amphibole / melt partition coefficients are those of run #02 of Dalpé (1997), except for Pb (Ionov et al., 1997). Garnet / melt partition coefficients are from Johnson (1998), except for Rb, Ba, Th, K and Pb (Halliday et al., 1995) and Tb and Ho (interpolated). Spinel / melt partition coefficients have been compiled by Kelemen et al. (1993). Ilmenite / melt partition coefficients are from Zack and Brumm (1998).

Table 4: Partition coefficients used in melting calculations

Kd	Clinopyroxene	Amphibole	Garnet	Spinel	Ilmenite
Rb	0.0047	0.23	0.0002	0.001	-
Ba	0.0007	0.14	0.00007	0.001	0.00034
Th	0.012	0.01	0.0021	-	0.00055
K	0.0072	0.71	0.013	0.001	-
Nb	0.0077	0.14	0.0031	0.01	2
La	0.0536	0.07	0.0016	0.0006	0.000029
Ce	0.0858	0.12	0.005	0.0006	0.000054
Pb	0.072	0.03	0.0003	-	-
Sr	0.1283	0.23	0.0025	0.001	-
Nd	0.1873	0.23	0.052	0.0006	0.00048
Sm	0.291	0.33	0.25	0.0006	0.00059
Zr	0.1234	0.25	0.27	0.07	0.29
Hf	0.256	0.44	0.24	0.05	0.38
Eu	0.36	0.33	0.4	0.0006	0.0011
Ti	0.384	1.2	0.29	0.15	11
Tb	0.42	0.33	1.4	0.0006	0.0067
Dy	0.442	0.33	2.2	0.0015	0.01
Y	0.467	0.36	3.1	0.001	-
Ho	0.43	0.32	2.8	0.0015	0.011
Er	0.387	0.34	3.6	0.003	-
Yb	0.43	0.35	6.6	0.0045	0.17
Lu	0.433	0.35	7.1	0.0045	0.084

Figure 11: Calculated source concentrations that could produce the composition of the melts at the kink in the K versus La diagram (Fig. 10), assuming that it corresponds to exhaustion of amphibole, using Shaw (1970)'s non modal melting equation $C_O = C_L * (D + F(1 - P))$ where P's were calculated from incongruent melting equations (1) and (2) in text. The source concentrations are compared with the average composition of natural vein amphiboles, with a mixture of amphibole and apatite, and with a mixture of amphibole, apatite and garnet. The trace element composition of amphibole in veins corresponds to average composition of Ionov and Hoffman (1995), Vaselli et al., (1995), Ionov et al. (1997), Witt-Eickschen et al. (1998), and unpublished data from D. Francis of amphibole pyroxenites from Kakanui. The apatite and garnet trace element composition corresponds to the average composition of respectively metasomatic apatite from O'Reilly and Griffin (2000), and garnet in pyroxenites from Kakanui (D. Francis, unpublished data).

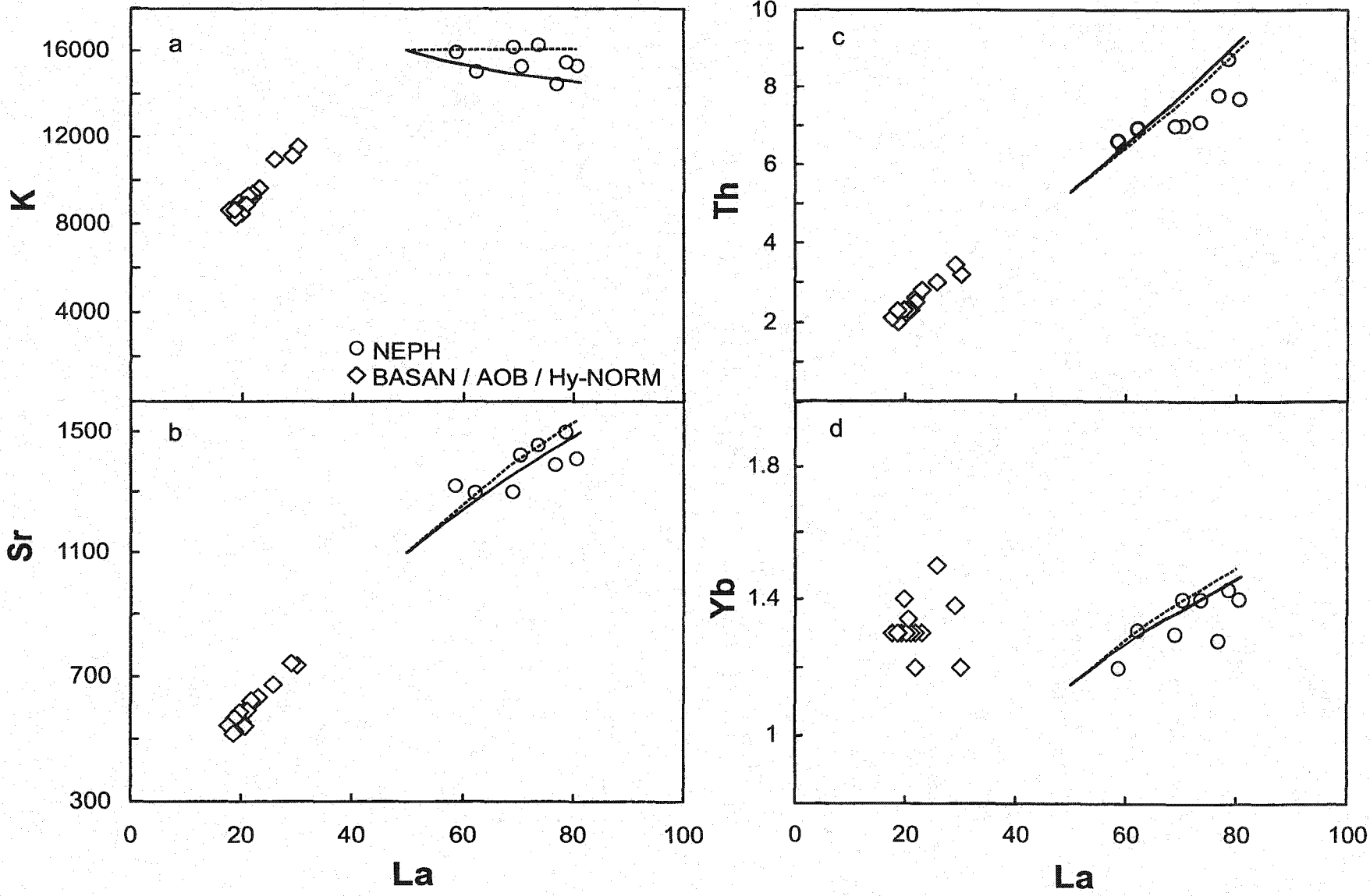


Hirschfeld NEPH in the garnet stability field differs from amphibole observed in mantle veins by its higher Th, LREE, P, and HREE contents (Fig. 11), which would require the presence of garnet in the initial source as well as apatite. The composition of the calculated source of the Hirschfeld NEPH magmas in the garnet stability field can be reproduced by a mixture of 20% garnet, 1% apatite and 79% amphibole, using the above mentioned compositions for apatite and amphibole in mantle veins, and Francis' unpublished Kakanui data for garnet (Fig. 11).

Using the calculated spinel and garnet source compositions, the range of melt compositions produced by incongruent melting can be compared to the compositional range observed in the NEPH lavas of Hirschfeld (Fig. 12). The results indicate that the relative behavior of all incompatible trace elements compared to La in the Hirschfeld intrusion are relatively well explained by incongruent melting of mantle amphibole in either the spinel or the garnet stability field.

As amphibole is often associated with pyroxene in mantle veins (e.g. Francis, 1976b; Witt-Eickschen and Harte, 1994, Xu X. et al. 1997), the effects of melting of amphibole-bearing pyroxenite veins were evaluated by using variable proportions of amphibole, clinopyroxene and spinel or garnet as analogues of amphibole-bearing pyroxenites. The trace element source compositions associated with these variable initial modes were calculated using Shaw (1970)'s melting equation and assuming that amphibole alone melts until its exhaustion at the kink in the K versus La plot, as would be expected under water-undersaturated conditions (Green, 1973). Partial melting models of these amphibole-bearing vein analogues indicate that, when the source vein contains less

Figure 12: a) K versus La, b) Sr versus La, c) Th versus La and d) Yb versus La for the Hirschfeld's data set (Francis and Ludden, 1995). The full heavy line corresponds to the spectrum of liquids produced by melting of garnet-amphibole veins, the dotted line corresponds to liquids produced by melting of amphibole veins in the spinel stability field.

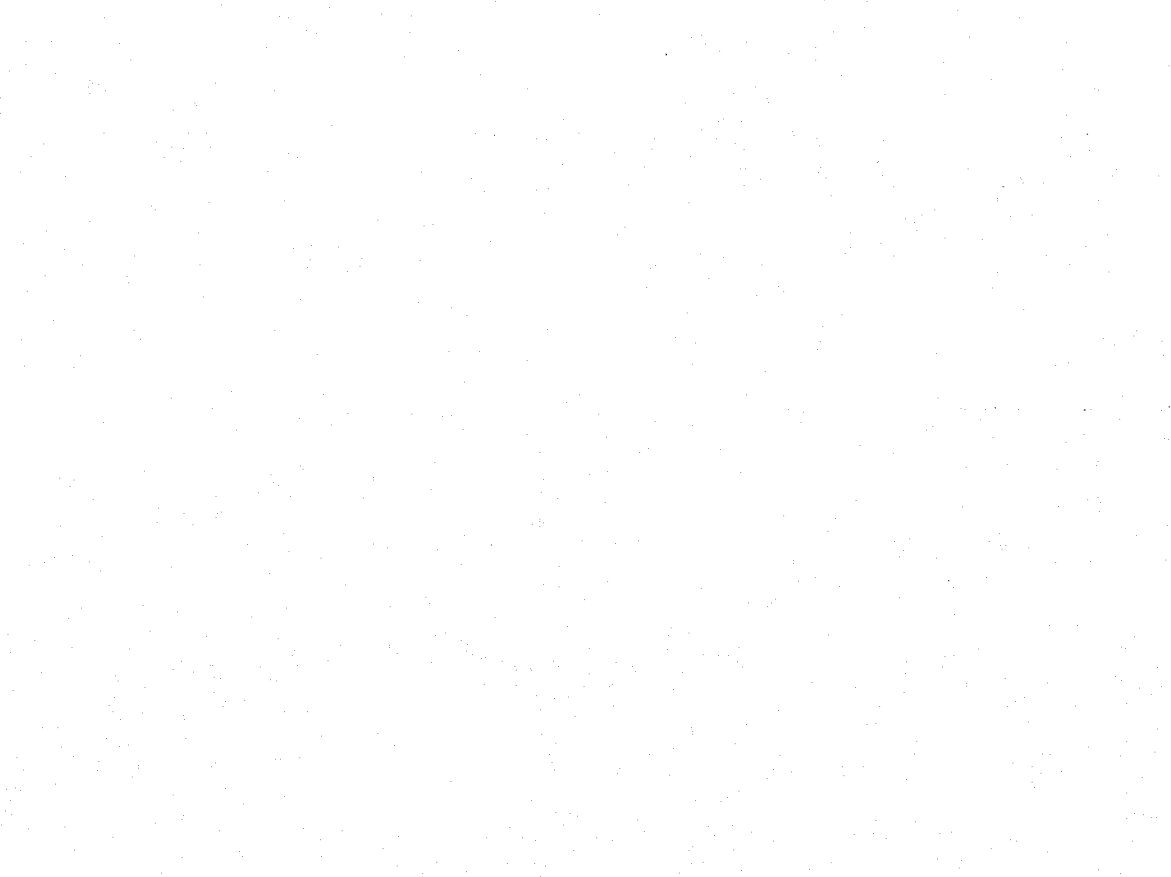


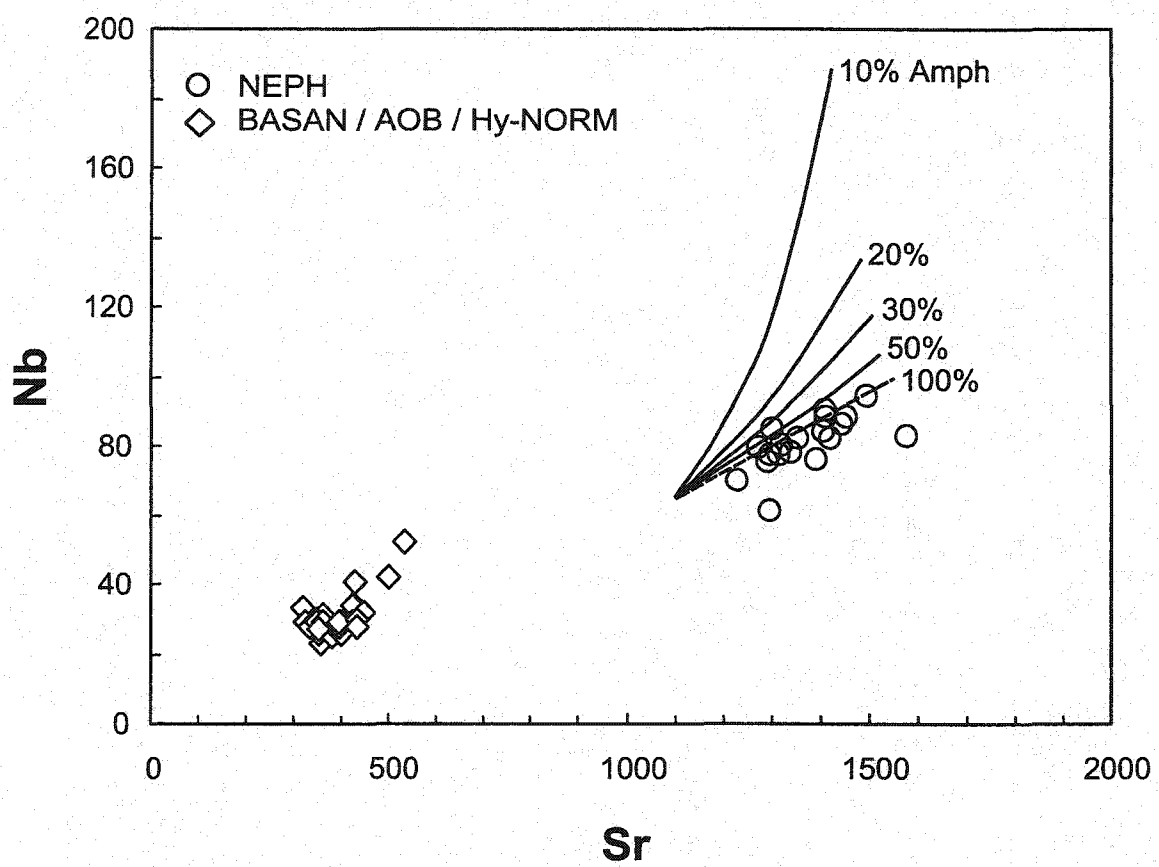
than approximately 50% amphibole, the melts produced will be more enriched in elements such as K, Rb, Ba, or Nb, that partition preferentially in amphibole, than NEPH lavas erupted at Hirschfeld (Fig. 13). This implies that the NEPH magmas represent relatively large degrees of partial melting of the amphibole-rich veins, the smallest degrees of partial melting being approximately 15 % in the garnet stability field, and 20 % in the spinel stability field.

The higher Nb but lower Ba contents of the NEPH lavas at Fort Selkirk compared to those at Hirschfeld (Fig. 6) can not be explained by smaller proportions of amphibole in the pyroxenite mantle source, because the melt produced should be more enriched in both these elements, which partition preferentially in amphibole. The chemical differences in trace elements such as HREE, Ba or Y between NEPH lavas erupted in different centres (Fig. 6) may better be attributed to differences in the composition of the amphibole. Indeed, amphiboles in mantle veins display a relatively large range of major and trace element compositions (e.g. Ionov et al., 1997; Vaselli et al., 1995; Witt-Eickschen et al., 1998) that might be related either to different stages of crystallization of the melt(s) that formed the veins (Harte et al., 1993), to different extents of solid-liquid exchange with the wall-rocks of the veins (Witt-Eickschen et al., 1998), or to different compositions of metasomatic melt or fluid (e.g. Francis, 1976b; Menzies et al., 1987) that produced them.

The isotopically homogeneous character of the NEPH lavas erupted in the Intermontane Belt, and the trend towards the NEPH end-member observed in the isotopic signature of BASAN lavas from the Omineca Belt (Fig. 7), indicate that the proposed

Figure 13: Nb versus Sr variations during partial melting of amphibole-bearing pyroxenites in the spinel stability field, with labels indicating the proportion of amphibole in the pyroxenites, compared to the Hirschfeld data set (Francis and Ludden, 1995).





amphibole-bearing vein source for the NEPH lavas may have been produced by a metasomatic event that affected the whole northern Canadian Cordillera. The isotopically depleted character of the Cordilleran NEPH lavas indicates that this event must be recent, and would be consistent with derivation of the amphibole-bearing veins from asthenospheric melts or fluids. An asthenospheric origin for mantle amphiboles has been proposed to the south, beneath Proterozoic mobile belts in the western United States (Ben Othman et al., 1990). The metasomatic event in the northern Cordillera may be related to the presence of a slab-window since the early Miocene (Thorkelson and Taylor, 1989), which has allowed the upwelling of mantle. Some studies of alkaline volcanic suites (e.g. Fitton, 1987; Kempton et al., 1991; Jung and Masberg, 1998; Prestvik et al., 1999; Jung and Hoernes, 2000; Edwards and Russell, 2000) have concluded that NEPH lavas are derived directly from asthenospheric mantle because of their isotopically depleted character. The amphibole signature of the Cordilleran NEPH lavas indicates, however, that they can not arise directly from the asthenospheric mantle. Small degrees partial melts derived from the asthenospheric mantle could, however, crystallize as amphibole-bearing veins in the lithospheric mantle, and subsequent melting of these veins would then generate the NEPH lavas. Derivation of the NEPH lavas from a metasomatized lithospheric source is consistent with many recent studies of alkaline volcanic suites, both in oceanic (e.g. Hoernle et al., 1991; Widom et al., 1997; Class et al., 1998), and continental settings (e.g. Wilson et al., 1995; Beccaluva et al., 1998; Zhang et al., 2001).

In summary, the chemical and isotopic signatures of NEPH lavas in the northern Canadian Cordillera are consistent with incongruent melting, in the lithospheric mantle, of recent amphibole-bearing veins containing more than 50% amphibole, small amounts

of apatite \pm garnet, and leaving clinopyroxene, ilmenite and spinel or garnet as residual phases. The most successful models indicate that extremely small degrees of partial melting are not required to explain the enriched trace element patterns of the NEPH lavas, which may represent about 15 % partial melting.

4.2. Mantle source of Hy-NORM basalts

The crystallization sequence of the Hy-NORM basalts is olivine, plagioclase, Cpx and opaques (Francis and Ludden, 1990), with plagioclase appearing as a phenocryst phase at ~8 wt.% MgO. This sequence has been confirmed using MELTS (Ghiorso and Sack, 1995) at 1 atm for a primitive Hy-NORM basalt (MH-19; Abraham et al., 2001) with 13.5 % MgO. MELTS results indicate that the first plagioclase crystallized at an MgO content of 7.5 wt.%. In the following, the effects of low pressure plagioclase and/or Cpx fractionation are avoided by considering only the most primitive Hy-NORM lavas, with MgO contents greater than 8 wt.%.

Primitive Hy-NORM basalts in the northern Canadian Cordillera have more restricted incompatible trace element compositions than the primitive NEPH lavas (Fig. 6). They display, however, larger ranges of Sr, Nd and Pb isotopic ratios than the NEPH lavas, and define domains of distinct isotopic signature that correlate with the tectonic belts of the northern Canadian Cordillera (Abraham et al., 2001). Hy-NORM basalts erupted in the Omineca Belt have higher Sr and Pb, and lower Nd isotopic ratios than Hy-NORM basalts erupted in the Intermontane Belt, and higher Sr, and lower Nd and Pb

isotopic ratios than Hy-NORM basalts erupted in the Coast Belt (Abraham et al., 2001). The differences in isotopic signatures between the Intermontane, Omineca and Coast belts Hy-NORM basalts could reflect contamination by distinct crustal material on their way to the surface. Granitoids of the Intermontane Belt have low initial Sr isotopic ratios (< 0.705; Armstrong, 1988), whereas granitoids of both the Coast and Omineca belts have high initial Sr initial ratios (> 0.705; Armstrong, 1988), and thus the Intermontane crust is expected to be less radiogenic in Sr than the crust of both the Omineca and Coast belts. Fractional crystallization and assimilation models using the most primitive Cordilleran Hy-NORM lavas and upper crustal granitoids, however, indicate that Hy-NORM basalts with enriched isotopic signatures ($^{87}\text{Sr}/^{86}\text{Sr} > 0.704$) and high MgO (~ 13 wt.%) cannot be produced by upper crustal contamination (Abraham et al., 2001). The possibility of lower crustal contamination is more difficult to assess due to the lack of lower crustal xenoliths in Cordilleran lavas. Recent seismic reflection data, however, reveal the presence of a westward tapering wedge (Fig. 2b) in the lower crust of the Omineca Belt and of the eastern part of the Intermontane Belt (Cache Creek terrane) that has been interpreted as North American Precambrian lower crust (Cook et al., 2001). The lack of correspondence in the position of the isotopic change between the Omineca and Intermontane belts lavas and the edge of this lower crustal wedge (Fig. 2b) argues against the isotopic provinciality reflecting contamination by lower crustal melts. If crustal contamination does not account for the isotopic differences between the Omineca and Intermontane Hy-NORM basalts, then these signatures must lie in the mantle. As the isotopic signature of asthenospheric mantle below the Canadian Cordillera should not correlate with crustal tectonic belts, the isotopic differences between Omineca and Intermontane Hy-NORM basalts most likely lie in the lithospheric mantle.

Hy-NORM basalts with more than 10 wt.% MgO would coexist with olivines with Fo contents of 86 ± 1 , assuming $\text{Fe}^{3+}/(\text{total Fe})=0.15$ and using an olivine-liquid Fe/Mg Kd of 0.3 (Roeder and Emslie, 1970). These Fo values are too low for primary lavas that have equilibrated with a pyrolite-like mantle ($\text{Fo}_{89.90}$; Ringwood, 1975) or Cordilleran lherzolite peridotites ($\text{Fo}_{89.92}$; Francis, 1987; Shi et al. 1998). However, the highest MgO Hy-NORM basalt (13.5 wt.%) have high Ni (350 ppm) and Cr (350 ppm) contents (Abraham et al., 2001), values that approach those expected for primary melts. We estimated the composition of primary Hy-NORM lavas by fractionally adding 2-14% olivine to the composition of primitive Hy-NORM lavas ($\text{MgO} > 8\text{wt.\%}$) until they reached a MgO content of 14 wt.%. These 14 wt.% MgO normalized lavas (later referred as Mg_{14} Hy-NORM) would coexist with olivines with Fo contents of 89 ± 1 , if $\text{Fe}^{3+}/(\text{total Fe})=0.15$, values within the range of olivine in pyrolite-like mantle and in Cordilleran lherzolite peridotites.

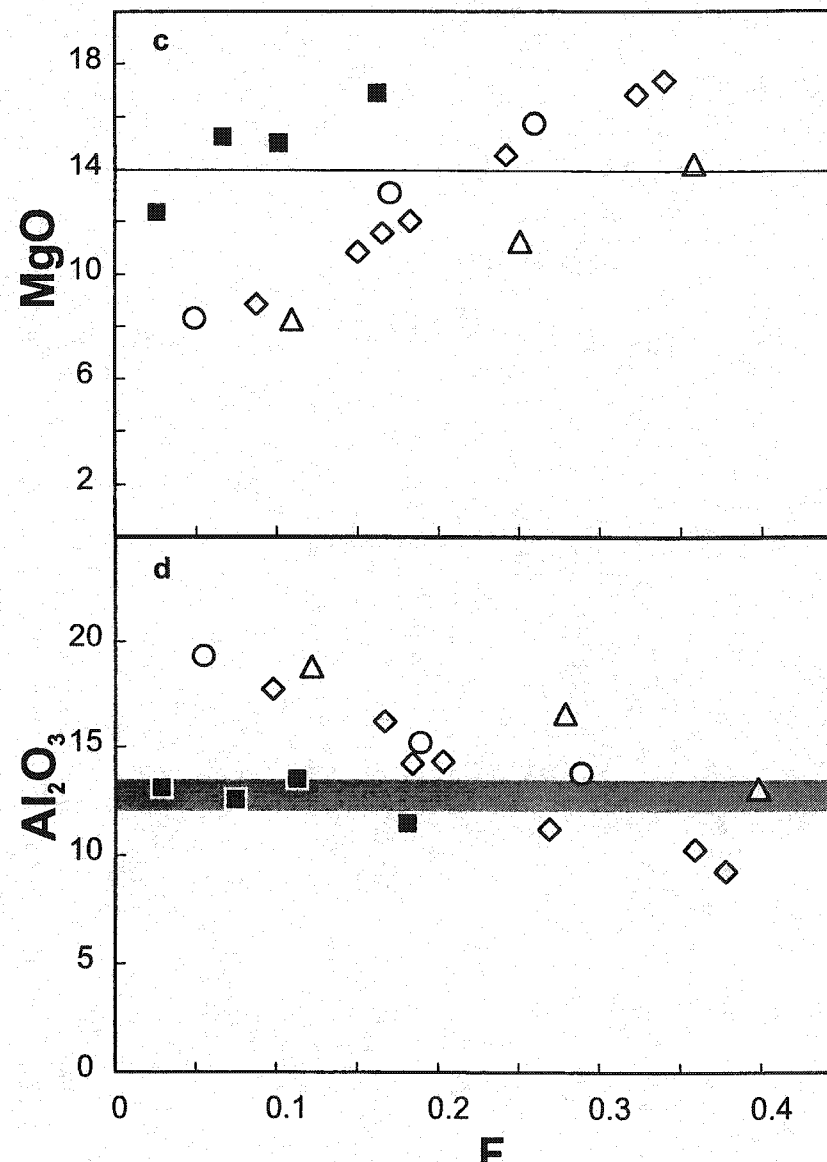
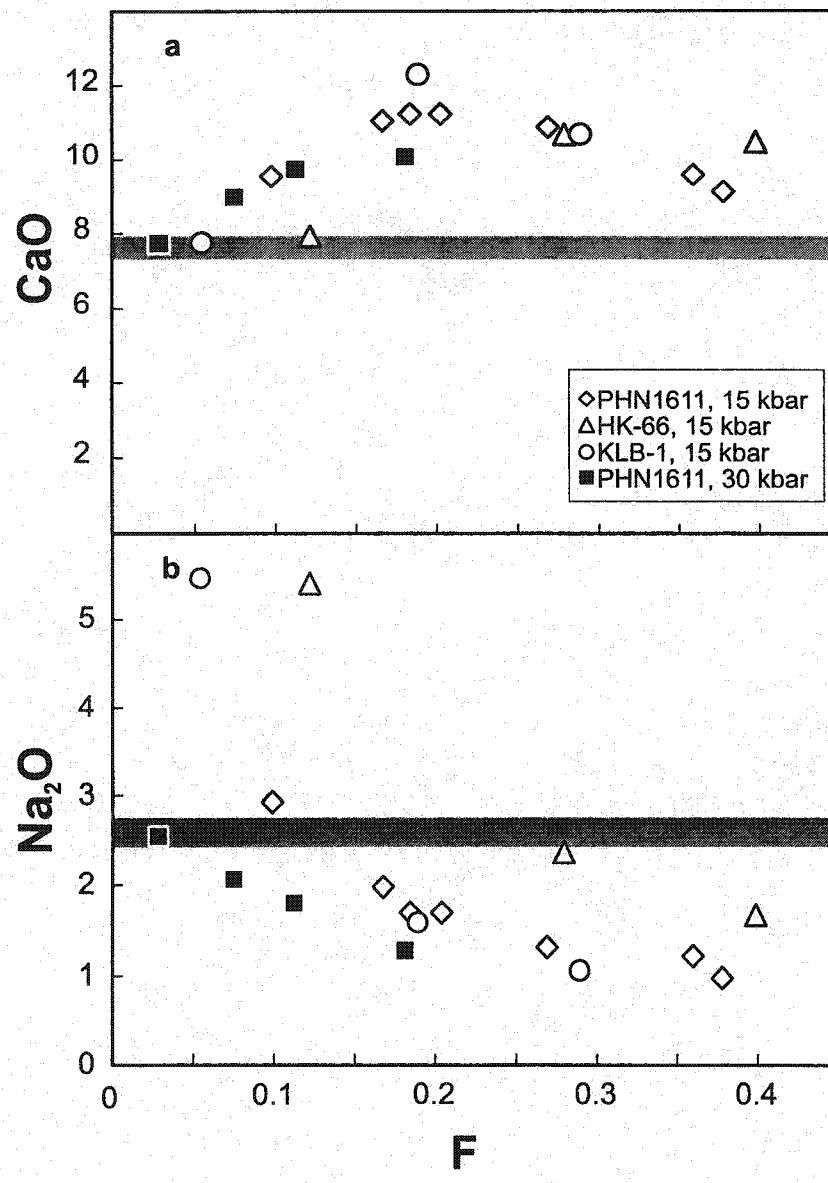
Mg_{14} Hy-NORM basalts in the Canadian Cordillera are characterized by low CaO contents (7.8 ± 0.3 wt.%) and high Na₂O contents (2.6 ± 0.2), features that also characterize basalts from other continental margin areas in contrast to the higher CaO and lower Na₂O contents of their equivalents in oceanic hot spot and MOR areas (Fig. 9a). The low CaO content of the Cordilleran Hy-NORM lavas is not consistent with high pressure crystal fractionation of Cpx because modeling with MELTS (Ghiorso and Sack, 1995) indicates that the liquidus phase at pressure > 5 kbar is Opx and not Cpx. In addition, the lack of Cpx phenocrysts in the high MgO Hy-NORM basalts, the lack of decrease of CaO/Al₂O₃ with decreasing MgO (Fig. 3), and the low CaO and Sc contents

in all Recent alkaline lava types in the northern Cordillera, even in those containing mantle xenoliths, argues against significant high pressure Cpx fractionation.

The CaO content of a melt derived from partial melting of a dry peridotite appears to be dependent on the degree of partial melting and on the source composition (e.g. Hirose and Kushiro, 1993; Hirschmann et al., 1999). CaO increases with increasing degrees of partial melting and decreasing Na₂O until the exhaustion of Cpx, at which point it begins to decrease (Fig. 14a and 14b). The low CaO content of the Mg₁₄ Hy-NORM basalts could thus be explained by either small (< 10%) or large (> 40%) degrees of partial melting of a dry mantle peridotite. At high degrees of partial melting (> 40%), however, melts derived from melting of a mantle lherzolite should have much higher MgO and much lower Na₂O contents than Mg₁₄ Hy-NORM basalts (Fig. 14b and 14c). In addition, experimental melts at high degrees of melting do not reach the low CaO contents of Hy-NORM basalts from the Canadian Cordillera and all other continental margin areas (Fig. 14a). Alternatively, the Mg₁₄ Hy-NORM basalts have similar CaO, but much lower Al₂O₃ (~ 12 wt.%) contents than small degrees partial melts (F ≤ 10%) of mantle lherzolites at P ~ 15 kbar (Fig. 14c). The Al₂O₃ content of the low degree partial melts would be lower, however, if garnet were present as a residual phase. The only experimental low-degree melts (3-8 %) of peridotite with residual garnet at pressures of 30 kbar are those performed on a fertile garnet lherzolite, PHN1611 (Kushiro, 1996). These melts have much lower Al contents (Al₂O₃ ~ 13 wt.%) than low degree melts of the same peridotite at lower pressure (at 15 kbar, Al₂O₃ ~ 18 wt.%; Fig. 14c). The low Al and Ca contents of Cordilleran Hy-NORM basalts may thus indicate that they represent



Figure 14: a) CaO, b) Na₂O, c) MgO, and d) Al₂O₃ versus degree of partial melting (F) for experimental melts produced by dry melting of peridotite at 15 and 30 kbar. PHN1611 from Kushiro (1996), HK-66 and KLB-1 from Hirose and Kushiro (1993). Grey area: range in Cordilleran Hy-NORM normalized to 14 wt.% MgO.



low degree partial melts (<10%) of a peridotite mantle at relatively high pressure, in the garnet stability field.

Experimental studies indicate that low Ca Hy-NORM basalts are not produced by melting of a carbonated peridotite because carbonated melts have higher CaO than partial melts without CO₂ at the same pressure (Hirose, 1997). Low Ca Hy-NORM basalts might be produced, however, by hydrous melting of peridotite, because, at high temperature, the composition of hydrous partial melts with < 2.5 wt.% H₂O is similar to that of melts produced under anhydrous conditions (Hirose and Kushiro, 1993; Hirose and Kawamoto, 1995). The major element characteristics of the Cordilleran Mg₁₄ Hy-NORM basalts are thus consistent with relatively small degrees partial melting of either an anhydrous or an hydrous amphibole-bearing peridotite.

Cordilleran and other continental margin Hy-NORM basalts have lower CaO and higher Na₂O contents than most Hy-NORM basalts from oceanic hot spots, which fall with MOR Hy-NORM basalts at high CaO and low Na₂O contents (Fig. 9a). The range of Na in MOR basalts has been explained by a range in the degree of partial melting (Klein and Langmuir, 1987) and a similar model has been proposed to explain the Na contents of arc lavas (Plank and Langmuir, 1988). The low Ca and high Na contents of continental margin Hy-NORM basalts compared to oceanic hot spot and MOR basalts may thus reflect the fact that they represent lower degrees of partial melting. The low Al content of continental margin areas and oceanic hot spot Hy-NORM basalts (Fig. 9b) indicates that melting occurred in the garnet stability field, whereas the higher Al contents

in MOR basalts suggest that they were generated at lower pressure, in the spinel stability field.

Continental lithospheric mantle is generally enriched in the highly incompatible trace elements relative to primitive mantle, and depleted in mildly incompatible elements such as HREE (McDonough, 1990). In mantle xenoliths from the northern Canadian Cordillera, the HREE do not appear to have been significantly modified by metasomatism (Shi et al., 1998), and the average HREE values in lherzolites with $\text{Al}_2\text{O}_3 = 3\text{-}4$ wt.% (Peslier, 1999), corresponding to the composition of the predominant mode in Cordilleran mantle xenoliths (Shi et al. 1998), were used as an estimate of the HREE content of the Hy-NORM basalts source. The best fit for the HREE concentration of northern Canadian Cordillera Hy-NORM basalts would correspond to $\sim 8\%$ partial melting of such a garnet-bearing source (Fig. 15a), consistent with the estimate of less than 10% melting based on CaO and Na₂O contents (Fig. 9a). The concentration in the other incompatible elements in the mantle source of Hy-NORM basalts erupted in the Intermontane and Omineca belts have been recalculated using this model (Fig. 15b; Table 5). The calculated incompatible element patterns of the Intermontane and Omineca belts mantle sources exhibit similar enrichment in incompatible trace element except for slightly higher Rb, Th and Pb values for the Omineca mantle source compared to that of the Intermontane Belt. These trace element enrichments might be related to metasomatism by small degree melts or fluids rising from the underlying asthenosphere.

The isotopic differences between the Hy-NORM basalts of the Intermontane and Omineca belts (Abraham et al., 2001) indicate that the mantle source of the Hy-NORM

Figure 15:

a) REE concentrations calculated from 4, 8 and 12% partial melting of a garnet peridotite (Ol: 0.6, Opx: 0.25, Cpx: 0.1, and Gnt: 0.05) using the REE concentrations in Cordilleran mantle xenoliths for the source composition (Peslier, 1999) and the melting mode of Ottonello et al. (1984) (Ol: -0.1, Opx: 0.3, Cpx: 0.4, and Gnt: 0.4), compared to average primitive Hy-NORM from the Intermontane and Omineca belts. b) Calculated sources for the Intermontane and Omineca Hy-NORM basalts assuming that the Hy-NORM basalts were generated by 8% partial melting of a garnet peridotite. Same source and melting modes as a).

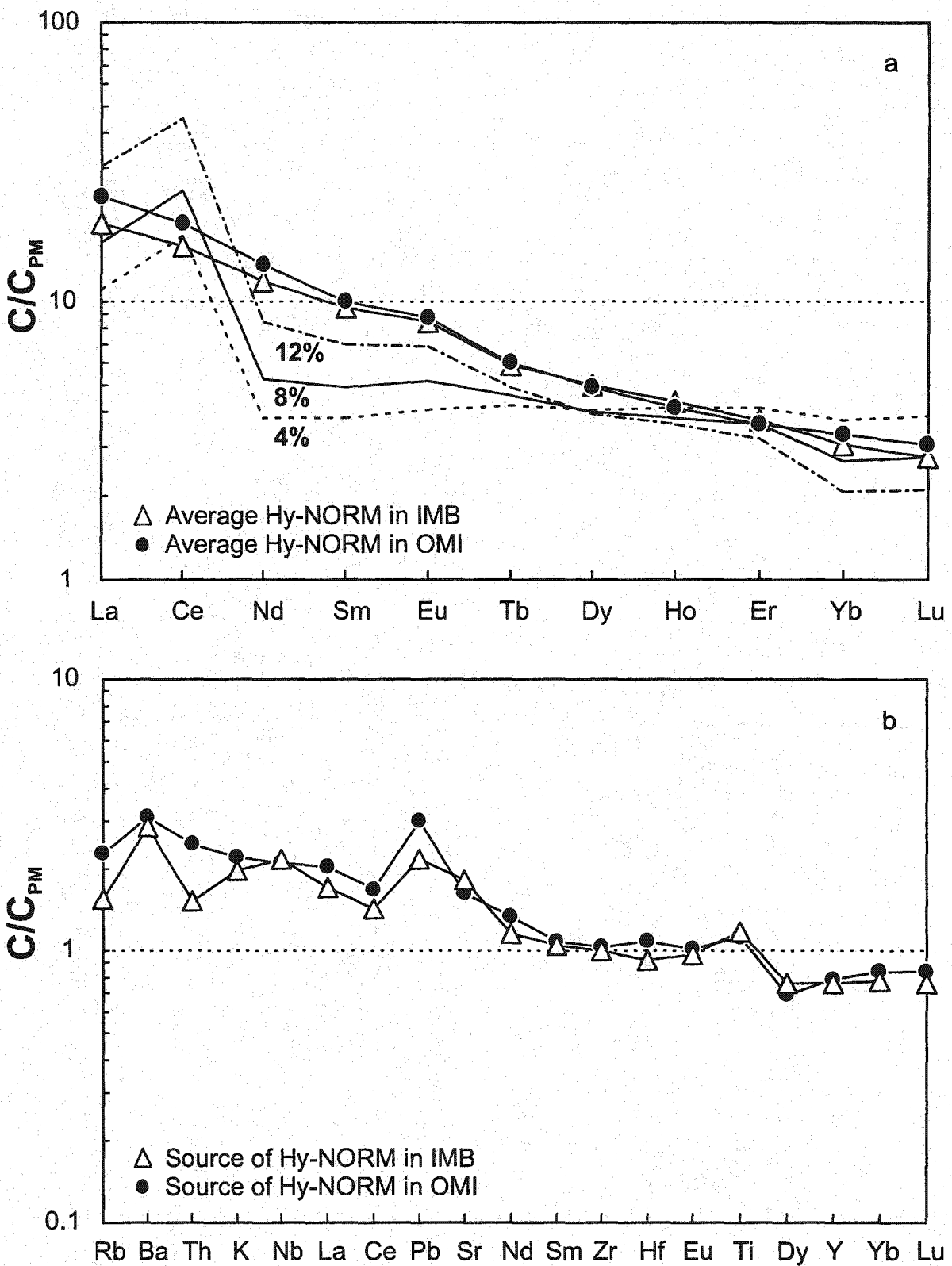


Table 5: Calculated compositions of the enriched mantle sources for Hy-NORM basalts from the Intermontane and Omineca belts.

Table 5: Calculated compositions of the enriched mantle sources for Hy-NORM basalts of the Intermontane and Omineca belts.

Element concentration in ppm	Omineca Belt enriched mantle	Intermontane Belt enriched mantle
Rb	1.46	0.99
Ba	21.7	19.9
Th	0.21	0.13
K	554	496
Nb	1.50	1.54
La	1.41	1.17
Ce	2.99	2.55
Pb	0.21	0.16
Sr	34.3	38.5
Nd	1.81	1.58
Sm	0.48	0.46
Zr	11.7	11.3
Hf	0.33	0.28
Eu	0.17	0.16
Ti	1458	1537
Dy	0.51	0.56
Y	3.55	3.45
Yb	0.41	0.38
Lu	0.06	0.06

basalts of the Omineca Belt is older and/or has been affected by an enrichment event that is different from the one that affected the mantle source of the Hy-NORM basalts of the Intermontane Belt. In other continental margin or rift related areas, such as in eastern Australia (McDonough et al., 1985), eastern China (Zhi et al., 1990; Song et al., 1990), or southern Kenya (Späth et al., 2001; Rogers et al., 2000), high $^{87}\text{Sr}/^{86}\text{Sr}$ signatures of the Hy-NORM end-members (Fig. 8) appear to reflect old enriched lithospheric mantle sources because crustal contamination alone can not produce the observed isotopic trends (see for example Price et al. (1997), or Zhang et al. (2001) in Australia). On the other hand, the low $^{87}\text{Sr}/^{86}\text{Sr}$ signatures of Hy-NORM basalts from alkaline suites such as the Comores (Class et al., 1998), the Canaries (Hoernle and Schmincke, 1993), or northern Kenya (Class et al., 1994; Rogers et al., 2000) are consistent with the absence of an old enriched component in their mantle source.

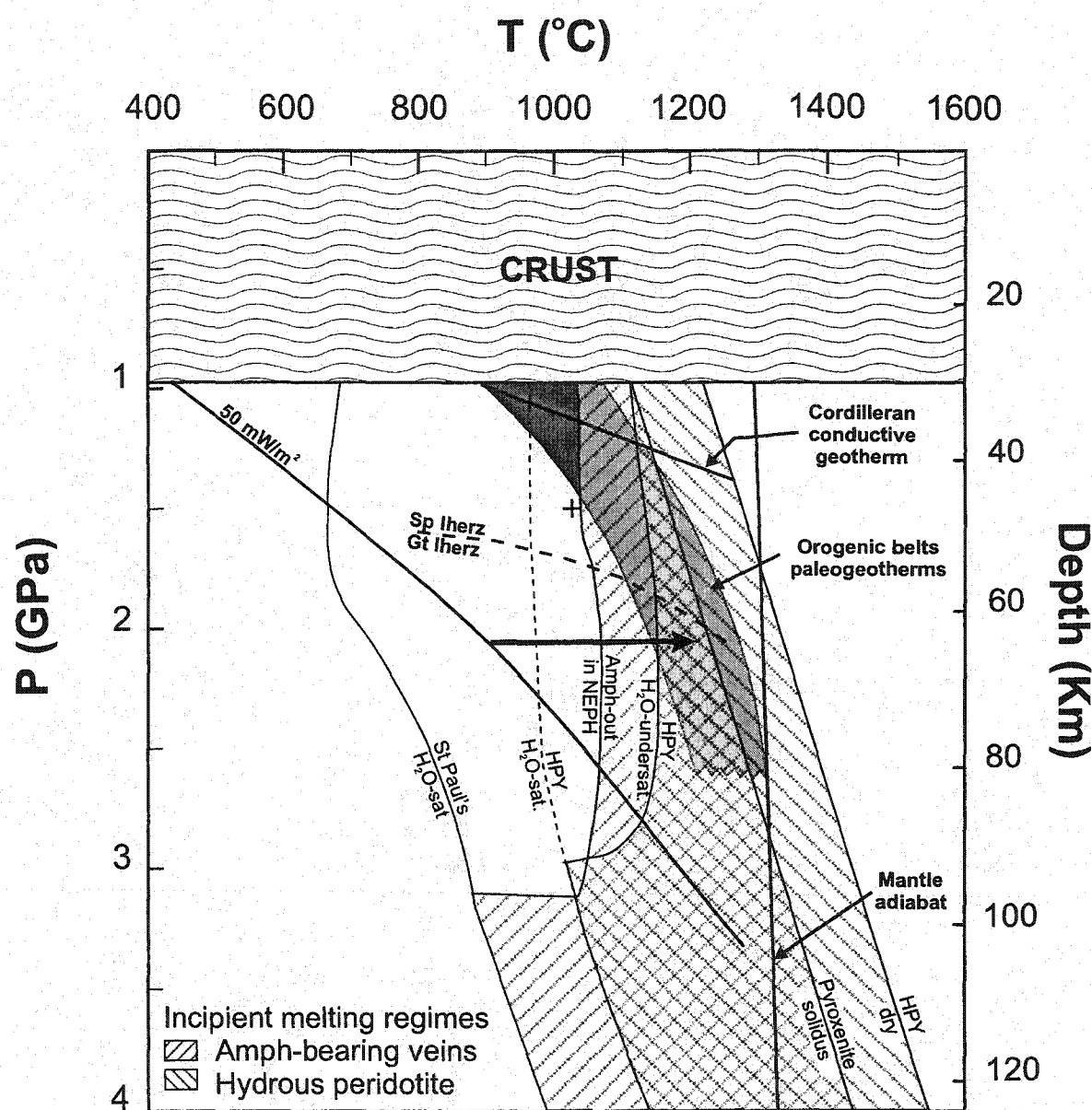
In conclusion, both the major and trace element characteristics of Hy-NORM basalts erupted in the northern Canadian Cordillera, and other continental margin areas, are consistent with relatively small degrees of partial melting (<10 %) of a garnet-bearing lithospheric mantle that is enriched in the most incompatible trace elements compared to primitive mantle.

4.3. The composition range from Hy-NORM to AOB and BASAN

The Hy-NORM to BASAN compositional range could be derived either by different degrees of partial melting of one common source, in which case the systematic isotopic

differences of the different magma types would represent later crustal contamination, or from binary mixing between melts derived from two isotopically distinct sources. Abraham et al. (2001) have demonstrated that the isotopic difference between the high-MgO Hy-NORM basalts of the Intermontane and Omineca belts could not be explained by fractional crystallization and assimilation models, indicating that the isotopic differences between primitive Hy-NORM basalts in the Omineca and Intermontane belts originate in the mantle. The systematic lower Sr and Pb isotopic ratios of AOB and BASAN lavas compared to Hy-NORM basalts in individual volcanic centres of the northern Canadian Cordillera, and in other continental mafic alkaline suites, and their trend towards the NEPH end-member in isotopic plots (Fig. 7 and 8) argue for mixing between Hy-NORM and NEPH melts, derived from garnet lherzolite and amphibole-bearing veins respectively. The entire chemical spectrum from NEPH to Hy-NORM lavas cannot, however, be explained by simple mixing between the NEPH and the Hy-NORM end-members (Francis and Ludden, 1995), and a two step melting process is required. The temperature difference between the H₂O-saturated solidi for mantle amphibolite (Millhollen and Wyllie, 1974) and Hawaii pyrolite (Green, 1973) indicates that, under water-saturated conditions, amphibole-bearing veins will melt at a lower temperature than their peridotite host (Fig. 16). Under water-undersaturated conditions, the temperature difference between the upper stability field of amphibole coexisting with olivine nephelinite (Allen et al., 1975), and the H₂O-undersaturated solidus for Hawaiian pyrolite (Green, 1973) also indicates that the amphibole-bearing veins will melt at a lower temperature than the peridotite host, which would begin to melt only after the exhaustion of amphibole in the vein (Fig. 16). The composition of the melts at the exhaustion of amphibole (corresponding to the kink in the Hirschfeld dataset in Fig. 10), will be less

Figure 16: P versus T diagram showing the conditions in the northern Cordilleran mantle. The 50 mW/m^2 geotherm corresponds to a conductive geotherm typical for Phanerozoic areas (Poudjom-Djomi et al., 2001). The incipient melting regime for hydrous peridotite corresponds to the P-T space between the water-undersaturated and dry solidus for Hawaiian pyrolite (Green, 1973). The incipient melting regime for amphibole-bearing veins corresponds to the P-T space between the amphibole-out curve for olivine nephelinite (Allen et al., 1975), and the H_2O -saturated solidus for mantle amphibole (St Paul's mylonite from Millhollen and Wyllie, 1974). The paleogeotherm field for orogenic belts includes geotherms derived from xenoliths from southeastern Australia (O'Reilly and Griffin, 1985), eastern China (Xu et al., 1996), and northwestern Spitsbergen (Amundsen et al., 1987). The Cordilleran conductive geotherm corresponds to the steady-state model used by Hyndman and Lewis (1999). The transition from the spinel to garnet lherzolite is taken from O'Neill (1981). The cross corresponds to the experimentally determined P-T conditions for amphibole in a NEPH lava from Hirschfeld (Dalgé, 1997). The heavy arrow indicates the proposed change in shape of the Phanerozoic geotherm due to lithospheric thinning.



enriched in trace elements than the initial NEPH end-member and simple mixing between this composition and Hy-NORM lavas can explain the chemical spectrum from Hy-NORM to BASAN compositions at Hirschfeld. This model indicates that, even in centres where no NEPH lavas have erupted, the presence of AOB and BASAN lavas requires the existence of amphibole-bearing veins in their mantle source, whose melt has been mixed with peridotite-derived melts.

4.4. Evidence for lithospheric thinning

The isotopic differences between primitive Hy-NORM basalts erupted in the Intermontane and Omineca belts in the northern Canadian Cordillera indicates that they are derived by melting of distinct lithospheric roots preserved since the accretion and translation of terranes along the North American continental margin (Abraham et al., 2001). Significant melting of anhydrous continental lithosphere is improbable because of the high solidus temperatures of refractory peridotite (Fig. 16; e.g. McKenzie and Bickle, 1988; Arndt and Christensen, 1992). The presence of small amounts of water (~ 0.4 %; Gallagher and Hawkesworth, 1992), and/or of mafic veins with lower solidus temperatures (Harry and Leeman, 1995), however, may enable the derivation of significant volumes of melt from the lithospheric mantle. This interpretation is consistent with the conclusion that the Cordilleran Hy-NORM magmas may be derived by low degrees of melting of an enriched, amphibole-bearing, lithospheric mantle (Fig. 15b).

The high heat flow data measured in the northern Canadian Cordillera indicate that the lithosphere beneath the Canadian Cordillera may be less than 50 km in thickness, assuming a steady state conductive geotherm (Fig. 16; Hyndman and Lewis, 1999). No paleogeotherm can be constructed for the Cordilleran lithospheric mantle because of the lack of garnet-bearing xenoliths. However, the need for garnet in the lithospheric mantle source of the Hy-NORM basalts to explain the low concentrations of HREE and Al_2O_3 indicates that the lithosphere beneath the Cordillera must extend into the garnet stability field. The Cordilleran geotherm might thus be similar to that under other Phanerozoic orogenic belts with active Neogene volcanism (Poudjom-Djoman et al., 2001), such as eastern Australian continental margin (O'Reilly and Griffin, 1985), eastern China (Xu et al. 1996), or in rift environments such as northwestern Spitsbergen (Amundsen et al., 1987). These strongly convex-upward geotherms appear to reflect advective rather than conductive heat transport, consistent with the transfer of heat from the underlying asthenosphere. Asthenospheric upwelling may be related to the presence of a slab window beneath the northern Canadian Cordillera since the early Miocene (Thorkelson and Taylor, 1989), or to incipient rifting of the continental margin of North America (Edwards and Russell, 1999). In either case, the Cordilleran geotherm may have changed from a conductive one corresponding to surface heat flows of about 50 mW/m^2 (Poudjom-Djoman et al., 2001) to a more convex-upward geotherm typical of alkaline basaltic provinces (Fig. 16). The temperature of the lower lithospheric mantle would be above the peridotite wet solidus, and the Tertiary to Recent alkaline lavas would reflect melting and thinning of the lithospheric mantle beneath the northern Canadian Cordillera. An interesting aspect of this model is that coeval NEPH and Hy-NORM lavas are likely to have a depth of origin relationship that is the inverse of that expected from simplistic

interpretations of experimental results. The NEPH lavas would be derived from similar or shallower depths than coeval Hy-NORM basalts.

As no NEPH lavas have been found in the Omineca or Coast belts of the northern Canadian Cordillera (Abraham et al., 2001), the degree of melting beneath these terranes might be such that the amphibole has totally melted out. This is consistent with the slightly higher heat flow values measured in the Omineca Belt indicating that the temperature at the base of the crust in the Omineca Belt might be up to 150°C hotter than that in the Intermontane Belt (Hyndman and Lewis, 1999). The absence of mantle xenoliths in the Omineca Belt may indicate that little lithospheric mantle remains under this belt.

5. Conclusion

Systematic correlations between major and trace elements, and Sr-Nd-Pb isotopic ratios in the northern Cordillera alkaline lavas indicate that two different mantle sources are involved in their generation. The presence of amphibole in the NEPH source and the existence of a terrane dependence in the isotopic signature of the Hy-NORM basalts (Abraham et al., 2001) suggest that the source of both end-members resides in the lithosphere.

The two mantle components identified in the Canadian Cordillera lithosphere are amphibole-bearing veins, which produced the NEPH lavas, and the surrounding hydrous

garnet peridotite, which produced the Hy-NORM basalts. The NEPH lavas represent relatively large degrees of partial melting (> 15%) of the amphibole-bearing veins, while the Hy-NORM basalts represent smaller degrees (< 10%) of the host lithospheric mantle. The high heat flow values reported in the northern Canadian Cordillera are consistent with a model in which ongoing melting and thinning of the lithospheric mantle is responsible for generating the mafic alkaline magmas. A slab window present beneath the northern Canadian Cordillera (Thorkelson and Taylor, 1989) might have allowed asthenospheric upwelling, which brought heat and volatiles to the base of the lithospheric mantle.

The low Ca and high Na contents of Cordilleran Hy-NORM basalts are characteristic of alkaline lavas erupted in continental margin or rift-related areas, in contrast to the high Ca and low Na character of Hy-NORM basalts associated with oceanic hot spots and mid-ocean ridges. A comparison with experimental melts of mantle peridotite indicates that continental Hy-NORM basalts in general may reflect smaller degrees of partial melting than Hy-NORM basalts associated with oceanic hot spots or mid-ocean ridges.

Acknowledgements

We thank Tariq Ahmedali and Glenna Keating for performing the XRF analyses, Bernard Reynier and Michel Valladon for assistance in obtaining the ICP-MS analysis, and Pierre Brunet for training and help with the TIMS analysis. This research was

supported by NSERC and LITHOPROBE grants to D. F and CNRS funds to M. P.

References

- Abraham, A.-C., Francis, D., Polv , M., 2001. Recent alkaline basalts as probes of the lithospheric mantle roots of the northern Canadian Cordillera. *Chem. Geol.* 175, 361-386.
- Adam, J., 1990. The geochemistry and experimental petrology of sodic alkaline basalts from Oatlands, Tasmania. *J. Petrol.* 31, 1201-1223.
- Albarede, F., Tamagnan, V., 1988. Modelling the recent geochemical evolution of the Piton de la Fournaise Volcano, Reunion Island, 1931-1986. *J. Petrol.* 29, 997-1030.
- Allen, J.C., Boettcher, A.L., Marland, G., 1975. Amphiboles in andesites and basalts: I. Stability as a function of P-T-fH₂O, *Am. Min.* 60, 1069-1085.
- Amundsen, H.E.F., Griffin, W.L., O'Reilly, S.Y., 1987. The lower crust and upper mantle beneath northwestern Spitsbergen: evidence from xenoliths and geophysics. *Tectonophys.* 139, 169-185.
- Armstrong, R.L., 1988. Mesozoic and early Cenozoic magmatic evolution of the Canadian Cordillera. *Geol. Soc. Am. Spec. Pap.* 218, 55-91.
- Arndt, N.T., Christensen, U., 1992. The role of lithospheric mantle in continental flood volcanism; thermal and geochemical constraints. *J. of Geophys. Res.* 97, 10967-10981.
- Baker, B. H., 1987. Outline of the petrology of the Kenya Rift alkaline province. In Alkaline igneous rocks, Fitton, J.G., and Upton, B.G.J. (ed.), *Geol. Soc. Special Publications* 30, 293-311.
- Barsikov, V.L., Kogarko, L.N., Polyakov, A.I., Ignatenko, K.I., Zinoveyev, A.I., 1979. Differentiation of basaltoid melts and formation of the volcanic rock series of the South Atlantic islands. *Geochemistry International.* 16, 1-12.

- Beard, B.L., Johnson, C.M., 1997. Hafnium isotope evidence for the origin of Cenozoic basaltic lavas from the Southwestern United States. *J. Geophys. Res.* 102, 20149-20178.
- Beccaluva, L., Siena, F., Coltorti, M. Di Grande, A., Lo Giudice, A., Macciotta, G., Tassinari, R., Vaccaro, C., 1998. Nephelinitic to tholeiitic magma generation in a transtensional tectonic setting: an integrated model for the Iblean volcanism, Sicily. *J. Petrol.* 39, 1547-1576.
- Bender, J.F., Langmuir, C.H., Hanson, G.N., 1984. Petrogenesis of basalt glasses from the Tamayo region, East Pacific Rise. *J. Petrol.* 25, 213-254.
- Ben Othman, D.B., Tilton, G.R., Menzies, M.A., 1990. Pb, Nd, & Sr isotopic investigations of kaersutite and clinopyroxene from ultramafic nodules and their host basalts: the nature of the subcontinental mantle. *Geochim. Cosmochim. Acta* 54, 3449-3460.
- Blanchard, D.P., Rhodes, J.M., Dungan, M.A., Rodgers, K.V. Donaldson, C.H., Brannon, J.C., Jacobs, J.W., Gibson, E.K., 1976. The chemistry and petrology of basalts from Leg 37 of the Deep-Sea Drilling Project. *J. Geophys. Res.* 81, 4231-4246.
- Bryan, W.B., Thompson, G., Ludden, J.N., 1981. Compositional variation in normal MORB from 22 degrees -25 degrees N; Mid-Atlantic Ridge and Kane fracture zone. *J. Geophys. Res.* 86, 11815-11836.
- Carignan, J., Ludden, J., Francis, D., 1994. Isotopic constraints on the mantle sources for Quaternary continental alkaline magmas in the northern Canadian Cordillera. *Earth Planet. Sci. Lett.* 128, 271-286.
- Cebria, J.M., Lopez Ruiz, J., 1995. Alkali basalts and leucitites in an extensional intracontinental plate setting; the late Cenozoic Calatrava volcanic province (central Spain). *Lithos.* 35, 27-46. 1995.
- Chaffey, D.J., Cliff, R.A., Wilson, B.M., 1989. Characterization of the St. Helena magma source. *Geol. Soc. Spec. Pub.* 42, 257-276. 1989.
- Chen, C.Y., Frey, F.A., 1985. Trace element and isotopic geochemistry of lavas from Haleakala Volcano, East Maui, Hawaii; implications for the origin of Hawaiian basalts. *J. of Geophys. Res.* 90, 8743-8768.

- Clague, D.A., Beeson, M.H., 1980. Trace element geochemistry of the East Molokai Volcanic Series, Hawaii. Am. J. Sci. 280-A, 820-844.
- Clague, D.A., Dalrymple, G.B., 1988. Age and petrology of alkalic postshield and rejuvenated-stage lava from Kauai, Hawaii. Contrib. Min. Pet. 99, 202-218.
- Clague, D. A., Frey, F. A., 1982. Petrology and trace element geochemistry of the Honolulu Volcanics, Oahu; implications for the oceanic mantle below Hawaii. J. Petrol., 23, 447-504.
- Class, C., Goldstein, S.L., 1997. Plume-lithosphere interactions in the ocean basins: constraints from the source mineralogy. Earth Planet. Sci. Let. 150, 245-260.
- Class, C., Altherr, R., Volker, F., Eberz, G., McCulloch, M.T., 1994. Geochemistry of Pliocene to Quaternary alkali basalts from the Huri Hills, northern Kenya. Chem. Geol. 113, 1-22.
- Class, C., Goldstein, S.L., Altherr, R., Bachèlery, P., 1998. The process of plume-lithosphere interactions in the ocean basins – the case of Grande Comore. J. Petrol. 39, 881-903.
- Clowes, R.M., 1993. Lithoprobe phase IV Proposal – Studies of the Evolution of a Continent. Published by the LITHOPROBE Secretariat, The University of British Columbia, Vancouver, B.C. 290 p.
- Cook, F.A., Clowes, R.M., Snyder, D.B., van der Velden, A.J., Hall, K.W., Erdmer, P., Evenchick, C.A., 2001. LITHOPROBE seismic reflection profiling of the northern Canadian Cordillera: First results of SNORCLE profiles 2 and 3. Lithoprobe Report 79, 1145-1200.
- Cousens, B.L., Bevier, M.L., 1995. Discerning asthenospheric, lithospheric and crustal influences on the geochemistry of Quaternary basalts from Iskut-Unuk rivers area, northwestern British Columbia. Can. J. Earth Sci. 32, 1451-1461.
- Cousens, B.L., Chase, R.L., Schilling, J.G., 1984. Basalt geochemistry of the Explorer Ridge area, northeast Pacific Ocean. Can. J. Earth Sci., 21, 157-170.
- Cousens, B.L., Allan, J.F., Leybourne, M.I., Chase, R.L., Van Wagoner, N., 1995. Mixing of magmas from enriched and depleted mantle sources in the northeast Pacific; West Valley segment, Juan de Fuca Ridge. Contrib. Min. Pet., 120, 337-357.

- Dalpé, C., 1997. Trace element partitioning between amphibole and basaltic melt. Unpublished PhD thesis, McGill Univ., Montréal, Canada.
- Devey, C.W., Garbe-Schönberg, C.D., Stoffers, P., Chauvel, C., Mertz, D.F., 1994. Geochemical effects of dynamic melting beneath ridges; reconciling major and trace element variations in Kolbeinsey (and global) mid-ocean ridge basalt. *J. Geophys. Res.* 99, 9077-9095.
- D'Orazio, M., Agostini, S., Mazzarini, F., Innocenti, F., Manetti, P., Haller, M.J., Lahsen, A., 2000. The Pali Aike Volcanic Field, Patagonia: slab-window magmatism near the tip of South America. *Tectonophys.* 321, 407-427.
- Edwards, B.R., Russell, J.K., 1999. Northern Cordilleran volcanic province; a northern Basin and Range? *Geology* 27, 243-246.
- Edwards, B.R., Russell, J.K., 2000. Distribution, nature, and origin of Neogene-Quaternary magmatism in the northern Cordilleran volcanic province, Canada. *Geol. Soc. of Am. Bulletin* 112, 1280-1295.
- Eiché, G., Francis, D., Ludden, J., 1987. Primary alkaline magmas in the Quaternary Alligator Lake volcanic complex, Yukon, Canada. *Contrib. Min. Pet.* 95, 191-201.
- Embey-Isztin, A., Downes, H., James, D.E., Upton, B.G.J., Dobosi, G., Ingram, G.A., Harmon, R.S., Scharbert, H.G., 1993. The petrogenesis of Pliocene alkaline volcanic rocks from the Pannonian basin, Eastern central Europe. *J. Petrol.* 34, 317-343.
- Ewart, A., Baxter, K., Ross, J.A., 1980. The petrology and petrogenesis of the Tertiary anorogenic mafic lavas of southern and central Queensland, Australia; possible implications for crustal thickening. *Contrib. Min. Pet.* 75, 129-152.
- Feigenson, M.D., 1984. Geochemistry of Kauai volcanics and a mixing model for the origin of Hawaiian alkali basalts. *Contrib. Min. Pet.* 87, 109-119.
- Feigenson, M.D., Hofmann, A.W., Spera, F.J., 1983. Case studies on the origin of basalt; II, The transition from tholeiitic to alkalic volcanism on Kohala Volcano, Hawaii. *Contrib. Min. Pet.* 84, 390-405.
- Fisk, M.R., Upton, B.G.J., Ford, C.E., White, W.M., 1988. Geochemical and experimental study of the genesis of magmas of Reunion Island, Indian Ocean. *J. Geophys. Res.* 93, 4933-4950.

- Fitton, J.G., 1987. The Cameroon Line, West Africa; a comparison between oceanic and continental alkaline volcanism. In: Alkaline igneous rocks, Fitton, J.G. and Upton, B.G.J (Eds.). Geol. Soc. Spec. Publi. 30, 273-291.
- Fitton, J.G., James, D., Leeman, W.P., 1991. Basic magmatism associated with late Cenozoic extension in the Western United States: compositional variations in space and time. *J. Geophys. Res.* 96, 13693-13711.
- Fodor, R. V., Frey, F. A., Bauer, G. R., Clague, D. A., 1992. Ages, rare-earth element enrichment, and petrogenesis of tholeiitic and alkalic basalts from Kahoolawe Island, Hawaii. *Contrib. Min. Pet.* 110, 442-462.
- Foley, S.F., Musselwhite, D.S., Van der Laan, S.R., 1999. Melt compositions from ultramafic vein assemblages in the lithospheric mantle; a comparison of cratonic and non-cratonic settings. In Proceedings of the International Kimberlite Conference 7, 238-246.
- Foley, S.F., Jackson, S.E., Fryer, B.J., Greenough, J.D., Jenner, G.A., 1996. Trace element partition coefficients for clinopyroxene and phlogopite in an alkaline lamprophyre from Newfoundland by LAM-ICP-MS. *Geochim. Cosmochim. Acta*. 60, 629-638.
- Francis, D., 1976a. The origin of amphibole in lherzolite xenoliths from Nunivak Island, Alaska. *J. Petrol.* 17, 357-378.
- Francis, D., 1976b. Amphibole pyroxenite xenoliths: cumulate or replacement phenomena from the upper mantle, Nunivak Island, Alaska. *Contrib. Min. Pet.* 58, 51-61.
- Francis, D., 1987. Mantle-melt interaction recorded in spinel lherzolite xenoliths from the Alligator Lake volcanic complex, Yukon, Canada. *J. Petrol.* 28, 569-597.
- Francis, D., Ludden, J., 1990. The mantle source for Olivine Nephelinite, Basanite, and Alkaline olivine basalt at Fort Selkirk, Yukon, Canada. *J. Petrol.* 31, 371-400.
- Francis, D., Ludden, J., 1995. The signature of amphibole in mafic alkaline lavas, a study in the northern Canadian Cordillera. *J. Petrol.* 36, 1171-1191.
- Frey, F.A., Clague, D.A., 1983. Geochemistry of diverse basalt types from Loihi Seamount, Hawaii; petrogenetic implications. *Earth Planet. Sci. Lett.*, 66, 337-355.
- Frey, F.A., Prinz, M., 1978. Ultramafic inclusions from San Carlos, Arizona: petrologic

- and geochemical data bearing on their petrogenesis. *Earth Planet. Sci. Lett.* 38, 129-176.
- Frey, F.A., Green, D.H., Roy, S.D., 1978. Integrated models of basalt petrogenesis; a study of quartz tholeiites to olivine melilitites from South eastern Australia utilizing geochemical and experimental petrological data. *J. Petrol.* 19, 463-513.
- Frey, F. A., Garcia, M. O., Wise, W. S., Kennedy, A., Gurriet, P., Albareda, F., 1991. The evolution of Mauna Kea Volcano, Hawaii; petrogenesis of tholeiitic and alkalic basalts. *J. Geophys. Res.* 96, 14347-14375.
- Frey, F.A., Wise, W.S., Garcia, M.O., West, H., Kwon, S.-T., Kennedy, A., 1990. Evolution of Mauna Kea Volcano, Hawaii: petrologic and geochemical constraints on postshield volcanism. *J. Geophys. Res.* 95, 1271-1300.
- Gallagher, K., Hawkesworth, C., 1992. Dehydration melting and the generation of continental flood basalts. *Nature* 358, 57-59.
- Garcia, M.O., Frey, F.A., Grooms, D.G., 1986. Petrology of volcanic rocks from Kaula Island, Hawaii; implications for the origin of Hawaiian phonolites. *Contrib. Min. Pet.* 94, 461-471.
- Ghiorso, M.S., Sack, R.O., 1995. Chemical mass transfer in magmatic processes: IV. A revised and internally consistent thermodynamic model for the interpolation and extrapolation of liquid-solid equilibria in magmatic systems at elevated temperatures and pressures. *Contrib. Min. Pet.* 119, 197-212.
- Gorring, M.L., Kay, S.M., 2001. Mantle processes and sources of Neogene slab window magmas from southern Patagonia, Argentina. *J. of Petrol.* 42, 1067-1094.
- Green, D.H., 1973. Experimental melting studies on a model upper mantle composition at high pressure under water-saturated and water-undersaturated conditions. *Earth Planet. Sci. Lett.* 19, 37-53.
- Green, D.H., Ringwood, A.E., 1967. The genesis of basaltic magmas. *Contrib. Min. Pet.* 15, 103-190.
- Halliday, A.N., Lee, D.C., Tommasini, S., Davies, G.R., Paslick, C.R., Fitton, J.G., James, D.E., 1995. Incompatible trace elements in OIB and MORB and source enrichment in the sub-oceanic mantle. *Earth Planet. Sci. Lett.* 133, 379-395.

- Hamilton, T.S., 1981. Late Cenozoic alkaline volcanics of the Level Mountain Range, northwestern British Columbia. Ph.D. thesis, University of Alberta, Canada.
- Harry, D.L., Leeman, W.P., 1995. Partial melting of melt metasomatized subcontinental mantle and the magma source potential of the lower lithosphere. *J. Geophys. Res.* 100, 10255-10269.
- Hart, S., Dunn, T., 1993. Experimental cpx / melt partitioning of 24 trace elements. *Contrib. Mineral. Petrol.* 113, 1-8.
- Harte, B., Hunter, R.H., Kinny, P.D., 1993. Melt geometry, movement and crystallization, in relation to mantle dykes, veins and metasomatism. *Phil. Trans. Royal Soc. London, Series A* 342: 1-21.
- Hauri, E.H., Wagner, T.P., Grove, T.L. 1994. Experimental and natural partitioning of Th, U, Pb and other trace elements between garnet, clinopyroxene and basaltic melts. *Chem. Geol.* 117, 149-166.
- Hirose, K., 1997. Partial melting compositions of carbonated peridotite at 3 GPa and role of CO₂ in alkali-basalt magma generation. *Geol. Res. Let.* 24, 2837-2840.
- Hirose, K., Kawamoto, T., 1995. Hydrous partial melting of lherzolite at 1 GPa: the effect of H₂O on the genesis of basaltic magmas. *Earth Planet. Sci. Lett.* 133, 463-473.
- Hirose, K., Kushiro, K., 1993. Partial melting of dry peridotites at high pressure: determination of compositions of melts segregated from peridotite using aggregates of diamond. *Earth Planet. Sci. Let.* 114, 477-489.
- Hirschmann, M.M., Ghiorso, M.S., Stolper, E.M., 1999. Calculation of peridotite partial melting from thermodynamic models of minerals and melts. II. Isobaric variation in melts near the solidus and owing to variable source composition. *J. Petrol.* 40, 297-313.
- Holloway, J.R., 1973. The system pargasite-H₂O-CO₂: a model for melting of hydrous mineral with a mixed-volatile fluid -I. Experimental results to 8 kbar. *Geochim. Cosmochim. Acta* 37, 651-666.
- Hoernle, K., Schmincke, H.-U., 1993. The petrology of the tholeiites through melilite nephelinites on Gran Canaria, Canary Islands: crystal fractionation, accumulation, and depths of melting. *J. Petrol.* 34, 573-597.
- Hoernle, K., Tilton, G., Schmincke, H.U., 1991. Sr-Nd-Pb isotopic evolution of Gran

- Canaria; evidence for shallow enriched mantle beneath the Canary Islands. *Earth Planet. Sci. Lett.* 106, 44-63.
- Hyndman, R. D., Lewis, T.J., 1999. Geophysical consequences of the Cordillera-Craton thermal transition in southwestern Canada. *Tectonophys.* 306, 397-422.
- Hyndman, R. D., Lewis, T.J., Flueck, P., 2000. The thermal regime of the SNORCLE Lithoprobe transect and tectonic consequences. *Lithoprobe Report* 72, 81-84.
- Ionov, D.A., Hofmann, A.W., 1995. Nb-Ta-rich mantle amphiboles and micas: implications for subduction-related metasomatism trace element fractionations. *Earth Planet. Sci. Lett.* 131, 341-356.
- Ionov, D.A., Griffin, W.L., O'Reilly, S.Y., 1997. Volatile-bearing minerals and lithophile trace elements in the upper mantle. *Chem. Geol.* 141, 153-184.
- Jakobsson, S.P., Jonsson, J., Shido, F., 1978. Petrology of the western Reykjanes Peninsula, Iceland. *J. Petrol.* 19, 669-705. 1978.
- Johnson, K.T.M., 1998. Experimental determination of partition coefficients for rare earth and high-field-strength elements between clinopyroxene, garnet, and basaltic melt at high pressures. *Contrib. Mineral. Petrol.* 133, 60-68.
- Jung, S., Hoernes, S., 2000. The major- and trace-element and isotope (Sr, Nd, O) geochemistry of Cenozoic alkaline rift-type volcanic rocks from the Rhön area (central Germany): petrology, mantle source characteristics and implications for asthenosphere-lithosphere interactions. *J. Volcanol. Geotherm. Res.* 99, 27-53.
- Jung, S., Masberg, P., 1998. Major- and trace-element systematics and isotope geochemistry of Cenozoic mafic volcanic rocks from the Vogelsberg (central Germany); constraints on the origin of continental alkaline and tholeiitic basalts and their mantle sources. *J. Volcanol. Geotherm. Res.* 86, 151-177.
- Kelemen, P.B., Shimizu, N., Dunn, T., 1993. Relative depletion of niobium in some arc magmas and the continental crust: partitioning of K, Nb, La and Ce during melt/rock reaction in the upper mantle. *Earth Planet. Sci. Lett.* 120, 111-134.
- Kempton, P.D., Fitton, J.G., Hawkesworth, C.J., Ormerod, D.S., 1991. Isotopic and trace element constraints on the composition and evolution of the lithosphere beneath the southwestern United States. *J. Geophys. Res.* 96, 13713-13735.
- Klein, E.M., Langmuir, C.H., 1987. Global correlations of ocean ridges basalt chemistry

- with axial depth and crustal thickness. *J. Geophys. Res.* 92, 8089-8115.
- Kushiro, I., 1996. Partial melting of a fertile mantle peridotite at high pressures; an experimental study using aggregates of diamond. In *Earth Processes: reading the isotopic code*, Basu, A., and Hart., S. (Eds.), *Geophysical monograph*, Am. Geophys. Union 95, 109-122.
- LaTourrette, T., Hervig, R.L., Holloway, J.R., 1995. Trace element partitioning between amphibole, phlogopite, and basanite melt. *Earth Planet. Sci. Lett.* 135, 13-30.
- Le Roex, A.P., Erlank, A.J., Needham, H.D., 1981. Geochemical and mineralogical evidence of the occurrence of at least, three distinct magma types in the "FAMOUS" region. *Contrib. Min. Pet.* 77, 24-34.
- Lorand, J.-P., Vétil J.-Y., Fabriès, J., 1990. Fe-Ti oxide assemblages of the Lherz and Freychinède amphibole-rich veins (French Pyrenees). First International Workshop on Lherzolites and Mantle processes, Montpellier, *Terra Abstr.* 2, 34.
- Lum, C.C.L., Leeman, W.P., Foland, K.A., Kargel, J.A., Fitton, J.G., 1989. Isotopic variations in continental basaltic lavas as indicators of mantle heterogeneity: examples from the western U.S. Cordillera. *J. Geophys. Res.* 94, 7871-7884.
- Maaloe, S., James, D., Smedley, P., Petersen, S., Garmann, L.B., 1992. The Koloa volcanic suite of Kauai, Hawaii. *J. Petrol.* 33, 761-784.
- Marzoli, A., Piccirillo, E.M., Renne, P.R., Bellieni, G., Iacumin, M., Nyobe, J.B., Tongwa, A.T., 2000. The Cameroon Volcanic Line revisited: petrogenesis of continental basaltic magmas from lithospheric and asthenospheric mantle sources. *J. Petrol.* 41, 87-109.
- McDonough, W.F., 1990. Constraints on the composition of the continental lithospheric mantle. *Earth Planet. Sci. Lett.* 101, 1-18.
- McDonough, W. F., McCulloch, M.T., Sun, S.S., 1985. Isotopic and geochemical systematics in Tertiary-Recent basalts from southeastern Australia and implications for the evolution of the sub-continental lithosphere. *Geochim. Cosmochim. Acta* 49, 2051-2067.
- McKenzie, D., Bickle, M.J., 1988. The volume and composition of melt generated by extension of the lithosphere. *J. Petrol.* 29, 625-679.

- Menzies, M.A., Rogers, N., Tindle, A., Hawkesworth, C.J., 1987. Metasomatic and enrichment processes in lithospheric peridotites, an effect of asthenosphere-lithosphere interaction. In: Mantle metasomatism, Menzies, M.A. and Hawkesworth C.J. (Eds.). pp. 313-361.
- Merrill, R.B., Wyllie, P.J., 1975. Kaersutite and kaersutite eclogite from Kakanui, New Zealand – Water-excess and water-deficient melting to 30 kilobars. Geol. Soc. Am. Bull. 86, 555-570.
- Millhollen, G.L., Wyllie, P.J., 1974. Melting relations of brown-hornblende mylonite from Saint Paul's Rocks under water-saturated and water-undersaturated conditions to 30 kilobars. J. Geol. 82, 589-606.
- Monger, J.W.H., Price, R.A., Tempelman-Kluit, D.J., 1982. Tectonic accretion and the origin of the two major metamorphic and welts in the Canadian Cordillera. Geology 10, 70-75.
- Olafsson, M., Eggler, D.H., 1983. Phase relations of amphibole, amphibole-carbonate, and phlogopite-carbonate peridotite: petrologic constraints on the asthenosphere. Earth Planet. Sci. Lett. 64, 305-315.
- O'Neill, H.S.C., 1981. The transition between spinel lherzolite and garnet lherzolite, and its use as a geobarometer. Contrib. Min. Pet. 77, 185-194.
- O'Reilly, S.Y., Griffin, W.L., 1985. A xenolith-derived geotherm for southeastern Australia and its geophysical implications. Tectonophys. 111, 41-63.
- O'Reilly, S.Y., Griffin, W.L., 2000. Apatite in the mantle: implications for metasomatic processes and high heat production in Phanerozoic mantle. Lithos 53, 217-232.
- O'Reilly, S.Y., Zhang, M., 1995. Geochemical characteristics of lava-field basalts from eastern Australia and inferred sources: connections with the subcontinental lithospheric mantle?. Contrib. Min. Pet. 121, 148-170.
- O'Reilly, S.Y., Griffin, W.L., Ryan, C.G., 1991. Residence of trace elements in metasomatized spinel lherzolite xenoliths: a proton-microprobe study. Contrib. Min. Pet. 109, 98-113.
- Ottanello, G., Ernst, W.G., Joron, J.-L., 1984. Rare earth and 3d transition element geochemistry of peridotitic rocks; I, Peridotites from the Western Alps. J. Petrol. 25, 343-372.

- Peslier, A.H., 1999. Pétrologie et géochimie isotopique de xénolites mantelliques de la Cordillère Canadienne. Ph.D thesis, Université de Montréal, Canada.
- Plank,T., Langmuir, C.H., 1988. An evaluation of the global variations in the major element chemistry of arc basalts. *Earth Planet. Sci. Lett.* 90, 349-370.
- Price, R.C., Gray, C.M., Frey, F.A., 1997. Strontium isotopic and trace element heterogeneity in the plains basalts of the Newer Volcanic Province, Victoria, Australia. *Geochim. Cosmochim. Acta* 61, 171-192.
- Poudjom-Djomi, Y.H., O'Reilly, S.Y., Griffin, W.L., Morgan, P., 2001. The density structure of subcontinental lithosphere through time. *Earth Planet. Sci. Lett.* 184, 605-621.
- Reiners, P.W., Nelson, B.K., 1998. Temporal-compositional-isotopic trends in rejuvenated-stage magmas of Kauai, Hawaii, and implications for mantle melting processes. *Geochim. Cosmochim. Acta* 62, 2347-2368.
- Ringwood, A.E. 1975. Composition and petrology of the Earth's mantle. McGraw- Hill, 188 pp.
- Roeder, P.L., Emslie, R.F., 1970. Olivine-liquid equilibrium. *Contrib. Min. Pet.* 29, 275-289.
- Rogers, N., Macdonald, R., Fitton, J.G., Rhiannon, G., Smith, M., Barreiro, B., 2000. Two mantle plumes beneath the East African Rift system; Sr, Nd and Pb isotope evidence from Kenya Rift basalts. *Earth Planet. Sci. Lett.* 176, 387-400.
- Rudnick, R.L., McDonough, W.F., O'Connell, R.J., 1998. Thermal structure, thickness and composition of continental lithosphere. *Chem. Geol.* 145, 395-411.
- Schmincke, H.U., 1982. Volcanic and chemical evolution of the Canary Islands. In: *Geology of the Northwest African continental margin*, von Rad, U., Hinz, K., Sarnthein, M., Seibold, E. (Eds), Springer-Verlag, Berlin, 273-306.
- Shaw, D.M., 1970. Trace element fractionation during anatexis. *Geochim. Cosmochim. Acta* 34, 237-243.
- Shi, L., Francis, D., Ludden, J., Frederiksen, A., Bostock, M., 1998. Xenolith evidence for lithospheric melting above anomalously hot mantle under the northern Canadian Cordillera. *Contrib. Min. Pet.* 131, 38-53.

- Sims, K.W.W., DePaolo, D.J., Murrell, M.T., Baldridge, W.S., Goldstein, S.J., Clague, D.A., 1995. Mechanisms of magma generation beneath Hawaii and mid-ocean ridges; uranium/ thorium and samarium/ neodymium isotopic evidence. *Science*. 267, 508-512.
- Song, Y., Frey, F.A., Zhi, X., 1990. Isotopic characteristics of Hannuoba basalts, eastern China: implications for their petrogenesis and the composition of the subcontinental mantle. *Chem. Geol.* 88, 35-52.
- Souther, J.G., 1992. The late Cenozoic Mount Edziza Volcanic Complex, British Columbia. *Geol. Surv. Can. Mem.* 420, 320p.
- Späth, A., Le Roex, A.P., Duncan, R.A., 1996. The geochemistry of lavas from the Comores Archipelago, western Indian Ocean; petrogenesis and mantle source region characteristics. *J. Petrol.* 37, 961-991.
- Späth, A., Le Roex, A.P., Opiyo-Akech, N., 2001. Plume-lithosphere interaction and the origin of continental rift-related alkaline volcanism – the Chyulu Hills volcanic province, Southern Kenya. *J. Petrol.* 42, 765-787.
- Strong, D.F., 1972. The Petrology of the Lavas of Grande Comore. *J. Petrol.* 13, 181-217.
- Sun, S.S, McDonough, W.F., 1989. Chemical and isotopic systematics of oceanic basalts: implications for mantle composition and processes. In: *Magmatism in the ocean basins*, Saunders, A.D., and Norry, M.J. (Eds). *Geol. Soc. Lond. Spec. Publ.* 42, 313-345.
- Thorkelson, D.J., Taylor, R.P., 1989. Cordilleran slab windows. *Geology* 17, 833-836.
- Vaselli, O., Downes, H., Thirwall, M., Dobosi, G., Coradossi, N., Seghedi, I., Szakacs, A., Vannucci, R., 1995. Ultramafic xenoliths in Plio-Pleistocene alkali basalts from the Eastern Transylvanian Basin: depleted mantle enriched by vein metasomatism. *J. Petrol.* 36, 23-53.
- Wheeler, J.O., McFeely, P., 1991 Tectonic assemblage map of the Canadian Cordillera and adjacent parts of the United States of America. *Geol. Surv. Canada Map* 1712A, scale 1:2000000.
- Widom, E., Carlson, R.W., Gill, J.B., Schmincke, H.-U., 1997. Th-Sr-Nd-Pb isotope and trace element evidence for the origin of the São Miguel, Azores, enriched mantle source. *Chem. Geol.*, 140, 49-68.

- Wilson, M., Downes, H., 1991. Tertiary-Quaternary extension-related alkaline magmatism in Western and Central Europe. *J. Petrol.* 32, 811-849.
- Wilson, M., Downes, H., Cebria, J.M., 1995. Contrasting fractionation trends in coexisting continental alkaline magmas series; Cantal, Massif Central, France. *J. Petrol.* 36, 1729-1753.
- Witt-Eickschen, G., Harte, B., 1994. Distribution of trace elements between amphibole and clinopyroxene from mantle peridotites of the Eifel (western Germany): an ion-microprobe study. *Chem. Geol.* 117, 235-250.
- Witt-Eickschen, G., Kaminsky, W., Kramm, U., Harte, B., 1998. The nature of young vein metasomatism in the lithosphere of the West Eifel (Germany): geochemical and isotopic constraints from composite mantle xenoliths from the Meerfelder Maar. *J. Petrol.* 39, 155-185.
- Xu, X., O'Reilly, S.Y., Zhou, X., Griffin, W.L., 1996. A xenolith-derived geotherm and the crust-mantle boundary at Qilin, southeastern China. *Lithos* 38, 41-62.
- Xu, X., Huang, Y., Xia, L., Xia, Z., 1997. Phlogopite-amphibole-pyroxenite xenoliths in Langao, Shaanxi province, China: evidence for mantle metasomatism. *Chin. J. Geochem.* 16, 318-328.
- Xu, Y., Mercier, J.C., Lin, C., 1997. Amphibole-bearing peridotite xenoliths from Nushan, Anhui province: evidence for melt percolation process in the upper mantle and lithospheric uplift. *Chin. J. Geochem.* 16, 213-229.
- Zack, T., Brumm, R., 1998. Ilmenite/liquid partition coefficients of 26 trace elements determined through ilmenite/clinopyroxene partitioning in garnet pyroxenites. Extended Abstract of the 7th International Kimberlite Conference, 986-988.
- Zhang, M., Stephenson, P.J., O'Reilly, S.Y., McCulloch, M.T., Norman M., 2001. Petrogenesis and geodynamic implications of Late Cenozoic basalts in North Queensland, Australia: trace-element and Sr-Nd-Pb isotope evidence. *J. Petrol.* 42, 685-719.
- Zhi, X., Song, Y., Frey, F.A., Feng, J., Zhai, M., 1990. Geochemistry of Hannuoba basalts, eastern China: constraints on the origin of continental alkalic and tholeiitic basalt. *Chem. Geol.* 88, 1-33.

- Zindler, A., Hart, S.R., Frey, F.A., Jakobsson, S.P., 1979. Nd and Sr isotope ratios and rare earth element abundances in Reykjanes Peninsula basalts; evidence for mantle heterogeneity beneath Iceland. *Earth Planet. Sci. Lett.* 45, 249-262.
- Zou, H., Zindler, A., Xu, X., Qi., Q., 2000. Major, trace element, and Nd, Sr and Pb isotope studies of Cenozoic basalts in SE China; mantle sources, regional variations, and tectonic significance. *Chem. Geol.* 171, 33-47.

CHAPTER V

General conclusion

This study explains the range of observed alkaline lava compositions in the northern Canadian Cordillera by the melting of two distinct lithospheric components, amphibole-rich veins on one hand, whose melting produces the NEPH end-member, and their host garnet lherzolite on the other hand, whose melting produces the Hy-NORM end-member. The high heat flow values reported in the northern Canadian Cordillera indicate that these mafic alkaline lavas might be generated by ongoing melting and thinning of the lithospheric mantle. This lithospheric thinning may result from asthenospheric upwelling in a slab window beneath the northern Canadian Cordillera, which brought heat and volatiles to the base of the lithospheric mantle.

The two components model indicates that the major and trace element contents of the NEPH lavas represent relatively large degrees of partial melting (> 15%) of amphibole-rich veins either in the spinel or garnet stability fields, whereas the low CaO, Al₂O₃ and HREE contents of the Hy-NORM basalts require relatively small degrees of partial melting (< 10%) of a garnet-bearing source. The NEPH lavas might thus be derived from larger degrees of partial melting at similar or shallower depths than the Hy-NORM basalts, contrary to what is expected from simplistic interpretations of experimental results that relate high alkalinity to smaller degrees of partial melting and greater depths.

NEPH lavas are only present in a few volcanic centres of the Intermontane Belt, and none has been found in the Omineca Belt of the northern Canadian Cordillera. In volcanic centres where NEPH lavas do not occur, the alkaline lavas nevertheless display systematic chemical and isotopic binary arrays between the Hy-NORM end-member,

which is present in most centres, and more alkaline and isotopically depleted compositions that approach that of the NEPH end-member. These binary arrays are explained by mixing between melts derived from two mantle components, amphibole-veins and garnet lherzolite, implying that, even in centres where no NEPH lavas have erupted, amphibole-bearing veins were present in the mantle source, and the melts derived from these veins have been mixed with peridotite-derived melts. The absence of NEPH lavas in the Omineca Belt may indicate that the amphibole-bearing veins have been melted out in the underlying lithosphere, which would be consistent with higher heat flow values in the Omineca Belt compared to the Intermontane Belt.

The presence of isotopic discontinuities in alkaline basalts at the boundaries between the North American craton and the Omineca belt, the Omineca and Intermontane belts, and the Intermontane and Coast belts, implies the juxtaposition of distinct lithospheric mantles along these tectonic boundaries of the northern Canadian Cordillera. The isotopic and chemical discontinuity across the Tintina fault separating the Omineca belt from the North American craton occurs between alkaline lavas separated by less than 5 km, indicating that the Tintina fault is a high angle feature, in agreement with recent geophysical survey across the Tintina Fault. The major isotopic discontinuity in alkaline basalts at the boundary between the Intermontane and Omineca belts occurs above the mid-point in a lower crustal wedge detected by recent seismic reflection data, arguing against the isotopic provinciality reflecting contamination by lower crustal melts. As the isotopic difference can not be explained by upper crustal contamination of asthenospheric-derived melts, the Intermontane and Omineca belts must have conserved distinct lithospheric mantle roots. To the west, an eastern displacement of the isotopic

discontinuity between alkaline basalts of the Intermontane and Coast belts indicates that the enriched lithospheric mantle source beneath the Coast Belt extends partly beneath the western margin of the Intermontane Belt. This enriched lithospheric mantle may be related to the presence of a thermal anomaly in the underlying asthenosphere, which was discovered teleseismically under this area.

Although the Hy-NORM basalts have isotopic signatures that indicate a terrane dependence, their major and trace elements exhibit only minor differences with respect to distinct terranes. All primitive Hy-NORM basalts of the northern Canadian Cordillera are characterized by low Ca and high Na contents compared to their equivalents in oceanic hot spots or associated with mid-ocean ridges. This low Ca and high Na signature also characterizes Hy-NORM basalts from other continental margin or rift-related areas. This worldwide signature of continental alkaline lavas has not been previously recognized, and a comparison with experimental melts of mantle peridotite indicates that continental Hy-NORM basalts in general may reflect smaller degrees of partial melting than Hy-NORM basalts associated with oceanic hot spots or mid-ocean ridges. Most experimental studies on mantle peridotite melting have focused, however, on melting spinel lherzolites because of their implications for genesis of mid-ocean ridge basalts. Only one experimental study reported the compositions of melts derived by less than 10 % partial melting of garnet peridotite and more experimental data are needed to confirm that small degree partial melts in the garnet stability field have the low Ca and Al, and high Na contents that characterize continental Hy-NORM basalts.

This study has shown that the generally accepted relationship between alkalinity and depth might have to be reassessed. Although some experimental studies have produced melts with olivine nephelinite composition by melting of amphibole pyroxenite, the composition of these melts have not been published. Experimental melting of both amphibole veins and amphibole pyroxenite veins in the spinel and garnet stability fields are required to obtain more information about melting reactions and the composition of partial melts.

The two components melting model proposes that NEPH lavas are derived from incongruent melting of amphibole in amphibole pyroxenite veins, whereas alkali olivine basalts and basanites are derived from mixing between amphibole-derived melts and Hy-NORM melts. As glass inclusions in single phenocrysts of olivine in MORB have been shown to preserve evidence of mixing between melts of distinct trace element and isotopic composition, the nature and the scale of mixing might be elucidated by a study of glass inclusions in olivine phenocrysts from each magma type.

Appendices

Table A-1-a: Classification of Mount Edziza mafic volcanic samples

Sample	Formation	Foid	Opx	Rock type
EZ-3	Raspberry	-	9.96	Hy-NORM
EZ-5	Raspberry	-	9.67	Hy-NORM
EZ-23	Armadillo	-	1.3	Hy-NORM
EZ-31	Nido	-	20.22	Hy-NORM
EZ-32	Nido	-	18.05	Hy-NORM
EZ-33	Nido	-	14.54	Hy-NORM
EZ-34	Ice Peak	-	4.15	Hy-NORM
EZ-36	Ice Peak	-	6.49	Hy-NORM
EZ-39	Ice Peak	2.18	-	AOB
EZ-41	Ice Peak	-	2.06	Hy-NORM
EZ-42	Ice Peak	-	1.93	Hy-NORM
EZ-43	Ice Peak	-	2.74	Hy-NORM
EZ-44	Ice Peak	-	4.08	Hy-NORM
EZ-45	Ice Peak	-	1.86	Hy-NORM
EZ-46	Ice Peak	0.4	-	AOB
EZ-47	Ice Peak	-	1.7	Hy-NORM
EZ-48	Ice Peak	-	6.81	Hy-NORM
EZ-49	Ice Peak	-	5.04	Hy-NORM
EZ-50	Ice Peak	-	4.36	Hy-NORM
EZ-37	Big Raven	-	7.89	Hy-NORM
EZ-40	Big Raven	0.42	-	AOB
EZ-606	Big Raven	-	5.43	Hy-NORM
EZ-1622	Big Raven	-	4.41	Hy-NORM
EZ-2518	Big Raven	-	2.35	Hy-NORM
EZ-2602	Big Raven	-	7.26	Hy-NORM
EZ-3102	Big Raven	1.54	-	AOB
EZ-3204	Big Raven	-	4.54	Hy-NORM
EZ-3602	Big Raven	0.6	-	AOB
EZ-3704	Big Raven	0.4	-	AOB
EZ-3717	Big Raven	-	5.44	Hy-NORM
EZ-3807	Big Raven	-	6.01	Hy-NORM
EZ-3913	Big Raven	0.06	-	AOB
EZ-4106	Big Raven	-	6.91	Hy-NORM
EZ-4203	Big Raven	-	1.67	Hy-NORM
EZ-4411	Big Raven	-	4.69	Hy-NORM
EZ-4412	Big Raven	0.06	-	AOB
EZ-4413	Big Raven	-	2.7	Hy-NORM
EZ-4414	Big Raven	-	5.95	Hy-NORM
EZ-4513	Big Raven	-	3.16	Hy-NORM
EZ-5106	Big Raven	-	13.51	Hy-NORM

Foid and Opx values are the normative contents of the lavas, assuming $\text{Fe}^{3+}/\text{Fe}_{\text{tot}}=0.15$.

Table A-1-b: Classification of Mount Edziza hawaiites and felsic volcanic samples

Sample	Formation	Qtz	Foid	Opx	Rock type
EZ-2	Raspberry	-	1.24	-	Haw
EZ-4	Raspberry	-	0.32	-	Haw
EZ-6	Raspberry	-	-	4.72	Haw
EZ-7	Raspberry	-	-	4.61	Haw
EZ-9	Raspberry	-	-	7.43	Haw
EZ-10	Raspberry	-	-	3.23	Haw
EZ-11	Raspberry	-	-	9.84	Haw
EZ-12	Raspberry	-	-	7.58	Haw
EZ-13	Raspberry	-	1.63	-	Haw
EZ-14	Raspberry	-	0	7.34	Haw
EZ-15	Raspberry	-	0	2.88	Haw
EZ-16	Raspberry	-	0.45	-	Haw
EZ-17	Raspberry	-	-	6.02	Haw
EZ-18	Raspberry	-	-	7.65	Haw
EZ-19	Raspberry	-	-	7.04	Haw
EZ-20	Raspberry	-	0.63	-	Haw
EZ-21	Armadillo	8.01	-	6.31	Qtz Trach
EZ-22	Armadillo	1.48	-	14.06	Haw
EZ-24	Armadillo	38.27	-	5.55	Rhyol
EZ-25	Armadillo	-	-	12.51	Haw
EZ-26	Armadillo	-	-	14.43	Haw
EZ-27	Armadillo	-	-	11.78	Haw
EZ-112	Armadillo	37.79	-	4.26	Rhyol
EZ-2514	Armadillo	27.2	-	4.06	Rhyol
EZ-29	Nido	-	-	10.88	Haw
EZ-30	Nido	2.51	-	13.99	Haw
EZ-38	Big Raven	-	-	4.68	Haw
EZ-2004	Big Raven	18.05	-	3.08	Rhyol
EZ-1208	Big Raven	36.64	-	0.87	Rhyol
EZ-2108	Big Raven	-	-	9.13	Haw
EZ-2218	Big Raven	-	-	2.94	Haw
EZ-2506	Big Raven	-	-	0.25	Haw
EZ-3109	Big Raven	33.11	-	1.31	Rhyol
EZ-3806	Big Raven	38	-	1.41	Rhyol
EZ-3809	Big Raven	35.76	-	1.85	Rhyol
EZ-4104	Big Raven	36.68	-	1.13	Rhyol
EZ-4509	Big Raven	37.07	-	1.58	Rhyol

Qtz, Foid and Opx values are the normative contents of the lavas, assuming $\text{Fe}^{3+}/\text{Fe}_{\text{tot}}=0.15$ for the hawaiites, and $\text{Fe}^{3+}/\text{Fe}_{\text{tot}}=0.3$ for the felsic lavas.

Abbreviations: Haw = hawaiite, Qtz Trach = quartz trachyte, Rhyol = rhyolite.

Table A-2-a: Location and classification of Level Mountain mafic volcanic samples

Sample	Longitude	Latitude	Elevation (m)	Foid	Opx	Rock type
LM-70	352000	6458100	1065	-	3.98	Hy-NORM
LM-67	351975	6458150	1080	-	12.72	Hy-NORM
LM-58	352280	6458710	1205	2.31	-	AOB
LM-57	352275	6458725	1215	-	-	Hy-NORM
LM-55	353275	6459850	1250	1.31	-	AOB
LM-49	353180	6460010	1325	0.07	-	AOB
LM-48	353170	6460025	1335	1.39	-	AOB
LM-47	353165	6460035	1340	0.49	-	AOB
LM-44	353135	6460085	1370	-	15.54	Hy-NORM
LM-42	353125	6460100	1375	-	13.57	Hy-NORM
LM-41	353025	6460475	1390	-	1.22	Hy-NORM
LM-24	356075	6482975	1750	-	5.96	Hy-NORM
LM-23	356050	6483000	1775	-	0.53	Hy-NORM
LM-22	356035	6483015	1785	0.6	-	AOB
LM-21	356025	6483025	1795	0.15	-	AOB
LM-6	357500	6482180	1895	-	0.71	Hy-NORM
LM-1	357500	6482275	1960	-	1	Hy-NORM
LM-15	357550	6484300	2010	2.77	-	AOB
LM-14	357600	6484285	2025	1.66	-	AOB
LM-13	357650	6484275	2035	1.45	1.45	AOB
LM-12	357725	6484250	2070	1.27	1.27	AOB
LM-11	358000	6484325	2145	1.16	1.16	AOB
LM-10	358000	6484350	2170	1.52	1.52	AOB

Foid and Opx values are the normative contents of the lavas, assuming $\text{Fe}^{3+}/\text{Fe}_{\text{tot}}=0.15$.

Longitude and latitude are the universal mercator transversal (UTM) coordinates.

Table A-2-b: Location and classification of Level Mountain hawaiites and felsic volcanic samples

Sample	Longitude	Latitude	Elevation (m)	Qtz	Foid	Opx	Rock type
LM-52	353220	6459940	1300	-	-	2.77	Haw
LM-50	353195	6459985	1315	-	5.47	-	Haw
LM-45	353145	6460065	1360	-	-	4.74	Haw
LM-39	356775	6480900	1580	-	-	3.42	Haw
LM-36	357125	6480800	1555	-	-	5.61	Haw
LM-40	356000	6482250	1600	-	-	0.6	Haw
LM-25	356000	6482250	1600	-	2.85	-	Trach
LM-35	357075	6481750	1670	-	7.08	-	Pho Trach
LM-34	357080	6481780	1690	-	7.4	-	Pho Trach
LM-33	357085	6481810	1710	-	6.79	-	Pho Trach
LM-32	357085	6481835	1735	-	6.04	-	Pho Trach
LM-31	357090	6481865	1755	-	6.58	-	Pho Trach
LM-29	357100	6481925	1795	-	4.02	-	Trach
LM-20	356075	6483150	1805	5.02	-	4.33	Qtz Trach
LM-26	357100	6481950	1815	-	5.85	-	Trach
LM-9	357500	6482075	1820	-	-	9.99	Haw
LM-27	357200	6482075	1820	-	0.59	-	Haw
LM-7	357500	6482115	1840	11.39	-	6.89	Qtz Trach
LM-19	356020	6483170	1855	1.05	-	5.72	Trach
LM-18	356000	6483175	1865	1.05	-	6.49	Trach
LM-17	355900	6483450	1915	-	0.62	-	Haw
LM-4	357500	6482215	1920	-	-	2.15	Trach
LM-3	357500	6482230	1930	0.25	-	1.92	Trach
LM-2	357500	6482260	1950	-	-	2.49	Haw

Qtz, Foid and Opx values are the normative contents of the lavas, assuming $\text{Fe}^{3+}/\text{Fe}_{\text{tot}}=0.15$ for the hawaiites, and $\text{Fe}^{3+}/\text{Fe}_{\text{tot}}=0.3$ for the felsic lavas.

Longitude and latitude are the universal mercator transversal (UTM) coordinates.

Abbreviations: Haw = hawaiite, Trach = trachyte, Pho Trach = phonolite trachyte, Qtz Trach = quartz trachyte.

Table A-3: Location and classification of Kawdy Mountain volcanic samples

Sample	Longitude	Latitude	Elevation (m)	Foid	Opx	Rock type
KM-1	374025	6531100	1415	-	0.14	Hy-NORM
KM-2	373525	6530850	1430	-	7.09	Hy-NORM
KM-3	373250	6530650	1440	-	6.6	Hy-NORM
KM-4	373300	6530600	1450	-	6.12	Hy-NORM
KM-5	373175	6530450	1460	-	6.51	Hy-NORM
KM-6	373125	6530350	1475	-	6.99	Hy-NORM
KM-7	373100	6530250	1500	-	6.2	Hy-NORM
KM-8	373625	6530025	1540	-	4.4	Hy-NORM
KM-10	373605	6529975	1575	1.08	-	AOB
KM-11	373600	6529950	1590	-	0.11	Hy-NORM
KM-15	373050	6529550	1670	-	0.59	Hy-NORM
KM-14	373075	6529625	1690	-	3.11	Hy-NORM
KM-13	373075	6529625	1715	1.44	-	AOB
KM-12	372925	6529600	1735	1.34	-	AOB
KM-22	371950	6528900	1810	1.45	-	AOB
KM-21	371925	6528872	1830	-	0.6	Hy-NORM
KM-20	371575	6528725	1875	0.89	-	AOB
KM-19	371175	6528750	1895	-	2.99	Hy-NORM
KM-18	371250	6528800	1910	-	1.84	Hy-NORM
KM-17	371325	6528825	1930	-	0.71	Hy-NORM

Foid and Opx values are the normative contents of the lavas, assuming $\text{Fe}^{3+}/\text{Fe}_{\text{tot}}=0.15$.

Longitude and latitude are the universal mercator transversal (UTM) coordinates.

Table A-4: Location and classification of Metahag Mountain volcanic samples

Sample	Longitude	Latitude	Elevation (m)	Foid	Opx	Rock type
MH-23	379550	6535275	1480	0.6	-	AOB
MH-22	379550	6533300	1490	0.4	-	AOB
MH-21	379545	6533330	1515	1.02	-	AOB
MH-19	379540	6533390	1550	-	1.07	Hy-NORM
MH-18	379535	6533420	1565	1.37	-	AOB
MH-17	379535	6533445	1575	0.89	-	AOB
MH-14	379525	6534525	1615	-	1.72	Hy-NORM
MH-13	378450	6532375	1650	-	5.07	Hy-NORM
MH-12	378510	6533420	1665	-	0.29	Hy-NORM
MH-11	378570	6533470	1680	-	3.62	Hy-NORM
MH-10	378630	6533515	1695	-	3.55	Hy-NORM
MH-9	378700	6533570	1715	-	4.94	Hy-NORM
MH-8	378770	6533625	1740	-	6.97	Hy-NORM
MH-7	378800	6532650	1745	-	6.56	Hy-NORM
MH-6	380500	6533575	1750	-	4.59	Hy-NORM
MH-5	380550	6533300	1765	-	5.77	Hy-NORM
MH-4	380535	6533275	1775	-	6.58	Hy-NORM
MH-3	380520	6533250	1790	-	2.99	Hy-NORM
MH-2	380505	6533225	1800	-	2.08	Hy-NORM

Foid and Opx values are the normative contents of the lavas, assuming $\text{Fe}^{3+}/\text{Fe}_{\text{tot}}=0.15$.

Longitude and latitude are the universal mercator transversal (UTM) coordinates.

Table A-5: Location and classification of Metah Mountain volcanic samples

Sample	Longitude	Latitude	Elevation (m)	Foid	Opx	Rock type
MM-40	367825	6549900	1165	-	4.45	Hy-NORM
MM-39	367750	6549900	1180	-	2.83	Hy-NORM
MM-37	367450	6549950	1305	3.73	-	AOB
MM-36	367325	6549925	1315	3.38	-	AOB
MM-34	367275	6549975	1340	2.81	-	AOB
MM-33	367225	6550025	1370	3.1	-	AOB
MM-31	367150	6550150	1480	1.89	-	AOB
MM-28	367150	6550175	1520	1.82	-	AOB
MM-27	367150	6550200	1530	0.31	-	AOB
MM-26	367150	6550225	1540	2.15	-	AOB
MM-21	367475	6550375	1560	-	0.98	Hy-NORM
MM-24	367150	6550275	1570	0.37	-	AOB
MM-20	367450	6550375	1580	1.58	-	AOB
MM-18	367425	6550400	1600	-	1.57	Hy-NORM
MM-17	367425	6550425	1610	1.56	-	AOB
MM-15	367400	6550450	1626	2.05	-	AOB
MM-13	367400	6550475	1630	1.29	-	AOB
MM-12	367400	6550500	1645	1.67	-	AOB
MM-11	367900	6550750	1660	1.27	-	AOB
MM-10	367875	6550800	1665	0.84	-	AOB
MM-8	367150	6552875	1680	0.37	-	AOB
MM-9	367150	6552875	1680	0.91	-	AOB
MM-6	367125	6553000	1730	2.07	-	AOB
MM-3	367125	6553225	1800	1.36	-	AOB
MM-2	367100	6553275	1805	0.59	-	AOB
MM-1	367125	6553700	1820	-	0.03	Hy-NORM

Foid and Opx values are the normative contents of the lavas, assuming $\text{Fe}^{3+}/\text{Fe}_{\text{tot}}=0.15$.

Longitude and latitude are the universal mercator transversal (UTM) coordinates.

Table A-6: Location and classification of Tuya Butte volcanic samples

Sample	Longitude	Latitude	Elevation (m)	Foid	Opx	Rock type
TB-31	411400	6556950	1290	-	17	Hy-NORM
TB-29	410175	6556550	1320	-	15.36	Hy-NORM
TB-18	409525	6556675	1340	-	3.3	Hy-NORM
TB-19	409550	6556600	1345	-	3	Hy-NORM
TB-20	409450	6556525	1365	-	3.48	Hy-NORM
TB-21	409500	6556500	1385	-	0.79	Hy-NORM
TB-22	409425	6556475	1405	-	3.09	Hy-NORM
TB-15	411100	6556375	1410	-	1.1	Hy-NORM
TB-23	409350	6556400	1425	-	1.28	Hy-NORM
TB-14	411000	6556350	1440	-	0.59	Hy-NORM
TB-24	409475	6556400	1450	-	3.67	Hy-NORM
TB-25	409500	6556350	1480	-	2.14	Hy-NORM
TB-26	409525	6556300	1495	-	1.95	Hy-NORM
TB-13	410675	6556375	1510	-	1.48	Hy-NORM
TB-28	409550	6556200	1520	-	2.49	Hy-NORM
TB-12	410650	6556350	1530	-	0.78	Hy-NORM
TB-11	410650	6556325	1540	-	6.98	Hy-NORM
TB-10	410625	6556300	1560	-	4.94	Hy-NORM
TB-7	410150	6556125	1585	-	1.59	Hy-NORM
TB-8	410150	6556125	1585	0.56	-	AOB
TB-6	410125	6556100	1600	-	0.94	Hy-NORM
TB-5	410100	6556075	1610	-	0.14	Hy-NORM
TB-4	410100	6556050	1620	-	2.36	Hy-NORM
TB-2	410075	6556000	1640	-	3.65	Hy-NORM
TB-1	410550	6556125	1650	-	1.81	Hy-NORM

Foid and Opx values are the normative contents of the lavas, assuming $\text{Fe}^{3+}/\text{Fe}_{\text{tot}}=0.15$.

Longitude and latitude are the universal mercator transversal (UTM) coordinates.

Table A-7: Location and classification of Tanzilla Volcano samples

Sample	Longitude	Latitude	Elevation (m)	Foid	Opx	Rock type
TV-37	419325	6546500	1440	-	9.57	Hy-NORM
TV-35	419625	6546450	1475	-	6.82	Hy-NORM
TV-34	419725	6546450	1485	-	8.79	Hy-NORM
TV-33	419800	6546450	1490	-	8.87	Hy-NORM
TV-31	420025	6546450	1520	-	9.68	Hy-NORM
TV-13	419725	6546150	1525	-	12.15	Hy-NORM
TV-29	419550	6546050	1540	-	8.07	Hy-NORM
TV-12	419700	6545975	1555	-	5.09	Hy-NORM
TV-28	419800	6545850	1580	0.89	-	AOB
TV-27	419850	6545875	1590	0.83	-	AOB
TV-26	420050	6545800	1635	-	4.97	Hy-NORM
TV-24	420175	6545750	1665	0.56	-	AOB
TV-23	420225	6545575	1680	0.66	-	AOB
TV-11	420275	6545650	1710	1.23	-	AOB
TV-20	421325	6546250	1710	0.8	-	AOB
TV-10	420325	6545600	1725	0.42	-	AOB
TV-8	420350	6545550	1750	1.12	-	AOB
TV-19	421250	6546200	1750	1.73	-	AOB
TV-18	421250	6546050	1775	0.85	-	AOB
TV-6	420425	6545425	1780	1.02	-	AOB
TV-16	421200	6545875	1810	2.45	-	AOB
TV-15	421175	6545800	1835	1.52	-	AOB
TV-5	420525	6545350	1855	3.05	-	AOB
TV-4	420600	6545300	1870	2.68	-	AOB
TV-3	420750	6545075	1900	1.39	-	AOB
TV-1	420600	6544875	1924	1.37	-	AOB

Foid and Opx values are the normative contents of the lavas, assuming $\text{Fe}^{3+}/\text{Fe}_{\text{tot}}=0.15$.

Longitude and latitude are the universal mercator transversal (UTM) coordinates.

Table A-8: Location and classification of Dome Mountain volcanic samples

Sample	Longitude	Latitude	Elevation (m)	Foid	Opx	Rock type
DM-1	465425	6479425	1890	15.92	-	NEPH
DM-2	465125	6480750	1815	13.18	-	BASAN
DM-4	465350	6480350	1735	12.99	-	BASAN
DM-5	465350	6480375	1720	11.89	-	BASAN
DM-6	465325	6480400	1670	10.69	-	BASAN
DM-7	465325	6480425	1665	9.28	-	BASAN
DM-8	465375	6480350	1765	10.43	-	BASAN
DM-9	465725	6480400	1720	8.61	-	BASAN
DM-10	465750	6480425	1705	10.77	-	BASAN
DM-11	465750	6480450	1700	12.35	-	BASAN
DM-12	465775	6480475	1670	11.63	-	BASAN
DM-13	465800	6480500	1660	12.17	-	BASAN
DM-14	465500	6480000	1840	11.39	-	BASAN
DM-15	465375	6479900	1900	8.89	-	BASAN

Foid and Opx values are the normative contents of the lavas, assuming $\text{Fe}^{3+}/\text{Fe}_{\text{tot}}=0.15$.

Longitude and latitude are the universal mercator transversal (UTM) coordinates.

Table A-9: Location and classification of Jennings River volcanic samples

Sample	Longitude	Latitude	Elevation (m)	Foid	Opx	Rock type
JR-1	368025	6594600	1110	-	11.65	Hy-NORM
JR-2	368040	6594610	1115	-	13.82	Hy-NORM
JR-3	368055	6594620	1117	-	13.12	Hy-NORM
JR-4	368075	6594630	1125	-	12.16	Hy-NORM
JR-5	368090	6594640	1128	-	11.87	Hy-NORM
JR-6	368105	6594650	1135	-	11.38	Hy-NORM
JR-7	368120	6594660	1150	-	11.66	Hy-NORM
JR-8	368135	6594670	1180	-	10.58	Hy-NORM
JR-9	368155	6594680	1195	-	9.23	Hy-NORM
JR-10	368170	6594690	1225	-	8.06	Hy-NORM
JR-11	368185	6594700	1227	-	8.39	Hy-NORM
JR-12	368200	6594710	1250	-	1.1	Hy-NORM
JR-13	368225	6594725	1265	-	7.32	Hy-NORM
JR-14	368425	6594750	1295	-	11.64	Hy-NORM
JR-25	369575	6595425	1330	2.39	-	AOB
JR-26	369600	6595350	1355	2.63	-	AOB
JR-27	369650	6595275	1385	0.94	-	AOB
JR-24	369775	6595225	1440	3.3	-	AOB
JR-16	369275	6594550	1470	8.94	-	BASAN
JR-17	369275	6594550	1470	5.23	-	BASAN
JR-19	370075	6594725	1495	10.8	-	BASAN
JR-21	370400	6594225	1500	13.03	-	BASAN
JR-20	370250	6594450	1520	12.98	-	BASAN
JR-22	370250	6594200	1530	15.12	-	BASAN

Foid and Opx values are the normative contents of the lavas, assuming $\text{Fe}^{3+}/\text{Fe}_{\text{tot}}=0.15$.

Longitude and latitude are the universal mercator transversal (UTM) coordinates.

Table A-10: Location and classification of Nome Cone volcanic samples

Sample	Longitude	Latitude	Elevation (m)	Foid	Opx	Rock type
NC-9	392525	6601300	1345	-	3.48	Hy-NORM
NC-10	392535	6601325	1355	-	4.89	Hy-NORM
NC-11	392545	6601355	1360	-	4.23	Hy-NORM
NC-12	392555	6601380	1375	-	5.35	Hy-NORM
NC-13	392565	6601405	1385	-	5.15	Hy-NORM
NC-14	392575	6601435	1390	-	5.55	Hy-NORM
NC-15	392600	6601500	1420	-	3.69	Hy-NORM
NC-16	393675	6602150	1480	2.36	-	AOB
NC-8	393825	6601850	1495	4.66	-	AOB
NC-19	393750	6601950	1510	-	4.91	Hy-NORM
NC-6	393800	6601860	1540	-	4.17	Hy-NORM
NC-5	393755	6601880	1555	-	4.6	Hy-NORM
NC-3	393720	6601895	1575	-	5.66	Hy-NORM
NC-1	393650	6601925	1595	-	12.68	Hy-NORM

Foid and Opx values are the normative contents of the lavas, assuming $\text{Fe}^{3+}/\text{Fe}_{\text{tot}}=0.15$.

Longitude and latitude are the universal mercator transversal (UTM) coordinates.

Table A-11: Location and classification of Little Rancheria volcanic samples

Sample	Longitude	Latitude	Elevation (m)	Foid	Opx	Rock type
LR-24A	423575	6621400	1420	0.53	-	AOB
LR-18	423900	6620900	1450	-	0.32	Hy-NORM
LR-17	423825	6620900	1470	-	0.24	Hy-NORM
LR-16	423800	6620900	1485	1.07	-	AOB
LR-14	423700	6620900	1505	1.03	-	AOB
LR-13	423650	6620900	1515	0.36	-	AOB
LR-12	423625	6620900	1520	1.03	-	AOB
LR-10	423575	6620900	1530	1.45	-	AOB
LR-23	422975	6621175	1545	-	0.55	Hy-NORM
LR-22	422800	6621125	1585	0.5	-	AOB
LR-21	422810	6221075	1600	0.24	-	AOB
LR-20	422815	6221050	1625	0.17	-	AOB
LR-9	422050	6620350	1630	-	6.65	Hy-NORM
LR-19	422825	6620975	1635	0.18	-	AOB
LR-8	422065	6620360	1642	-	8.46	Hy-NORM
LR-7	422075	6620365	1645	-	8.38	Hy-NORM
LR-5	422100	6620380	1660	-	8.85	Hy-NORM
LR-4	422125	6620395	1682	-	2.11	Hy-NORM
LR-3	422135	6620400	1685	0.28	-	AOB
LR-2	422160	6620415	1700	-	3.92	Hy-NORM
LR-1	422175	6620425	1710	0.04	-	AOB

Foid and Opx values are the normative contents of the lavas, assuming $\text{Fe}^{3+}/\text{Fe}_{\text{tot}}=0.15$.

Longitude and latitude are the universal mercator transversal (UTM) coordinates.

Table A-12: Location and classification of Blue River volcanic samples

Sample	Longitude	Latitude	Elevation (m)	Foid	Opx	Rock type
BR-10	428000	6575750	1360	-	11.93	Hy-NORM
BR-13	428225	6575800	1405	-	13.09	Hy-NORM
BR-14	428300	6575800	1425	-	11.28	Hy-NORM
BR-15	428375	6575800	1450	-	11.74	Hy-NORM
BR-16	428575	6575850	1530	-	10.98	Hy-NORM
BR-17	428600	6575850	1540	-	9.11	Hy-NORM
BR-18	428650	6575950	1625	-	1.91	Hy-NORM
BR-19	428675	6575950	1635	-	3.69	Hy-NORM
BR-34	428625	6575475	1650	1.26	-	AOB
BR-35	428750	6575575	1680	0.62	-	AOB
BR-36	428800	6575750	1705	-	0.9	Hy-NORM
BR-33	430325	6575300	1735	-	2.51	Hy-NORM
BR-37	428900	6575900	1745	0.38	-	AOB
BR-32	430275	6575325	1760	-	2.92	Hy-NORM
BR-7	430225	6575650	1790	-	0.36	Hy-NORM
BR-31	430225	6575325	1790	-	2.13	Hy-NORM
BR-30	430150	6575400	1800	-	2.25	Hy-NORM
BR-29	430075	6575700	1850	0.17	-	AOB
BR-28	430050	6575700	1860	-	1.19	Hy-NORM
BR-26	430050	6575725	1880	-	0.51	Hy-NORM
BR-25	430025	6575725	1890	0.87	-	AOB
BR-6	430125	6575800	1910	2.44	-	AOB
BR-23	430025	6575775	1910	0.8	-	AOB
BR-4	430100	6575850	1930	2.23	-	AOB
BR-22	430000	6575775	1930	0.78	-	AOB
BR-20	429955	6575800	1945	-	0.55	Hy-NORM
BR-3	430000	6575975	1950	0.37	-	AOB
BR-1	429975	6575950	1960	1.21	-	AOB

Foid and Opx values are the normative contents of the lavas, assuming $\text{Fe}^{3+}/\text{Fe}_{\text{tot}}=0.15$.

Longitude and latitude are the universal mercator transversal (UTM) coordinates.

Table A-13: Location and classification of Caribou Tuya volcanic samples

Sample	Longitude	Latitude	Elevation (m)	Foid	Opx	Rock type
CT-17	31275	83250	1690	-	8.06	Hy-NORM
CT-18	31900	83275	1695	-	9.07	Hy-NORM
CT-19	31900	83400	1710	-	7.86	Hy-NORM
CT-20	31900	83525	1720	-	10.72	Hy-NORM
CT-21	31900	83600	1730	-	7.55	Hy-NORM
CT-1	31900	84150	1740	-	5.67	Hy-NORM
CT-2	32000	84050	1760	-	10.26	Hy-NORM
CT-3	32000	84000	1780	-	11.59	Hy-NORM
CT-4	32050	83900	1835	-	9.48	Hy-NORM
CT-5	32075	83875	1840	-	11.87	Hy-NORM
CT-6	32100	83900	1855	-	10.33	Hy-NORM
CT-7	32100	83850	1875	-	0.67	Hy-NORM
CT-8	32125	83825	1885	-	2.48	Hy-NORM
CT-9	32225	83775	1910	-	1.4	Hy-NORM
CT-10	32275	83775	1920	-	2.62	Hy-NORM
CT-11	32375	83775	1940	-	2.49	Hy-NORM
CT-12	32450	83775	1965	-	1.52	Hy-NORM
CT-13	32575	83775	1985	-	9.45	Hy-NORM
CT-14	32750	83775	2000	-	8.62	Hy-NORM
CT-15	32800	83800	2015	-	10.27	Hy-NORM
CT-16	32825	83825	2020	-	8.62	Hy-NORM

Foid and Opx values are the normative contents of the lavas, assuming $\text{Fe}^{3+}/\text{Fe}_{\text{tot}}=0.15$.

Longitude and latitude are the universal mercator transversal (UTM) coordinates.

Table A-14: Location and classification of Rancheria area volcanic samples

Sample	Longitude	Latitude	Site	Foid	Opx	Rock type
RA-8	373125	6645425	Swan Lake	-	8.62	Hy-NORM
RA-9	373125	6645425	Swan Lake	-	12.3	Hy-NORM
RA-1	408250	6657500	Rancheria R.	10.82	-	BASAN
RA-2	408250	6657500	Rancheria R.	11.99	-	BASAN
RA-3	408250	6657500	Rancheria R.	16.81	-	BASAN
RA-4	408250	6657500	Rancheria R.	8.58	-	BASAN
RA-5	408260	6657500	Rancheria R.	6.38	-	BASAN
RA-6	408260	6657500	Rancheria R.	5.72	-	BASAN
RA-7	408260	6657500	Rancheria R.	2.04	-	AOB
RA-10	413750	6660500	Rancheria R.	14.55	-	BASAN
RA-11	413750	6660500	Rancheria R.	3.21	-	AOB
RA-12	432300	6665400	Rancheria R.	4.18	-	AOB
RA-13	432300	6665400	Rancheria R.	3.82	-	AOB
RA-14	432300	6665400	Rancheria R.	5.53	-	BASAN
RA-15	460750	6669200	Big Creek	0.77	-	AOB
RA-16	460250	6667800	Big Creek	-	0.19	Hy-NORM
RA-17	461100	6669250	Big Creek	0.27	-	AOB
RA-18	461100	6669250	Big Creek	0.5	-	AOB
RA-19	461000	6662675	Big Creek	-	4.37	Hy-NORM
WT-3	491600	6676075	Liard R.	-	15.41	Hy-NORM
WT-4	491575	6676050	Liard R.	-	11.19	Hy-NORM
WT-5	491550	6676025	Liard R.	-	17.54	Hy-NORM
WT-6	505825	6658000	Liard R.	-	14.23	Hy-NORM
WT-7	505825	6658000	Liard R.	-	13.73	Hy-NORM
WT-10	503425	6653875	Liard R.	-	2.11	Hy-NORM
WT-11	503425	6653875	Liard R.	-	3.57	Hy-NORM
WT-12	503375	6653900	Liard R.	-	2.26	Hy-NORM

Foid and Opx values are the normative contents of the lavas, assuming $\text{Fe}^{3+}/\text{Fe}_{\text{tot}}=0.15$.

Longitude and latitude are the universal mercator transversal (UTM) coordinates.

Table A-15: Location and classification of Watson Lake area volcanic samples

Sample	Longitude	Latitude	Foid	Opx	Rock type
RA-20	509250	6656925	2.36	-	AOB
RA-21	514300	6659000	3.61	-	AOB
RA-22	514300	6659000	1.89	-	AOB
WT-1	511400	6661325	-	0.31	Hy-NORM
WT-2	511250	6661250	0.84	-	AOB
WT-13	509100	6656875	2.26	-	AOB

Foid and Opx values are the normative contents of the lavas, assuming $\text{Fe}^{3+}/\text{Fe}_{\text{tot}}=0.15$.

Longitude and latitude are the universal mercator transversal (UTM) coordinates.

Table B-1-a: Whole rock analyses of Mount Edziza mafic volcanic samples

Sample	EZ-3	EZ-5	EZ-23	EZ-31	EZ-32	EZ-33	EZ-34	EZ-36	EZ-39
Rock type	Hy-NORM	Hy-NORM	Hy-NORM	Hy-NORM	Hy-NORM	Hy-NORM	Hy-NORM	Hy-NORM	AOB
Formation	Raspberry	Raspberry	Armadillo	Nido	Nido	Nido	Ice Peak	Ice Peak	Ice Peak
SiO ₂	46.57	46.92	45.78	48.24	46.83	47.69	45.65	46.34	46.53
TiO ₂	2.34	2.69	3.4	2.91	3.02	3.02	3.55	3.54	2.2
Al ₂ O ₃	16.4	16.81	15.93	15.94	14.8	15.34	15.35	16.27	15.2
Fe ₂ O ₃ T	12.31	12.84	13.29	12.35	13.2	12.88	13.92	12.98	11.47
MnO	0.18	0.19	0.19	0.17	0.19	0.17	0.2	0.19	0.17
MgO	7.12	5.95	5.41	6.38	6.54	5.98	5.64	5.54	8.64
CaO	8.7	8.39	9.83	9.63	9.88	10.15	9.93	9.87	9.32
Na ₂ O	2.71	2.87	2.99	2.42	2.32	2.62	2.79	2.83	3.01
K ₂ O	0.81	1.09	0.96	0.69	0.56	0.58	0.95	0.93	1.21
P ₂ O ₅	0.37	0.48	0.76	0.32	0.34	0.34	0.81	0.76	0.45
LOI	2.45	2.67	0.35	3.66	3.41	2.4	0.51	0.83	0.3
Total	99.96	100.9	98.89	102.71	101.09	101.16	99.3	100.08	98.5
Rb	11	17	13	50	4	5	12	11	21
Sr	505	546	571	1398	376	417	551	561	548
Ba	389	416	426	236	234	234	473	436	331
Sc	23	-	-	-	26	-	26	-	23
Cr	27	34	69	113	111	110	73	74	311
Co	46	-	-	-	43	-	48	-	51
Ni	42	43	45	67	64	72	45	45	104
Zn	108	123	109	114	113	114	120	121	64
Cu	31	31	51	31	44	65	49	46	31
Y	30	32	34	32	29	28	34	33	29
Zr	166	213	176	134	138	143	176	171	220
Nb	19.33	25.45	30.8	16.13	16.93	18.22	25.56	25.69	33.96
La	17.4	-	21.9	-	13.7	-	22.6	-	25.6
Ce	35.6	-	45.4	-	27.6	-	46.1	-	46.8
Nd	19.3	-	25	-	15.1	-	24.6	-	22.6
Sm	5.7	-	7.1	-	5.1	-	7.5	-	6.5
Eu	1.72	-	2.56	-	1.73	-	2.67	-	1.85
Tb	0.82	-	0.81	-	0.73	-	0.95	-	0.69
Ho	0.91	-	0.82	-	0.74	-	0.85	-	0.88
Yb	1.82	-	1.79	-	1.59	-	1.8	-	1.87
Lu	0.16	-	0.13	-	0.21	-	0.15	-	0.08
⁸⁷ Sr/ ⁸⁶ Sr	0.70306	-	0.70293	-	0.70276	-	0.70297	-	0.70289
¹⁴³ Nd/ ¹⁴⁴ Nd	0.51307	-	-	-	0.51301	-	0.51299	-	0.51296
²⁰⁶ Pb/ ²⁰⁴ Pb	19.339	-	19.175	-	19.272	-	-	-	19.341
²⁰⁷ Pb/ ²⁰⁴ Pb	15.57	-	15.556	-	15.532	-	-	-	15.594
²⁰⁸ Pb/ ²⁰⁴ Pb	38.68	-	38.562	-	38.525	-	-	-	38.694

Major elements in wt.%, trace elements in ppm.

Table B-1-a: Whole rock analyses of Mount Edziza mafic volcanic samples (cont'd)

Sample	EZ-41	EZ-42	EZ-43	EZ-44	EZ-45	EZ-46	EZ-47	EZ-48	EZ-49
Rock type	Hy-NORM	Hy-NORM	Hy-NORM	Hy-NORM	Hy-NORM	AOB	Hy-NORM	Hy-NORM	Hy-NORM
Formation	Ice Peak								
SiO ₂	45.89	46.06	46.15	45.57	45.44	45.95	45.12	45.78	45.57
TiO ₂	3.52	3.4	3.48	3.47	3.34	3.5	3.74	3.43	3.43
Al ₂ O ₃	15.88	16.38	16.41	16.03	15.63	16.37	15.83	16.13	15.68
Fe ₂ O ₃ ^T	13.43	13.08	13.29	13.11	13.11	13.39	13.82	12.99	13.35
MnO	0.19	0.19	0.2	0.19	0.2	0.2	0.19	0.2	0.2
MgO	5.74	5.47	5.25	5.17	5.45	5.57	6.05	5.83	6.16
CaO	9.84	9.94	9.95	9.8	9.65	9.94	9.84	9.84	9.78
Na ₂ O	2.93	2.99	2.98	2.9	2.97	3.08	2.79	2.69	2.72
K ₂ O	0.94	0.92	0.96	0.93	0.99	0.96	0.9	0.9	0.87
P ₂ O ₅	0.74	0.78	0.84	0.8	0.81	0.79	0.76	0.74	0.7
LOI	0.52	0.35	0.22	0.31	0.34	0.52	0.31	0.38	0.66
Total	99.62	99.56	99.72	98.27	97.93	100.27	99.35	98.92	99.12
Rb	14	13	14	13	14	13	13	13	13
Sr	553	573	579	570	563	564	553	554	532
Ba	404	432	452	440	437	442	401	415	391
Sc	-	-	-	-	-	-	-	-	-
Cr	72	71	66	66	67	76	77	77	86
Co	-	-	-	-	-	-	-	-	-
Ni	44	45	39	37	41	44	47	43	50
Zn	111	108	110	110	109	116	108	111	119
Cu	42	48	40	30	41	44	48	45	48
Y	34	32	33	33	34	33	33	34	31
Zr	169	166	170	167	173	169	161	171	166
Nb	23.06	24.68	25.58	26.23	30.98	28.98	22.9	24.63	23.63
La	-	-	-	-	-	-	-	-	-
Ce	-	-	-	-	-	-	-	-	-
Nd	-	-	-	-	-	-	-	-	-
Sm	-	-	-	-	-	-	-	-	-
Eu	-	-	-	-	-	-	-	-	-
Tb	-	-	-	-	-	-	-	-	-
Ho	-	-	-	-	-	-	-	-	-
Yb	-	-	-	-	-	-	-	-	-
Lu	-	-	-	-	-	-	-	-	-
⁸⁷ Sr/ ⁸⁶ Sr	-	-	-	-	-	-	-	-	-
¹⁴³ Nd/ ¹⁴⁴ Nd	-	-	-	-	-	-	-	-	-
²⁰⁶ Pb/ ²⁰⁴ Pb	-	-	-	-	-	-	-	-	-
²⁰⁷ Pb/ ²⁰⁴ Pb	-	-	-	-	-	-	-	-	-
²⁰⁸ Pb/ ²⁰⁴ Pb	-	-	-	-	-	-	-	-	-

Major elements in wt.%, trace elements in ppm.

Table B-1-a: Whole rock analyses of Mount Edziza mafic volcanic samples (cont'd)

Sample	EZ-50	EZ-37	EZ-40	EZ-606	EZ-1622	EZ-2518	EZ-2602	EZ-3102	EZ-3204
Rock type	Hy-NORM Ice Peak	Hy-NORM Big Raven	AOB Big Raven	Hy-NORM Big Raven	Hy-NORM Big Raven	Hy-NORM Big Raven	Hy-NORM Big Raven	AOB Big Raven	Hy-NORM Big Raven
Formation									
SiO ₂	45.97	46.87	46.36	46.23	46.47	49.83	48.56	46.83	47.49
TiO ₂	3.49	2.3	2.78	2.51	2.85	2.3	1.95	2.07	2.26
Al ₂ O ₃	16.22	15.3	16.09	16.54	16.24	16.72	15.03	14.41	15.83
Fe ₂ O ₃ T	13.11	12	12.41	11.53	12.37	10.6	10.48	11.51	11.97
MnO	0.2	0.18	0.17	0.16	0.19	0.02	0.17	0.17	0.18
MgO	5.07	6.63	6.24	5.84	5.8	5.15	7.9	9.13	7.07
CaO	9.74	9.83	10.19	10.41	10.23	8.18	8.63	8.02	10.14
Na ₂ O	2.94	2.68	2.81	2.62	2.64	3.71	2.94	3.3	2.81
K ₂ O	1	0.81	1.04	0.77	0.98	1.64	1.33	1.22	0.75
P ₂ O ₅	0.81	0.37	0.4	0.37	0.42	0.44	0.35	0.41	0.36
LOI	0.48	0.21	0.23	0.28	0.41	0.29	0.34	0.24	0.72
Total	99.03	97.18	98.72	97.26	98.6	98.87	97.68	97.31	99.58
Rb	15	11	15	11	16	26.2	24	19	10
Sr	571	460	560	523	542	462	446	456	464
Ba	441	235	292	226	291	454	389	335	225
Sc	-	24	-	-	-	-	-	19.5	-
Cr	62	170	100	78	119	174	315	274	187
Co	-	-	-	-	-	-	-	58.8	-
Ni	40	169	48	53	53	71.9	142	247	81
Zn	112	110	96	94	113	104.4	101	108	115
Cu	47	57	55	54	56	49.3	57	66	58
Y	35	30	31	28	31	31.5	27	28	29
Zr	181	177	191	148	188	256	207	191	154
Nb	29.44	26.16	29.64	22.44	32.61	35	33.69	30.15	27.47
La	-	18.4	-	-	-	-	-	23.9	-
Ce	-	36.6	-	-	-	-	-	48	-
Nd	-	19.7	-	-	-	-	-	23	-
Sm	-	5.9	-	-	-	-	-	6.15	-
Eu	-	1.6	-	-	-	-	-	1.9	-
Tb	-	0.84	-	-	-	-	-	0.85	-
Ho	-	0.79	-	-	-	-	-	0.8	-
Yb	-	1.83	-	-	-	-	-	2	-
Lu	-	0.14	-	-	-	-	-	0.31	-
⁸⁷ Sr/ ⁸⁶ Sr	-	0.70284	-	-	-	-	-	-	-
¹⁴³ Nd/ ¹⁴⁴ Nd	-	0.51294	-	-	-	-	-	-	-
²⁰⁶ Pb/ ²⁰⁴ Pb	-	19.2	-	-	-	-	-	-	-
²⁰⁷ Pb/ ²⁰⁴ Pb	-	15.534	-	-	-	-	-	-	-
²⁰⁸ Pb/ ²⁰⁴ Pb	-	38.516	-	-	-	-	-	-	-

Major elements in wt.%, trace elements in ppm.

Table B-1-a: Whole rock analyses of Mount Edziza mafic volcanic samples (cont'd)

Sample	EZ-3602	EZ-3704	EZ-3717	EZ-3807	EZ-3913	EZ-4106	EZ-4203	EZ-4411	EZ-4412
Rock type	AOB	AOB	Hy-NORM	Hy-NORM	AOB	Hy-NORM	Hy-NORM	Hy-NORM	AOB
Formation	Big Raven								
SiO ₂	46.44	46.51	47.32	45.18	46.55	47.73	46.34	48.39	47.92
TiO ₂	2.48	2.41	2.22	2	2.88	1.98	2.42	2.15	2.25
Al ₂ O ₃	15.63	15.7	14.57	13.03	16.33	15.47	15.66	15.99	15.81
Fe ₂ O ₃ ^T	11.49	11.02	11.67	11.96	12.37	10.69	11.03	10.69	11.23
MnO	0.17	0.17	0.18	0.18	0.18	0.17	0.17	0.17	0.18
MgO	8.3	7.57	8.2	12.11	6.13	6.74	7.62	6.2	6.03
CaO	9.48	9.57	8.2	8.74	10.13	9.62	9.37	9.55	9.39
Na ₂ O	2.77	2.85	2.97	2.16	2.83	2.84	2.72	3.07	3.24
K ₂ O	1.16	1.16	1.22	0.73	1.04	1.03	1.18	1.16	1.26
P ₂ O ₅	0.42	0.43	0.44	0.31	0.42	0.37	0.44	0.38	0.44
LOI	0.35	0.35	0.44	0.5	0.28	0.49	0.52	0.54	0.63
Total	98.69	97.74	97.43	96.9	99.14	97.13	97.47	98.29	98.38
Rb	20	20	19	11	16	19	19	20.5	26
Sr	566	577	428	422	546	479	564	488.5	480
Ba	307	336	317	203	283	321	315	330.5	395
Sc	-	-	-	23.3	-	-	-	-	-
Cr	317	291	310	451	105	301	300	257.5	231
Co	-	-	-	74.5	-	-	-	-	-
Ni	147	135	186	322	51	83	144	73.5	71
Zn	113	93	113	98	109	99	99	103	109
Cu	61	56	54	65	52	51	54	54.5	56
Y	28	28	33	23	30	27	29	27	30
Zr	203	207	211	144	192	165	211	165.5	194
Nb	32.09	33.16	28.72	21.74	31.4	28.07	36.5	31.65	41.78
La	-	-	-	16.7	-	-	-	-	-
Ce	-	-	-	34	-	-	-	-	-
Nd	-	-	-	18	-	-	-	-	-
Sm	-	-	-	4.8	-	-	-	-	-
Eu	-	-	-	1.6	-	-	-	-	-
Tb	-	-	-	0.8	-	-	-	-	-
Ho	-	-	-	1.2	-	-	-	-	-
Yb	-	-	-	1.7	-	-	-	-	-
Lu	-	-	-	0.22	-	-	-	-	-
⁸⁷ Sr/ ⁸⁶ Sr	-	-	-	-	-	-	-	-	-
¹⁴³ Nd/ ¹⁴⁴ Nd	-	-	-	-	-	-	-	-	-
²⁰⁶ Pb/ ²⁰⁴ Pb	-	-	-	-	-	-	-	-	-
²⁰⁷ Pb/ ²⁰⁴ Pb	-	-	-	-	-	-	-	-	-
²⁰⁸ Pb/ ²⁰⁴ Pb	-	-	-	-	-	-	-	-	-

Major elements in wt.%, trace elements in ppm.

Table B-1-a: Whole rock analyses of Mount Edziza mafic volcanic samples (cont'd)

Sample	EZ-4413	EZ-4414	EZ-4513	EZ-5106
Rock type	Hy-NORM	Hy-NORM	Hy-NORM	Hy-NORM
Formation	Big Raven	Big Raven	Big Raven	Big Raven
SiO ₂	46.42	47.43	49.14	52.44
TiO ₂	3.29	2.25	1.97	1.51
Al ₂ O ₃	16.17	15.32	14.94	16.63
Fe ₂ O ₃ ^T	12.63	11.32	10.97	9
MnO	0.19	0.19	0.18	0.15
MgO	5.87	6.38	7.45	5.08
CaO	9.84	9.4	7.38	8.09
Na ₂ O	2.85	2.92	3.49	3.54
K ₂ O	1.02	1.08	1.65	1.78
P ₂ O ₅	0.5	0.41	0.43	0.29
LOI	1.22	0.85	0.37	0.47
Total	100	97.55	97.97	98.97
Rb	17	21	28	30
Sr	536	453	389	495
Ba	359	330	414	426
Sc	-	-	-	-
Cr	116	280	-	179
Co	-	-	-	-
Ni	54	86	187	53
Zn	123	115	110	85
Cu	45	62	45	45
Y	30	29	36	23
Zr	186	182	254	130
Nb	33.69	34.9	33.06	19.69
La	-	-	-	-
Ce	-	-	-	-
Nd	-	-	-	-
Sm	-	-	-	-
Eu	-	-	-	-
Tb	-	-	-	-
Ho	-	-	-	-
Yb	-	-	-	-
Lu	-	-	-	-
⁸⁷ Sr/ ⁸⁶ Sr	-	-	-	-
¹⁴³ Nd/ ¹⁴⁴ Nd	-	-	-	-
²⁰⁶ Pb/ ²⁰⁴ Pb	-	-	-	-
²⁰⁷ Pb/ ²⁰⁴ Pb	-	-	-	-
²⁰⁸ Pb/ ²⁰⁴ Pb	-	-	-	-

Major elements in wt %, trace elements in ppm.

Table B-1-b: Whole rock analyses of Mount Edziza hawaiites and felsic volcanic samples

Sample	EZ-2	EZ-4	EZ-6	EZ-7	EZ-9	EZ-10	EZ-11	EZ-12	EZ-13
Rock type	Haw								
Formation	Raspberry								
SiO ₂	47.28	46.17	46.44	48.2	47.04	47.34	48.07	47.71	46.47
TiO ₂	2.78	2.86	3.15	3.03	3.09	3.1	3.19	3	3.11
Al ₂ O ₃	17.04	16.68	15.46	16.42	16.53	16.45	16.91	16.99	16.34
Fe ₂ O ₃ T	12.93	13.44	14.19	13.03	13.44	13.47	13.6	12.21	14.05
MnO	0.18	0.2	0.24	0.23	0.24	0.21	0.17	0.22	0.24
MgO	4.78	4.35	3.85	3.37	3.23	3.53	2.34	2.7	3.79
CaO	8.18	9.23	7.05	7.75	7.82	7.91	7.79	7.92	8.18
Na ₂ O	3.68	3.16	3.53	3.61	3.43	3.57	3.56	3.61	3.62
K ₂ O	1.34	1.21	1.74	1.88	1.51	1.63	1.62	1.51	1.7
P ₂ O ₅	0.53	0.55	1.01	1.01	0.86	0.91	0.91	0.79	0.9
LOI	4.06	5.4	3.87	5.43	4.82	4.8	5.87	5.74	5.06
Total	102.78	103.25	100.53	103.96	102.02	102.92	104.03	102.4	103.45
Rb	18	16	22	24	17	23	20	22	26
Sr	688	635	577	1397	689	678	653	667	612
Ba	740	831	960	1390	1012	1290	990	919	791
Sc	-	-	-	-	-	-	-	-	-
Cr	28	19	2	2	4	5	5	8	3
Co	-	-	-	-	-	-	-	-	-
Ni	41	36	12	16	17	19	17	20	14
Zn	117	132	150	159	150	142	159	141	134
Cu	33	34	32	33	31	33	35	31	37
Y	30	31	49	32	44	42	44	39	42
Zr	243	229	291	321	281	284	295	272	305
Nb	29.33	29.47	39.17	39.66	37.95	37.15	36.56	34.09	40.35
La	-	-	-	-	-	-	-	-	-
Ce	-	-	-	-	-	-	-	-	-
Nd	-	-	-	-	-	-	-	-	-
Sm	-	-	-	-	-	-	-	-	-
Eu	-	-	-	-	-	-	-	-	-
Tb	-	-	-	-	-	-	-	-	-
Ho	-	-	-	-	-	-	-	-	-
Yb	-	-	-	-	-	-	-	-	-
Lu	-	-	-	-	-	-	-	-	-
⁸⁷ Sr/ ⁸⁶ Sr	-	-	-	-	-	-	-	-	-
¹⁴³ Nd/ ¹⁴⁴ Nd	-	-	-	-	-	-	-	-	-
²⁰⁶ Pb/ ²⁰⁴ Pb	-	-	-	-	-	-	-	-	-
²⁰⁷ Pb/ ²⁰⁴ Pb	-	-	-	-	-	-	-	-	-
²⁰⁸ Pb/ ²⁰⁴ Pb	-	-	-	-	-	-	-	-	-

Major elements in wt.%, trace elements in ppm.

Table B-1-b: Whole rock analyses of Mount Edziza hawaiites and felsic volcanic samples (cont'd)

Sample	EZ-24	EZ-25	EZ-26	EZ-27	EZ-112	EZ-2514	EZ-29	EZ-30	EZ-38
Rock type	Rhyol	Haw	Haw	Haw	Rhyol	Rhyol	Haw	Haw	Haw
Formation	Armadillo	Armadillo	Armadillo	Armadillo	Armadillo	Armadillo	Nido	Nido	Big Raven
SiO ₂	73.42	46.42	48.01	47.34	73.7	67.11	47.24	48.73	48.65
TiO ₂	0.37	4.11	3.23	3.2	0.33	0.35	2.94	3.16	2.4
Al ₂ O ₃	8.65	14.16	15	14.83	9.36	15.96	15.44	16.84	16.73
Fe ₂ O ₃ T	6.23	14.9	13.11	12.84	5.01	5.28	12.67	12.43	11.64
MnO	0.13	0.46	0.26	0.24	0.1	0.14	0.22	0.13	0.18
MgO	0.05	3.35	4.5	4.86	0.01	0.07	4.58	3.39	4.78
CaO	0.28	9.15	10.69	10	0.27	1.42	11.14	9.7	9.78
Na ₂ O	5.17	3.17	2.67	2.86	4.85	2.3	2.59	2.79	3.27
K ₂ O	4.34	1.32	0.7	0.72	4.5	6.36	0.63	0.75	1
P ₂ O ₅	0.02	1.62	0.35	0.36	0.02	0.07	0.34	0.31	0.38
LOI	2.09	4.07	3.47	2.42	0.68	5.76	3.76	1.76	0.51
Total	100.75	102.73	101.98	99.68	98.83	104.82	101.55	100	99.32
Rb	123	20	9	11	144	129	7	9	14
Sr	1	490	422	424	1	33	438	429	454
Ba	171	846	301	318	146	876	246	276	283
Sc	-	-	-	-	-	-	-	-	-
Cr	-	10	119	116	-	-	104	129	70
Co	-	-	-	-	-	-	-	-	-
Ni	8	19	69	56	7	8	73	44	18
Zn	382	167	125	146	330	181	104	101	75
Cu	8	31	49	41	7	7	41	41	23
Y	150	51	28	30	145	71	26	31	32
Zr	1178	252	137	144	1232	1254	135	163	189
Nb	101.9	24.92	16.99	18.17	115	79.17	16.52	19.66	29.32
La	-	-	-	-	-	-	-	-	-
Ce	-	-	-	-	-	-	-	-	-
Nd	-	-	-	-	-	-	-	-	-
Sm	-	-	-	-	-	-	-	-	-
Eu	-	-	-	-	-	-	-	-	-
Tb	-	-	-	-	-	-	-	-	-
Ho	-	-	-	-	-	-	-	-	-
Yb	-	-	-	-	-	-	-	-	-
Lu	-	-	-	-	-	-	-	-	-
⁸⁷ Sr/ ⁸⁶ Sr	-	-	-	-	-	-	-	-	-
¹⁴³ Nd/ ¹⁴⁴ Nd	-	-	-	-	-	-	-	-	-
²⁰⁶ Pb/ ²⁰⁴ Pb	-	-	-	-	-	-	-	-	-
²⁰⁷ Pb/ ²⁰⁴ Pb	-	-	-	-	-	-	-	-	-
²⁰⁸ Pb/ ²⁰⁴ Pb	-	-	-	-	-	-	-	-	-

Major elements in wt.%, trace elements in ppm.

Table B-1-b: Whole rock analyses of Mount Edziza hawaiites and felsic volcanic samples (cont'd)

Sample	EZ-2004	EZ-1208	EZ-2108	EZ-2218	EZ-2506	EZ-3109	EZ-3806	EZ-3809	EZ-4104
Rock type	Rhyol	Rhyol	Haw	Haw	Haw	Rhyol	Rhyol	Rhyol	Rhyol
Formation	Big Raven								
SiO ₂	67.09	76.65	51.52	49.74	50.23	74.45	75.9	75.75	76.59
TiO ₂	0.34	0.09	1.76	2.17	2.09	0.15	0.1	0.1	0.08
Al ₂ O ₃	15.98	11.84	16.51	17.34	16.48	12.22	11.22	11.74	12.05
Fe ₂ O ₃ ^T	3.7	1.66	9.15	10.08	10.06	2.37	2.05	2.05	1.59
MnO	0.08	0.02	0.16	0.16	0.17	0.05	0.03	0.03	0.02
MgO	0.25	0.04	4.2	4.74	4.9	0.03	0.01	-	-
CaO	1.82	0.26	7.37	8.59	8.52	0.28	0.2	0.21	-
Na ₂ O	4.33	4.26	3.63	3.61	3.78	4.15	4.07	4.51	4.39
K ₂ O	5.3	4.5	2.29	1.57	1.74	4.96	4.4	4.35	4.4
P ₂ O ₅	0.07	0.01	0.31	0.42	0.44	0.01	0.01	0.33	0.05
LOI	0.2	0.83	0.25	0.17	0	1.05	0.33	0.18	0.25
Total	99.15	100.17	97.14	98.59	98.41	99.72	98.33	99.26	99.42
Rb	131	318	33	25	32	213	324	307	317
Sr	182	-	377	557	450	8	-	8	-
Ba	1024	52.98	575	508	452	119	62.54	86.86	44.34
Sc	4.53	-	-	-	-	-	-	-	-
Cr	-	-	129	121	129	-	-	-	-
Co	10.1	-	-	-	-	-	-	-	-
Ni	8	8	51	53	48	8	8	8	9
Zn	78	217	96	95	109	198	215	210	149
Cu	5	3	45	47	46	4	3	3	5
Y	55	153	28	26	32	140	168	141	130
Zr	538	470	252	202	261	679	715	534	450
Nb	54.99	134	34.65	26.79	35.25	131	161	131	133
La	55	-	26.3	-	-	-	-	-	-
Ce	103	-	50.3	-	-	-	-	-	-
Nd	42	-	22	-	-	-	-	-	-
Sm	9.8	-	6.1	-	-	-	-	-	-
Eu	1.6	-	2.1	-	-	-	-	-	-
Tb	1.4	-	0.82	-	-	-	-	-	-
Ho	2.4	-	1.1	-	-	-	-	-	-
Yb	4.7	-	2.19	-	-	-	-	-	-
Lu	0.73	-	0.3	-	-	-	-	-	-
⁸⁷ Sr/ ⁸⁶ Sr	-	-	-	-	-	-	-	-	-
¹⁴³ Nd/ ¹⁴⁴ Nd	-	-	-	-	-	-	-	-	-
²⁰⁶ Pb/ ²⁰⁴ Pb	-	-	-	-	-	-	-	-	-
²⁰⁷ Pb/ ²⁰⁴ Pb	-	-	-	-	-	-	-	-	-
²⁰⁸ Pb/ ²⁰⁴ Pb	-	-	-	-	-	-	-	-	-

Major elements in wt.%, trace elements in ppm.

Table B-1-b: Whole rock analyses of Mount Edziza hawaiites and felsic volcanic samples (cont'd)

Sample	EZ-4509
Rock type	Rhyol
Formation	Big Raven
SiO ₂	75.33
TiO ₂	0.09
Al ₂ O ₃	11.31
Fe ₂ O ₃ T	1.99
MnO	0.02
MgO	-
CaO	0.12
Na ₂ O	4.34
K ₂ O	4.16
P ₂ O ₅	0.01
LOI	0.35
Total	97.72
Rb	350
Sr	0.17
Ba	26.29
Sc	-
Cr	-
Co	-
Ni	7.1
Zn	243
Cu	3.5
Y	62.5
Zr	667
Nb	164
La	-
Ce	-
Nd	-
Sm	-
Eu	-
Tb	-
Ho	-
Yb	-
Lu	-
⁸⁷ Sr/ ⁸⁶ Sr	-
¹⁴³ Nd/ ¹⁴⁴ Nd	-
²⁰⁶ Pb/ ²⁰⁴ Pb	-
²⁰⁷ Pb/ ²⁰⁴ Pb	-
²⁰⁸ Pb/ ²⁰⁴ Pb	-

Major elements in wt.%, trace elements in ppm.

Table B-2-a: Whole rock analyses of Level Mountain mafic volcanic samples

Sample Rock type	LM-70 Hy-NORM	LM-67 Hy-NORM	LM-58 AOB	LM-57 Hy-NORM	LM-55 AOB	LM-49 AOB	LM-48 AOB	LM-47 AOB	LM-44 Hy-NORM
SiO ₂	49.2	49.23	46.96	50.92	46.23	47.64	46.66	47	47.07
TiO ₂	2.02	2.1	1.88	1.33	2.32	2.68	3.11	2.89	1.91
Al ₂ O ₃	14.24	14.34	13.87	15.02	13.99	16.15	16.01	15.2	14.18
Fe ₂ O ₃ T	10.59	12.06	11	9.28	13.06	12.73	13.38	14.02	12.75
MnO	0.14	0.14	0.18	0.14	0.19	0.17	0.19	0.2	0.18
MgO	8.04	7.19	9.09	9.08	9.42	5.66	5.31	5.2	9.21
CaO	8.51	8.39	9.86	9.47	9.42	8.24	8.16	7.86	8.42
Na ₂ O	3.59	3.21	3.03	3.06	2.76	3.61	3.71	3.81	2.62
K ₂ O	0.85	0.87	1.05	0.86	0.97	1.19	1.38	1.4	0.38
P ₂ O ₅	0.32	0.33	0.37	0.27	0.32	0.59	0.95	1.17	0.25
LOI	1.93	1.83	2.01	0.17	0.47	0.36	-	0.11	1.5
Total	99.43	99.68	99.3	99.6	99.16	99.03	98.87	98.87	98.46
Rb	11.4	11.9	19.2	16.2	13.3	17	18.8	21.3	2.7
Cs	0.1	0.1	0.3	0.2	0.1	-	-	-	0.2
Sr	514.6	514.8	637.4	579.5	711.8	650.4	760.9	610.9	393.5
Ba	293.1	293.1	367.4	322.2	268.3	381.9	497.7	426.3	194.8
Sc	14	26	26	16	18	22	26	12	21
V	214	222	214	158	273	195	191	164	207
Cr	260.7	231.9	304.5	236.7	275	91	59.5	94.4	338
Co	-	-	58	55	55	46	37	32	57
Ni	119	94	224	220	212	67	57	56	276
Zn	-	-	120	105	133	135	149	159	137
Cu	-	-	78	59	67	38	51	43	77
Ga	20.6	21.4	20.4	19.6	23.2	25.4	25.4	26.2	21.2
Y	21.9	40	19.6	14.9	18.9	27.2	28.5	35.4	20.7
Zr	100.2	124.4	126.3	94.8	131.8	211.6	215.2	257.9	115.2
Nb	17.3	17.8	27.2	19.7	22.1	29.5	35	38.5	17.1
Hf	2.5	2.8	2.6	2.1	2.9	-	-	-	2.6
Ta	1	1	1.4	0.9	1.3	-	-	-	0.9
Th	1.2	1.3	2	2.1	1.6	-	-	-	1.6
U	0.2	0.3	0.6	0.7	0.6	-	-	-	0.4
Pb	1.8	1.7	2.2	3.1	2	-	-	-	2
La	13.29	23.33	17.69	14.19	15.31	-	-	-	12.01
Ce	30.43	33.45	37.12	29.02	33.37	-	-	-	24.99
Pr	4.2	5.52	4.75	3.7	4.38	-	-	-	3.43
Nd	18.84	25.38	19.93	15.64	18.81	-	-	-	15.26
Sm	4.87	6.43	4.73	3.69	4.68	-	-	-	4.21
Eu	1.63	2.15	1.52	1.25	1.55	-	-	-	1.47
Gd	4.5	6.8	4.18	3.27	4.46	-	-	-	4.32
Tb	0.68	0.95	0.61	0.48	0.63	-	-	-	0.65
Dy	3.94	5.36	3.45	2.72	3.59	-	-	-	3.74
Ho	0.76	1.09	0.65	0.51	0.69	-	-	-	0.73
Er	1.94	2.61	1.64	1.3	1.68	-	-	-	1.87
Tm	0.25	0.32	0.2	0.16	0.21	-	-	-	0.23
Yb	1.63	2.05	1.39	1.11	1.35	-	-	-	1.56
Lu	0.22	0.27	0.18	0.14	0.18	-	-	-	0.21
⁸⁷ Sr/ ⁸⁶ Sr	0.703775	-	-	0.703256	0.703137	-	-	-	0.703047
¹⁴³ Nd/ ¹⁴⁴ Nd	0.512841	-	-	0.512973	0.512954	-	-	-	0.512956
²⁰⁶ Pb/ ²⁰⁴ Pb	18.805	-	-	18.995	18.88	-	-	-	19.004
²⁰⁷ Pb/ ²⁰⁴ Pb	15.549	-	-	15.558	15.541	-	-	-	15.559
²⁰⁸ Pb/ ²⁰⁴ Pb	38.243	-	-	38.331	38.232	-	-	-	38.357

Major elements in wt.%, trace elements in ppm.

Table B-2-a: Whole rock analyses of Level Mountain mafic volcanic samples (cont'd)

Sample Rock type	LM-42 Hy-NORM	LM-41 Hy-NORM	LM-24 Hy-NORM	LM-23 Hy-NORM	LM-22 AOB	LM-21 AOB	LM-6 Hy-NORM	LM-1 Hy-NORM	LM-15 AOB
SiO ₂	48.78	46.66	48.07	46.83	48.41	46.17	46.85	47.3	45.78
TiO ₂	1.65	3.07	1.97	2.89	2.68	2.92	2.69	2.77	3.69
Al ₂ O ₃	14.62	15.31	15.15	16.17	16.21	16.3	15.5	16.06	14.72
Fe ₂ O ₃ T	12.67	12.37	11.62	14.05	13.1	13.93	12.51	13.42	14.49
MnO	0.18	0.18	0.15	0.19	0.19	0.19	0.17	0.19	0.21
MgO	8.51	6.7	6.95	5.56	5.05	5.98	6.12	5.51	5.76
CaO	9.22	8.99	7.84	8.45	8.05	8.64	8.73	8.11	8.73
Na ₂ O	2.89	3.19	3.39	3.42	3.89	3.27	3.32	3.56	3.66
K ₂ O	0.26	1.07	1.13	0.93	1.2	0.85	1.04	1.09	1.05
P ₂ O ₅	0.15	0.68	0.47	0.45	0.45	0.42	0.5	0.54	0.64
LOI	0.07	0.77	2.29	0.34	0	0	1.54	0.46	0
Total	99	98.99	99.03	99.28	99.22	98.67	98.97	99.01	98.73
Rb	1.8	15.7	16.1	12.2	19.3	12.1	15.8	13.9	15.9
Cs	-	-	0.2	-	-	-	-	-	-
Sr	292.9	689.7	564.3	585.6	573	597.6	522.1	558.2	511.7
Ba	132.2	304.7	271.9	316.4	373.1	278.5	282.2	352.1	349.9
Sc	24	16	20	23	18	20	19	23	21
V	200	243	155	259	240	258	215	238	308
Cr	299.7	149.2	223.7	21.2	18.5	21.2	117	24	83.5
Co	52	44	48	48	36	53	47	45	39
Ni	227	109	174	42	36	52	73	28	73
Zn	134	129	131	143	148	144	129	147	146
Cu	88	57	58	30	42	41	44	43	31
Ga	21.8	23.2	22.3	24	23.8	24.1	24.2	23.8	25.9
Y	19	26.7	20.2	28	30	27.6	25.4	31.2	32.1
Zr	79.7	217.8	210.1	192.6	219.1	186	186.1	220.2	216
Nb	7.3	29.5	27.2	22.1	24.2	22.6	25.3	26.5	29.4
Hf	2	-	4.1	-	-	-	-	-	-
Ta	0.5	-	1.6	-	-	-	-	-	-
Th	0.9	-	2.3	-	-	-	-	-	-
U	0.3	-	1.1	-	-	-	-	-	-
Pb	1.5	-	2	-	-	-	-	-	-
La	6.35	-	20.35	-	-	-	-	-	-
Ce	14.68	-	44.31	-	-	-	-	-	-
Pr	2.08	-	5.69	-	-	-	-	-	-
Nd	10.21	-	24.25	-	-	-	-	-	-
Sm	3.24	-	5.79	-	-	-	-	-	-
Eu	1.18	-	1.95	-	-	-	-	-	-
Gd	3.56	-	5.36	-	-	-	-	-	-
Tb	0.58	-	0.75	-	-	-	-	-	-
Dy	3.47	-	4.09	-	-	-	-	-	-
Ho	0.7	-	0.73	-	-	-	-	-	-
Er	1.79	-	1.78	-	-	-	-	-	-
Tm	0.22	-	0.22	-	-	-	-	-	-
Yb	1.56	-	1.38	-	-	-	-	-	-
Lu	0.22	-	0.18	-	-	-	-	-	-
⁸⁷ Sr/ ⁸⁶ Sr	0.703068	-	-	-	-	-	-	-	-
¹⁴³ Nd/ ¹⁴⁴ Nd	0.512974	-	-	-	-	-	-	-	-
²⁰⁶ Pb/ ²⁰⁴ Pb	19.045	-	-	-	-	-	-	-	-
²⁰⁷ Pb/ ²⁰⁴ Pb	15.584	-	-	-	-	-	-	-	-
²⁰⁸ Pb/ ²⁰⁴ Pb	38.463	-	-	-	-	-	-	-	-

Major elements in wt.%, trace elements in ppm.

Table B-2-a: Whole rock analyses of Level Mountain mafic volcanic samples (cont'd)

Sample Rock type	LM-14 AOB	LM-13 AOB	LM-12 AOB	LM-11 AOB	LM-10 AOB
SiO ₂	45.85	46	45.85	46.08	46.15
TiO ₂	3.76	3.75	3.79	3.76	3.58
Al ₂ O ₃	14.88	14.81	14.87	14.79	14.66
Fe ₂ O ₃	14.55	14.56	14.54	14.58	14.34
MnO	0.21	0.21	0.21	0.22	0.2
MgO	5.54	5.51	5.5	5.47	6.11
CaO	8.71	8.59	8.72	8.84	8.9
Na ₂ O	3.54	3.58	3.48	3.48	3.47
K ₂ O	1.05	1.07	1.05	1.05	1
P ₂ O ₅	0.66	0.69	0.64	0.65	0.62
LOI	0	0	0	0	0
Total	98.74	98.77	98.64	98.91	99.03
Rb	16.3	14.4	15.6	15.2	14.7
Cs	-	-	-	-	-
Sr	513	513.7	503.1	513.7	503.9
Ba	390.9	352.7	398.2	341.8	339.6
Sc	24	20	27	15	27
V	319	312	315	311	308
Cr	99	71.2	89	68.4	108.8
Co	43	42	44	46	52
Ni	57	52	47	57	75
Zn	154	152	156	151	154
Cu	56	42	51	56	52
Ga	25.5	26	25.1	25.8	25.3
Y	32.4	33.1	32.1	33.2	31.5
Zr	223	225.9	220.1	222.8	205.9
Nb	30.7	31.4	30.7	30.8	28.1
Hf	-	-	-	-	-
Ta	-	-	-	-	-
Th	-	-	-	-	-
U	-	-	-	-	-
Pb	-	-	-	-	-
La	-	-	-	-	-
Ce	-	-	-	-	-
Pr	-	-	-	-	-
Nd	-	-	-	-	-
Sm	-	-	-	-	-
Eu	-	-	-	-	-
Gd	-	-	-	-	-
Tb	-	-	-	-	-
Dy	-	-	-	-	-
Ho	-	-	-	-	-
Er	-	-	-	-	-
Tm	-	-	-	-	-
Yb	-	-	-	-	-
Lu	-	-	-	-	-
⁸⁷ Sr/ ⁸⁶ Sr	-	-	-	-	-
¹⁴³ Nd/ ¹⁴⁴ Nd	-	-	-	-	-
²⁰⁶ Pb/ ²⁰⁴ Pb	-	-	-	-	-
²⁰⁷ Pb/ ²⁰⁴ Pb	-	-	-	-	-
²⁰⁸ Pb/ ²⁰⁴ Pb	-	-	-	-	-

Major elements in wt.%, trace elements in ppm.

Table B-2-b: Whole rock analyses of Level Mountain hawaiites and felsic volcanic samples

Sample Rock type	LM-52 Haw	LM-50 Haw	LM-45 Haw	LM-39 Haw	LM-36 Haw	LM-40 Haw	LM-25 Trach	LM-35 Pho Tra	LM-34 Pho Tra
SiO ₂	46.94	48.41	50.87	48.93	47.86	48.11	58.49	58.92	58.94
TiO ₂	2.83	2.55	1.98	2.55	2.61	2.63	0.37	0.36	0.35
Al ₂ O ₃	15.95	16.31	16.04	15.2	14.92	15.01	17.07	17.26	17.27
Fe ₂ O ₃ T	13.39	13.44	10.93	12.58	13.08	12.88	7.42	7.5	7.5
MnO	0.2	0.21	0.17	0.2	0.19	0.22	0.21	0.22	0.22
MgO	4.39	3.29	4.68	3.25	4.02	3.66	0.31	0.2	0.27
CaO	6.08	6.49	6.48	6.33	6.1	6.15	2.42	2.15	2.21
Na ₂ O	3.98	5.02	4.05	4.3	4.04	4.37	5.95	6.75	6.78
K ₂ O	1.66	2.05	2.09	2.22	2.04	2.08	5.31	5.36	5.36
P ₂ O ₅	0.98	1.14	0.44	1.47	1.41	1.46	0.18	0.17	0.17
LOI	2.38	-	0.88	1.91	2.43	2.05	1.56	0.24	0.34
Total	98.78	98.92	98.62	98.95	98.7	98.62	99.3	99.12	99.42
Rb	24.6	36	22	28.6	26.1	29.3	102.3	102.4	102.1
Cs	-	0.5	-	-	-	-	-	0.8	-
Sr	615.1	732.1	458.1	602.9	519.7	550.1	81	40.9	45.9
Ba	462.7	482.4	529	799.8	754	782.7	375.3	351.3	352.1
Sc	15	14	15	15	-	-	-	-	-
V	125	91	156	99	102	97	11	-	-
Cr	-	-	164.9	8.9	39	-	-	-	-
Co	22	25	34	26	28	24	-	-	-
Ni	-	-	102	24	25	-	-	-	-
Zn	163	171	137	171	171	168	200	212	212
Cu	33	37	54	31	31	27	10	11	20
Ga	25.4	29.4	24.7	27.3	25.4	25.2	36.3	39.5	39.3
Y	43	43	25.6	47.8	45.9	48.3	66.7	68.5	68.5
Zr	380	403.6	186.3	330	312.7	313.8	933.8	1001	997
Nb	49.9	55.1	26.1	50.2	47.5	46.7	116.6	122.2	119.5
Hf	-	8.2	-	-	-	-	-	-	-
Ta	-	3.6	-	-	-	-	-	-	-
Th	-	5.2	-	-	-	-	-	-	-
U	-	1.4	-	-	-	-	-	-	-
Pb	-	4	-	-	-	-	-	-	-
La	-	45.81	-	-	-	-	-	42.79	-
Ce	-	99.39	-	-	-	-	-	101.2	-
Pr	-	12.83	-	-	-	-	-	12.74	-
Nd	-	53.37	-	-	-	-	-	51.5	-
Sm	-	12.27	-	-	-	-	-	11.67	-
Eu	-	3.72	-	-	-	-	-	2.31	-
Gd	-	10.76	-	-	-	-	-	9.51	-
Tb	-	1.53	-	-	-	-	-	1.52	-
Dy	-	8.41	-	-	-	-	-	9.13	-
Ho	-	1.55	-	-	-	-	-	1.75	-
Er	-	3.86	-	-	-	-	-	4.69	-
Tm	-	0.47	-	-	-	-	-	0.61	-
Yb	-	3.15	-	-	-	-	-	4.58	-
Lu	-	0.43	-	-	-	-	-	0.63	-
⁸⁷ Sr/ ⁸⁶ Sr	-	-	-	-	-	-	-	-	0.703897
¹⁴³ Nd/ ¹⁴⁴ Nd	-	-	-	-	-	-	-	-	0.512971
²⁰⁶ Pb/ ²⁰⁴ Pb	-	-	-	-	-	-	-	-	19.17
²⁰⁷ Pb/ ²⁰⁴ Pb	-	-	-	-	-	-	-	-	15.572
²⁰⁸ Pb/ ²⁰⁴ Pb	-	-	-	-	-	-	-	-	38.504

Major elements in wt.%, trace elements in ppm.

Table B-2-b: Whole rock analyses of Level Mountain hawaiites and felsic volcanic samples (cont'd)

Sample Rock type	LM-33 Pho Tra	LM-32 Pho Tra	LM-31 Pho Tra	LM-29 Trach	LM-20 Qtz Tra	LM-26 Trach	LM-9 Haw	LM-27 Haw	LM-7 Qtz Tra
SiO ₂	58.66	58.94	58.94	58.83	62.55	57.55	45.67	45.12	64.33
TiO ₂	0.43	0.37	0.37	0.39	0.76	0.36	3.3	3.7	0.55
Al ₂ O ₃	17.15	17.24	17.29	17.17	15.67	16.83	12.94	13.05	12.51
Fe ₂ O ₃ T	7.64	7.57	7.54	7.41	7	7.86	14.11	15.01	8.06
MnO	0.22	0.22	0.24	0.21	0.24	0.31	0.19	0.3	0.15
MgO	0.3	0.21	0.25	0.25	0.51	0.21	3.59	3.37	0.35
CaO	2.3	2.18	2.14	2.21	1.71	2.47	7.75	9.65	1.04
Na ₂ O	6.69	6.62	6.71	6.31	5.68	6.33	3.57	3.69	5.93
K ₂ O	5.25	5.3	5.3	5.25	5.08	5.14	1.52	1.31	4.54
P ₂ O ₅	0.21	0.17	0.17	0.18	0.2	0.17	1.78	2.02	0.05
LOI	0.4	0.54	0.51	1.13	0.1	2.04	3.22	1.87	1.62
Total	99.25	99.36	99.46	99.35	99.51	99.27	97.65	99.09	99.13
Rb	104.5	94.1	97.4	106.7	74.7	102.3	19.6	20.6	132.9
Cs	-	-	-	-	0.4	-	-	-	1.7
Sr	41.4	41.8	41	42.4	19.8	38.6	511.4	567.1	9.2
Ba	363.7	368.1	360.8	383.4	1416	325.1	1215	724.1	61.8
Sc	-	-	-	10	17	-	17	21	-
V	-	-	-	14	-	-	133	175	14
Cr	-	-	-	-	-	-	-	-	-
Co	-	-	-	-	-	-	30	32	-
Ni	-	-	-	-	-	-	-	-	-
Zn	206	204	208	203	156	239	167	155	297
Cu	21	18	14	34	15	25	28	26	18
Ga	39.5	38.9	39.2	37.4	28	39.3	26.1	24.1	47.5
Y	67.5	65.5	67.5	66.8	49.6	82.5	51.7	51.8	87.7
Zr	972.9	939.8	974.2	914.4	467.8	1115	224.1	256.1	1381
Nb	120.6	116.7	119.5	115.3	47.7	137.3	35.7	32.6	155.2
Hf	-	-	-	-	12.6	-	-	-	36.7
Ta	-	-	-	-	5.1	-	-	-	16
Th	-	-	-	-	7.6	-	-	-	15.4
U	-	-	-	-	2.4	-	-	-	2.5
Pb	-	-	-	-	9.9	-	-	-	15.7
La	-	-	-	-	40.66	-	-	-	82.53
Ce	-	-	-	-	85.84	-	-	-	178.8
Pr	-	-	-	-	10.87	-	-	-	22.43
Nd	-	-	-	-	43.79	-	-	-	91.73
Sm	-	-	-	-	9.97	-	-	-	21.57
Eu	-	-	-	-	3.28	-	-	-	2.66
Gd	-	-	-	-	9.12	-	-	-	19.87
Tb	-	-	-	-	1.41	-	-	-	3.27
Dy	-	-	-	-	8.53	-	-	-	19
Ho	-	-	-	-	1.74	-	-	-	3.59
Er	-	-	-	-	5.09	-	-	-	9.65
Tm	-	-	-	-	0.79	-	-	-	1.34
Yb	-	-	-	-	4.88	-	-	-	8.75
Lu	-	-	-	-	0.74	-	-	-	1.27
⁸⁷ Sr/ ⁸⁶ Sr	-	-	-	-	0.704884	-	-	-	0.706988
¹⁴³ Nd/ ¹⁴⁴ Nd	-	-	-	-	0.51297	-	-	-	0.513037
²⁰⁶ Pb/ ²⁰⁴ Pb	-	-	-	-	18.992	-	-	-	19.031
²⁰⁷ Pb/ ²⁰⁴ Pb	-	-	-	-	15.576	-	-	-	15.562
²⁰⁸ Pb/ ²⁰⁴ Pb	-	-	-	-	38.377	-	-	-	38.316

Major elements in wt.%, trace elements in ppm.

Table B-2-b: Whole rock analyses of Level Mountain hawaiites and felsic volcanic samples (cont'd)

Sample Rock type	LM-19 Trach	LM-18 Trach	LM-17 Haw	LM-4 Trach	LM-3 Trach	LM-2 Haw
SiO ₂	58.92	58.04	46.3	61.96	62.58	48.71
TiO ₂	1.17	1.24	3.26	0.54	0.55	2.48
Al ₂ O ₃	16.15	16.3	14.5	16.39	16.11	16.09
Fe ₂ O ₃ T	8.21	8.45	14.36	6.29	5.91	11.8
MnO	0.22	0.21	0.25	0.14	0.11	0.15
MgO	1.05	1.23	4.96	0.28	0.3	4.8
CaO	2.95	3.27	8.68	1.84	1.86	8.28
Na ₂ O	5.9	5.7	3.58	6.49	6.61	3.67
K ₂ O	3.94	3.74	1.33	5.01	5.04	1.42
P ₂ O ₅	0.49	0.5	1.19	0.1	0.1	0.57
LOI	0.17	0.38	0	0.41	0.67	1.45
Total	99.16	99.07	98.41	99.45	99.84	99.42
Rb	48.7	40.2	18	66.2	65	19.4
Cs	0.4	-	0.3	-	-	-
Sr	247.8	275.3	543.2	99.3	82.3	647.9
Ba	4117	3953	636.1	274.1	231.9	405.9
Sc	-	12	24	-	-	12
V	-	12	214	14	-	178
Cr	-	-	99.2	-	-	162.8
Co	-	-	0.3	-	-	34
Ni	-	-	43	-	-	76
Zn	160	162	159	167	144	145
Cu	18	24	55	20	20	58
Ga	25.9	26.1	24.9	36.8	37.2	25.4
Y	42.6	47.8	41.9	72.2	33.3	24.3
Zr	389.4	445.9	204.2	620.6	622.3	234.9
Nb	47.4	49	28.6	64.5	70.8	29.6
Hf	-	-	4.3	-	-	-
Ta	-	-	1.8	-	-	-
Th	-	-	2.4	-	-	-
U	-	-	1	-	-	-
Pb	-	-	2.1	-	-	-
La	36.94	-	29.12	-	-	-
Ce	81.16	-	63.89	-	-	-
Pr	9.92	-	9.12	-	-	-
Nd	41.92	-	42.9	-	-	-
Sm	9.81	-	10.51	-	-	-
Eu	4.42	-	3.83	-	-	-
Gd	8.34	-	10.54	-	-	-
Tb	1.27	-	1.52	-	-	-
Dy	7.35	-	8.24	-	-	-
Ho	1.46	-	1.51	-	-	-
Er	3.66	-	3.96	-	-	-
Tm	0.47	-	0.52	-	-	-
Yb	3.48	-	2.88	-	-	-
Lu	0.49	-	0.44	-	-	-
⁸⁷ Sr/ ⁸⁶ Sr	-	-	-	-	-	-
¹⁴³ Nd/ ¹⁴⁴ Nd	-	-	-	-	-	-
²⁰⁶ Pb/ ²⁰⁴ Pb	-	-	-	-	-	-
²⁰⁷ Pb/ ²⁰⁴ Pb	-	-	-	-	-	-
²⁰⁸ Pb/ ²⁰⁴ Pb	-	-	-	-	-	-

Major elements in wt.%, trace elements in ppm.

Table B-3: Whole rock analyses of Kawdy Mountain volcanic samples

Sample Rock type	KM-1 Hy-NORM	KM-2 Hy-NORM	KM-3 Hy-NORM	KM-4 Hy-NORM	KM-5 Hy-NORM	KM-6 Hy-NORM	KM-7 Hy-NORM	KM-8 Hy-NORM	KM-10 Hy-NORM	AOB
SiO ₂	49.05	48.05	48.09	48.07	48.5	47.81	48.67	48.22	48.31	
TiO ₂	2.22	2.03	2.1	1.99	2.15	2.04	2.2	2.18	2.48	
Al ₂ O ₃	15.46	13.8	14.02	13.95	14.73	13.86	14.72	14.27	15.5	
Fe ₂ O ₃ ^T	12.65	14.23	14.08	14.09	13.74	14.24	13.75	13.98	12.84	
MnO	0.17	0.17	0.18	0.17	0.17	0.18	0.17	0.17	0.17	
MgO	5.96	9.59	8.81	9.62	7.36	9.43	7.24	8.12	6.22	
CaO	9.85	9	9.22	9.01	9.62	9.02	9.64	9.45	9.89	
Na ₂ O	3.46	2.82	2.9	2.88	3.03	2.81	3.08	3.04	3.38	
K ₂ O	0.99	0.71	0.71	0.68	0.74	0.69	0.76	0.75	1.13	
P ₂ O ₅	0.36	0.29	0.3	0.29	0.31	0.3	0.31	0.31	0.42	
LOI	-	-	-	-	-	-	-	-	0.19	
Total	100.17	100.69	100.41	100.75	100.35	100.38	100.54	100.49	100.53	
Rb	12.8	9.4	9.3	8.9	9.7	8.8	9.8	9.6	17.6	
Cs	0.05	0.16	0.15	-	-	-	0.16	-	-	
Sr	514.8	389.1	396.1	395.4	425.3	397.7	422.5	401.2	608.4	
Ba	389.2	211.5	200.6	202	234.1	204.9	216.6	225.3	413.2	
Sc	24	22	19	27	19	18	21	17	30	
V	241	202	203	193	208	197	222	211	245	
Cr	211.4	268.9	267.5	262	292.2	262.7	282.6	263.4	185.4	
Co	49	50	58	62	55	53	63	55	47	
Ni	58	224	189	217	126	212	114	146	57	
Zn	131	138	142	133	137	141	136	136	131	
Cu	57	66	80	58	80	63	73	65	54	
Ga	22.9	22.04	21	20.6	22.4	20.9	22.2	22.6	22.6	
Y	21.5	18.8	19.1	18.5	20.5	19	20.6	20.2	21.3	
Zr	147.4	116.3	118.2	113.2	122.8	116.1	125.6	123.5	169.2	
Nb	25.1	18.5	19.1	18.5	18.8	18.9	19.7	19.5	29.7	
Hf	3.03	2.94	2.55	-	-	-	2.71	-	-	
Ta	1.32	0.96	1.28	-	-	-	1.06	-	-	
Th	1.68	1.12	1.09	-	-	-	1.16	-	-	
U	0.4	0.41	0.35	-	-	-	0.37	-	-	
Pb	1.83	1.03	1.08	-	-	-	1.14	-	-	
La	16	11.94	11.58	-	-	-	12.46	-	-	
Ce	35.17	27.26	26.08	-	-	-	27.94	-	-	
Pr	4.64	3.69	3.53	-	-	-	3.77	-	-	
Nd	19.87	17.17	15.67	-	-	-	16.94	-	-	
Sm	5.1	4.35	4.22	-	-	-	4.8	-	-	
Eu	1.68	1.56	1.42	-	-	-	1.54	-	-	
Gd	4.96	4.61	4.3	-	-	-	4.59	-	-	
Tb	0.72	0.71	0.63	-	-	-	0.69	-	-	
Dy	4.07	4.01	3.58	-	-	-	3.85	-	-	
Ho	0.77	0.73	0.68	-	-	-	0.72	-	-	
Er	1.93	1.86	1.68	-	-	-	1.79	-	-	
Tm	0.24	0.23	0.2	-	-	-	0.22	-	-	
Yb	1.62	1.42	1.36	-	-	-	1.48	-	-	
Lu	0.22	0.2	0.19	-	-	-	0.19	-	-	
⁸⁷ Sr/ ⁸⁶ Sr	-	0.702997	-	-	-	-	-	-	-	
¹⁴³ Nd/ ¹⁴⁴ Nd	-	0.513032	-	-	-	-	-	-	-	
²⁰⁶ Pb/ ²⁰⁴ Pb	-	19.094	-	-	-	-	-	-	-	
²⁰⁷ Pb/ ²⁰⁴ Pb	-	15.56	-	-	-	-	-	-	-	
²⁰⁸ Pb/ ²⁰⁴ Pb	-	38.434	-	-	-	-	-	-	-	

Major elements in wt.%, trace elements in ppm.

Table B-3: Whole rock analyses of Kawdy Mountain volcanic samples (cont'd)

Sample Rock type	KM-11 Hy-NORM	KM-15 Hy-NORM	KM-14 Hy-NORM	KM-13 AOB	KM-12 AOB	KM-22 AOB	KM-21 Hy-NORM	KM-20 AOB	KM-19 Hy-NORM
SiO ₂	47.64	47.62	47.77	48.22	47.92	46.55	47.3	47.71	47.71
TiO ₂	2.39	2.44	2.48	2.55	2.5	2.21	2.55	2.69	2.53
Al ₂ O ₃	15.09	15.08	15.25	15.64	15.44	13.99	15.24	15.33	15.34
Fe ₂ O ₃ T	13.02	13.1	13.05	12.9	13.07	14.83	12.76	12.68	12.71
MnO	0.17	0.17	0.17	0.17	0.17	0.18	0.17	0.17	0.17
MgO	7.55	6.91	6.59	5.93	6.47	8.49	5.87	5.08	5.89
CaO	9.67	9.97	10.21	10.11	10.19	8.93	10.08	10.35	10.23
Na ₂ O	3.03	3.03	2.94	3.41	3.28	3.19	2.98	3.24	2.92
K ₂ O	1.01	0.99	0.93	1.1	1.03	0.85	1.18	1.22	1.12
P ₂ O ₅	0.37	0.41	0.41	0.43	0.42	0.35	0.43	0.46	0.43
LOI	0.41	0.75	0.87	-	0.28	1.33	1.85	1.3	1.2
Total	100.35	100.47	100.67	100.46	100.77	100.9	100.41	100.23	100.25
Rb	15.1	9.7	8.1	14.3	14	10	12.3	15.3	10.5
Cs	0.2	-	-	-	-	0.08	-	-	-
Sr	640.4	644.6	638.7	637.5	602.1	625.8	804.4	842	841.5
Ba	372.4	416.1	397.9	400.1	419.1	215.2	558	421.9	419.1
Sc	16	24	26	25	21	25	20	25	21
V	241	233	236	240	247	246	243	265	234
Cr	242.2	220.3	208	177.9	187.5	262.7	190.2	153.3	178.6
Co	48	50	48	43	45	56	39	32	38
Ni	91	73	66	48	57	184	47	28	82
Zn	127	127	125	128	129	146	126	132	127
Cu	52	48	55	48	55	70	47	61	52
Ga	22.9	21.4	22.1	22.7	23	21.5	21.1	22.7	22.5
Y	19.3	20.7	20.6	21.9	21.2	18	20.9	23.1	20.7
Zr	148.5	166.6	165	172.8	170.6	131	172.4	185.6	168.1
Nb	26.6	29.4	28.6	30	29.2	22	30.3	32.8	29.5
Hf	3.11	-	-	-	-	2.83	-	-	-
Ta	1.44	-	-	-	-	1.2	-	-	-
Th	1.64	-	-	-	-	1.35	-	-	-
U	0.45	-	-	-	-	0.43	-	-	-
Pb	1.67	-	-	-	-	1.17	-	-	-
La	16.12	-	-	-	-	14.21	-	-	-
Ce	35.44	-	-	-	-	31.87	-	-	-
Pr	4.67	-	-	-	-	4.2	-	-	-
Nd	20.04	-	-	-	-	18.25	-	-	-
Sm	4.99	-	-	-	-	4.73	-	-	-
Eu	1.66	-	-	-	-	1.57	-	-	-
Gd	4.65	-	-	-	-	4.46	-	-	-
Tb	0.68	-	-	-	-	0.66	-	-	-
Dy	3.66	-	-	-	-	3.66	-	-	-
Ho	0.7	-	-	-	-	0.68	-	-	-
Er	1.7	-	-	-	-	1.64	-	-	-
Tm	0.2	-	-	-	-	0.2	-	-	-
Yb	1.33	-	-	-	-	1.3	-	-	-
Lu	0.17	-	-	-	-	0.18	-	-	-
⁸⁷ Sr/ ⁸⁶ Sr	-	-	-	-	-	0.702999	-	-	-
¹⁴³ Nd/ ¹⁴⁴ Nd	-	-	-	-	-	0.513011	-	-	-
²⁰⁶ Pb/ ²⁰⁴ Pb	-	-	-	-	-	19.031	-	-	-
²⁰⁷ Pb/ ²⁰⁴ Pb	-	-	-	-	-	15.528	-	-	-
²⁰⁸ Pb/ ²⁰⁴ Pb	-	-	-	-	-	38.282	-	-	-

Major elements in wt.%, trace elements in ppm.

Table B-3: Whole rock analyses of Kawdy Mountain volcanic samples (cont'd)

Sample	KM-18	KM-17
Rock type	Hy-NORM	Hy-NORM
SiO ₂	47.64	47.28
TiO ₂	2.63	2.59
Al ₂ O ₃	14.95	14.77
Fe ₂ O ₃	12.84	13.03
MnO	0.17	0.17
MgO	6.4	6.98
CaO	10.23	10.05
Na ₂ O	2.9	2.88
K ₂ O	1.16	1.12
P ₂ O ₅	0.45	0.44
LOI	1.03	1.05
Total	100.4	100.36
Rb	10.8	10.6
Cs	0.09	0.08
Sr	690.6	744.6
Ba	402.3	397.9
Sc	25	16
V	256	269
Cr	200.5	218.3
Co	46	43
Ni	71	70
Zn	128	121
Cu	40	41
Ga	21.2	20.6
Y	20.3	20.6
Zr	175.7	175.9
Nb	31.8	31.9
Hf	3.61	3.55
Ta	1.75	1.72
Th	2.07	2.02
U	0.63	0.53
Pb	1.72	1.88
La	19.72	19.39
Ce	43.04	42.18
Pr	5.6	5.53
Nd	23.76	23.45
Sm	5.73	5.78
Eu	1.89	1.87
Gd	5.28	5.21
Tb	0.75	0.75
Dy	4.12	4.07
Ho	0.76	0.75
Er	1.84	1.83
Tm	0.22	0.22
Yb	1.46	1.4
Lu	0.19	0.19
⁸⁷ Sr/ ⁸⁶ Sr	-	0.703198
¹⁴³ Nd/ ¹⁴⁴ Nd	-	0.513035
²⁰⁶ Pb/ ²⁰⁴ Pb	-	19.05
²⁰⁷ Pb/ ²⁰⁴ Pb	-	15.571
²⁰⁸ Pb/ ²⁰⁴ Pb	-	38.489

Major elements in wt.%, trace elements in ppm.

Table B-4: Whole rock analyses of Metahag Mountain volcanic samples

Sample Rock type	MH-23 AOB	MH-22 AOB	MH-21 AOB	MH-19 Hy-NORM	MH-18 AOB	MH-17 AOB	MH-14 Hy-NORM	MH-13 Hy-NORM	MH-12 Hy-NORM
SiO ₂	46.25	46.06	46.7	46.02	47.71	46.85	47.69	48.22	47.49
TiO ₂	2.63	2.4	2.6	1.87	2.43	1.98	1.9	2.06	1.87
Al ₂ O ₃	14.7	13.46	14.6	11.94	15.04	12.76	13.62	14.35	13.23
Fe ₂ O ₃ T	14.19	14.48	14.1	15.04	13.32	14.5	13.95	13.39	14.17
MnO	0.18	0.18	0.17	0.19	0.17	0.18	0.18	0.17	0.18
MgO	7.28	9.98	7.33	13.89	5.96	12.17	10.57	8.29	11.2
CaO	10.53	9.64	10.38	8.29	10.23	8.82	8.88	9.52	8.68
Na ₂ O	2.68	2.57	2.86	2.41	3.35	2.81	2.91	2.92	2.94
K ₂ O	1	0.93	1.02	0.73	0.98	0.77	0.78	0.86	0.75
P ₂ O ₅	0.51	0.47	0.51	0.35	0.45	0.37	0.34	0.36	0.32
LOI	0.54	0.25	0.34	-	0.18	-	-	0.26	-
Total	100.49	100.43	100.62	100.72	99.82	101.21	100.82	100.41	100.83
Rb	25.7	17.2	20.2	13	20.2	15.2	11.1	14.9	12.8
Cs	0.29	0.18	-	0.12	-	0.19	-	0.23	0.18
Sr	644.1	605.9	632.1	475.7	586.3	494.7	494.2	507.8	479.1
Ba	395	363.7	394.3	278.5	387	310.5	330.2	359.3	307.6
Sc	17	24	27	16	25	16	25	21	24
V	254	221	256	205	254	199	203	216	204
Cr	247.7	268.2	209.4	340	236	275.7	291.5	331.2	312.7
Co	48	60	44	80	44	68	64	54	62
Ni	107	212	117	346	68	286	218	493	242
Zn	136	140	132	135	132	128	128	133	132
Cu	77	65	55	61	68	41	64	70	70
Ga	22.9	22.6	22.8	18.8	22.4	19.2	20.7	20.8	19.9
Y	23	22.3	22.7	18.3	23.2	19.2	18.9	21.3	18.6
Zr	150.3	142.9	150.4	112.6	145.3	119.7	115.9	125.2	112
Nb	33.7	32.3	33.3	23.6	29.8	24.5	22.5	24.2	21.6
Hf	3.21	3.05	-	2.4	-	2.54	-	2.72	2.4
Ta	1.75	1.64	-	1.22	-	1.22	-	1.21	1.09
Th	2.17	2.03	-	1.65	-	1.71	-	1.8	1.44
U	0.57	0.73	-	0.38	-	0.36	-	0.53	0.37
Pb	1.69	1.56	-	1.39	-	1.44	-	1.73	1.74
La	21.7	20.48	-	15.45	-	15.92	-	16.21	14.29
Ce	46.44	43.76	-	33.46	-	34.16	-	34.95	31.13
Pr	6	5.59	-	4.27	-	4.34	-	4.52	4
Nd	25.93	24.13	-	17.9	-	18.64	-	19.24	17.44
Sm	6.26	5.7	-	4.49	-	4.65	-	4.86	4.45
Eu	1.98	1.86	-	1.47	-	1.52	-	1.57	1.46
Gd	5.78	5.13	-	4.2	-	4.35	-	4.61	4.2
Tb	0.81	0.76	-	0.6	-	0.64	-	0.68	0.61
Dy	4.53	4.19	-	3.41	-	3.55	-	3.95	3.47
Ho	0.81	0.76	-	0.65	-	0.67	-	0.76	0.67
Er	1.96	1.86	-	1.56	-	1.64	-	1.87	1.63
Tm	0.24	0.23	-	0.2	-	0.19	-	0.23	0.2
Yb	1.55	1.47	-	1.21	-	1.29	-	1.5	1.32
Lu	0.21	0.18	-	0.17	-	0.17	-	0.2	0.18
⁸⁷ Sr/ ⁸⁶ Sr	0.703023	-	-	0.703089	-	-	-	-	-
¹⁴³ Nd/ ¹⁴⁴ Nd	0.513018	-	-	0.512996	-	-	-	-	-
²⁰⁶ Pb/ ²⁰⁴ Pb	18.935	-	-	18.964	-	-	-	-	-
²⁰⁷ Pb/ ²⁰⁴ Pb	15.536	-	-	15.56	-	-	-	-	-
²⁰⁸ Pb/ ²⁰⁴ Pb	38.267	-	-	38.377	-	-	-	-	-

Major elements in wt.%, trace elements in ppm.

Table B-4: Whole rock analyses of Metahag Mountain volcanic samples (cont'd)

Sample Rock type	MH-11 Hy-NORM	MH-10 Hy-NORM	MH-9 Hy-NORM	MH-8 Hy-NORM	MH-7 Hy-NORM	MH-6 Hy-NORM	MH-5 Hy-NORM	MH-4 Hy-NORM	MH-3 Hy-NORM
SiO ₂	49.01	47.92	48.73	49.08	48.56	49.89	49.29	49.23	48.35
TiO ₂	2.15	1.89	2.02	2.08	1.91	2.18	2.23	2.22	2.24
Al ₂ O ₃	15.29	13.55	15.08	15.19	14.66	15.65	15.43	15.37	15.24
Fe ₂ O ₃ ^T	12.81	13.86	12.87	12.63	13.12	12.4	12.6	12.48	12.47
MnO	0.17	0.17	0.17	0.17	0.17	0.16	0.16	0.16	0.15
MgO	6.61	10.35	7.39	6.59	8.67	6	5.8	5.82	5.97
CaO	10.13	8.92	9.79	9.87	9.39	10.15	9.94	9.86	10
Na ₂ O	3.16	2.9	3.06	3.06	2.85	3.33	3.17	3.18	3.18
K ₂ O	0.9	0.75	0.84	0.94	0.89	0.94	1.08	1.03	0.99
P ₂ O ₅	0.37	0.32	0.34	0.35	0.32	0.37	0.39	0.39	0.41
LOI	0.03	-	0.08	0.16	0.04	-	0.71	0.52	1.57
Total	100.63	100.63	100.37	100.11	100.59	101.07	100.8	100.26	100.57
Rb	14.9	11.7	15.4	17.3	19.5	12.7	20.3	20.2	17.5
Cs	-	0.1	-	-	0.25	0.16	-	-	-
Sr	544.7	464	515.9	516.2	499.3	562.4	561.3	557.5	596.7
Ba	367.4	299.6	345.5	354.2	312	392.1	402.3	411	400.1
Sc	32	14	27	23	19	22	23	17	22
V	237	214	212	219	207	232	226	234	225
Cr	257.3	315.4	265.5	245.6	285.3	247.7	217.6	231.9	218.3
Co	42	66	51	48	49	36	40	36	29
Ni	86	200	108	74	139	43	52	51	43
Zn	127	129	125	126	125	119	124	131	122
Cu	43	59	57	52	52	38	48	47	46
Ga	21.8	20.5	21.2	21.7	20.2	22.2	22.3	21.5	22.1
Y	21.9	19.2	20.7	21.2	19.7	20	21.8	21.5	21.2
Zr	129.4	109.4	118.3	122.6	109.6	132	136.6	135.6	139
Nb	24.6	20.4	22.1	22.8	20.7	25	26.4	25.7	28.3
Hf	-	2.32	-	-	2.37	2.82	-	-	-
Ta	-	1.03	-	-	1.01	1.28	-	-	-
Th	-	1.35	-	-	1.41	1.73	-	-	-
U	-	0.49	-	-	0.42	0.7	-	-	-
Pb	-	1.42	-	-	1.43	1.76	-	-	-
La	-	13.63	-	-	14.1	15.64	-	-	-
Ce	-	29.36	-	-	30.13	34.74	-	-	-
Pr	-	3.8	-	-	3.94	4.52	-	-	-
Nd	-	16.55	-	-	16.95	19.32	-	-	-
Sm	-	4.25	-	-	4.31	4.92	-	-	-
Eu	-	1.42	-	-	1.45	1.67	-	-	-
Gd	-	4.12	-	-	4.17	4.66	-	-	-
Tb	-	0.61	-	-	0.62	0.69	-	-	-
Dy	-	3.46	-	-	3.55	3.92	-	-	-
Ho	-	0.66	-	-	0.69	0.73	-	-	-
Er	-	1.63	-	-	1.68	1.78	-	-	-
Tm	-	0.2	-	-	0.21	0.22	-	-	-
Yb	-	1.34	-	-	1.38	1.47	-	-	-
Lu	-	0.18	-	-	0.18	0.2	-	-	-
⁸⁷ Sr/ ⁸⁶ Sr	-	0.703219	-	-	-	-	-	-	-
¹⁴³ Nd/ ¹⁴⁴ Nd	-	0.512976	-	-	-	-	-	-	-
²⁰⁶ Pb/ ²⁰⁴ Pb	-	19.016	-	-	-	-	-	-	-
²⁰⁷ Pb/ ²⁰⁴ Pb	-	15.587	-	-	-	-	-	-	-
²⁰⁸ Pb/ ²⁰⁴ Pb	-	38.509	-	-	-	-	-	-	-

Major elements in wt.%, trace elements in ppm.

Table B-4: Whole rock analyses of Metahag Mountain samples (cont'd)

Sample	MH-2
Rock type	Hy-NORM
SiO ₂	49.14
TiO ₂	2.3
Al ₂ O ₃	15.54
Fe ₂ O ₃ ^T	12.55
MnO	0.16
MgO	5.74
CaO	10.01
Na ₂ O	3.34
K ₂ O	1.06
P ₂ O ₅	0.41
LOI	0.27
Total	100.52
Rb	19.5
Cs	-
Sr	602.3
Ba	427.8
Sc	16
V	236
Cr	226.5
Co	42
Ni	35
Zn	122
Cu	31
Ga	22.4
Y	21.4
Zr	143.9
Nb	28.6
Hf	-
Ta	-
Th	-
U	-
Pb	-
La	-
Ce	-
Pr	-
Nd	-
Sm	-
Eu	-
Gd	-
Tb	-
Dy	-
Ho	-
Er	-
Tm	-
Yb	-
Lu	-
⁸⁷ Sr/ ⁸⁶ Sr	-
¹⁴³ Nd/ ¹⁴⁴ Nd	-
²⁰⁶ Pb/ ²⁰⁴ Pb	-
²⁰⁷ Pb/ ²⁰⁴ Pb	-
²⁰⁸ Pb/ ²⁰⁴ Pb	-

Major elements in wt.%, trace elements in ppm.

Table B-5: Whole rock analyses of Metah Mountain volcanic samples

Sample Rock type	MM-40 Hy-NORM	MM-39 Hy-NORM	MM-37 AOB	MM-36 AOB	MM-34 AOB	MM-33 AOB	MM-31 AOB	MM-28 AOB	MM-27 AOB
SiO ₂	48.14	48.18	46.27	45.87	45.87	45.7	45.85	45.63	47.39
TiO ₂	1.86	1.86	2.61	2.59	2.58	2.57	2.58	2.59	2.32
Al ₂ O ₃	14.05	14.09	13.95	13.91	13.89	13.85	13.74	13.73	13.87
Fe ₂ O ₃ T	12.65	13.23	14.5	14.47	14.47	14.44	14.45	14.45	14.33
MnO	0.17	0.16	0.19	0.19	0.19	0.19	0.18	0.19	0.18
MgO	9.44	9	9.11	9.09	9.19	9.16	9.34	9.14	8.76
CaO	8.72	8.77	9.87	9.92	9.84	9.9	10	10.22	9.4
Na ₂ O	2.92	3.03	3.08	2.93	2.88	2.9	2.78	2.65	3.05
K ₂ O	1.07	1.06	1.03	1.05	1.01	0.98	0.85	0.91	0.83
P ₂ O ₅	0.35	0.35	0.45	0.46	0.46	0.46	0.46	0.45	0.35
LOI	0.97	0.78	-	0.1	0.22	0.37	0.92	0.65	0.02
Total	100.34	100.51	101.06	100.58	100.59	100.51	101.15	100.62	100.49
Rb	14	14	17.7	17.3	16.9	14.6	11.8	11.4	14.1
Cs	0.14	-	0.18	-	-	0.18	-	0.09	-
Sr	567.2	536.7	612	617.4	607.9	623.4	739.6	743.6	476.2
Ba	350.6	354.9	362.2	347	349.2	353.5	327.3	318.6	283.6
Sc	23	19	14	31	16	25	19	23	26
V	199	198	235	242	236	231	242	239	226
Cr	343.5	347.6	261.4	259.3	257.9	262	272.3	286	271.6
Co	-	-	-	-	-	-	-	-	-
Ni	215	214	189	190	199	194	194	185	169
Zn	-	-	-	-	-	-	-	-	-
Cu	-	-	-	-	-	-	-	-	-
Ga	21	20.7	21.5	22	21.4	21.4	21.7	21.2	20.8
Y	18.2	18.4	22.2	22.3	22	22.4	21.2	21.6	21.6
Zr	128	129.3	163.2	163.1	161.2	161.4	153.3	144.7	118.1
Nb	23.3	23.6	33	32.6	32.3	32.7	31.5	30.2	22.8
Hf	2.9	-	3.78	-	-	3.44	-	3.29	-
Ta	1.42	-	2.02	-	-	1.87	-	1.97	-
Th	2.14	-	2.55	-	-	2.38	-	1.96	-
U	0.72	-	0.81	-	-	0.75	-	0.62	-
Pb	2.15	-	1.86	-	-	1.57	-	1.43	-
La	18.65	-	25.69	-	-	24.21	-	21.29	-
Ce	38.04	-	53.38	-	-	49.82	-	45.04	-
Pr	4.74	-	6.66	-	-	6.2	-	5.67	-
Nd	19.89	-	27.82	-	-	25.73	-	23.95	-
Sm	4.72	-	6.48	-	-	6.13	-	5.78	-
Eu	1.5	-	2.18	-	-	2	-	1.9	-
Gd	4.35	-	5.77	-	-	5.77	-	5.44	-
Tb	0.67	-	0.87	-	-	0.83	-	0.79	-
Dy	3.67	-	4.94	-	-	4.37	-	4.3	-
Ho	0.68	-	0.9	-	-	0.82	-	0.79	-
Er	1.68	-	2.14	-	-	1.94	-	1.89	-
Tm	0.21	-	0.25	-	-	0.23	-	0.22	-
Yb	1.37	-	1.63	-	-	1.48	-	1.42	-
Lu	0.18	-	0.22	-	-	0.2	-	0.2	-
⁸⁷ Sr/ ⁸⁶ Sr	0.703244	-	0.703003	-	-	-	-	-	-
¹⁴³ Nd/ ¹⁴⁴ Nd	0.512964	-	0.51305	-	-	-	-	-	-
²⁰⁶ Pb/ ²⁰⁴ Pb	19.007	-	18.993	-	-	-	-	-	-
²⁰⁷ Pb/ ²⁰⁴ Pb	15.597	-	15.542	-	-	-	-	-	-
²⁰⁸ Pb/ ²⁰⁴ Pb	38.535	-	38.327	-	-	-	-	-	-

Major elements in wt.%, trace elements in ppm.

Table B-5: Whole rock analyses of Metah Mountain volcanic samples (cont'd)

Sample Rock type	MM-26 AOB	MM-21 Hy-NORM	MM-24 AOB	MM-20 AOB	MM-18 Hy-NORM	MM-17 AOB	MM-15 AOB	MM-13 AOB	MM-12 AOB
SiO ₂	46	49.23	47.51	48.82	49.16	48.35	48.24	47.92	48.35
TiO ₂	2.6	2.35	2.32	2.44	2.34	2.35	2.39	2.35	2.47
Al ₂ O ₃	13.77	14.63	14.02	14.67	14.76	14.77	14.8	14.89	14.89
Fe ₂ O ₃ T	14.53	13.43	14.33	13.74	13.59	13.83	13.85	13.85	13.73
MnO	0.19	0.17	0.18	0.18	0.18	0.18	0.18	0.18	0.18
MgO	9.33	6.76	8.82	6.76	7	7.18	7.03	7.05	6.61
CaO	10.08	9.2	9.44	9.32	9.55	9.45	9.47	9.77	9.66
Na ₂ O	2.77	3.59	3.1	3.74	3.44	3.58	3.65	3.41	3.61
K ₂ O	0.93	0.97	0.76	1	0.88	0.9	0.91	0.82	0.93
P ₂ O ₅	0.46	0.44	0.34	0.45	0.41	0.4	0.41	0.36	0.42
LOI	0.42	-	-	-	-	-	-	-	-
Total	101.06	100.77	100.83	101.11	101.31	100.99	100.94	100.6	100.85
Rb	12.8	15.1	10.5	14.5	12.5	14.7	14.9	13.9	15.8
Cs	-	-	0.12	-	0.11	-	0.06	-	-
Sr	688.5	583.3	481.8	588.1	592.8	592.6	601.3	623.7	619.5
Ba	344	380.5	280	386.2	338.9	351.3	345.5	330.9	349.2
Sc	24	12	23	19	22	25	18	15	24
V	241	208	231	219	221	230	225	232	224
Cr	273.7	231.3	280.5	213.5	252.5	244.9	247	262.7	226.5
Co	-	-	-	-	-	-	-	-	-
Ni	197	90	165	82	86	95	87	81	71
Zn	-	-	-	-	-	-	-	-	-
Cu	-	-	-	-	-	-	-	-	-
Ga	21	21.8	21.3	21.9	22.2	22.6	21.8	23.2	22.9
Y	21.4	22.7	21.6	24	21.6	21.8	22.1	20.5	23.4
Zr	154.3	142.6	118.1	149	129.8	129.6	129.8	113.6	132.7
Nb	31.6	29.1	22.5	29.8	27.1	26.1	25.8	22.1	25.4
Hf	-	-	2.74	-	3.02	-	3.1	-	-
Ta	-	-	1.28	-	1.48	-	1.55	-	-
Th	-	-	1.43	-	1.86	-	1.83	-	-
U	-	-	0.46	-	0.57	-	0.43	-	-
Pb	-	-	1.21	-	1.08	-	1.42	-	-
La	-	-	14.7	-	18.74	-	18.95	-	-
Ce	-	-	31.91	-	40.12	-	40.94	-	-
Pr	-	-	4.16	-	5.21	-	5.27	-	-
Nd	-	-	18.34	-	22.27	-	23.2	-	-
Sm	-	-	4.84	-	5.78	-	5.93	-	-
Eu	-	-	1.62	-	1.87	-	1.93	-	-
Gd	-	-	4.79	-	5.09	-	5.28	-	-
Tb	-	-	0.72	-	0.8	-	0.82	-	-
Dy	-	-	3.95	-	4.38	-	4.43	-	-
Ho	-	-	0.76	-	0.82	-	0.83	-	-
Er	-	-	1.8	-	1.99	-	2.02	-	-
Tm	-	-	0.23	-	0.24	-	0.24	-	-
Yb	-	-	1.48	-	1.54	-	1.6	-	-
Lu	-	-	0.2	-	0.2	-	0.21	-	-
⁸⁷ Sr/ ⁸⁶ Sr	-	-	0.702977	-	-	-	-	-	-
¹⁴³ Nd/ ¹⁴⁴ Nd	-	-	0.513046	-	-	-	-	-	-
²⁰⁶ Pb/ ²⁰⁴ Pb	-	-	19.036	-	-	-	-	-	-
²⁰⁷ Pb/ ²⁰⁴ Pb	-	-	15.573	-	-	-	-	-	-
²⁰⁸ Pb/ ²⁰⁴ Pb	-	-	38.458	-	-	-	-	-	-

Major elements in wt.%, trace elements in ppm.

Table B-5: Whole rock analyses of Metah Mountain volcanic samples (cont'd)

Sample Rock type	MM-11 AOB	MM-10 AOB	MM-8 AOB	MM-9 AOB	MM-6 AOB	MM-3 AOB	MM-2 AOB	MM-1 Hy-NORM
SiO ₂	47.99	47.96	45.63	46.85	47.11	46.77	46.55	46.64
TiO ₂	2.53	2.11	2.15	2.5	3	2.9	2.94	2.76
Al ₂ O ₃	14.7	15.29	11.87	14.13	15.81	15.07	14.9	15.02
Fe ₂ O ₃ T	14.33	13.24	14.51	13.08	13.17	13.57	13.28	13.54
MnO	0.18	0.17	0.18	0.17	0.16	0.17	0.16	0.17
MgO	7.01	7.6	13.19	6.71	5.55	6.53	6.4	6.42
CaO	9.62	9.7	8.62	10.15	10.76	10.31	10.71	9.95
Na ₂ O	3.45	3.31	2.44	3.08	3.08	2.93	2.64	2.9
K ₂ O	0.85	0.78	0.84	1	1.26	1.22	1.32	1.09
P ₂ O ₅	0.36	0.35	0.38	0.42	0.49	0.46	0.48	0.45
LOI	-	-	1.45	2.44	0.61	0.92	1.62	1.43
Total	101.02	100.51	101.27		101.01	100.85	101.01	100.36
Rb	14.4	12.5	12.4	14.6	15.1	18.1	19.6	18.7
Cs	-	-	0.2	-	0.11	-	-	-
Sr	617.8	635.4	450.5	528.1	659.1	595.9	652.2	600.2
Ba	325.8	296.7	358.6	629.6	494	461.3	475.8	445.3
Sc	20	25	23	27	17	23	27	18
V	242	210	212	246	278	273	277	257
Cr	232.6	280.5	340.7	266.2	119.7	147.1	195	169.7
Co	-	-	-	-	-	-	-	-
Ni	84	105	345	107	31	54	47	62
Zn	-	-	-	-	-	-	-	-
Cu	-	-	-	-	-	-	-	-
Ga	22.8	23.1	18.3	20.9	23.6	22.6	22.4	22
Y	21.3	19.9	18.5	21.7	22	21.1	21	21.4
Zr	121.8	109.9	114.5	134.7	155.6	150.3	156.8	146.9
Nb	23.2	22.1	28.1	31.6	35.2	32.6	35.9	32.5
Hf	-	-	2.8	-	3.93	-	-	-
Ta	-	-	1.64	-	2.23	-	-	-
Th	-	-	2.2	-	2.66	-	-	-
U	-	-	0.5	-	1.02	-	-	-
Pb	-	-	1.84	-	2.21	-	-	-
La	-	-	17.75	-	23.37	-	-	-
Ce	-	-	37.68	-	50.26	-	-	-
Pr	-	-	4.8	-	6.52	-	-	-
Nd	-	-	20.45	-	27.94	-	-	-
Sm	-	-	5.01	-	6.67	-	-	-
Eu	-	-	1.66	-	2.26	-	-	-
Gd	-	-	4.55	-	5.94	-	-	-
Tb	-	-	0.68	-	0.89	-	-	-
Dy	-	-	3.88	-	5.03	-	-	-
Ho	-	-	0.71	-	0.92	-	-	-
Er	-	-	1.72	-	2.17	-	-	-
Tm	-	-	0.21	-	0.26	-	-	-
Yb	-	-	1.37	-	1.68	-	-	-
Lu	-	-	0.19	-	0.24	-	-	-
⁸⁷ Sr/ ⁸⁶ Sr	-	-	-	-	-	-	-	-
¹⁴³ Nd/ ¹⁴⁴ Nd	-	-	-	-	-	-	-	-
²⁰⁶ Pb/ ²⁰⁴ Pb	-	-	-	-	-	-	-	-
²⁰⁷ Pb/ ²⁰⁴ Pb	-	-	-	-	-	-	-	-
²⁰⁸ Pb/ ²⁰⁴ Pb	-	-	-	-	-	-	-	-

Major elements in wt.%, trace elements in ppm.

Table B-6: Whole rock analyses of Tuya Butte volcanic samples

Sample Rock type	TB-31	TB-29	TB-18	TB-19	TB-20	TB-21	TB-22	TB-15	TB-23
	Hy-NORM	Hy-NORM	Hy-NORM	Hy-NORM	Hy-NORM	Hy-NORM	Hy-NORM	Hy-NORM	Hy-NORM
SiO ₂	49.44	50.49	48.88	48.97	49.8	49.53	49.63	48.71	49.7
TiO ₂	1.66	1.7	2.07	2.07	2.2	2.1	2.2	2.11	2.23
Al ₂ O ₃	13.9	14.73	14.44	14.5	15.47	14.66	15.48	14.31	15.68
Fe ₂ O ₃	13.9	13.45	13.61	13.43	12.98	13.65	13	14.08	13.01
MnO	0.18	0.17	0.16	0.16	0.17	0.18	0.17	0.17	0.17
MgO	8.26	7.41	7.08	6.95	5.84	6.82	5.81	7.71	5.67
CaO	8.55	8.93	9.03	8.92	9.43	9.19	9.38	8.84	9.38
Na ₂ O	2.89	3.12	3.4	3.47	3.48	3.59	3.5	3.36	3.65
K ₂ O	0.69	0.72	1.01	1.04	1.15	1.06	1.12	1.12	1.07
P ₂ O ₅	0.27	0.26	0.51	0.51	0.44	0.51	0.43	0.52	0.43
LOI	1.07	-	0.68	0.95	-	-	-	0.01	-
Total	100.81	100.98	100.88	100.97	100.98	101.29	100.73	100.94	101
Rb	12.4	13.1	16.3	16.9	18	17.4	17.9	16.8	15.1
Cs	0.21	0.21	-	-	-	-	-	-	-
Sr	341.8	330.8	573.5	568.8	535.5	587	531.9	634.1	542
Ba	213	211.5	322.2	317.9	333.1	320.7	331.7	328	351.3
Sc	20	14	23	19	25	20	23	17	24
V	178	183	201	193	211	207	219	198	220
Cr	283.9	286.7	270.3	275.7	205.3	264.1	220.3	291.5	181.3
Co	-	-	-	-	-	-	-	-	-
Ni	208	139	103	107	46	96	49	136	40
Zn	-	-	-	-	-	-	-	-	-
Cu	-	-	-	-	-	-	-	-	-
Ga	20.1	20.5	22.8	22.4	23.1	22.6	23	22.7	22.7
Y	21.1	25.3	22.1	22.2	22.3	22.4	22.3	21.2	23.3
Zr	120.3	110.4	169.9	169.6	176	172.4	174.2	175.8	181.2
Nb	17.1	15.2	28.1	28.2	25.5	28	25.7	29.2	26.6
Hf	2.89	2.94	-	-	-	-	-	-	-
Ta	1.22	0.97	-	-	-	-	-	-	-
Th	1.96	1.93	-	-	-	-	-	-	-
U	0.55	0.55	-	-	-	-	-	-	-
Pb	2.04	2.01	-	-	-	-	-	-	-
La	13.49	12.87	-	-	-	-	-	-	-
Ce	28.99	27.73	-	-	-	-	-	-	-
Pr	3.75	3.64	-	-	-	-	-	-	-
Nd	16.19	15.71	-	-	-	-	-	-	-
Sm	4.25	4.24	-	-	-	-	-	-	-
Eu	1.47	1.5	-	-	-	-	-	-	-
Gd	4.16	4.36	-	-	-	-	-	-	-
Tb	0.7	0.72	-	-	-	-	-	-	-
Dy	4.07	4.31	-	-	-	-	-	-	-
Ho	0.78	0.81	-	-	-	-	-	-	-
Er	1.99	2.09	-	-	-	-	-	-	-
Tm	0.25	0.27	-	-	-	-	-	-	-
Yb	1.7	1.83	-	-	-	-	-	-	-
Lu	0.24	0.24	-	-	-	-	-	-	-
⁸⁷ Sr/ ⁸⁶ Sr	0.703595	-	-	-	-	-	-	-	-
¹⁴³ Nd/ ¹⁴⁴ Nd	0.51294	-	-	-	-	-	-	-	-
²⁰⁶ Pb/ ²⁰⁴ Pb	19.242	-	-	-	-	-	-	-	-
²⁰⁷ Pb/ ²⁰⁴ Pb	15.63	-	-	-	-	-	-	-	-
²⁰⁸ Pb/ ²⁰⁴ Pb	38.889	-	-	-	-	-	-	-	-

Major elements in wt.%, trace elements in ppm.

Table B-6: Whole rock analyses of Tuya Butte volcanic samples (cont'd)

Sample Rock type	TB-14 Hy-NORM	TB-24 Hy-NORM	TB-25 Hy-NORM	TB-26 Hy-NORM	TB-13 Hy-NORM	TB-28 Hy-NORM	TB-12 Hy-NORM	TB-11 Hy-NORM	TB-10 Hy-NORM
SiO ₂	48.46	49.85	49.78	49.5	49.27	49.89	49.18	49.93	48.88
TiO ₂	2.12	2.18	2.22	2.12	2.18	2.26	2.09	2.01	2.09
Al ₂ O ₃	14.34	15.5	15.59	15.64	15.62	15.72	14.6	14.59	14.45
Fe ₂ O ₃ T	14.02	13.01	13.02	12.88	13.13	12.96	13.68	13.23	13.67
MnO	0.18	0.17	0.17	0.17	0.17	0.17	0.18	0.17	0.17
MgO	7.4	6.03	5.83	6.29	6.06	5.42	6.97	7.13	6.87
CaO	8.99	9.4	9.48	9.45	9.37	9.49	9.1	8.99	8.78
Na ₂ O	3.33	3.5	3.56	3.5	3.52	3.62	3.55	3.39	3.38
K ₂ O	1.13	1.07	1.09	1.01	1.03	1.08	1.03	1.01	1.07
P ₂ O ₅	0.51	0.42	0.43	0.4	0.41	0.43	0.51	0.44	0.51
LOI	0.16	-	-	-	-	-	-	-	0.88
Total	100.63	101.13	101.18	100.96	100.76	101.04	100.89	100.89	100.76
Rb	16.1	17.5	17.1	13.7	12.2	14.5	15.8	16.4	16.1
Cs	-	-	-	0.12	-	-	-	0.28	-
Sr	689.8	535.5	535.1	544.6	539	542.7	589.5	534	548.5
Ba	320	327.3	349.2	323.6	312.7	344	323.6	316.4	314.9
Sc	13	20	32	21	22	27	20	26	26
V	203	212	214	212	208	221	208	206	199
Cr	273	210.7	200.5	218.9	168.3	171	276.4	295.6	270.3
Co	-	-	-	-	-	-	-	-	-
Ni	127	45	42	56	52	40	102	99	106
Zn	-	-	-	-	-	-	-	-	-
Cu	-	-	-	-	-	-	-	-	-
Ga	22.8	23.5	23.2	23.7	24	24.3	22.9	23.1	22.3
Y	20.9	22.6	22.5	22.3	21.9	23.2	22.2	22.2	22.7
Zr	175.1	173.4	175.4	167.7	170.6	179.5	173.3	166.3	174.9
Nb	29.8	25.5	26.4	24.8	25.5	26.3	28	25.1	28.2
Hf	-	-	-	3.92	-	-	-	3.46	-
Ta	-	-	-	1.57	-	-	-	1.46	-
Th	-	-	-	2.83	-	-	-	2.94	-
U	-	-	-	1.34	-	-	-	0.69	-
Pb	-	-	-	2.68	-	-	-	2.73	-
La	-	-	-	21.76	-	-	-	22.88	-
Ce	-	-	-	45.8	-	-	-	47.8	-
Pr	-	-	-	5.73	-	-	-	5.87	-
Nd	-	-	-	24.27	-	-	-	24.74	-
Sm	-	-	-	5.83	-	-	-	5.83	-
Eu	-	-	-	1.97	-	-	-	1.92	-
Gd	-	-	-	5.25	-	-	-	5.56	-
Tb	-	-	-	0.8	-	-	-	0.8	-
Dy	-	-	-	4.69	-	-	-	4.35	-
Ho	-	-	-	0.87	-	-	-	0.81	-
Er	-	-	-	2.18	-	-	-	1.95	-
Tm	-	-	-	0.26	-	-	-	0.23	-
Yb	-	-	-	1.78	-	-	-	1.61	-
Lu	-	-	-	0.24	-	-	-	0.21	-
⁸⁷ Sr/ ⁸⁶ Sr	-	-	-	-	-	-	-	-	-
¹⁴³ Nd/ ¹⁴⁴ Nd	-	-	-	-	-	-	-	-	-
²⁰⁶ Pb/ ²⁰⁴ Pb	-	-	-	-	-	-	-	-	-
²⁰⁷ Pb/ ²⁰⁴ Pb	-	-	-	-	-	-	-	-	-
²⁰⁸ Pb/ ²⁰⁴ Pb	-	-	-	-	-	-	-	-	-

Major elements in wt.%, trace elements in ppm.

Table B-6: Whole rock analyses of Tuya Butte volcanic samples (cont'd)

Sample Rock type	TB-8 AOB	TB-6 Hy-NORM	TB-5 Hy-NORM	TB-4 Hy-NORM	TB-2 Hy-NORM	TB-1 Hy-NORM
SiO ₂	48.56	48.86	48.78	48.88	49.1	49.31
TiO ₂	2.03	2.14	2.16	1.96	1.92	1.99
Al ₂ O ₃	14.76	14.69	14.44	14.59	14.39	14.43
Fe ₂ O ₃ T	13.69	13.88	14.16	13.49	13.64	13.71
MnO	0.17	0.18	0.18	0.17	0.17	0.18
MgO	7.21	6.95	7.19	7.15	7.71	7.55
CaO	9.12	9.07	8.95	8.99	8.88	8.9
Na ₂ O	3.45	3.44	3.43	3.45	3.38	3.53
K ₂ O	1.1	1.1	1.16	0.97	0.96	0.96
P ₂ O ₅	0.48	0.52	0.53	0.47	0.46	0.46
LOI	-	-	-	-	-	-
Total	100.58	100.83	100.98	100.13	100.6	101.02
Rb	19.3	16.3	24.3	14.2	16.2	14.4
Cs	0.34	-	0.28	-	0.19	-
Sr	675.1	634.4	610.3	582.8	570.4	561.4
Ba	298.2	313.5	332.4	304.7	285.1	304
Sc	27	20	27	21	19	21
V	199	201	198	196	203	197
Cr	287.4	271.6	273	291.5	308.6	314.7
Co	-	-	-	-	-	-
Ni	119	106	121	107	127	123
Zn	-	-	-	-	-	-
Cu	-	-	-	-	-	-
Ga	22.9	22.8	24	23.5	22.2	23.4
Y	20.4	22.2	22.1	21.2	21.7	21.8
Zr	167.3	182.2	184.1	163	159.1	163.6
Nb	28.2	30.1	29.6	25.6	25.3	25.8
Hf	3.49	-	4.11	-	3.55	-
Ta	1.61	-	1.8	-	1.61	-
Th	2.81	-	3.02	-	2.7	-
U	0.58	-	0.66	-	0.67	-
Pb	2.43	-	2.69	-	2.47	-
La	24.65	-	27.68	-	24.13	-
Ce	51.67	-	57.06	-	49.34	-
Pr	6.25	-	7.02	-	6.1	-
Nd	26.24	-	28.99	-	25.23	-
Sm	6.07	-	6.7	-	5.95	-
Eu	1.97	-	2.18	-	1.95	-
Gd	5.53	-	6.09	-	5.44	-
Tb	0.79	-	0.89	-	0.82	-
Dy	4.32	-	4.81	-	4.52	-
Ho	0.76	-	0.87	-	0.82	-
Er	1.81	-	2.08	-	2.02	-
Tm	0.22	-	0.25	-	0.24	-
Yb	1.46	-	1.67	-	1.59	-
Lu	0.2	-	0.23	-	0.21	-
⁸⁷ Sr/ ⁸⁶ Sr	-	-	0.703272	-	0.703389	-
¹⁴³ Nd/ ¹⁴⁴ Nd	-	-	0.512889	-	0.51294	-
²⁰⁶ Pb/ ²⁰⁴ Pb	-	-	19.136	-	19.162	-
²⁰⁷ Pb/ ²⁰⁴ Pb	-	-	15.598	-	15.609	-
²⁰⁸ Pb/ ²⁰⁴ Pb	-	-	38.708	-	38.777	-

Major elements in wt.%, trace elements in ppm.

Table B-7: Whole rock analyses of Tanzilla Volcano samples

Sample Rock type	TV-37 Hy-NORM	TV-35 Hy-NORM	TV-34 Hy-NORM	TV-33 Hy-NORM	TV-31 Hy-NORM	TV-13 Hy-NORM	TV-29 Hy-NORM	TV-12 Hy-NORM	TV-28 AOB
SiO ₂	48.61	48.67	48.95	49.14	48.78	49.59	49.16	49.76	47.9
TiO ₂	1.71	1.72	1.83	1.82	1.73	1.81	1.76	2.04	1.93
Al ₂ O ₃	14.31	13.89	14.26	14.23	14.32	13.46	14.5	15.04	14.12
Fe ₂ O ₃ T	13.7	13.22	13.13	13.17	13.59	13.72	13	12.81	13.22
MnO	0.17	0.17	0.17	0.17	0.17	0.18	0.17	0.17	0.17
MgO	9.5	9.94	8.74	9.18	9.37	9.69	9.06	7.12	9.75
CaO	8.94	8.74	9.04	9.05	8.95	8.68	9.09	9.49	9.17
Na ₂ O	2.84	2.94	2.93	2.86	2.85	2.91	2.95	3.3	3.17
K ₂ O	0.63	0.81	0.87	0.92	0.7	0.78	0.84	0.97	0.86
P ₂ O ₅	0.25	0.29	0.31	0.31	0.27	0.29	0.3	0.36	0.36
LOI	0.12	-	0.14	0.16	-	0.05	0.01	-	-
Total	100.78	100.39	100.37	101.01	100.73	101.16	100.85	101.06	100.65
Rb	11.7	16.7	15.5	23.4	13.6	13.7	15.3	16.4	13.8
Cs	0.18	-	0.31	-	0.26	0.27	-	-	0.14
Sr	357.7	419.5	430.4	431	371.2	357.5	437.5	472.4	531.4
Ba	209.3	263.2	275.6	285.7	226.8	242.1	274.1	337.4	348.4
Sc	23	21	12	22	21	17	29	28	22
V	185	192	200	199	192	201	195	213	207
Cr	290.8	381.8	385.9	377	327.7	357.2	352.4	282.6	476.9
Co	-	-	-	-	-	-	-	-	-
Ni	267	266	240	226	300	266	206	131	204
Zn	-	-	-	-	-	-	-	-	-
Cu	-	-	-	-	-	-	-	-	-
Ga	19.8	19.4	19.9	20.2	19.9	19.6	19.7	22	20.2
Y	19.9	19.1	20.6	19.8	20.5	20.6	18.9	21.9	19
Zr	106.1	121.3	131	128.5	112.2	121.4	125.8	148.7	138.9
Nb	15.6	18.3	20.2	19.7	16.6	17.3	19	21.9	23
Hf	2.44	-	2.95	-	2.6	2.61	-	-	3.27
Ta	0.87	-	1.13	-	0.94	0.93	-	-	1.42
Th	1.35	-	1.81	-	1.47	1.49	-	-	1.9
U	0.56	-	0.76	-	0.59	0.66	-	-	0.64
Pb	1.61	-	2.12	-	1.76	1.89	-	-	2.01
La	11.77	-	16.01	-	13.7	13.45	-	-	17.64
Ce	24.98	-	33.71	-	28.02	28.32	-	-	38.01
Pr	3.26	-	4.29	-	3.64	3.61	-	-	4.91
Nd	13.99	-	18.31	-	15.57	15.57	-	-	20.86
Sm	3.79	-	4.62	-	4.12	4.08	-	-	5.11
Eu	1.33	-	1.55	-	1.41	1.38	-	-	1.69
Gd	3.83	-	4.41	-	4.13	4	-	-	4.67
Tb	0.61	-	0.68	-	0.67	0.65	-	-	0.69
Dy	3.69	-	4.01	-	3.89	3.76	-	-	3.93
Ho	0.7	-	0.76	-	0.75	0.73	-	-	0.72
Er	1.77	-	1.88	-	1.87	1.81	-	-	1.83
Tm	0.22	-	0.22	-	0.24	0.23	-	-	0.23
Yb	1.46	-	1.55	-	1.57	1.5	-	-	1.5
Lu	0.21	-	0.21	-	0.21	0.21	-	-	0.2
⁸⁷ Sr/ ⁸⁶ Sr	0.703401	-	-	-	-	-	-	-	-
¹⁴³ Nd/ ¹⁴⁴ Nd	0.512933	-	-	-	-	-	-	-	-
²⁰⁶ Pb/ ²⁰⁴ Pb	19.282	-	-	-	-	-	-	-	-
²⁰⁷ Pb/ ²⁰⁴ Pb	15.597	-	-	-	-	-	-	-	-
²⁰⁸ Pb/ ²⁰⁴ Pb	38.625	-	-	-	-	-	-	-	-

Major elements in wt.%, trace elements in ppm.

Table B-7: Whole rock analyses of Tanzilla volcano samples (cont'd)

Sample Rock type	TV-27 AOB	TV-26 Hy-NORM	TV-24 AOB	TV-23 AOB	TV-11 AOB	TV-20 AOB	TV-10 AOB	TV-8 AOB	TV-19 AOB
SiO ₂	48.56	49.42	48.82	49.33	48.78	49.08	48.52	48.69	48.48
TiO ₂	2.06	1.95	2.23	2.31	2.29	2.43	2.34	2.38	2.45
Al ₂ O ₃	14.68	15.29	15.14	15.54	16.33	16.07	16.29	16.72	16.13
Fe ₂ O ₃ T	12.96	12.4	12.81	12.48	12.09	12.43	12.32	12.25	12.56
MnO	0.17	0.16	0.17	0.17	0.16	0.17	0.16	0.16	0.16
MgO	8.52	7.22	7.15	6.03	5.62	5.35	5.73	5.33	6.09
CaO	9.55	9.65	9.77	10.03	10.19	10.18	10.27	10.06	10.21
Na ₂ O	3.32	3.18	3.38	3.57	3.54	3.56	3.39	3.57	3.53
K ₂ O	0.9	0.97	1.02	1.03	1.03	1.07	0.93	1.04	0.97
P ₂ O ₅	0.38	0.35	0.42	0.43	0.44	0.46	0.45	0.47	0.45
LOI	-	0.19	0.07	-	0.46	-	0.39	-	-
Total	101.11	100.78	100.97	100.92	100.93	100.79	100.78	100.68	101.03
Rb	13.7	19.6	19.2	16.5	18.1	18	17.2	18.2	15.2
Cs	0.11	0.33	0.33	-	-	-	-	-	-
Sr	551.4	505.5	557.9	587.7	642.6	640.1	653.8	678.5	648.6
Ba	389.9	332.4	405.2	428.5	418.3	437.2	404.4	425.6	378.3
Sc	23	18	21	30	24	22	13	32	32
V	203	215	229	230	229	238	227	228	239
Cr	398.2	290.8	302.4	223.7	179.3	170.4	214.2	154.6	171
Co	-	-	-	-	-	-	-	-	-
Ni	159	128	112	78	61	48	65	51	64
Zn	-	-	-	-	-	-	-	-	-
Cu	-	-	-	-	-	-	-	-	-
Ga	21.2	21.4	21.2	22.8	22.6	23.2	22.7	23.4	22.2
Y	20	20.9	21.5	22.2	21.6	22.6	21.8	22	22.2
Zr	147.6	141.8	162	168.9	167.6	178.5	170.4	177	177.2
Nb	24.4	22.6	27.2	27.6	27.8	29.1	28.8	29.6	28.2
Hf	3.11	3.13	3.51	-	-	-	-	-	-
Ta	1.34	1.28	1.54	-	-	-	-	-	-
Th	1.86	1.91	2.17	-	-	-	-	-	-
U	0.68	0.77	0.84	-	-	-	-	-	-
Pb	2.01	2.15	2.34	-	-	-	-	-	-
La	17.95	18.45	21.21	-	-	-	-	-	-
Ce	38.92	38.17	45.39	-	-	-	-	-	-
Pr	4.99	4.89	5.83	-	-	-	-	-	-
Nd	21.29	20.66	24.71	-	-	-	-	-	-
Sm	5.32	5.1	5.88	-	-	-	-	-	-
Eu	1.67	1.7	1.87	-	-	-	-	-	-
Gd	4.49	4.75	5.12	-	-	-	-	-	-
Tb	0.7	0.73	0.81	-	-	-	-	-	-
Dy	3.83	4.11	4.44	-	-	-	-	-	-
Ho	0.71	0.78	0.83	-	-	-	-	-	-
Er	1.76	1.92	2.03	-	-	-	-	-	-
Tm	0.22	0.23	0.25	-	-	-	-	-	-
Yb	1.42	1.59	1.61	-	-	-	-	-	-
Lu	0.18	0.21	0.22	-	-	-	-	-	-
⁸⁷ Sr/ ⁸⁶ Sr	-	-	0.703308	-	-	-	-	-	-
¹⁴³ Nd/ ¹⁴⁴ Nd	-	-	0.512945	-	-	-	-	-	-
²⁰⁶ Pb/ ²⁰⁴ Pb	-	-	19.203	-	-	-	-	-	-
²⁰⁷ Pb/ ²⁰⁴ Pb	-	-	15.59	-	-	-	-	-	-
²⁰⁸ Pb/ ²⁰⁴ Pb	-	-	38.572	-	-	-	-	-	-

Major elements in wt.%, trace elements in ppm.

Table B-7: Whole rock analyses of Tanzilla volcano samples (cont'd)

Sample Rock type	TV-18 AOB	TV-6 AOB	TV-16 AOB	TV-15 AOB	TV-5 AOB	TV-4 AOB	TV-3 AOB	TV-1 AOB
SiO ₂	48.69	48.05	48.41	48.76	48.24	48.41	48.67	48.43
TiO ₂	2.33	2.22	2.48	2.61	2.26	2.26	2.64	2.71
Al ₂ O ₃	17.02	16.91	16.63	16.28	16.7	16.72	15.81	15.77
Fe ₂ O ₃ T	12.12	12.24	12.55	12.77	12.2	12.12	13.01	13.12
MnO	0.16	0.16	0.17	0.17	0.16	0.16	0.17	0.17
MgO	5.51	6.41	5.34	4.9	6.24	6.06	5.52	5.39
CaO	10.05	9.96	9.94	9.98	9.96	10.06	10.27	10.23
Na ₂ O	3.52	3.38	3.72	3.7	3.72	3.7	3.54	3.52
K ₂ O	0.99	0.88	1.1	1.12	0.96	0.95	1.06	1.07
P ₂ O ₅	0.46	0.42	0.49	0.51	0.43	0.43	0.49	0.5
LOI	0.05	0.09	-	-	-	-	0.05	-
Total	100.89	100.72	100.83	100.79	100.87	100.88	101.24	100.92
Rb	16.6	14.8	18.1	18.3	15.3	14.5	15.7	16.2
Cs	-	-	-	0.18	0.2	-	-	-
Sr	689	677.8	673.7	660.1	658.4	662.6	628.3	636.9
Ba	408.8	370.2	434.4	460.5	361.5	365.9	409.6	428.5
Sc	20	17	23	17	19	20	22	18
V	216	221	240	248	213	216	250	268
Cr	170.4	163.5	145.1	140.9	177.2	188.8	120.4	123.8
Co	-	-	-	-	-	-	-	-
Ni	59	82	47	38	75	71	45	48
Zn	-	-	-	-	-	-	-	-
Cu	-	-	-	-	-	-	-	-
Ga	23.3	22.4	23.1	23.5	22.3	21.9	23.1	23.8
Y	21.7	20.5	22.8	23.8	20.7	20.9	24.3	24.5
Zr	174.1	160.9	186	196.8	164	165	191.6	197.5
Nb	28.8	26.5	31.2	32	26.9	26.9	30.1	31.4
Hf	-	-	-	4.05	3.43	-	-	-
Ta	-	-	-	1.84	1.55	-	-	-
Th	-	-	-	2.37	1.89	-	-	-
U	-	-	-	0.68	0.63	-	-	-
Pb	-	-	-	2.12	1.72	-	-	-
La	-	-	-	24.86	20.52	-	-	-
Ce	-	-	-	53.08	44.44	-	-	-
Pr	-	-	-	6.64	5.62	-	-	-
Nd	-	-	-	27.95	23.97	-	-	-
Sm	-	-	-	6.6	5.68	-	-	-
Eu	-	-	-	2.07	1.9	-	-	-
Gd	-	-	-	5.75	4.97	-	-	-
Tb	-	-	-	0.86	0.76	-	-	-
Dy	-	-	-	4.86	4.15	-	-	-
Ho	-	-	-	0.91	0.8	-	-	-
Er	-	-	-	2.24	1.96	-	-	-
Tm	-	-	-	0.27	0.23	-	-	-
Yb	-	-	-	1.76	1.53	-	-	-
Lu	-	-	-	0.23	0.21	-	-	-
⁸⁷ Sr/ ⁸⁶ Sr	-	-	-	-	0.703196	-	-	-
¹⁴³ Nd/ ¹⁴⁴ Nd	-	-	-	-	0.512973	-	-	-
²⁰⁶ Pb/ ²⁰⁴ Pb	-	-	-	-	19.102	-	-	-
²⁰⁷ Pb/ ²⁰⁴ Pb	-	-	-	-	15.548	-	-	-
²⁰⁸ Pb/ ²⁰⁴ Pb	-	-	-	-	38.425	-	-	-

Major elements in wt.%, trace elements in ppm.

Table B-8: Whole rock analyses of Dome Mountain volcanic samples

Sample Rock type	DM-1 NEPH	DM-2 BASAN	DM-4 BASAN	DM-5 BASAN	DM-6 BASAN	DM-7 BASAN	DM-8 BASAN	DM-9 BASAN	DM-10 BASAN
SiO ₂	44.18	45.25	45.27	45.74	45.25	45.31	45.61	45.42	45.14
TiO ₂	3.07	2.32	2.44	2.5	2.33	2.44	2.49	2.39	2.26
Al ₂ O ₃	13.01	13.32	13.97	13.96	13.18	13.98	14.07	13.48	12.8
Fe ₂ O ₃ T	15.7	14.81	14.88	14.93	14.88	14.51	14.71	14.68	14.55
MnO	0.17	0.19	0.19	0.18	0.19	0.18	0.18	0.18	0.18
MgO	10.18	10.18	8.16	8.39	10.64	8.27	8.43	9.86	11.25
CaO	6.78	7.33	7.58	7.55	7.34	8.06	7.59	7.62	6.8
Na ₂ O	4.65	4.57	4.66	4.55	4.15	3.97	4.3	3.89	4.17
K ₂ O	2.24	1.85	1.92	1.95	1.8	1.92	1.92	1.75	1.95
P ₂ O ₅	0.85	0.95	0.95	0.93	0.91	0.96	0.91	0.86	0.98
LOI	-	-	-	-	-	1.14	-	0.35	0.51
Total	100.83	100.77	100.02	100.68	100.67	100.74	100.21	100.48	100.59
Rb	42.5	34.9	36.1	36.5	33.1	39.2	35.5	31.6	36.8
Cs	0.4	-	-	0.4	0.3	-	-	-	0.4
Sr	952.5	949.8	969.9	974.3	904.6	1109	941.2	1508	1164
Ba	752.3	617.1	669.1	674.4	618	727.3	647.6	606.4	650.2
Sc	18	18	22	17	20	11	15	15	19
V	165	155	165	157	152	160	163	156	139
Cr	381.1	476.9	293.5	299	459.8	316.1	384.5	465.3	553.5
Co	-	-	-	-	-	-	-	-	-
Ni	327	316	198	210	352	220	238	305	420
Zn	-	-	-	-	-	-	-	-	-
Cu	-	-	-	-	-	-	-	-	-
Ga	25	23.1	23.6	23.7	21.5	23.1	22.8	22	22.8
Y	19	24	25	24.6	24	24.9	24.8	22.6	21.3
Zr	323	294.2	300.5	300.9	278.4	291	298.7	266.3	300.4
Nb	66.7	59.2	60.3	60.2	56.6	58	58.6	53.9	62.4
Hf	6.4	-	-	5.9	5.2	-	-	-	5.6
Ta	4.2	-	-	3.7	3.3	4.3	4.5	2.2	3.5
Th	5.2	-	-	5.5	5.2	-	-	-	5.7
U	1.6	2.2	2.6	1.8	1.5	1.6	2.7	0	1.7
Pb	3.2	5.4	6.7	3.6	3.2	6.4	6.2	6.7	3.6
La	45.68	-	-	51.66	47.3	-	-	-	51.16
Ce	93.68	-	-	102.3	91.6	-	-	-	100.9
Pr	11.33	-	-	11.99	10.72	-	-	-	11.95
Nd	44.84	-	-	45.89	41.31	-	-	-	45.43
Sm	9.6	-	-	9.75	8.79	-	-	-	9.31
Eu	2.82	-	-	2.93	2.62	-	-	-	2.78
Gd	7.79	-	-	8.42	7.52	-	-	-	7.79
Tb	1	-	-	1.14	1.01	-	-	-	1.04
Dy	4.86	-	-	5.9	5.27	-	-	-	5.12
Ho	0.75	-	-	1.04	0.93	-	-	-	0.87
Er	1.6	-	-	2.36	2.2	-	-	-	1.97
Tm	0.17	-	-	0.27	0.24	-	-	-	0.21
Yb	1.03	-	-	1.64	1.61	-	-	-	1.31
Lu	0.13	-	-	0.21	0.21	-	-	-	0.16
⁸⁷ Sr/ ⁸⁶ Sr	0.702839	-	-	-	-	-	-	-	-
¹⁴³ Nd/ ¹⁴⁴ Nd	0.512985	-	-	-	-	-	-	-	-
²⁰⁶ Pb/ ²⁰⁴ Pb	19.173	-	-	-	-	-	-	-	-
²⁰⁷ Pb/ ²⁰⁴ Pb	15.535	-	-	-	-	-	-	-	-
²⁰⁸ Pb/ ²⁰⁴ Pb	38.452	-	-	-	-	-	-	-	-

Major elements in wt.%, trace elements in ppm.

Table B-8: Whole rock analyses of Dome Mountain volcanic samples (cont'd)

Sample Rock type	DM-11 BASAN	DM-12 BASAN	DM-13 BASAN	DM-14 BASAN	DM-15 BASAN
SiO ₂	45.14	45.01	45.31	45.44	44.69
TiO ₂	2.2	2.24	2.26	2.25	2.36
Al ₂ O ₃	12.54	12.88	12.97	12.72	13.34
Fe ₂ O ₃ T	14.45	14.53	14.58	14.54	14.54
MnO	0.18	0.18	0.18	0.18	0.19
MgO	12.02	11.13	11.04	11.94	10.46
CaO	6.55	6.84	6.92	6.73	7.79
Na ₂ O	4.4	4.29	4.41	4.26	3.75
K ₂ O	1.93	1.9	1.91	1.95	1.56
P ₂ O ₅	0.95	0.93	0.93	0.96	0.73
LOI	-	-	-	-	1.11
Total	100.36	99.93	100.51	100.97	100.52
Rb	36.3	35.7	35.5	36.8	27.3
Cs	0.4	-	0.4	-	0.3
Sr	955.1	930.4	935.2	969.9	774.9
Ba	627	632.3	612.6	636.8	547.2
Sc	14	21	20	17	16
V	125	152	152	141	173
Cr	598.7	536.4	562.4	634.9	436.5
Co	-	-	-	-	-
Ni	464	408	401	453	349
Zn	-	-	-	-	-
Cu	-	-	-	-	-
Ga	21.8	22.6	22.7	22.9	19.8
Y	21.9	22.7	22.2	22.7	27.7
Zr	297.6	295.6	291.4	297.4	242.7
Nb	61	59.6	59.1	60.4	46.6
Hf	5.5	-	5.6	-	4.4
Ta	3.5	3.6	3.5	2.8	2.6
Th	5.6	-	5.6	-	4.2
U	1.7	2.7	1.7	2.6	1.1
Pb	3.4	6.2	3.4	6	2.5
La	49.95	-	49.73	-	37.16
Ce	98.23	-	97.5	-	73.68
Pr	11.5	-	11.4	-	8.72
Nd	43.7	-	43.2	-	33.9
Sm	9.15	-	9.13	-	7.5
Eu	2.71	-	2.72	-	2.34
Gd	7.59	-	7.58	-	6.8
Tb	1.01	-	1	-	0.98
Dy	4.99	-	5.2	-	5.45
Ho	0.85	-	0.91	-	1.05
Er	1.91	-	2.06	-	2.55
Tm	0.21	-	0.22	-	0.3
Yb	1.3	-	1.44	-	1.98
Lu	0.18	-	0.19	-	0.26
⁸⁷ Sr/ ⁸⁶ Sr	-	-	0.702900	-	0.702886
¹⁴³ Nd/ ¹⁴⁴ Nd	-	-	0.513006	-	0.513016
²⁰⁶ Pb/ ²⁰⁴ Pb	-	-	19.135	-	19.13
²⁰⁷ Pb/ ²⁰⁴ Pb	-	-	15.523	-	15.541
²⁰⁸ Pb/ ²⁰⁴ Pb	-	-	38.394	-	38.436

Major elements in wt.%, trace elements in ppm.

Table B-9: Whole rock analyses of Jennings River volcanic samples

Sample Rock type	JR-1 Hy-NORM	JR-2 Hy-NORM	JR-3 Hy-NORM	JR-4 Hy-NORM	JR-5 Hy-NORM	JR-6 Hy-NORM	JR-7 Hy-NORM	JR-8 Hy-NORM	JR-9 Hy-NORM
SiO ₂	49.57	49.65	47.96	49.44	48.71	49.78	49.59	49.38	49.59
TiO ₂	1.61	1.7	1.5	1.71	1.53	1.77	1.74	1.72	1.73
Al ₂ O ₃	14.98	14.71	12.46	14.66	14.14	14.93	14.88	14.69	15.01
Fe ₂ O ₃ ^T	12.53	12.77	13.87	12.76	12.99	12.54	12.62	12.62	12.41
MnO	0.17	0.17	0.18	0.17	0.17	0.17	0.17	0.17	0.17
MgO	8.42	8.3	13	8.3	10.46	7.77	8.02	8.41	7.95
CaO	9.39	9.48	8.18	9.44	9.02	9.72	9.68	9.54	9.76
Na ₂ O	2.99	2.89	2.43	2.95	2.69	2.89	2.95	2.96	3.04
K ₂ O	0.56	0.57	0.51	0.58	0.51	0.82	0.61	0.61	0.64
P ₂ O ₅	0.24	0.25	0.23	0.26	0.23	0.27	0.27	0.26	0.26
LOI	-	-	-	-	-	-	-	-	-
Total	100.46	100.5	100.32	100.27	100.46	100.67	100.53	100.36	100.55
Rb	8.4	9	9.7	9.6	7.4	13.8	10.1	9.8	9.6
Cs	0.14	-	0.13	-	-	-	0.15	-	-
Sr	386.1	376.8	330.4	378.4	370.2	407.9	393.5	396.8	415.6
Ba	208.6	228.3	188.9	222.4	204.2	250.1	245	234.1	234.1
Sc	22	24	14	33	25	34	32	19	20
V	196	192	176	189	178	207	208	205	200
Cr	299.7	309.9	428.3	300.4	363.3	294.2	320.9	329.8	331.8
Co	44	39	77	47	57	39	52	49	48
Ni	147	165	335	142	216	97	115	118	98
Zn	132	125	138	135	128	124	121	130	129
Cu	82	81	88	103	68	54	57	66	89
Ga	20.9	19.9	17.7	19.8	19.4	20.7	20	19.9	20
Y	18.6	19.9	18	19.1	17.4	20.7	19.3	19.7	19.9
Zr	98.9	106.2	93.8	104.8	94.4	115.1	109.1	110.8	109.9
Nb	14.3	15.9	14.2	15.9	14	18.1	17	17.7	18.1
Hf	2.24	-	2.11	-	-	-	2.49	-	-
Ta	0.74	-	0.74	-	-	-	0.91	-	-
Th	1.17	-	1.12	-	-	-	1.43	-	-
U	0.55	-	0.46	-	-	-	0.47	-	-
Pb	1.96	-	1.61	-	-	-	1.76	-	-
La	10.71	-	10.04	-	-	-	12.14	-	-
Ce	23.1	-	22.03	-	-	-	26.19	-	-
Pr	3.04	-	2.87	-	-	-	3.38	-	-
Nd	13.23	-	12.92	-	-	-	15.2	-	-
Sm	3.75	-	3.55	-	-	-	4.13	-	-
Eu	1.33	-	1.21	-	-	-	1.43	-	-
Gd	3.86	-	3.49	-	-	-	4.1	-	-
Tb	0.59	-	0.56	-	-	-	0.65	-	-
Dy	3.42	-	3.24	-	-	-	3.76	-	-
Ho	0.68	-	0.65	-	-	-	0.76	-	-
Er	1.72	-	1.64	-	-	-	1.9	-	-
Tm	0.22	-	0.2	-	-	-	0.24	-	-
Yb	1.47	-	1.42	-	-	-	1.69	-	-
Lu	0.21	-	0.2	-	-	-	0.23	-	-
⁸⁷ Sr/ ⁸⁶ Sr	-	-	0.703212	-	-	-	0.703173	-	-
¹⁴³ Nd/ ¹⁴⁴ Nd	-	-	0.512974	-	-	-	-	-	-
²⁰⁶ Pb/ ²⁰⁴ Pb	-	-	18.978	-	-	-	19.016	-	-
²⁰⁷ Pb/ ²⁰⁴ Pb	-	-	15.587	-	-	-	15.567	-	-
²⁰⁸ Pb/ ²⁰⁴ Pb	-	-	38.468	-	-	-	38.441	-	-

Major elements in wt.%, trace elements in ppm.

Table B-9: Whole rock analyses of Jennings River volcanic samples (cont'd)

Sample Rock type	JR-10 Hy-NORM	JR-11 Hy-NORM	JR-12 Hy-NORM	JR-13 Hy-NORM	JR-14 Hy-NORM	JR-25 AOB	JR-26 AOB	JR-27 AOB	JR-24 AOB
SiO ₂	49.35	49.55	49.29	49.91	49.46	47.92	47.45	47.41	47.84
TiO ₂	1.79	1.78	2.08	1.99	1.82	1.92	2.06	2.05	2.31
Al ₂ O ₃	15.24	14.91	15.27	15.34	15.13	14.56	14.45	14.68	15.3
Fe ₂ O ₃ T	12.24	12.41	12.42	12.3	12.19	12.62	12.72	12.57	12.51
MnO	0.17	0.17	0.17	0.17	0.17	0.17	0.18	0.17	0.18
MgO	7.44	7.77	6.45	6.43	6.8	9.14	9.01	8.77	6.67
CaO	10.01	9.68	10.34	10.22	10.09	9.75	10.19	10.41	10.73
Na ₂ O	3.04	3.13	3.35	3.18	2.88	3.31	3.09	2.82	3.34
K ₂ O	0.67	0.66	0.83	0.82	0.79	0.87	0.99	0.93	1.12
P ₂ O ₅	0.27	0.28	0.33	0.31	0.28	0.34	0.38	0.38	0.43
LOI	-	0.22	-	0.15	0.75	-	-	-	-
Total	100.23	100.56	100.54	100.82	100.37	100.61	100.52	100.19	100.42
Rb	11.1	10.6	13.7	13.2	14.8	16.1	18.8	17.8	22
Cs	-	0.09	-	-	-	0.19	-	0.19	-
Sr	439.2	428.8	504.6	456.6	449.1	535.2	579.1	636.9	647.6
Ba	261	266.9	403.1	299.6	269	360	382.7	455.1	446.7
Sc	28	22	21	28	29	19	26	14	23
V	206	214	239	224	221	222	234	234	259
Cr	301.7	331.2	379	273.7	297.6	450.2	443.4	618	255.9
Co	52	57	32	40	31	55	46	48	46
Ni	79	99	53	57	76	119	123	123	75
Zn	115	125	124	116	123	117	127	124	122
Cu	45	62	46	37	57	55	99	59	61
Ga	20.6	20.6	22	21.7	20.3	20.3	20.4	20.5	21.8
Y	19.9	19.9	22.1	20.6	20.9	19.6	19.8	19.9	22.2
Zr	112.2	114.7	136.6	124.4	117.8	126.1	136.2	134.3	155.6
Nb	19	18.7	23.9	20.6	18.7	26.3	30.8	30	36.4
Hf	-	2.54	-	-	-	2.75	-	2.99	-
Ta	-	1.02	-	-	-	1.42	-	1.71	-
Th	-	1.52	-	-	-	1.92	-	2.23	-
U	-	0.49	-	-	-	0.47	-	0.56	-
Pb	-	1.84	-	-	-	1.87	-	1.95	-
La	-	13.14	-	-	-	16.81	-	19.48	-
Ce	-	28.19	-	-	-	35.57	-	40.34	-
Pr	-	3.66	-	-	-	4.62	-	5.15	-
Nd	-	16.05	-	-	-	19.58	-	21.75	-
Sm	-	4.34	-	-	-	4.86	-	5.33	-
Eu	-	1.46	-	-	-	1.6	-	1.73	-
Gd	-	4.2	-	-	-	4.32	-	4.53	-
Tb	-	0.66	-	-	-	0.66	-	0.7	-
Dy	-	3.8	-	-	-	3.79	-	3.93	-
Ho	-	0.77	-	-	-	0.74	-	0.75	-
Er	-	1.96	-	-	-	1.86	-	1.85	-
Tm	-	0.24	-	-	-	0.23	-	0.23	-
Yb	-	1.67	-	-	-	1.51	-	1.54	-
Lu	-	0.22	-	-	-	0.21	-	0.21	-
⁸⁷ Sr/ ⁸⁶ Sr	-	-	-	-	-	0.703284	-	-	-
¹⁴³ Nd/ ¹⁴⁴ Nd	-	-	-	-	-	0.512956	-	-	-
²⁰⁶ Pb/ ²⁰⁴ Pb	-	-	-	-	-	18.968	-	-	-
²⁰⁷ Pb/ ²⁰⁴ Pb	-	-	-	-	-	15.559	-	-	-
²⁰⁸ Pb/ ²⁰⁴ Pb	-	-	-	-	-	38.381	-	-	-

Major elements in wt.%, trace elements in ppm.

Table B-9: Whole rock analyses of Jennings River volcanic samples (cont'd)

Sample Rock type	JR-16 BASAN	JR-17 BASAN	JR-19 BASAN	JR-21 BASAN	JR-20 BASAN	JR-22 BASAN
SiO ₂	45.05	44.63	45.23	45.46	45.72	45.48
TiO ₂	2.31	2.37	2.75	2.75	2.81	2.76
Al ₂ O ₃	12.94	13.3	15.87	15.64	16.05	15.66
Fe ₂ O ₃ ^T	13.19	12.73	12.83	12.8	12.79	12.76
MnO	0.18	0.18	0.18	0.18	0.19	0.18
MgO	10.41	9.17	5	5.48	5.09	5.61
CaO	11.49	12.15	11.62	11.46	11.45	11.53
Na ₂ O	2.98	2.36	3.7	4.03	4.11	4.34
K ₂ O	1.18	1.12	1.54	1.62	1.65	1.59
P ₂ O ₅	0.49	0.51	0.63	0.63	0.65	0.63
LOI	0.33	1.61	0.86	-	-	-
Total	100.56	100.13	100.21	100.05	100.5	100.55
Rb	23.9	21.2	32.4	33.9	34	34
Cs	0.31	0.33	-	-	-	-
Sr	681.4	720.4	863.1	839.1	863.9	852
Ba	471.4	499.9	617.9	631.7	638.9	643.3
Sc	23	24	27	19	19	20
V	260	262	276	294	284	285
Cr	493.3	429.7	62.26	110.8	81.42	118.4
Co	59	46	38	47	32	35
Ni	151	119	52	40	38	47
Zn	116	118	138	129	132	138
Cu	58	65	83	97	80	95
Ga	19.5	20.4	23.2	22.7	23.8	23.5
Y	20.1	20.8	24.7	24.5	24.2	24.4
Zr	157.8	162.6	197.6	191.6	200.8	195.7
Nb	47.6	49.2	63.5	60.6	62.4	61.5
Hf	3.31	3.55	-	-	-	-
Ta	2.57	2.64	-	-	-	-
Th	3.21	3.42	-	-	-	-
U	0.87	0.87	-	-	-	-
Pb	2.15	2.18	-	-	-	-
La	27.06	27.92	-	-	-	-
Ce	54.11	55.9	-	-	-	-
Pr	6.65	6.95	-	-	-	-
Nd	26.92	28.53	-	-	-	-
Sm	6.31	6.61	-	-	-	-
Eu	2	2.12	-	-	-	-
Gd	5.43	5.44	-	-	-	-
Tb	0.76	0.8	-	-	-	-
Dy	4.15	4.3	-	-	-	-
Ho	0.75	0.78	-	-	-	-
Er	1.82	1.92	-	-	-	-
Tm	0.22	0.23	-	-	-	-
Yb	1.47	1.48	-	-	-	-
Lu	0.19	0.2	-	-	-	-
⁸⁷ Sr/ ⁸⁶ Sr	0.703152	-	-	-	-	-
¹⁴³ Nd/ ¹⁴⁴ Nd	0.513016	-	-	-	-	-
²⁰⁶ Pb/ ²⁰⁴ Pb	18.832	-	-	-	-	-
²⁰⁷ Pb/ ²⁰⁴ Pb	15.529	-	-	-	-	-
²⁰⁸ Pb/ ²⁰⁴ Pb	38.165	-	-	-	-	-

Major elements in wt.%, trace elements in ppm.

Table B-10: Whole rock analyses of Nome Cone volcanic samples

Sample Rock type	NC-9 Hy-NORM	NC-10 Hy-NORM	NC-11 Hy-NORM	NC-12 Hy-NORM	NC-13 Hy-NORM	NC-14 Hy-NORM	NC-15 Hy-NORM	NC-16 AOB	NC-8 AOB
SiO ₂	48.37	48.33	48.2	48.33	48.56	48.33	48.05	45.67	46.02
TiO ₂	1.8	1.77	1.78	1.79	1.84	1.78	1.73	2.41	2.4
Al ₂ O ₃	14.9	14.78	14.74	14.83	15.09	14.77	14.77	14.17	14.27
Fe ₂ O ₃ ^T	14.19	14.23	14.22	14.2	14.01	14.18	14.12	14.65	14.55
MnO	0.18	0.19	0.18	0.18	0.18	0.18	0.18	0.18	0.18
MgO	8.07	8.43	8.39	8.3	7.49	8.28	8.5	8.73	8.7
CaO	9.29	9.22	9.21	9.27	9.48	9.25	9.18	9.28	9.05
Na ₂ O	3.16	3.06	3.08	3.05	3.15	3.04	3.09	3	3.41
K ₂ O	0.63	0.62	0.62	0.6	0.61	0.62	0.59	1.02	1.13
P ₂ O ₅	0.27	0.28	0.27	0.27	0.27	0.27	0.26	0.57	0.54
LOI	-	-	-	-	-	-	-	0.88	0.4
Total	100.87	100.9	100.69	100.82	100.68	100.7	100.47	100.56	100.65
Rb	11.2	11.2	11.4	10.1	10.9	10.8	10.5	13.5	17.9
Cs	-	-	0.16	-	-	-	0.16	0.13	0.18
Sr	381.4	382.4	377.1	379.5	390.7	377.7	379.6	872.7	655.6
Ba	295.6	180.2	168.5	161.3	299.1	162.7	172.9	294.5	284.4
Sc	22	26	31	16	22	22	28	-	21
V	202	198	198	202	216	199	193	206	210
Cr	253.2	255.9	258.6	255.2	255.9	255.2	261.4	225.1	224.4
Co	55	53	52	57	47	52	50	58	62
Ni	161	173	172	169	140	173	175	196	194
Zn	140	142	141	137	141	139	138	149	151
Cu	77	95	81	81	73	84	71	70	88
Ga	22	21.5	21.5	21.6	22.6	21.6	21.3	23.7	23.1
Y	21.4	21.2	21.1	21.6	22.4	21.2	20.7	19.1	21
Zr	120.7	120.6	120.7	118.8	124.7	118.8	115.3	208.1	208.6
Nb	15.9	16.1	16.3	16.3	16.1	16.1	15.3	36	35.3
Hf	-	-	2.6	-	-	-	2.56	4.12	4.16
Ta	-	-	0.83	-	-	-	0.82	2.12	1.96
Th	-	-	1.62	-	-	-	1.59	2.85	2.75
U	-	-	0.41	-	-	-	0.44	0.86	0.86
Pb	-	-	1.68	-	-	-	1.69	2.07	1.97
La	-	-	13.09	-	-	-	12.69	27.12	25.49
Ce	-	-	28.64	-	-	-	27.84	56.78	53.61
Pr	-	-	3.68	-	-	-	3.59	7.04	6.73
Nd	-	-	16.18	-	-	-	15.78	28.69	27.9
Sm	-	-	4.17	-	-	-	4.09	6.8	6.6
Eu	-	-	1.45	-	-	-	1.42	2.1	2.05
Gd	-	-	4.15	-	-	-	4.11	5.57	5.49
Tb	-	-	0.66	-	-	-	0.66	0.78	0.81
Dy	-	-	3.86	-	-	-	3.81	4.23	4.28
Ho	-	-	0.76	-	-	-	0.75	0.76	0.79
Er	-	-	1.97	-	-	-	1.92	1.76	1.83
Tm	-	-	0.24	-	-	-	0.25	0.21	0.22
Yb	-	-	1.71	-	-	-	1.7	1.32	1.38
Lu	-	-	0.23	-	-	-	0.23	0.17	0.19
⁸⁷ Sr/ ⁸⁶ Sr	-	-	0.703716	-	-	-	-	0.703067	
¹⁴³ Nd/ ¹⁴⁴ Nd	-	-	0.512902	-	-	-	-	0.512958	
²⁰⁶ Pb/ ²⁰⁴ Pb	-	-	19.235	-	-	-	-	19.121	
²⁰⁷ Pb/ ²⁰⁴ Pb	-	-	15.628	-	-	-	-	15.574	
²⁰⁸ Pb/ ²⁰⁴ Pb	-	-	38.933	-	-	-	-	38.584	

Major elements in wt.%, trace elements in ppm.

Table B-10: Whole rock analyses of Nome Cone volcanic samples

Sample Rock type	NC-19 Hy-NORM	NC-6 Hy-NORM	NC-5 Hy-NORM	NC-3 Hy-NORM	NC-1 Hy-NORM
SiO ₂	48.41	48.2	48.33	48.24	49.1
TiO ₂	1.77	1.74	1.8	1.74	1.68
Al ₂ O ₃	14.75	14.81	14.77	14.87	14.67
Fe ₂ O ₃ T	14.15	14.14	14.24	14.17	13.88
MnO	0.19	0.18	0.19	0.18	0.18
MgO	8.27	8.34	8.29	8.38	8.18
CaO	9.28	9.28	9.23	9.25	9.21
Na ₂ O	3.09	3.09	3.08	3.02	2.92
K ₂ O	0.61	0.58	0.64	0.58	0.5
P ₂ O ₅	0.27	0.26	0.28	0.26	0.22
LOI	-	-	-	-	-
Total	100.79	100.63	100.84	100.7	100.54
Rb	9.1	10.7	10.5	10.7	9.6
Cs	-	-	-	0.15	0.16
Sr	386.4	376.7	389.1	380.1	328.1
Ba	176.6	162	182.4	172.2	148.2
Sc	30	16	29	24	34
V	200	194	204	199	198
Cr	274.4	260.7	256.6	294.2	243.6
Co	54	56	58	52	52
Ni	171	170	167	294	172
Zn	136	142	141	137	141
Cu	70	84	86	68	95
Ga	21.6	21.8	22.7	21.2	20.8
Y	21.4	21.4	21.2	20.8	21.5
Zr	121.5	117.8	123.1	117.6	104.6
Nb	16.7	16.1	16.3	15.5	13.1
Hf	-	-	-	2.66	2.47
Ta	-	-	-	0.85	0.65
Th	-	-	-	1.65	1.48
U	-	-	-	0.43	0.37
Pb	-	-	-	1.68	1.69
La	-	-	-	12.68	10.79
Ce	-	-	-	27.61	23.67
Pr	-	-	-	3.61	3.13
Nd	-	-	-	15.56	13.8
Sm	-	-	-	4.23	4.02
Eu	-	-	-	1.41	1.34
Gd	-	-	-	4.04	4
Tb	-	-	-	0.64	0.66
Dy	-	-	-	3.87	3.97
Ho	-	-	-	0.78	0.79
Er	-	-	-	2.02	2.02
Tm	-	-	-	0.24	0.26
Yb	-	-	-	1.69	1.78
Lu	-	-	-	0.24	0.25
⁸⁷ Sr/ ⁸⁶ Sr	-	-	-	-	0.703932
¹⁴³ Nd/ ¹⁴⁴ Nd	-	-	-	-	0.512841
²⁰⁶ Pb/ ²⁰⁴ Pb	-	-	-	-	19.24
²⁰⁷ Pb/ ²⁰⁴ Pb	-	-	-	-	15.646
²⁰⁸ Pb/ ²⁰⁴ Pb	-	-	-	-	39.017

Major elements in wt.%, trace elements in ppm.

Table B-11: Whole rock analyses of Little Rancheria volcanic samples

Sample Rock type	LR-24A AOB	LR-18 Hy-NORM	LR-17 Hy-NORM	LR-16 AOB	LR-14 AOB	LR-13 AOB	LR-12 AOB	LR-10 AOB	LR-23 Hy-NORM
SiO ₂	48.99	49.46	49.42	49.12	48.84	49.2	49.05	48.76	49.29
TiO ₂	2.32	2.31	2.34	2.36	2.36	2.31	2.36	2.26	2.31
Al ₂ O ₃	15.63	15.82	15.79	15.78	15.68	15.8	15.72	15.88	15.72
Fe ₂ O ₃ T	12.33	12.03	12.3	12.34	12.41	12.27	12.29	11.96	12.19
MnO	0.17	0.16	0.17	0.17	0.17	0.17	0.17	0.17	0.17
MgO	5.93	5.95	5.84	5.63	5.92	5.89	5.74	5.74	5.86
CaO	10	10.14	10.09	10.01	9.98	10.07	10.08	10.1	9.98
Na ₂ O	3.38	3.34	3.36	3.51	3.42	3.38	3.46	3.49	3.33
K ₂ O	1.22	1.2	1.2	1.24	1.24	1.21	1.24	1.19	1.24
P ₂ O ₅	0.41	0.41	0.42	0.42	0.42	0.42	0.42	0.4	0.41
LOI	-	-	-	-	-	-	-	-	-
Total	100.37	100.82	100.93	100.59	100.44	100.72	100.53	99.95	100.5
Rb	25.5	21.2	21.7	25.5	23.9	25.2	25.8	24.8	26.4
Cs	-	-	-	-	0.1	-	0.16	0.17	-
Sr	594.8	599.7	608.3	620.4	620.4	619.4	611.6	620.2	594.7
Ba	412.5	417.6	406.6	425.6	420.5	409.6	427.8	403	427
Sc	24	31	31	24	26	20	23	28	28
V	249	253	248	255	242	246	260	249	250
Cr	125.9	138.9	125.2	105.4	130	127.3	124.5	132.7	112.2
Co	34	45	41	34	38	38	32	35	32
Ni	34	36	27	29	32	34	31	38	33
Zn	126	124	122	125	127	124	124	118	124
Cu	56	48	47	48	53	52	61	45	45
Ga	22.7	22.9	22.9	24.1	23.1	21.8	23.5	23	22.4
Y	24.1	23.3	23.6	23.8	23.9	22.9	23.6	23.5	22.6
Zr	161.2	152.6	157	159	157.6	157.4	159.3	151.5	155
Nb	33.2	32.3	32.8	33.2	33.5	31.9	33.7	31.8	32.8
Hf	-	-	-	-	3.23	-	3.36	3.19	-
Ta	-	-	-	-	1.77	-	1.78	1.82	-
Th	-	-	-	-	3.14	-	3.11	2.92	-
U	-	-	-	-	0.85	-	0.81	0.69	-
Pb	-	-	-	-	2.28	-	2.34	2.01	-
La	-	-	-	-	23.21	-	23.25	22.42	-
Ce	-	-	-	-	48.18	-	48.91	46.56	-
Pr	-	-	-	-	5.97	-	6.15	5.82	-
Nd	-	-	-	-	24.62	-	25.77	23.97	-
Sm	-	-	-	-	5.87	-	5.94	5.77	-
Eu	-	-	-	-	1.85	-	1.93	1.83	-
Gd	-	-	-	-	5.21	-	5.27	5.04	-
Tb	-	-	-	-	0.77	-	0.79	0.75	-
Dy	-	-	-	-	4.25	-	4.51	4.25	-
Ho	-	-	-	-	0.85	-	0.85	0.8	-
Er	-	-	-	-	2.09	-	2.17	2.03	-
Tm	-	-	-	-	0.27	-	0.27	0.25	-
Yb	-	-	-	-	1.72	-	1.79	1.69	-
Lu	-	-	-	-	0.23	-	0.24	0.22	-
⁸⁷ Sr/ ⁸⁶ Sr	-	-	-	-	-	-	0.704126	-	-
¹⁴³ Nd/ ¹⁴⁴ Nd	-	-	-	-	-	-	0.512849	-	-
²⁰⁶ Pb/ ²⁰⁴ Pb	-	-	-	-	-	-	19.212	-	-
²⁰⁷ Pb/ ²⁰⁴ Pb	-	-	-	-	-	-	15.613	-	-
²⁰⁸ Pb/ ²⁰⁴ Pb	-	-	-	-	-	-	39.009	-	-

Major elements in wt.%, trace elements in ppm.

Table B-11: Whole rock analyses of Little Rancheria volcanic samples (cont'd)

Sample Rock type	LR-22 AOB	LR-21 AOB	LR-20 AOB	LR-19 AOB	LR-9 Hy-NORM	LR-8 Hy-NORM	LR-7 Hy-NORM	LR-5 Hy-NORM	LR-4 Hy-NORM
SiO ₂	49.35	49.55	49.38	48.99	49.63	50.06	49.95	50.02	49.44
TiO ₂	2.22	2.26	2.29	2.26	1.96	1.94	1.93	1.93	2.09
Al ₂ O ₃	15.56	15.62	15.77	15.72	14.85	14.9	14.96	14.93	15.14
Fe ₂ O ₃ T	12.24	12.27	12.18	12.16	12.36	12.28	12.22	12.3	11.9
MnO	0.17	0.17	0.17	0.17	0.17	0.17	0.17	0.16	0.17
MgO	6.16	5.86	5.81	5.95	7.1	7.09	7.01	7.03	6.24
CaO	9.97	9.85	9.93	9.99	9.65	9.62	9.64	9.69	10.19
Na ₂ O	3.38	3.44	3.41	3.32	3.12	3.09	3.09	3.07	3.18
K ₂ O	1.27	1.3	1.25	1.22	1.04	1.08	1.06	1.04	1.24
P ₂ O ₅	0.39	0.41	0.41	0.4	0.32	0.32	0.31	0.31	0.37
LOI	-	-	-	0.13	-	-	0.14	0.01	0.65
Total	100.72	100.73	100.59	100.32	100.2	100.54	100.49	100.5	100.6
Rb	26	28.8	24	26.1	24.1	24.3	24.5	23.6	29.4
Cs	-	0.25	-	0.24	0.22	0.23	-	0.23	-
Sr	595.5	592	600.9	603.7	510.3	499.6	498.5	504.7	564
Ba	482.7	437.9	416.9	422.7	360	365.9	369.5	344.8	419.1
Sc	25	27	19	15	27	25	25	20	21
V	244	243	248	239	225	220	216	223	251
Cr	200	122.5	101.9	115.6	310.6	321.6	307.2	317.5	234
Co	32	41	35	39	50	50	39	37	40
Ni	43	32	39	36	69	61	63	63	44
Zn	122	130	120	123	127	124	116	122	121
Cu	57	90	47	49	62	58	41	45	54
Ga	22.3	23.1	22.8	22.5	21.3	20.8	21.2	21.5	22.4
Y	23.1	23.2	23.5	22.9	21.9	22.7	21.7	21.8	22.5
Zr	157.6	160.7	160	155.4	145	142.2	141.8	142.8	149.1
Nb	32.2	33.2	33.2	31.3	24.3	23.6	23.6	23.6	30.5
Hf	-	3.38	-	3.27	2.98	3.01	-	2.96	-
Ta	-	1.73	-	1.69	1.27	1.19	-	1.21	-
Th	-	3.69	-	3.2	3.08	3.22	-	3.14	-
U	-	0.75	-	0.37	0.59	0.64	-	0.59	-
Pb	-	2.6	-	2.33	2.37	2.85	-	2.71	-
La	-	24.96	-	23.31	21.41	21.75	-	21.56	-
Ce	-	51.94	-	48.63	43.87	44.79	-	44.37	-
Pr	-	6.33	-	5.96	5.34	5.48	-	5.39	-
Nd	-	25.64	-	24.22	21.62	21.88	-	21.58	-
Sm	-	5.97	-	5.7	5.19	5.2	-	5.11	-
Eu	-	1.86	-	1.84	1.62	1.6	-	1.59	-
Gd	-	5.28	-	5.26	4.57	4.58	-	4.51	-
Tb	-	0.76	-	0.75	0.69	0.71	-	0.68	-
Dy	-	4.35	-	4.25	3.96	3.93	-	3.91	-
Ho	-	0.83	-	0.81	0.79	0.76	-	0.76	-
Er	-	2.13	-	2.02	1.97	1.93	-	1.91	-
Tm	-	0.26	-	0.25	0.24	0.24	-	0.23	-
Yb	-	1.83	-	1.72	1.63	1.63	-	1.6	-
Lu	-	0.24	-	0.23	0.22	0.23	-	0.23	-
⁸⁷ Sr/ ⁸⁶ Sr	-	0.704488	-	-	-	0.705007	-	-	-
¹⁴³ Nd/ ¹⁴⁴ Nd	-	0.512738	-	-	-	0.512696	-	-	-
²⁰⁶ Pb/ ²⁰⁴ Pb	-	19.282	-	-	-	19.372	-	-	-
²⁰⁷ Pb/ ²⁰⁴ Pb	-	15.634	-	-	-	15.664	-	-	-
²⁰⁸ Pb/ ²⁰⁴ Pb	-	39.207	-	-	-	39.43	-	-	-

Major elements in wt.%, trace elements in ppm.

Table B-11: Whole rock analyses of Little Rancheria volcanic samples (cont'd)

Sample Rock type	LR-3 AOB	LR-2 Hy-NORM	LR-1 AOB
SiO ₂	49.72	49.72	49.48
TiO ₂	2.1	2.13	2.21
Al ₂ O ₃	15.18	15.43	15.68
Fe ₂ O ₃ T	11.91	11.81	12.09
MnO	0.16	0.16	0.17
MgO	6.29	5.44	5.5
CaO	10.28	10.33	10.02
Na ₂ O	3.34	3.19	3.4
K ₂ O	1.25	1.26	1.29
P ₂ O ₅	0.37	0.38	0.4
LOI	0.07	0.58	0.23
Total	100.67	100.43	100.47
Rb	29.2	29.6	26.8
Cs	-	0.18	-
Sr	563.5	578	592.2
Ba	411.8	435.1	437.9
Sc	24	25	20
V	242	281	247
Cr	241.5	251.1	132.1
Co	38	40	41
Ni	43	47	37
Zn	120	123	126
Cu	54	54	44
Ga	20.9	21.6	21.8
Y	21.7	22.8	23.4
Zr	149.5	151	157.5
Nb	30.3	30.9	32
Hf	-	3.21	-
Ta	-	1.64	-
Th	-	3.62	-
U	-	0.9	-
Pb	-	2.52	-
La	-	24.57	-
Ce	-	50.52	-
Pr	-	6.15	-
Nd	-	25.13	-
Sm	-	5.6	-
Eu	-	1.76	-
Gd	-	4.77	-
Tb	-	0.73	-
Dy	-	4.11	-
Ho	-	0.78	-
Er	-	1.96	-
Tm	-	0.24	-
Yb	-	1.67	-
Lu	-	0.22	-
⁸⁷ Sr/ ⁸⁶ Sr	-	-	-
¹⁴³ Nd/ ¹⁴⁴ Nd	-	-	-
²⁰⁶ Pb/ ²⁰⁴ Pb	-	-	-
²⁰⁷ Pb/ ²⁰⁴ Pb	-	-	-
²⁰⁸ Pb/ ²⁰⁴ Pb	-	-	-

Major elements in wt.%, trace elements in ppm.

Table B-12: Whole rock analyses of Blue River volcanic samples

Sample Rock type	BR-10 Hy-NORM	BR-13 Hy-NORM	BR-14 Hy-NORM	BR-15 Hy-NORM	BR-16 Hy-NORM	BR-17 Hy-NORM	BR-18 Hy-NORM	BR-19 Hy-NORM	BR-34 AOB
SiO ₂	49.08	49.7	48.39	48.14	48.43	48.03	48.61	48.46	47.41
TiO ₂	1.57	1.68	1.62	1.62	1.61	1.6	1.95	1.92	2.06
Al ₂ O ₃	14.06	14.34	14.04	13.83	13.64	13.6	14.24	14.19	14.11
Fe ₂ O ₃ T	13.75	13.65	13.37	13.2	13.42	13.19	12.69	12.83	12.32
MnO	0.18	0.17	0.17	0.17	0.18	0.19	0.18	0.16	0.17
MgO	9.56	8.31	7.88	7.66	8.66	7.95	8.15	8.13	7.32
CaO	8.45	8.78	9.07	9.19	9.15	9.68	9.27	9.12	10.43
Na ₂ O	2.85	2.99	2.81	2.79	2.76	2.75	3.14	3.08	3.02
K ₂ O	0.76	0.75	0.81	0.76	0.74	0.72	1.06	1.04	1.06
P ₂ O ₅	0.21	0.22	0.22	0.21	0.21	0.22	0.31	0.32	0.36
LOI	0.31	0.5	2.53	3.01	1.7	2.89	1.04	1.16	2.48
Total	100.78	101.09	100.91	100.58	100.51	100.82	100.63	100.41	100.74
Rb	17.6	17.1	17.5	15.7	16.6	15.6	21.1	18.8	25.9
Cs	0.29	0.27	-	-	0.28	-	-	0.28	-
Sr	313.2	313.5	317.7	330.3	318.2	325.7	437.3	439.5	501.8
Ba	183.9	210.8	185.3	178.7	202.7	189.6	314.2	317.1	345.5
Sc	22	26	21	29	22	29	23	20	20
V	181	187	182	185	186	188	201	207	209
Cr	286	264.8	249.7	257.9	273	269.6	321.6	326.4	309.9
Co	-	-	-	-	-	-	-	-	-
Ni	246	191	171	192	230	246	169	182	176
Zn	-	-	-	-	-	-	-	-	-
Cu	-	-	-	-	-	-	-	-	-
Ga	20.1	19.4	20	19	19.3	19	21.5	20.4	20.2
Y	19.7	21	20.4	20.5	20.1	20.2	20.7	20.5	20.6
Zr	99.2	106	102.3	103.7	102.1	100.9	128.3	123.3	139.1
Nb	14.4	15	14.5	14.6	15.5	15.4	24.5	23.7	27.6
Hf	2.54	2.49	-	-	2.59	-	-	3.14	-
Ta	0.85	0.84	-	-	0.89	-	-	1.45	-
Th	2.31	2.29	-	-	2.42	-	-	3.01	-
U	0.63	0.55	-	-	0.58	-	-	-	-
Pb	2.71	2.73	-	-	2.83	-	-	3.26	-
La	12.8	13.49	-	-	13.44	-	-	17.95	-
Ce	26.99	28.38	-	-	28.01	-	-	38.17	-
Pr	3.44	3.61	-	-	3.54	-	-	4.9	-
Nd	14.58	15.27	-	-	15.02	-	-	20.69	-
Sm	3.84	3.94	-	-	3.99	-	-	5.18	-
Eu	1.27	1.32	-	-	1.28	-	-	1.64	-
Gd	3.85	4.13	-	-	3.93	-	-	4.85	-
Tb	0.63	0.67	-	-	0.65	-	-	0.73	-
Dy	3.75	3.86	-	-	3.87	-	-	4.24	-
Ho	0.75	0.76	-	-	0.74	-	-	0.82	-
Er	1.88	1.96	-	-	1.89	-	-	1.98	-
Tm	0.24	0.25	-	-	0.24	-	-	0.25	-
Yb	1.69	1.65	-	-	1.7	-	-	1.69	-
Lu	0.22	0.22	-	-	0.23	-	-	0.23	-
⁸⁷ Sr/ ⁸⁶ Sr	0.704693	-	-	-	-	-	-	-	-
¹⁴³ Nd/ ¹⁴⁴ Nd	0.512752	-	-	-	-	-	-	-	-
²⁰⁶ Pb/ ²⁰⁴ Pb	19.289	-	-	-	-	-	-	-	-
²⁰⁷ Pb/ ²⁰⁴ Pb	15.669	-	-	-	-	-	-	-	-
²⁰⁸ Pb/ ²⁰⁴ Pb	39.219	-	-	-	-	-	-	-	-

Major elements in wt.%, trace elements in ppm.

Table B-12: Whole rock analyses of Blue River volcanic samples (cont'd)

Sample Rock type	BR-35 AOB	BR-36 Hy-NORM	BR-33 Hy-NORM	BR-37 AOB	BR-32 Hy-NORM	BR-31 Hy-NORM	BR-7 Hy-NORM	BR-30 Hy-NORM	BR-29 AOB
SiO ₂	47.84	48.63	49.12	48.33	49.12	49.08	49.35	49.12	48.97
TiO ₂	2.04	1.99	2.03	2.09	2	1.97	2.1	2.03	1.97
Al ₂ O ₃	14.18	14.17	14.5	14.24	14.54	14.39	14.57	14.51	14.46
Fe ₂ O ₃ ^T	12.58	12.87	13.07	13.11	12.89	13.09	12.81	12.92	12.98
MnO	0.17	0.16	0.17	0.17	0.17	0.17	0.17	0.17	0.17
MgO	7.98	8.08	8.23	8.96	8.37	8.64	7.86	8.23	8.6
CaO	9.99	9.4	9.1	9.29	9.14	8.99	9.13	9.07	9.04
Na ₂ O	3.01	3.14	3.22	3.13	3.18	3.22	3.37	3.24	3.33
K ₂ O	1.08	1.11	1.06	1.06	1.05	1.04	1.17	1.08	1.04
P ₂ O ₅	0.36	0.34	0.33	0.37	0.33	0.32	0.36	0.34	0.33
LOI	1.74	1.1	-	0.12	-	-	-	-	-
Total	100.96	100.99	100.83	100.86	100.79	100.91	100.89	100.71	100.89
Rb	22.6	23.8	21	20.4	17.6	19.8	25.9	22.4	20.4
Cs	0.33	-	0.18	-	-	-	-	-	-
Sr	537.7	469.6	453.5	499	452	455.5	488.1	459.4	462.3
Ba	328.7	336	329.5	332.4	324.4	318.6	341.1	336	312
Sc	28	16	25	26	24	31	15	24	27
V	210	213	220	214	219	207	225	213	215
Cr	331.8	315.4	327	335.3	319.5	339.4	283.3	309.9	327.7
Co	-	-	-	-	-	-	-	-	-
Ni	183	175	156	190	159	173	151	172	181
Zn	-	-	-	-	-	-	-	-	-
Cu	-	-	-	-	-	-	-	-	-
Ga	21.1	20.9	20.9	20.1	20.8	20.5	22.3	21	21.2
Y	23.8	20.4	21.9	20.4	21.2	20.8	21.7	21.4	21.4
Zr	124.6	132.4	136.8	140.9	132.4	131.5	143.3	137.6	130.2
Nb	26.8	25.6	24.7	27.5	24.6	24.1	26.5	25.6	24.1
Hf	3.26	-	3.05	-	-	-	-	-	-
Ta	1.6	-	1.37	-	-	-	-	-	-
Th	2.7	-	2.75	-	-	-	-	-	-
U	-	-	0.57	-	-	-	-	-	-
Pb	2.6	-	2.71	-	-	-	-	-	-
La	18.94	-	18.03	-	-	-	-	-	-
Ce	39.82	-	38.43	-	-	-	-	-	-
Pr	5.1	-	4.91	-	-	-	-	-	-
Nd	21.45	-	20.6	-	-	-	-	-	-
Sm	5.29	-	4.91	-	-	-	-	-	-
Eu	1.69	-	1.57	-	-	-	-	-	-
Gd	4.83	-	4.56	-	-	-	-	-	-
Tb	0.73	-	0.72	-	-	-	-	-	-
Dy	4.16	-	4.15	-	-	-	-	-	-
Ho	0.78	-	0.78	-	-	-	-	-	-
Er	1.88	-	1.91	-	-	-	-	-	-
Tm	0.24	-	0.24	-	-	-	-	-	-
Yb	1.6	-	1.6	-	-	-	-	-	-
Lu	0.22	-	0.22	-	-	-	-	-	-
⁸⁷ Sr/ ⁸⁶ Sr	-	-	0.704284	-	-	-	-	-	-
¹⁴³ Nd/ ¹⁴⁴ Nd	-	-	0.512837	-	-	-	-	-	-
²⁰⁶ Pb/ ²⁰⁴ Pb	-	-	19.251	-	-	-	-	-	-
²⁰⁷ Pb/ ²⁰⁴ Pb	-	-	15.652	-	-	-	-	-	-
²⁰⁸ Pb/ ²⁰⁴ Pb	-	-	39.098	-	-	-	-	-	-

Major elements in wt.%, trace elements in ppm.

Table B-12: Whole rock analyses of Blue River volcanic samples (cont'd)

Sample Rock type	BR-28 Hy-NORM	BR-26 Hy-NORM	BR-25 AOB	BR-23 AOB	BR-6 AOB	BR-22 AOB	BR-4 AOB	BR-20 Hy-NORM	BR-3 AOB
SiO ₂	48.93	49.1	49.05	48.37	48.52	48.31	48.35	49.38	48.8
TiO ₂	2.01	2.06	2.25	2.14	2.12	2.03	2.26	2.15	2.16
Al ₂ O ₃	14.38	14.5	14.87	14.34	14.4	14.23	15.53	14.62	14.36
Fe ₂ O ₃ ^T	13.01	12.93	12.83	13.3	13.18	13.23	12.84	12.85	13.18
MnO	0.17	0.17	0.17	0.17	0.17	0.17	0.16	0.17	0.17
MgO	8.54	8.28	7.28	8.44	8.5	9.08	7.11	7.9	8.23
CaO	9.05	9.04	9.43	9.2	9.16	9.26	9.28	8.83	8.76
Na ₂ O	3.21	3.29	3.44	3.25	3.48	3.17	3.56	3.38	3.36
K ₂ O	1.1	1.15	1.2	1.12	1.21	1.04	1.19	1.29	1.24
P ₂ O ₅	0.34	0.35	0.38	0.37	0.37	0.33	0.4	0.38	0.38
LOI	-	-	-	-	-	-	-	-	-
Total	100.74	100.87	100.91	100.7	101.12	100.85	100.68	100.95	100.64
Rb	23.8	24.4	26.3	24.1	25.5	21.7	25.4	30.2	29.3
Cs	-	-	0.4	-	0.3	-	-	-	-
Sr	482.1	489	520.7	497.9	503.5	505.7	610.4	524.8	520.8
Ba	321.4	328	363.7	335.3	334.6	309.8	370.2	341.1	338.2
Sc	25	23	22	24	23	15	26	21	16
V	209	215	224	215	229	215	231	212	211
Cr	334.6	314.7	275	316.1	299.7	336.6	209.4	249.7	248.4
Co	-	-	-	-	-	-	-	-	-
Ni	172	161	129	166	177	183	134	160	169
Zn	-	-	-	-	-	-	-	-	-
Cu	-	-	-	-	-	-	-	-	-
Ga	21.6	22	22.8	21	20.4	21.7	23.8	22.7	20.9
Y	20.9	21.6	22.4	21.7	20.9	20.3	21.3	21.1	21.9
Zr	136.1	142.4	153.8	144.5	145.9	132.2	149.5	149.2	147.5
Nb	24.7	25.5	28.2	27.3	28.4	24.6	28.6	28.2	28
Hf	-	-	3.4	-	3.48	-	-	-	-
Ta	-	-	1.68	-	1.7	-	-	-	-
Th	-	-	2.95	-	3.08	-	-	-	-
U	-	-	0.79	-	0.8	-	-	-	-
Pb	-	-	2.81	-	3.41	-	-	-	-
La	-	-	20.37	-	20.16	-	-	-	-
Ce	-	-	43.71	-	42.14	-	-	-	-
Pr	-	-	5.56	-	5.4	-	-	-	-
Nd	-	-	23.04	-	22.75	-	-	-	-
Sm	-	-	5.49	-	5.5	-	-	-	-
Eu	-	-	1.74	-	1.77	-	-	-	-
Gd	-	-	5.15	-	5.16	-	-	-	-
Tb	-	-	0.78	-	0.79	-	-	-	-
Dy	-	-	4.43	-	4.41	-	-	-	-
Ho	-	-	0.84	-	0.83	-	-	-	-
Er	-	-	2.06	-	2.06	-	-	-	-
Tm	-	-	0.25	-	0.25	-	-	-	-
Yb	-	-	1.65	-	1.69	-	-	-	-
Lu	-	-	0.22	-	0.23	-	-	-	-
⁸⁷ Sr/ ⁸⁶ Sr	-	-	-	-	0.703909	-	-	-	-
¹⁴³ Nd/ ¹⁴⁴ Nd	-	-	-	-	0.51286	-	-	-	-
²⁰⁶ Pb/ ²⁰⁴ Pb	-	-	-	-	19.189	-	-	-	-
²⁰⁷ Pb/ ²⁰⁴ Pb	-	-	-	-	15.626	-	-	-	-
²⁰⁸ Pb/ ²⁰⁴ Pb	-	-	-	-	38.931	-	-	-	-

Major elements in wt.%, trace elements in ppm.

Table B-12: Whole rock analyses of Blue River volcanic samples (cont'd)

Sample Rock type	BR-1 AOB
SiO ₂	49.1
TiO ₂	2.27
Al ₂ O ₃	14.81
Fe ₂ O ₃ T	13.02
MnO	0.17
MgO	7.56
CaO	9
Na ₂ O	3.52
K ₂ O	1.32
P ₂ O ₅	0.42
LOI	-
Total	101.19
Rb	29.9
Cs	0.5
Sr	530.9
Ba	385.6
Sc	24
V	219
Cr	232.6
Co	-
Ni	148
Zn	-
Cu	-
Ga	21.7
Y	22.4
Zr	159.7
Nb	30.5
Hf	3.88
Ta	1.97
Th	3.75
U	0.99
Pb	3.87
La	22.8
Ce	47.54
Pr	6.03
Nd	25.13
Sm	6.02
Eu	1.91
Gd	5.5
Tb	0.85
Dy	4.76
Ho	0.9
Er	2.2
Tm	0.27
Yb	1.8
Lu	0.26
⁸⁷ Sr/ ⁸⁶ Sr	-
¹⁴³ Nd/ ¹⁴⁴ Nd	-
²⁰⁶ Pb/ ²⁰⁴ Pb	-
²⁰⁷ Pb/ ²⁰⁴ Pb	-
²⁰⁸ Pb/ ²⁰⁴ Pb	-

Major elements in wt.%, trace elements in ppm.

Table B-13: Whole rock analyses of Caribou Tuya volcanic samples

Sample Rock type	CT-17	CT-18	CT-19	CT-20	CT-21	CT-1	CT-2	CT-3	CT-4
	Hy-NORM	Hy-NORM	Hy-NORM	Hy-NORM	Hy-NORM	Hy-NORM	Hy-NORM	Hy-NORM	Hy-NORM
SiO ₂	49.08	49.5	50.04	50.17	49.93	49.12	50.17	50.1	50.02
TiO ₂	1.82	1.79	1.87	1.85	1.8	1.79	1.87	1.67	1.73
Al ₂ O ₃	15.22	14.98	15.03	15.44	15.23	15.13	15.52	14.84	14.77
Fe ₂ O ₃ T	12.79	12.65	12.35	12.2	12.31	12.65	12.2	12.75	12.85
MnO	0.16	0.16	0.16	0.16	0.16	0.16	0.16	0.16	0.16
MgO	7.32	7.66	7.62	6.96	7.54	7.29	6.45	7.77	7.55
CaO	9.35	9.21	9.35	9.47	9.25	9.18	9.45	8.77	8.7
Na ₂ O	3.08	3.12	3.22	3.17	3.25	3.28	3.24	3.17	3.29
K ₂ O	0.84	0.84	0.91	0.86	0.9	0.83	0.91	0.89	0.94
P ₂ O ₅	0.31	0.31	0.32	0.32	0.31	0.3	0.33	0.28	0.29
LOI	0.29	0.02	-	0.04	-	-	-	-	-
Total	100.26	100.25	100.87	100.64	100.69	99.73	100.29	100.41	100.31
Rb	15.6	17.3	17.9	17.5	18.3	17.1	18.1	23	24.4
Cs	0.21	-	-	-	0.2	0.23	0.22	-	-
Sr	475.7	465.1	465.7	476.5	469.4	470.5	485.2	414.5	419
Ba	271.9	269.7	277.8	285.1	263.2	278.5	267.6	243.5	254.4
Sc	15	24	18	21	18	24	20	24	22
V	195	200	194	200	192	197	191	181	181
Cr	283.3	293.5	308.6	270.9	294.2	281.9	246.3	253.2	252.5
Co	-	-	-	-	-	-	-	-	-
Ni	100	110	115	90	118	105	73	128	120
Zn	-	-	-	-	-	-	-	-	-
Cu	-	-	-	-	-	-	-	-	-
Ga	21.8	21.3	21.1	21.8	21.8	21.6	21.5	21.6	21.4
Y	21.1	19.6	21	20.7	19.7	19.9	20.3	19.8	19.8
Zr	128.8	124.8	130.5	130.3	128.3	124.8	136	127.2	131.7
Nb	19.6	19.5	20.2	19.7	19.7	19.7	20.2	18.3	19.3
Hf	3	-	-	-	2.53	2.81	3	-	-
Ta	1.12	-	-	-	0.9	1.04	1.09	-	-
Th	2.56	-	-	-	2.05	2.45	2.35	-	-
U	0.64	-	-	-	0.82	0.53	0.64	-	-
Pb	2.55	-	-	-	2.1	2.43	2.35	-	-
La	20.43	-	-	-	17.01	19.08	20.65	-	-
Ce	41.19	-	-	-	34.94	39.88	42.81	-	-
Pr	5.22	-	-	-	4.31	4.88	5.3	-	-
Nd	21.05	-	-	-	17.5	19.91	21.59	-	-
Sm	5.03	-	-	-	4.15	4.91	5.1	-	-
Eu	1.63	-	-	-	1.36	1.54	1.6	-	-
Gd	4.58	-	-	-	3.72	4.29	4.85	-	-
Tb	0.72	-	-	-	0.59	0.68	0.7	-	-
Dy	4.12	-	-	-	3.37	3.79	3.99	-	-
Ho	0.77	-	-	-	0.64	0.74	0.75	-	-
Er	1.95	-	-	-	1.6	1.82	1.9	-	-
Tm	0.24	-	-	-	0.2	0.23	0.22	-	-
Yb	1.63	-	-	-	1.32	1.52	1.54	-	-
Lu	0.22	-	-	-	0.18	0.2	0.21	-	-
⁸⁷ Sr/ ⁸⁶ Sr	-	-	-	-	0.704215	-	-	-	-
¹⁴³ Nd/ ¹⁴⁴ Nd	-	-	-	-	0.512763	-	-	-	-
²⁰⁶ Pb/ ²⁰⁴ Pb	-	-	-	-	19.292	-	-	-	-
²⁰⁷ Pb/ ²⁰⁴ Pb	-	-	-	-	15.639	-	-	-	-
²⁰⁸ Pb/ ²⁰⁴ Pb	-	-	-	-	39.137	-	-	-	-

Major elements in wt.%, trace elements in ppm.

Table B-13: Whole rock analyses of Caribou Tuya volcanic samples (cont'd)

Sample Rock type	CT-5 Hy-NORM	CT-6 Hy-NORM	CT-7 Hy-NORM	CT-8 Hy-NORM	CT-9 Hy-NORM	CT-10 Hy-NORM	CT-11 Hy-NORM	CT-12 Hy-NORM	CT-13 Hy-NORM
SiO ₂	49.74	50.21	49.78	49.61	49.55	49.7	50.27	49.5	49.68
TiO ₂	1.62	1.69	1.99	1.98	1.94	1.99	2.01	1.95	1.59
Al ₂ O ₃	14.97	14.98	14.92	14.95	14.91	15.04	14.98	15.21	14.79
Fe ₂ O ₃ T	12.49	12.63	11.97	12.03	11.9	11.98	12.05	11.95	12.93
MnO	0.16	0.16	0.16	0.16	0.16	0.16	0.16	0.16	0.17
MgO	7.8	7.63	6.98	7.05	7.05	6.98	7.01	6.96	8.33
CaO	8.71	8.81	9.52	9.48	9.39	9.44	9.56	9.61	8.73
Na ₂ O	3.12	3.25	3.43	3.3	3.37	3.33	3.39	3.32	3.18
K ₂ O	0.87	0.91	1.23	1.23	1.24	1.23	1.25	1.18	0.79
P ₂ O ₅	0.28	0.29	0.38	0.38	0.38	0.38	0.38	0.37	0.26
LOI	-	-	-	-	-	-	-	-	-
Total	99.76	100.56	100.37	100.16	99.88	100.23	101.07	100.22	100.44
Rb	23.1	23.5	30.2	30.3	30.1	28.2	32	26.2	21
Cs	-	-	-	0.41	-	-	-	0.14	0.32
Sr	426.4	429.7	540.3	538.5	534.5	538.3	539.9	561.2	406.8
Ba	228.3	253	379	384.8	384.8	386.2	373.1	381.9	215.9
Sc	24	24	20	21	27	26	23	23	25
V	177	187	214	211	210	216	219	208	173
Cr	260.7	261.4	317.5	309.3	307.2	318.8	296.9	296.9	271.6
Co	-	-	-	-	-	-	-	-	-
Ni	131	123	110	93	88	86	81	78	141
Zn	-	-	-	-	-	-	-	-	-
Cu	-	-	-	-	-	-	-	-	-
Ga	21.3	21.6	22	21.6	21	21.5	22.6	22.6	20.6
Y	19	19.5	21	20.2	20.9	21.1	20.8	20.5	19.3
Zr	123.7	128.1	156.5	155.3	155.4	156.6	156.5	151.2	115.7
Nb	18.4	19.2	28.1	28.8	28.4	28.4	28.6	27.9	17.5
Hf	-	-	-	3.39	-	-	-	3.4	2.86
Ta	-	-	-	1.57	-	-	-	1.58	1
Th	-	-	-	3.54	-	-	-	3.35	2.8
U	-	-	-	0.98	-	-	-	0.85	0.79
Pb	-	-	-	3.22	-	-	-	2.75	2.81
La	-	-	-	25.04	-	-	-	26.8	17.54
Ce	-	-	-	50.87	-	-	-	53.48	35.85
Pr	-	-	-	6.2	-	-	-	6.45	4.43
Nd	-	-	-	24.73	-	-	-	25.25	18.2
Sm	-	-	-	5.64	-	-	-	5.78	4.45
Eu	-	-	-	1.7	-	-	-	1.8	1.48
Gd	-	-	-	5.2	-	-	-	5.47	4.14
Tb	-	-	-	0.76	-	-	-	0.78	0.64
Dy	-	-	-	4.11	-	-	-	4.23	3.78
Ho	-	-	-	0.76	-	-	-	0.8	0.73
Er	-	-	-	1.89	-	-	-	1.94	1.81
Tm	-	-	-	0.23	-	-	-	0.23	0.23
Yb	-	-	-	1.57	-	-	-	1.58	1.55
Lu	-	-	-	0.21	-	-	-	0.21	0.2
⁸⁷ Sr/ ⁸⁶ Sr	-	-	-	0.704182	-	-	-	-	-
¹⁴³ Nd/ ¹⁴⁴ Nd	-	-	-	0.512764	-	-	-	-	-
²⁰⁶ Pb/ ²⁰⁴ Pb	-	-	-	19.296	-	-	-	-	19.3
²⁰⁷ Pb/ ²⁰⁴ Pb	-	-	-	15.65	-	-	-	-	15.655
²⁰⁸ Pb/ ²⁰⁴ Pb	-	-	-	39.19	-	-	-	-	39.205

Major elements in wt.%, trace elements in ppm.

Table B-13: Whole rock analyses of Caribou Tuya volcanic samples (cont'd)

Sample	CT-14	CT-15	CT-16
Rock type	Hy-NORM	Hy-NORM	Hy-NORM
SiO ₂	49.85	50.19	49.59
TiO ₂	1.72	1.62	1.61
Al ₂ O ₃	14.93	14.93	14.89
Fe ₂ O ₃	12.91	12.81	12.85
MnO	0.16	0.17	0.17
MgO	7.47	8.02	8.06
CaO	8.84	8.87	8.86
Na ₂ O	3.3	3.21	3.2
K ₂ O	0.87	0.83	0.8
P ₂ O ₅	0.28	0.27	0.26
LOI	-	-	-
Total	100.33	100.92	100.29
Rb	22.4	21.6	20.3
Cs	0.34	-	-
Sr	406	412	410.3
Ba	254.4	232.7	212.2
Sc	31	20	18
V	198	188	192
Cr	259.3	262.7	281.9
Co	-	-	-
Ni	118	132	131
Zn	-	-	-
Cu	-	-	-
Ga	21.6	20.9	21.6
Y	20.3	19.4	19.5
Zr	126.4	119.1	116.7
Nb	18.1	17.4	17.7
Hf	2.8	-	-
Ta	1.01	-	-
Th	2.81	-	-
U	0.79	-	-
Pb	2.75	-	-
La	18.18	-	-
Ce	37.34	-	-
Pr	4.56	-	-
Nd	18.65	-	-
Sm	4.56	-	-
Eu	1.46	-	-
Gd	4.55	-	-
Tb	0.68	-	-
Dy	3.84	-	-
Ho	0.72	-	-
Er	1.86	-	-
Tm	0.23	-	-
Yb	1.53	-	-
Lu	0.2	-	-
⁸⁷ Sr/ ⁸⁶ Sr	0.704216	-	-
¹⁴³ Nd/ ¹⁴⁴ Nd	0.512699	-	-
²⁰⁶ Pb/ ²⁰⁴ Pb	-	-	-
²⁰⁷ Pb/ ²⁰⁴ Pb	-	-	-
²⁰⁸ Pb/ ²⁰⁴ Pb	-	-	-

Major elements in wt.%, trace elements in ppm.

Table B-14: Whole rock analyses of Rancheria area volcanic samples

Sample Rock type Location	RA-8 Hy-NORM Swan L.	RA-9 Hy-NORM Swan L.	RA-1 BASAN Ranch. R	RA-2 BASAN Ranch. R	RA-3 BASAN Ranch. R	RA-4 BASAN Ranch. R	RA-5 BASAN Ranch. R	RA-6 BASAN Ranch. R	RA-7 AOB Ranch. R
SiO ₂	49.12	49.93	45.55	44.8	44.01	45.61	46.36	46.47	44.82
TiO ₂	1.74	1.68	2.32	2.42	2.49	2.12	2.11	2.04	1.73
Al ₂ O ₃	14.69	14.74	13.64	13.53	13.84	13.4	13.67	13.42	11.21
Fe ₂ O ₃ T	13.61	13.41	13.76	13.91	14.01	13.6	13.35	13.4	14.73
MnO	0.17	0.17	0.19	0.19	0.2	0.18	0.19	0.18	0.19
MgO	8.26	8.16	9.18	8.83	8.29	10.48	10.76	11.17	16.31
CaO	9.06	9	10.52	10.87	11.05	9.78	9.95	9.59	8.18
Na ₂ O	3.06	3.05	3.6	3.6	4.07	3.42	3.17	3.13	2.15
K ₂ O	0.72	0.71	1.47	1.47	1.67	1.3	1.24	1.25	0.95
P ₂ O ₅	0.27	0.24	0.58	0.67	0.76	0.53	0.49	0.46	0.36
LOI	0.01	0.01	0.01	0.52	0.01	0.01	0.01	0.01	0.01
Total	100.71	101.1	100.82	100.81	100.39	100.43	101.3	101.12	100.64
Rb	14	15	29	32	31	26	27	28	20
Cs	0.15	-	0.33	-	0.59	0.48	-	0.35	0.45
Sr	370	332	726	1024	902	679	662	620	529
Ba	215	221.2	588.5	564.3	565.2	407.5	490.8	475.6	434.4
Sc	23.61	-	21.87	-	22.06	23.17	-	23.27	21.49
V	201	194	230	263	246	238	248	229	203
Cr	253.2	251.1	278.5	244.3	210.7	315.4	308.6	351.7	548
Co	54.93	-	52.91	-	50.65	59.14	-	60.97	76.26
Ni	139	136	167	148	117	213	215	237	381
Zn	132	-	-	-	136	-	-	-	121
Cu	54	-	-	-	65	-	-	-	45
Ga	21.7	-	-	-	22.3	-	-	-	17.3
Y	20	21	23	25	25	21	21	21	17
Zr	118	108	175	195	213	155	148	142	109
Nb	16	14	52	55	60	42	40	37	28
Hf	2.73	-	4.65	-	5.07	3.87	-	3.71	2.91
Th	2.56	-	4.58	-	5.39	3.95	-	3.74	2.61
U	0.46	-	2.6	-	1.77	1.26	-	0.68	1.04
Pb	1.93	-	-	-	-	-	-	-	-
La	16.06	-	36.19	-	46.32	29.37	-	27.32	19.95
Ce	34.35	-	66.51	-	87.98	59.78	-	52.73	39.4
Pr	4.3	-	-	-	-	-	-	-	-
Nd	17.76	-	31.44	-	41.13	27.22	-	21.96	16.4
Sm	4.45	-	7.41	-	8.6	6.2	-	6.45	4.96
Eu	1.4	-	2.32	-	2.75	2.01	-	1.93	1.56
Gd	4.2	-	-	-	-	-	-	-	-
Tb	0.65	-	0.67	-	0.85	0.71	-	0.63	0.53
Dy	3.75	-	-	-	-	-	-	-	-
Ho	0.74	-	-	-	-	-	-	-	-
Er	1.84	-	-	-	-	-	-	-	-
Tm	0.23	-	-	-	-	-	-	-	-
Yb	1.56	-	2.07	-	1.93	1.62	-	1.97	1.29
Lu	0.22	-	0.23	-	0.21	0.2	-	0.21	0.14
⁸⁷ Sr/ ⁸⁶ Sr	0.704318	-	-	-	0.703467	-	-	-	0.704271
¹⁴³ Nd/ ¹⁴⁴ Nd	0.512768	-	-	-	0.512946	-	-	-	0.512828
²⁰⁶ Pb/ ²⁰⁴ Pb	19.328	-	-	-	18.951	-	-	-	19.159
²⁰⁷ Pb/ ²⁰⁴ Pb	15.646	-	-	-	15.581	-	-	-	15.629
²⁰⁸ Pb/ ²⁰⁴ Pb	39.242	-	-	-	38.475	-	-	-	38.882

Major elements in wt.%, trace elements in ppm.

Table B-14: Whole rock analyses of Rancheria area volcanic samples (cont'd)

Sample Rock type Location	RA-10 BASAN Ranch. R	RA-11 AOB Ranch. R	RA-12 AOB Ranch. R	RA-13 AOB Ranch. R	RA-14 BASAN Ranch. R	RA-15 AOB Big Creek	RA-16 Hy-NORM Big Creek	RA-17 AOB Big Creek	RA-18 AOB Big Creek
SiO ₂	44.78	46.4	46.42	46.53	46.3	47.75	47.47	48.28	47.39
TiO ₂	2.43	2.02	2.15	2.04	2.08	1.82	1.74	1.92	1.74
Al ₂ O ₃	13.57	13.21	13.72	13.36	13.35	12.85	12.57	13.72	12.49
Fe ₂ O ₃ ^T	13.9	13.42	13.2	13.41	13.35	13.8	13.87	13.46	13.83
MnO	0.2	0.18	0.18	0.18	0.18	0.18	0.18	0.17	0.17
MgO	9.02	10.96	9.85	10.97	10.82	11.36	12.42	9.58	12.31
CaO	10.81	9.39	9.97	9.66	9.53	8.87	8.61	9.4	8.66
Na ₂ O	3.9	2.86	2.91	2.87	3.12	2.97	2.75	3.07	2.82
K ₂ O	1.6	1.19	1.33	1.23	1.27	0.92	0.87	0.92	0.88
P ₂ O ₅	0.68	0.43	0.48	0.45	0.44	0.32	0.3	0.35	0.3
LOI	0.01	0.01	0.33	0.01	0.01	0.01	0.01	0.01	0.01
Total	100.9	100.07	100.54	100.71	100.44	100.85	100.79	100.88	100.59
Rb	32	25	29	25	27	18	17	17	18
Cs	-	-	-	0.15	0.18	-	0.05	0.04	0.08
Sr	833	576	633	600	589	415	405	459	409
Ba	514.1	367.2	390.5	497.1	445.2	258.9	301	402.2	378
Sc	-	23.19	-	23.99	23.67	-	21.98	-	-
V	267	230	245	236	249	216	185	203	211
Cr	258.6	395.5	347.6	374.3	356.5	363.3	396.8	353.7	405.7
Co	-	58.52	-	60.49	59.03	-	63.69	-	-
Ni	131	258	208	232	237	268	322	220	328
Zn	-	-	-	124	125	-	124	-	-
Cu	-	-	-	56	64	-	58	-	-
Ga	-	-	-	20.3	20.8	-	20	-	-
Y	24	21	22	21	21	20	19	20	18
Zr	198	139	149	144	144	121	111	130	112
Nb	55	34	38	36	35	25	23	27	23
Hf	-	3.76	-	3.76	2.19	-	3.08	1.68	3.17
Th	-	3.48	-	3.70	3.64	-	2.70	3.12	2.73
U	-	1.16	-	0.84	0.92	-	0.35	0.28	0.42
Pb	-	-	-	2.60	2.58	-	1.78	2.08	1.98
La	-	25.14	-	27.09	23.85	-	19.91	21.1	19.87
Ce	-	47.9	-	55.26	48.1	-	40.65	41.68	40.82
Pr	-	-	-	6.66	6.45	-	5.03	5.63	4.99
Nd	-	24.62	-	28.22	25.23	-	21.39	21.91	21.31
Sm	-	5.93	-	6.07	5.54	-	4.77	5.07	4.78
Eu	-	1.92	-	1.92	1.78	-	1.56	1.66	1.55
Gd	-	-	-	5.38	5.18	-	4.71	5.01	4.56
Tb	-	0.66	-	0.77	0.75	-	0.71	0.75	0.70
Dy	-	-	-	4.39	4.01	-	4.09	4.17	4.00
Ho	-	-	-	0.81	0.71	-	0.75	0.77	0.75
Er	-	-	-	2.02	1.85	-	1.97	1.95	1.92
Tm	-	-	-	0.26	0.27	-	0.25	0.28	0.25
Yb	-	1.61	-	1.57	1.55	-	1.56	1.64	1.53
Lu	-	0.29	-	0.22	0.22	-	0.23	0.24	0.22
⁸⁷ Sr/ ⁸⁶ Sr	-	-	-	0.704067	0.704011	-	0.704484	-	0.704517
¹⁴³ Nd/ ¹⁴⁴ Nd	-	-	-	0.512885	0.512826	-	0.512773	-	0.512883
²⁰⁶ Pb/ ²⁰⁴ Pb	-	-	-	19.188	19.14	-	19.336	-	19.366
²⁰⁷ Pb/ ²⁰⁴ Pb	-	-	-	15.644	15.599	-	15.627	-	15.644
²⁰⁸ Pb/ ²⁰⁴ Pb	-	-	-	38.894	38.828	-	39.228	-	39.287

Major elements in wt.%, trace elements in ppm.

Table B-14: Whole rock analyses of Rancheria area volcanic samples (cont'd)

Sample	RA-19	WT-3	WT-4	WT-5	WT-6	WT-7	WT-10	WT-11	WT-12
Rock type	Hy-NORM	Hy-NORM	Hy-NORM	Hy-NORM	Hy-NORM	Hy-NORM	Hy-NORM	Hy-NORM	Hy-NORM
Location	Big Creek	Liard R.							
SiO ₂	48.69	49.68	49.78	50.06	49.7	49.85	48.78	48.28	48.5
TiO ₂	1.68	1.61	1.75	1.66	1.86	1.89	1.81	1.69	1.74
Al ₂ O ₃	13.85	14.64	14.75	14.8	14.43	14.51	14.72	14.77	14.73
Fe ₂ O ₃ ^T	13.58	13.23	13.17	13.2	13.59	13.23	14.05	14.07	13.98
MnO	0.16	0.18	0.18	0.17	0.17	0.18	0.18	0.18	0.18
MgO	10.11	8.79	8.08	8.18	8.24	8.07	8.54	9.15	8.62
CaO	8.69	9.05	9.36	9.3	8.58	8.68	8.89	8.77	8.9
Na ₂ O	3	2.8	3.04	2.74	2.92	2.95	3.29	3.1	3.23
K ₂ O	0.85	0.63	0.64	0.67	0.91	0.96	0.78	0.71	0.74
P ₂ O ₅	0.25	0.24	0.23	0.24	0.26	0.26	0.3	0.28	0.27
LOI	0.01	-	-	-	-	-	-	-	-
Total	100.87	100.84	100.98	101.02	100.66	100.58	101.34	101.01	100.89
Rb	19	13	13	22.9	13.4	23.5	12.2	10.5	10.6
Cs	0.26	0.14	-	-	-	0.68	-	-	-
Sr	395	369.3	376.4	380.7	374.3	379.2	387.9	392.1	394.1
Ba	251.7	303.6	284.8	271.4	337.7	349.3	276.7	257.9	263.3
Sc	-	27	22	21	18	20	19	25	21
V	203	184	206	209	197	194	191	182	179
Cr	353.7	271.6	265.5	272.3	270.3	272.3	258.6	277.8	274.4
Co	-	55	59	69	59	62	59	47	54
Ni	194	181	148	155	178	180	207	246	211
Zn	-	105	102	103	111	113	151	141	149
Cu	-	103	96	123	83	95	54	37	97
Ga	-	20.9	20.8	22.3	21.1	21.8	22.6	21.6	21
Y	18	20.4	20.3	21.1	20.8	20.9	20.2	17.8	19.9
Zr	106	119	118.2	141.8	120.4	145.1	116.8	101.2	118
Nb	17	14.6	14.8	19.1	14.6	19.4	18.7	17.7	17.7
Hf	2.43	2.91	-	-	-	3.56	-	-	-
Th	3.06	2.20	-	-	-	2.84	-	-	-
U	0.67	0.47	-	-	-	1.10	-	-	-
Pb	2.38	1.79	-	-	-	3.27	-	-	-
La	16.03	14.67	-	-	-	17.12	-	-	-
Ce	32.54	31.67	-	-	-	36.32	-	-	-
Pr	4.49	4.03	-	-	-	4.51	-	-	-
Nd	17.74	17.78	-	-	-	19.78	-	-	-
Sm	4.17	4.39	-	-	-	4.74	-	-	-
Eu	1.4	1.53	-	-	-	1.57	-	-	-
Gd	4.11	4.55	-	-	-	4.73	-	-	-
Tb	0.63	0.71	-	-	-	0.70	-	-	-
Dy	3.7	4.09	-	-	-	4.11	-	-	-
Ho	0.7	0.76	-	-	-	0.76	-	-	-
Er	1.75	1.99	-	-	-	1.99	-	-	-
Tm	0.26	0.26	-	-	-	0.26	-	-	-
Yb	1.51	1.58	-	-	-	1.54	-	-	-
Lu	0.23	0.23	-	-	-	0.22	-	-	-
⁸⁷ Sr/ ⁸⁶ Sr	-	0.704212	-	-	-	0.704218	-	-	-
¹⁴³ Nd/ ¹⁴⁴ Nd	-	0.512881	-	-	-	0.512805	-	-	-
²⁰⁶ Pb/ ²⁰⁴ Pb	-	19.408	-	-	-	19.504	-	-	-
²⁰⁷ Pb/ ²⁰⁴ Pb	-	15.666	-	-	-	15.706	-	-	-
²⁰⁸ Pb/ ²⁰⁴ Pb	-	39.4	-	-	-	39.455	-	-	-

Major elements in wt.%, trace elements in ppm.

Table B-15: Whole rock analyses of Watson Lake area volcanic samples

Sample Rock type	RA-20 AOB	RA-21 AOB	RA-22 AOB	WT-1 AOB	WT-2 AOB	WT-13 AOB
SiO ₂	48.01	47.94	47.79	48.22	48.05	47.75
TiO ₂	2.15	2.15	2.12	2.17	2.17	2.11
Al ₂ O ₃	13.59	13.88	13.77	14.1	14.16	14.28
Fe ₂ O ₃ T	14.38	14.19	14.51	14.31	14.26	14.02
MnO	0.16	0.16	0.16	0.17	0.17	0.17
MgO	9.08	8.29	8.89	8.42	8.34	8.23
CaO	8.05	8.07	7.98	8.07	8.13	8.04
Na ₂ O	3.62	3.82	3.51	3.3	3.41	3.57
K ₂ O	1.26	1.39	1.31	1.34	1.33	1.41
P ₂ O ₅	0.5	0.53	0.52	0.52	0.52	0.54
LOI	0.01	0.01	0.01	-	-	-
Total	100.81	100.43	100.57	100.62	100.54	100.12
Rb	25	26	24	24.8	24.3	26.8
Cs	0.45	-	0.33	-	-	-
Sr	604	639	633	636.9	647.5	716.8
Ba	312.6	309.9	327.8	443.3	472.9	327.8
Sc	16.72	16.7	-	15	17	17
V	209	186	189	176	179	175
Cr	280.5	255.9	277.8	247	253.2	235.4
Co	61.5	58.02	-	67	66	50
Ni	245	215	226	217	208	196
Zn	150	154	-	130	132	166
Cu	69	77	-	154	116	72
Ga	25.5	25.4	-	24.4	24.7	24.6
Y	18	19	19	20.8	20.3	19.3
Zr	185	200	194	214.1	217.4	219.4
Nb	31	34	33	33.8	34	35.5
Hf	4.27	-	3.63	-	-	-
Th	3.63	-	3.38	-	-	-
U	1.19	-	0.9	-	-	-
Pb	3.03	-	2.9	-	-	-
La	24.58	29.03	25.35	-	-	-
Ce	51.81	57.53	51.47	-	-	-
Pr	6.53	-	7.01	-	-	-
Nd	26.92	25.74	27.38	-	-	-
Sm	6.2	7.25	6.27	-	-	-
Eu	1.99	2.3	2.03	-	-	-
Gd	5.41	-	5.67	-	-	-
Tb	0.75	0.64	0.84	-	-	-
Dy	3.96	-	4.01	-	-	-
Ho	0.7	-	0.69	-	-	-
Er	1.63	-	1.7	-	-	-
Tm	0.2	-	0.22	-	-	-
Yb	1.22	1.44	1.26	-	-	-
Lu	0.17	0.2	0.17	-	-	-
⁸⁷ Sr/ ⁸⁶ Sr	0.703446	0.703517	-	-	-	-
¹⁴³ Nd/ ¹⁴⁴ Nd	0.512961	0.512996	-	-	-	-
²⁰⁶ Pb/ ²⁰⁴ Pb	19.22	19.287	-	-	-	-
²⁰⁷ Pb/ ²⁰⁴ Pb	15.622	15.621	-	-	-	-
²⁰⁸ Pb/ ²⁰⁴ Pb	38.921	38.932	-	-	-	-

Major elements in wt.%, trace elements in ppm.

Table C: Whole rock analyses of granitoid samples from the northern Canadian Cordillera

Sample Rock: Site	Omineca Belt		Intermontane Belt			CO-3 MsGd Pluton	HF-40 Chert Xenolith-Hirschfeld
	CA-1 Gr Pluton Cassiar	CA-2 Gr Pluton Cassiar	PC Gr Pluton Parallel Creek	LG-40 Gd Pluton Llangorse			
SiO ₂	73.66	72.42	76.16	64.14	64.42	89.89	
TiO ₂	0.18	0.32	0.06	0.58	0.63	0.1	
Al ₂ O ₃	14.52	14.69	12.91	16.11	15.93	2.16	
Fe ₂ O ₃ ^T	1.43	1.97	1.24	5.49	4.93	1.22	
MnO	0.04	0.04	0.08	0.12	0.1	0.12	
MgO	0.29	0.45	0.06	2.08	1.95	0.9	
CaO	1.33	1.42	0.48	5.46	4.82	1.21	
Na ₂ O	3.45	3	4.3	2.99	3.09	0.35	
K ₂ O	4.19	4.74	4.48	2.08	2.21	0.7	
P ₂ O ₅	0.12	0.12	0.02	0.14	0.17	0.02	
LOI	0.62	0.63	0.32	0.96	1.27	1.5	
Total	99.82	99.8	100.1	100.15	99.52	98.17	
Rb	169.7	217.3	219.4	46.2	56.7	26	
Cs	-	-	-	1.47	-	-	
Sr	269.2	166.5	6.4	529.7	434.3	80	
Ba	1014	880	16.45	1635	1660	504.3	
V	-	23	-	90	67	24	
Cr	-	-	13	17.1	26	34.89	
Co	-	-	-	-	-	-	
Ni	-	-	-	-	-	12	
Zn	-	-	-	-	71	-	
Cu	-	-	-	-	-	-	
Ga	17.2	18.7	17.1	16	16.4	-	
Y	10.8	11.6	32.2	17.6	20.1	2	
Zr	103.4	169.8	57.7	88.2	133.3	15	
Nb	13.6	16.8	29.5	10.5	15.3	3	
Hf	-	-	-	-	5.1	-	
Ta	-	2.3	1.2	-	1.06	-	
Th	16.13	24.1	28.88	2.09	8.31	-	
U	5.6	3.94	8.94	2.08	3.58	-	
Pb	27.97	21.65	18.66	5.17	7.99	-	
La	28.91	39.88	10.16	7.64	27.82	-	
Ce	52.85	77.93	23.23	17.08	53.11	-	
Pr	5.5	8.7	3.25	2.49	6.24	-	
Nd	19.49	31.25	13.55	11.22	24.07	-	
Sm	3.5	5.73	4.2	2.33	4.57	-	
Eu	0.56	0.9	0.05	0.62	1.36	-	
Gd	2.58	4.16	4.9	2.7	4.14	-	
Tb	0.4	0.53	0.93	0.43	0.64	-	
Dy	2.36	2.72	6	2.73	3.84	-	
Ho	0.46	0.46	1.25	0.56	0.77	-	
Er	1.35	1.34	3.7	1.78	2.24	-	
Tm	0.19	0.18	0.58	0.27	0.32	-	
Yb	1.18	1.18	3.93	1.65	2.18	-	
Lu	0.18	0.18	0.63	0.24	0.35	-	
⁸⁷ Sr/ ⁸⁶ Sr	0.714022	0.723522	0.96327	0.704719	0.70494	-	
¹⁴³ Nd/ ¹⁴⁴ Nd	-	0.511916	0.512869	0.512665	0.512634	-	
²⁰⁶ Pb/ ²⁰⁴ Pb	19.609	19.58	19.585	19.823	19.732	-	
²⁰⁷ Pb/ ²⁰⁴ Pb	15.713	15.703	15.637	15.694	15.68	-	
²⁰⁸ Pb/ ²⁰⁴ Pb	39.373	39.624	38.986	38.871	39.165	-	

Table C: continued

Coast Belt						
Sample	AL-105	AL-173	AL-106	AL-109	AL-300	AL-301
Rock:	Gr Xenolith	Gr Xenolith	Gr Xenolith	Gr Xenolith	Gr Xenolith	Gr Xenolith
Site	Alligator Lake					
SiO ₂	75.05	72.22	75.18	76.01	71.86	66.92
TiO ₂	0.11	0.38	0.08	0.09	0.14	0.5
Al ₂ O ₃	12.78	15.93	12.73	12.95	15.02	16
Fe ₂ O ₃	1.66	1.81	1.24	1.42	0.84	4.24
MnO	0.03	0.01	0.01	0.01	0.01	0.07
MgO	0	0.58	0	0.03	0.96	1.21
CaO	0.2	0.51	0.26	0.27	1.16	3.05
Na ₂ O	4.04	5.73	2.73	3.84	4.63	4.43
K ₂ O	4.66	1.35	5.52	4.78	4.62	3.66
P ₂ O ₅	0.02	0.17	0.02	0.01	0.04	0.17
LOI	0.65	1.77	2.11	0.2	0.6	0.31
Total	99.2	100.46	99.87	99.61	99.88	100.56
Rb	133	48	145	151	119	118
Cs	-	-	-	-	-	-
Sr	37	192	35	31	314	314
Ba	1087	172	279	382	522	1304
V	-	50	-	-	-	-
Cr	-	64	-	-	-	-
Co	-	-	-	-	-	-
Ni	-	33	-	-	-	-
Zn	-	-	-	-	-	-
Cu	-	-	-	-	-	-
Ga	-	-	-	-	-	-
Y	32	5	36	35	4	19
Zr	237	103	145	187	91	166
Nb	19	11	17	-	9	11
Hf	6.71	-	-	-	-	3.97
Ta	-	-	-	-	-	-
Th	21.84	4.02	-	-	17.74	65.13
U	4.83	1.37	-	-	4.15	8.81
Pb	17.4	4.68	-	-	34.07	12.88
La	47.33	8.69	-	-	21.19	68.59
Ce	92.73	17.83	-	-	41.72	131.7
Pr	11.84	2.12	-	-	4.83	14.16
Nd	47.11	8.23	-	-	17.83	47.35
Sm	9.08	1.5	-	-	3.71	6.85
Eu	0.64	0.34	-	-	0.59	0.87
Gd	8.52	0.98	-	-	2.57	4.74
Tb	1.27	0.13	-	-	0.27	0.63
Dy	8.13	0.86	-	-	1.11	3.64
Ho	1.59	0.18	-	-	0.16	0.75
Er	4.61	0.5	-	-	0.32	2.04
Tm	0.68	0.07	-	-	0.04	0.31
Yb	4.58	0.44	-	-	0.27	2.13
Lu	0.69	0.09	-	-	0.05	0.36
⁸⁷ Sr/ ⁸⁶ Sr	0.713892	0.705095	-	-	0.706545	-
¹⁴³ Nd/ ¹⁴⁴ Nd	0.512532	-	-	-	-	-
²⁰⁶ Pb/ ²⁰⁴ Pb	19.355	19.302	-	-	19.189	-
²⁰⁷ Pb/ ²⁰⁴ Pb	15.673	15.645	-	-	15.652	-
²⁰⁸ Pb/ ²⁰⁴ Pb	39.25	39.218	-	-	38.897	-

Table C: continued

	Coast Belt		
Sample	SG-21	SG-13	SG-35
Rock:	BtGd	BtGd	Gr
	Pluton	Pluton	Pluton
Site	Skagway Road	Skagway Road	Skagway Road
SiO ₂	67.86	67.54	75.2
TiO ₂	0.47	0.45	0.1
Al ₂ O ₃	15.8	15.96	13.27
Fe ₂ O ₃ ^T	3.49	3.4	1.53
MnO	0.07	0.07	0.05
MgO	1.1	0.99	0.15
CaO	2.75	2.77	0.93
Na ₂ O	3.9	3.8	3.72
K ₂ O	4.26	4.26	4.38
P ₂ O ₅	0.18	0.17	0.03
LOI	0.32	0.43	0.62
Total	100.19	99.83	99.97
Rb	121.7	134.8	109.8
Cs	-	-	-
Sr	393.9	394.3	94.8
Ba	1817	1902	1405
V	54	46	-
Cr	-	11.63	-
Co	13	12	-
Ni	-	4	-
Zn	59	62	36
Cu	21	40	2
Ga	16	16.3	14.7
Y	16	16.7	17.7
Zr	153.8	162.5	94.5
Nb	12.7	13.7	11.4
Hf	-	-	-
Ta	-	-	-
Th	19.8	-	-
U	4.64	-	-
Pb	23.58	-	-
La	40.66	-	-
Ce	73.22	-	-
Pr	7.61	-	-
Nd	26.7	-	-
Sm	4.56	-	-
Eu	1.1	-	-
Gd	3.59	-	-
Tb	0.51	-	-
Dy	2.98	-	-
Ho	0.58	-	-
Er	1.71	-	-
Tm	0.24	-	-
Yb	1.62	-	-
Lu	0.26	-	-
⁸⁷ Sr/ ⁸⁶ Sr	0.706159	0.706303	0.708145
¹⁴³ Nd/ ¹⁴⁴ Nd	0.512592	0.512585	0.512602
²⁰⁶ Pb/ ²⁰⁴ Pb	19.38	19.364	19.324
²⁰⁷ Pb/ ²⁰⁴ Pb	15.658	15.667	15.672
²⁰⁸ Pb/ ²⁰⁴ Pb	38.966	39.006	39.004